Characterisation of Psychoactive Substances on Paper Using Various Analytical and Chemometrics Approaches.

Giorgia Vaccaro

Thesis

Submitted to the University of Hertfordshire in partial fulfillment of the requirements of the degree

Doctor of Philosophy

The University of Hertfordshire

School of Life and Medical Science

Department of Clinical, Pharmaceutical and Biological Science

August, 2022

Table of Contents

Table of Tables

Table of Figures

Abbreviations

4-MEC	4-methylethcathinone
5F-PB-22 P	5F-PB-22 Product
Ace	Acetone
AMP	D-Amphetamine
ANOVA	Analysis of Variance
AU	Arbitrary Units
AUC	Area Under the Curve
BBD	Box-Behnken Design
BEN	Benzocaine
BP	Blank Paper
$CaCO_3$	Calcium carbonate
CAF	Caffeine
CC	Calibration Curve
CCD	Charge-Couples Device
CD3OD	Deuterated Methanol
CE	Collision Energy
CHN	Carbon Hydrogen Nitrogen
CL	Confidence Limit
CNS	Central Nervous System
COC	Cocaine
DIA	Diazepam
DLS	Dynamic Light Scattering
DoE	Design of Experiment
DW	Deionised Water
ECF	Elemental chlorine free
EDND	European Database on New Drugs
EI	Electron Impact
EMCDDA	European Monitoring Centre for Drugs and Drug Addiction
ESI	Electro Spray Ionisation
EtOAc	Ethyl acetate
EtOH	Ethanol

FFD	Full Factorial Design
FrFD	Fractional Factorial Design
FTIR	Fourier Transform Infra-Red
GC	Gas Chromatography
GC-MS	Gas Chromatography-Mass Spectrometry
GCxGC	Two-dimensional gas chromatography
GHB	Gamma-hydroxybutyrate
GHV	Gamma-hydroxyvalerate
HCl	Hydrochloric acid/ Hydrochloride
HMP	Her Majesty's Prison
HMIP	Her Majesty Inspectorate of Prisons
HMPPS	Her Majesty's Prison and Probation Services
HPLC	High-Performance Liquid Chromatography
HR	High-Resolution
HRMS	High-Resolution Mass Spectrometry
ICH	International Conference of Harmonization
IMS	Ion Mobility Spectrometry
IR	Infra-Red
IS	Inside the Spot
ITMS	Ion Trap Mobility Spectrometers
K_0	Reduced Mobility Time
LC	Liquid Chromatography
LC-HRMS/MS	High-Resolution Mass Spectrometry/Mass Spectrometry
LLE	Liquid-Liquid Extraction
LOD	Limit of Detection
LOQ	Limit of Quantification
LTQ-Orbitrap	Linear Trap Quadrupole-Orbitrap
m/z	Mass to charge ratio
MC	Microcrystalline Cellulose
MDMA	3,4-Methylenedioxymethamphetamine
MDT	Mandatory Drug Testing
MeOH	Methanol

MIP	Molecularly Imprinted Polymer
MRM	Multiple Reaction Monitoring
MS	Mass Spectrometry
MS/MS	Tandem Mass Spectrometry
MVA	Multivariate Data Analysis
MW	Millipore Water/ Molecular weight
NIST	National Institute of Standards and Technology
NMR	Nuclear Magnetic Resonance
NPS	New Psychoactive Substances
OFAT	One-Factor-At-Time
oLOD	Observed Limit of Detection
OS	Outside the Spot
OTC	Over The Counter
PAR	Paracetamol
PBD	Plackett-Burman Design
PC	Principal Components
PCA	Principal Component Analysis
PdA	Photodiode Array
PFTE	Polytetrafluoroethylene
pH	Potential of Hydrogen
PLS	Partial Least Square
POC	Point of Care
POM	Prescription Only Medicine
PRISMA-S	Preferred Reporting Items for Systematic Reviews and Meta-Analyses
PTFE	Polytetrafluoroethylene
QDa	Quadrupole Dalton
QLIT	Quadrupole Linear Ion Trap
QToF	Quadrupole-Time of Flight
RMA	Rigaku Mixtures Algorithm
RSD	Relative Standard Deviation
RT	Retention Time

SCRA	Synthetic Cannabinoids Receptor Agonists
SCX	Strong Cation Exchange
SERS	Surface Enhanced Raman Spectroscopy
SOP	Standard Operating Procedures
SPE	Solid-Phase Extraction
SPSS	Statistical Package for Social Sciences
SRM	Selected Reaction Monitoring
SS	Stock Solution
SWDRUG	Scientific Working Group for the Analysis of Seized Drugs
TCF	Totally Chlorine Free
TD	Thermal Desorption
TdA	Traditional Drugs of Abuse
TIC	Total Ion Chromatogram
ToF	Time of Flight
TRIS	Trisaminomethane
UH	University of Hertfordshire
UHPLC	Ultra-High-Performance Liquid Chromatography
UHSOP	University Hertfordshire Standard Operating Procedure
UNODC	United Nations Office on Drugs and Crime
UPLC	Ultra-Performance Liquid Chromatography
UV	Ultraviolet
UV-Vis	Ultraviolet-Visible
VDT	Voluntary Drug Testing
WCC	Wavelet Correlation Coefficient
WEDINOS	Welsh Emerging Drugs & Identification of Novel Substances Project
WWA	Wastewater Analysis

Abstract

In recent years, the growing popularity of NPS within the prison system has contributed to the increase in violence, psychotic episodes and self-harm, undermining the rehabilitation of prisoners. A systematic literature review on the detection of NPS in prison settings was carried out to establish an understanding of current research in the field. MEDLINE, Scopus, PubMed, and Web of Science databases and the grey literature were consulted in line with the PRISMA-S guidelines leading to the identification of 50 articles which met the inclusion criteria. Findings showed that the most prevalent NPS class reported in prison was synthetic cannabinoids mainly deposited on paper matrices and smuggled through the postal services. Laboratory-based techniques i.e., LC-HRMS/MS and GC-MS were predominantly employed for the detection of NPS. The IMS was the only technique used for in-field analysis, highlighting a gap in knowledge for specific and selective in-field analytical techniques for such samples. Therefore, the aim of the thesis was the development of an extraction method of psychoactive substances from paper samples which can be used to facilitate the development of a minimally invasive, highly sensitive, in-field detection technique of psychoactive substances on such samples.

Basic extraction properties of paper impregnated with psychoactive substances were investigated to gain knowledge of the process and the percentage recovery using traditional analytical techniques such as LC-UV-Vis and UPLC-PdA-QDa-MS. An extraction method using simulated paper samples impregnated with paracetamol employed as a model substance was optimised and led to the extraction of 80.1 ± 0.7% of paracetamol, over two consecutive extractions. The extraction method was then applied to simulated paper samples impregnated with a ternary mixture of caffeine + cocaine + THJ-018 and the percentage recovery was calculated at 74.7 ± 1.3%, over one extraction. Qualitative analysis of a seized paper sample from prison was carried out to gain insight into the concentration found on such samples, using corroborative analytical techniques i.e., HPLC-PdA-QDa-MS, GC-MS, and NMR, leading to the identification of 5F-ADB. Following up, 5F-ABD was found on another seized paper sample from prison from the same evidence bag as the previous one and was quantified using an optimised and validated UPLC-PdA-QDA-MS method. Concentrations of 5F-ADB calculated on 39 subunits of the sample after three consecutive extractions ranged between 0.00026-0.055 mg/cm^2. Furthermore, the percentage recovery of 5F-ADB from simulated paper samples (n=15) was calculated at three concentrations (C1=20 µL of 1 mg/mL, C2=50

µL of 0.1 mg/mL and C3=10 µL 0.1 mg/mL) over five consecutive extractions, this was found to be 98.7 ± 0.8%. A matrix effect study evaluating five paper matrices impregnated with 5F-ADB was performed, the low RSD calculated over the measurement for each type of paper was of suggested that no matrix effect arises when quantifying 5F-ADB on these specific types of samples.

A PCA model was developed to understand if Raman spectra of psychoactive substances and cutting agents/adulterants i.e., 5F-PB-22, amphetamine, benzocaine, caffeine, cocaine, diazepam, and paracetamol, as a single neat reference standard, as neat binary mixtures and as soaked or pipetted on simulated paper samples, could have been discriminated. Good discrimination could be achieved between the spectra of neat psychoactive substances and related adulterant/cutting agents reference standard analysed. Discrimination using PCA of the Raman spectra of mixtures of psychoactive substances and related adulterant/cutting agents reference standard has been proved challenging due to the impact of the orientation of oscillations of light waves of the excitation laser irradiating the molecules and the different Raman scattering properties of the compounds in the mixtures. While most of the paper samples impregnated with psychoactive substances and related adulterant/cutting agents formed a 'mega cluster' in the scores plot near the BP samples, due to the paper background present in the spectra. However, observation of Raman spectra of such samples showed potential for their discrimination. For instance, when the line plot of the psychoactive substances i.e., 5F-PB-22, amphetamine, cocaine and diazepam reference standard pipetted on the simulated paper samples at five concentrations and collected using Raman Rigaku were examined characteristic peaks of the related reference standard were visible at the highest concentration e.g., 5F-PB-22 pipetted on paper at 20 and 15 mg/mL; cocaine pipetted on paper at 60, 40, 35 and 30 mg/mL.

Finally, a minimally invasive extraction of 5F-PB-22 from simulated paper samples using agar gel was developed and optimised using Design of Experiments techniques. This was performed to facilitate the development of a minimally invasive, highly sensitive, in-field NPS detection technique. The screening phase performed using a 2^5 full-factorial design led to the selection of two statistically significant factors in the process i.e., agar concentration and sonication time. The optimisation phase was then carried out using a two-factor CCD, in which the maximum of the AUC was sought. This identified the optimum agar concentration and sonication time at 2% and 10.95 min, respectively. The extraction time, weight applied, and extraction number

were fixed at 120 sec, 85 grams, and 2 extractions, respectively. The model was successfully validated by running five confirmation experiments using the same parameters as the optimised conditions. A 99.67% increase in the extraction of 5F-PB-22 from simulated paper samples was achieved (unoptimised vs. optimised process 1.20 ± 0.09% vs. 2.36 ± 0.19%). Furthermore, the optimised extraction method has also been successfully applied to a seized paper sample known to contain 5F-ADB.

Keywords: New Psychoactive Substances, NPS, synthetic cannabinoids, prisons

1. Introduction

In recent years, the increasing popularity of New Psychoactive Substances (NPS), especially synthetic cannabinoids, within the prison system, both UK and international, has contributed dramatically to the reduction of the welfare of the prisoners [1–3]. The use of synthetic cannabinoids in prison contributes to violence, psychotic episodes, self-harm, undermining the rehabilitation, and recovery of prisoners. This thesis focuses on the characterisation of smuggled paper matrices into UK prisons impregnated with psychoactive substances specifically synthetic cannabinoids, and related adulterant/cutting agents using various wet-analytical techniques, and on the development of extraction methods with the support of chemometric techniques that support the use of new in-field analytical techniques with a particular focus on Raman spectrometry. This introduction is aimed to give an overview of the thesis by outlining its structure chapter by chapter.

The second Chapter of the thesis "NPS detection in Prison: A Systematic Literature Review of Use, Drug Form, and Analytical Approaches" aimed at identifying the most predominant NPS group reported, their forms, and the analytical methods used to detect them in prisons. It was found that the synthetic cannabinoids were the most predominant NPS group described in the literature. In the last five years, paper matrices impregnated with synthetic cannabinoids were most commonly used to smuggle synthetic cannabinoids as they are easily introduced into prisons via the postal service [4]. Laboratory techniques such as Liquid Chromatography-High Resolution Mass Spectrometry/Mass Spectrometry (LC-HRMS/MS) and Gas Chromatography-Mass Spectrometry (GC-MS) were found to be used for the characterisation of such samples [4]. Since synthetic cannabinoids are smuggled sprayed on paper in low concentrations and often in mixtures, in-field analytical approaches have shown limited ability to identify them. Therefore, a gap in knowledge for specific and selective in-field analytical techniques suitable for the detection of paper samples impregnated with psychoactive substances was highlighted in the literature. Moreover, at the time this project started only one study on qualitative analysis was available in the literature [5], but since then, the knowledge has increased during the lifetime of this project. However, there is still a lack of comprehensive studies, regarding the properties of these new drugs on paper matrices, their extraction in the presence of mixtures, and the use of different paper matrices.

Chapter 3 “Extraction and Qualitative Analysis of Psychoactive Substances from Prison Letters using Corroborative Analytical Techniques” investigated a preliminary method for confirmatory analysis of seized paper samples. A model mixture containing a synthetic cannabinoid (THJ-018) was used to look at the basic extraction properties of paper impregnated with psychoactive substances using traditional standards analytical techniques such as Liquid Chromatography-Ultraviolet-Visible (LC-UV-Vis) and LC-MS. The synthetic cannabinoid 5F-ADB was identified and confirmed in the seized paper samples using UPLC-PdA-QDa-MS, GC-MS, and Nuclear Magnetic Resonance (NMR), thus, this was used in Chapter 4. Challenges related to the use of a low sensitivity MS instrument e.g., UPLC-PdA-QDa-MS, which could not detect the 5F-ADB in a 1 cm^2 piece of paper sampled, highlighted the need for more extracts to be combined. Therefore, a more comprehensive study was carried out in Chapter 4 (“Screening and Quantitative Analysis of Psychoactive Substances from seized paper Prison sample using High-Performance Liquid Chromatography- Mass Spectrometry”). A prison sample, from the same seizure as the one analysed in Chapter 3, was screened using the more sensitive UPLC-PdA-QToF-MS instrument, to see if additional substances were present. Also, sample preparation and analytical methods were optimised to achieve better recovery values and to evaluate different paper matrices impregnated with 5F-ADB. Furthermore, in Chapter 4 quantification of 5F-ADB impregnated on paper was performed with an optimised and validated UPLC-PdA-QDa-MS.

As mentioned above, the use of Raman was investigated as a potential in-field method for the detection of psychoactive substances and related adulterants/cutting agents on paper. In the fifth Chapter “Use of Raman Renishaw InVia and Rigaku Progeny coupled with Chemometric for the Detection and Classification of Psychoactive Substance Impregnated on Papers” using the information on the characteristic concentrations of synthetic cannabinoids found o on the paper sample from Chapter 4, the capabilities of Raman were evaluated on paper samples impregnated with psychoactive substances , specifically the model synthetic cannabinoids 5F-PB-22, and related adulterant/cutting agents. From Chapter 5 onward the model synthetic cannabinoid was changed to the 5F-PB-22 purified product due to a large amount of NPS reference standard being expensive. This represents an additional challenge within this research field. Limitations of Raman instruments in detecting psychoactive substances and adulterants/cutting agents, especially at low concentrations found on seized paper samples were highlighted. In most Raman spectra, resulting from the analysis of simulated paper samples,

the background from the paper itself dominated the spectra hindering the detection of substances on this matrix. Thus, in Chapter 6 "Optimisation of minimally invasive agar-gel extraction of 5F-PB-22 from simulated paper samples using Design of Experiment" it was of interest to investigate methods to extract drugs from paper in a minimally invasive way. The minimally invasive extraction method that was optimised and validated involved the use of agar gel, which preserves the integrity of samples that might be needed in court. Such technique would be highly suitable to be coupled with Surface Enhanced Raman Spectroscopy (SERS), which is a method to enhance the Raman signal of low concentration analyte. Therefore, Chapter 6 work, was aimed to facilitate the development of a minimally invasive, highly sensitive, in-field NPS detection technique e.g., SERS.

2. NPS detection in Prison: A Systematic Literature Review of Use, Drug Form, and Analytical Approaches.

The systematic literature review on the detection of NPS in prison settings, was carried out to establish an understanding of current research in the field to inform and help the development of the experimental chapters of the thesis. The objectives of the systematic literature review were to identify i) the most frequently reported NPS class ii) the routes and forms used for smuggling, and iii) the methods employed to analyse biological and non-biological samples. The aim of the systematic literature review was to identify what has already been done and the gaps in the knowledge within the field.

2.1. Introduction

In recent years, the use of NPS in prison settings has become a cause of concern internationally [1,6–13]. The situation reported by 24 countries including the United Kingdom (UK), Germany, Sweden, Hungary, Latvia, Australia, and the United States of America (USA) [2,13,14] has proven particularly challenging. It has been reported that the use of NPS in prisons has led to increased levels of violence, organized crime, bullying, aggression, and debt[2,12,13,15]. Although initial measures including training modules for staff, implementation of Mandatory Drug Testing (MDT), infrastructural changes, and/or legislative restrictions [13], NPS use in prison remains an issue of major concern [16]. Whilst there is evidence suggesting that the use of NPS worldwide may be declining, this trend is not observed in marginalized groups, including prison populations[17]. Use has increased among such populations, for instance, seizures of NPS in UK prisons have increased from 4,560 in 2017 to 9,114 in 2021[18]. Thus, timely and collated information focused on the identification of NPS in the prison environment is critical to further understand and ultimately tackle NPS use in this setting.

NPS are defined by the United Nation Office on Drugs and Crime (UNODC) and European Monitoring Centre on Drugs and Drugs Abuse (EMCDDA) as "substances of abuse, either in a pure form or a preparation, that are not controlled by the 1961 Single Convention on Narcotic Drugs or the 1971 Convention on Psychotropic Substances, but which may pose a public health threat" [6,19]. In addition, NPS use has been associated with public health risks similar to Traditional Drugs of Abuse (TdA), and they have also been shown to induce unpredictable health risks. The World Drug Report 2020 further specifies that "the term 'new' does not

necessarily refer to new inventions, but to substances that have recently become available" [19]. Due to the structural diversity of NPS, they are largely classified according to their substance groups e.g., aminoindanes, phencyclidine-type substances, phenethylamines, piperazines, plant-based substances, synthetic cannabinoids, synthetic cathinones, tryptamines, and 'other' substances such as designer opioids and benzodiazepines [19].

The use of NPS in prisons was first reported in the UK around 2013 [20] and in the years to follow in other European and non-European countries [13]. These compounds represented a valid alternative to TdA because of their low price, ease of availability, and undetectability [2,7,8,11–13]. In addition, high potency NPS such as synthetic cannabinoids are popular amongst prisoners as the desired effect can be achieved with a lesser amount of substance and hence for a cheaper price [6,12,21]. In particular, synthetic cannabinoids are used in this environment to aid in coping with imprisonment, sustaining existing habits, and for self-medication or pleasure [1]. Until a few years ago NPS in the UK were not normally screened in routine MDT [2], making them an attractive alternative to TdA. Despite that some NPS are now included in MDT, their structures are continuously being altered by producers to avoid detection [42].

The market availability of specific NPS is strictly connected to countries' respective legislation in place at the time of production and/or consumption [22,23]. This results in a constantly evolving market of NPS which presents the main analytical challenge for in-field instruments and laboratories in charge to detect and quantify these substances. The large number of structurally diverse NPS available (~ 950 registered by UNODC [24] and > 4200 on the web [25]), and the pace at which these appear on the market (one new NPS per week [26]) are also contributing factors challenging detection, due to a lag in certified reference standard availability [7,8]. Low concentrations of potent NPS e.g., synthetic cannabinoids or opioids combined with inhomogeneous distribution on new matrices or formulations, employed to facilitate smuggling in prisons, are also factors making difficult their detection and identification [27].

Currently, there are no universal globally agreed Standard Operating Procedures (SOP) in place to identify TdA as well as NPS in prison. Drugs of abuse are often confiscated in this setting via cell, inmate, or visitor searches performed by prison officers [28]. In some countries, such as the UK, USA, and Canada, the use of sniffer dogs has also been reported for the detection of TdA[28] as well as synthetic cannabinoids [5,27]. However, due to the ever-changing nature of the NPS market, it is difficult to maintain the long-term effectiveness of sniffer dogs with these

substances [13]. Once samples suspected to contain drugs are identified, these are screened using in-field analytical techniques such as Ion Mobility Spectrometry (IMS) [29] and/or sent to external forensic laboratories for confirmatory analysis. External forensic laboratories employ traditional analytical techniques such as Gas Chromatography-Mass Spectrometry (GC-MS), Liquid Chromatography-Mass Spectrometry (LC-MS), and Nuclear Magnetic Resonance (NMR), which are costly and time-consuming [30], but can give meaningful information even in the absence of reference standard. In addition, drug use can be identified by analysis of prisoners' biological specimens [28], which are also commonly sent to external forensic laboratories for testing.

This Chapter aims to investigate the current state of chemical detection and identification of NPS in prisons based on the available literature, looking at i) the most predominant groups and specific NPS which have been reported in prison; ii) the routes and forms through which these were smuggled into prison, and ii) the analytical methods employed to detect and identify NPS in biological and non-biological samples from prisons. A particular focus will be given to the UK situation for points i) and ii). Recommendations are then presented in the future works section based on the findings of this review. To the best of the authors' knowledge, this marks the first systematic literature review examining detection in the prison setting for this complex and emerging group of substances.

2.2. Methodology

The methodology has been developed in line with the Preferred Reporting Items for Systematic reviews and Meta-Analyses literature search extension (PRISMA-S) [31], which is a checklist employed to ensure that each component of a systematic literature search is completely reported, hence reproducible. Search words belonging to group 1 (including keywords such as NPS, NPS classes, and their synonyms) were combined using the Boolean operator AND to search words belonging to group 2 (including keywords such as prison and its synonyms), while the Boolean operator OR was used to combine words within a group, to give a search string, listed in full in Appendix 1.1. No other Boolean operator were used. The search was carried out between May 2020 and December 2021 using MEDLINE (EBSCO), Scopus (ELSEVIER), PubMed (NCBI) and Web of Science (Clarivate) databases. A total of 493 citations were added to the review from the string search strategy. No study registries were searched. The grey literature search was carried out between May 2020 and December 2021

and included targeted hand-searching of additional websites. A particular focus was on UK government and/or research organization websites, while European and global agencies' websites were also consulted (Appendix 1.1). A total of 272 additional citations were added to the review from the grey literature search. The selected articles related to the topic were manually cross-referenced to identify additional studies. A total of 1937 additional citations were added to the review from the cross-referencing search. Some organizations were also contacted to enquire about the latest reports and/or additional unpublished data (e.g., UK focal point on drugs, Welsh Emerging Drugs & Identification of Novel Substances Project (WEDINOS), Office for National Statistics UK, and (EMCDDA). No additional information sources or search methods were used. The search was not limited to any time or geographical restrictions. All languages were included in the search results; however, non-English results were excluded during the review process. All document types available were searched on the databases, however, opinion/discussion papers, press releases/magazines/websites articles, published conference abstracts, leaflets, posters, theses, protocols, and patents were excluded. No published filters were used in database searches, while some filters were used for the grey literature search (Appendix 1.1). The comprehensive literature search on Scopus was finalized in December 2021, alerts were set up to provide updates of the literature in the form of weekly e-mails, until the end of April 2021. While the other three databases were added at a later date and, for consistency the time limit was set to April 2021. The duplicates were removed using Microsoft Excel (Version 16.0.13426.20274) function to find and remove duplicates. The general methodology is outlined in the PRISMA flow diagram (Figure 2.1), while the details are reported in Appendix 1.1.

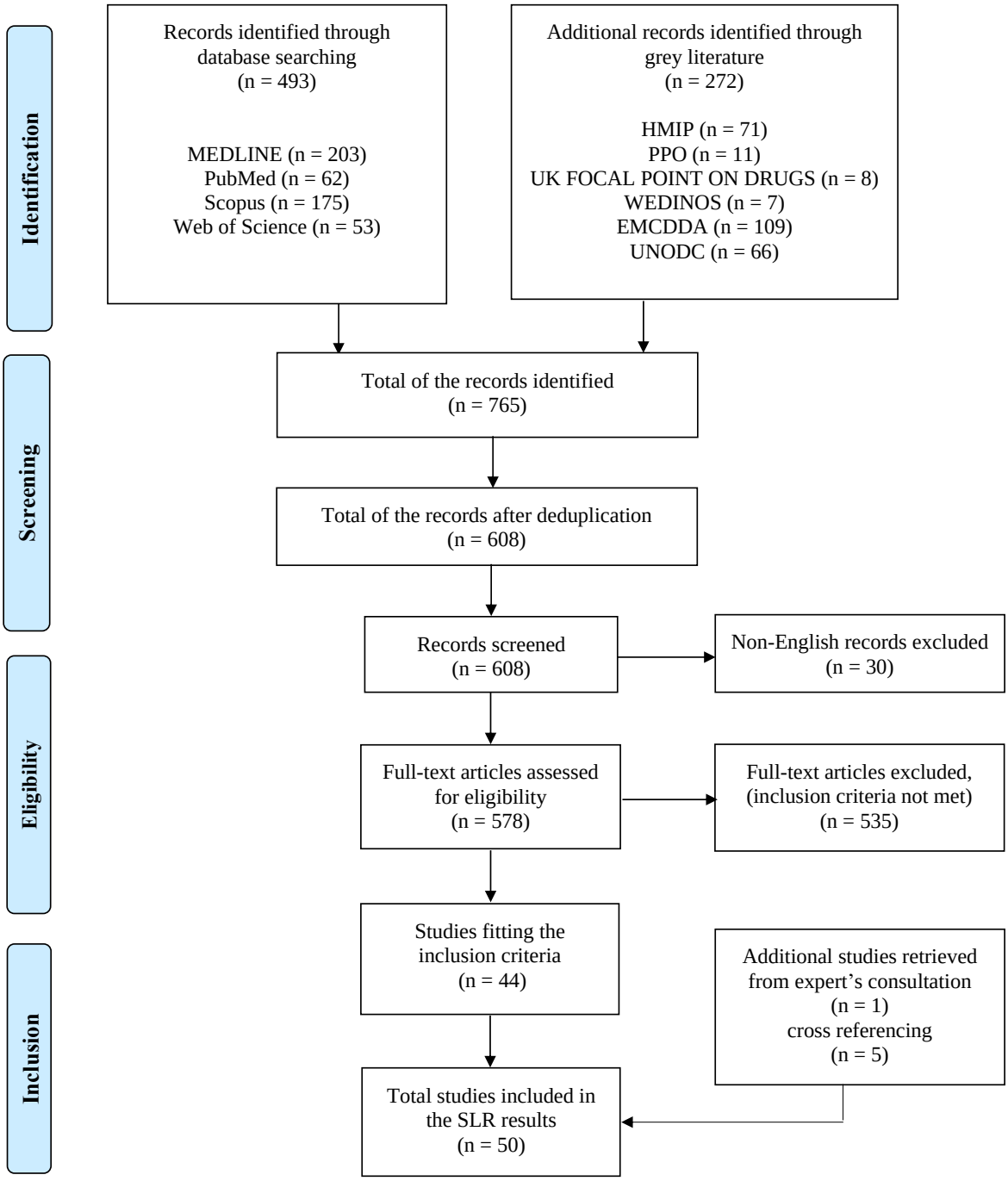

Figure 2.1. PRISMA flow diagram.

2.3. Results and discussion

A total of 50 articles were identified via the systematic review process. Despite the global search, articles have been found to come only from a limited number of countries. Results, which can be divided among the three key themes, are presented and discussed below. Specific aspects of the literature may be presented in different sections for comparison purposes, to present key information according to each theme.

2.3.1. An overview of NPS reported in prisons

To have effective detection approaches, the NPS prisons' scene should be evaluated. This section provides an overview of NPS reported in the prison setting to date, based on the available resources. A variety of sources were identified including quantitative/qualitative self-reporting studies, analytical studies of biological/non-biological samples, organizational reports, and generic publications on NPS in prison. These were used to establish the NPS groups, as well as the specific compounds reported in prisons. Although some of the studies may be different in nature, the information on the NPS group or the specific name was collated to highlight overall observed trends in the literature. The number of publications related to NPS found in prison settings from 1978-2020 has increased from *ca.* 2010 to the present (Appendix 1.3). No articles were found prior to 1978 and those found after 2010 mostly refer to the newly reported NPS phenomena. Most of the articles were quantitative/qualitative self-reporting studies or generic publications on the topic, however, since 2017, interest in the chemical analysis of NPS seized in prisons has increased. For example, approximately 18% (n=2) of the articles published in 2019 had an analytical perspective which increased to almost 38% (n=6) in 2020. Overall, the increasing number of publications demonstrates the growing interest in this topic.

An overview of the types of NPS reported in prisons is shown in Table 2.1.

Table 2.1. NPS reported in prison identified via the systematic literature review.

NPS group[1], subgroup[2] and name	Country	Reference
SYNTHETIC CANNABINOIDS		
Alkoylindoles		
5F-UR-144	England	[32]
FUB 144 (AKA FUB-UR-144)	Germany	[23]
UR-144	England	[32]
Benzoylindoles		
AM-694	England	[32]
Carbazoles		
EG-018	Germany	[23]
γ-carbolines		
5F-CUMYL-PEGACLONE	Germany	[23,33]
CUMYL-CBMEGACLONE	Germany	[23]
CUMYL-PEGACLONE	Germany	[23,29]
Indole carboxylates		
5F-PB-22	England, Wales	[23,32,34]
PB-22 (AKA QUPIC)	England, Germany, Scotland	[29,32,35]
QUCHIC (AKA BB-22)	England	[32]
Indole carboxamides		
5F-MPP-PICA	Scotland	[23,35]
FUB-PB-22 (AKA QUFUBIC)	England	[32]
a) Adamantly derived		
STS-135 (AKA 5F-APICA)	England	[32,36]
b) Cumylamine derived		
5F-CUMYL-PICA	Germany	[23]
CUMYL-CBMICA	Germany	[23]
c) Valinate derived		
5F-EMB-PICA (AKA EMB-2201)	Scotland	[23,35,37,38]
AMB-4EN-PICA (AKA MMB-4 EN-PICA)	Germany	[23]
AMB-FUBICA	Germany	[23]
MMB-2201	Germany	[29]
MMB-CHMICA (AKA AMB-CHMICA)	England, Scotland, USA	[3,10,23,27,32,35]
d) Tert-leucinamide derived		
5F-ABICA[3]	Germany	[23]
e) Tert-leucinate derived		
4F-MDMB-BICA	Belgium, Cyprus, France, Hungary, Lithuania, Slovenia, UK	[23,35,37,38]
5F-MDMB-PICA[3]	Germany, UK, USA	[3,10,13,23,35,37–41]
(R)-5F-MDMB-PICA	Scotland	[22]
MDMB-CHMICA	England, Germany, Wales	[5,23,32,34,42,43]

Indazole Carboxamides		
THJ-2201	England	[32]
a) Adamantly derived		
5F-APINACA (AKA 5F-AKB-48)	England, Wales	[5,23,32,34,36]
APINACA (AKA AKB-48)	England, Germany	[23,29,32,36]
FUB-APINACA	Germany	[23]
b) Cumylamine derived		
5F-CUMYL-PINACA	England	[32]
CUMYL-4CN-BINACA (AKA CUMYL-CYBINACA)	Germany, Lithuania, UK, USA	[10,23,44]
CUMYL-CBMINACA	Germany	[23]
c) Valinamide derived		
AB-CHMINACA	Germany, Lithuania, UK, USA	
AMB-FUBINACA (AKA FUB-AMB, MMB-FUBINACA)	England, Germany, Scotland, Wales, USA	[3,9,10,23,27,29]
d) Valinate derived		
5F-AMB (AKA 5F-MMB-PINACA, 5F-AMB-PINACA)	England, USA	[9,32]
e) Tert-leucinamide derived		
5F-AB-PINACA	England, Germany	[23,32]
5F-ADB (AKA 5F-MDMB-PINACA)	Germany, UK, USA	[3,9,10,23,29,34,35,39,45]
(R)-5F-ADB (AKA (R)-5F-MDMB-PINACA)	Scotland	[22]
5FADB-PINACA	England, G-ermany	[23,32]
AB-FUBINACA[3]	England, Germany	[5,23,32,42]
ADB-BINACA	Germany	[23]
ADB-CHMINACA	Germany	[23,42]
ADB-FUBINACA	Germany, USA	[23,42,46]
f) Tert-leucinate derived		
4F-MDMB-BINACA (AKA 4F-MDMB-BUTINACA)[3]	Germany, Scotland, Wales	[3,23,33,35,38,39,41,47]
(R)-4F-MDMB-BINACA	Scotland	[22]
MDMB-4EN-PINACA[3]	Belgium, Cyprus, France, Germany, Hungary, Lithuania, Slovenia, UK, USA	[3,35,37,38,48]
(R)-MDMB-4EN-PINACA	Scotland	[22]
MDMB-CHMINACA	Germany	[23]
MDMB-FUBINACA (AKA FUB-MDMB, MDMB-BZ-F)	USA	[9]
Naphthoylindoles		
AM-2201	Germany, England, Norway	[32,42,49]
JWH-018	Norway	[23,49]

JWH-081	Germany	[23]
JWH-122	Germany	[23]
JWH-210	Germany	[23]
MAM-2201	England	[32]
7-Azaindole carboxamides		
5F-MDMB-P7AICA	Germany	[23]
CUMYL-4CN-B7AICA	Germany	[23]
Non-specific (e.g., 'Spice')	Croatia, Cyprus, Czech Republic, Finland, France, Germany, Hungary Ireland, Italy, Latvia, Lithuania, Norway, Poland, Slovenia, Sweden and UK	[1,2,12–14,20,50–62]
SYNTHETIC CATHINONES		
4F-PHP	Scotland	[3]
4-MEC	England	[32]
Mephedrone	Australia, England	[32,63,64]
Methylone	Australia	[64]
Non-specific	Cyprus, Czech Republic, Finland, France, Germany, Hungary, Latvia, Lithuania, Poland, Sweden	[13]
OPIOIDS		
Acryloylfentanyl	Latvia	[65]
Carfentanil	Latvia	[66]
Cyclopropylfentanyl	Latvia	[67]
Non-specific	Czech Republic, Finland, Italy, Latvia, Poland, Sweden	[13]
STIMULANTS		
4-methylmethamphetamine	England	[32]
Ethylphenidate	England	[5,32]
Methylhexaneamine	England	[5,32]
Methiopropamine	England	[5,32]
BENZODIAZEPINES		
Etizolam	England	[5]
Non-specific	Finland, Italy, Latvia, Poland	[13]
PIPERAZINES		
1-benzylpiperazine	Sweden	[68]
PLANT-BASED		
Dihydrokavain	England	[32]

PHENCYCLIDINE-TYPE		
Methoxphenidine	England	[5]

[1] The NPS groups were adapted from UNODC Word Drug Report 2020 [19]
[2] The NPS subgroups were adapted from Abate *et al.* [69]
[3] Includes the NPS and its metabolites

The NPS substance groups, reported in order of prevalence, were synthetic cannabinoids, synthetic cathinones, synthetic opioids, benzodiazepines, stimulants, piperazines, and plant-based substances. The predominant group of NPS that have been reported in prison were synthetic cannabinoids, with a total of 63 different synthetic cannabinoids and/or their metabolites. Due to the large number of synthetic cannabinoids reported, this specific group was further divided into the 9 relevant subgroups of alkoylindoles, benzoylindoles, carbazoles, γ-carbolines, indole carboxylates, indole carboxamides, indazole carboxamides, naphthoylindoles, and 7-azaindole carboxamides [69]. The carboxamides were further divided into adamantly, cumylamine, valinamide, valinate, tert-leucinamide and tert-valinate derived groups (Table 2.1). The most frequently referenced synthetic cannabinoids were 4F-MDMB-BINACA (aka 4F-MDMB-BUTINACA), [3,23,33,35,38,39,41,47], 5F-MDMB-PICA [5,35,36,38,39,41–9], 5F-ADB (aka 5F-MDMB-PINACA) [3,9,10,23,29,34,35,39,71], AB-CHMINACA [9,23,29,32,42,72], AMB-FUBINACA (aka FUB-AMB, MMB-FUBINACA) [3,9,10,23,27,29] and MDMB-CHMICA [5,23,32,34,42,43] (Figure 2.2).

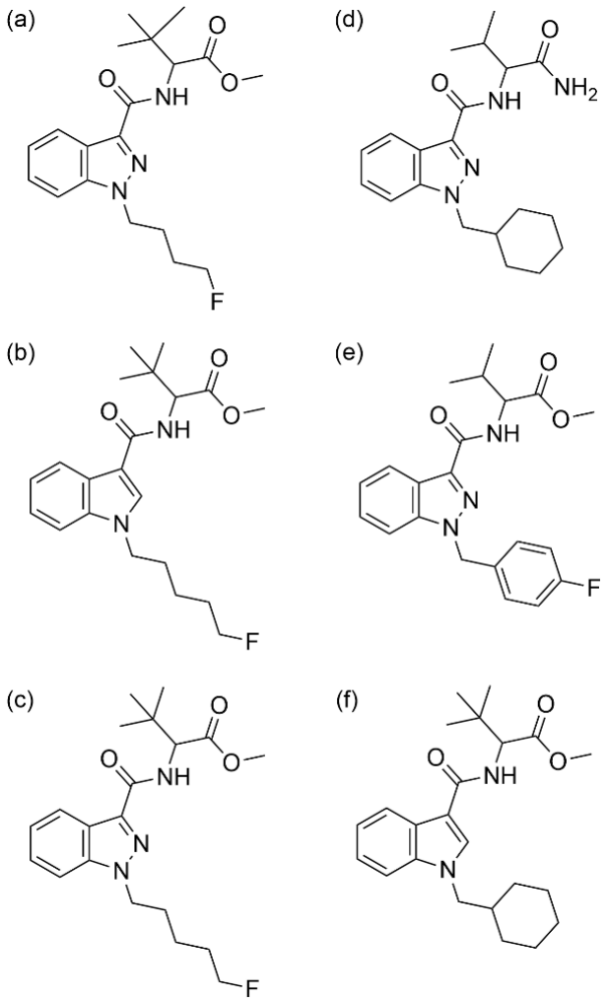

Figure 2.2. Structures of the most reported NPS a) 4F-MDMB-BINACA b) 5F-MDMB-PICA c) 5F-ADB d) AB-CHMINACA e) AMB-FUBINACA and f) MDMB-CHMICA. (Chemdraw Professional, version 16.0, UK).

These all belong to the indazole and indole carboxamide subgroups of tert-leucinamide, tert-leucinate, valinamide and valinate derived. The majority of studies were reported by Germany, the UK, and the USA. The availability of specific synthetic cannabinoids is connected to the legislation related to their production, import, and export countries [22]. For instance, when the People's Republic of China in 2018 placed 32 NPS under control, including 5F-ADB, ADB-FUBINACA, and AMB-FUBINACA a reduction in findings of these substances was registered across different countries [3,23]. A year later new synthetic cannabinoids, structurally related to the latter but not covered by the legislative control e.g., MDMB-4en-PINACA and 4F-MDMB-BINACA, made their appearance on the market [3,23,40,41,47,48]. This highlights the evolving nature of the synthetic cannabinoid market, where trends are also reflected in the prison drug market

[3,23]. Another example of the evolving synthetic cannabinoid market is related to the current loss of popularity of 5F-PB-22, which emerged and peaked from 2013-2015 in the USA [73] and English prisons [32]. The disappearance of 5F-PB-22 from the market was again due to its placement under control by the People's Republic of China in October 2015. Table 2.1 also identifies less common yet more recent synthetic cannabinoids. In January 2019 in Germany, the γ-carbolines derived 5F-cumyl-PEGACLONE was found for the first time in the post-mortem blood and urine of a prisoner [33]. The same synthetic cannabinoid was later found also in urine from German prisons along with cumyl-CBMEGACLONE and cumyl-PEGACLONE, also belonging to the γ-carbolines [23]. Other newly emerging synthetic cannabinoids belonging to the subgroup 7-azaindole carboxamides were 5F-MDMB-P7AICA and cumyl-4CN-B7AICA, also detected for the first time by urinalysis in German prisons in 2021 [23].

Synthetic cannabinoids were also often reported in general studies but referred to by their street name "Spice"; these studies are collated under the "non-specific" subgroup in Table 2.1. A high level of self-reported use of synthetic cannabinoids in England was documented by the "Spice awareness project" (unpublished work) [12] undertaken in a category C prison in November 2014, by a charity. It reported that 80% of prisoners tried "Spice" during their current sentence, while around 65% admitted to using "Spice" currently [12]. Similar results were found in a report published in May 2016, which surveyed 684 prisoners across nine English prisons. It found that 33% of prisoners reported having used "Spice" in the last month, making it the most popular misused substance amongst hooch (illegally brewed alcohol), cannabis, heroin substitutes, and heroin. Interestingly, around 66% of survey respondents thought that more than half of the prisoners in their prison used "Spice". In contrast, a survey by Her Majesty Inspectorate of Prisons (HMPI) distributed to inmates in eight prisons between June and November 2014 (n=1,376) reported that only 10% had used "Spice" during their current sentence [12]. The discrepancies in the results of the self-reported studies might be confounded by the differing level of trust prisoners exhibit towards the organizations conducting the studies [1].

Synthetic cathinones, synthetic opioids, new benzodiazepines, and stimulants were also found. In 2017 ten European countries reported synthetic cathinones being used in their prisons according to the EMCDDA [13]. Additionally, two subsequent studies reported the detection of mephedrone [32,63,64] and 4-methylethcathinone (4-MEC) [32] in English prisons. Synthetic cathinones were also reported in an Australian wastewater analysis (WWA) study, which

identified methylone and mephedrone in a small prison facility [64]. Synthetic opioids were less reported in European prisons in comparison to synthetic cannabinoids and cathinones. Studies reporting opioid usage were confined mainly to the North-Eastern area of Europe and Italy [13]. Specifically, a total of ten seizures of synthetic opioids were reported from prisons in Latvia, including acryloylfentanyl, carfentanil, and cyclopropylfentanyl [65–67]. In England, etizolam was identified sprayed onto letters that were seized and analysed in 2015 [5], where up to three synthetic cannabinoids, stimulant NPS such as ethylphenidate, methoxphenidine, methiopropramine, and adulterants were also detected. It is not well understood why low potency NPS, and adulterants were found in conjunction with synthetic cannabinoids in this matrix, and it was not possible to ascertain whether these were intentionally added to achieve enhanced desirable effects [5] or perhaps to hinder identification.

To a lesser extent, substances belonging to the NPS groups of piperazines, plant-based, and phencyclidine-type have also been reported in prison settings. For example, the NPS 1-benzylpiperazine was detected in Sweden between 2000 and 2002 in 11 post-mortem biological samples [68]. In some of the analysed specimens, traces of amphetamines were also found. It was unclear whether the prisoners intended to take the piperazine analogue or believed that it was amphetamine. Kava (*Piper methysticum)* is a plant that grows in the South Pacific Islands with both stimulant and depressant effects on the Central Nervous System (CNS); its kavalactone, dihydrokavain, was found in three pre-release and one Voluntary Drug Testing (VDT) urine specimens in a prison near Manchester (UK) in 2015 [32]. A thematic report by HMPI, suggests that despite some differences, drug use in prison reflects, to some extent, the use in the general population [12]. Generally, in both prison and the general population, drugs with a depressant effect on the CNS are preferred over their stimulant counterparts [74]. Yet, higher use of stimulants in the general population is suggested by Bonds and Hudson's study (2015) where the results of urinalysis, showed a 3.5-fold increase in stimulant detection for prisoner admission ("on reception" samples) versus incarcerated residents ("pre-release", MDT and VDT samples) [32]. Despite the latter study took place in 2015, it is the only study available reporting data on different NPS classes, including stimulants, in the prison setting. The results from Table 2.1, including literature/reports outside of the UK, also follow an NPS prison trend favouring synthetic cannabinoids, used to relieve stress and boredom of imprisonment [1,2,12].

2.3.2. NPS smuggling routes and forms

Knowledge of potential smuggling routes and forms, which may differ from that of TdA [75,76], could help inform and support the prison security system in tackling the detection and identification of NPS. A total of 26 studies related to NPS smuggling routes and forms, employed to illegally introduce NPS in prisons, were retrieved from the literature.

Seventeen out of 26 studies applied to the NPS smuggling routes employed in prisons and were divided into seven groups (Appendix 1.4- Figure A1). The postal service was highlighted as the most prevalent smuggling route (n=14) for bringing NPS into prisons through parcels or mail [8,10,24,26,39–42,9,49,53,62,67,68]. Due to the trend of spraying NPS on paper, some UK prisons photocopied prisoners' correspondence, which reduced smuggling but was time-consuming. However, in some circumstances (e.g., English and Welsh prison "Rule 39" [78] and Scotland "Legal Mail" [79]) legal confidential correspondence can only be opened and inspected by prison staff in specific situations, which makes photocopying and routine checks more complicated [80]. The second most reported NPS smuggling routes, each described in five articles, were concealment inside the body and transportation over prison walls. Concealment in body orifices [1,2,46,59,76] e.g., gastrointestinal system, rectum, or vagina, is particularly challenging to detect [75], new prisoners were found to smuggle up to 280 g of synthetic cannabinoids through this route [2]. X-ray body scanners able to detect drugs concealed inside the body or under clothes are being introduced in more UK prisons to tackle the issue. Transportation over prison walls was also reported via drones [6,8,10,9,67] or using catapults [12]. NPS thrown over the wall were found to be concealed also in unusual items, such as carcasses of birds [6,9], or oranges [13]. To overcome this issue some prisons installed nets around the perimeters or used radar systems to intercept drones. Lesser reported NPS smuggling routes included via new prisoners or prisoners who were released on bail [1,2,76], prison staff [1,2,12], visitors [8,10,9], and external contractors [13] including cleaning companies, waste disposal trucks, and canteen distributors.

Twenty-five studies detailed the forms in which NPS are smuggled into prisons. The forms reported for NPS in prison (Appendix 1.4- Figure A2) were via paper matrices, herbal mixtures, food and drinks, solid materials, clothes, cosmetics, and e-liquids. Paper matrices (n=19), commonly delivered by postal services or during social visits, were the main form reported that was used to smuggle NPS [1,2,15,47,58–60,76,77] as confirmed by analytical studies performed on seized samples [3,5,10,22,23,27,29,35,40]. The term "paper matrices" is used to encompass letters,

children's drawings, blank paper sheets, greeting cards, photographs, books, documents, poems, blotters, paper snippets, Bible pages, online printed catalogues, rice paper, crossword, and sudoku puzzles [1–3,5,10,15,22,23,27,29,35,40,47,58–60,76,77,81]. Prisoners are believed to take NPS, specifically synthetic cannabinoids, by licking, chewing, swallowing, smoking [5] or placing in eyes [23] the paper, which is usually cut into 1 cm^2 or smaller pieces [29]. When in this formulation and size, such samples are easily concealed, carried, and traded between inmates [3]. Synthetic cannabinoids are commonly produced in solid form, then dissolved in an organic solvent such as acetone, and easily sprayed onto paper matrices [2] or herbal material [32]. Recently, other general reports also highlight paper matrices as the most popular form to smuggle NPS in prison across Europe, especially in Finland, Germany, Hungary, Lithuania, Poland, and Sweden [5,9] because of the challenges in detection [12]. The second most prevalent form reported was herbal mixtures [3,23,29,32,45,63,66,77] (n=8). In particular, herbal/plant material such as marshmallow (*Althea officinalis*) leaves [32] or tobacco [29,63] were mixed or sprayed with synthetic cannabinoids. In UK prisons, inmates were found smoking cigarettes laced with synthetic cannabinoids infused herbs [3], yet after the smoking ban was implemented (2018), NPS were found infused in paper inserted between the heating constituent and the cartridge of e-cigarettes [23]. The increased risk of fatal and non-fatal overdoses, related to the consumption of synthetic cannabinoids in the forms discussed, could also be due to their heterogeneous distribution on the matrices [40]. Areas with a high drug concentration on paper are known as "hot-spots" [13], while those on herbal mixtures are known as "hot-pockets" [82]. Moreover, this has implications for chemical detection, making representative sampling by the analyst challenging [3,32]. Apirakkan *et al.* determined analytically the presence of synthetic cannabinoids dissolved in vaping liquid [27], purchased from internet retailers before the 2016 UK 'legal high ban'. In 2021 synthetic cannabinoids in vaping liquid were also found in Welsh prisons, accounting for only 0.6% of synthetic cannabinoid samples analysed [23]; however, the popularity of this new formulation could grow due to detection difficulty and will require monitoring in the future. NPS were also found in the lid of soft drinks [2] and in the form of pre-sealed food packages such as crackers, coffee, and instant noodles [9]. synthetic cannabinoids were also seized in solid, powder, and crystalline forms [23,32,67] as well as found sprayed on clothing [59] and textiles [29] in prison settings. Lastly, acryloylfentanyl, a new synthetic opioid, was detected in a cosmetic cream in a Latvian prison [65].

2.3.3. NPS detected in non-biological and biological prison samples

The studies in which NPS were detected in non-biological and biological samples from prisons are summarized in Tables 2.2 and 2.3, respectively.

Table 2.2. Summary of NPS detected in non-biological prison samples.

NPS detected	Sample form	Analytical technique	Method	Country	Sample's Year	Reference
AMB-FUBINACA and MMB-CHMICA	Paper	UHPLC-MS/ Q-Orbitrap[1]	Qualitative	England	N.A.	[27]
5F-AKB-48, AB-FUBINACA, ethylphenidate, etizolam, MDMB-CHMICA, methiopropamine, methylphenidate and methoxphenidine	Paper	UPLC-MS/QToF[2]	Qualitative	England	2016	[5]
(S) and (R)-4F-MDMB-BINACA, (S) and (R)-5F-MDMB-PICA, (S) and (R)-5F-MDMB-PINACA, (S) and (R)-MDMB-4en-PINACA	Paper	Chiral HPLC-MS/QToF	Qualitative	Scotland	2018-2020	[22]
4F-PHP, 4F-MDMB-BINACA, 5F-MDMB-PICA, 5F-MDMB-PINACA, AMB-CHMICA, AMB-FUBINACA and MDMB-4en-PINACA	Paper	GC-MS[3]; UPLC-MS/QToF and NMR[4]	Qualitative	Scotland	2018-2019	[3]
4F-MDMB-BINACA and 5F-MDMB-PICA	Paper	GC-MS and HPLC-MS/QtoF	Qualitative	Germany	2019	[40]
4F-MDMB-BUTINACA, 4F-MDMB-BUTINACA 2'-indazole isomer, 5F-ADB and 5F-MDMB-PICA	Paper	GC-MS	Qualitative	USA	2019	[10]
4F-MDMB-BICA, 4F-MDMB-BINACA, 5F-EMB-PICA, 5F-MDMB-PICA, 5F-MPP-PICA, 5F-MDMB-PINACA, AMB-CHMICA, MDMB-4en-PINACA and PB-22.	Paper	IMS[5]; GC-MS and UPLC-MS/QtoF	Qualitative	Scotland	2018-2020	[35]
4F-MDMB-BICA, 4F-MDMB-BINACA, 5F-EMB-PICA, 5F-MDMB-PICA, 5F-MDMB-	Paper	GC-MS and UPLC-MS/QtoF	Qualitative	Scotland	2018-2020	[23]

PINACA, 5F-MPP-PICA and MDMB-4en-PINACA						
4F-MDMB-BINACA, 5F-APINACA, 5F-MDMB-PINACA, 5F-PB-22, AMB-FUBINACA, MDMB-4en-PINACA and MDMB-CHMICA	Herbal mixture, solid, paper, e-liquid	UPLC-MS/QtoF	Qualitative	Wales		
5F-ADB (5F-MDMB-PINACA), AB-CHMINACA, APINACA, cumyl-PEGaClone, FUB-AMB, MMB-2201 and PB-22	Herbal mixture, paper	IMS and GC-MS	Qualitative	Germany	N.A.	[29]
5F-AKB-48, 5F-AMB, 5F-PB-22, 5F-UR-144, AB-CHMINACA, AB-FUBINACA, AKB-48, AM-2201, FUB PB-22, MAM-2201, MDMB-CHMICA, PB-22, QUCHIC, STS-135 and UR-144	Herbal mixtures	GC-MS	Qualitative	England	2014-2015	[32]
5F-AKB-48, 5F-PB-22, AB-FUBINACA, AKB-48, AM-2201, mephedrone, PB-22 and STS-135	Herbal mixtures	UPLC-MS/QtoF	Qualitative	England	2014-2015	[63]

[1]Ultra-High Performance Liquid Chromatography-Mass Spectrometry/Quadrupole-Orbitrap

[2]Ultra-Performance Liquid Chromatography-Mass Spectrometry/Quadrupole Time of Flight

[3]Gas Chromatography-Mass Spectrometry

[4] Nuclear Magnetic Resonance

[5] Ion Mobility Spectrometry

Table 2.3. Summary of NPS detected in biological prison samples.

NPS detected	Sample Form	Analytical technique	Method	Country	Sample's Year	Reference
4-MEC, 4-methylmethamphetamine, 5F-AB-PINACA, 5F-ADB-PINACA, 5F-AKB-48, 5F-PB-22, 5F-UR-144, AB-CHMINACA, AB-FUBINACA, ADB-FUBINACA, AKB-48, AM-2201, AM-694, cumyl-5F-PINACA, ethylphenidate, FAM-2201, dihydrokavain, mephedrone, methiopropamine, methylhexaneamine. MAM-220, MDMB-CHMICA, STS-135, THJ-018, THJ-2201 and UR-144	Urine	UHPLC-MS/ LTQ-Orbitrap[1] and UHPLC-MS/ Q-Orbitrap	Qualitative	England	2014-2015	[32]
SCRAs	Urine	Immunoassay				
3rd generation adamantly SCRA	Urine	UPLC-MS/QToF	Qualitative	England	N.A.	[36]
4F-MDMB-BICA, 4F-MDMB-BINACA, 5F-ABICA amide hydrolysis metabolite, 5F-AB-PINACA, 5F-ADB-PINACA, 5F- cumyl-PEGACLONE, 5F-cumyl-PICA, 5F-MDMB-P7AICA, 5F-MDMB-PICA, 5F-MDMB-PINACA, AB-FUBINACA amide hydrolysis metabolite , AB-CHMINACA, ADB-BINACA, ADB-CHMINACA, ADB-FUBINACA, AMB-4en-PICA, AMB-CHMICA, AMB-FUBICA , cumyl-4CN-B7AICA, cumyl-4CN-BINACA, cumyl-CBMEGACLONE, cumyl-CBMICA,	Urine	UHPLC-MS/TQ[2]	Qualitative	Germany	2018-2020	[23]

cumyl-CBMINACA, cumyl-PEGACLONE, EG-018, FUB-144, FUB-APINACA, JWH-081, JWH-122, JWH-210, MDMB-4en-PINACA, MDMB-CHMINACA						
4F-MDMB-BINACA 3,3-dimethylbutanoic acid and 5F-MDMB-PICA 3,3-dimethylbutanoic acid	Urine	UHPLC-MS/QToF	Qualitative	USA	2019	
1-benzylpiperazine	Urine	GC-MS	Qualitative	Sweden	2000-2002	[68]
5F-ADB[3], 5F-AMB[3], AB-CHMINACA[3], FUB-AMB[3] and MDMB-FUBINACA[3]	Blood, urine	UPLC-MS/TQ	Quantitative	USA	2017-201	[9]
5F-cumyl-PEGACLONE and 5F-cumyl-PEGACLONE[4]	Blood, urine	UHPLC- QLIT[5]	Quantitative	Germany	2019	[33]
ADB-FUBINACA	Blood, urine	UHPLC-MS/QToF	Quantitative	USA	N.A.	[46]
MDMB-4en-PINACA 3,3-dimethylbutanoic acid	Blood	UHPLC-MS/QToF	Qualitative	USA	2019	[48]
4F-MDMB-BINACA and 5F-MDMB-PICA	Blood	GC-MS and HPLC-MS/QToF	Quantitative	Germany	N.A.	[41]
MDMB-CHMICA	Blood	UPLC-MS/QToF	Qualitative	England	N.A.	[43]
AM-2201 and JWH-018	Saliva	UPLC- MS/TQ	Qualitative	Norway	N.A.	[49]
Mephedrone and methylone	Wastewater	UHPLC-MS/QLIT	Quantitative	Australia	2013	[64]

[1]Ultra-High Performance Liquid Chromatography-Mass Spectrometry/Linear Trap Quadrupole-Orbitrap

[2] Ultra-Performance Liquid Chromatography®- Mass Spectrometry/Triple Quadrupole

[3]Identified by their butanoic acid conjugated metabolites

[4]Metabolites

[5]Ultra-High Performance Liquid Chromatography-Mass Spectrometry/Quadrupole Linear Ion Trap

Synthetic cannabinoids were the most reported group of NPS in both samples' matrices [3,9,10,22,23,32,33,35,36,40,41,43,46,48,49]. Based on the results of our review 5F-APINACA (aka 5F-AKB-48) (337 findings), 4F-MDMB-BINACA (aka 4F-MDMB-BUTINACA) (273 findings), 5F-PB-22 (273 findings), MDMB-4en-PINACA (246 findings), 5F-MDMB-PICA (141 findings) 5F-ADB (aka 5F-MDMB-PINACA) (131 findings) were the most reported NPS in seizures. While the most detected synthetic cannabinoids in biological samples were 5F-AKB-48 (1449 findings), MDMB-CHMICA (584 findings), and 5F-MDMB-PICA (388 findings), 4F-MDMB-BINACA (301 findings), MDMB-4en-PINACA (166 findings) and AB-FUBINACA (124 findings). The above specific synthetic cannabinoids results are skewed by the extensive number of samples analysed in the study carried out by Bonds and Hudson in English prisons, where 39% of seized samples (n=1088) and 17.9%/16.9% of phase I (n=7395) /phase II (n=1833) urine samples tested positive for synthetic cannabinoids [32]. Although this study gives an indication of the extent synthetic cannabinoids are used in prisons it is dated back to 2015 and does not necessarily reflect current prison trends on specific synthetic cannabinoids. A more recent study by Norman *et al.* (2021) reported about synthetic cannabinoids found in prison seizures between 2018 and 2020 in Scotland and Wales [23]. In this study, the most prevalent were 4F-MDMB-BINACA (aka 4F-MDMB-BUTINACA) (244 findings) MDMB-4en-PINACA (209 findings) and 5F-ADB (aka 5F-MDMB-PINACA) (179 findings). The same study also reported a 33.6% incidence of synthetic cannabinoids detection in urine samples from German prisons [23] of which 5F-MDMB-PICA (376 findings), 4F-MDMB-BINACA (aka 4F-MDMB-BUTINACA) (297 findings) MDMB-4en-PINACA (165 findings) were the most reported. This study, carried out internationally, showed that some similarities between countries such as Germany, England, Wales and the USA, were present, e.g., high prevalence of 5F-MDMB-PINACA, which are usually driven by legislation in countries producing NPS and international control. However, differences are seen as well; for instance, γ-carboline synthetic cannabinoids were often found in Germany, yet rarely seen in UK and USA prisons.

2.3.3.1. Analysis and sample preparation for NPS in non-biological matrices

Seized NPS were mainly found impregnated into paper or herbal material in the prison setting (Table 2.2). Literature findings revealed that the mainstay analytical techniques employed for the analysis of non-biological prison samples were Liquid Chromatography (LC) [3,5,22,23,27,35,40,63] or Gas Chromatography (GC)[3,10,23,29,32,35,40] coupled with mass spectrometry

(MS), which are regarded as highly discriminatory techniques for forensic analysis of drugs [83]. Table 2.2 shows a prevalence for the use of High-Resolution Mass Spectrometry (HRMS) such as QtoF [3,5,22,23,35,40,63] and quadrupole-orbitrap [27]. In seven studies GC-MS was employed either as a stand-alone [10,32] or alongside other techniques [3,23,29,35,40]. The in-field technique IMS was evaluated in two studies screening for synthetic cannabinoids in prison [29,35].

Bond and Hudson developed an analytical workflow for general seized material in prison [32]. Firstly, unknown powders were analysed by colourimetric tests while tablets were compared against the TICTAC database, then in some cases further analysed either by IR or GC-MS. Herbal matrices were analysed by GC-MS. Only 15 different synthetic cannabinoids in the form of herbal material were detected, and no other NPS were found in these prison seizures [32]. Herbal matrices were reported in an additional three studies where extraction was performed using pure methanol [23,29,63] or ethanol [32]. Some studies reported centrifugation and withdrawal of supernatant [63] or filtration of the extracts [29] to reduce impurities introduced in the chromatographic column. Ford and Berg (2016) were able to detect a wide range of substances with different polarities in seized herbs using UPLC-MS/ Quadrupole Time of Flight (QToF) with two simultaneous screening methods [63], a "NOIDS screen" (>100 synthetic cannabinoids) and a "general screen" (>1300 drugs and metabolites). It was more common to see samples containing only one synthetic cannabinoid [23,29,32,63], however, some samples contained multiple synthetic cannabinoids. Up to eight synthetic cannabinoids were found in one sample by Bond and Hudson [32]. The majority of studies found in Table 2.2, characterized NPS on paper seized in prison. Ford and Berg (2018) were the first to present analytical evidence of NPS smuggled on paper. In this study, as well as Apirakkan *et al.*, sniffer dogs were used initially to detect synthetic cannabinoids on paper samples which were then sent for further analysis [29,35]. In general, paper matrices were sampled using areas ranging from 0.70-1 cm^2 [3,5,10,22,29,40]; for example, a biopsy punch was employed by Norman *et al.* to ensure sampling consistency. Samples were extracted for 5 to 20 min [3,5,27,40] in either pure methanol [3,5,10,22,27,29,40] or a combination of methanol and dichloromethane (25:75) [3], in order to cover compounds with different polarities. To extract substances from paper one extraction was used in most studies [3,5,10,22,27,29,40]. McKenzie and co-workers [3] spiked paper with known quantities of synthetic cannabinoids (i.e., 5F-MDMB-PICA, 4F-MDMB-BINACA, 5F-MDMB-PINACA, AMB-FUBINACA and AMB-CHMICA) and showed that 94.16-98.43% was recovered after one extraction in 25:75 methanol/dichloromethane with *ca.* 100% recovery when three consecutive

extractions were performed. In the case of Hascimi *et al.*, a paper sample was seized from a deceased inmate's cell who tested positive for 4F-MDMB-BINACA metabolite in urine. Analysis of the paper sample showed no synthetic cannabinoids using GC-MS, however further analysis with the more sensitive HPLC-MS/QtoF identified 4F-MDMB-BINACA and 5F-MDMB-PICA[40]. This case highlights the importance of determining typical concentrations for NPS and specifically synthetic cannabinoids on paper to determine which methods/techniques are the most suitable for these sample types. To this end, McKenzie and co-workers used a combination of two techniques for the identification and quantification of synthetic cannabinoids infused in paper seized in Scottish prisons between 2018-2019 [3]. This was the first report on synthetic cannabinoid concentrations in paper samples (n=145). The synthetic cannabinoids quantified by GC-MS, collected by 3x extraction, were the following: 5F-MDMB-PICA (n=59, <0.08 ± 0.01 to 0.76 ± 0.11 mg/cm^2 paper); 4F-MDMB-BINACA (n=45, <0.09 ± 0.01 to 0.94 ± 0.14 mg/cm^2 paper); 5F-ADB (n=42, <0.05 ± 0.01 to 1.17 ± 0.17 mg/cm^2 paper); MDMB-4en-PINACA (n=22, <0.07 ± 0.01 to 0.58 ± 0.09 mg/cm^2 paper); AMB-FUBINACA (n=5, 0.20 ± 0.03 to 1.16 ± 0.17 mg/cm^2 paper) and AMB-CHMICA (n=1, 0.58 ± 0.09 mg/cm^2 paper) [3]. Furthermore, concentration mapping showed a 5-fold variability of AMB-CHMICA concentration across a seized paper sample ranging between 0.47-2.38 mg/cm^2 [3] demonstrating the inhomogeneity of synthetic cannabinoids across paper samples linked to the drying process employed. A study by Caterino *et al.* evaluated the impact of latent fingerprint detection (i.e., exposure to 1,8-diazaflouren-9-one (DFO) and ninhydrin) on the extraction and detection of synthetic cannabinoid impregnated paper [10]. The presence of four synthetic cannabinoids, 4F-MDMB-BUTINACA, 5F-ADB, 5F-MDMB-PICA, and the 2'-indazole isomer of 4F-MDMB- BUTINACA, were successfully identified by GC-MS before and after fingerprint analysis, as well as in the ninhydrin run-off. Although synthetic cannabinoids were detected in all three scenarios, the quantitative analysis would be helpful to assess the concentration reductions encountered due to this type of processing. In an effort to distinguish synthetic cannabinoid optical isomers found on paper, Antonides *et al.* used two chiral columns (i.e., a Phenomenex Lux® Amylose-1 and Lux® i-Cellulose-5 (5 μm, 4.6 × 100 mm)) coupled to an HPLC-photo diode array (PDA)-MS/QToF method to analyse 177 synthetic cannabinoid infused paper samples seized in Scottish prisons between 2018 and 2020 [22]. synthetic cannabinoids were the enantiopure (*S*)-enantiomer in > 89% of the samples, although in 2-16% the (*R*)-enantiomer was detected as well. This study highlighted the

potential for chiral profiling of chiral valinate and *tert*-leucinate based synthetic cannabinoids to distinguish production batches of drugs for intelligence purposes.

The in-field technique IMS was evaluated in two studies screening for synthetic cannabinoids in prison [29,35]. Generally, laboratory-based hyphenated techniques are regarded as confirmatory techniques, while in-field techniques are employed as a preliminary test. Quick, minimal, and non-destructive sample preparation makes IMS well-suited for in-field analysis by non-expert users; for example, the analytes were collected by rubbing a Teflon sample trap on the sample's surface [29,35]. Metternich *et al.* evaluated both simulated and prison casework samples using the IMS IONSCAN600® [29]. The simulated samples contained mixtures of 5F-ADB, and five TdA/ Prescription Only Medicine (POM) (100 ng for each compound) concealed in cosmetic and food samples, while 36 casework samples were mainly in herbal and paper form. The IMS identified 5F-ADB in most of the matrices evaluated (i.e., 9 of 11), but failed in highly viscous matrices (e.g., toothpaste or liquid soap). For the casework samples, 12 samples (mainly herbal material) tested positive for synthetic cannabinoids which were confirmed by GC-MS analysis. In contrast, Norman *et al.* focused on the detection of synthetic cannabinoids in seized paper samples (n=392) to evaluate the operational reliability of two Ion Trap Mobility Spectrometers (ITMS®), the Rapiscan Itemiser® 3E and 4DN [35]. Sampling was performed on paper of varying sizes which resulted in high trap loading variability [35]. A limited but tailored IMS library, comprised of nine "Spice alarms", was employed to detect the synthetic cannabinoids using the reduced mobility (K_0) [29] and drift time [35]. The study found that the level of agreement between ITMS® and GC-MS results was 91.1% for the Itemiser® 3E and 92.9% for the Itemiser® 4DN instruments. Reasons for disagreement included false negative (e.g., no IMS alarm generated for trace or multiple synthetic cannabinoids present) and false positive (e.g., Spice, buprenorphine, and cocaine alarms generated by IMS, but not detected by GC-MS). The Itemiser® 3E was more suitable for the detection of synthetic cannabinoids due to its ability to detect cumyl compounds (cumyl-4CN-BINACA and 5F-cumyl-PEGACLONE), compared to the Itemiser® 4DN. The observed LODs (oLOD) were determined for nine synthetic cannabinoids and ranged from 0.5 to 100 ng and 5 to 500 ng for the Itemiser® 3E and Itemiser® 4DN (Region 0) instruments, respectively. It was highlighted that variability of the K_0 values for the compounds between different instruments could lead to misidentification or false negatives [35]. Reduced selectivity can occur as substances that exhibit a difference < 0.025 $cm^2 V^{-1} s^{-1}$ in their K_0 values cannot be discriminated unambiguously [84] e.g., 5F-PB-22 and AB-

CHMINACA with K_0 values of 0.9995 and 0.9975 $cm^2 V^{-1} s^{-1}$, respectively [29]. On the other hand, newly emerging synthetic cannabinoids with structural similarity to the compounds already in the library can potentially be identified [35], based on the overlapping K_0 values [84]. Nonetheless, IMS has difficulty when detecting more than one analyte in a mixture, where only the analyte with higher peak intensity is detected by the instrument e.g., in a sample containing a mixture of AB-CHMINACA, APINACA, 5F-ADB, MMB-2201 and caffeine only 5F-ADB was detected [29]. Additionally, the low LOD, in the ng range [29,35], could lead to false positives due to cross-contamination, arising from papers collected and stored in the same evidence bag [35].

2.3.3.2. Analysis and sample preparation of NPS in biological matrices

In this section, articles including post-mortem analysis of specimen [9,33,41,48], case studies of prisoners admitted to hospital following NPS intake [36,43,46], as well urine [23,32,68], saliva [49] or wastewater [64] analysis carried out on prison samples are presented (Table 2.3). In general, biological samples were pre-treated, before NPS extraction, by the addition of buffers (i.e., acetate,[32] phosphate,[23,32,41] or carbonate [23,33,36]) and/or pH manipulation by addition of sodium hydroxide [68] or trisaminomethane (TRIS) HCl [9,48] to reduce enzymatic activity and preserve the NPS. The main analytical technique employed for the analysis of biological samples (i.e., 12 out of 13 studies) was liquid chromatography coupled with mass spectrometry (LC-MS) or tandem mass spectrometry (MS/MS). Different MS analysers or their combination such as triple quadrupole [9,23,49], QToF [23,36,41,43,46,48], linear trap quadrupole-orbitrap [32], quadrupole-linear ion trap [64] were employed. These analysers are all equipped with HRMS-MS capabilities except for the triple quadrupole. Additionally, the use of GC-MS [41,68] and one immunoassay [32] was also reported.

Urine was the biological matrix most reported for antemortem detection of NPS consumed by prisoners [23,32,36,46,68]. The preference for this matrix can be explained by the low invasiveness of the collection technique, and the longer detection window of drug metabolites (days-weeks), when compared to blood matrices (hours-day). However, urine is susceptible to factors including quantity collected, pH, and differences in individual metabolism which may influence the quantitative results [85]. Additionally, urinalysis leads to minimal parent drug detection, while being more useful for the identification of metabolites. For instance, different synthetic cannabinoids can undergo different metabolic reactions in the human liver and form

the same metabolite; thus, making the identification of the exact synthetic cannabinoid ambiguous e.g., 5F-ADBICA amide hydrolysis metabolite may result from 5F-ABICA, 5F-AMB-PICA, or 5F-EMB-PICA metabolism [23]. However, in a clinical rather than a forensic context this is not always disadvantageous as demonstrated by Rook *et al.*, which employed the metabolite 1-adamantylamine as a urine marker to quickly identify adamantly-type synthetic cannabinoids e.g., 5F-AKB-48, AKB-48 and STS-135 in an emergency context [36]. Extraction of the NPS from urine samples was performed by standard techniques such as precipitation, filtration, Liquid-Liquid Extraction (LLE) [32,36,68], and Solid-Phase Extraction (SPE) [23,32,41]. Bonds and Hudson employed a reversed-phase SPE (i.e., Agilent Nexus polymer sorbent) and extracted analytes with different polarities such as non-synthetic cannabinoids NPS, Over the Counter (OTC)/POM, and TdA [32]. Similarly, a SPE cartridge based on a bimodal non-polar and Strong Cation Exchange (SCX) mechanism (i.e., Agilent Bond Elut Certify cartridge) was also effective at extracting synthetic cannabinoids along with other drugs (e.g., cocaine and amphetamine-like substances) [41]. Lastly, Norman *et al.* employed a non-polar and anion exchange SPE cartridge (i.e., Agilent Bond Elut Plexa PAX) effective for synthetic cannabinoids and their metabolites [23]. In an effort to recover NPS for quantification purposes, β-glucuronidase enzymes [9,23,32] were often added to urine samples to hydrolyse glucuronide metabolites back to the parent drug. Rook *et al.* employed the UPLC-MS/QToF qualitative methods previously described by Ford and Berg (2016) [36] for the analysis of non-biological samples. Similar to Ford and Berg (2016), Bond and Hudson employed simultaneously two screening methods with a UHPLC-MS/ LTQ-Orbitrap and a UHPLC-MS/ Q-Orbitrapto to detect NPS in urine specimens (i.e., a "general screen" and a "SCRA screen" respectively) to cover a wider range of substances with different polarities, increasing the chance of positive detection [32]. The UHPLC-MS/TQ system, employed for the analysis of urine samples from German prisons, successfully identified, on full scan, 31 synthetic cannabinoids and metabolites, which were then confirmed in multiple reaction monitoring (MRM) mode [23]. Several studies also utilized a stable isotopically labelled (SIL) IS to correct for analyte loss during sample preparation [9,32,68] e.g., hydroxypentyl JWH-018-d5. synthetic cannabinoids in biological matrices are not usually detected through GC-MS methods [9] due to low concentration and the requirement of a derivatization step before analysis. In one case, GC-MS was successfully employed to analyse urine samples (i.e., derivatization via fluorinated anhydride) from 11 prisoners for the emerging NPS, 1-benzylpiperazine [68]. A Point of Care (POC) test was also trialled for the screening of urine samples from prisons. The 'Spice'

immunoassay ‘dip and read’ was externally validated on urine samples (n=514); it gave a positive synthetic cannabinoid match for only 1.4% of the samples tested vs 20% confirmed by UPLC-MS/MS [32]. A high number of results (n=96) were likely false negatives, while 0.2% false positives were recorded. This highlighted limitations in coverage and sensitivity; therefore, the authors did not recommend the use of such immunoassay [32]. When performing immunoassays, the usefulness of false positives, which may be due to the cross-reactivity of substances present in a sample that have similar characteristics, must be noted.

Blood samples were used in post-mortem [9,33,41] or antemortem analysis in hospitalized and unresponsive prisoners [43,46] as it involves a more invasive collection by trained staff. In general blood, specimens are more challenging to handle and store due to putrefaction and autolysis processes [85] especially when post-mortem. Blood analysis enables mainly detection of the parent drug in contrast to urine analysis [85], however, it is possible to detect the metabolite in blood as well e.g., MDMB-4en-PINACA 3,3-dimethylbutanoic acid detected in postmortem femoral blood [48]. The characteristic and quality (i.e., pH level, presence of clots, and water quantity) of blood specimen is strictly related to the site of blood collection e.g., central, or peripheral. Central blood, due to post-mortem redistribution, contains increased drug levels [33], which may compromise exact quantification, hence analysis of femoral blood is preferable. For example, Giorgetti *et al.* found a higher quantity of the novel synthetic cannabinoid 5F-cumyl-PEGACLONE in central (0.22 ng/mL) vs femoral (0.12 ng/mL) blood [33]. The addition of SIL IS e.g., JWH-200-d5 in this case was employed for accurate quantification purposes of synthetic cannabinoids. This study also highlighted the challenges related to the lack of data on post-mortem redistribution and toxic concentration ranges in the assessment of the toxicological significance score of synthetic cannabinoids. In contrast, higher concentrations (34-17 ng/mL) of the synthetic cannabinoid ADB-FUBINACA were detected in the serum of a “body packer” after the containment was compromised [46]. To target low synthetic cannabinoid concentrations Kleis *et al.* [41] reported an LC-MS/QToF qualitative screening approach run in auto-MS/MS, a data-independent acquisition (DIA) scan mode in conjunction with a preferred synthetic cannabinoids list. This was used to identify 5F-MDMB-PICA and 4F-MDMB-BINACA in the femoral blood of an inmate, which were then quantified and found to be 0.14 and 0.48 ng/mL respectively. In addition, Krotulski *et al.* also used a DIA scan mode termed MS/MS^{ALL} with SWATH® acquisition which records the MS/MS of every molecule in the sample which led to the detection of MDMB-4en-PINACA metabolite in a forensic

toxicological case of an inmate [48]. A data mining approach which is the retrospective analysis of data files acquired under non-targeted conditions to determine the presence of drugs that were not tested for at the time of first data processing was also applied to the samples analysed by these authors. Meyyappan *et al.* employed the same UPLC-MS/QToF qualitative methods previously described by Ford and Berg (2016) [36] and Rook *et al.* [36].

Lastly, NPS were also detected in saliva and wastewater. As the need for easy and non-invasive collection of biological specimens is increasing Øiestad *et al.* [49] validated a screening method for synthetic cannabinoids using a commercially available oral fluid collection device. Time to sampling was highlighted as a key factor for the analysis of this matrix, due to the high enzymatic activity in the saliva. However, stability issues were overcome by the addition of a preservative solution in the vial of the collection device made of chlorhexidine digluconate, Tween® 20, Flag Blue dye and deionized water, followed by storage at 4°C. During the analysis a large ion enhancement of up to 6000% was recorded, due to the use of the preservative solution. A diazepam-d5 IS was added during sample preparation, yet was not useful as it eluted earlier in the run, highlighting the importance of the accurate selection of IS. This method also offered the advantage of detecting the parent drugs instead of the metabolite, however, the potential for adulteration or contamination should be considered. Wastewater analysis (WWA) was carried out in a small Australian prison to assess drug use and to compare its result to urinalyses [64]. This approach allowed a daily representation of drugs used by prisoners; for instance, on day 12, 537 mg (3-5 daily doses) of methylone were detected. Mephedrone was also detected but concentrations were below the quantification limit (<0.0001–<0.025 μg/L) of the UHPLC-MS/quadrupole linear ion trap (QLIT) employed. When WWA and urinalyses were compared, no methylone was detected by urinalyses due to the different types of sampling. This highlights the advantage of WWA in gaining a daily picture of the overall use of drugs in contrast to routine urinalyses, which are often targeted. However, it was unfeasible to discern between the prisoner and staff/visitor's contributions [64].

2.4. Conclusions

This study reviewed the NPS reported in prisons, ways and forms in which they are smuggled, and analytical methods used to detect them synthetic cannabinoids were by far the dominant NPS group reported, followed to a lesser extent by synthetic cathinones, synthetic opioids, new benzodiazepines, and stimulants. Specifically, synthetic cannabinoids belonging to the last

generation subclasses of the tert-leucinate indazole carboxamides (i.e., 4F-MDMB-BINACA and MDMB-4en-PINACA) tert-leucinate indole carboxamides (i.e., 5F-MDMB-PICA) and tert-leucinamide indazole carboxamides (i.e., 5F-ADB) were the most reported in recent findings. The literature suggests that most NPS, in particular synthetic cannabinoids, are smuggled via paper and herbal matrices into prison, predominantly using postal services. For paper samples, one solvent extraction was sufficient for identification via chromatography-mass spectrometry (i.e., LC-HRMS/MS and GC-MS), while synthetic cannabinoid quantitative studies reported concentrations between 0.05-1.17 mg/cm^2 providing parameters for further development of in-field methods. In particular, in-field monitoring by sniffer dogs and IMS were able to detect synthetic cannabinoids on paper and shows promise for rapid NPS detection on this matrix. However, IMS suffers from reduced selectivity where substances cannot be discriminated unambiguously [84]. Laboratory-based technique, chromatography-mass spectrometry was the most often employed for the analysis of NPS in biological (i.e., LC-HRMS/MS) from prison. Whilst detection of the exact NPS in a forensic context is important to gather intelligence; in a clinical/emergency context of decision making, identification of metabolites as being quicker can be more useful. The application of sample mining and data mining approaches to seized and urine samples can help gain a bigger picture of emerging NPS and their metabolites and to determine when a substance first appeared.

The authors would like to highlight the following limitations of the study: i) a particular focus was given to the UK grey literature (e.g., Her Majesty Prison and Probation Services and Prison and Probation Ombudsman reports) and ii) it was not possible to determine NPS trends in prison overtime due to a lack of details reported in the available literature (e.g., different seizure years or missing years).

2.5. Future work

Based on the outcomes of this review, specific areas are suggested for future work. As synthetic cannabinoids were smuggled principally via paper and herbal matrices, rapid and accurate in-field analysis of these sample forms would improve real-time decision-making. Due to the evolving market, the focus should be given to monitoring the effectiveness of current in-field techniques for identifying new emerging synthetic cannabinoids. For instance, when IMS fail to identify synthetic cannabinoids in suspected samples producing peaks in the typical synthetic cannabinoids detection range which do not generate any alarm, should be used in conjunction

with the laboratory-based prison drugs monitoring program [35]. As a result of the reduced selectivity and inability of IMS to detect more than one substance in a mixture, future research should also focus on other in-field technologies. It should be noted that spectroscopic techniques such as Raman and FTIR, are powerful analytical techniques [30], that can discriminate between NPS in tablet and powder forms, and between NPS isomers. These are also non-destructive and available in handheld technology, however, they struggle with interfering matrices, especially if containing a low amount of NPS, such as herbal material [32], paper matrices or tobacco [29]. The use of approaches such as SERS using minimally invasive sampling methods could be investigated to promote the practical application of synthetic cannabinoids detection on paper and herbal matrices. Of particular interest is the application of SERS swabs and colloids, embedded with metal nanoparticles to enhance the Raman signal, already employed for the screening of TdA and NPS [86]. A methcathinone spectrum was obtained in the study performed by Lee *et al.* where 23 µg of the analyte was deposited into SERS active films made of hydroxyethylcellulose polymer and aggregated silver nanoparticles. The samples were wiped with a cotton bud wetted and then pressed onto a pre-swelled SERS substrate. Conveniently, the film when dry is similar to paper and can be stored for a year and cut to size when needed [87]. While Yu *et al.* designed paper-based inkjet-printed SERS swabs able to collect trace amounts of analyte from large surface areas, which can be concentrated into a small-volume SERS-active region by lateral-flow concentration. The swabs were validated for the detection of 5 µg of heroin and 5 µg of cocaine on glass slides. The measurements show that the technique is quantitative and is repeatable across multiple swabs [88]. The easy sampling approach similar to IMS could allow rapid yet selective identification of NPS in herbal and paper matrices.

As immunoassays lacked accuracy, there is still a need to develop sensitive, real-time and non-invasive POC testing to screen for synthetic cannabinoids in biological samples (i.e., urine and oral fluids) for use in a decision-making context during on-site intoxication and emergencies. The IMS (IONSCAN LS®) with a high-pressure injection system [89] was proven effective for detecting TdA gamma-hydroxybutyrate (GHB) and gamma hydroxyvalerate (GHV) in synthetic urine at *ca.* 3 µg/mL which suggests the method could potentially work for saliva samples. More recently the same instrument was employed for the detection of cocaine in saliva [90]. However, their field collection device, based on a cotton swab with an indicator and a molecularly imprinted polymer (MIP) sorbent, was designed to selectively retain cocaine.

Therefore, the adaptation of such device to retain synthetic cannabinoids would be needed. Moreover, fluorescence spectral fingerprinting combined with numerical modelling could be used to identify the likely presence of synthetic cannabinoids, as well as provide more specific information on structural class and concentration (~1 μg/mL). This approach can detect both parent and combusted material, and it is practical for detecting synthetic cannabinoids in oral fluids [91]. All the procedures mentioned in the above studies [89–91] could be employed by non-specialized personnel. For the development of new laboratory-based LC-MS detection methods for detection of NPS in biological samples, HRMS incorporating DIA should be preferred, as this will allow the application of sample mining and data mining. While to monitor NPS general trends in prisons and for intelligence purposes, WWA analysis would provide a more representative picture of the overall extent of substance use, compared to MDT. WWA is already used for TdA in Australia and trialled in the USA and Spain [28]. This approach compared to MDT is more cost-effective and less invasive. Recently an air monitoring approach, already employed for the detection of NPS [92] was evaluated for the detection of synthetic cannabinoids. Paul *et al.* [93] employed a combination of fixed and mobile sampling units, worn by prison officers, coupled with Thermal Desorption (TD) sorbent tubes, allowing for multiple location sampling. A two-dimensional gas chromatography (GCxGC)-MS/ToF method was validated for AB-FUBINACA, UR144, MDMB-4en-PINACA, and MDMB-CHMCA, however, these synthetic cannabinoids were not found in the collected samples. Therefore, further investigation on the wide applicability of the technique to detect synthetic cannabinoids in prisons should be considered.

2.6. Aims and objectives of the PhD thesis

Thus, based on the systematic literature review , there is a need to develop more specific and selective in-field analytical techniques and it was suggested that certain vibrational spectroscopic techniques can give that specificity and selectivity, hence their use should be investigated to be used on paper samples impregnated with psychoactive substances.

Hypothesis:

The use of vibrational spectroscopy such as Raman coupled with a minimally invasive extraction method could allow for the specific and selective detection of psychoactive substances on prison paper samples.

Aim:

To develop a minimally invasive extraction method of psychoactive substances from paper samples applicable in conjunction with a highly sensitive in-field detection technique.

Objectives:

i) Characterise the extraction process of psychoactive substances and adulterants/cutting agents and their ternary mixtures from simulated paper samples.

ii) Analyse qualitatively and quantitatively a seized paper sample from prison.

iii) Evaluate Raman instruments' capabilities coupled with Principal Component Analysis (PCA) in identifying psychoactive substances, cutting agents/adulterants and their mixtures on simulated paper samples.

iv) Optimise the agar-gel extraction of the model synthetic cannabinoid 5F-PB-22 from simulated paper samples using Design of Experiment (DoE).

3. Extraction and Qualitative Analysis of a Psychoactive Substance from Prison Letters using Corroborative Analytical Techniques

From Chapter 2 "NPS detection in Prison: A Systematic Literature Review of Use, Drug Form, and Analytical Approaches" we learned that i) the most predominant group reported in prisons was the synthetic cannabinoids ; ii) paper matrices impregnated with synthetic cannabinoids were being used to smuggle most psychoactive substances into prison via the postal services and iii) laboratory techniques such as Liquid Chromatography-High Resolution Mass Spectrometry/Mass Spectrometry (LC-HRMS/MS) and Gas Chromatography-Mass Spectrometry (GC-MS) were used for the characterisation of such samples. To facilitate the development of new in-field detection approaches for synthetic cannabinoids and related compounds on paper, such as handheld Raman spectroscopy, we need to first probe the extraction characteristics of these substances on paper, using standard analytical techniques. The studies in this chapter were performed using simulated prison paper samples before these methods were applied to the preliminary analysis of a seized prison paper.

3.1. Introduction

In the past five years paper matrices have begun to be increasingly used as a support to facilitate the smuggling of NPS into prisons [2,94]. Amongst NPS the most popular class smuggled in this manner is the synthetic cannabinoids. Most of the compounds are highly lipophilic and show good solubility in non-polar or medium-polarity organic solvents such as methanol, ethanol, acetonitrile, ethyl acetate, acetone and isooctane [95]. Therefore, synthetic cannabinoids are dissolved in such solvents and the solutions are used to impregnate paper matrices e.g., books, letters and children's drawings. Paper matrices are then smuggled through the mail system or during social visits into prisons thus, challenging NPS in-field detection. Such samples, seized in prison are sent to laboratories which use laboratory-based technologies such as GC-MS and HPLC-MS for comprehensive characterisation of substances [96]. To perform laboratory analysis on paper matrices, it is necessary first to extract the drugs. Literature findings revealed that the extraction of NPS from paper was performed in most of the cases using pure methanol [3,5,10,29,40,81] although in one instance a mix of methanol and dichloromethane (25:75) was employed [3]. Extraction was performed for variable times ranging from 5 to 20 min [3,5,27,40] on paper matrices with areas ranging from 0.70-1 cm^2 [3,5,10,40,81]. In most of the studies, the piece

of paper was sampled using scissors or a scalpel [10], in one case a biopsy punch was employed to ensure consistency of the area sampled for quantification purposes [3]. From the literature review, it also emerged that seized paper samples are likely to contain mixtures of different NPS, traditional drugs of abuse and adulterants/cutting agents. Ford and Berg found a mixture of three synthetic cannabinoids, cocaine, other four NPS (ethylphenidate, methoxphenidine, methiopropramine, etizolam), benzocaine and lignocaine on one letter seized in a UK prison mail room [5]. The presence of a complex mixture on paper samples adds a further challenge to the in-field detection of NPS, especially if the technique used has difficulty in the detection of more than one analyte in a mixture. For instance, when a paper sample containing a mixture of five synthetic cannabinoids and caffeine was analysed by Ion Mobility Spectrometry (IMS), only 5F-ADB which had the higher peak intensity was detected [29]. Therefore, is important to work towards the development of new in-field detection approaches for synthetic cannabinoids and related compounds on paper, able to overcome this issue.

This study aims to qualitatively analyse a prison letter impregnated with psychoactive substances using corroborative analytical techniques. The objectives are to i) develop and optimise an extraction method using simulated paper samples impregnated with paracetamol employed as a model substance, ii) develop and optimise a detection method for simulated paper samples impregnated with a ternary mixture of caffeine, cocaine and THJ-018 iii) apply the optimised method to the extraction and analysis of psychoactive substances from a seized paper samples from prison using HPLC-PdA-QDa-MS, GC-MS and NMR analysis. To our knowledge, this study was the first to evaluate the recovery of a mixture of psychoactive substances and a cutting agent from the simulated paper sample which mimics the way NPS are smuggled into UK prisons.

3.2. Materials and methods

3.2.1. Chemicals and reagents

Caffeine, cocaine, paracetamol reference standards (all ≥ 99% purity) and formic acid (≥ 98% purity) were obtained from Sigma-Aldrich (Gillingham, UK). THJ-018 (≥ 99% purity) certified reference standard was obtained from Chiron AS (Trondheim, Norway). HPLC grade methanol (MeOH) and common grade acetone (Ace) (both ≥ 99% purity) were obtained by Fisher Scientific (Loughborough, UK). Deuterated methanol (d-MeOH), (≥ 99% purity) was obtained

from Cambridge Isotope Laboratories (Cambridge, UK). Ultra-high purity Millipore Water (MW) (18 MΩ cm^{-1}) was obtained from the Milli-Q water purification system (Merck, UK). A common A4 printing 80 g/m^2 density paper sheet (Envirocopy A4 500 sheet; ECF; 100% Recyclable paper; ISO 9706 Long Life paper) was employed for the preparation of simulated paper samples.

3.2.2. Instrumentation

3.2.2.1. UV lamp

A UVGL-58 handheld UV lamp (UVP, UK), equipped with a combination of a long and a short wavelength of 365/ 254 nm (6 Watt; 230 V; 012 Amps), was used to initially evaluate the seized paper sample. The UV lamp facilitated the identification of solvents by fluorescence e.g., MeOH or Ace containing psychoactive substances used to impregnate seized paper samples.

3.2.2.2. High-Performance Liquid Chromatography-Ultraviolet-Visible

An Agilent 1260 Infinity series High-Performance Liquid Chromatography-Ultraviolet-Visible (HPLC) coupled to an Agilent 1200 Infinity Series Ultraviolet-Visible (UV-Vis) detector (Santa Clara, CA, USA), running under OpenLab software V.01.06.111, was employed to detect the paracetamol extracted from simulated paper samples, to optimise the extraction method. The mobile phase was 25:75 MeOH: MW with a 0.01 M phosphate buffer (PB) and a pH of 3.5 ± 0.1 reached by the addition of orthophosphoric acid. A flow rate of 1 mL/min and sample volume of 10 µL was employed with a Phenomenex Luna C18 column (100Å 150 x 46 mm x 5 µm particle size (Macclesfield, UK) for a total run time of six min at 30 °C. A 246 nm wavelength was employed. The HPLC method was validated for the paracetamol using the UH Standard Operating Procedures (SOP) for validation of LC methods, based on the International Conference of Harmonization (ICH) guidelines [97–99] for the following parameters: system suitability; linearity and range; Limit of Detection (LOD) and Limit of Quantification (LOQ), precision and accuracy.

3.2.2.3. Ultra-Performance Liquid Chromatography-Photodiode Array Detector-Quadrupole Dalton-Mass Spectrometry

A Waters Acquity® Ultra-Performance Liquid Chromatography (UPLC) coupled to a Waters Acquity® Photodiode Array (PdA) and a Waters Acquity® QDa® (Quadrupole Dalton) Mass Spectrometer (MS) (Milford, MA, USA), running under MassLynx V.4.2 was employed to develop a method to identify and quantify psychoactive substances present in the seized paper sample. Mobile phases used were (A) MW with 0.1% v/v formic acid and (B) MeOH with 0.1% v/v formic acid. The solvents were individually filtered through a 0.22 µm membrane filter (Whatman, UK) and then sonicated using Decon Ultrasonic Heater (Decon Laboratories Ltd, UK) for 20 mins. The gradient used was 75:25 A:B from 0.0-0.5 min, 10:90 A:B from 0.5-3.5 min, held for one min, 50:50 A:B from 4.5-5.5 min, held for 0.5 min, and 75:25 A:B from 6.0-7.0 min. A flow rate of 0.6 mL/min and a sample volume of 0.7 µl was employed with a Phenomenex Kinetex C_{18} 100Å 100 x 2.1 mm x 2.6 µm particle size column and a KrudKatcher™ Ultra HPLC in-Line filter 0.5 µm depth filter both sourced from Phenomenex (Macclesfield, UK). Sample vials were kept at 15 °C and a temperature of analysis of 30 °C was used. Chromatograms were produced using the PdA® detector in Total Ion Current (TIC) at 20 sampling points per sec, with a resolution of 1.2 nm across 190-400 nm range and the negative absorbance margin was set at -0.15 AU. The Qda® analysis was conducted using Electrospray Ionisation (ESI) in positive mode from 99-900 m/z range with a sampling frequency of 8.0 sec and a capillary voltage at 0.8 V. The mass spectrometer detector recorded a signal every 0.080 sec, with a cone voltage of 20 V and a probe temperature of 600°C. UPLC-PdA-QDa-MS method was validated for caffeine, cocaine and THJ-18 reference standard using the UH SOP for validation of LC methods, based on the International Conference of Harmonization (ICH) guidelines [97–99] for the following parameters: system suitability; linearity and range; Limit of Detection (LOD) and Limit of Quantification (LOQ), precision and accuracy.

3.2.2.4. Gas Chromatography-Mass Spectrometry

A Varian 450-GC gas chromatography system coupled to a Varian 240-MS mass spectrometer, from Agilent Technologies (Santa Clara, CA, USA), running Varian MS Data Review Software, V.6.9.2, was used to corroborate the results from the UPLC-PdA-QDa-MS and NMR analysis of the seized paper sample. An Agilent Technologies 50:50 phenyl:

methylpolysiloxane 30 m x 0.25 mm x 0.25 µm particle size column (Santa Clara, CA, USA) was employed as a stationary phase along with helium gas mobile phase with a flow rate of 1 mL/min. The Electronic Flow Controller (EFC) injector was held at 275 ºC and was used in split mode (50:1) with triplicate 1µL sample injections. The method was adopted from Assi *et al.* [100] where a 50 ºC holding temperature was ramped to 150 ºC and held for 3 mins, this was then ramped to 250 ºC and further held for 1.33 min, and the final stage increasing to 310 ºC and held for 6 min giving a total run time per sample of 20 mins. The mass spectrometer operated in Electron Ionisation (EI) mode at 70 eV over a scan range of 40-700 m/z. All mass spectra obtained were initially compared to the installed NIST library V.2.0.

3.2.2.5. Nuclear Magnetic Resonance

A JEOL 600 MHz NMR spectrometer (JEOL Ltd., Japan) equipped with a CHN probe, running Delta software v.5.3.1, was employed to analyse the seized paper sample. ^{1}H frequency was 600.17 MHz respectively. The sample compartment temperature was set to 19 °C. The number of scans was set on 64 for ^{1}H-NMR and 1024. Chemical shifts were related to 0.0 ppm for Tetramethyl silane (TMS) or to residual solvent peaks. The NMR spectrometer was tuned prior analysis.

3.2.3. Samples

Prior to sample preparation and analysis, all glassware, spatulae and tweezers were carefully washed and rinsed first with Deionised Water (DW) and then with pure MeOH. In addition, working surfaces were cleaned with pure MeOH.

3.2.3.1. HPLC reference standard solutions preparation

Approximately 2 mg of paracetamol, caffeine, cocaine and THJ-018 reference standard were weighted separately on the analytical balance Sartorius Practum (Sartorius AS, Germany) and dissolved in a 20 mL volumetric flask containing MeOH to obtain a working standard stock (WSS) solution of around 0.1 mg/mL. The reference standard solutions were vortexed using VORTEX-GENIE2 (Scientific industries, Inc., USA) for two minutes to reach complete solubilisation. By dilution of the WSS using different graduated pipettes and volumetric flasks, a range of six concentrations (0.1-0.01 mg/mL) was obtained (Table 3.1).

Table 3.1. Paracetamol, caffeine, cocaine and THJ-018 calibration curve concentration range.

Sample	Concentration (mg/mL)	Concentration (µg/mL)	Dilutions
Analyte C1	0.1	100	1 mg in 10 mL vial (WSS)
Analyte C2	0.067	67	2 mL WWS in 3 mL vial
Analyte C3	0.04	40	2 mL WSS in 5 mL vial
Analyte C4	0.033	33	1 mL WSS in 3 mL vial
Analyte C5	0.02	20	1 mL WSS in 5 mL vial
Analyte C6	0.01	10	1 mL WSS in 10 mL vial

The solutions were drawn directly from the volumetric flask with a 1 mL syringe and needle. The solutions were then filtered through a 0.22 µm pore size PTFE hydrophobic filter and transferred into labelled HPLC vials for the analysis. A blank MeOH was run between the different concentration vials. Six replicate injections per concentration were evaluated.

3.2.3.2. Simulated paper sample

3.2.3.2.1. Paracetamol simulated paper samples preparation and extraction for HPLC-UV-Vis analysis

Paracetamol simulated paper samples were prepared and then extracted in pure MeOH using different parameters to optimise the extraction methods. Twenty-one paper samples of 1 cm^2 were prepared by cutting common A4 printing using a manual tile cutter to obtain 1 cm x 29.7 cm paper strips, first and then 1 cm^2 clear plastic stencil and scissors were used to cut the strips into 1 cm^2 pieces. Approximately 1 g of paracetamol was dissolved in acetone to obtain a 20 mg/mL solution. The solution was poured into a glass beaker and each of the 1 cm^2 piece of paper was laid flat and soaked into the 20 mg/mL paracetamol solution for approximately 30 sec ("soaking method"). Each of the 1 cm^2 piece of paper was left to dry for *ca.* 2 min while held by a tweezer form a corner, to avoid any loss of paracetamol by contact with surfaces. To perform the extraction of the drug from paper, each of the 1 cm^2 paper samples was placed in a plastic reaction tube with 0.5 mL MeOH. Both sonication and centrifugation (6000 rpm) were evaluated for optimum extraction of paracetamol from the simulated paper samples (Table 3.2).

Table 3.2. Set of parameters evaluated for paracetamol extraction.

Set	Sonication (min)	Centrifugation (min)
1st	10	5
2nd	10	10
3rd	20	5
4th	20	10
5th	60	5
6th	60	10

Following paracetamol extraction, the solutions were drawn from the reaction tube with a 1 mL syringe, filtered through a 0.2 µm polytetrafluoroethylene (PTFE) hydrophobic filter and then transferred into HPLC vials for analysis. The analysis of each set of parameters was performed on the same day on three replicate samples and from each vial, three injections were evaluated. A 1 cm^2 blank printing paper treated using the 6th set of parameters and positive control of paracetamol solution at 0.1 mg/mL were also analysed. To note that when the "soaking method" was used to prepare the simulated paper samples, it did not allow calculation of the paracetamol percentage recovery, as the quantity of paracetamol absorbed by the paper after soaking it in the solution, was unknown.

The percentage recovery needed to be calculated to evaluate the efficiency of the developed paracetamol extraction method. To this end, the "pipetting method" was employed to prepare the simulated paper samples as allowed for the calculation of the recovery percentage. A solution of 0.580 mg/mL of paracetamol in acetone was prepared and 0.5 mL transferred with a graduated pipette onto the 1 cm^2 piece of paper. Paracetamol simulated paper samples were extracted in 0.5 mL MeOH using the 1st set of parameters (sonication 10 min and centrifugation 5 min) and analysed via HPLC-UV-Vis. A second extraction was then carried out on the same paracetamol simulated paper samples by repeating the above method. The same procedure was performed in triplicate. A mobile MeOH blank was injected after the analysis of each extract to check for any carryover.

Caffeine, cocaine and THJ-018 mixtures simulated paper samples preparation and extraction for UPLC-PdA-QDa-MS

Extraction of single (caffeine), binary (caffeine +cocaine) and ternary (caffeine +cocaine+THJ-018) mixtures from simulated paper samples was performed via 10 min sonication followed by 5 min centrifugation (Section 3.2.3.2.1.). Evaluation of the percentage recovery of single (caffeine), binary (caffeine +cocaine) and ternary (caffeine +cocaine+THJ-018) mixtures on simulated paper samples were also carried out, to better mimic seized paper samples, likely to contain a mixture of substances. Solutions of these substances and mixtures, were prepared at concentrations of 0.1 mg/mL, with the exact solution concertation being 0.1365 mg/mL for caffeine, 0.161 and 0.164 mg/mL for caffeine +cocaine, and 0.163, 0.117 and 0.08 mg/mL for caffeine +cocaine+THJ-018. Using a graduated pipette 0.5 mL of the solutions were transferred onto the 1 cm^2 piece of paper. The simulated paper samples were extracted in 0.5 mL MeOH using the 1^{st} set of parameters (sonication 10 min and centrifugation 5 min) and then the MeOH extracts were quantified using UPLC-PdA-QDa-MS. A MeOH blank was injected after the analysis of each extract to check for any carryover.

3.2.3.3. Seized paper samples

Non-judicial seized paper samples in tamperproof polythene evidence bags from an English prison were received at the University of Hertfordshire (UH) in October 2018. The evidence bags were labelled according to the UH standard operating procedures (SOP) UM028(003) "Handling, Storage and Disposal of Controlled Substances" and stored securely in a safe. The evidence bag UHSOP/2018/PR025 (Figure 3.1 a) consisted of an envelope (Figure 3.1 b), marked with the wording "Rule 39", referring to confidential legal correspondence [79], containing multiple paper sheets. Additionally, the evidence bag contained the IMS slip result, resulting from IMS screening performed by prison officers. In the seized paper sample traces of 'Spice' and cocaine were detected by the IMS. One of the A5 printing paper sheets was chosen from the envelope for the analysis.

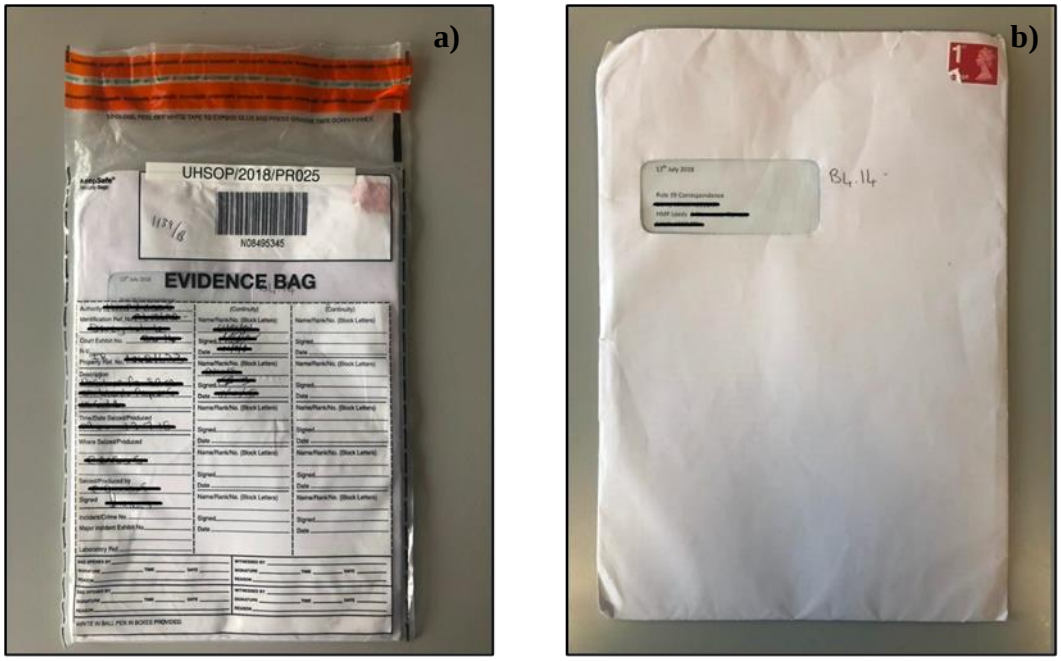

Figure 3.1. UHSOP/2018/PR025 a) evidence bag and b) envelope showing 'Rule 39' wording.

3.2.3.3.1. Seized paper samples preparation and extractions

Initially, two 1 cm^2 pieces of paper samples were accurately cut from the central spot (Section 3.3.3.1.) of the seized paper sample and then extracted according to Section 3.2.3.2.1**.** However, due to the low concentration of the analytes in the extract, it was necessary to sample additional eight 1 cm^2 and then other 66 x 1 cm^2 pieces of paper from the central area inside the spot (I.S.), for a total of 76 x 1 cm^2 pieces of paper sampled. The same number of samples i.e., 2, 8, and 66 x 1 cm^2 samples were taken from the area outside the spot (O.S.) of the seized paper sample (Figure 3.2), and from a Blank printing Paper sheet (BP extract).

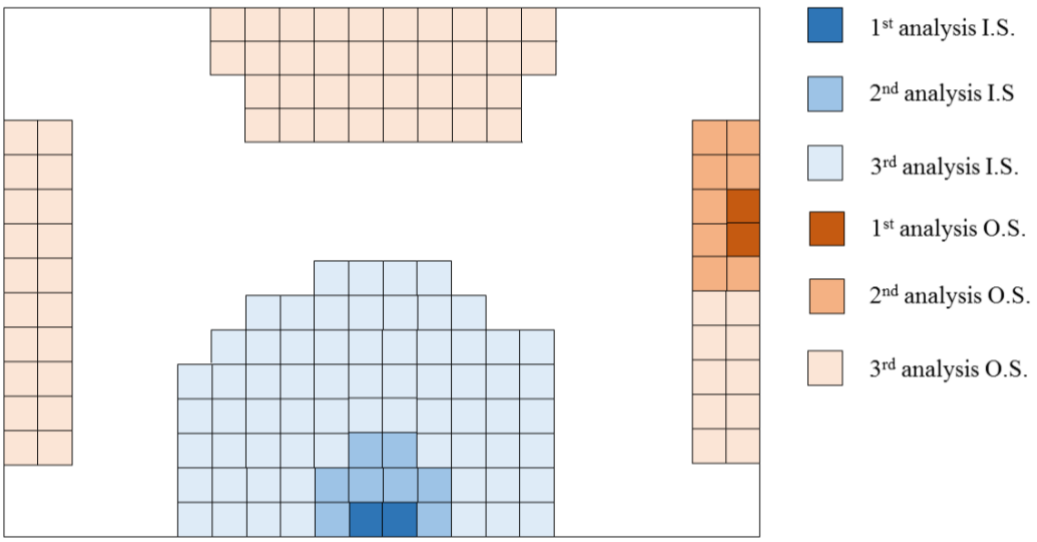

Figure 3.2. Diagram of the sampling of the UHSOP/2018/PR025 seized paper sample.

Extracts from each of the 76 x 1 cm^2 pieces of paper were combined, concentrated to 0.5 mL volume, and used for UPLC-PdA-QDa-MS and GC-MS analysis. While for NMR analysis, the samples were dried under N_2 flux, reconstituted with 0.75 mL of d-MeOH, transferred in an NMR borosilicate glass tube 5 mm (Sigma-Aldrich, UK) and analysed for ^{1}H, and ^{13}C.

3.3. Results and discussion

3.3.1. Selection of psychoactive substances and adulterants/cutting agents

The psychoactive substances and adulterants/cutting agents (Figure 3.3) were selected based on the findings from the literature review (Chapter 2). The paracetamol, employed as a model substance to optimise extraction from paper, was chosen as it is relatively inexpensive and one of the most used adulterants in Traditional Drugs of Abuse (TDA) and NPS [100,101]. For the same reasons, caffeine was chosen for the simulated paper samples containing a ternary mixture [100,101,102]. Cocaine was used as traces were identified in the UHSOP/2018/PR025 prison sample as per the IMS analysis performed by prison officers. Moreover, cocaine was also detected in three prison paper samples analysed by Antonides *et al.* [81]. The synthetic cannabinoid model substance, THJ-018 was chosen for this study as it belongs to the sub-group of the indazole carboxamide which includes many synthetic cannabinoids seized in prison in recent years such as 5F-APINACA, APINACA and 5F-ADB [35].

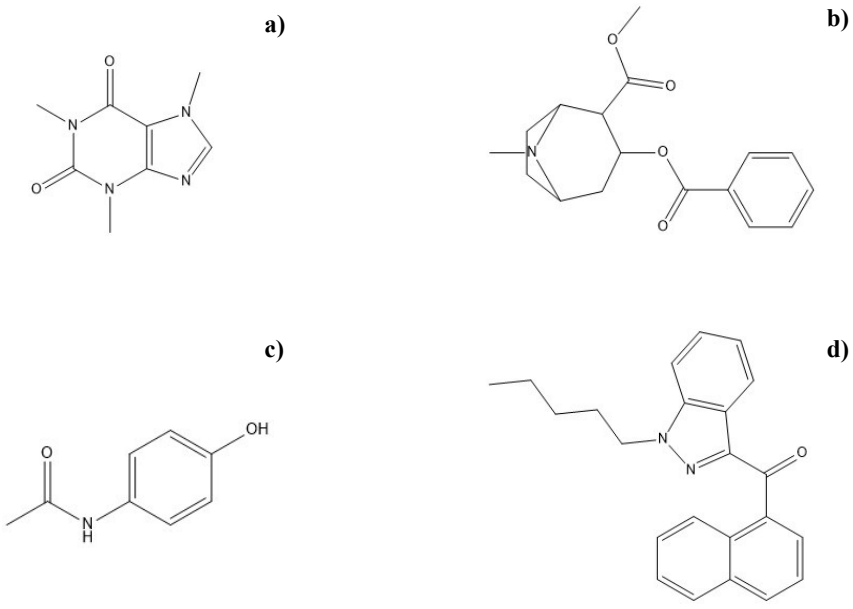

Figure 3.3. Chemical structures of a) caffeine b) cocaine c) paracetamol and d) THJ-018. (Chemdraw Professional, version 16.0, UK).

3.3.2. Optimisation and validation of methods

3.3.2.1. High-Performance Liquid Chromatography-Ultraviolet-Visible

To optimise the HPLC-UV-Vis method for the detection and quantification of paracetamol simulated paper samples mobile phases MeOH: MW ratios, pH range, injection volume and absorption wavelengths were evaluated (Table 3.3). Optimum parameters which improved the peak shape were a 25:75 MeOH: MW mobile phase mixture with a pH of 3.5, an injection volume of 10 µL, and a detector absorption wavelength of 246 nm.

Table 3.3. Parameters optimised in the HPLC-UV method development.

Parameters optimised	
MeOH: MW ratios (%) isocratic method	75:25 50:50 25:75
pH range	3.5 to 6.5
Injection volume (µL)	5; 10 and 20
Detector wavelengths (nm)	250; 254; 246 and 243

The retention time for paracetamol was found to be 3.6 ± 0.1 min (Appendix 2.1.-Figure A1). All parameters evaluated for the HPLC-UV-Vis method validation of paracetamol were found to be within the acceptance criteria (Appendix 2.2.-Table A1) as defined by the UH SOP for validation of LC methods, in line with the International Conference of Harmonization (ICH) guidelines [97–99]. The calibration curves were built by plotting the concentration ranges against the instrument response, Area Under the Curve (AUC), which satisfies the minimum requests for the linearity: five points and $R^2 > 0.9990$. The theoretical plate number is in the correct range thus a good column efficiency is achieved. The tailing factor values of the peaks related to the three different calibration curves are < 2. Therefore, the chromatographic shapes of the peaks are acceptable, without broad or split peaks. The RSD values calculated for the injection repeatability are all < 2%, meaning a good reproducibility between the peaks related to different injections of the same sample. The LOD and LOQ were calculated for the three calibration curves. The system suitability test parameters were evaluated by making six replicate injections of the reference standard solutions.

3.3.2.2. Ultra-Performance Liquid Chromatography-Photodiode Array Detector-Mass Spectrometry

To optimise the UPLC-PdA-QDa-MS method for the detection and quantification of caffeine +cocaine+THJ-018 mixture extracted from paper, various mobile phase ratios, flow rate and injection volume were evaluated (Table 3.4.). Optimum parameters which improved the shape of the peaks were a mobile phase mixture of (A) HPLC grade MeOH and (B) MW using a gradient of 75:25 A:B from 0.0-0.5 min, 10:90 A:B from 0.5-3.5 min, held for one min, 50:50 A:B from 4.5-5.5 min, held for 0.5 min, and 75:25 A:B from 6.0-7.0 min with a flow rate of 0.6 mL/min and a sample volume of 0.7 µL.

Table 3.4. Parameters optimised in the UPLC-PdA-QDa-MS method development.

Parameters optimised		
Mobile phases ratios gradient method (from 0.00-0.50 min)	(A) MW + 0.1% FA	(B) MeOH + 0.1%FA
	65	35
	67.5	32.5
	70	30
	72.5	27.5
	75	25
	77.5	22.5
	80	20
Flow rate (mL/min)	0.500; 0.600 and 0.700	
Injection volume (µL)	0.300; 0.500; 0.700; 0.850; 1.000	

The retention time of caffeine was 1.1 ± 0.1 min, cocaine was 1.6 ± 0.1 min THJ-018 was 4.5 ± 0.1 min. All the parameters evaluated for the UPLC-PdA-Qda-MS method validation of caffeine, cocaine and THJ-018 were found to be within the acceptance criteria (Appendix 2.2-Tables A2 to A4) as defined by the UH SOP for validation of LC methods, based on the International Conference of Harmonization (ICH) guidelines [97–99].

3.3.3. Simulated paper samples analysis

3.3.3.1. High-Pressure Liquid Chromatography-Ultraviolet-Visible paracetamol simulated paper samples analysis

The extraction of paracetamol from simulated paper samples prepared either by soaking or pipetting was evaluated. In both cases, the paracetamol was successfully extracted and quantified using the calibration curve built on the day of the experiment. The quantity of paracetamol extracted from the 1 cm^2 simulated paper samples prepared using the "soaking method" ranged between 0.31-0.58 mg/mL. Please note that the paracetamol theoretical concentration i.e., the quantity of paracetamol absorbed by the paper after soaking in the solution, was unknown. Therefore, when the "soaking method" was used to prepare the simulated paper samples, it was not possible to calculate the paracetamol percentage recovery. Furthermore, the concentration values (AUC) of the replicate samples showed a low reproducibility (RSD *ca.* 20%). This made this simulated paper samples preparation method unsuitable for quantification purposes.

When simulated paper samples were prepared using the "pipetting method" it was possible to calculate the percentage of the paracetamol concentration extracted, using Equation (3.1).

$$\left(\frac{Theoretical\ concentration}{Experimental\ concentration}\right) x\ 100 \qquad \text{Equation (3.1)}$$

The quantity of paracetamol extracted was 0.421 mg/mL ± 0.005 mg/mL, meaning that 72.2 ± 0.8% of the total amount of paracetamol transferred on the paper was successfully extracted. The re-extraction of the same simulated paper samples contributed to a further 0.0465 mg/mL ± 0.0009 mg/mL paracetamol recovery meaning that 7.9 ± 0.1% of paracetamol was extracted, for a total of 80.1 ± 0.7% of paracetamol extracted over two consecutive extractions and three replicate samples. This confirms that the first extraction is the main contribution to the recovery of the paracetamol from paper. It must be noted that the behaviour of the paracetamol during the MeOH extraction might not reflect the behaviour of other psychoactive substances found on paper, as it depends mainly on the solubility of the psychoactive substances in the solvent employed.

Having obtained the data, three replicates for each set of parameters (Table 3.2) were submitted to IBM Statistical Package for Social Sciences (SPSS) (version 26) for a two-way ANOVA test to assess how the two independent variable (sonication and centrifugation) and their interaction relate to the response (AUC) [102]. This was performed to explore if a specific set of parameters could be statistically significant compared to the others in the extraction process, thus facilitating the extraction of a higher amount of analyte from the paper. No statistically significant difference was found between the different sets of parameters evaluated, as the p-value was always $p > 0.05$, thus for the following experiment only the 1st set of parameters was evaluated.

3.3.3.2. Ultra-Performance Liquid Chromatography-Photodiode Array Detector-Quadrupole Dalton-Mass Spectrometry caffeine, cocaine and THJ-018 simulated paper samples analysis

The percentage of the recovery extraction was evaluated on the single substance caffeine, then on the binary mixture caffeine+cocaine and, finally on the tertiary mixture caffeine+cocaine+THJ-018. This was done to mimic seized paper samples which are likely to contain a mixture of different substances. An example of the UPLC-PdA chromatogram resulting from the analysis of caffeine +cocaine+THJ-018 paper extract is presented in Figure 3.4.

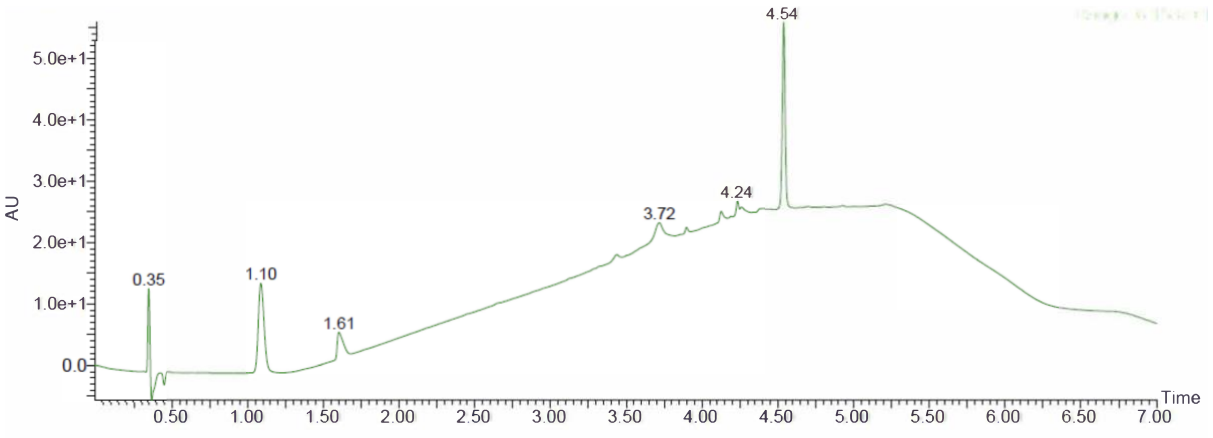

Figure 3.4. Photodiode array chromatogram of caffeine +cocaine+THJ-018 paper extract, eluting at 1.10, 1.61 and 4.54 min, respectively.

The quantity of caffeine extracted from the three simulated paper samples was 0.098 ± 1.0 mg/mL, meaning that 76 ± 1% of the total amount of caffeine pipetted on the simulated paper samples was successfully extracted. While the quantity of caffeine +cocaine extracted from the three simulated paper samples was 0.117 ± 0.002 mg/mL and 0.119 ± 0.003 mg/mL, meaning that the 75.3 ± 1.1 % and 73.4 ± 1.7% of the total amounts of caffeine +cocaine pipetted on the simulated paper samples was successfully extracted, respectively. Lastly, the quantity of caffeine +cocaine+THJ-018 extracted from the three simulated paper samples was 0.119 ± 0.001 mg/mL, 0.085 ± 0.001 mg/mL and 0.065 ± 0.008 mg/mL, meaning that the 74.3 ± 0.2%, 73.7 ± 1.0% and the 75.8 ± 1.0% of the total amounts of caffeine +cocaine+THJ-018 pipetted on the simulated paper samples was successfully extracted, respectively. Although three substances are present in the simulated sample, none of these is influenced by the other regarding retention times and AUC of the peaks, hence the quantity of substance extracted. The percentage of caffeine, cocaine or THJ-018 recovered was approximately the same in a single substance, binary and ternary mixture simulated samples (Appendix 2.3- Table A1), probably because the different substances are similarly retained by the paper, and all soluble in MeOH. At the time this study was carried out, only one study on qualitative analysis was available in the literature [5], however a similar study has become available since. Our results are compared to McKenzie and co-workers in the conclusions [3].

3.3.4. Seized paper samples analysis

3.3.4.1. UV lamp seized paper samples analysis

One of the A5 paper sheets was selected to carry out the analysis, as a semicircle-shaped spot was visible under handheld UV lamp light UVGL-58 wavelength 254 nm (Figure 3.5) suggesting that a solution potentially containing drugs was pipetted on the centre of an A4 paper and then cut in half.

Figure 3.5. Seized paper sample UHSOP/2018/PR025 under a UV lamp λ =254 nm.

3.3.4.2. Ultra-Performance Liquid Chromatography-Photodiode Array Detector-Mass Spectrometry seized paper samples analysis

No compounds were detected in the BP extract prepared. No caffeine, cocaine or THJ-018, which were used as model substances to develop the method, were found in any of the samples, although on the IMS slip traces of cocaine were recorded. This might be due to the IMS sample trap being wiped on multiple paper sheets present in the envelope, or to the lowest sensitivity of the UPLC-PdA-Qda-MS. In Table 3.5, are reported the elution times of the peaks of the BP extract and O.S and I.S of the seized paper samples found in the chromatograms (Figure 3.6).

Table 3.5. Summary of peaks retention times of the BP extract, O.S and I.S of the seized paper sample.

Summary of peaks retention time (min)															
CTRL	3.35	3.37	3.65	3.83	-	4.07	4.17	4.19	4.31	4.33	4.42	4.47	4.58	4.75	5.02
O.S	3.33	3.38	3.65	3.83	3.92	4.06	4.17	4.19	4.30	4.33	4.42	4.46	4.58	4.75	4.97
I.S.	3.33	3.38	3.65	3.83	3.91	4.08	4.17	4.19	4.30	4.33	4.41	4.46	4.58	4.75	4.97

The peaks reported in Table 3.5 were observed by zooming the diode array chromatograms of the BP extract and O.S and I.S samples (Figure 3.5) using the Waters MassLynx software. All the peaks reported in Table 3.5, except the one eluting at 3.91-3.92 min, have low-intensity *ca.* 5 Arbitrary Units (AU) and are present also in the BP extract, meaning that these peaks could be related to the trace level of substances extracted from the paper to the instrument background, or impurity present in the column used. For these reasons a blank MeOH is needed for comparison, and it was observed that the same peaks were consistently found in the MeOH sample (Appendix 2.4- Figure A1). Therefore, it is more likely that these are related to the instrument background or impurity present in the column used. Only the two peaks eluting at 3.91-3.92 min (Figure 3.6 b and c) are related to an unknown analyte present in both O.S and I.S areas of the seized paper sample analysed. Although the quantification of the samples was not performed, the intensity of the peak at *ca.* 3.9 min indicates a 3.5-fold increase between the O.S. (Figure 3.6 b) and I.S. (Figure 3.6 c) samples. As the analyte eluted at a retention time when the gradient consisted of 90:10 MeOH:MW it is possible to hypothesise that the analyte has relatively non-polar and lipophilic characteristics.

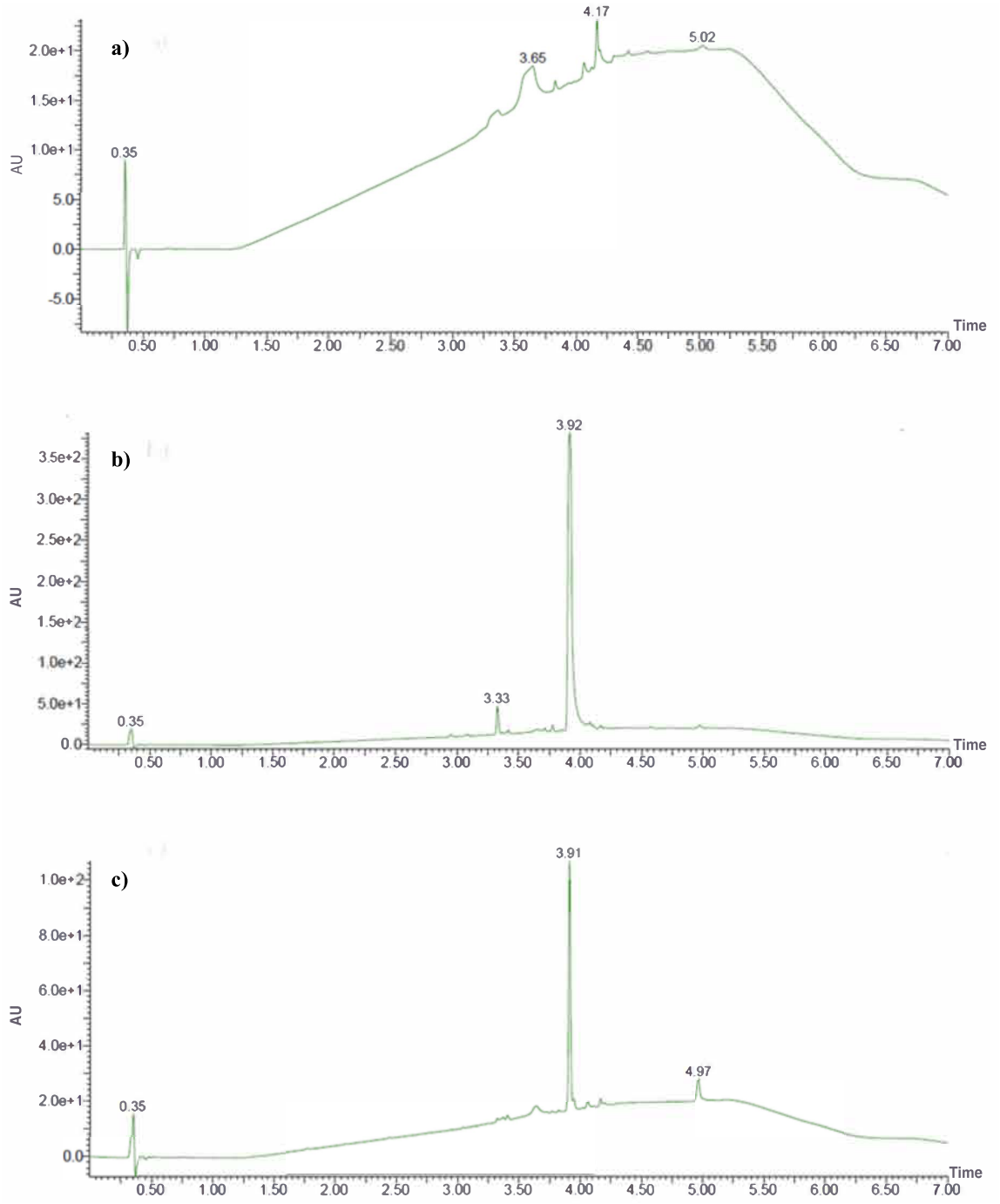

Figure 3.6. PdA chromatograms of a) BP extract b) O.S area and c) I.S area of the seized paper sample.

By checking the MS related to the unknown analyte eluting at 3.91-3.92 min (Figure 3.6 a and b) the base peak is the one with an m/z value of 378.0 in both cases. As the instrument was set on ESI^+ mode values obtained are referred to as $[M+H]^+$ ions, so it is necessary to subtract the

atomic mass of 1H (1.00784 Da) from the value displayed on the MS, hence the molecule of interest will have a molecular weight of *ca.* 377 g/mol.

In both of the mass spectra (Figure 3.7 a and b) is visible a second ion at 400.0 m/z with lower relative intensity compared to the ion at 378.0 m/z, which could be attributed to the presence of the Na salt with an MW of 377 g/mol.

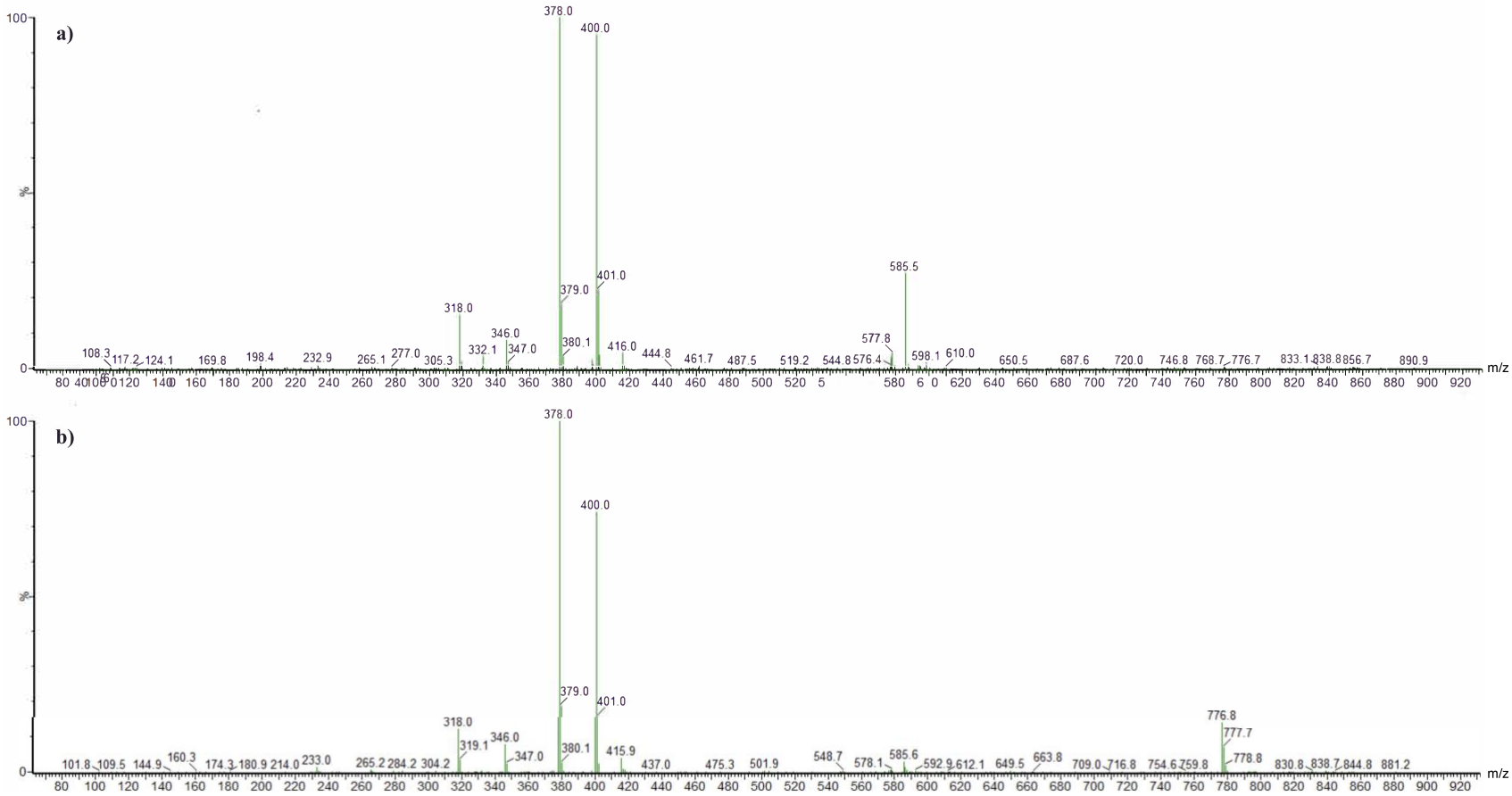

Figure 3.7. ESI mass spectra of unknown analytes eluting at 3.91-3.92 with a molecular weight of ca. 377 g/mol) a) I.S. and b) O.S samples.

Moreover, to confirm the presence of 5F-ADB in the seized paper sample, a direct comparison with a 5F-ADB reference standard solution at 0.1 mg/mL concentration was performed, which showed the elution peak at 3.93 min (Figure 3.8 a) and a molecular ion at 378.0 m/z (Figure 3.8 b).

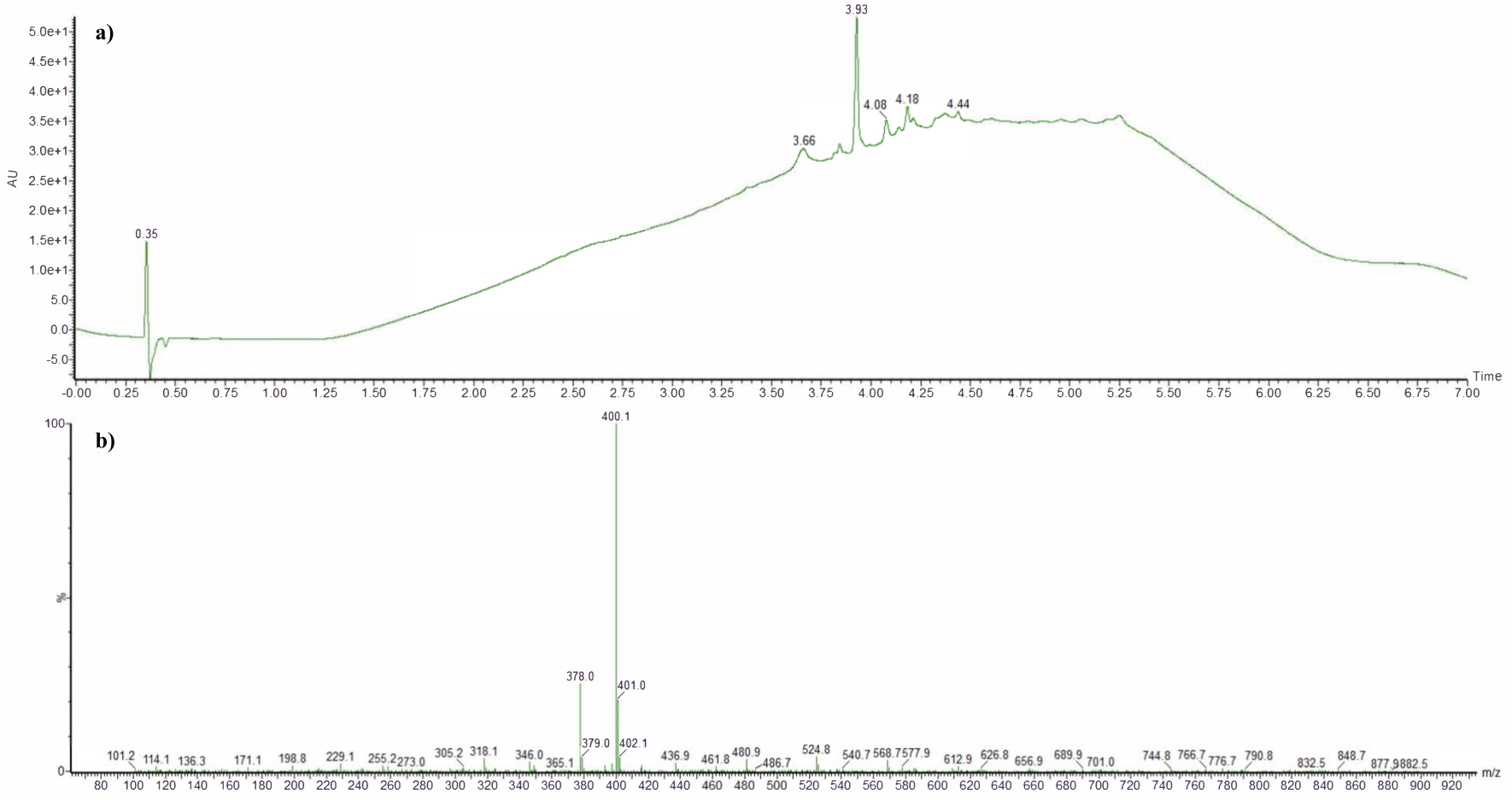

Figure 3.8. 5F-ADB reference standard a) PdA chromatogram eluting at 3.93 min and b) ESI mass spectrum showing a molecular ion at 378.0 m/z

3.3.4.3. Gas Chromatography-Mass Spectrometry seized paper sample analysis

The gas chromatograms of both the O.S. and I.S. areas of the seized paper sample showed a main peak with a retention time of 14.00 min and two smaller identical peaks with a retention time of 10.50 and 10.68 min (Figure 3.9), respectively. The BP extract and MeOH samples did not show any peaks with the same elution times reported for the seized paper sample.

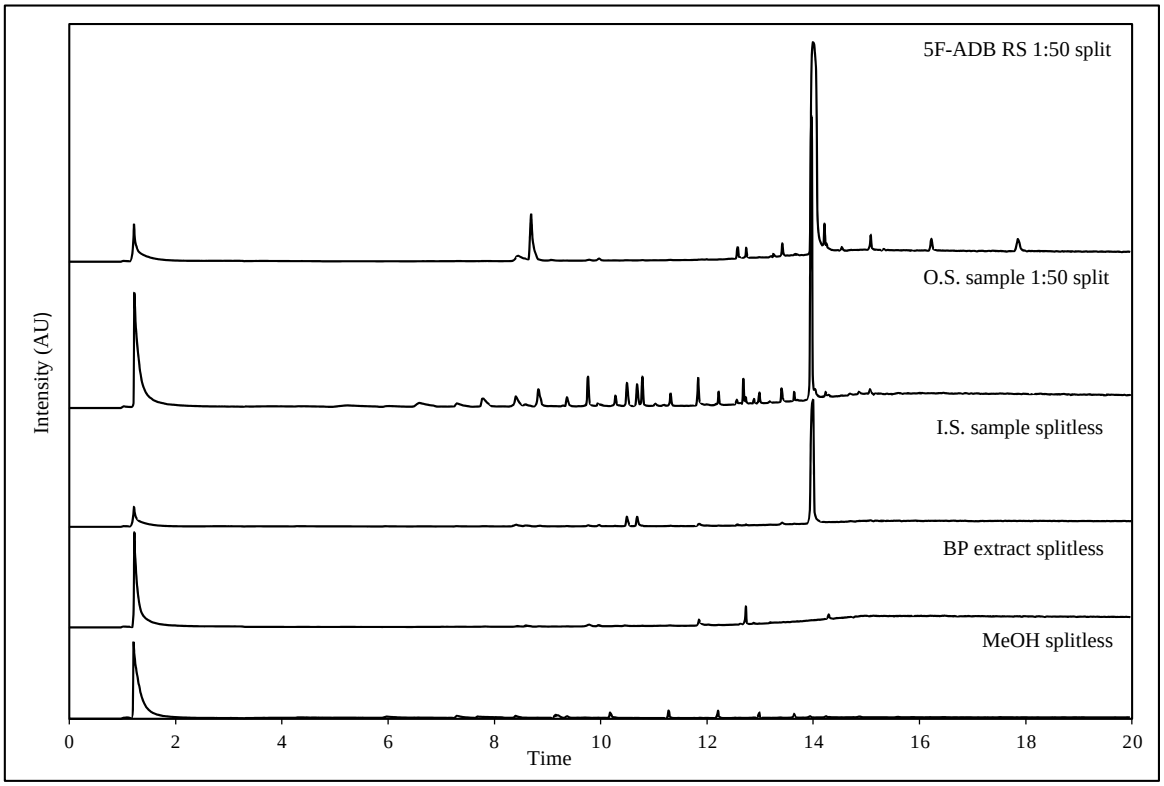

Figure 3.9. Gas chromatograms of MeOH blank, BP extract, I.S. and O.S. of the seized paper sample, and 5F-ADB reference standard.

In the EI mass spectrum related to the unknown analyte present in the O.S. sample eluting at 14.00 min (Figure 3.9) are displayed its molecular ion at 377 m/z and its fragmentation ions at 321, 291, 247, 234, 147 and 69 m/z (Figure 3.10).

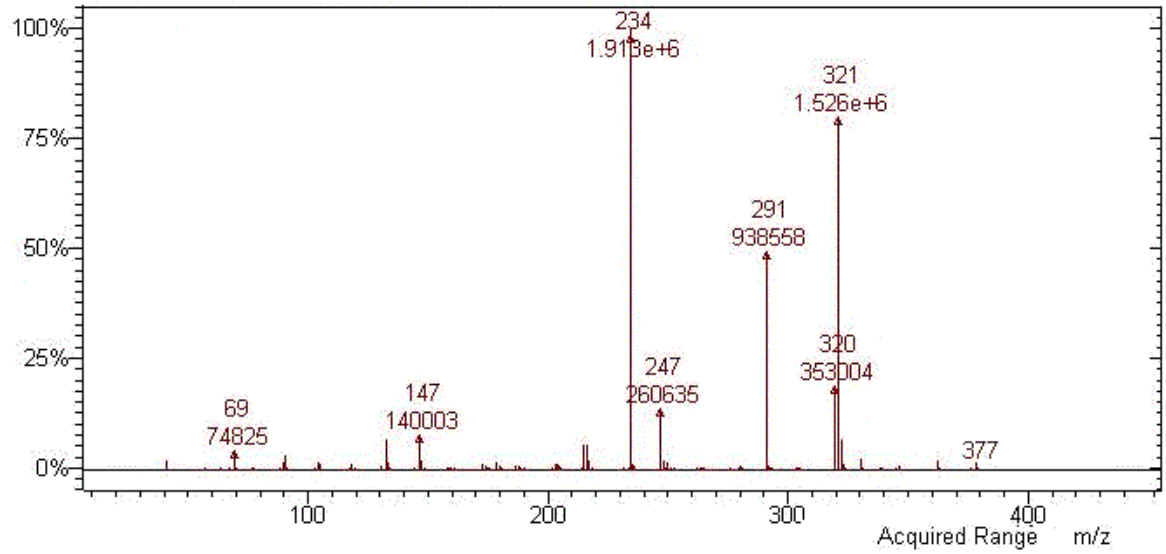

Figure 3.10. EI mass spectrum and fragmentation pattern of the O.S. sample containing the unknown analyte with a molecular weight of ca. 377 g/mol.

In the EI mass spectrum related to the unknown analytes present in the O.S. sample eluting at 10.50 and 10.68 min (Figure 3.9) are displayed their molecular ion at 373 m/z and its fragmentation ions at 316, 286, 257, 190, 89 and 41 m/z (Figure 3.11).

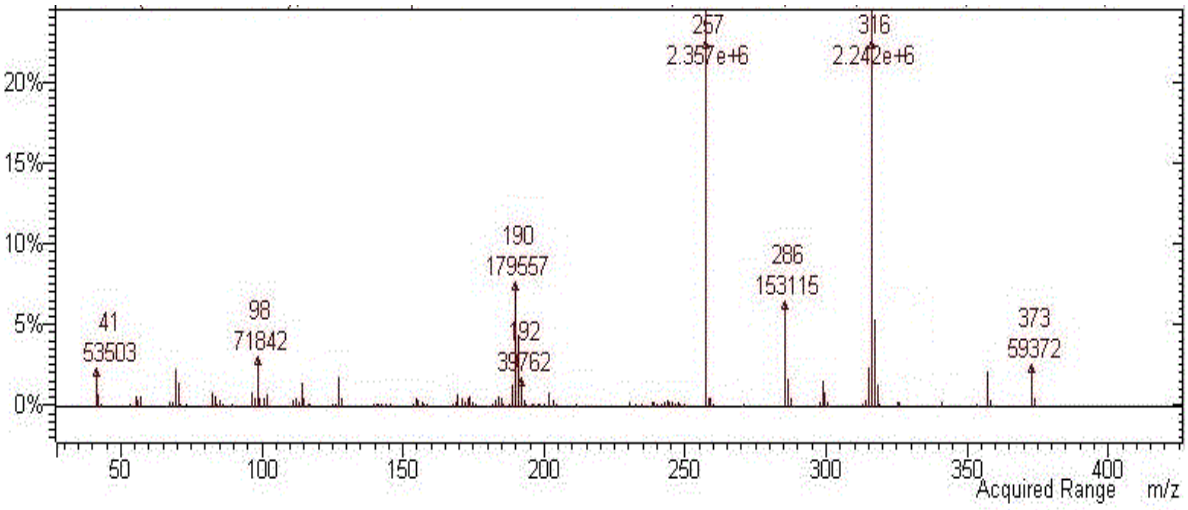

Figure 3.11. EI mass spectrum and fragmentation pattern of the O.S. sample containing the unknown analyte with a molecular weight of ca. 373 g/mol.

National Institute of Standards and Technology (NIST) and Scientific Working Group for the Analysis of Seized Drugs (SWGDRUG) libraries were consulted and did not match the unknown analytes to any known substances in the database. Moreover, the European Database on New Drugs (EDND) was consulted filtering by molecular weight. No match was found for the analyte with a molecular weight of *ca.* 373 g/mol While possible matches to four synthetic cannabinoids (Table 3.6) were found for the analyte with a molecular weight of *ca.* 377 g/mol.

Table 3.6. Possible synthetic cannabinoids candidates matching the unknown analyte found in the seized paper sample.

Synthetic cannabinoids candidates	Molecular formulae	Molecular Weight (g/mol)
5F-EMB-PINACA	$C_{20}H_{28}FN_3O_3$	377.45
5F-MDMB-PINACA aka 5F-ADB	$C_{20}H_{28}FN_3O_3$	377.45
CUMYL-THPINACA	$C_{23}H_{27}N_3O_2$	377.48
5F-PB-22 indazole analogue	$C_{22}H_{20}FN_3O_2$	377.41

The Cayman spectral library was searched for the GC-MS spectra of the synthetic cannabinoids in Table 6. Among the latter, the synthetic cannabinoid 5F-ADB GC-MS spectrum (Figure 3.12) showed a similar fragmentation pattern of the unknown analyte eluting at 14.00 min.

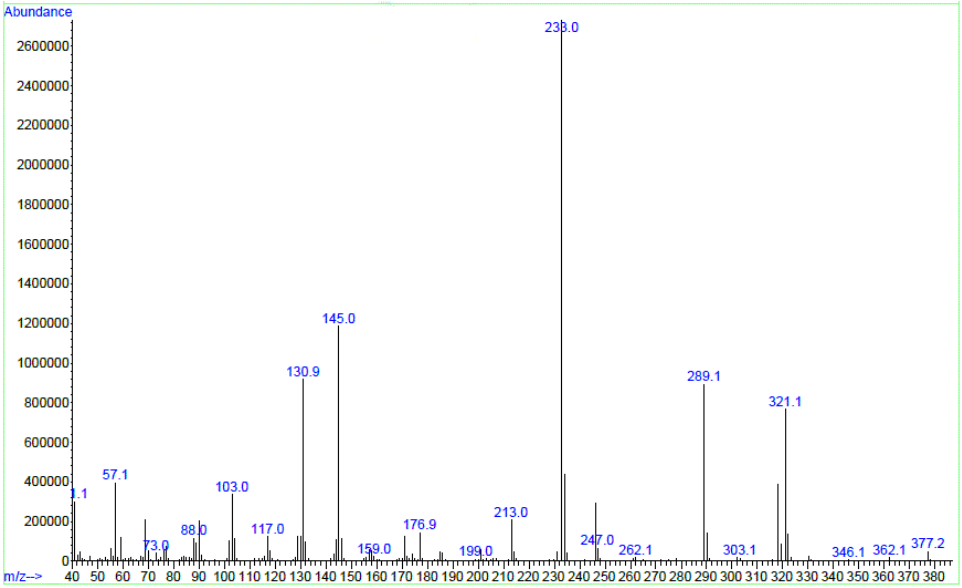

Figure 3.12. EI GC-MS fragmentation pattern of the compound 5F-ADB reference standard. From Cayman Chemical database.

Based on the Cayman EI CG-MS of 5F-ADB a fragmentation pattern has been proposed in Figure 3.13 [103]. The ion $[C_{13}H_{14}FN_2O]^+$ with an m/z of 233 is the base peak, which has formed following the break of the bond between C and N of the carboxamide group on the molecular ion. The base peak with an m/z of 233 loses i) the pentyl fluoride chain by break of the bond with the N of the indazole, forming the ion $[C_8H_5N_2O]^+$ with an m/z of 213 ii) the F atom by break of the bond between the pentyl chain and the F atom, rearranging and forming the ion $[C_{13}H_{13}N_2O]^+$ with an m/z of 213. While the ion $[C_{13}H_{19}N_3O_3]^+$ with an m/z of 289 has formed by the breaking of the pentyl fluoride chain bonded to the N atom of the indazole of the molecular ion. The ion $[C_{16}H_{20}FN_3O_3]^+$ with an m/z of 321 has formed after the loss and rearrangement of the tert-butyl chain bonded to the β-carbon of the molecular ion. The latter further lose C_4H_8F from the pentyl fluoride chain, forming the ion $[C_{12}H_{12}N_3O_3]^+$ with an m/z of 246. The ion $[C_{19}H_{28}FN_3O]^+$ with an m/z of 319 has formed after the break of the bond between the C and the $COOCH_3^-$ of the ester group and a rearrangement between the C and the N atom of the indazole core.

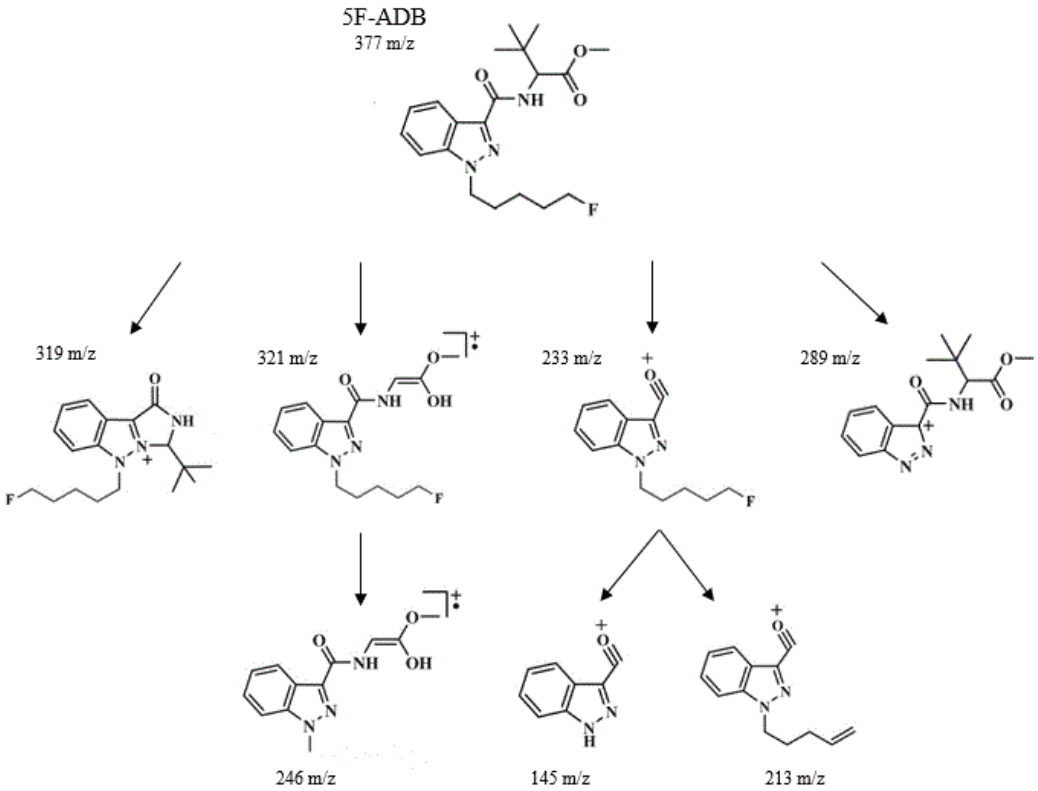

Figure 3.13. Proposed fragmentation pattern of the 5F-ADB reference standard.

Given the differences between the m/z fragments of the GC-MS spectra of the seized paper samples and the 5F-ADB Cayman reference standard, to confirm unambiguously the presence of 5F-ADB, in the seized paper sample, a 5F-ADB reference standard (100 ppm) was run using the same GC-MS method. The 5F-ADB reference standard showed an elution peak at 14.06 min (Figure 3.8) and the same fragmentation pattern of the samples (Figure 3.14) confirming the presence of the 5F-ADB in the seized paper sample.

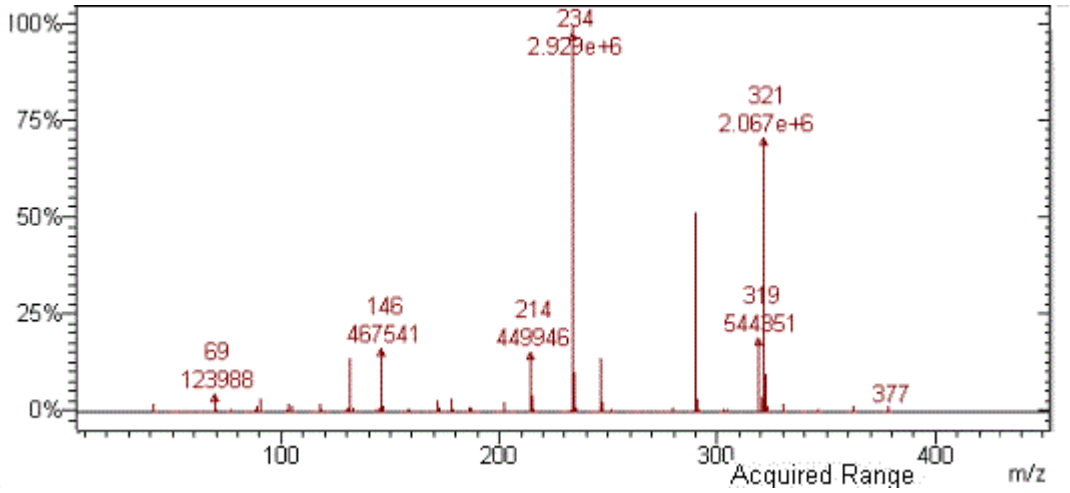

Figure 3.14. EI-MS and fragmentation pattern of 5F-ADB reference standard.

The two analytes eluting at 10.50 and 10.68 min, share the same molecular ion and fragmentation pattern (Figure 3.10), which might suggest an isomeric form of the same analyte. In the literature, the synthetic cannabinoid AB-CHFUPYCA (MW ~ 400) showed a similar fragmentation pattern up to the fragment with an m/z of 316, which might suggest that the unknown substance is a pyrazole-carbamoxide synthetic cannabinoid type [104].

3.3.4.4. Nuclear Magnetic Resonance seized paper samples analysis

The NMR analysis was carried out to confirm and elucidate the structure of the analytes in seized paper sample. d-MeOH was employed as a solvent for the analysis of the seized prison sample, as this was found to be used in the literature to analyse the synthetic cannabinoid 5F-ADB [105]. The presence of 5F-ADB was confirmed in both areas of the seized paper sample. Figure 3.15 shows the stacked ^{1}H NMR spectra of the BP extract, O.S. and I.S. area. Characteristic signals of d-MeOH can be distinguished at 3.31 (multiplex) and 4.87 (singlet) ppm [106]. Also, in all the samples analysed including the BP extract, low concentration peaks were found e.g., around 8.5 ppm, which could be attributed either to compounds/impurities extracted from the paper, or impurity present in the d-MeOH.

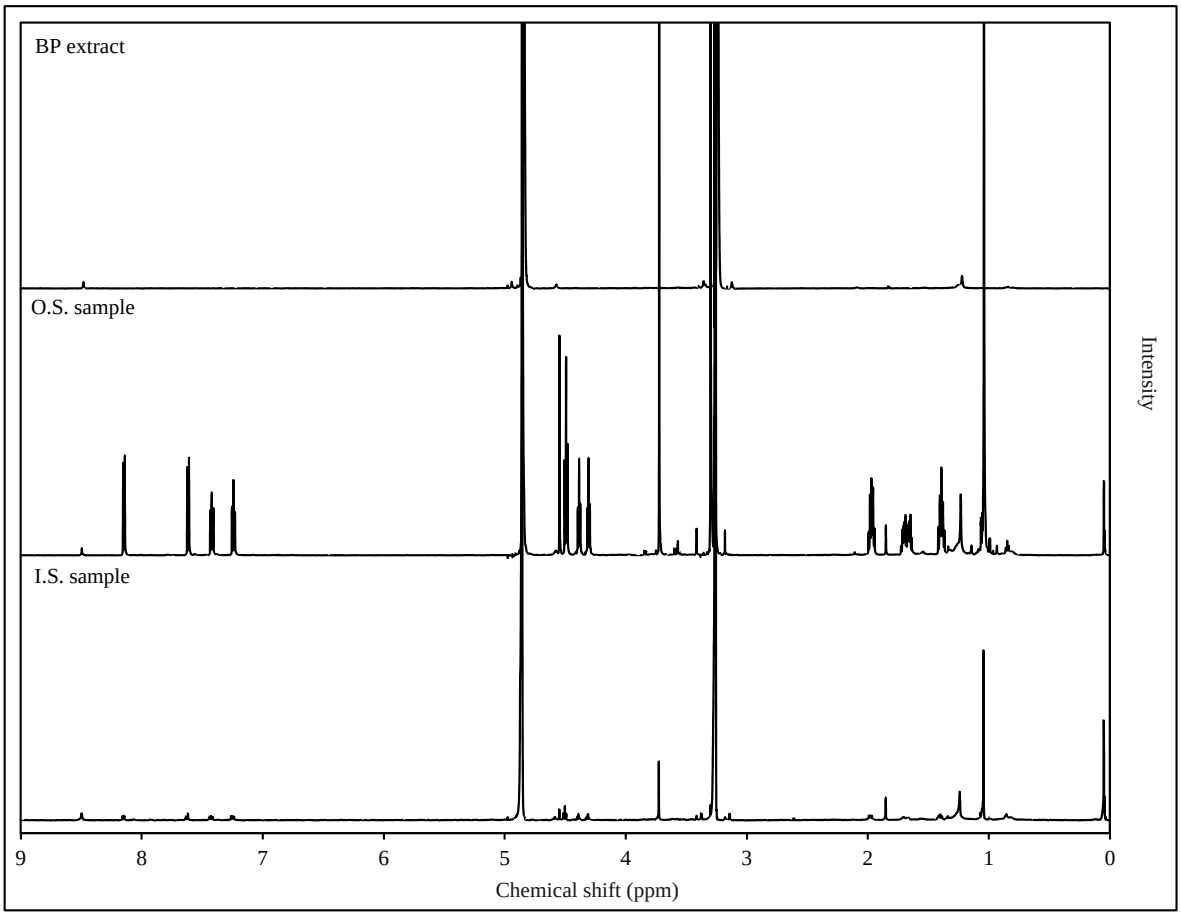

Figure 3.15. BP extract, O.S. and I.S. samples ^{1}H NMR stacked spectra in d-MeOH.

The chemical shifts (ppm), multiplicity, integral, J coupling and intensity values of the analyte found in the seized paper sample are presented in Table 3.7. When comparing the ^{1}H NMR spectra of the I.S and the O.S. the signal positions are aligned, while the intensity is higher in the O.S area of the sample, suggesting a higher concentration of the analyte in the O.S. area of the sample, consistently with the results from the other analysis (Sections 3.3.3.2. and 3.3.3.3.). Moreover, no additional peaks related to the unknown substances are visible in the NMR spectra. This is possibly due to their low concentrations in the sample.

Table 3.7. Summary of comparison between I.S. and O.S 1H NMR spectra of the seized paper sample.

Ppm	**Multiplicity**	**Position**	**Region**	**Integral**	**J coupling (Hz)**	**Intensity I.S.**	**Intensity O.S.**
0.10	Singlet	Si grease	-	-	-	0.55	0.74
1.04	Singlet	4" ($3xCH_3$)	Alkanes	9.46	-	1.25	17.33
1.40	Multiplex (5)	3"'	Alkanes	1.93	7.56	0.04	0.61
1.68	Multiplex (5)	4""	Alkanes	2.06	6.87	0.02	0.18
1.97	Multiplex (5)	2"'	Alkanes	2.02	7.56-6.87	0.05	0.57
3.31	Triplet	d-MeOH	Alkanes	2.88	1.70	16.90	38.79
3.72	Singlet	5"	$CO-OCH_3$	3	-	0.45	6.21
4.31	Triplet	5"'	$F-CH_2$	0.96	6.19	0.05	0.72
4.39	Triplet	5"'	$F-CH_2$	0.95	6.19	0.05	0.72
4.49	Triplet	1"'	$N-CH_2$	1.9	7.56	0.10	1.47
4.55	Singlet	2"	$NH-CH-COOCH_3$	0.92	-	0.06	1.64
4.87	Singlet	d-MeOH	OH	1.12	-	32.72	26.79
7.24	Triplet	5'	Aromatic	1	7.56	0.03	0.56
7.42	Triplet	6'	Aromatic	1	7.56-8.25	0.03	0.46
7.62	Doublet	7'	Aromatic	0.99	8.25	0.05	0.73
8.15	Doublet	4'	Aromatic	0.97	8.25	0.05	0.74

The position of the chemical shift values of the different protons of the 5F-ADB molecule is shown in Figure 3.16. The values were also confirmed by comparison to the available literature [105].

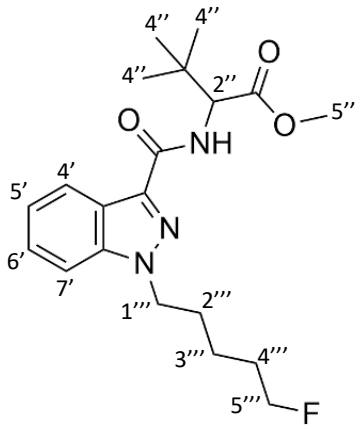

Figure 3.16. Position of chemical shift values of the different protons of the 5F-ADB. (Chemdraw Professional, version 16.0, UK).

NMR analysis confirmed 5F-ADB on the seized paper samples component, which is known to be the most prevalent synthetic cannabinoid identified in prison estate and homelessness services in the last five years [96,107]. While the presence of the other unknown analyte was not detected by the NMR since in low concentration.

3.4. Conclusions

A solid-liquid extraction method was developed to extract the model substance paracetamol from simulated paper samples. The solid-liquid extraction method was optimised by changing the sonication and centrifugation parameters, producing six different sets of parameters. The response (AUC) was evaluated using a two-way ANOVA analysis, which found no statistically significant difference (p-value <0.05) between the sets of parameters evaluated. Therefore, the sonication and centrifugation time chosen was the lowest evaluated, 10 min and 5 min, respectively. A percentage recovery study was conducted on paracetamol simulated paper samples which found that after two consecutive extractions an average of 80.1 ± 0.7% of paracetamol was extracted, with the highest amount of paracetamol (72.3 ± 1.6%) recovered during the first extraction.

A UPLC-PdA-QDa-MS method for the simultaneous detection and quantification of the caffeine +cocaine+THJ-018 mixture was optimised and successfully validated. Extractions of the single substance caffeine, then of the binary mixture caffeine +cocaine and, finally of the tertiary mixture caffeine +cocaine+THJ-018 pipetted on simulated paper samples were evaluated, using the parameters optimised for the extraction of paracetamol. On average 74.7 ± 1.3% of the analytes were successfully extracted on the first extraction, meaning that the method could be further optimised. The percentage recovered of caffeine, cocaine, and THJ-018 was consistent when complexity was added, suggesting that recovery does not seem to be impacted greatly for the mixtures evaluated. However, future work should be done to evaluate other NPS mixtures e.g., other reference standard and quaternary mixtures. To our knowledge, this study was the first to evaluate the recovery of a mixture of psychoactive substances and a cutting agent from the simulated paper sample which mimics the way substances are smuggled into UK prisons. After this study was completed, the percentage recovery values were compared to the work done by McKenzie and co-workers who successfully recovered 94-98% of synthetic cannabinoids after one extraction and *ca.* 100% after three consecutive extractions [3]. A difference of around 20% in the percentage of psychoactive substances recovered between McKenzie and co-workers and our study was recorded. This could be due to the different way the samples have been prepared. For instance, McKenzie and co-workers transferred 75 μL of 1 mg/mL solution of analytes to the 1cm^2 piece of paper using a single channel micropipette [3], while in our study 0.5 mL of 0.1 mg/mL solution of analyte was transferred using a graduated pipette. Due to the larger volume employed in our study, it could be likely that part of the solution could have been lost while being transferred onto the simulated paper samples, or diffused onto the tweezers. In the next chapter, this aspect was corrected to achieve better recovery values.

The extraction method optimised for paracetamol was also employed to extract unknown analytes from the one paper sheet of the evidence bag UHSOP/2018/PR025 seized from prison. When the extraction method was used to extract 1 cm^2 pieces from the seized paper sample, a quantity of analytes not detectable by the instrument was extracted. Hence the number of 1 cm^2 subunits of paper taken from the seized paper sample and extracted was increased up to 1 cm^2 x 76. The extracts were combined, and the solution evaporated down to *ca.* 0.5 mL to generate a peak in the chromatogram related to an unknown analyte. Combining extracts could have been avoided if more sensitive instrumentation such as UPLC-PdA-Time of Flight (ToF)-MS

were used. The UPLC-PdA-QDa-MS and NMR methods were developed using caffeine, cocaine and THJ-018 ternary model mixture and employed to analyse seized paper samples from a UK prison. Additionally, an already validated GC-MS method [100] was used to confirm the findings and gain insight into the fragmentation pattern of the analyte. The use of corroborative laboratory based techniques identified the ultra-potent synthetic cannabinoid 5F-ADB as the main component. While another possible psychoactive substances with an m/z of 373 was found in the samples but this is yet to be identified and confirmed.

Despite the IMS slip found in the evidence bag UHSOP/2018/PR025 reported traces of cocaine, previously identified by IMS screening in prison, cocaine was not found on the sheet selected and analysed in our laboratory. This might have occurred since the evidence bag contained an envelope with multiple paper sheets, and the IMS sample trap sample could have been wiped on multiple or all the paper sheets in the envelope. Wiping the IMS sample trap on large surfaces e.g., multiple paper sheets will result in a high loading of analytes in the sample trap. This is especially true if the whole sampling area covered by the IMS sample trap is compared to the few cm^2 analysed by UPLC-PdA-QDa-MS. Moreover, the sensitivity of the instruments employed in our study e.g., UPLC-PdA-QDa-MS is lower compared to IMS employed in prison. Therefore, in the next Chapter a prison sample, from the same evidence bag used in this Chapter, was screened using the more sensitive UPLC-PdA-QToF-MS instrument, to see if additional substances were present.

Furthermore, the UPLC-PdA-QDa-MS instrument, available at the time this study was carried out, used for the analysis of seized paper samples did not offer high resolution and high mass accuracy measurements, as opposed to UPLC-PdA-ToF-MS. High mass accuracy would allow limiting the number of possible molecular formulae significantly based on the accurate mass measurement, hence reducing the time of identification of an unknown. The use of MS/MS technique, available on the UPLC-PdA-ToF-MS instrument, would also reduce the time of analysis and identification of unknown since the analyte's fragmentation pattern would be available on the same instrument without the need to use EI GC-MS.

An additional limitation is that only one common printing paper was evaluated for the simulated samples prepared in this study, therefore, one of the next Chapter's objectives is to evaluate different paper matrices impregnated with 5F-ADB.

4. Screening and Quantitative Analysis of Psychoactive Substances from seized paper Prison sample using High-Performance Liquid Chromatography- Mass Spectrometry

As we learned from the previous Chapter 3 i) on average 75% of caffeine, cocaine and THJ-018 were successfully extracted on the first extraction when presented as a mixture, meaning that the recovery does not seem to be impacted greatly when substances are present together on paper ii) 5F-ADB was the main component in the seized paper sample analysed even though traces of cocaine were reported on the IMS slip found in the evidence bag UHSOP/2018/PR025. Before reaching the final aim, in this Chapter, an additional A5 paper sheet randomly selected from the same seizure employed in Chapter 3 was qualitatively and quantitatively analysed. The initial qualitative analysis was performed using the more powerful UPLC-PdA-QToF-MS instrument, to screen for additional substances. The quantification work, carried out using UPLC-PdA-QDA-MS, was performed to gain knowledge on the quantity of such NPS in seized paper samples, which is paramount for the future development of in-field screening techniques.

4.1. Introduction

At the time this study was performed no published literature on synthetic cannabinoids quantification of seized paper samples from prison was available. In 2020, McKenzie and co-workers were the first to report on the concentration of synthetic cannabinoids in seized paper samples from prison (n=145). In their study, six main synthetic cannabinoids (5F-MDMB-PICA; 4F-MDMB-BINACA; 5F-ADB; MDMB-4en-PINACA; AMB-FUBINACA; AMB-CHMICA) were quantified by GC-MS, collected by three consecutive extractions from seized paper samples [3]. A percentage recovery study was also carried out by spiking simulated paper samples with known quantities of synthetic cannabinoids (5F-MDMB-PICA, 4F-MDMB-BINACA, 5F-ADB, AMB-FUBINACA and AMB-CHMICA) and evaluated over five consecutive extractions [3]. The percentage recovery of synthetic cannabinoids obtained by McKenzie and co-workers was found to be 94-98% after one extraction and *ca.* 100% after three consecutive extractions, which was found to be *ca.* 20% higher than the one achieved in Chapter 3. The reason for the discrepancy could be due to the different way the samples have been prepared. McKenzie and co-workers transferred 75 μL of 1 mg/mL solution of analytes

to the 1cm^2 piece of paper using a single channel micropipette [3], while in our study 0.5 mL of 0.1 mg/mL solution of analyte was transferred using graduated pipettes. Due to the larger volume employed in our study, it could be likely that part of the solution could have been lost while being transferred onto the simulated paper samples or diffused onto the tweezers. This aspect was addressed in this chapter to achieve better recovery values. In this chapter, McKenzie and co-workers' findings are compared to the ones from our study, where quantification of an A5 paper sheet randomly selected from the same envelope in the evidence bag UHSOP/2018/PR025 employed in Chapter 3 was performed. The quantification analysis was carried out using a UPLC-PdA-QDa-MS method previously developed, optimised and used to quantify caffeine, cocaine and THJ-018 in Chapter 3 (Section 3.3.1.2.), which was further optimised specifically for quantification of the synthetic cannabinoid 5F-ADB and validated. The percentage recovery of 5F-ADB was calculated on three sets of concentrations, over five consecutive extractions for five replicates simulated samples each (n=15). The three concentrations employed to prepare the simulated paper samples were chosen to mirror the range of synthetic cannabinoids found on seized paper samples, and to expand on McKenzie and co-workers' study, which was performed on compounds at a higher concentration. Gaps in the knowledge were highlighted from the literature concerning the impact of the type of paper in the quantification of analytes, which was evaluated in this chapter using five different types of paper. The work performed in this Chapter, especially on the quantification of synthetic cannabinoids was of greatest importance to increase knowledge and improve future method development of in-field detection approaches.

This study aims to analyse a seized prison paper impregnated with psychoactive substances, specifically the synthetic cannabinoid 5F-ADB, using Ultra-Performance Liquid Chromatography-Photodiode Array Detector-Quadrupole Time of Flight-Mass Spectrometry (UPLC-PdA-QToF-MS) and Ultra-Performance Liquid Chromatography-Photodiode Array Detector-Quadrupole Dalton-Mass Spectrometry (UPLC-PdA-QDA-MS) methods. The objectives are to i) screen the seized paper samples for psychoactive substances using a UPLC-PdA-QToF-MS method; ii) quantify the 5F-ADB found in the seized paper samples using a further optimised and validated UPLC-PdA-QDA-MS method from Chapter 3; iii) calculate the percentage recovery of 5F-ADB over five consecutive extractions and five replicates simulated samples and iv) evaluate the matrix effect of five paper matrices impregnated with 5F-ADB.

4.2. Material and methods

4.2.1. Chemicals and reagents

5F-ADB and APINACA (both 99% purity) certified reference standard was obtained from Chiron AS (Trondheim, Norway). HPLC grade methanol (MeOH) and common grade acetone (both 99% purity) were obtained by Fisher Scientific (Loughborough, UK). Ultra-high purity Millipore Water (MW) (18 MΩ cm^{-1}) was obtained from Milli-Q water purification system (Merck, UK). Common A4 printing 80 g/m^2 density paper sheet (Type 1: Envirocopy A4 500 sheet; ECF; 100% Recyclable paper. Type 2: Evolution, A4 500 sheet, TCF, 75% Recycled paper), paper from ruled notebook 80 g/m^2 density (Pukka Pad), weighted paper 120 g/m^2 density (Evolution) was employed for the preparation of simulated paper samples.

4.2.2. Instrumentation

4.2.2.1. Ultra-Performance Liquid Chromatography-Photodiode Array Detector-Quadrupole Time of Flight-Mass Spectrometry

A Waters Acquity® Ultra-Performance Liquid Chromatography (UPLC) coupled to a Waters Xevo G2S Quadrupole Time of Flight (QtoF) Mass Spectrometer (MS) (Milford, MA, USA), running under MassLynx V.4.2 was employed to screen for psychoactive substances present in the seized paper sample. The method employed to screen the sample for psychoactive substances was adapted from Von Cüpper *et.al.* [108] . Mobile phases used were (A) 5 mM of aqueous ammonium formate buffer, pH 3 (formic acid) and (B) acetonitrile with 0.1% v/v formic acid. Both solvents were filtered through a 0.22 µm membrane filter (Whatman, UK) and then sonicated using Decon Ultrasonic Heater (Decon Laboratories Ltd, UK). The gradient was (% B): 0 to 0.5 min: 13% (B), from 0.5 to 10 min: 13 to 50% (B), from 10 to 10.75 min: 50 to 95% (B), from 10.75 to 12.25 min: 95% (B), from 12.25 to 15 min: 95 to 13% (B) and from 15 to 20 held at 13% (B), for a total run time of 20 min. A flow rate of 0.4 mL/min and a sample volume of 5 µL was employed with a Waters Acquity UPLC HSS T3 C18 150 x 2.1 mm x 1.8 µm particle size column. Sample vials were kept by the sample manager at 15 °C and a temperature of analysis of 50 °C was used. The analysis was conducted using positive Electrospray Ionisation (+ ESI) in the 50.0-950.0 m/z range. The instrument settings were the following: desolvation gas, argon 800 L/h, with a temperature of 400 °C; cone gas flow 20 L/h;

source temperature 150 °C; capillary voltage 800 V; and cone voltage 25 V. The QtoF was operated in the Data Independent Acquisition (DIA) MS^E with elevated collision energy (CE). The low CE (4 eV) was alternated with high CE (ramped from 10 to 40 eV), allowing the simultaneous collection of precursor and product ion data. The DIA was performed in both resolution and sensitivity modes. Further fragment spectra were acquired in MS/MS Selected Reaction Monitoring (SRM) on the precursor ion of interest to confirm the relationship between precursor and product ions formed. A direct comparison between the spectra of the identified substance and its certified reference standard was performed as well. The method was not fully validated using Standard Operating Procedure (SOP) for HPLC method validation, as it was only used for screening purposes. However, a QC sample comprised of APINACA and 5F-ADB reference standards 500 ng/mL) at the beginning at the end of the run was employed to check if mass accuracy, peak shape and RT, were appropriate remaining consistent during the sample analysis. MeOH blank was run before and after the QC samples, to check for any carryover.

4.2.2.2. HighResNPS.com

Access to the online mass spectral database for Liquid Chromatography-High Resolution Mass Spectrometry LC-HRMS HighResNPS.com was granted. This allowed accurate mass search by setting specific parameters e.g., a precursor ion and fragment ions with an m/z tolerance of 5 ppm. Compounds that were selected by the library search were compared with the ones observed experimentally and labelled as potential candidates.

4.2.2.3. Ultra-Performance Liquid Chromatography-Photodiode Array Detector-Quadrupole Dalton-Mass Spectrometry

A Waters Acquity® Ultra-Performance Liquid Chromatography (UPLC) coupled to a Waters Acquity® Photodiode Array (PdA) and a Waters Acquity® Qda® (Quadrupole Dalton) MS (Milford, MA, USA), running under MassLynx V.4.2 was employed to quantify the 5F-ADB present in the seized paper sample. Mobile phases used were (A) MW with 0.1% v/v formic acid and (B) MeOH with 0.1% v/v formic acid. Both solvents were filtered through a 0.22 μm membrane filter and then sonicated for 20 mins. The gradient used was 75:25 A:B from 0.0-0.5 min, 10:90 A:B from 0.5-3.5 min, 5:95 A:B from 3.5-6.0 min, 50:50 A:B from 6.0-6.5 min, 75:25 A:B from 6.5-7.0 min and held for 2 min. A flow rate of 0.6 mL/min was employed with

a Phenomenex Kinetex C_{18} 100Å 100 x 2.1 mm x 2.6 µm particle size column (SN: H21-249406) and SecurityGuard ULTRA UHPLC holder and cartridge, C_{18} 2.1 mm, filter both sourced from Phenomenex (Macclesfield, UK). The injection volume was set at 1 µL. The post-injection was performed for 6 min needle with MeOH. Sample vials were kept by the Sample Manager at 5 °C and a temperature of analysis of 30 °C was used. Chromatograms were produced using the PdA® detector in Total Ion Current (TIC) at 20 sampling points per sec, with a resolution of 1.2 nm across the 190-400 nm range and the negative absorbance margin was set at -0.15 AU. The Qda® analysis was conducted using Electrospray Ionisation (ESI) in positive mode from 99-900 m/z range with a sampling frequency of 8.0 sec and a capillary voltage at 0.8 V. The mass spectrometer detector recorded a signal every 0.080 sec, with a cone voltage of 20 V and a probe temperature of 600°C. UPLC method was validated for 5F-ADB using the UNODC "Guidance for the Validation of Analytical Methodology and Calibration of Equipment used for Testing of Illicit Drugs in Seized Materials and Biological Specimens" [109] for the following parameters: system suitability; linearity and working range; Limit of Detection (LOD) and Limit of Quantification (LOQ), precision under repeatability and reproducibility conditions, accuracy and recovery.

4.2.3. Samples

Prior to sample preparation and analysis, all glassware, spatulae and tweezers were carefully washed and rinsed first with Deionised Water (DW) and then with pure MeOH. In addition, working surfaces were cleaned with pure MeOH.

4.2.3.1. UPLC reference standard solutions preparation

A series of calibration standards (50-1 µg/mL) were prepared for the quantification of 5F-ADB, and also to calculate the linearity as part of the method validation. The Stock Solution 1 (SS1) was prepared by weighting *ca.* 2 mg of 5F-ADB reference standard in a Sartorius Practum (Sartorius AS, Germany) analytical balance and adding them to a 2 mL volumetric flask. MeOH was added to reach the 2 mL final volume, to give a concentration of *ca.* 1 mg/mL. The SS1 was vortexed using VORTEX-GENIE2 (Scientific industries, Inc., USA) for two minutes to reach complete solubilisation. An SS2 was prepared by diluting 100 µL of SS1 into 900 µL of MeOH. A range of six calibration standards was obtained by dilution of either SS1 or SS2

(Table 4.1) by pipetting diluent and spiking volume directly into the labelled HPLC vials, which were then immediately sealed.

Table 4.1. UPLC-PdA-QDa-MS 5F-ADB calibration curve concentration range.

Sample	Conc (mg/mL)	Conc (µg/mL)	Conc (ng/mL)	Spiking volume (µL)		Diluent (µL)
				SS1*	SS2*	
5F-ADB C1	0.05	50	50,000	50		950
5F-ADB C2	0.02	20	20,000	20		980
5F-ADB C3	0.01	10	10,000	10		990
5F-ADB C4	0.005	5	5,000		50	950
5F-ADB C5	0.002	2	2,000		20	980
5F-ADB C6	0.001	1	1,000		10	990

*Stock Solution 1 concentration 1 mg/mL= 1000 µg/mL=1,000,000 ng/mL

*Stock Solution 2 concentration 0.1 mg/mL= 100 µg/mL= 100,000 ng/mL

The HPLC vials were, vortexed and submitted for analysis. A blank MeOH was run between the different concentration vials. Six replicate injections per concentration were evaluated.

4.2.3.2. Seized paper samples

An additional A5 paper sheet from the evidence bag labelled UHSOP/2018/PR025 was randomly chosen for the analysis. See Chapter 3, Section 3.2.3.2.

4.2.3.3. Seized paper samples sampling strategy, preparation, and extraction

An A5 paper sheet was divided into roughly 316 units (N) of 1 cm^2, to make a sampling grid. The seized paper sample from the evidence bag UHSOP/2018/PR025, was laid on top of the sampling grid, and the 1 cm^2 subunits were cut with the help of a scalpel. For the UPLC-PdA-QToF-MS screening analysis, three subunits of 1cm^2 were analysed to find out about the psychoactive substances present and to have a general idea of their concentration range, used to build the calibration curves for the quantification. The three subunits were cut from the middle of the sheet at the bottom (11A), middle (11E), and top (11M) positions which are highlighted in red in Figure 4.1.

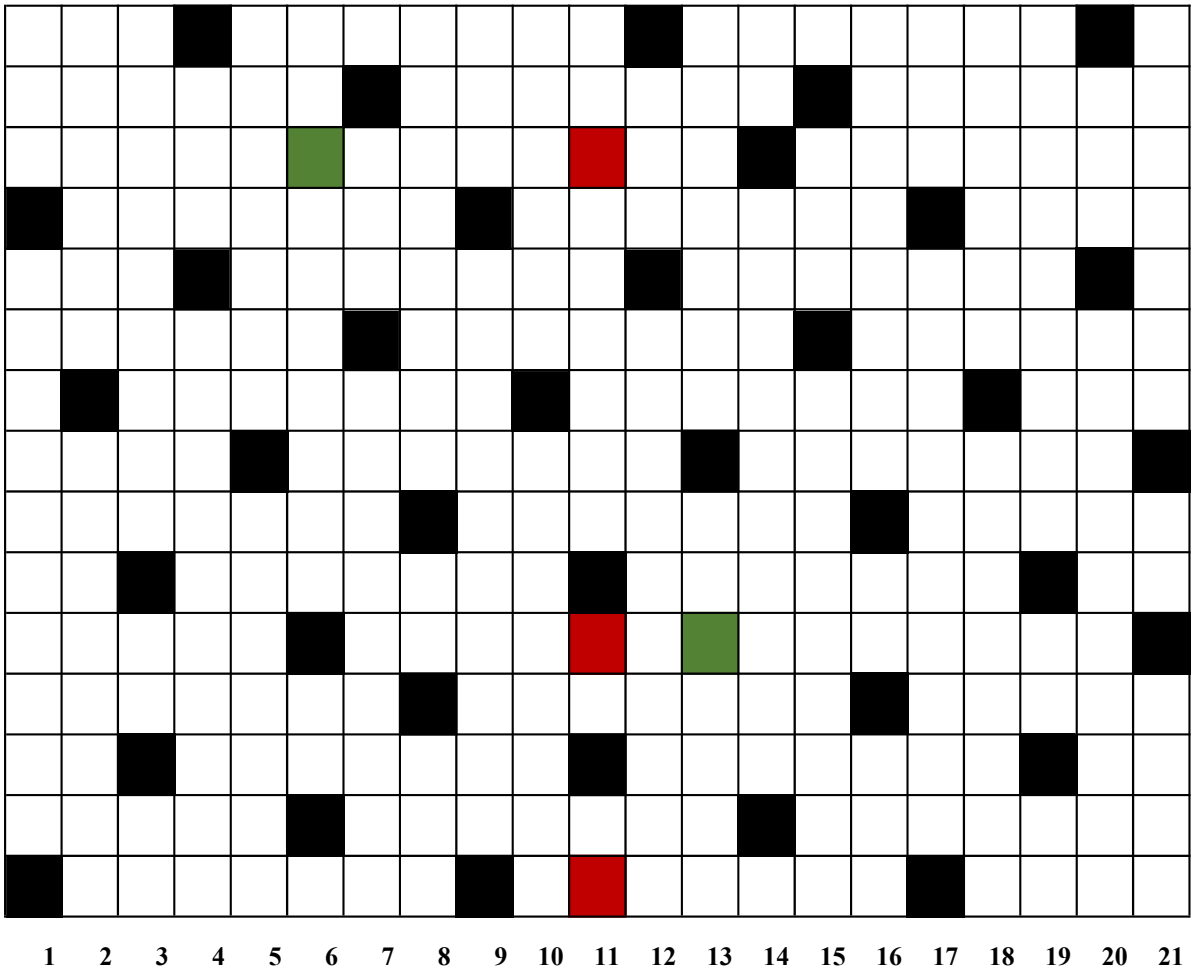

Figure 4.1. Sampling grid of the prison sample. The red subunits were used for the initial UPLC-PdA-QToF-MS screening analysis. The green subunits were used as the two starting sampling points while the black were the other subunits sampled for UPLC-PdA-QDa-MS qua.

To initially extract the analytes from the paper, each of the 1 cm^2 paper samples (11A, 11E and 11M) was placed in a reaction tube with 0.5 mL MeOH. The reaction tubes were sonicated and centrifugated for 10 and 5 min, respectively. This process was carried out three times using fresh MeOH. The extracts were drawn from the reaction tube with a 1 mL syringe, filtered through a 0.2 µm polytetrafluoroethylene (PTFE) hydrophobic filter, transferred into HPLC vials, dried under N_2 and reconstituted with 0.5 mL of MeOH. The same procedure was applied to 1 cm^2 blank paper (BP) samples cut from a common A4 printing paper sheet, and then the BP extract was analysed. A pure MeOH control sample was also analysed.

To establish the sample size on which to perform the quantification analysis a statistical frequentist approach using the hypergeometric distribution was employed to determine the number of subunits to analyse to achieve representative sampling [110]. The frequentist approach was chosen as it assumes that a fixed but unknown proportion of the seizure contains drugs, as opposed to a Bayesian approach which assumes that the sample proportion is fixed and known. To guarantee with 99% confidence that at least 90% of the subunits contain illicit substances, 40 (n) subunits should be sampled (Table 4.2).

Table 4.2. Hypergeometric distribution. From UNODC-Guidelines on representative sampling [110].

Population size *N*	95% confidence			99% confidence		
	k=0.5	*k*=0.7	*k*=0.9	*k*=0.5	*k*=0.7	*k*=0.9
300	5	9	27	7	13	40
400	5	9	27	7	13	41
500	5	9	28	7	13	41
600	5	9	28	7	13	42
700	5	9	28	7	13	42
800	5	9	28	7	13	42
900	5	9	28	7	13	43
1 000	5	9	28	7	13	43
5 000	5	9	29	7	13	44
10 000	5	9	29	7	13	44

The systematic sampling design is a probability sampling method where the subunits in the population are selected at regular intervals starting from a random point. This offers the advantages of ease of execution, convenience, and obtaining a more even spread of samples compared to random sampling. While simple random sampling offers less risk of data manipulation it is often less efficient and less precise than other designs. The sampling interval (k) was calculated using Equation (4.1) below.

$$k = \frac{N}{n} \qquad Equation\ (4.1)$$

Where N is the total population size and n is the subunits sampled [111]. Meaning each sample was taken at an interval of 8 subunits. Two random subunits 13E and 6M, coloured in green in Figure 4.1, were selected as started sampling points, using the random function on Excel (version 2015, build 14026.20308), so that the variance and the standard error estimates could be determined without bias [111].

To extract the analytes from the paper, each of the 1 cm^2 paper samples was placed in a reaction tube with 0.5 mL MeOH. The reaction tubes were sonicated and centrifugated for 10 and 5 min, respectively. This process was carried out three consecutive times using fresh MeOH. The extracts were drawn from the reaction tube with a 1 mL syringe, filtered through a 0.2 µm polytetrafluoroethylene (PTFE) hydrophobic filter, transferred into HPLC vials, and analysed using the UPLC-PdA-QDa-MS. A MeOH control sample was also analysed. A blank MeOH was run every 6 samples, to ensure that no carry-over issues were present.

4.2.3.4. Simulated paper samples

Simulated paper samples were prepared to evaluate i) percentage recovery of the substance and ii) the paper matrix effect impact during the quantification with the UPLC-PdA-QDa-MS.

4.2.3.5. 5F-ADB simulated paper samples preparation and extraction for percentage recovery study

The percentage recovery study was performed as part of the HPLC method validation to prove the reproducibility of the method within ± 15% as per HPLC method validation (UNODC) criteria, and to verify how many sequential extractions were needed to extract 5F-ADB from paper. Simulated paper samples were prepared using the target analyte 5F-ADB, which was

found on the seized paper sample by screening with UPLC-PdA-QtoF-MS analysis. Five replicate samples were prepared at three different concentrations using a typical matrix, and five consecutive extractions were performed on them. Therefore, fifteen pieces of paper of 1 cm^2 were cut from common printing A4 80 g/m^2 density paper sheets with the help of a stencil. Approximately 2 mg (2.14 mg) of 5F-ADB were weighed and dissolved in 2 mL of MeOH to obtain 1.07 mg/mL stock solution 1 (SS1). The SS1 was further diluted by drawing 100 µL and diluting in 900 µL of MeOH to obtain a 0.1 mg/mL stock solution 2 (SS2). For the first concentration (C1) employed, 20 µL of SS1 were pipetted onto a 1 cm^2 piece of paper. For the second concentration (C2) 50 µL of SS2 were pipetted onto a 1 cm^2 piece of paper. For the last concentration (C3) 10 µL of SS2 were pipetted onto a 1 cm^2 piece of paper. Each of the three concentrations was used to prepare five replicate simulated paper samples. The solutions were pipetted onto the paper while they were held carefully in a corner by a pair of tweezers between a clamp. The simulated paper samples were allowed to dry completely in the same position to avoid any loss of solution containing 5F-ADB by contact with surfaces. Each piece of paper was placed in a separate reaction tube with 1 mL of MeOH, sonicated and centrifugated for 10 and 5 min, respectively. This process was repeated five times using fresh MeOH. Each extract was drawn from the reaction tube with a 1 mL syringe, filtered through a 0.2 µm polytetrafluoroethylene (PTFE) hydrophobic filter, transferred into an HPLC vial, and analysed using the UPLC-PdA-QDa-MS. A blank MeOH was run every 6 samples, to ensure that no carry-over issues were present. The peak areas resulting from each extract were collected, converted into a concentration and the percentage recovery was calculated using Equation (4.2) below.

$$\left(\frac{Theoretical\ concentration}{Experimental\ concentration}\right) x\ 100 \qquad \text{Equation (4.2)}$$

4.2.3.6. 5F-ADB simulated paper samples preparation and extraction for matrix effect evaluation

The study on the paper matrix was performed to verify if other compounds present in the different types of paper, used to smuggle synthetic cannabinoid in prison, could lead to alteration of the ionisation efficiency hence influence the quantification of the target analyte. To this end, simulated paper samples were prepared using different paper matrices spiked with the same amount of 5F-ADB, which was then quantified. The paper matrices employed (Figure 4.2) were the following: type 1 common printing paper 80 g/m^2 density (Envirocopy), type 2 common printing paper 80 g/m^2 density (Evolution), type 3 paper from ruled notebook 80 g/m^2 density (Pukka Pad), type 4 weighted paper 120 g/m^2 density (Evolution), and type 5 black ink printed common printing paper 80 g/m^2 density (Envirocopy).

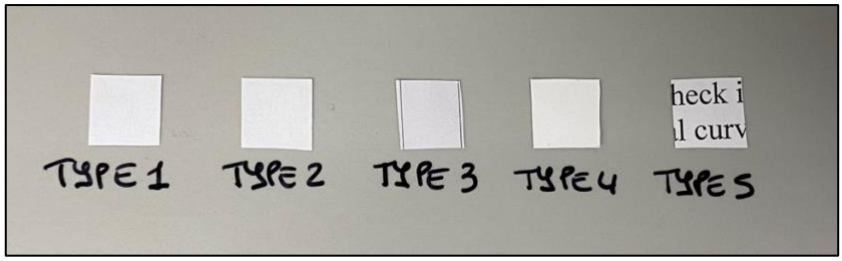

Figure 4.2. Different types of paper matrix evaluated for the study.

Using the same procedure described in section 4.2.3.3.1. 20 µL of a 1 mg/mL 5F-ADB reference standard solution were pipetted onto the five different paper matrices, extracted, and analysed using the UPLC-PdA-QDa-MS. The peak areas of each extraction were collected, quantified, and compared to each other's using the Relative Standard Deviation (RSD), to verify if there was any big fluctuation in the quantity of 5F-ADB extracted when different paper matrices were employed to prepare the simulated paper samples.

4.3. Results and discussion

4.3.1. Optimisation and validation of Ultra-Performance Liquid Chromatography-Photodiode Array Detector- Quadrupole Dalton-Mass Spectrometry method

The UPLC-PdA-QDa-MS method previously developed, optimised and used to quantify caffeine, cocaine and THJ-018 in Chapter 3 (Section 3.3.1.2.), was adapted for 5F-ADB detection and quantification, and re-optimised to produce symmetrical peaks. The mobile phase A and B composition remained the same, while the gradient was changed slightly, to have a wider apolar interval of the two solvents (from 3.5-6.0 min) for the elution of 5F-ADB and a wider equilibration interval (7.0-9.0 min) (Table 4.3). This increased the analysis time from 6 min to 9 min total runtime.

Table 4.3. Comparison of UPLC-PdA-QDa-MS gradient method employed in Chapters 3 and 4.

Gradient (min)	Mobile phases ratios Chapter 4		Gradient (min)	Mobile phases ratios Chapter 3	
	(A) MW + 0.1% FA	(B) MeOH + 0.1%FA		(A) MW + 0.1% FA	(B) MeOH + 0.1%FA
0.0-0.5	75	25	**0.0-0.5**	75	25
0.5-3.5	10	90	**0.5-3.5**	10	90
3.5-4.5	10	90	**3.5-6.0**	5	95
4.5-5.5	50	50	**6.0-6.5**	50	50
5.5-6.0	75	25	**6.5-7.0**	75	25
			7.0-9.0	75	25

The flow rate remained the same at 0.6 µL/min, while the injection volume was set to 1 µL. The retention time of 5F-ADB was 3.99 ± 0.05 min. Linearity r^2, LOD and LOQ values calculated on six calibration curves, were found to be comprised between 0.998 ± 0.001, 0.059 ± 0.027 ng/mL and 0.181 ± 0.082 ng/mL, respectively. All the parameters evaluated for the UPLC-PdA-MS method validation of 5F-ADB were found to be within the acceptance criteria (Appendix 3.1- Table A1) as defined by the UNODC "Guidance for the Validation of Analytical Methodology and Calibration of Equipment used for Testing of Illicit Drugs in Seized Materials and Biological Specimens" [109].

4.3.2. Seized paper samples analysis

4.3.2.1. Screening of seized paper samples using Ultra-Performance Liquid Chromatography-Photodiode Array Detector-Quadrupole Time of Flight-Mass Spectrometry.

The MS was operated in the Data Independent Acquisition (DIA) MS^E mode which offers the advantage of a generic, non-biased screening method to acquire data, ideal for identification of analyte in unknown samples/mixtures. The fragmentation spectra were acquired using MS/MS Selected Reaction Monitoring (SRM). Therefore, the approach employed in this section consisted of the combination of accurate mass and fragmentation patterns. Using the accurate measurement of the protonated molecule $[M+H]^+$ the number of potential substances in a database can be drastically reduced. The synthetic cannabinoid 5F-ADB was found in the three subunits (Section 4.2.3.2.1) of the A5 paper sheets randomly selected from the evidence bag UHSOP/2018/PR025. The total ion chromatograms (TIC), in both resolution and sensitivity mode of the top (11M), middle (11E), bottom (11A), BP extract and pure MeOH samples were compared to each other's using Waters software package MassLynx V.4.2 to highlight peaks present in a sample but absent in other ones. Firstly, the BP extract was compared to a pure MeOH sample (Figure 4.3).

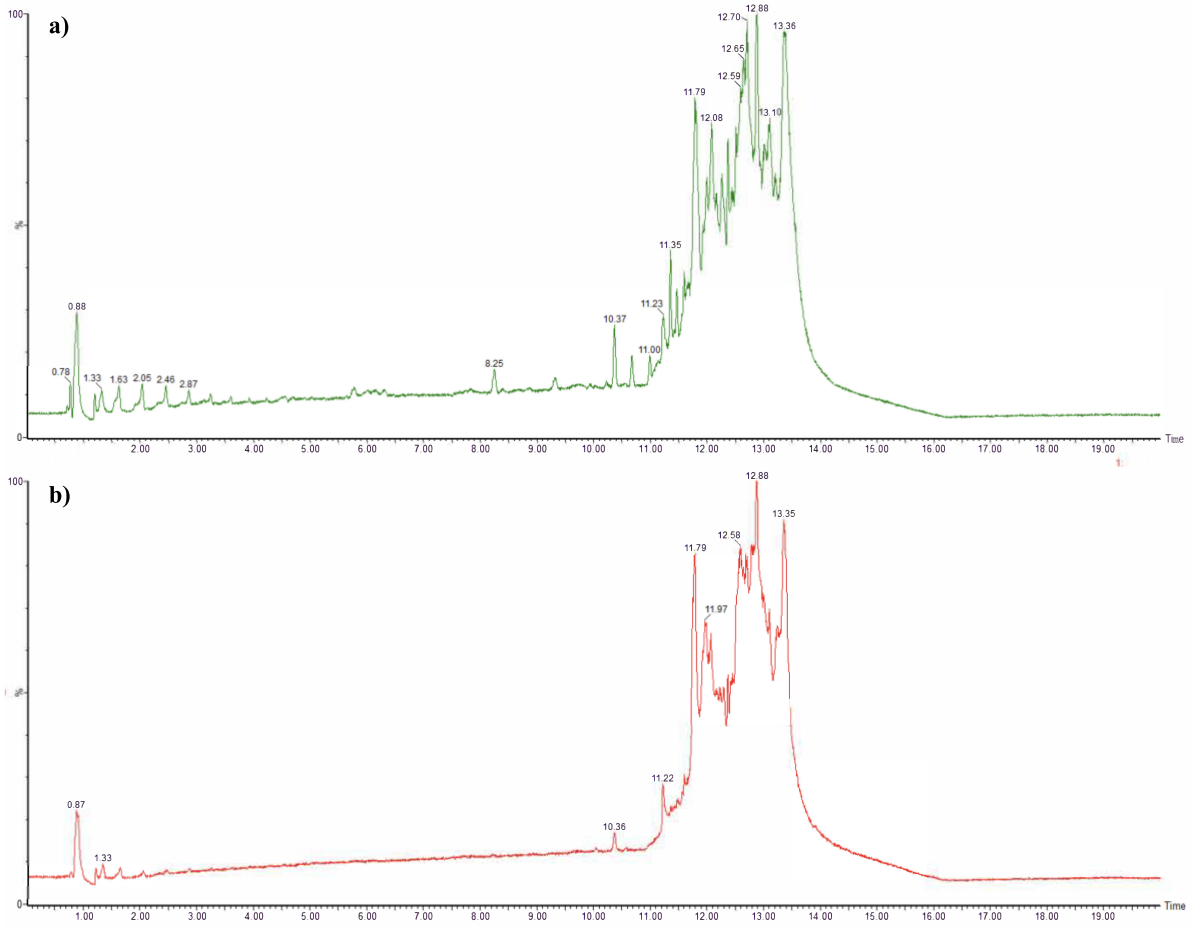

Figure 4.3. TIC in resolution mode of a) BP extract vs. b) MeOH blank samples, highlighting no peaks differences between the two samples.

No differences were found between the TIC chromatograms of the BP extract and the MeOH blank samples. Although from visual observation of the two chromatograms it seems that some peaks were present in the BP extract but not in the MeOH blank sample, this was carefully checked by enlarging and comparing every single peak throughout the chromatograms. This was due to differences in the absolute intensity of the BP extract and the MeOH blank samples analysed, which were 4.61×10^7 and 4.08×10^7 AU, respectively.

Then the 1st replicate of the sample 11M was compared to the BP extract sample (Figure 4.4).

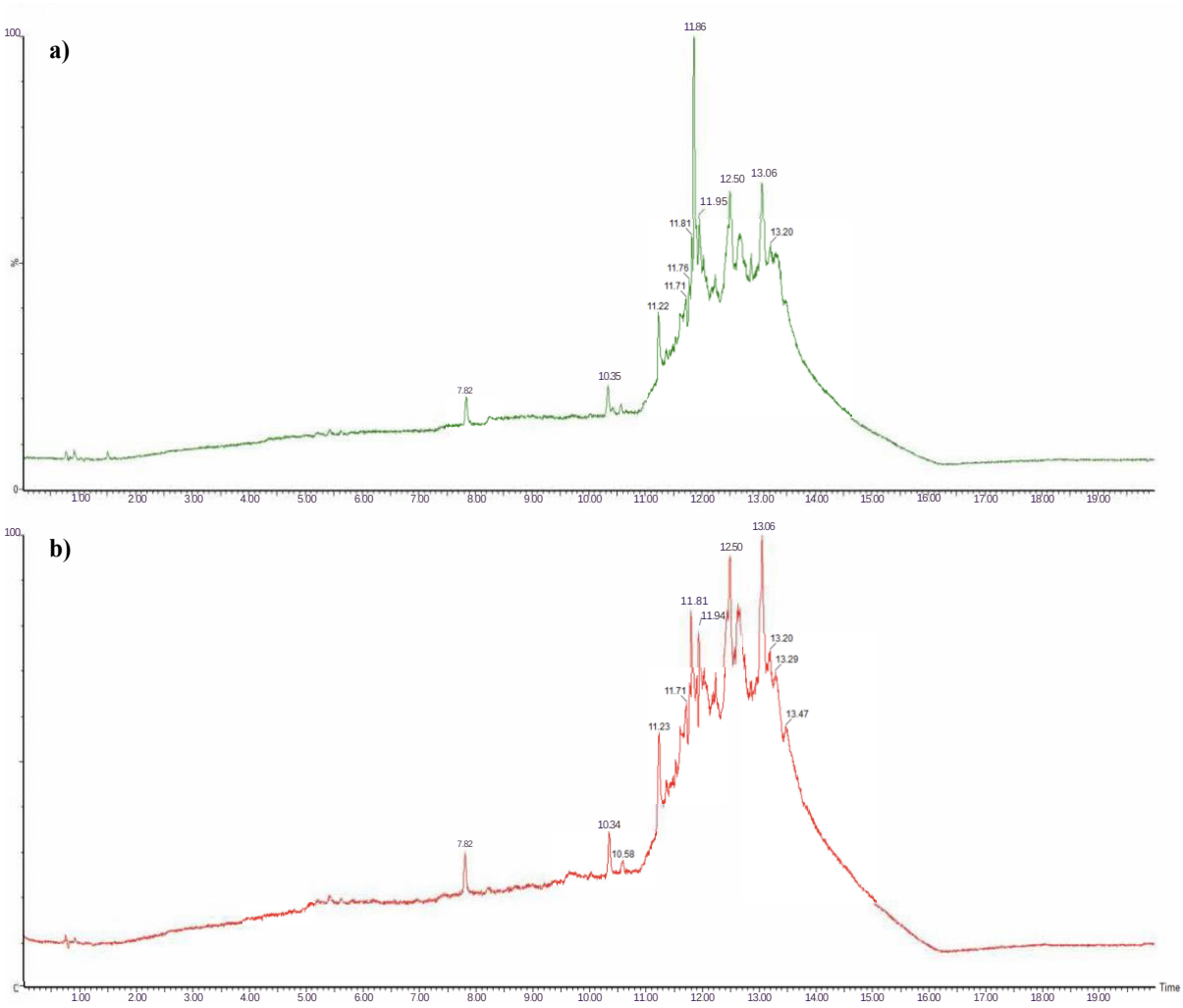

Figure 4.4. TIC in resolution mode of a) 11M replicate 1 vs. b) BP extract samples, highlighting a peak at 11.86 min present in 11M R1 but not in BP extract sample.

Two additional peaks with a RT of 1.51 and 11.86 min and absolute intensity of 8.53×10^6 and 2.32×10^7 were found in all the 11M replicate 1. The retention time 1.51 and 11.86 min were associated with the protonated molecules 157.1148 and 378.2206 m/z, respectively. Both accurate masses with a tolerance of ± 5 ppm were input into the HighResNPS database. The accurate mass 157.1148 m/z did not match any entry, while 378.2206 m/z corresponded to 9 entries in the database (Table 4.4), which are all structural isomers of 5F-ADB. The absolute intensity of the 11 M replicate 1 and the BP extract samples, were 2.32×10^7 and 1.59×10^7 AU, respectively.

Lastly, the three replicates of the sample 11M were compared to each other's (Figure 4.5).

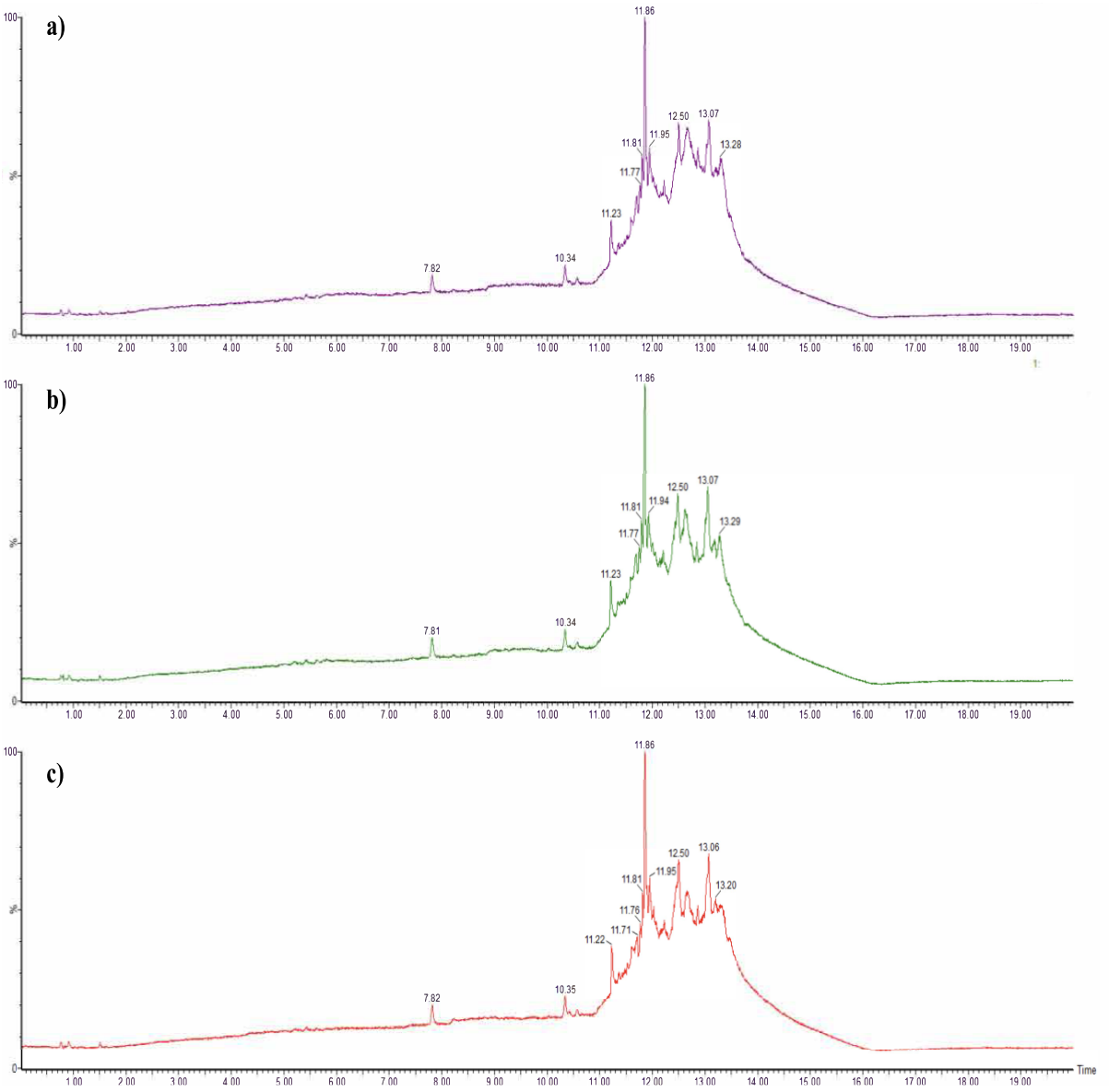

Figure 4.5. TIC in resolution mode of a) 11M replicate 3 vs. b) replicate 2 and c) replicate 1 sample, highlighting no peaks differences between the three samples.

The two peaks found in the sample 11M replicate 1 were consistently found in the other two 11M replicate samples. The RT, the absolute intensity, and the m/z of the protonated ion of the two peaks found in the three 11M replicate samples were compared and found to be 1.51 ± 0.00 min and 11.86 ± 0.00 min, 8.11 ± 0.37 AU and 2.41×10^{6} ± 0.09 AU, and 157.1148 ± 5.77×10^{-5} m/z and 378.2206 ± 2.5×10^{-4} m/z, respectively.

An example of the peak related to the protonated ion 378.2206 m/z eluting at 11.86 min is presented in Figure 4.6.

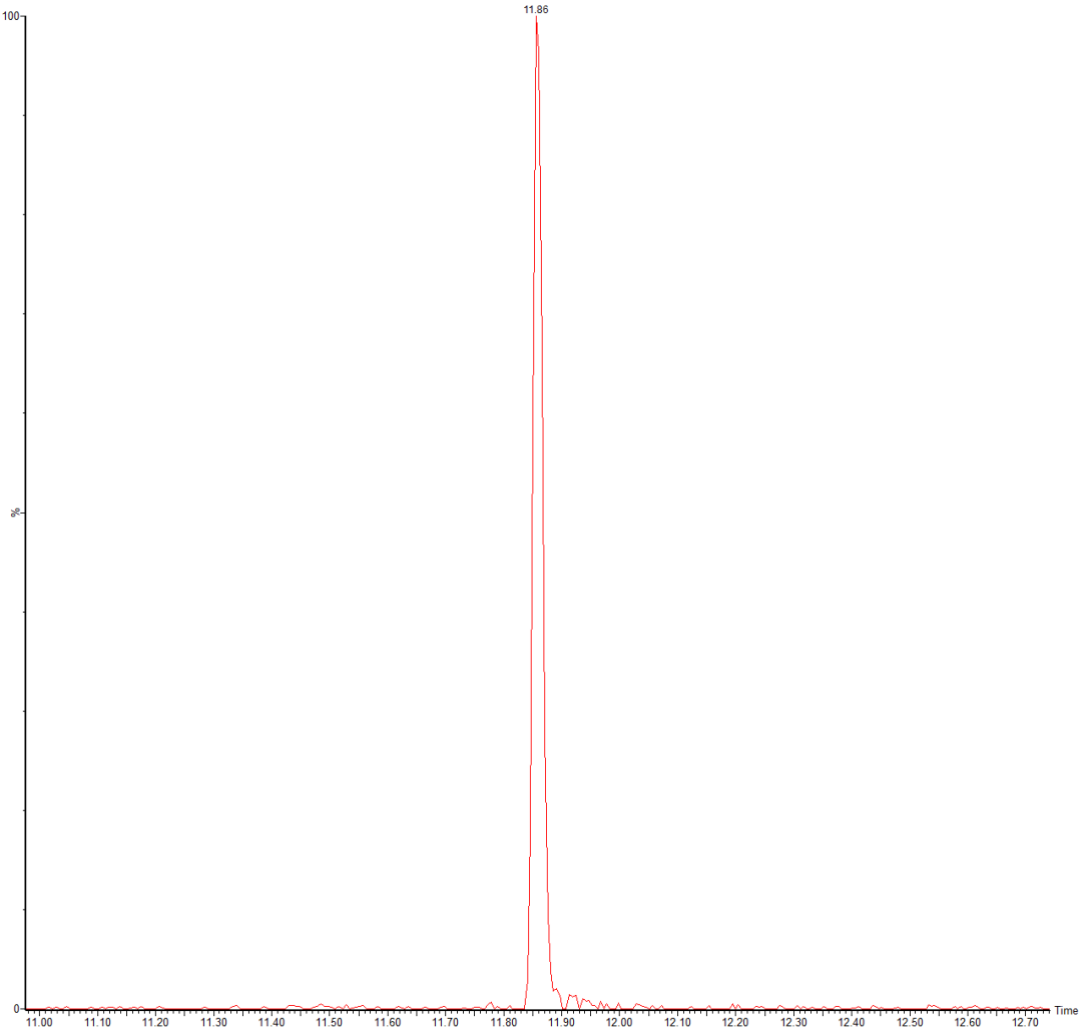

Figure 4.6. Peak related to the unknown protonated ion 378.2206 m/z eluting at 11.86 min.

The comparison presented above for sample 11M was repeated for samples 11A (Appendix 3.2- Figure A1 and A2) and 11E (Appendix 3.2- Figure A3 and A4), analysed in resolution mode and for samples 11A (Appendix 3.2- Figure A5, A6 and A7), 11E (Appendix 3.2- Figure A8 and A9), and 11M (Appendix 3.2-Figure A10 and A11) in sensitivity mode. No additional analytes were identified by comparison of the samples 11E and 11A with the BP extract.

The accurate mass 378.2206 ± 5 ppm m/z found in the 11M replicate samples corresponded to 9 entries in the HighResNPS database (Table 4.4). The 9 entries reported by the HighResNPS database had all the same accurate mass of 378.2187 m/z, which means a difference of 2.38 ppm between the m/z in the database and the one observed in this study (378.2206 m/z). The 9 database entries were related to positional isomers.

Table 4.4. Compounds with molecular formula $C_{20}H_{28}FN_3O_3$ and 378.2187 m/z mass from found on HighResNPS.com.

Compounds	Molecular formula	P mass	F1 mass	F2 mass	F3 mass	F4 mass	F5 mass	F6 mass
2F-ADB	$C_{20}H_{28}FN_3O_3$	378.2187	233.1085	318.1976	145.0396	-	-	-
3F-ADB			233.1085	318.1976	145.0396	-	-	-
4F-EDMB-BUTINACA			-	-	-	-	-	-
4F-ADB			233.1085	213.1022	145.0396	69.0699	-	-
5F-ADB			233.1085	318.1976	213.1022	145.0396	251.119	69.0699
5F-AEB			233.1085	213.1022	304.1819	251.119	145.0396	69.0699
5F-ADB 2'-indazole isomer			-	-	-	-	-	-
5F-MDMB-P4AICA			233.1085	-	-	-	-	-
5F-MDMB-P7AICA			233.1085	318.1976	145.0396	-	-	-

Some information about the fragmentation pattern of the 9 entries (Table 4.4), sharing the molecular formula $C_{20}H_{28}FN_3O_3$ was reported by the HighResNPS database. However, not all the fragmentation patterns were reported, and the majority shared fragment ions since all the compounds were structural isomers. In this case, unambiguous identification of the compound present in the sample was not possible using only the fragmentation patterns reported in the HighResNPS database. Therefore, to confirm the compound present in the sample a direct comparison between the sample 11M replicate 1 and 5F-ADB reference standard was necessary.

The RT and the protonated parent ion of 5F-ADB reference standard resulting from the MS^E method were 11.86 min and 378.2191 m/z, respectively. The RT and protonated parent ion of the unknown compound were 11.86 min and 378.2206 m/z, respectively, in line with the one found for 5F-ADB reference standard. A discrepancy of 3.96 ppm was found between the two protonated parent ions. While the MS/MS SRM method was used to monitor the protonated ion 378.2206 m/z, to reveal its fragmentation pattern and compare it to the one of the reference standard 5F-ADB (Figure 4.7).

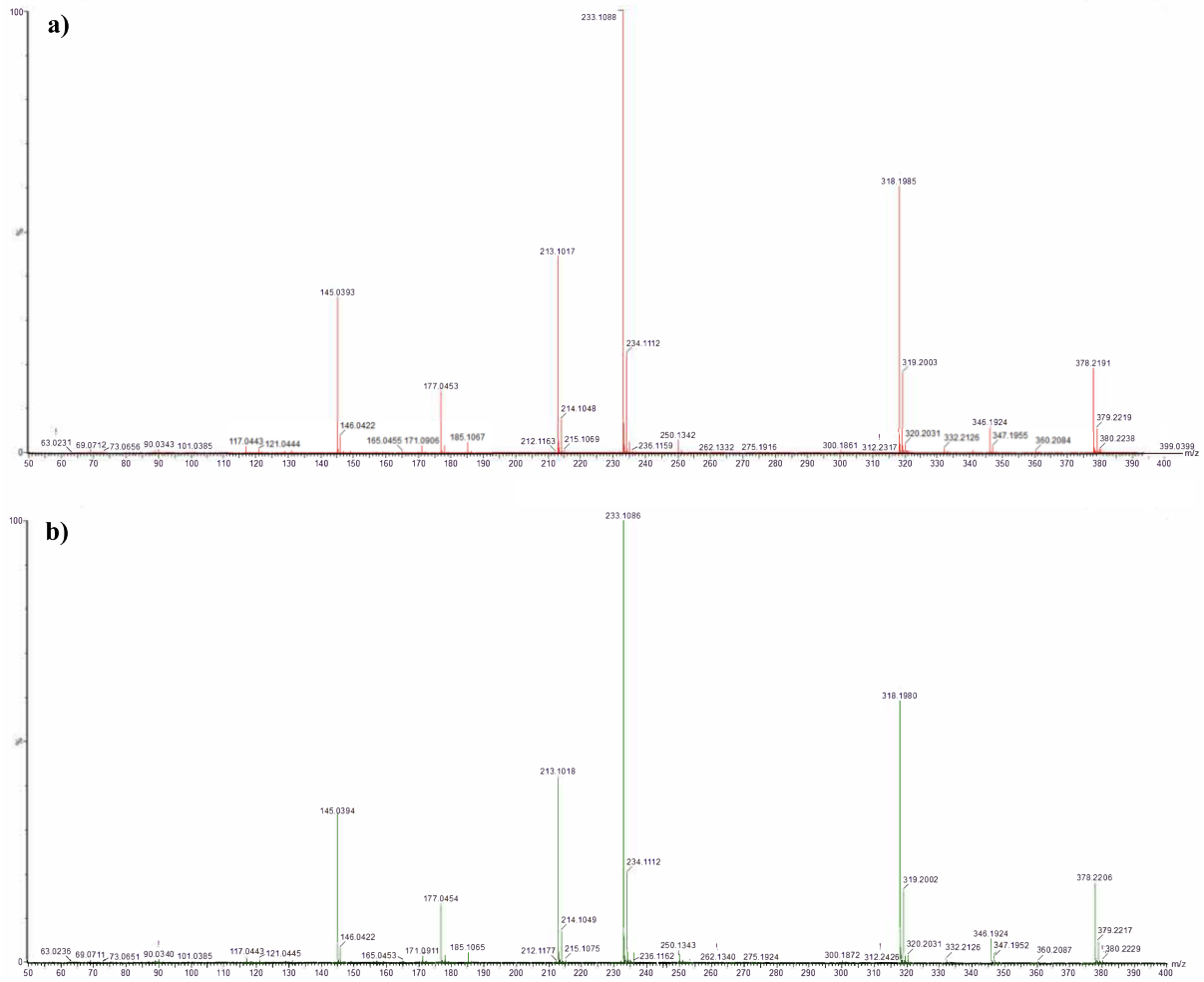

Figure 4.7. ESI MS/MS showing fragmentation patterns of a) 5F-ADB reference standard and b) sample 11M replicate 1.

The following fragment ions 233.1086, 318.1980, 213.1018, 145.0394, 177.0454 m/z belonged to the protonated ion 378.2206 m/z, while 233.1088, 318.1985, 213.1017, 145.0393, 177.0453 m/z belonged to the protonated ion 378.2191 m/z resulting from the analysis of the 5F-ADB

reference standard. Between all the fragment ions a discrepancy of less than 5 ppm was found, which was the criterion used for identification.

4.3.2.2. Quantification of psychoactive substances found on seized paper samples using Ultra-Performance Liquid Chromatography-Photodiode Array Detector-Quadrupole Dalton-Mass Spectrometry.

The synthetic cannabinoid 5F-ADB was detected on one of the A5 paper sheets part of the evidence bag UHSOP/2018/PR025 was quantified using the optimised and validated UPLC-PdA-QDa-MS method. The quantification of the sample's subunits was carried out using a calibration curve performed on the day of the analysis. The quantity of 5F-ADB found on each of the 39 x 1 cm^2 subunit after three consecutive extractions ranged between 0.1103-0.0005 mg/mL The quantity of 5F-ADB found on each of the subunits analysed was 0.016 ± 0.019 mg/mL showing a significant degree of variability of the concentration across the seized paper sampled. The quantification results are fully reported in Table 4.5.

Table 4.5. Quantification of 5F-ADB found in the 39 subunits of the seized prison sample analysed.

Sample's unit name	Concentration mg/mL	Concentration mg/cm^2
1A	0.0124	0.0062
1L	0.0394	0.020
2I	0.0162	0.0081
3C	0.0146	0.0073
3F	0.0184	0.0092
4K	0.0239	0.012
4O	0.0103	0.0051
5H	0.0161	0.0081
6B	0.0008	0.00041
6E	0.0018	0.00091
6M	0.0100	0.0050
7J	0.0216	0.011
7N	0.0199	0.0099
8D	0.0007	0.00037
8G	0.0012	0.00061
9A	0.0007	0.00035
9L	0.0116	0.0058
10I	0.0106	0.0053

11C	0.0005	0.00026
11F	0.0014	0.00068
12K	0.0170	0.0085
12O	0.0665	0.033
13E	0.0008	0.00038
13H	0.0191	0.0095
14B	0.0015	0.00073
14M	0.0205	0.010
15J	0.0206	0.010
15N	0.0176	0.0088
16D	0.0024	0.0012
16G	0.0202	0.010
17A	0.1103	0.055
17L	0.0147	0.0074
18I	0.0102	0.0051
19C	0.016	0.0080
19F	0.0089	0.0045
20K	0.0255	0.013
20O	0.013	0.0065
21E	0.0163	0.0081
21H	0.0119	0.0059

The concentrations of 5F-ADB found on the 39 subunits analysed were converted from mg/mL to mg/cm^2 to compare our findings to the one obtained by McKenzie and co-workers. The 5F-ADB concentration found on seized prison samples in our study ranged between 0.00026-0.055 mg/cm^2, while McKenzie and co-worker found concentration of synthetic cannabinoids (5F-MDMB-PICA; 4F-MDMB-BINACA; 5F-ADB; MDMB-4en-PINACA; AMB-FUBINACA; AMB-CHMICA) ranging between 0.05-1.17 mg/cm^2 [3]. The two ranges overlap at the lower end, and this could be due to the wider number of seized prison samples analysed (n=145) by McKenzie and co-workers. In this part of their study, McKenzie and co-workers quantified only two subunits which were taken in the two opposite corners of the samples with a 3 mm hole-puncher. However, they also performed a concentration mapping study which showed significant concentration variability across two seized paper samples [3]. Concentration ranged between 0.47-2.38 and 0.48-1.34 mg/cm^2 for samples one and two containing the synthetic

cannabinoids AMB-CHMICA and 5F-ADB, respectively. This data demonstrates high variability of the synthetic cannabinoid concentrations across seized paper samples since the process employed to prepare such samples by drug dealers is neither controlled nor consistent, hence do not ensure uniform distribution of the drug on paper. Moreover, the starting concentration of the synthetic cannabinoid employed to prepare such samples is not known and based on the findings of the quantification studies can be highly variable. In sample two, used for their mapping study, 5F-ADB was detected with the highest concentrations of *ca.* 1.3 mg/cm^2 in one corner of the paper and the middle of the opposite long side of the sample (Figure 4.8), which conflict with their hypothesis of the "paper having been soaked and then held at one corner to drip dry and then dried flat or held at one corner and dried hanging up" proposed by McKenzie and co-workers [3].

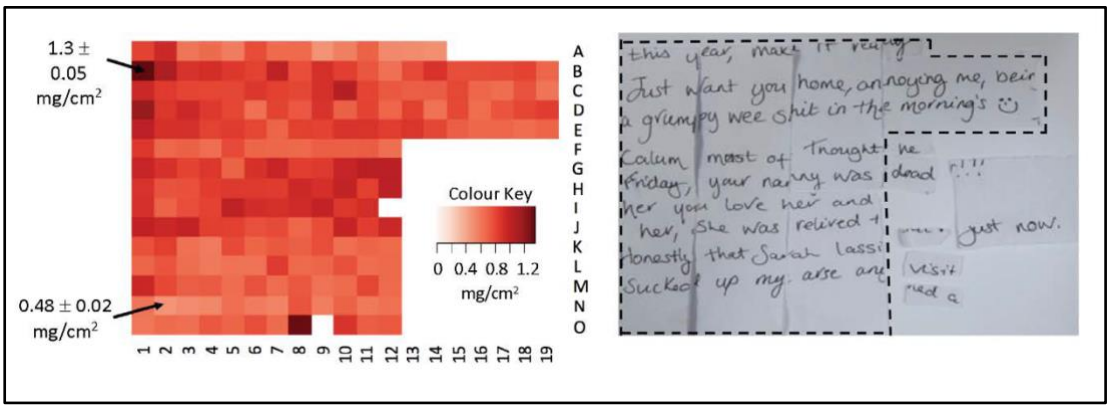

Figure 4.8. Heat-map resulting from GC-MS quantification of the seized paper sample performed by McKenzie and co-workers [3]

For the sample analysed in our study, a partial mapping of the concentration of 5F-ADB across the seized papers samples was carried out. The sampling strategy employed a statistical approach to gain knowledge on the concentration of the synthetic cannabinoid while considering budget and time constraints. A heat-map resulting from UPLC-PdA-QDa-MS quantification of the seized paper sample and showing the concentration of 5F-ADB over the 39 subunits quantitatively analysed is reported in Figure 4.9.

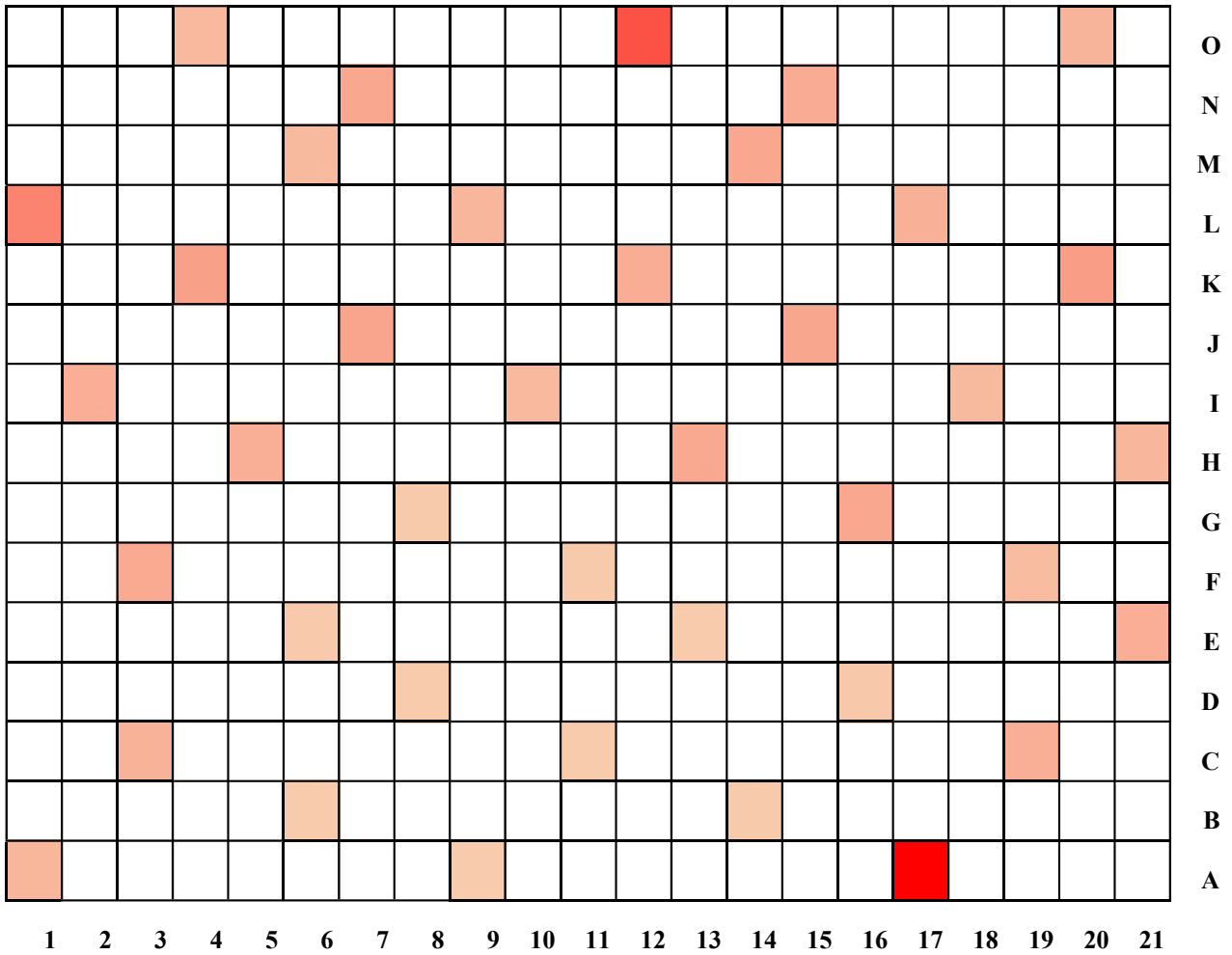

Figure 4.9. Heat-map resulting from UPLC-PdA-QDa-MS quantification of the seized paper sample, where the red subunit (17A) was the area with the highest concentration of 5F-ADB while the pale pink subunit (11C) was the area with the lowest one.

4.3.3. Simulated paper samples analysis

4.3.3.1. 5F-ADB percentage recovery study performed on paper type 1

The 5F-ADB percentage recovery was calculated at three different concentrations (C1 was 20 µL of 1 mg/mL, C2 was 50 µL of 0.1 mg/mL and C3 was of 10 µL 0.1 mg/mL solutions) over five simulated paper sample replicates for each of the concentration prepared using the paper type 1 (n=15). After three consecutive MeOH extraction the percentage quantity of 5F-ADB extracted was 98.4 ± 0.6%, 98.9 ± 0.6 %, and 98 ± 1% for C1, C2 and C3, respectively. Since the concentration of the 5F-ADB extracted after the 4th and 5th extraction was lower than the Limit of Quantification (LOQ) these values were excluded. This finding is in agreement with McKenzie and co-workers, who verified that three consecutive extractions were sufficient to extract synthetic cannabinoids. The full summary of results is reported in Table 4.6.

Table 4.6. Summary of the percentage recoveries evaluated at three concentrations over five consecutive extractions of simulated paper samples spiked with 5F-ADB.

Concentration 1 20 µL 1 mg/mL	**Simulated paper sample R1**	**Simulated paper sample R2**	**Simulated paper sample R3**	**Simulated paper sample R4**	**Simulated paper sample R5**
1st extraction %	85.8	84.7	81.3	83.4	82.4
2nd extraction %	10.9	13.4	15.9	15.1	16.1
3rd extraction %	1.01	0.211	0.875	0.407	0.582
4th extraction %	< LOQ	< LOQ	< LOQ	< LOQ	< LOQ
5th extraction %	< LOQ	< LOQ	< LOQ	< LOQ	< LOQ
Total %	97.7	98.3	98.1	98.9	99.1
Concentration 2 50 µL 0.1 mg/mL	**Simulated paper sample R1**	**Simulated paper sample R2**	**Simulated paper sample R3**	**Simulated paper sample R3**	**Simulated paper sample R5**
1st extraction %	84.3	77.7	87.3	82.9	81.2
2nd extraction %	13	19.7	10.7	14.1	15.7
3rd extraction %	1.87	1.64	1.52	1.08	1.76
4th extraction %	< LOQ	< LOQ	< LOQ	< LOQ	< LOQ
5th extraction %	< LOQ	< LOQ	< LOQ	< LOQ	< LOQ
Total %	99.2	99.1	99.6	98.1	98.6

Concentration 3 10 µL 0.1 mg/mL	**Simulated paper sample R1**	**Simulated paper sample R2**	**Simulated paper sample R3**	**Simulated paper sample R4**	**Simulated paper sample R5**
1st extraction %	90.1	86.5	85	83.1	87.4
2nd extraction %	8.40	11.6	11.3	13.1	8.89
3rd extraction %	0.742	0.757	1.82	1.10	0.785
4th extraction %	< LOQ	< LOQ	< LOQ	< LOQ	< LOQ
5th extraction %	< LOQ	< LOQ	< LOQ	< LOQ	< LOQ
Total %	99.3	98.9	98.2	97.3	97.1

The RSD of the 5F-ADB percentage recovery from fifteen simulated paper samples at three different concentrations is 0.78%, was in line with the ± 15% values of the "Guidance for the Validation of Analytical Methodology and Calibration of Equipment used for Testing of Illicit Drugs in Seized Materials and Biological Specimens" (UNODC).

The percentage recovery of 5F-ADB obtained as a result of the first extraction is 84.2 ± 3 %, which compared to the one achieved for Chapter 3 (74.7 ± 1.3%) show an increase of *ca.* 10%, highlighting a good improvement of the process. However, the percentage recovery of 5F-ADB obtained from the three consecutive extraction 98.7 ± 0.8%, is slightly lower than the one obtained by McKenzie and co-workers who extracted *ca.*100% of the synthetic cannabinoids. A reason for the discrepancy could be found in i) the use of a different extraction solvents and in ii) the addition of the IS. Since most of synthetic cannabinoids have solubility in solvents with low polarity e.g., isooctane as well as medium polar organic solvents e.g., in methanol, acetonitrile, acetone [95], the different solvents employed by McKenzie and co-workers might have played a role in enhancing the extraction of 5F-ADB from simulated paper samples. The addition of dichloromethane to methanol employed by McKenzie and co-workers reduced the polarity of the overall solvent mixture when compared to the pure methanol employed in our previous study. However, the main reason why dichloromethane was used was to solubilise the Internal Standard (IS) tridecane, which is not soluble in pure methanol [3]. An additional reason could be found in the addition of the IS, which aims also to correct for analyte loss during the extraction and quantification process. Therefore, to investigate the remaining percentage of the unextracted 5F-ADB amount our study should be repeated under the same conditions. It must be noted that in McKenzie's study the simulated paper samples (n=3) were spiked with 75 µL of a 1 mg/mL synthetic cannabinoids

solution [3], whilst in this study lower concentrations of the spiking solutions (C1 to C3) containing 5F-ADB were evaluated over a larger number of simulated paper samples (n=15).

4.3.3.2. Paper matrix effect evaluation

The five paper matrices evaluated in this study (type 1 common printing paper 80 g/m^2 density (Envirocopy), type 2 common printing paper 80 g/m^2 density (Evolution), type 3 paper from ruled notebook 80 g/m^2 density (Pukka Pad), type 4 weighted paper 120 g/m^2 density (Evolution), and type 5 black ink printed common printing paper 80 g/m^2 density (Envirocopy) employed to prepare the simulated paper samples spiked with 20 µL of a 1 mg/mL 5F-ADB reference standard solution did not lead to alteration of the ionisation efficiency of the target analyte quantified. The full summary of results is reported in Table 4.7.

Table 4.7. Summary of results of the five paper matrices evaluated in the paper matrix evaluation study.

Samples	Average AUC (AU)	Average concentration (ng/mL)	Average recovery (%)	RSD AUC (%)	RSD concentration (%)	RSD recovery (%)
Type 1 paper	115057	17446	81.5	2.2	2.3	2.5
Type 2 paper	113808	17218	80.4			
Type 3 paper	116676	17668	82.6			
Type 4 paper	118216	17928	83.8			
Type 5 paper	120807	17835	85.7			

The RSD between the AUC resulting from the analysis of the different types of paper matrices was 2.2%. While the RSD between the 5F-ADB concentration was 2.3%, and the RSD between the percentage recovery was 2.5%. it is important to note that the data collected are limited (n=1), as no replicates were evaluated for each type of paper used, and this study only intended to estimate the spread of the results to gain insight into the behaviour of different paper matrices. The low RSD calculated over the five types of paper, suggests that no matrix effect arises when quantifying these specific types of samples. No studies investigating different paper matrices are available in the literature, making this the first one to shed light on the impact of different paper matrices during the quantification of analytes extracts from paper. However, more replicates, and additional paper

matrices should be systematically evaluated in the future to ensure statistically valid conclusions are reached.

4.4. Conclusions

A UPLC-PdA-QToF-MS method, adapted from the literature [108], was employed to qualitatively screen a seized paper sample from prison. The sample was randomly selected from the same seizure (UHSOP/2018/PR025) employed in Chapter 3. The protonated ion 378.2006 m/z was found, by the UPLC-PdA-QToF-MS MS^E method, in the sample analysed. The accurate mass search was performed on the HighResNPS LC-HRMS database, leading to 9 candidates. The possible candidates were all positional isomers, and the complete fragmentation pattern for each of the candidates was not reported in the database. Hence, unambiguous identification of the substance using only the accurate mass and the fragmentation pattern was not possible. The MS/MS spectra of the 5F-ADB reference standard and the unknown analyte with the ionised mass of 378.2006 m/z were compared to each other. Comparison of the RT, parent ion and fragmentation pattern led to the identification of the 5F-ADB in the samples, which was already known to be in another A5 sheet present in the same evidence bag. Despite the fact a more sensitive analytical technique UPLC-PdA-QToF-MS compared to the UPLC-PdA-QDa-MS employed in Chapter 3, was used for the screening of the seized prison sample, no other analytes e.g., cocaine reported in the IMS slip, were identified.

A UPLC-PdA-QDa-MS method previously developed, optimised and used to quantify caffeine, cocaine and THJ-018 in Chapter 3 (Section 3.3.1.2.), was further optimised for 5F-ADB quantification and validated. The content of 5F-ADB found in the 39 subunits of the sample after three consecutive extractions ranged between 0.00026-0.055 mg/cm^2. While McKenzie and co-workers found higher synthetic cannabinoids concentrations ranging between 0.05-1.17 mg/cm^2, with a slight overlap between the two ranges detected [3]. These data demonstrate high variability of the synthetic cannabinoids concentration across seized paper samples, since the process employed for preparation is not controlled, consistent and the starting concentration of the synthetic cannabinoid employed to prepare such samples is not known and can be highly variable. High variability of synthetic cannabinoids concentration on these types of samples poses additional challenges to take into account working on new methods development of analytical techniques.

Furthermore, a percentage recovery study of the synthetic cannabinoid 5F-ADB on simulated paper samples was performed and the findings obtained were compared to our Chapter 3 study and to McKenzie and co-workers' study [95], The percentage recovery of 5F-ADB obtained after the first extraction in this study was 84.2 ± 3 %, showing an increase of *ca.* 10% from the one achieved in Chapter 3 (74.7 ± 1.3%) highlighting a good improvement of the process. While the percentage recovery of 5F-ADB obtained from the three consecutive extraction 98.7 ± 0.8% in this study, is slightly lower than the one obtained by McKenzie and co-workers who extracted *ca.*100% of the synthetic cannabinoids. A reason for the discrepancy could be found in i) the use of a different extraction solvents and in ii) the addition of the IS. Since most of synthetic cannabinoids have solubility in solvents with low polarity e.g., isooctane as well as medium polar organic solvents e.g., in methanol, acetonitrile, acetone [95], the different solvents employed by McKenzie and co-workers might have played a role in enhancing the extraction of 5F-ADB from simulated paper samples. The addition of dichloromethane to methanol employed by McKenzie and co-workers reduced the polarity of the overall solvent mixture when compared to the pure methanol employed in our previous study. However, the main reason why dichloromethane was used was to solubilise the Internal Standard (IS) tridecane, which is not soluble in pure methanol [3]. An additional reason could be found in the addition of the IS, which aims also to correct for analyte loss during the extraction and quantification process. Therefore, to investigate the remaining percentage of the unextracted 5F-ADB amount our study should be repeated under the same conditions. In agreement with McKenzie and co-workers finding, it can be concluded that three consecutive extractions were sufficient to extract synthetic cannabinoids from paper and should be employed to achieve accurate quantification. No studies investigating the impact of different paper matrices during quantification of analytes extracts from the paper were available in the literature, thus the last study of this Chapter aimed to estimate the spread of the results to gain insight. The low RSD calculated over the five types of paper evaluated, suggests that no matrix effect arises when quantifying 5F-ADB on these specific types of samples.

Once information on quantification values was gathered in this chapter and compared to the study of McKenzie and co-workers, in Chapter 5 the capabilities of Raman were evaluated on paper samples impregnated with psychoactive substances specifically the model synthetic cannabinoid 5F-PB-22, and related adulterant/cutting agents. It was paramount to ascertain the range of synthetic cannabinoids found on seized paper samples from prison, to work towards the future development of in-field detection approaches.

5. Use of Raman Renishaw InVia and Rigaku Progeny coupled with Chemometric for the Detection and Classification of Psychoactive Substance Impregnated on Papers

In Chapter 4, typical quantities of the synthetic cannabinoid 5F-ADB found on paper sample seized in prisons was determined using standard lab-based methods. In this Chapter, we focus on the evaluation of a technique with a high degree of molecular specificity, Raman Spectrometry. The capabilities of two Raman instruments, handheld and benchtop, in detecting psychoactive substances specifically the model synthetic cannabinoid 5F-PB-22, and related adulterant/cutting agents in simulated paper samples were evaluated. In Chapter 4 the content of 5F-ADB found in the 39 subunits of the sample analysed ranged between 0.00026-0.055 mg/cm^2. While McKenzie and co-workers found concentration of synthetic cannabinoids (5F-MDMB-PICA; 4F-MDMB-BINACA; 5F-ADB; MDMB-4en-PINACA; AMB-FUBINACA; AMB-CHMICA) ranging between 0.05-1.17 mg/cm^2. However, in the concentration mapping study, McKenzie and co-workers found a higher concentration of AMB-CHMICA across a seized paper sample, ranging between 0.47-2.38 mg/cm^2 [3]. These findings informed us of the synthetic cannabinoid 5F-PB-22 concentrations to employ in our study to prepare simulated paper samples, which ranged between 0.25-1 mg/cm^2.

5.1. Introduction

A range of analytical approaches was found to be used in the detection of psychoactive substances in prison samples (see Chapter 1). The only in-field instrument employed, documented in the literature review was ion mobility spectrometry (IMS) [3,29]. The IMS offer the advantage of rapid in-field screening of samples. However, IMS can sometimes lead to misidentification or false negatives, due to the K_0 values variability between different instruments [3], it also has difficulty in detecting more than one analyte in a mixture [29]. Other in-field approaches which have never been investigated before for the screening and rapid identification of paper impregnated with psychoactive substances are vibrational spectroscopic techniques, such as IR (Infra-Red) and Raman [30].

Raman spectroscopy is a technique that uses inelastic scattering effects of the interaction between a monochromatic radiation of a laser source of and the molecular vibration of a samples analysed, resulting in the scattering of the photons in all direction. Only one photon

out of 10^6 is scattered with a difference between the frequency of the incident radiation and the scattered radiation, with an exchange of energy between the photon and the molecule resulting in spectral fingerprint which enable the identification of molecules based on their peak positions (Raman shifts) and shape [112,113]. Raman spectroscopy has shown to be beneficial where rapid, non-destructive, non-invasive identification of psychoactive substances is required. Therefore, based on the previous studies showing successful identification of psychoactive substances and their mixtures in the solid form [100], the use of Raman to detect psychoactive substances on paper samples could be advantageous to detect drugs detection in prison.

Despite Raman spectroscopy has been shown to successfully identify psychoactive substances due to variation issues such as i) instrument artefacts such as noise (Charge-Couples Device (CCD) noise, background noise, etc.), instrument or room temperature, and laser power fluctuations; ii) analysis effects such as different opacity of the analysed sample, interference from the sample holder, variations in the focal distance; iii) sample effects such as the vibrational frequency of scattering molecules, the number of scattering groups, presence of fluorescing species; and iv) environmental effects (e.g., ambient light, cosmic rays, etc.) Raman spectral analysis is often coupled with chemometrics [112,113].

Chemometrics is defined by the International Chemometrics Society as "the science of relating measurement made on a chemical system or process to the state of the system via application of mathematical or statistical methods" [114]. Chemometrics techniques extract useful information, removing noise interferences and meaningless data in order to show patterns from large data sets e.g., spectroscopic data [115]. One of the most common chemometric approaches applied to Raman spectral data is Multivariate Data Analysis (MVA) where data are usually pre-processed before these applications. Pre-processing enables the maximum extraction of meaningful Raman data from both noise and fluorescence interference, hence, enabling the identification of target drugs in complex matrices or mixtures. Principal Component Analysis (PCA) is one of the most common MVA techniques employed to highlight patterns from large data sets [115–117]. PCA reduces the dimensionality of a wide data set, retaining the most relevant information related to the variance in Raman data [117]. This is possible by reducing the data matrix into discrete Principal Components (PC), where each PC explains a percentage of the total amount of variance contained in the original data set, with the first PC explaining the largest proportion of the variance [118]. PCA has been successfully applied in the analysis and

classification of illicit drugs mixtures [116,119–126]. Raman spectroscopy's key advantage is achieving discriminatory information for similar compounds and mixtures, which other in-field analysis techniques lack e.g., Ion Mobility Spectroscopy (IMS). However, for paper samples, there is a concentration issue as Raman is not a very sensitive technique. Therefore, the use of Raman coupled with PCA may assist to accentuate classification for these challenging samples on paper.

In this Chapter, we will refer to psychoactive substances as substances that when taken or administered, affect mental processes such as perception, consciousness, cognition, mood and emotions [127] including traditional drugs of abuse and NPS. This is a comprehensive systematic study to evaluate the different Raman instruments' capabilities and limitations when coupled with PCA in identifying psychoactive substances, cutting agents/adulterants and their mixtures on paper, and simulating prison samples. The objectives are to evaluate i) spectral pre-processing protocols ii) the capabilities of two Raman instruments 785 nm (benchtop) and 1064 nm (handheld) in detecting psychoactive substances iii) the impact of the sample preparation method on identifying impregnated psychoactive substances and mixtures using Raman spectroscopy coupled with chemometrics, and iv) the RMA capabilities in the identification of binary mixture components in simulated paper samples. The overall aim of the study was to determine if Raman instruments coupled with PCA could help identify psychoactive substances and/or cutting agents/adulterants of interest used in this study, i.e., 5F-PB-22, amphetamine, benzocaine, caffeine, cocaine, diazepam and paracetamol soaked or pipetted on paper samples.

5.2. Material and methods

5.2.1. Chemicals and reagents

Benzocaine, caffeine, cocaine hydrochloride, d-amphetamine sulphate, diazepam, and paracetamol certified reference standards in neat form (≥ 99% purity), acetone (Ace), ethanol (EtOH), and methanol (MeOH) (> 99.5% purity) were obtained from Sigma-Aldrich (Missouri, United States). The synthetic cannabinoid 5F-PB-22 reference standard (> 99% purity) was obtained from CHIRON. While 5F-PB-22 product (P) (UHSOP/2016/P071 ~92% purity) was purified (UHSOP/2020/P003, > 99% purity) and used for the preparation of the simulated paper sample. The confirmation of the structure and the purity of the 5F-PB-22 product were evaluated using Nuclear Magnetic Resonance (NMR) and High-Performance Liquid Chromatography- Ultraviolet-Visible (HPLC-UV-Vis), respectively. The data obtained were directly compared to the 5F-PB-22 certified reference standard (Chiron AS, Norway). A common A4 printing 80 g/m^2 density paper sheet (Envirocopy A4 500 sheet; ECF; 100% Recyclable paper; ISO 9706 Long Life paper) was employed to cut 83 one cm^2 pieces of paper to prepare the simulated paper samples and for the negative control also known as blank paper (BP).

5.2.2. Instrumentation

5.2.2.1. Nuclear Magnetic Resonance

For instrument and parameters employed see Chapter 3 Section 3.2.2.5**.**

5.2.2.2. High-Performance Liquid Chromatography-Ultraviolet-Visible

An Agilent 1260 Infinity series High-Performance Liquid Chromatography (HPLC) coupled with an Agilent 1200 Infinity Ultraviolet-Visible (UV-Vis) detector (Santa Clara, CA, USA), running under OpenLab software, was employed to validate the HPLC-UV method to detect the 5F-PB-22 extracted from simulated paper samples using agar gel. A mobile phase of (A) acetonitrile and (B) Millipore Water (MW) (70:30) with a pH adjusted to 2.1 ± 0.1 by dropwise addition of orthophosphoric acid was employed. A flow rate of 1.50 mL/min and sample volume of 20 µl were employed with an ACE UltraCore C_{18} 150 x 4.6 mm x 5 µm particle size (Aberdeen, Scotland) and an Agilent pursuit metaguard C_{18} 4.6 mm internal diameter x 5 µm particle size (Santa Clara, CA, USA) for a total run time of four minutes with a temperature of

analysis of 25 °C. A 226 nm wavelength was employed. The HPLC-UV-Vis method was validated for 5F-PB-22 in line with the International Conference of Harmonization (ICH) [97–99] for the following parameters: system suitability; linearity and range; limit of detection (LOD) and limit of quantification (LOQ), precision and accuracy.

5.2.2.3. Raman spectroscopy

The two Raman instruments InVia™ (Renishaw, UK) and Progeny™ (Rigaku, USA) were evaluated for the analysis of the samples. Specifications of the instruments are described in Table 5.1.

Table 5.1. Summary of the specification of the two Raman instruments evaluated.

Raman Instrument specifications	Renishaw InVia ™ (Benchtop)	Rigaku Progeny ™ (Handheld)
Instrument Image		
Laser type	High Power NIR Diode	Nd:YAG (neodymium-doped yttrium aluminium garnet)
Laser wavelength (λ)	785 nm	1064 nm
Laser output power	300 mW at the source 170 mW at sample	30-490 mW at the source
Laser spot diameter	1.20 µm	20 µm
Spectral resolution	0.3 cm^{-1}	8-11 cm^{-1}
Spectral range	5-3300 cm^{-1}	200-2500 cm^{-1}
Numerical aperture	0.4	0.25
Grating	transmission volume phase (VPG) 1200 lines/mm	transmission volume phase (VPG) 818 lines/mm
Detector	TE Cooled CCD 576 × 384 pixels	TE Cooled InGaAs 512 pixel
Exposure time	Adjustable	Adjustable 5ms to 30 sec.
Calibration standard	Silicone	Benzonitrile
Library	N/A	Standard library (12290) and user library
Operational and analysis software	Wi.RE	RRT Progeny software version 0.001-26 140521
Data analysis	Grams, Unscrambler X	Grams, Unscrambler X
Data export format	.Wxd, .spc and .txt	PDF, .xml and .txt
Algorithms	N/A	WCC and Rigaku mixtures

Operating temperature	-70 ºC	-20/+50 ºC
Battery	electricity plug	Switchable Li-ion battery (4-5 hours)
Others	x10 x20 x50 and x100 objective lenses	Adjustable nozzle

*Instrument images were reproduced with courtesy of SciMed, Rigaku, USA, and Renishaw, UK.

The benchtop Renishaw InVia ^{TM} Raman was set up with the following parameters: ten seconds exposure time, one accumulation and a laser power output of 50% (85 mW at the sample). However, for strong Raman scatter psychoactive substances such as benzocaine and diazepam the laser power output was reduced to 10% to avoid saturation of the detector. A 20x objective lens (spot radius 1.2 µm) was used, and any cosmic rays were removed automatically by the instrument. The calibration of the instrument was carried out on a static scan, at the beginning of each day, before starting analysis and after every time the instrument was switched off. The calibration Reference standard always matched to silicone, identifiable by its characteristic sharp peak at 520 ± 0.6 cm^{-1}. Spectra were acquired over a range of 100-3200 cm^{-1}. Three replicate measurements (R1 to R3) were taken in different spots for the single reference standard, the binary mixtures and the simulated paper samples.

The handheld Raman Rigaku Progeny^{TM} was set up using a developed and validated method [125], with the following parameters: exposure time of 2000 ms, ten averages, and a laser power output of 490 mW. However, for strong Raman scatterers, such as benzocaine and diazepam the laser power output had to be reduced to 185 mW to avoid saturation of the detector. The spectral baseline correction was applied, and the dark background was subtracted automatically by the instrument. The performance verification of the instrument was carried out at the beginning of the day, before starting analysing the substances and every time the instrument was switched on. The calibration reference standard always matched to benzonitrile with a Wavelet Correlation Coefficient (WCC) ≥ 0.99. Spectra were acquired over a range of 141-2470 cm^{-1}. Three replicate measurements were taken in different spots for the single reference standard, the binary mixtures, and the simulated paper samples. Moreover, the Raman Rigaku Progeny has two in-build algorithms aimed at enhancing rapid in-field identification of the unknown substance. The Wavelet Correlation Coefficient (WCC) algorithm is used to match pure substances to reference standard spectra. The WCC involves two pre-processing steps where interference from Raman spectral background and noise are reduced while the Raman signal is enhanced. These transformations improve the classification by identification of 'wavelet coefficients' representing specific Raman peaks, with high activity in unknown samples [128,129]. While the 'Rigaku Mixtures Algorithm' (RMA) is a proprietary algorithm, and its method of computation is not fully disclosed. The RMA identifies individual substances in a mixture, assigning a high weight to the spectral contribution rather than the relative amount of each constituent [128]. These algorithms, WCC and RMA also calculate the correlation

between an unknown and substances that are present in the spectral library. The closer the value to 1.00, the higher the correlation with the library reference spectra. The RMA has been evaluated in this study for the identification of binary neat reference standard mixtures and simulated paper samples impregnated with reference standard.

In both cases, the raw spectral data were exported as a text file format (.txt) and then saved on a Microsoft Excel spreadsheet. The raw data were then imported to the Unscrambler X 10.5.1 (Camo, Norway).

5.2.2.3.1. Raman activity ranking

To rank the Raman activity of the seven reference standards, a unified method using Raman Rigaku Progeny™ was employed. A method with a constant laser power output of 185 mW was used, to avoid saturation of the detector for high Raman scattering substances, while all the other parameters remained the same as above. Three replicate measurements were recorded for each substance in different spots without varying the focal distance of the laser from the sample. The measurements were all taken under the same condition on the same day. Spectral data were exported as text files format (.txt), saved on a Microsoft Excel spreadsheet, truncated in the fingerprint region (250-1750 cm^{-1}), the three replicates were averaged, the spectra were plotted, and the absolute intensity values were noted.

5.2.3. Sample preparation and analysis

Prior to analysis, all glassware, spatulae and tweezers were carefully washed and rinsed first with Deionised Water (DW) and then with pure MeOH In addition, working surfaces were cleaned with pure MeOH. Samples were analysed in their pure forms (powders), simulated binary mixtures and simulated paper samples of pure and mixtures solution employing two preparation methods.

5.2.3.1. 5F-PB-22 product purification

The recrystallisation of the 5F-PB-22 P. UHSOP/2016/P071 was performed using the protocol described by Hardwood and Moody [130]. Initially, a solubility test was carried out to select the appropriate solvent Around 1 mg of a yellowish powder of 5F-PB-22 P. was placed in a vial and a few drops of cold EtOAc were added. EtOAc was chosen as i) it is easily removed from the solution through evaporation, ii) it has a melting point lower than the melting point of the

5F-PB-22, and iii) 5F-PB-22 was highly soluble in the hot solvent and insoluble when cold. The steps of the recrystallisation process are summarised in Figure 5.1.

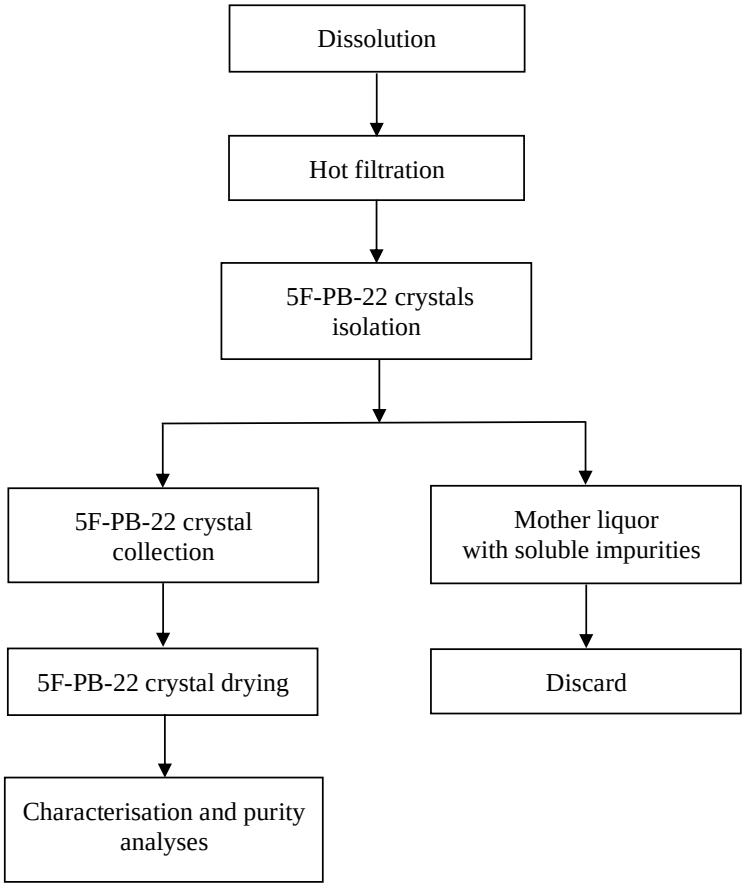

Figure 5.1. Flowchart of 5F-PB-22 product purification.

For the dissolution step, 1.9 g of 5F-PB-22 P was weighed and slowly added to the boiling EtOAc (B.P. 77.1 °C), swirling the flask after each addition. This was performed until the 5F-PB-22 was completely dissolved in the minimum quantity of hot EtOAc possible, to minimise the amount of material loss by retention in the chilled solvent. The hot filtration was carried out, to remove possible insoluble impurities present. Then the flask was covered with a watch glass and was left untouched until it cooled to room temperature for ~1 hour. Once the crystals had formed, the solution was placed in an ice bath for ~30 minutes to maximise the amounts of crystals obtained. The 5F-PB-22 P crystals were then isolated by scratching from the bottom of the flask using a spatula and placed in a Büchner funnel containing a 70 mm filter paper (Whatman, UK) to promote their recovery. The crystals were rinsed with a small amount of fresh, cold EtOAc to remove impurities. The crystals were pressed onto the filter and the air

was drawn through the Büchner funnel for 5 min. The crystals from the first crop, with a whitish crystalline powder appearance, were placed into a big vial in an electrically heated desiccator for *ca.* 3-4 hours. The filtered mother liquor was discarded. The purity of the 5F-PB-22 product UHSOP/2020/P003 was assessed after the recrystallisation using HPLC-UV.

5.2.3.2. Reference standards sample preparation and analysis (Raman Rigaku Progeny ™)

A square piece (2 x 2 cm) was cut from an aluminium plate (Thermo-Fisher, UK) and labelled on the bottom with the name or the UH code of the uncontrolled and controlled substance, respectively. Approximately 5 mg of the substance was weighed directly on the aluminium sample holder, placed on the working bench and with the help of a micro spatula, the powder was flattened. For the 21 binary mixtures (5F-PB-22/amphetamine; 5F-PB-22/ benzocaine; 5F-PB-22/caffeine; 5F-PB-22/cocaine; 5F-PB-22/diazepam, 5F-PB-22/paracetamol; amphetamine/benzocaine; amphetamine/caffeine; amphetamine/cocaine; amphetamine/diazepam; amphetamine/paracetamol; benzocaine/caffeine; benzocaine/cocaine; benzocaine/diazepam; benzocaine/paracetamol; caffeine /cocaine; caffeine/diazepam; caffeine/paracetamol; cocaine/diazepam; cocaine/paracetamol and diazepam/paracetamol) approximately 2.5 mg of each substance were weighed on a separate sample holder and then ground together in a quartz micro mortar and pestle, to homogenise the mixture. A micro-cover glass was laid on top of the sample holder and some tape was placed around it, without covering the sample (Figure 5.2). The sample was then taped to the instrument's nozzle, covered with blackout material and the analysis was performed. The position of the nozzle was changed between replicate analysis.

Figure 5.2.Picture of a sample holder used to analyse reference standard with Raman Rigaku Progeny ™.

5.2.3.3. Reference standards sample preparation and analysis (Renishaw InVia ™)

The sample prepared for Raman Rigaku Progeny™ (Section 5.2.3.2.) was cut around the edges and the glass removed, with the help of a scalpel. The reference standard powders were all white/off-white, which suggests no fluorescence should arise from them. These were re-compacted and flattened on the sample holder with a spatula. The sample holder was placed on a glass microscope slide on the microscope stage of the instrument, which was moved in the x, y and z positions, then, the focal distance was re-adjusted between analyses. The position of the microscope stage was moved between replicate analysis. At the end of the analysis, the micro-cover glass was laid on top of the sample again and stored back in the controlled drugs safe or discarded in the solid chemical waste, for controlled and uncontrolled substances, respectively.

5.2.3.4. Preparation of simulated paper samples and analysis

A total of 83 x 1 cm^2 pieces of paper were prepared by cutting common A4 printing paper using the manual tile cutter to obtain paper strips of 1 x 29.7 cm, then 1 cm^2 clear plastic stencil and scissors were used to cut the strips in 1 cm^2 square. Solutions of 5F-PB-22, amphetamine, benzocaine, caffeine, cocaine, diazepam and paracetamol at different concentrations (Table 5.2) were prepared in either ethanol (EtOH) or acetone (Ace) depending upon the solubility of the compounds. The highest concentration achievable for each solution was used to prepare the simulated paper samples. Subsequently, lower concentrations of each solution were iteratively applied to paper and spectra were obtained until a concentration was identified for each substance where the characteristic peaks related to reference standards were not observed.

Table 5.2. Sample concentration range evaluated for the two methods.

Reference standards	Highest to lowest concentration (mg/mL)				
5F-PB-22	20	15	10	7.5	5
Amphetamine	30	15	12.5	10	7.5
Benzocaine	10	6.5	5	3.5	2.5
Caffeine	15	10	8	6.5	5
Cocaine	60	40	35	30	20
Diazepam	30	20	15	10	5
Paracetamol	60	40	30	20	15

Solutions were prepared by dissolving a known quantity of the reference standard in the relevant solvent and then preparing the different concentrations using a serial dilution. Sample preparation was carried out following two different methods: "pipetting" and "soaking". The "pipetting method" involved carefully holding a 1 cm^2 piece of paper flat from a corner with a tweezer, which was placed between a clamp. Then 50 µL of the solution was pipetted, and the piece of paper was left to dry. In contrast, the "soaking method" involved laying flat a 1 cm^2 paper piece in 1 mL of solution for approximately 30 seconds. The 1 cm^2 infused piece of paper was carefully removed from the solution held in a corner by a pair of tweezers, taking care to keep it flat. The tweezer was then placed between a clamp to allow the piece of paper to dry while being suspended flat. It was important to keep the piece of paper suspended flat during the drying procedure to obtain a more homogeneous and less variable distribution of the reference standard onto the paper surface and to minimise loss of reference standard by contact with surfaces. Both procedures were repeated for each of the seven substances at five different concentrations, making a total of 70 simulated paper samples, plus one blank paper sample as the negative control. Triplicate spectra of the simulated and blank paper samples were collected using both Raman instruments.

After evaluating both instruments' capabilities to analyse simulated paper samples impregnated with a single psychoactive substances, samples impregnated with six binary mixtures (5F-PB-22/amphetamine; 5F-PB-22/ benzocaine; 5F-PB-22/caffeine; 5F-PB-22/cocaine; 5F-PB-22/diazepam, 5F-PB-22/paracetamol) were evaluated, using both "pipetting" and "soaking" methods. Binary mixture solutions were made by combining the synthetic cannabinoid 5F-PB-22 with the other six psychoactive substances and cutting agents/adulterant reference standards e.g., amphetamine, benzocaine, caffeine, cocaine, diazepam, and paracetamol . These were prepared by weighing around 40 mg of the two substances separately to give a final concentration of 20 mg/mL each in either Ace or MeOH

depending upon the solubility of the reference standards. The binary mixtures were analysed in triplicate using both Raman instruments.

The analysis of simulated paper samples was carried out with the Raman Renishaw and Rigaku accordingly to the description in Sections 5.2.3.2. and 5.2.3.3., respectively.

5.2.4. Chemometrics

5.2.4.1. Treatment of the Raman spectra

In this study, the stepwise process employed to treat the Raman spectra is summarised in Figure 5.3.

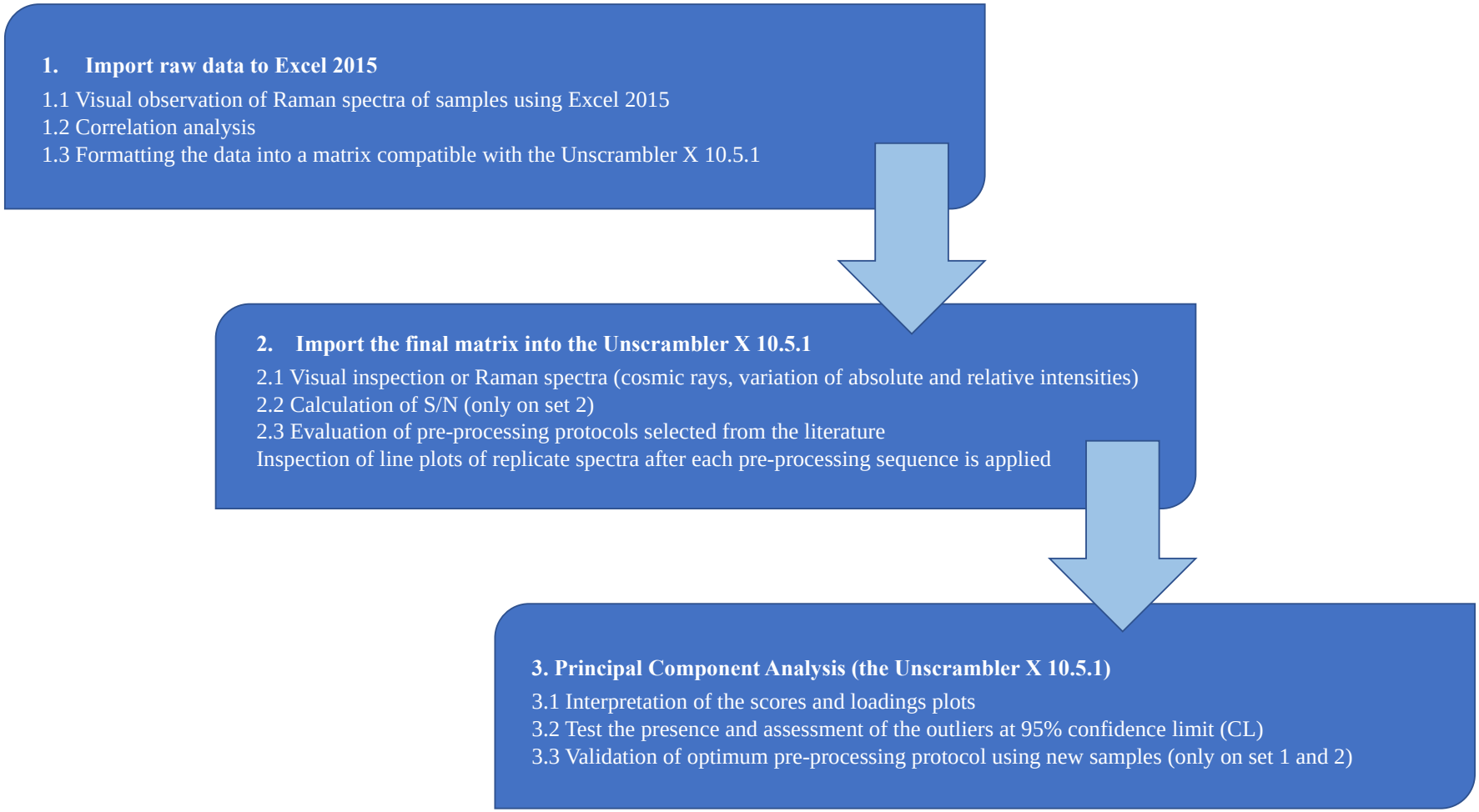

Figure 5.3. Flow chart outlining the stepwise treatment of Raman spectra. Figure adapted from Guirguis, 2017 [125].

5.2.4.2. Datasets

Table 5.3 summarises the data sets employed for the application of pre-processing protocols and performance of the PCA. In all cases samples were analysed using both Raman Renishaw InVia™ (odd data set numbering) and Raman Rigaku Progeny ™ (even data set numbering). The full labelling approach for each dataset is presented in Appendix 4.1 (Tables A1 to A5).

Table 5.3. Summary of the data sets employed in the study.

Data set	Experiment	Samples type
1	Calibration	7 reference standards (RS) + Blank paper (BP)
3	Validation	7 RS + BP
5	Classification	21 mixtures of the 7 RS
7	Classification	21 mixtures of the 7 RS + 7 RS + BP
9	Classification	7 RS pipetted on paper at 5 concentrations + 7 RS + BP
11	Classification	7 RS soaked on paper at 5 concentrations + 7 RS + BP
13	Classification	7 RS soaked and pipetted on paper at 5 concentrations + 7 RS + BP
15	Classification	5F-BP-22 + its mixtures with 6 RS pipetted on paper + BP
17	Classification	5F-BP-22 + its mixtures with 6 RS soaked on paper + BP

5.2.4.3. Pre-processing protocols

'The Unscrambler X' 10.5.1 (CAMO PROCESS AS, Oslo, Norway) software, was used to perform pre-processing of the data sets. Eight pre-processing protocols applied on Raman spectral data related to either psychoactive substances and/or adulterants/cutting agents were identified from the literature (Table 5.4). The pre-processing protocols were evaluated using the calibration data set 1 (Table 5.3).

Table 5.4. Summary of pre-processing protocols selected from the literature.

Pre-processing protocols	References
1) Spectral data truncation (450-1100 cm^{-1}) → Multiplicative Scatter Correction (MSC)	121
2) Savitzky-Golay 1st derivative, seven-point averaging → Maximum normalisation	131
3) Savitzky–Golay smoothing, 15-point smoothing window and a 2nd order deconvolution → Standard Normal Variate (SNV)	132

4) Spectral data truncation (750-1900 cm^{-1}) → Savitzky–Golay 1st derivative, nine-point averaging	120
5) Spectra data truncation (200-1800 cm^{-1}) → Unit normalisation → Linear baseline correction	123
6) Baseline offset → Mean normalisation	125
7) Cosmic ray removal → Spectra truncation (250-1750 cm^{-1}) → Savitzky–Golay smoothing, 21 smoothing points and 4th order derivative → Baseline subtraction 2nd derivative → Zero negative points → Maximum normalisation	124
8) Spectral data truncation (250-1750 cm^{-1}) → Average replicates → Standard Normal Variate (SNV)	133

5.2.4.4. Principal component analysis

'The Unscrambler X' 10.5.1 (CAMO PROCESS AS, Oslo, Norway) software, was used to perform the PCA on the data sets. The Non-linear Iterative Partial Least Squares (NIPALS) algorithm, useful for large data sets and for matrices that might contain missing variables [134], was used to calculate the PCA. It is common for spectroscopic data to have missing variables, originating during data acquisition, or pre-processing. Imputation algorithms such as NIPALS can handle missing variables by predicting them. The model was created by mean centring the data which is calculated when a PCA is performed by subtracting the mean from the values of the variables. This method calculates deviations from the mean, thus, reducing the number of PCs in the data set. The number of maximum iterations for the NIPALS algorithm was set to 1000. When this method was run, the default maximum PCs of seven were used. The model was validated using full cross-validation (leave one out method), which is the best method to employ when an independent test set for validation cannot be obtained, and where all the variables are equally weighted at a value of one.

The PCA outcomes are represented by different plots including the explained variance, scores, loading, Hotelling T^2 influence and leverage plots. The PCA explained variance plot will reveal the number of components or factors in the model. The plot shows its fit (blue line) and predictive ability (red line), also known as the full cross-validated and the calibrated variance, respectively. In the explained variance plot (Figure 5.4), the model is said to be well explained

by the PCs, when the values between the full cross-validated (red) validated and calibrated (blue) variance lines are close to each other [135].

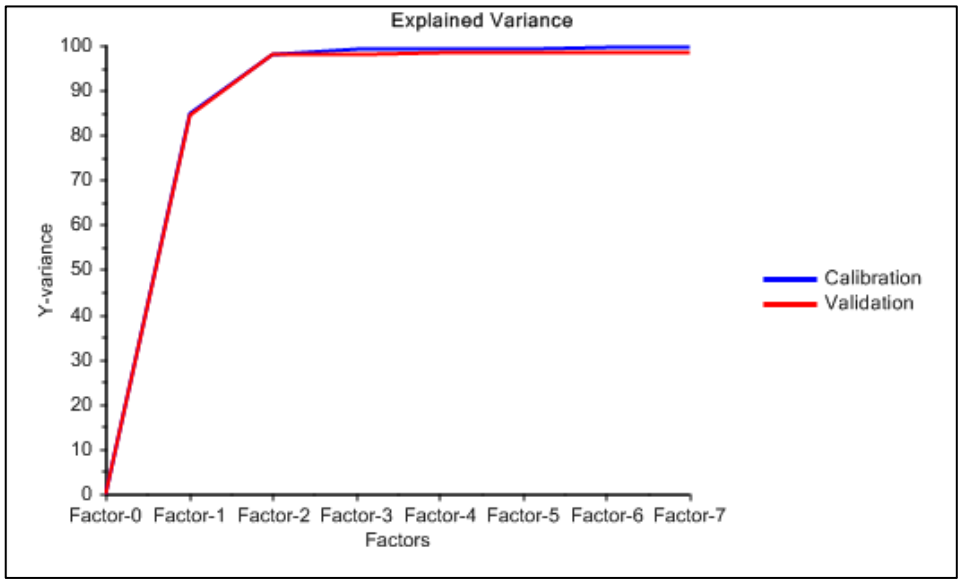

Figure 5.4. Explained variance plot showing the full cross-validated (red) vs calibrated (blue) variance lines close together, meaning the model is well explained by the PCs. Figure from The Unscrambler X user manual v10.3, CAMO 135.

The PC-1 vs PC-2 2D scores plot (Figure 5.5) describes the patterns of the analysed samples, showing their differences and similarities. Each sample has a score on each PC, these are also the coordinates of the sample on the plot. The score describes the main features of the sample related to the data point (variables) with high loadings on the same PC. Samples with a close score on the same PC are similar, while samples with different scores are dissimilar. The Hotelling T^2 ellipse in the scores plot (Figure 5.5) is a good way to detect outliers. This represents the samples within the critical statistical limit, which is by default set at the 95% Confidence Limit (CL). The samples that lie outside the ellipse are said to be statically different from the others inside the ellipse e.g., samples F and B in the top left quadrant. In addition, the scores plot also displays the total variation of each of the components explains expressed by the relative importance in parentheses next to the axis name (%) for each PC. If the sum of the explained variances for the 2 PC is large (for instance 60-80%), the plot shows a large portion of the information in the data, so the relationships can be interpreted with a high degree of certainty [135]. When such a large portion of the information in the data is explained by the first two PC it would be enough to consider only the two first PC when analysing the data.

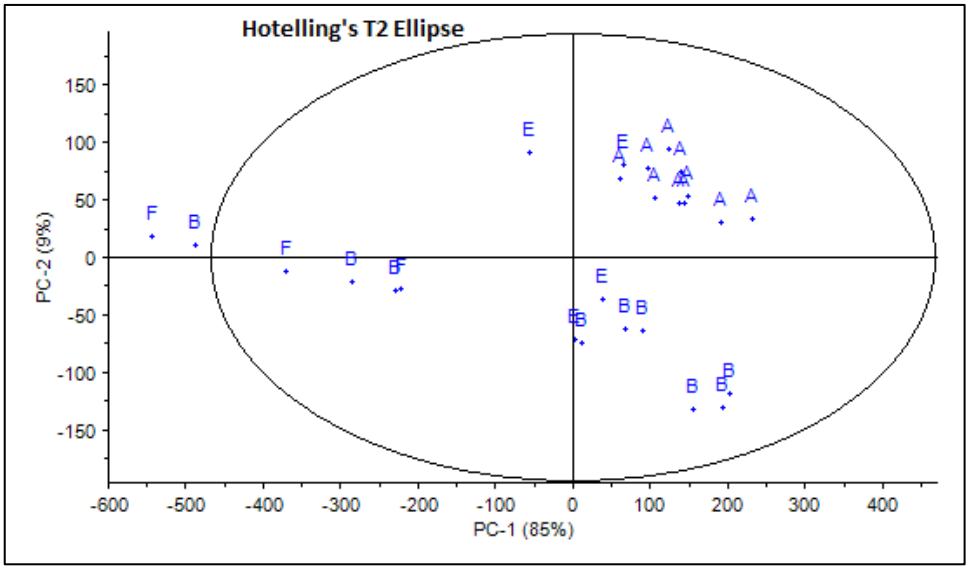

Figure 5.5. PC-1 vs PC-2 2D scores plot showing the differences and similarities between samples analysed. Figure from The Unscrambler X user manual v10.3, CAMO [135].

The loadings plot (Figure 5.6) cannot be interpreted without the scores plot and vice versa. The loadings plot looks at the data in terms of variable contributions and correlations. Each sample analysed has a loading on each PC, which explain how much the sample contributes to that PC, and how well the PC considers the variance contained in that sample. In other words, variables that are highly 'loaded' either in a positive or negative direction on the x-axis for a given PC are responsible for the greatest difference between the samples present in the dataset. The loadings can be plotted as PC-1 vs PC-2, which is more complicated to interpret, especially in the case of complex spectroscopic data. For spectral data e.g., Raman data it is common to plot the loadings as a line graph for each of the PC which highlights the important regions (Raman wavelengths or wavenumbers) that explain the variance for a specified PC.

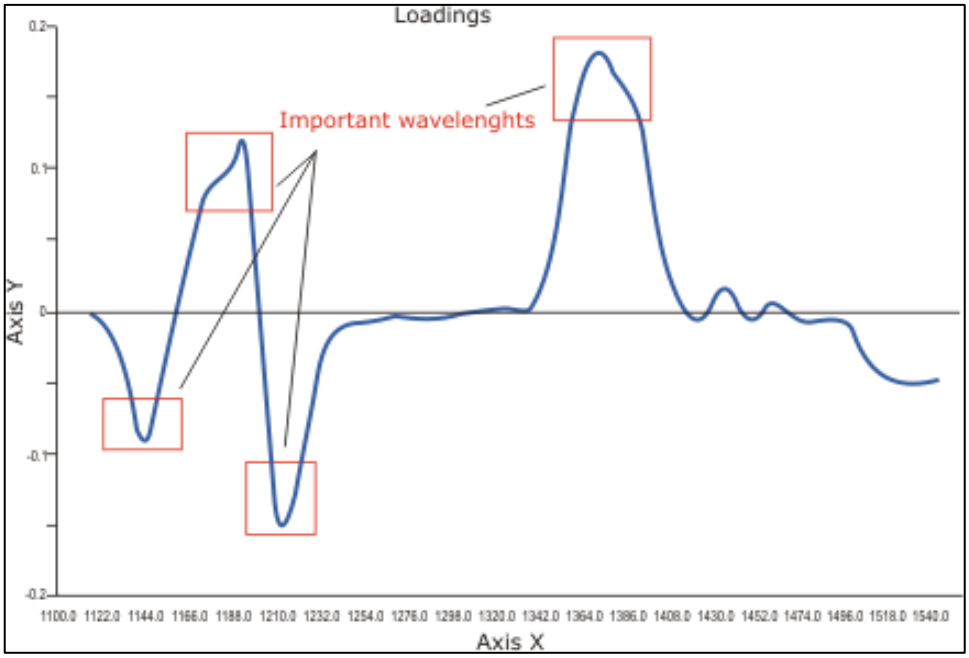

Figure 5.6. PC-1 loading plot highlighting important wavelengths explaining the variance in the region of the spectra being most different between samples. Figure from The Unscrambler X user manual v10.3, CAMO [135].

The influence plot explains the distance of the samples to the model centre as described by the PCs, against the statistical critical limits. Residual (y-axis) can be displayed as F or Q-residuals while leverage (x-axis) can be displayed as leverage per se or as Hotelling's T^2. The influence plot (Figure 5.7) explains whether the samples fit the model, influence the model, or could be potential outliers. Average samples (blue dots), which have low residuals and low leverage fit the model well. Samples in the bottom-right region (green dot) of the plot are extreme samples in the model and can potentially influence it, these have high leverage however fit the model well. Samples in the top-left (yellow dot) region of the plot are not extreme in the model and have low leverage however they do not fit the model well. Finally, samples in the top-right region (red dot) of the plot are extreme and do not fit the model well, having high leverage and high residuals, and as such are most likely outliers. In this Chapter the F-residuals vs Hotelling T^2 influence plot has been used.

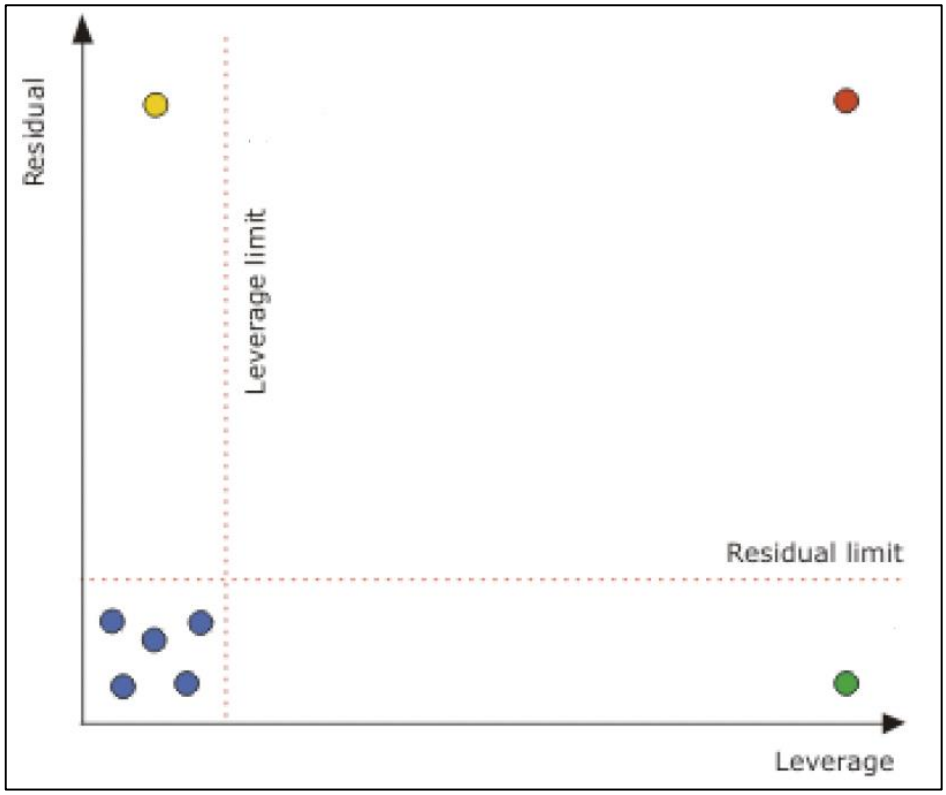

Figure 5.7. Influence plot, showing if samples fit the model, influence the model, or could be potential outliers. Figure from The Unscrambler X user manual v10.3, CAMO [135].

The Leverage plot (Figure 5.8) is useful to detect samples which are far from the centre within the space described by the model. Samples with high leverage are different from the average samples and could be outliers. High leverage also means high influence on the model. The leverage is based on an *ad-hoc* limit and varies from experiment to experiment.

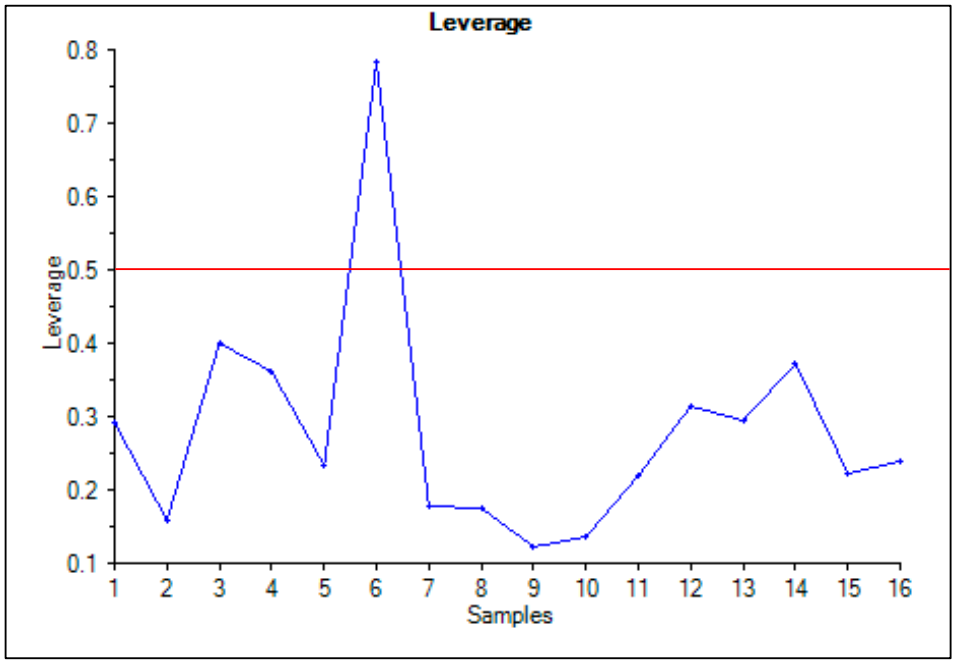

Figure 5.8. PC-1 leverage line plot, showing if samples leverage is above or below the critical limit (red line). Figure from The Unscrambler X user manual v10.3, CAMO [135].

Hotelling's T2 statistic plot (Figure 5.9) has a linear relationship to the leverage for a given sample. The difference between Leverage and Hotelling's T^2 is only a scaling factor. The critical limit for Leverage is based on an ad-hoc rule whereas Hotelling's T^2 critical limit is based on the assumption of a student-t distribution. This is used to identify outliers or detect situations where a process is operating outside normal conditions. In the plot below the limit for the PC-3 is 9.30, hence the sample circled in red, is above this limit (and likely to be an outlier).

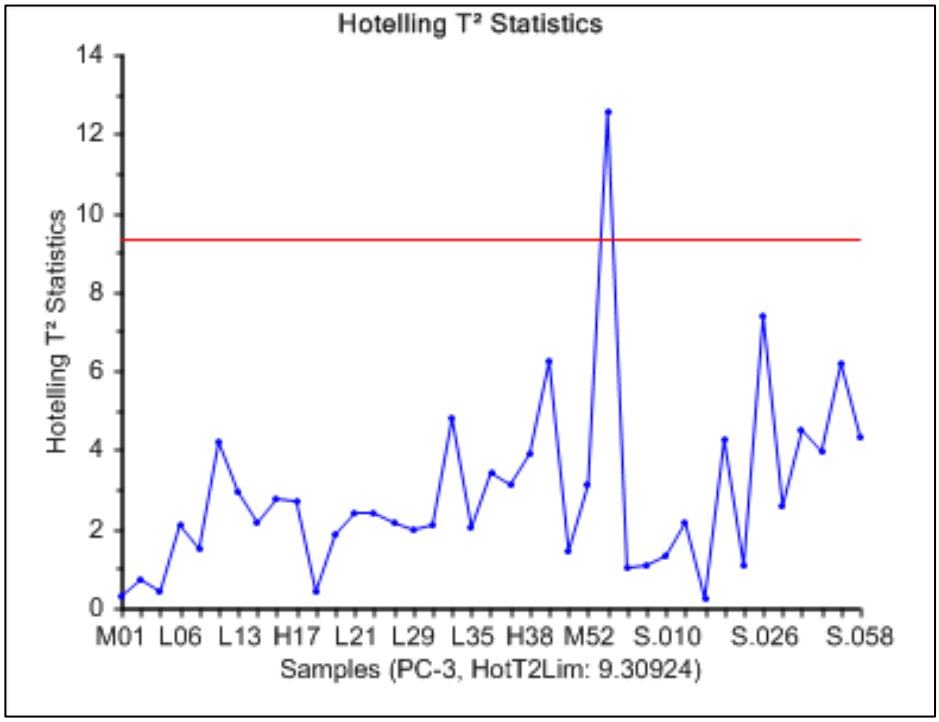

Figure 5.9. PC-1 Hotelling's T2 line plot, showing if samples are above or below the critical limit (red line). Figure from The Unscrambler X user manual v10.3, CAMO [135].

5.3. Results and discussion

5.3.1. Selection of psychoactive substances and adulterants/cutting agents

The psychoactive substances and adulterants/cutting agents (Section 5.2.1) were selected based on the findings from the literature review [5,29,81] and confidential information acquired during meetings with Her Majesty's Prison and Probation Service (HMPPS). Ford and Berg (2018) analysed five letters seized in English prisons and identified synthetic cannabinoids, novel stimulants and benzodiazepines mixed with traditional drugs of abuse such as cocaine and adulterants such as benzocaine and lignocaine [5]. From this chapter onward the model synthetic cannabinoid was changed to 5F-PB-22 due to NPS reference standards being expensive e.g., 10 mg of 5F-PB-22 reference standard cost around £150 vs 50 g at £150 "street sample". Typically, when a large amount of NPS is required for the work, they are either synthesised or purchased as "street samples" online to be then purified and characterised. In our case, the 5F-PB-22 "street sample" also known as product was readily available, therefore purified and employed in the study. This represents an additional challenge within this research field. Moreover, Metternich *et al.* identified the synthetic cannabinoids PB-22 infused in paper matrices, seized in prison [29]. Since the synthetic cannabinoid 5F-PB-22 was readily available and is the fluorinated analogue of the indole carboxylate PB-22, it was employed in this study. In contrast, Antonides *et al.* identified traces of controlled drugs on three paper samples cocaine, amphetamine and ketamine/ 2-fluorodeschloroketamine [81]. For these reasons, the following psychoactive substances were selected 5F-PB-22, amphetamine, cocaine and diazepam while the common adulterants/cutting agents used were benzocaine, caffeine, and paracetamol [100,101] (Figure 5.10).

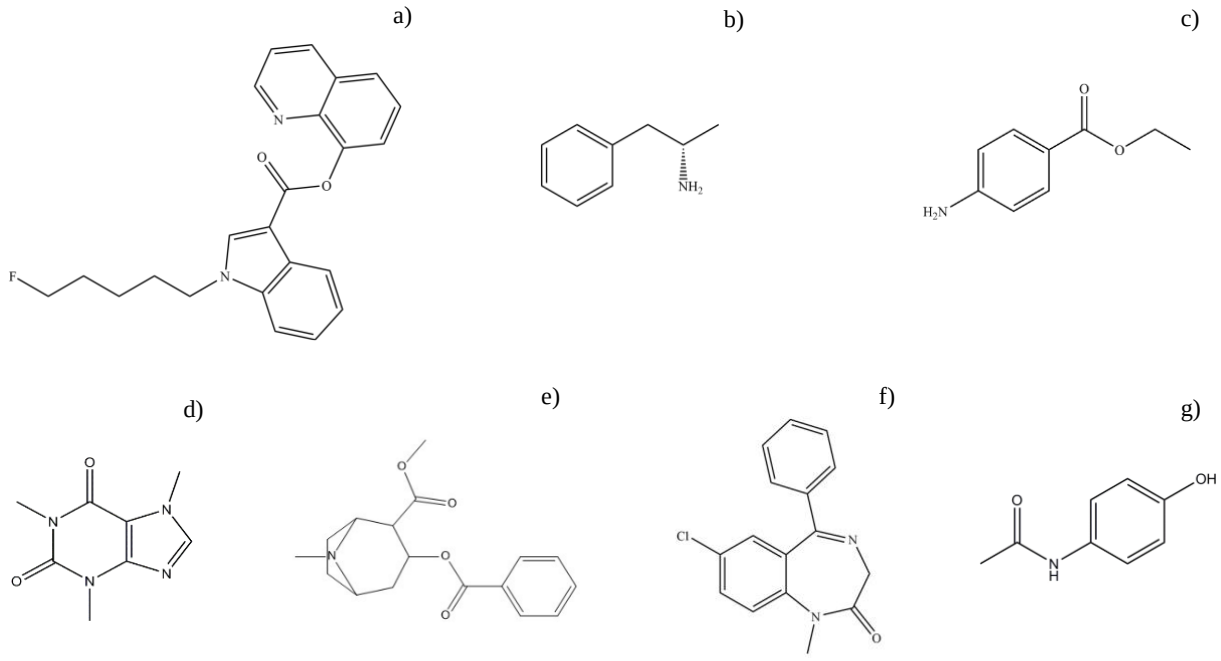

Figure 5.10. Chemical structures of a) 5F-PB-22 b) amphetamine c) benzocaine d) caffeine e) cocaine f) diazepam and g) paracetamol.

5.3.2. High-Performance Liquid Chromatography-Ultraviolet-Visible method optimisation and validation

The HPLC-UV-Vis method for the detection and quantification of 5F-PB-22 was adapted from a previous method developed by the University of Hertfordshire (UH) NPS research group for the detection of 5F-PB-22 reference standard [125].The experimental conditions, such as the mobile phases, the flow rate and the type of column were maintained the same. Whilst the Agilent pursuit metaguard was added to preserve the life of the column and the following injection volumes were evaluated 10 µl, 15 µl and 20 µl. The full description of the HPLC-UV-Vis method can be found in Chapter 5 Section 5.2.2.2. An example of the HPLC-UV-Vis chromatogram resulting from the analysis of 5F-PB-22 showing a retention time of 1.88 ± 0.05 is shown in Appendix 4.2- Figure A1. All the parameters evaluated for the HPLC-UV method validation of 5F-PB-22 were found to be within the acceptance criteria (Appendix 4.2- Table A1) as defined by the UH SOP for validation of LC methods, based on the International Conference of Harmonization (ICH) guidelines [97–99].

5.3.3. 5F-PB-22 product characterisation and purification

A total of 1.1 g of the 5F-PB-22 purified product was recovered, leading to a 57.9% yield. The purity of the re-crystallised 5F-PB-22 product was assessed through HPLC-UV and NMR and was > 99%. This was calculated on three independent analyses of aliquots of the 5F-PB-22 purified P.

5.3.4. Selection of the pre-processing protocol and validation

The pre-processing sequences (Table 5.4) were performed step by step on set 1 and the outcomes were evaluated through interpretation of the PCA's explained variance, scores, loadings and influence plots (Appendix 4.3). Guirguis's pre-processing protocol (Guirguis, 2017) led to improved clustering of the samples within the ellipse at 95% CL. 68% of the cumulative variance was accounted for in the first two PCs and the explained variance plot with calibrated and validated variances demonstrated close values (68% and 66% respectively). These metrics were better when compared to those achieved via the other methods. For this reason, protocol number 6 (Table 5.4), which consisted of the application of a baseline offset correction and mean normalisation of the intensity on the full spectral data range (3200-100 cm^{-1}), was applied to all the remaining datasets (Table 5.3). The baseline offsets, which are common spectroscopic instrumental artefacts, are usually corrected before applying spectral normalisation (Afseth *et al.* 2006). The baseline offset was calculated by subtracting the minimum absolute intensity value from all intensity values across the spectrum, removing the baseline offset and bringing the spectrum down to zero. Mean normalisation normalises spectra by dividing all intensities of individual spectra by the average of intensities, thus describing the relative intensities around the mean. The pre-processing protocol selected (Guirguis, 2017) was successfully validated by comparing the calibration set (sets 1-2) to a new set of independent samples called validation sets (sets 3-4). The validation was performed to ascertain whether the same substances belonging to the two independent sets were clustering together and to ensure that the model is not over-fitted to the data (Appendix 4.4 and 4.5).

5.3.5. Comparison between PCA of unprocessed and pre-processed Raman Renishaw (set 1) and Rigaku (set 2) spectra

In this section, the comparison between the PCA plots of the unprocessed and pre-processed data for Raman instruments is presented to offer an insight into the evaluation of the impact of the pre-processing protocol 6 on the data with the PCA classification. A correlation matrix study was performed in Excel (version 2015, build 14026.20308), using the Raman Renishaw dataset, before pre-processing, to gain an overview of the data and to confirm if pre-processing of the Raman spectral data would have been necessary. The correlation matrix (Appendix 4.5-Table A1) showed a positive correlation between the spectra obtained and the reference spectra of 5F-PB-22 (0.99-0.1), benzocaine (0.99-0.1), caffeine (0.97-0.1), cocaine (0.99-0.1), diazepam (0.99-0.1), paracetamol (0.99-0.1) and the negative control BP (0.99-0.1). A strong positive correlation (≥ 0.99) between replicate spectra of the same substance was expected and indicates that the spectra are similar to each other. However, a slightly lower correlation (0.97) between caffeine replicate spectra was observed. This was unexpected and might have resulted from a reduced intensity of the caffeine replicate 1 (CD-R1). This is supported by the results obtained by the PCA (influence and scores plots). Poor correlation (≤ 0.80) between the spectra of different substances was observed, meaning that the method should be able to distinguish between the different substances employed in the study. A good correlation was found between cocaine and amphetamine (≥ 0.80) which indicated that the spectra have a certain degree of similarity, therefore distinction between these two substances might be challenging.

Visual inspection of the line plot of the unprocessed spectra did not show any errors related to detector saturation and/or presence of cosmic rays, as such spectra would have been removed just after the analysis. However, issues such as raised baseline and significant variation in the overall peak intensities for caffeine samples (CD-R2 and R3 vs. R1) were observed (Appendix 4.6). These types of variation can be related to instrument artefacts such as noise, fluctuations in spectrometer performance, laser power and temperature, changes in optics geometry or analysis effects such as different mounting on the sample holder or variations in focal distance. Therefore, pre-processing is paramount to extract the Raman data from the noise (dark and detector). No spectral interpolation was applied as all the spectra had the same x-axis. The S/N ratio was manually calculated (Appendix 4.7) for all the sample replicates and ranged between 26-516 AU. In another study, Heraud *et al.* rejected spectra with a maximum signal less than 5,000 AU [136], while in this report the lowest minimum signal was around 16,000 AU.

In the PCA performed to both unprocessed and pre-processed set 1 collected using the Raman Renishaw seven PCs were required to achieve 100% of the explained variance. Both explained variance plots (Figure 5.11 a and b) showed a % residual validation variance not much larger than the residual calibration variance. An abnormal drop between calibrated and validated explained variance was present at the PC-4 (Figure 5.11 a) of the unprocessed set, meaning that the model may not be representative of new samples, for PC-4. However, the first two Principal Components (PCs) explained a sufficiently large amount of information, given the complexity of the information and the samples e.g., 68 and 66% of the variance within the dataset for the unprocessed and pre-processed data, respectively. The relationships between PC-1 and PC-2 can be interpreted with a high degree of certainty, and the model will be representative of unknown samples. The PCA calculated after pre-processing showed a slightly improved explained variance plot (Figure 5.11 b). In other words, after pre-processing validation and calibration lines are closer together, meaning that the PCA model built on pre-processed data would be more representative in explaining new samples.

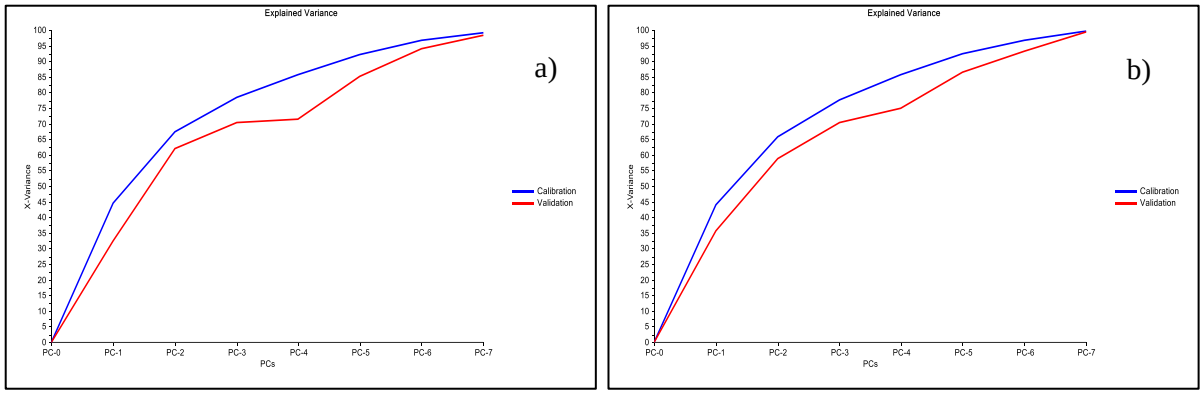

Figure 5.11. Explained variance plots a) unprocessed and b) pre-processed set 1

The caffeine R1 (CD-R1) in the PC-1 vs PC-2 2D scores plot (Figure 5.12 a) of unprocessed data was not clustering with the other two caffeine replicates (CD-R2 and R3). Visual inspection of the three caffeine replicates (Appendix 4.6) showed a raised baseline issue and a significant variation in the overall peak intensities for caffeine R1 and R2 (CD-R2 and R3) whilst caffeine R1 (CD-R1) displayed the lowest absolute intensity compared to the other two caffeine replicates (S/N = 67904). These factors might be responsible for their lack of clustering. After the application of mean normalisation and baseline offset removal, which minimise differences due to the variation in intensity in the raw data, caffeine replicates clustered together (Figure 5.12 b), also an overall closer clustering is obtained on a narrower x and y-axis scale. benzocaine (CC-R1 to R3) and diazepam (CF-R1 to R3) samples placed in the upper right (+ PC-2 and + PC-1 values) and lower right (- PC-2 and + PC-1 values) quadrants respectively, are dissimilar from the other samples in the set. This could be due to the difference in the intensities, the unique peaks in the sample's spectra, or both. When their pre-processed spectra were investigated, their intensity was higher compared to the other samples in the dataset, which could explain such dissimilarity. However, given that these were still within the ellipse at 95% CL, these are said to be not significantly different from the other samples and therefore are not outliers which would skew subsequent analysis and model interpretation (Figure 5.12 b).

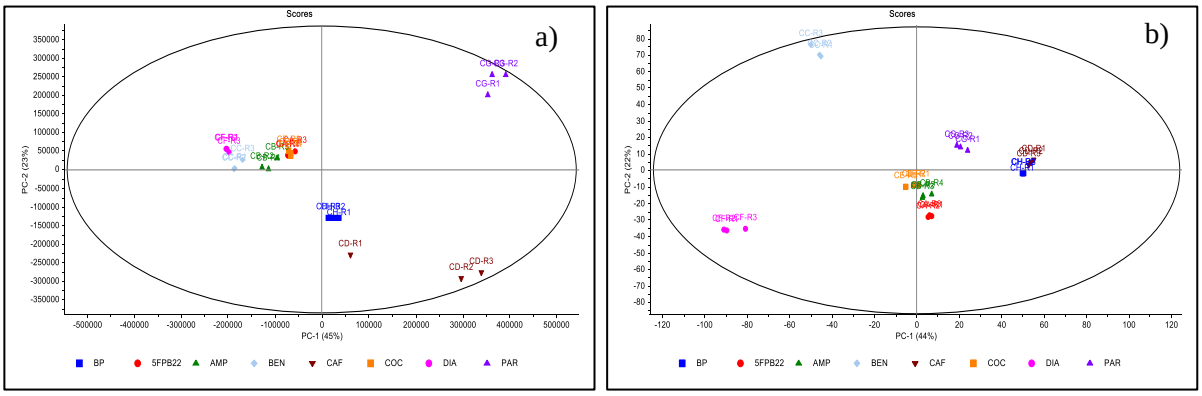

Figure 5.12. PC-1 vs PC-2 2D scores plot of the a) unprocessed and b) pre-processed set 1.

PC-1 and PC-2 F-residuals vs Hotelling T^2 influence plots were examined, to assess the presence of high leverage and/or high residuals samples. The PC-1 (Figure 5.13 a) and PC-2 (Appendix 4.8- Figure A1) plots of the unprocessed data set showed that caffeine R2 and R3 (CD-R2 and R3) and paracetamol R1 to R3 (CG-R1 to R3) samples have higher leverage on the model, meaning that the sample scores may have very high or low values for some components compared to the rest of the samples. While the influence plots of the pre-processed data set showed that diazepam R2 and R3 (CF-R1 R2 and R3) for PC-1 (Figure 5.13 b) and diazepam R2 and R3 (CF-R1 R2 and R3) and benzocaine R1 to R3 (CC-R1 to R3) for PC-2 (Appendix 4.8- Figure A2) samples have higher leverage on the model compared to the rest of the samples. However, in both cases, the sample's leverage is within the critical limit, so these are not skewing the model.

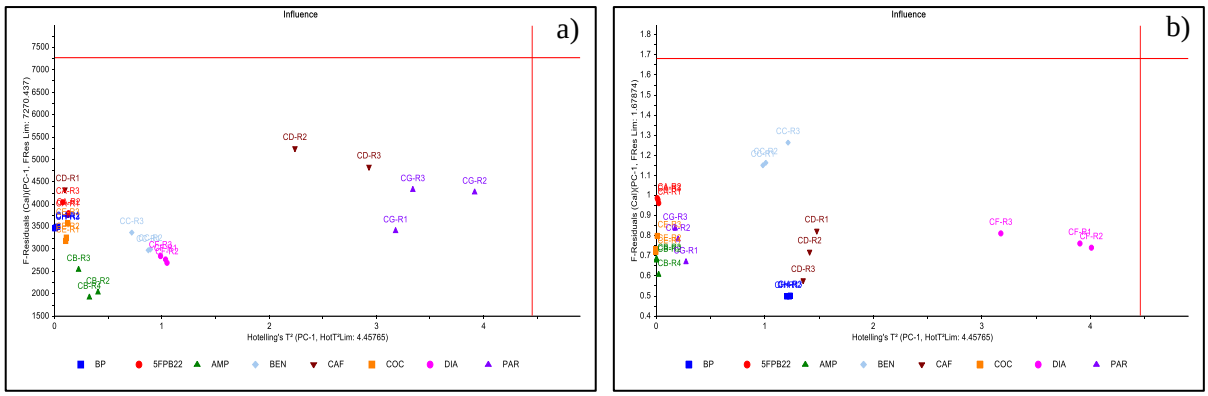

Figure 5.13. PC-1 F-residuals vs Hotelling T2 influence plots of the a) unprocessed and b) pre-processed set 1.

The PC-1 loadings plot (Figure 5.14 a) of the unprocessed data highlighted heavily loaded wavenumbers related to caffeine (554.41 cm^{-1}) and paracetamol spectra (856.84, 1236.69, 1325.71 and 1649.29 cm^{-1}). While the PC-2 loadings plot (Appendix 4.8- Figure A3) highlighted heavily loaded wavenumbers in common with PC-1 (554.41 and 856.84 cm^{-1}) and additional wavenumbers related to diazepam (1168.44 cm^{-1}) and paracetamol (1611.14 cm^{-1}) spectra. The 554.41 cm^{-1} heavily loaded wavenumber of caffeine spectra is related to the very strong intensity peak arising from the bending and rocking of the pyrimidine ring [137]. The 856.84, 1236.69, 1325.71, 1611.14 and 1649.29 cm^{-1} heavily loaded wavenumbers of paracetamol samples are related to the strong/very strong intensity peaks arising from the C-N-C ring 'breathing', C-C ring stretching, RCNR'R" amide III and II mode, respectively. The

1168.44 cm^{-1} heavily loaded wavenumber of diazepam samples is related to the C-N symmetric stretching [138].

After pre-processing, the loading plot did not show heavily loaded wavenumbers related to caffeine and paracetamol spectra which displayed issues with raised baseline and variations in absolute intensities. The new heavily loaded wavenumbers highlighted by the PC-1 loading plot (Figure 5.14 b) are related to benzocaine (861.76, 1604.32 and 1682.13 cm^{-1}) and diazepam (1168.44, 1313.08 and 1593.23 cm^{-1}) spectra. While the PC-2 loadings plot (Appendix 4.8- Figure A4) highlighted heavily loaded wavenumbers in common with the PC-1 (998.95, 1605.18 and 1681.13 cm-^{1}) and additional wavenumbers related to benzocaine (861.76 and 1281.39 cm^{-1}) spectra. The 861.76, 1281.39, 1604.32 and 1682.13 cm^{-1} heavily loaded wavenumbers of benzocaine spectra are related to the medium intensity peak arising from the out of plane C-H (ring) stretching and the very strong peaks arising from the C-N and C-O-C, C=C (ring) and C=O stretching, respectively [139]. The 1168.44, 1313.08 and 1593.23 cm^{-1} heavily loaded wavenumbers of diazepam spectra are related to C-N symmetric stretching C-C and C=N stretching, respectively [138] All the experimental and literature peak assignments related to the heavily loaded wavenumbers are summarised in Appendix 4.9.

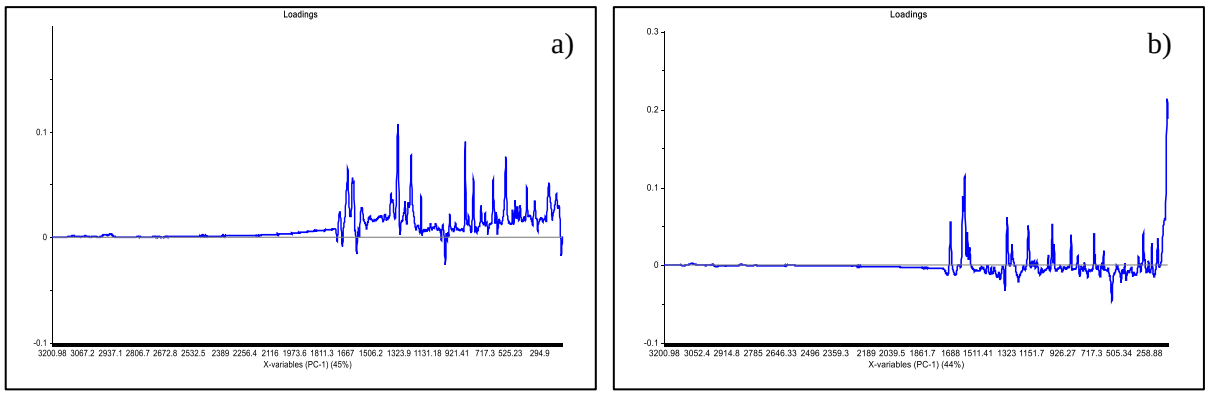

Figure 5.14. PC-1 loadings plots of the a) unprocessed and b) pre-processed set 1.

The additional Raman Renishaw PCA plots of unprocessed and pre-processed set 1 are available in Appendix 4.8.

The compounds in set 1 were also analysed using the Raman Rigaku (denoted set 2). The first two PCs of set 2 explained a smaller amount of variance within the dataset e.g., 67 and 48% for the unprocessed and pre-processed data, respectively, vs. 68 and 66% of the Raman Renishaw.

There is only a 1% difference between the variances of the two unprocessed datasets. However, after pre-processing is carried out the differences between the variance increase to 18%. This can be explained by the different spectral ranges covered by the two Raman instruments (Rigaku 200-2500 cm^{-1} vs Renishaw 5-3300 cm^{-1}). The region between 2500-3300 cm^{-1} which is only present in the Raman Renishaw spectra does not have any prominent peaks, however, some noise is visible between 2800-3200 cm^{-1}. Moreover, the Raman Renishaw have a spectral resolution of 0.3 cm^{-1} cm vs. 8-11 cm^{-1} of the Raman Rigaku, which allows more variance to be captured. The differences between % calibrated and validated explained variance of the Raman Rigaku pre-processed data was bigger than the Raman Renishaw instrument, e.g., 18 vs 10%, respectively, meaning that the PCA model built using the Raman Rigaku would be less representative in explaining new samples compared to the Raman Renishaw. Caution should be used when comparing results from the different instruments, due to their different specification (Table 5.1). All the samples after pre-processing fell and clustered well within the ellipse at 95% CL (Appendix 4.10- Figure A2). benzocaine R1 to R3 (CC-R1 to R2) replicates are placed in the lower right (+ PC-1 and - PC-2 and values) quadrant while BP R1 to R3 (CH-R1 to R3) replicate are placed in the lower left quadrant (- PC-1 and - PC-2 and values), apart from the other samples. This means that benzocaine and BP are dissimilar to each other's and the other samples, however, this is not statistically significant.

The F-residuals vs Hotelling T^2 influence plots (Appendix 4.10- Figure A5 and A6) of the pre-processed set 2 consistently show higher leverage of benzocaine compared to the other samples, also within the critical limit. This could be due to the strong Raman scattering property of benzocaine. The heavily positive loaded wavenumbers in the PC-1 loading plot (Appendix 4.10- Figure A9) are related to benzocaine (864.59, 1279.5, 1607.98 and 1685.35 cm^{-1}) while the heavily negative loaded wavenumber is attributed to BP (1088.35 cm^{-1}). The 864.59, 1279.5, 1607.98 and 1685.35 cm^{-1} heavily loaded wavenumbers of benzocaine samples are related to the medium intensity peak arising from the out of plane C-H (ring) stretching and the very strong peaks arising from the C-N and C-O-C, C=C (ring) and C=O stretching, respectively [139].These were the same wavenumbers (± 5 cm^{-1} shift) highlighted also for the Raman Renishaw dataset 1. The 1088.35 cm^{-1} heavily loaded wavenumber of BP samples is related to the very strong intensity peak arising from the C=O (CaCO3) symmetric stretching [140]. While the heavily positive loaded wavenumbers in the PC-2 loading plot (Appendix 4.10- Figure A10) are related to diazepam (1594.07 cm^{-1}) and cocaine (1027.98 and 1720.89 cm^{-1}) samples, while the heavily

negative loaded to paracetamol (858.89 $cm^{-1)}$, BP (1088.35 cm^{-1}), benzocaine (1607.98 cm^{-1}) and caffeine (1284.71 cm^{-1}) samples. The 1027.98 and 1720.89 cm^{-1} heavily loaded wavenumbers of cocaine samples are related to the asymmetric stretching of the aromatic ring and the C=O symmetric stretching, respectively. The 1594.07 cm^{-1} heavily loaded wavenumber of diazepam samples is related to the very strong peak arising from the C=N stretching. The 858.89 cm^{-1} heavily loaded wavenumber of paracetamol samples is related to the very strong peak arising from the C-N-C ring breathing. An additional highly positive loaded wavenumber for PC-2 is 1000.24 cm^{-1} which is almost three times more heavily loaded compared to the rest of the wavenumbers. This could be either attributed to the symmetric stretching and 'breathing' of the aromatic ring of cocaine or the C-N-C asymmetric stretching of diazepam, as both substances display peaks at that wavenumber. All the experimental and literature peak assignments related to the heavily loaded wavenumbers are summarised in Appendix 4.9.

The additional Raman Rigaku PCA plots of unprocessed and pre-processed set 2 are available in Appendix 4.10.

Raman spectral pre-processing was successfully performed to improve the classification of selected pure substances of known composition analysed with both Raman Renishaw and Rigaku. The optimal combined pre-processing protocol for this study [125], consisted of a two consecutive step process, namely baseline offset followed by mean normalisation. The application of the pre-processing protocol successfully improved the clustering of the substances in the scores plot while the explained validated and calibrated variance plot remained almost invariant. The difference between the variances % of the unprocessed dataset achieved with Raman Renishaw and Rigaku could be due to the different spectral ranges and resolutions covered by the different instruments.

5.3.5.1. Ranking of the Raman activity

Ranking of the Raman activity has been performed to experimentally determine strong/weak Raman scattering substances and to better understand the reason behind samples' position in the PCA scores plots. The Raman activity of the seven reference standards (Section 5.2.1) was ranked based on the maximum peak absolute intensity of the data acquired with the Raman Rigaku using a constant laser power of 185 mW. The seven reference standard spectral data were imported into Excel, the triplicate averaged, truncated in the (250-1750 cm^{-1}) and the spectra

were individually plotted (Appendix 4.9). The Raman activity was then ranked from stronger to weaker Raman scatterer as follows: benzocaine (~ 58000 A.U. at ~ 1605 cm^{-1}), 5F-PB-22 (~ 35000 A.U. at ~ 1713 cm^{-1}), diazepam (~ 30000 A.U. at ~ 1592 cm^{-1}), caffeine (~ 21000 A.U. at ~ 555 cm^{-1}), paracetamol (~ 13000 A.U. at ~ 858 cm^{-1}), cocaine (~ 6000 A.U. at ~ 1596 cm^{-1}), amphetamine (~ 2500 A.U. at ~ 1005 cm^{-1}).

5.3.6. PCA classification of Raman spectra of solid mixtures

In the sections below the pre-processing protocol [125] was applied to i) 21 binary mixture spectra taken with Raman Renishaw (set 5) and Rigaku (set 6) and ii) 21 binary mixtures plus seven reference standard spectra taken with Raman Renishaw (set 7) and Rigaku (set 8). This set of experiments was performed to evaluate the impact of different substances and instruments on the PCA model.

5.3.6.1. PCA classification of 21 binary mixtures spectra taken with Raman Renishaw (set 5) and Rigaku (set 6)

Set 5 PC-1 vs PC-2 2D scores plot (Figure 5.15) shows the first two PCs explaining a considerable amount of information, 60% of the variance within the dataset. All the samples fall into the 95% ellipse CL, except for amphetamine/caffeine R2 and R3 (M8-R2 and R3). Across the PC-1 vs PC-2 2D scores plot some replicate samples cluster closely together e.g., caffeine /diazepam (M17), amphetamine/diazepam (M10), diazepam/paracetamol (M21), while others e.g., benzocaine/cocaine (M13) and amphetamine/benzocaine (M7) are more disparate. This can be expected when analysing mixtures in replicate due to the inhomogeneous distribution of the two compounds (intra samples) and the impact of the orientation of oscillations (state of polarisation) of light waves of the excitation laser irradiating the molecules in the mixtures [141]. Due to the lack of reference standards in this data set, it is not possible to ascertain which mixture sample replicate is closer to the single reference standard than the others, which would be important to understand the behaviour of the mixtures and for identification purposes.

The benzocaine/paracetamol R1 (M15-R1) cluster with the benzocaine/caffeine R1 to R3 (M12-R1 to R3), while the benzocaine/paracetamol R2 and R3 (M15-R2 and R3) cluster with the 5F-PB-22/benzocaine R1 to R3 (M2-R1 to R3). All these samples share the main benzocaine spectra characteristic features including a strong intensity peak at 864 cm^{-1} due to the out-of-plane stretching of the C-H in the aromatic ring; a strong intensity peak at 1285 cm^{-1} due to the stretching of the C-N & C-O-C and a very strong intensity peak at 1608 cm^{-1} due to the C=C ring stretching. benzocaine is a strong Raman scattering substance, meaning that its signal is dominating, swamping the signal of the other substances in the mixtures e.g., paracetamol, caffeine, and 5F-PB-22. Although all these samples share benzocaine spectra

characteristic features, they cluster separately, due to differences in their intensities. The maximum peak intensities of benzocaine/paracetamol R1 (M15-R1) and benzocaine/caffeine R1 to R3 (M12 R1 to R3) are higher than 24 AU, while the benzocaine/paracetamol R2 and R3 (M15-R2 and R3) and 5F-PB-22/benzocaine R1 to R3 (M2 R1 to R3) is lower than 20 AU.

The amphetamine/caffeine (M8) replicate samples (Appendix 4.11- Figure A1) have prominent peaks in a different region of the spectra which causes them to be in a different region of the scores plot and some to be outside the 95% ellipse CL. For instance, the samples amphetamine/caffeine R2 and R3 (M8-R2 and R3) show the caffeine characteristic very strong intensity peak at 557 cm^{-1}, causing them to cluster with caffeine/diazepam (M17) replicate samples, as these share the features of caffeine spectra. However, amphetamine/caffeine R2 and R3 (M8-R2 and R3) are outside the 95% ellipse CL as the intensities of their peaks are higher than caffeine/diazepam (M17) replicate samples. While amphetamine/caffeine R1 (M8-R) shows the amphetamine characteristic strong, very strong and medium intensities peaks at 976, 1002 and 1033 cm^{-1}, respectively. Causing this sample to cluster near amphetamine/paracetamol R3 (M11-R3), as these share features of amphetamine spectra.

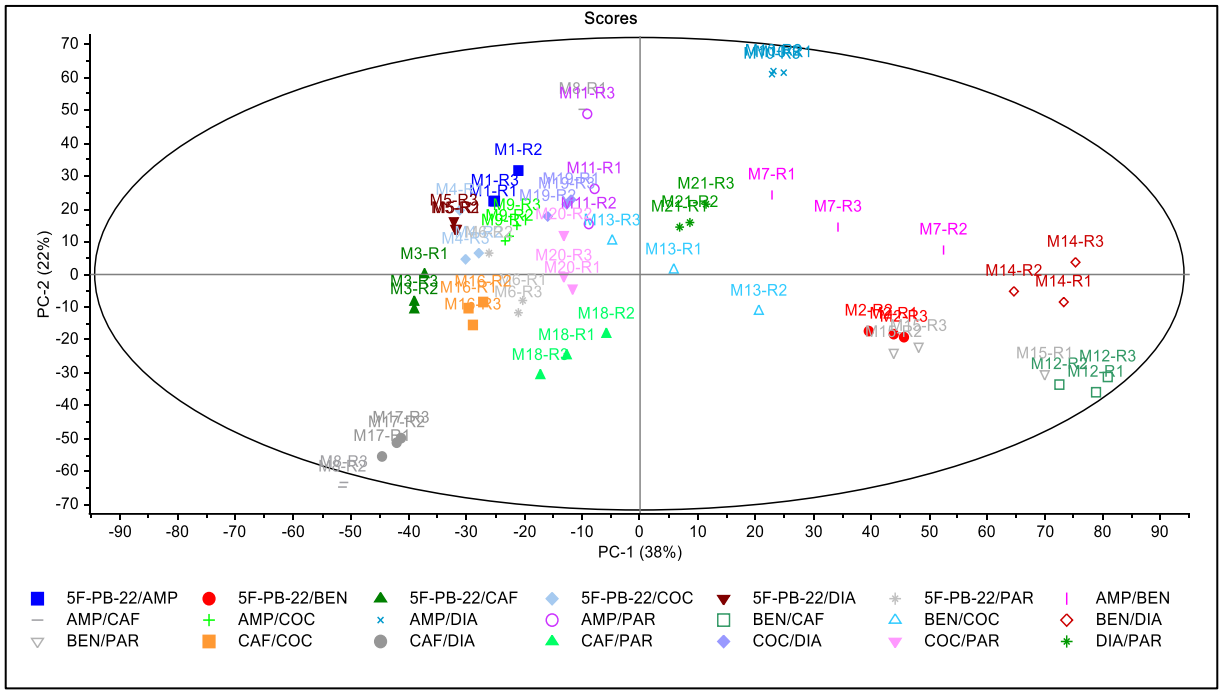

Figure 5.15. Set 5 PC-1 vs PC-2 2D scores plot.

The set 5 PC-1 F-residuals vs Hotelling T^2 influence plot (Figure 5.16 a) shows that benzocaine/diazepam R3 (M14-R3), benzocaine/caffeine R1 and R3 (M12-R1 and R3) have high leverage on the model. The overlaid spectra of benzocaine/diazepam (M14) sample replicates, show that the R3 has a more marked peak at 800 cm^{-1} (Appendix 4.11- Figure A2), which could explain the higher leverage on the model compared to the other replicate samples. The same case applies to benzocaine/caffeine R1 and R2 (M12-R1 and R2) samples which have a higher relative intensity compared to the R2 sample. However, if we look at the PC-1 leverage plot (Appendix 4.12- Figure A1) the samples benzocaine/diazepam R3 (M14-R3), benzocaine/caffeine R1 and R3 (M12-R1 and R3) are below the critical limit (<0.095). These samples have a higher Hotelling T^2 value above the critical limit (>4.059) in the PC-1 Hotelling T^2 influence plot (Appendix 4.12- Figure A2). The set 5 PC-2 F-residuals vs Hotelling T^2 influence plot (Figure 5.15 b) shows that amphetamine/caffeine R2 and R3 (M8-R2 and R3) have high leverage on the model, for the reason already mentioned at the beginning of the Section 5.3.4.1. Similarly, to the samples with high leverage on PC-1, if we look at the PC-2 leverage plot (Appendix 4.12- Figure A3) the samples amphetamine/caffeine R2 and R3 (M8-R2 and R3) are below the limit (<0.14) These samples have though a high Hotelling T^2 value above the limit (>6.50) in the PC-2 Hotelling T^2 influence plot (Appendix 4.12- Figure A4) While the PC-2 F-residuals vs Hotelling T^2 influence plot (Figure 5.16 b) shows that amphetamine/caffeine R2 and R3 (M8-R2 and R3) have high leverage on the model.

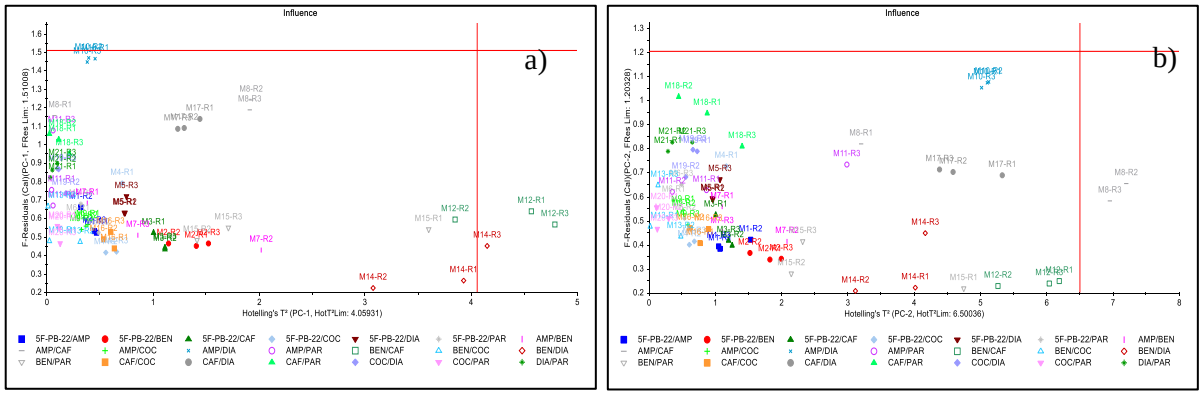

Figure 5.16. Set 5 F-residuals vs Hotelling T2 influence plots for a) PC-1 and b) PC-2.

Consistently with the above findings, the PC-1 loadings plot (Appendix 12- Figure A5) highlighted highly positive loaded wavenumbers belonging to benzocaine (861.76, 1281.39, 1171.2, 1604.32 and 1681.39 cm^{-1}), and highly negative loaded wavenumbers belonging to caffeine (554.41 cm^{-1}) spectrum. While the PC-2 loadings plot (Appendix 4.12- Figure A6) highlighted highly negative loaded wavenumbers also belonging to benzocaine (861.76, 1281.39 and 1604.32 cm^{-1}) and caffeine (554.41 and 1328.39 cm^{-1}) spectra. Moreover, an additional highly positive loaded wavelength was identified at 1000.56 cm^{-1} which belongs either to cocaine or diazepam spectrum. The relation between heavily loaded wavenumbers (Raman peaks) of the PCs loading plot and the vibration of the functional groups has been already discussed in section 5.3.3 for benzocaine. The 554.4 and 1328.39 cm^{-1} heavily loaded wavenumbers of the caffeine spectrum are related to the very strong and strong intensity peaks arising from the bending and rocking of the pyrimidine ring and the stretching of the imidazole ring, respectively [137]. While the heavily loaded wavenumber of the cocaine sample is related to the strong intensity peak arising from the symmetric stretching/breathing of the aromatic ring [142].

The additional Raman Renishaw PCA plots of set 5 are available in Appendix 4.12.

The set 6 PC-1 vs PC-2 2D scores plot (Figure 5.17) shows the two first PCs explaining a considerable amount of information, 65% of the variance within the dataset, similarly to the results achieved with the Raman Renishaw for set 5 (60%). All the samples fall into the 95% ellipse CL. benzocaine/cocaine (M13) replicate samples are spread similarly to Raman Renishaw scores plot data (Figure 5.15). There is almost a net separation between samples containing benzocaine, on the right side of the scores plot, and samples that do not contain benzocaine, except for 5F-PB-22/benzocaine (M2) replicate samples, which are placed in the middle. This trend could be due to the strong Raman scattering property of benzocaine, and to the 5F-PB-22 being the second strongest Raman scatter substance amongst those analysed.

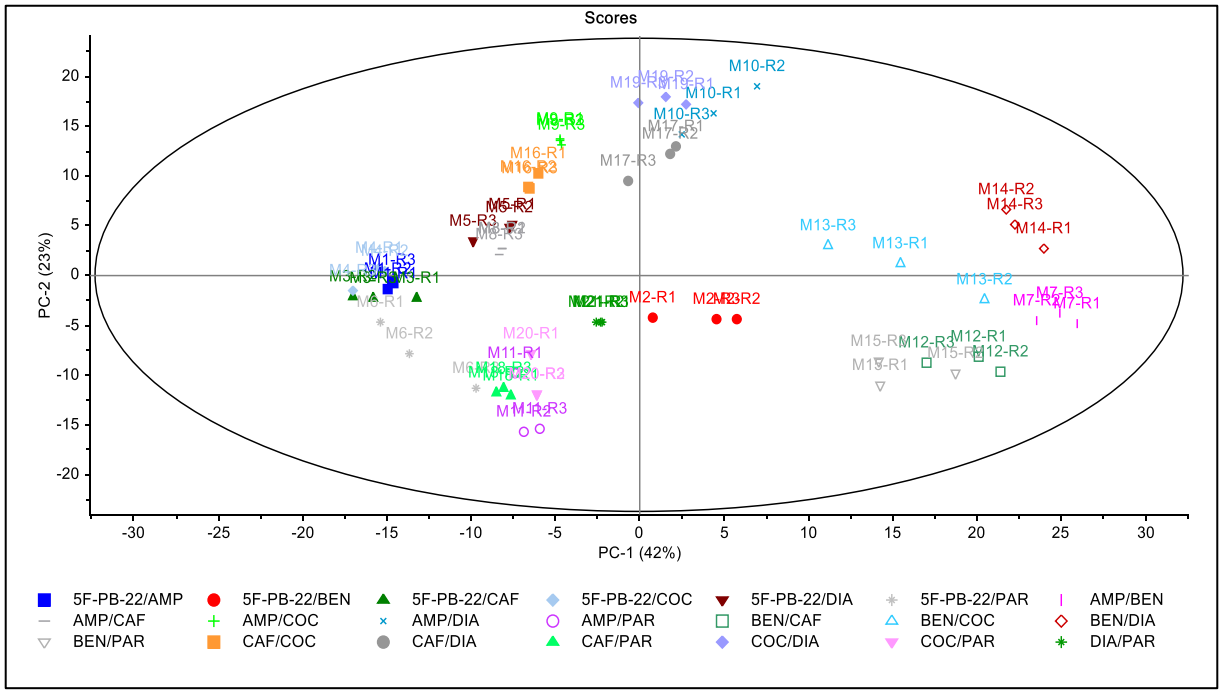

Figure 5.17. Set 6 PC-1 vs PC-2 2D scores plot.

The set 6 PC-1 F-residuals vs Hotelling T^2 influence plot (Figure 5.18 a) shows that amphetamine/benzocaine R1 (M7-R1), have high leverage on the model, and is statistically different from the remainder of the samples. An explanation for this behaviour is that the amphetamine/benzocaine R1 (M7-R1) has a slightly higher intensity of the following peaks 864.59, 1279.54, 1685.35 cm^{-1} in the spectra compared to the other samples amphetamine/benzocaine R2 and R2 (M7-R2 and R3). The set 6 PC-2 F-residuals vs Hotelling T^2 influence plot (Figure 5.18 b) did not show any samples with high residuals or high leverage on the model.

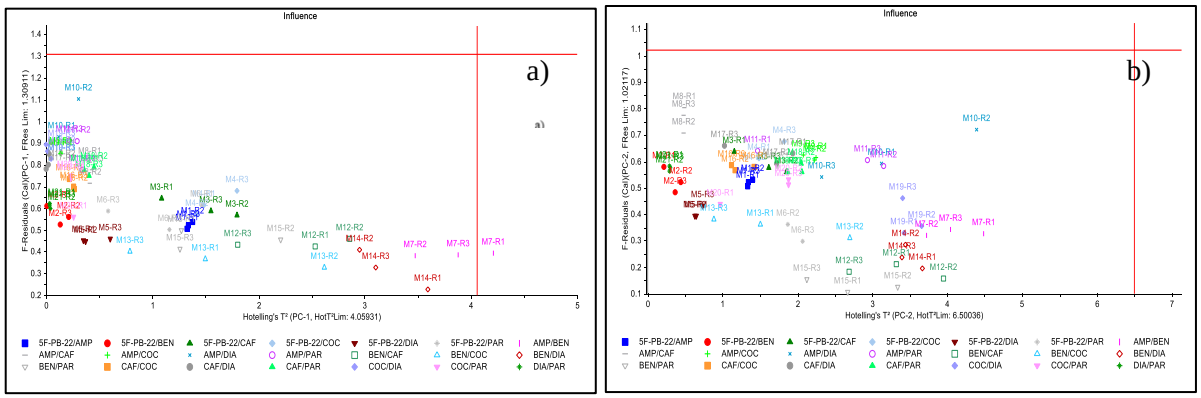

Figure 5.18. Set 6 F-residuals vs Hotelling T2 influence plots for a) PC-1 and b) PC-2.

Consistent with the PC-1 F-residuals vs Hotelling T^2 influence plot findings, the PC-1 loading plot (Appendix 4.13- Figure A1) showed the following highly positive loaded wavenumbers at 864.59, 1279.54, 1685.35 cm^{-1} characteristic of benzocaine spectrum, belonging to the amphetamine/benzocaine R1 (M7-R1). Additionally, the wavenumber at 1716.48 cm^{-1} related to the C=O symmetric stretching of the cocaine was found to be highly negative loaded for the PC-1. While PC-2 loading plot (Appendix 4.13- Figure A2) showed wavenumber 858.85 cm-1 (C-N-C ring breathing) related to the paracetamol spectrum having high negative loadings. Wavenumber 1594.07 (C=N stretching) cm^{-1} is related to diazepam, and wavenumber 1000.24 cm-1 is related either to cocaine or diazepam spectra, both have high positive loadings on PC-2.

Moreover, the instrument, equipped with the in-built RMA provided three matches with a decreasing CC from the 1st to the 3rd, if at least one of the 3 matches contained the correct mixture of substances it was considered a positive result. Both components of the mixture were correctly identified in 86% (54/63) of the samples with a CC ranging between 0.99-0.69 (Appendix 4.14) which represents a promising outcome. The nine mixture samples not correctly identified were 5F-PB-22/amphetamine R1 to R3; 5F-PB-22/diazepam R3; 5F-PB-22/paracetamol R1 and R2; amphetamine/benzocaine R1 and caffeine/diazepam R1 and R2. 5F-PB-22 is a strong Raman scatterer compared to the amphetamine, which probably swamped its signal. Mixtures of 5F-PB-22/amphetamine were matched mainly to a mixture of 5F-PB-22 and BB-22, another synthetic cannabinoid. In one replicate only, amphetamine was identified as one of the components in a mixture with BB-22. 5F-PB-22 and BB-22 differ from each other concerning the R group on the indole, and therefore, will have similar Raman spectra. The 5F-PB-22/diazepam R3 and 5F-PB-22/paracetamol R1 were matched to a ternary mixture made up of the two constituents of the samples plus BB-22. While in the other cases (amphetamine/benzocaine and caffeine/diazepam) the strongest Raman scattering substance of the mixture (benzocaine and diazepam) was correctly identified as a single substance in the 1st match and in the 2nd match the other single component was identified (amphetamine and caffeine).

The additional Raman Rigaku PCA plots of set 6 are available in Appendix 4.13.

The two PCA models built using the same samples analysed using Raman Renishaw and Rigaku are performing differently e.g., Raman Rigaku set 6 showed a higher explained

variance for the first two PCs and all the samples falling into the 95% ellipse CL. The differences in the performance could be explained by the reduced spectral range (200-2500 vs 5-3300 cm-1) and resolution (8-11 vs 0.3 cm^{-1}) of the Raman Rigaku instrument.

5.3.6.2. PCA classification of 21 binary mixtures and seven reference standard spectra taken with Raman Renishaw (set 7) and Rigaku (set 8).

Following the addition of the single neat reference standards to the 21 mixtures (set 5) the PCA was performed (set 7). The two first PCs explained variance went up by 1% leading to 61%. In the PC-1 vs PC-2 scores plot. The benzocaine/caffeine R1 and R3 (M12-R1 and R3), amphetamine/diazepam R1 to R3 (M10-R1 to R3) and diazepam R1 to R3 (CF-R1 to R3) samples fell just outside, or on the edge of the 95% ellipse CL (Figure 5.19), which was further investigated using the PC-1 and PC-2 F-residuals vs Hotelling's T^2 influence plots. The addition of the reference standards shows that the samples in the top right quadrant of the scores plot, which all have benzocaine in common in the mixture, cluster near the benzocaine reference standard. This suggests that if in a mixture is present a strong Raman scattering substance e.g., benzocaine, this is likely to swamp the signal of the other component, dominating the Raman spectra, hence making identification of other components in the mixture challenging.

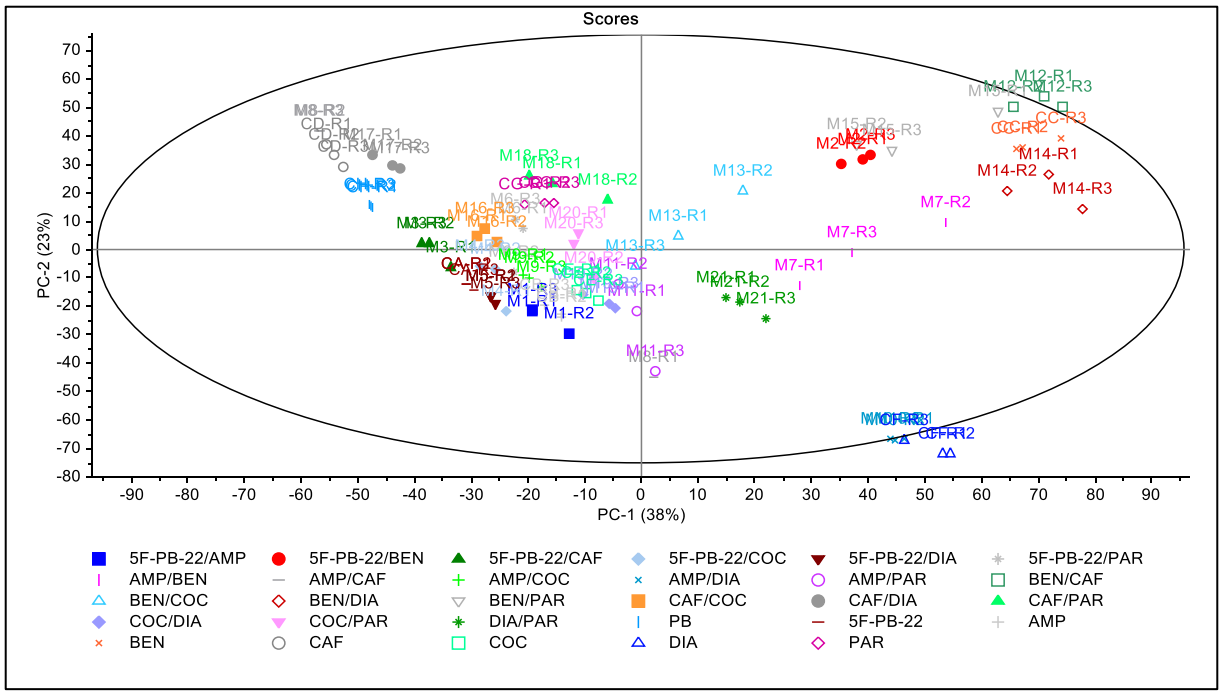

Figure 5.19. Set 7 PC-1 vs PC-2 2D scores plot.

The samples falling outside or on the edge of the 95% ellipse CL on the right side of the scores plot benzocaine/caffeine R1 and R3 (M12-R1 and R3), amphetamine/diazepam R1 to R3 (M10-R1 to R3) and diazepam R1 to R3 (CF-R1 to R3) also have high leverage on PC-2 (Figure 5.20 b). Samples such as benzocaine/caffeine R1 and R3 (M12-R1 and R3), amphetamine/diazepam R1 to R3 (M10-R1 to R3) were also close to the 95% ellipse CL in the scores plot of the data set 5 (Figure 5.15), and benzocaine/caffeine M12-R1 and R3 had also high leverage on the PC-1 of the previous model calculated (Figure 5.20 a).

After the addition of the single reference standard samples to the dataset, benzocaine/caffeine R1 and R3 (M12-R1 and R3), amphetamine/diazepam R1 to R3 (M10-R1 to R3), all fall further outside or just on the edge of the 95% ellipse CL. Additionally, the diazepam R1 to R3 (CF-R1 to R3) fall outside of the 95% ellipse CL but also cluster with the amphetamine/diazepam R1 to R3 (M10 R1 to R3) in the right bottom region of the scores plot. When diazepam and amphetamine/diazepam M10 replicate spectra were overlaid (Appendix 4.15), all their diazepam characteristics peaks were aligned, resulting in almost identical spectra except for some intensity variation. This means that the diazepam in the diazepam/amphetamine (M10) samples is likely to be swamping the signal of the amphetamine, consistent with their relative Raman activity ranking. Moreover, the benzocaine/diazepam R3 (M14-R3) has high leverage on the PC-1 model due to the higher intensity of a peak, which was something already investigated in Section 5.3.4.1.

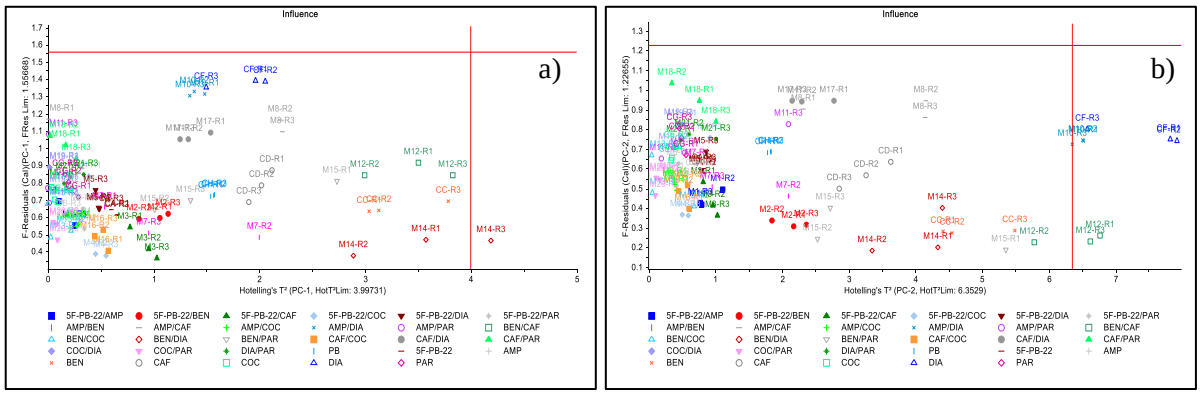

Figure 5.20. Set 7 F-residuals vs Hotelling T2 influence plots for a) PC-1 and b) PC-2.

The same heavily loaded wavenumbers found in the set 5 PC-1 loading plot (Appendix 4.16-Figure A1), were also highlighted for set 7 belonging to benzocaine (861.76, 1281.39, 1171.2, 1604.32 and 1681.39 cm^{-1}) spectra, having high positive loadings on PC-1, and to caffeine (554.41 cm^{-1}) spectra, having high negative loadings on PC-1. While the PC-2 loadings plot (Appendix 4.16- Figure A2) highlighted high negative loadings wavenumbers also belonging to benzocaine (861.76, 1281.39 and 1604.32 cm^{-1}) spectra, and high positive loadings wavenumbers belonging to diazepam (999.60 and 1592.38 cm^{-1}) spectra.

The additional Raman Renishaw PCA plots of set 7 are available in Appendix 4.16.

Following the addition of the single neat reference standard to the 21 mixtures (set 6) another PCA was performed (set 8). The first two PCs explained variance went down to 56% and all the samples fall into the 95% ellipse CL (Figure 5.21). It is interesting that when using the Raman Rigaku instrument (vs Raman Renishaw) the percentage of the explained variance is smaller. This could be due to the smaller spectral range of the instrument, which does not capture the noise at the lower wavenumbers, reducing the inherent variation in the dataset and hence making it more difficult to capture the variance in the first two PCs.

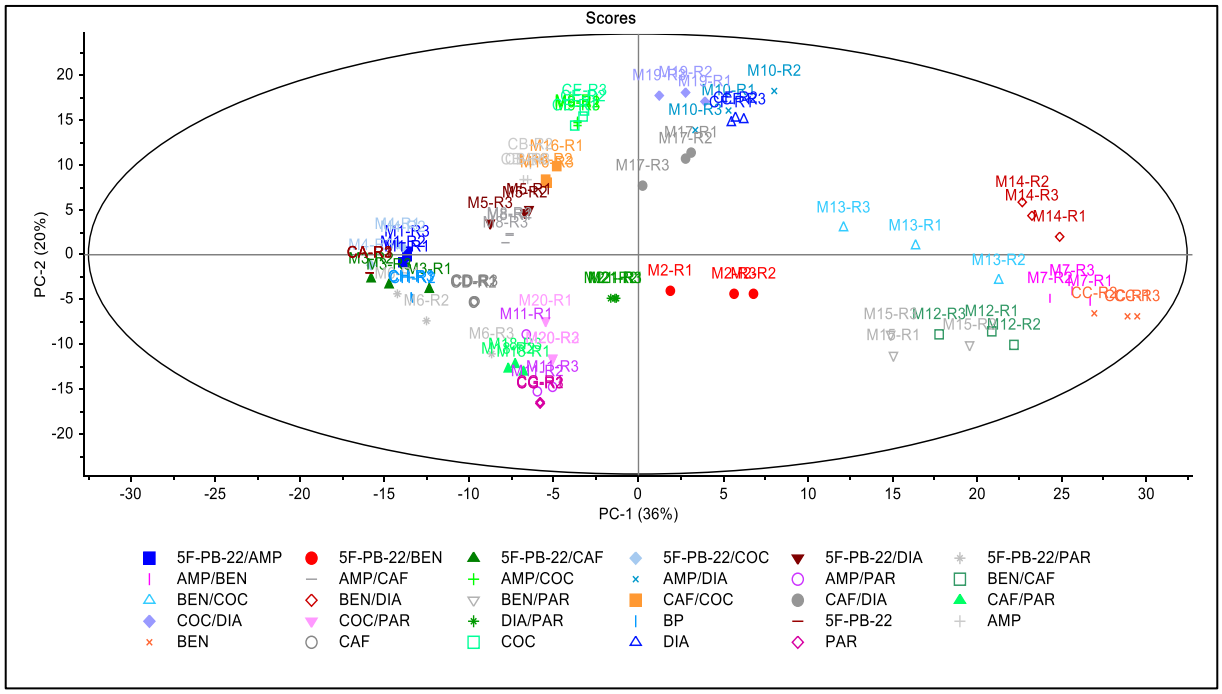

Figure 5.21. Set 8 PC-1 vs PC-2 2D scores plot.

The set 8 PC-1 F-residuals vs Hotelling T^2 influence plot (Figure 5.22 a) shows that benzocaine R1 to R3 (CC-R1 to R3) and amphetamine/benzocaine R1 (M7-R1) samples have high leverage. amphetamine/benzocaine R1 (M7-R1) had also high leverage in the influence plot of set 6, due to the change of intensity of some peaks related to benzocaine when compared to the other replicates. While benzocaine R1 to R3 (CC-R1 to R3) have high leverage as benzocaine is a strong Raman scatterer, hence their intensity is higher compared to the average samples. The set 8 PC-2 F-residuals vs Hotelling T^2 influence plot (Figure 5.22 b) shows BP R1 to R3 (CH-R1 to R3) having high residuals compared to the average samples, very strong intensity peak around 1088 cm^{-1}, and absence of any other significant peaks in the of the pre-processed spectra, meaning that these samples do not fit the model very well.

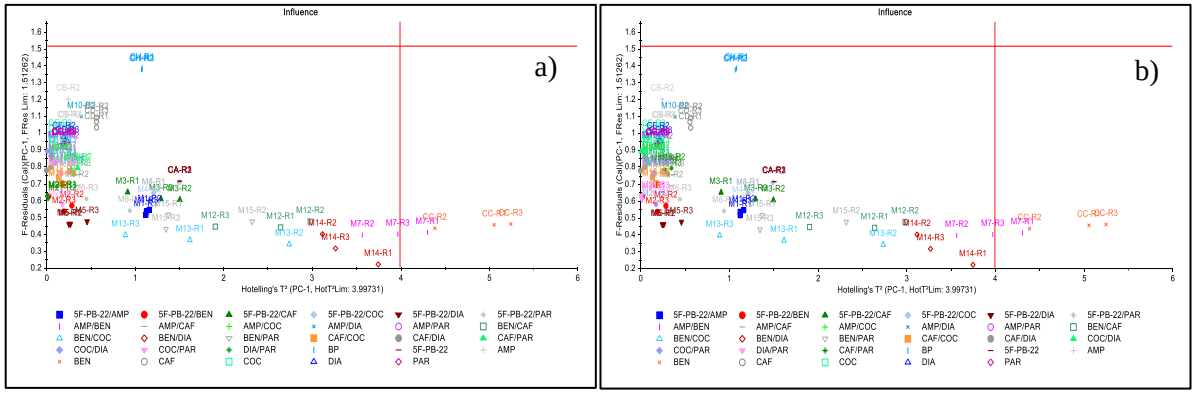

Figure 5.22. Set 8 F-residuals vs Hotelling T2 influence plots for a) PC-1 and b) PC-2.

The same heavily positive loaded wavenumbers found in the set 6 PC-1 loadings plot were also highlighted for this set PC-1 loadings plot (Appendix 4.17- Figure A1) showing the following wavenumbers 864.59, 1279.54, 1607.98, 1685.35 cm^{-1}, belonging to amphetamine/benzocaine R1 and benzocaine replicate spectra. Additionally, the cocaine wavenumber 1716.48 cm^{-1} (C=O symmetric stretching) was found to have a high negative loading on the PC-1. The PC-2 loadings plot (Appendix 4.17- Figure A2) showed highly negative loaded wavenumber 858.85 cm^{-1} (C-N-C ring breathing) related to paracetamol and highly positive loaded wavenumber 1594.07 cm^{-1} (C=N stretching) related to diazepam, while 1000.24 cm^{-1} is a common wavenumber for cocaine and diazepam related to small and medium intensity peaks, respectively.

The additional Raman Rigaku PCA plots of set 8 are available in Appendix 4.17.

5.3.7. PCA classification of Raman spectra of single reference standards pipetted or soaked paper.

In the sections below, the pre-processing protocol [125] is applied to i) the spectra of seven reference standards pipetted on paper at five different concentrations and the seven neat reference standards taken with Raman Renishaw (set 9) and Rigaku (set 10) ii) the spectra of seven reference standards soaked on paper at five different concentrations and the seven neat reference standards taken with Raman Renishaw (set 11) and Rigaku (set 12) iii) the spectra of seven reference standards pipetted and soaked on paper at five different concentrations taken with Raman Renishaw (set 13) and Rigaku (set 14**).** This set of experiments was performed to evaluate the impact of the instruments and sample preparation methods employed.

5.3.8. PCA classification of seven reference standards pipetted on paper at five different concentrations and seven neat spectra taken with Raman Renishaw (set 9) and Rigaku (set 10).

The set 9 PC-1 vs PC-2 2D scores plot (Figure 5.23) shows the two first PCs explaining 73% of the variance within the dataset. Most of the samples analysed cluster in the left region of the scores plot in the proximity of the BP replicate samples, while fewer are spreading into the right region. The samples falling out of the 95% ellipse CL are benzocaine R1 to R3 (CC-R1 to R3), diazepam (CF-R1 to R3), amphetamine 30 mg/mL R2 (PB-30-R2), benzocaine 10 mg/mL R2 (PC-10-R2), diazepam 30 mg/mL (PF-30-R1 to R3) pipetted on paper. Single reference standards, having high Raman scattering properties e.g., benzocaine and diazepam, are found outside of the ellipse at 95% CL, which is already known to have high leverage from previous models. Some of their related samples pipetted on paper at the highest concentration analysed are also found outside the ellipse at 95% CL e.g., benzocaine 10 mg/mL R2 (PC-10-R2) and diazepam 30mg/mL R1 to R3 (PF-30-R1 to R3). In addition, the R2 sample of the amphetamine 30 mg/mL pipetted on paper (PB-30-R2), falls outside the ellipse at 95% CL, and it is disparate from the remaining replicates as its relative intensity is higher. The reason most of the samples are located near BP is related to the low capabilities of the instrumentMost of the samples are located near BP due to the instrument's low capabilities to detect substances that have been pipetted on paper at lower concentrations. Low concentration solutions pipetted

on paper are barely detectable and will share the major features of the spectra of the BP samples.

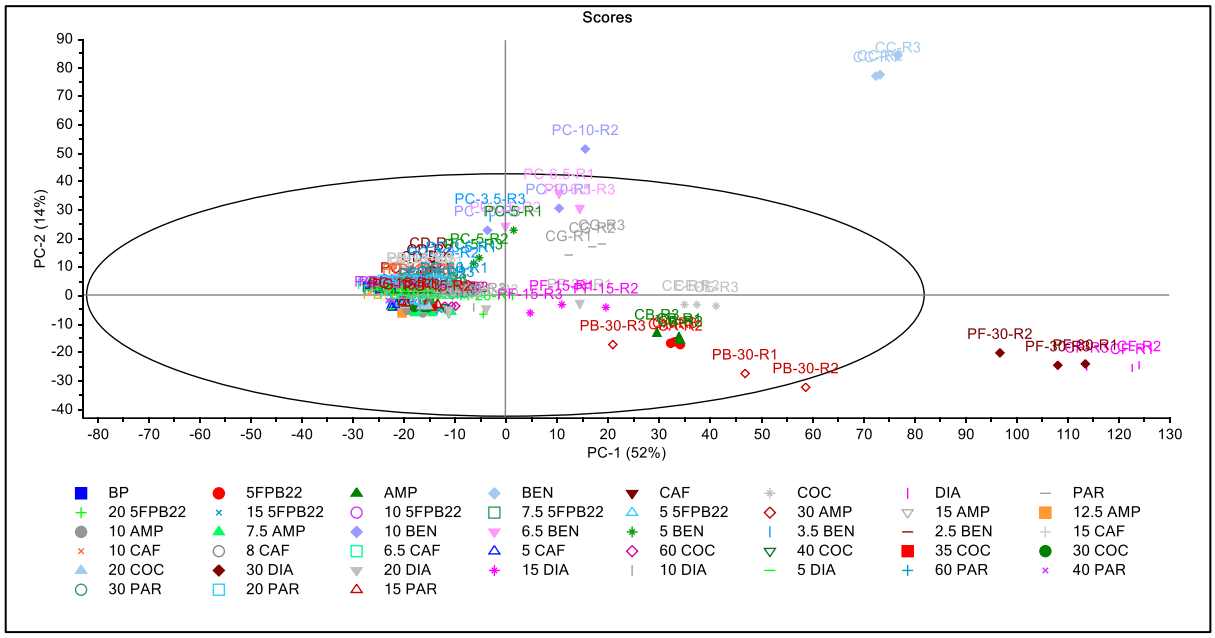

Figure 5.23. Set 9 PC-1 vs PC-2 2D scores plot.

The most concerning outliers which have both high leverage and do not fit the model very well were identified using the PC-1 and PC-2 F-residuals vs Hotelling T^2 influence plots (Figure 5.24 a and b). Of all the samples falling outside the 95% ellipse CL the most concerning were found to be benzocaine R1 to R3 (CC-R1 to R3) and diazepam 30 mg/mL R1 (PF-30-R1) for PC-1 and diazepam 30 mg/mL R1 and R2 (PF-30-R1 and R2) and amphetamine 30 mg/mL R2 (PB-30-R2) pipetted on paper.

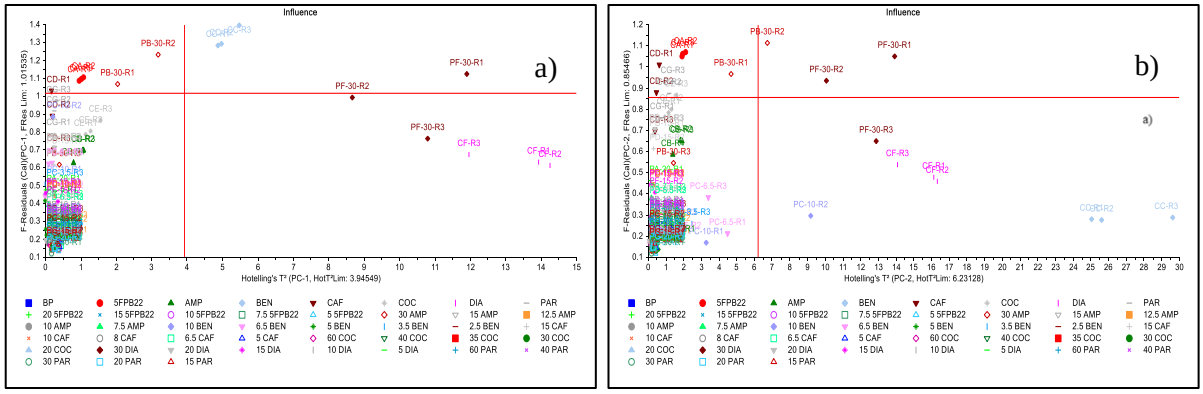

Figure 5.24. Set 9 F-residuals vs Hotelling T2 influence plots for a) PC-1 and b) PC-2.

The set 9 loading plots showed positive heavily loaded wavenumbers at 1593.23 and 105.77 cm^{-1} for PC-1 (Appendix 4.18- Figure A1) and 1681.29, 1605.18, 1281.39 and 861.76 cm^{-1} for PC-2 (Appendix 4.18- Figure A2). Wavenumbers 1681.29, 1605.18, 1281.39 and 861.76 cm^{-1} are all related to benzocaine, and their modes were all previously described. While wavenumber 1593.23 cm^{-1} is related to C=N stretching of the diazepam. In a Raman spectrum, the fingerprint region (250-1750 cm^{-1}) is a group of wavenumbers used for identification based on the peak position related to the modes of the functional groups for a given substance. This region in PCA is subject to large variation which explains the differences between the models generated for each of the instruments and the percentage variance explained in the first two PCs. The heavily loaded wavenumber 105.77 cm^{-1} does not belong to the fingerprint wavenumber of the Raman spectra.

The additional Raman Renishaw PCA plots of set 9 are available in Appendix 4.18.

Once identified the most concerning outliers, benzocaine R1 to R3 (CC-R1 to R3) and diazepam 30 mg/mL R1 and R2 (PF-30-R1 and R2) amphetamine 30 mg/mL R2 (PB-30-R2) pipetted on paper were removed from the dataset, and the PCA recalculated. The newly generated PC-1 vs PC-2 2D scores plot (Figure 5.25) of set 9 represented a reduced variance within the new dataset (61% vs 73%) for the two first PCs, which is expected when removing outliers, as the samples in the dataset are more like each other and less likely to be easily resolved by the first two PCs. Often removing outliers from a model, will result in generating other outliers in the recalculated model. Removing more and more outliers each time can cause overfitting of the data to the model built. A possible solution would be trying to obtain more samples of the same type to stabilize the model or build a separate model only for samples like the outliers.

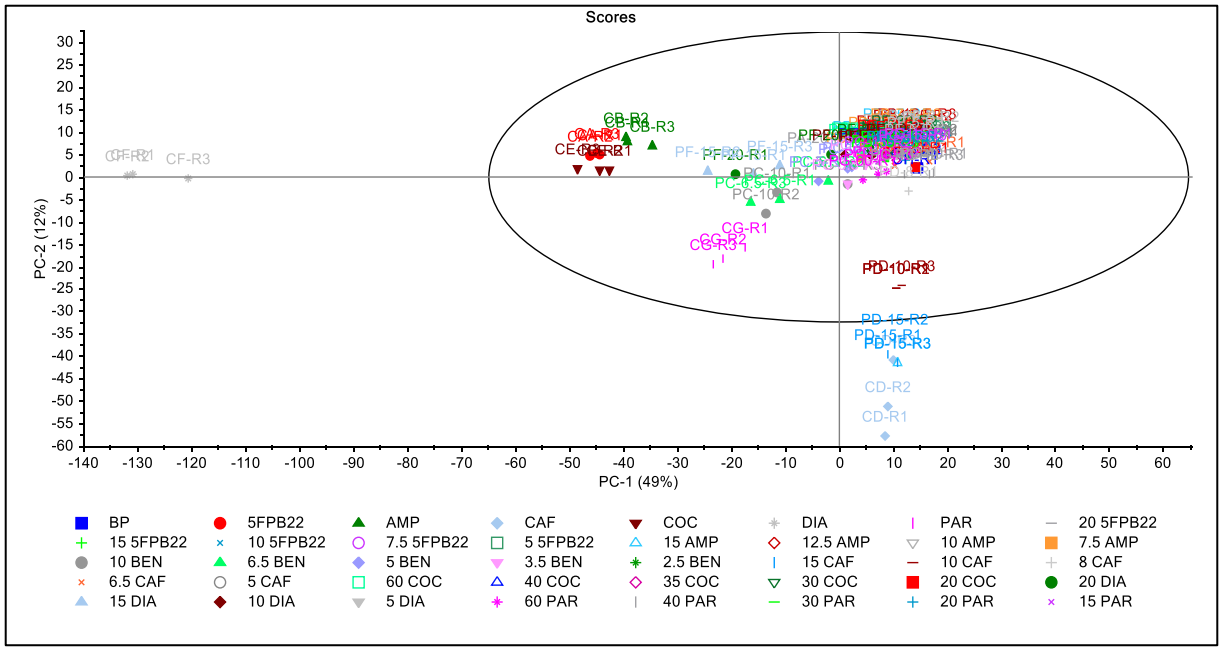

Figure 5.25. Set 9 PC-1 vs PC-2 2D scores plot after removing outliers.

Having removed the initial problematic samples, other samples are now falling outside the 95% ellipse CL, namely diazepam R1 to R3 (CF-R1 to R3), caffeine R1 to R3 (CD-R1 to R3) and caffeine pipetted on paper at 15mg/mL R1 to R3 (PD-15-R1 to R3). These samples all have high leverage on the PC-2. Additionally, diazepam has also high leverage on the PC-1, however, these fit the model very well (Figure 5.26 a and b). It is important to note that diazepam and caffeine are the third and fourth strongest Raman scatterer substances considered in this study, which makes them 'different' from the other paper samples, because of the dominance of the blank paper peaks in most of the remaining samples.

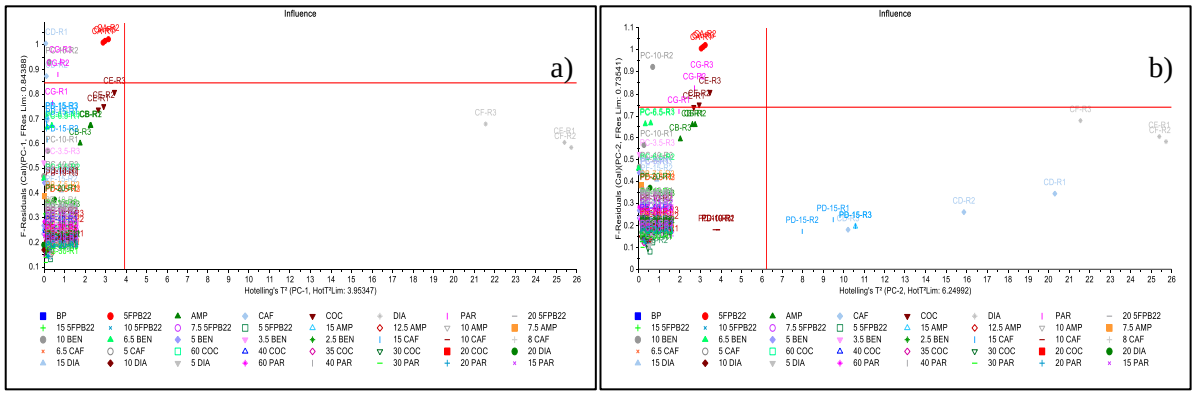

Figure 5.26. Set 9 F-residuals vs Hotelling T2 influence plots for a) PC-1 and b) PC-2 after removing outliers.

The additional Raman Renishaw PCA plots of set 9 recalculated without outliers are available in Appendix 4.19.

The set 10 PC-1 vs PC-2 2D scores plot (Figure 5.27) shows the first two PCs explaining 57% of the variance within the dataset, compared to 73% achieved analysing the same dataset with the Raman Renishaw. In this case, the samples are more evenly distributed in the scores plot. This appears related to the different capabilities of the Raman Rigaku instrument related to its spectral range and resolution. The samples falling out of the 95% ellipse CL are benzocaine R1 to R3 (CC-R1 to R3) and, benzocaine 10 mg/mL pipetted on paper R1 (PC-10-R1). The benzocaine R1 to R3 (CC-R1 to R3) fall outside the 95% ellipse CL, as known for the strong Raman scattering property, which means having higher intensity spectra, compared to the other samples, even after the normalisation is performed. While benzocaine pipetted on paper at 10 mg/mL R1 (PC-10-R1) which is one of the three replicates at the highest concentration benzocaine has been pipetted on the paper samples also falls outside the ellipse at 95% CL.

When benzocaine R1 to R3 (PC-10-R1 to R3) spectra are compared to each other, all share the characteristic peaks position with the neat benzocaine reference standard at 862, 1281, 1608 and 1685 cm^{-1} but also the BP peak at 1088 cm^{-1}. However, the benzocaine 10 mg/mL pipetted on paper R1 (PC-10-R1) has a higher intensity of benzocaine peaks, and lower intensity of BP peaks, this is followed by R2 and then R3, which displays the higher intensity of BP and lower benzocaine peaks (Appendix 4.20- Figure A1). The more the benzocaine peaks are intense in the spectra of the simulated paper sample pipetted with benzocaine at 10 mg/mL R1 (PC-10-R1) the more this cluster near the benzocaine reference standard replicates. Changes in the intensity of benzocaine or BP characteristic peaks could be attributed to different factors such as the inhomogeneous distribution of a substance on paper (intra sample) and the impact of the orientation of oscillations (state of polarisation) of light waves of the excitation laser irradiating the molecules [141]. These factors will determine the different positions of the replicate samples in the scores plot, but also the different positions between different samples. Other contributing factors are the initial simulated sample solution concentration employed, and the functional groups of the substance used to prepare the solution, which results in its strong/weak Raman activity.

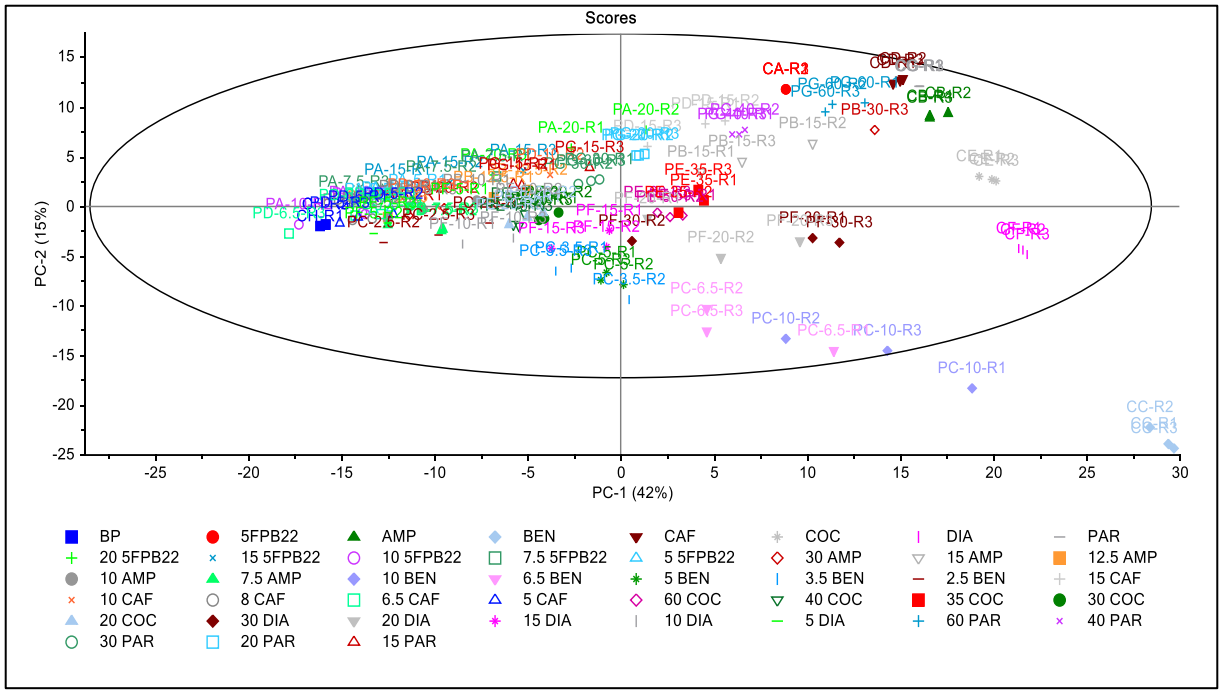

Figure 5.27. Set 10 PC-1 vs PC-2 2D scores plot.

Of all the samples falling outside the ellipse at 95% CL the most concerning outliers, which have high leverage and do not fit the model well, are benzocaine R1 and R3 (CC-R1 and R3) for PC-1 (Figure 5.28 a). benzocaine samples were also found to be outliers in set 9, due to benzocaine being a strong Raman scattering substance, which can skew the model. benzocaine R2 (CC-R2) was found to fit the model and have high leverage because its relative intensity is lower compared to the other two replicates.

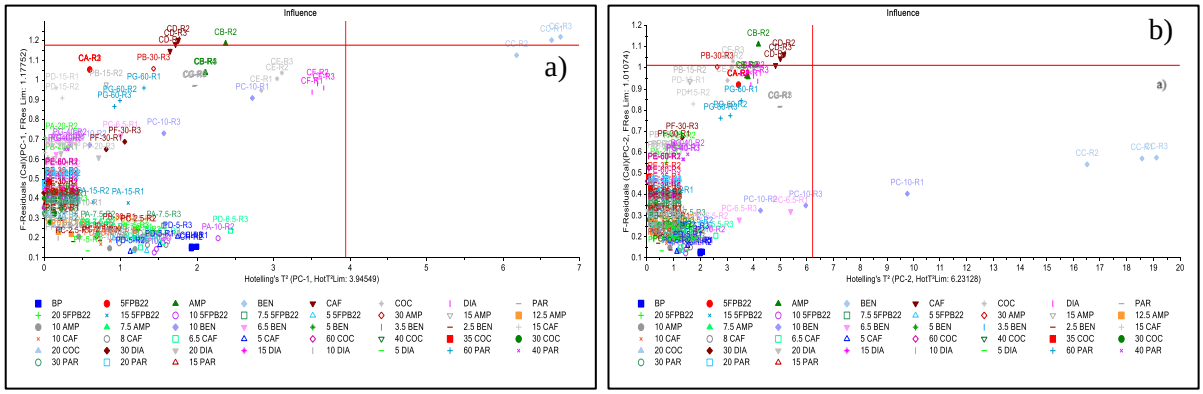

Figure 5.28. Set 10 F-residuals vs Hotelling T2 influence plots for a) PC-1 and b) PC-2.

The set 10 PC-1 loadings plot (Appendix 4.21- Figure A1) showed a positive heavily loaded wavenumber between 1603.35-1607.98 cm^{-1}, and a negative heavily loaded wavenumber at 1088.35 cm^{-1}. While the PC-2 loadings plot (Appendix 4.21- Figure A2) showed positive heavily loaded wavenumbers at 556.94 and 1325.77 cm^{-1}, and negative heavily loaded wavenumber at 1279.54, 1603.35 and 1685.35 cm^{-1}. The region between 1603.35-1607.98 cm^{-1} is related to caffeine (~1604 cm^{-1}) and both amphetamine and benzocaine (~1608 cm^{-1}) characteristic peaks. While wavenumbers at 556.94, 1088.35 and 1685.35 cm^{-1} are related to caffeine, BP and benzocaine, respectively. While wavenumbers at 1279.54 and 1325.77 cm^{-1} do not seem to be related to any characteristic peak of the samples.

The additional Raman Rigaku PCA plots of set 10 are available in Appendix 4.21.

The most concerning outliers are benzocaine R1 and R3 (CC-R1 and R3), and also benzocaine-R2 (CC-R3), as this appears near the critical limit and clusters near the other two problematic replicates, were removed from the dataset, and the PCA recalculated. The newly generated PC-1 vs PC-2 2D scores plot (Appendix 4.22- Figure A1) of set 10 explained a higher variance within the new dataset (58% vs 57%) for the two first PCs. However, other samples are now falling outside the 95% ellipse CL, namely diazepam R1 to R2 (CF-R1 to R2), cocaine R1 to R2 (CE-R1 to R2), paracetamol R1 and R3 (CG-R1 and R3) and paracetamol pipetted on paper at 60 mg/mL R1 to R3 (PG-60-R1 to R3). These samples have all high leverage on the PC-2 model, however, fit the model well. In addition, amphetamine (CB-R2) has high leverage and does not fit the model, hence becoming a concerning outlier.

The additional Raman Rigaku PCA plots of set 10 recalculated without outliers are available in Appendix 4.22.

Moreover, looking at the result obtained with the Raman Rigaku using the in-built RMA 42% (40/105) identification for any of the psychoactive substances and adulterants/cutting agents was achieved for set 10 (Appendix 4.14- Table A2) with a CC ranging between 0.99-0.55. A result was marked as positive if one of the three matches included the reference standards pipetted on the simulated paper sample or the reference standard plus microcrystalline cellulose (MC) and/or calcium carbonate ($CaCO_3$) since simulated paper samples could be seen as a mixture of the substance plus the paper. This assumption was based on Udristoiu and colleagues' findings, which described the paper composition as 80% cellulose, 5-15% $CaCO_3$ filler and other minor variable components such as kaolin, calcium sulphate ($CaSO_4$) and alumina trihydrate ($Al(OH)_3$) [140]. The 40 substances identified were 5F-PB-22 at 20 and 15 mg/mL, amphetamine at 15 mg/mL,

benzocaine at 10mg/mL, caffeine at 15 mg/mL, cocaine at 60 and 35 (only R2) mg/mL diazepam mg/mL at 30, 20 (only R1 and R2),15 and 10 (only R1 and R2) and paracetamol at 60, 40, 30 and 20 mg/mL sample replicates pipetted on paper. Most of the samples identified as a positive match by the instrument were at the highest concentration analysed, except for amphetamine which at the highest concentration of 30 mg/mL analysed did not give a positive match.

The line plots of the seven psychoactive substances and cutting agents and adulterant reference standards on simulated paper samples at five concentrations were built using Excel. The illustrative examples of the spectra of the psychoactive substances (5F-PB-22, amphetamine, cocaine and diazepam) pipetted on simulated paper samples and collected using Raman Rigaku are reported in Figures 5.29 to 5.32. below

From the top of the bottom of Figure 5.29, the Raman Rigaku spectra of the following samples are reported: 5F-PB-22, 5F-PB-22 pipetted on paper at the decreasing concentration of 20, 15, 10, 7.5 and 5 mg/mL, and BP. In the simulated paper samples that have been pipetted with the highest concentrations of 5F-PB-22 solutions i.e., 5F-PB-22 pipetted on paper at 20 and 15 mg/mL, characteristics peaks of 5F-PB-22 reference standard at ~1716 (red line), ~1528 (green line), ~1381 (light blue line), and ~778 (purple line) cm^{-1} are visible [143]. While the intensity of the characteristic peak of BP at ~1088 (black line) cm^{-1} decreases [140], remaining visible though when the concentration of 5F-PB-22 increases on the simulated paper samples.

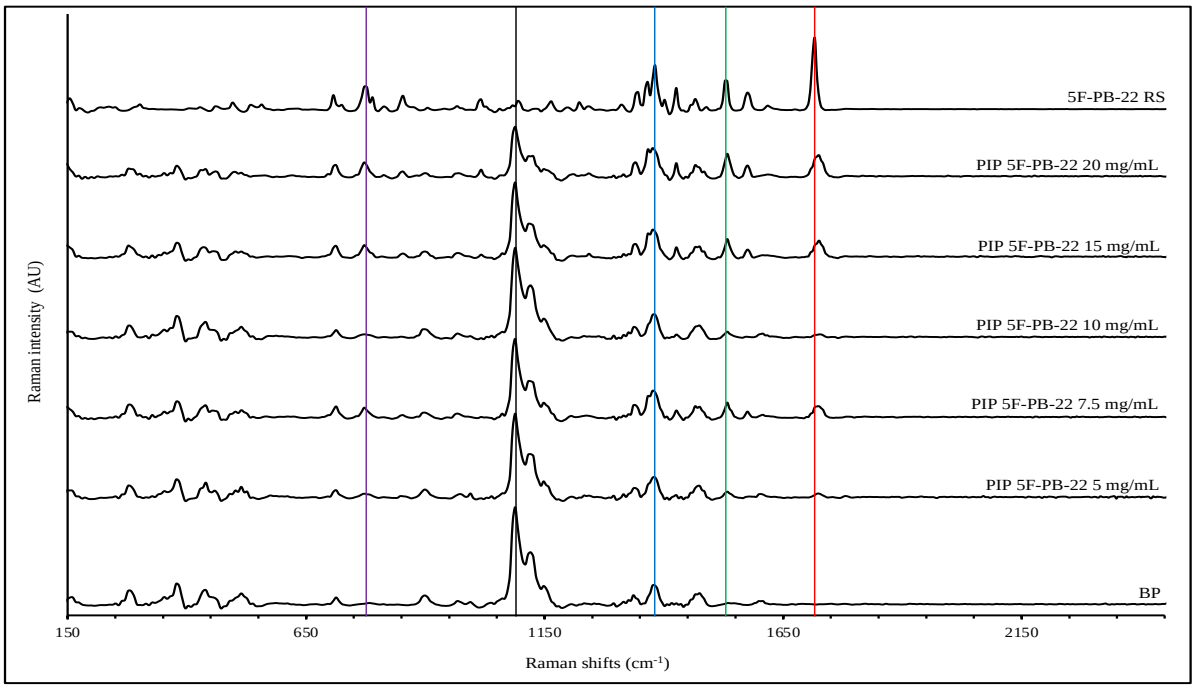

Figure 5.29. Raman Rigaku spectra of 5F-PB-22 reference standard, 5F-PB-22 pipetted on paper at 20, 15, 10, 7.5 and 5 mg/mL and BP (from top to bottom).

From the top of the bottom of Figure 5.30, the Raman Rigaku spectra of the following samples are reported: amphetamine reference standard, amphetamine reference standard pipetted on paper at the decreasing concentration of 30, 15, 12.5, 10 and 7.5 mg/mL, and BP. In the simulated paper samples that have been pipetted with the highest concentrations of amphetamine reference standard solutions i.e., amphetamine reference standard pipetted on paper at 30 and 15 mg/mL, characteristics peaks of amphetamine reference standard at ~1608 (red line), ~1212 (green line), ~1066 (light blue line), and ~978 (purple line) cm^{-1} are visible [144]. While the intensity of the characteristic peak of BP at ~1088 (black line) cm^{-1} decreases [140], remaining visible though when the concentration of amphetamine reference standard increases on the simulated paper samples.

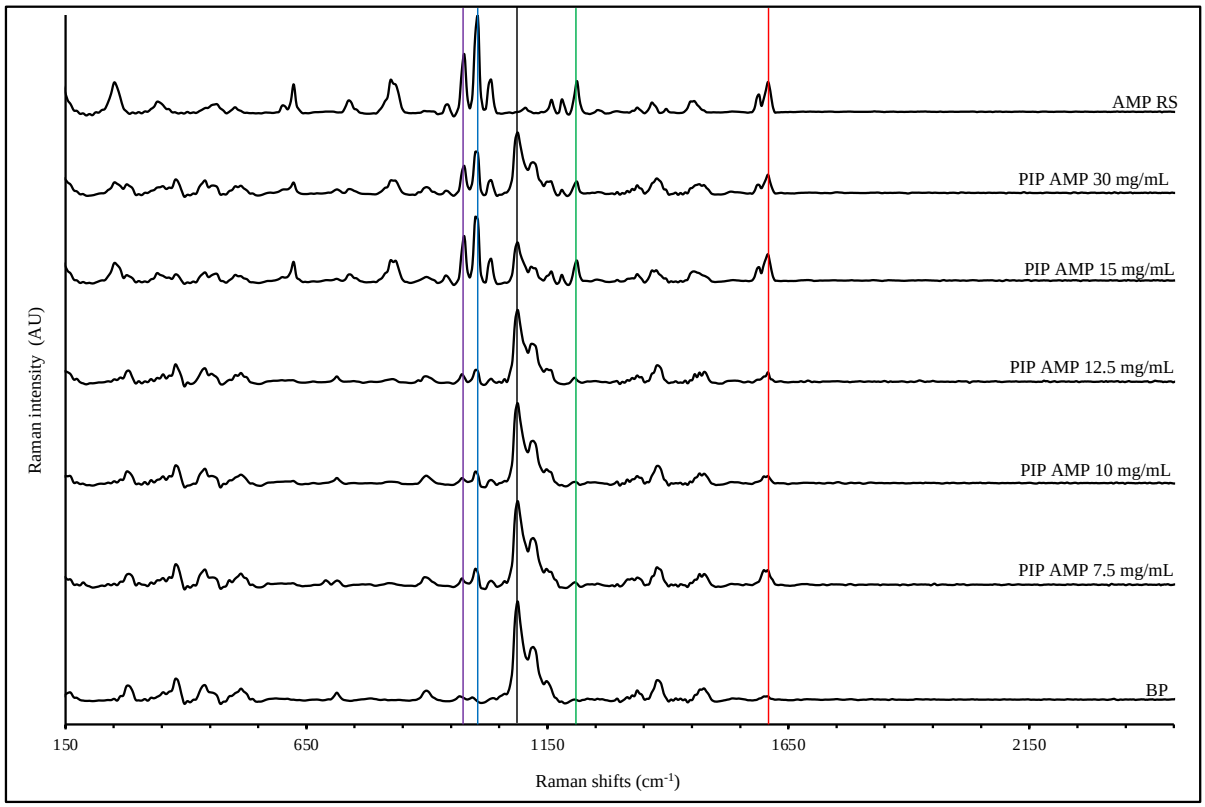

Figure 5.30. Raman Rigaku spectra of amphetamine reference standard, amphetamine pipetted on paper at 30, 15, 12.5, 10 and 7.5 mg/mL and BP (from top to bottom).

From the top of the bottom of Figure 5.31, the Raman Rigaku spectra of the following samples are reported: cocaine reference standard, cocaine reference standard pipetted on paper at the decreasing concentration of 60, 40, 35, 30 and 20 mg/mL, and BP. In the simulated paper samples that have been pipetted with the highest concentrations of cocaine reference standard solutions i.e., cocaine pipetted on paper at 60, 40, 35 and 30 mg/mL, characteristics peaks of cocaine reference standard at ~1716 (red line), ~1598 (green line), ~1274 (light blue line), ~1000 (purple line), and ~1028 (yellow line) cm^{-1} are visible [142]. While the intensity of the characteristic peak of BP at ~1088 (black line) cm^{-1} decreases [140], remaining visible though when the concentration of cocaine reference standard increases on the simulated paper samples.

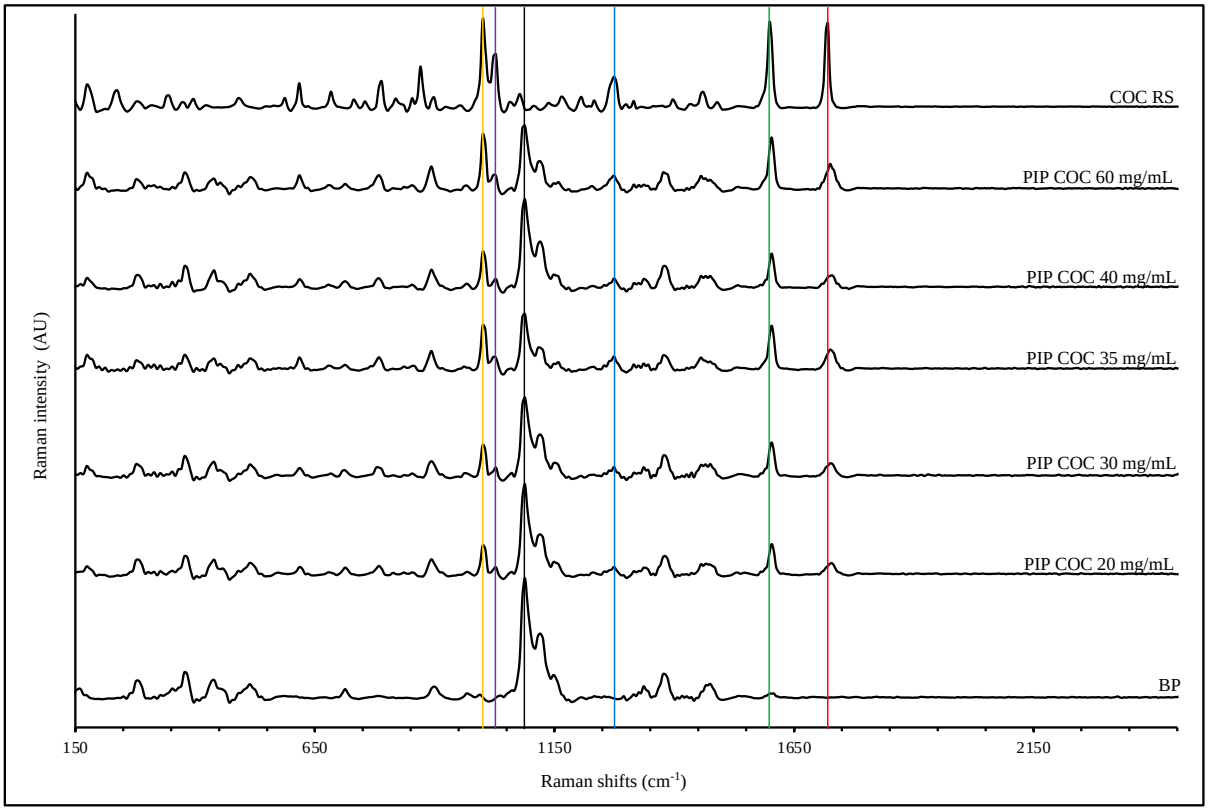

Figure 5.31. Raman Rigaku spectra of cocaine reference standard, cocaine pipetted on paper at 60, 40, 35, 30 and 20 mg/mL and BP (from top to bottom).

From the top of the bottom of Figure 5.32, the Raman Rigaku spectra of the following samples are reported: diazepam reference standard, diazepam reference standard pipetted on paper at the decreasing concentration of 30, 20, 15, 10 and 5 mg/mL, and BP. In the simulated paper samples that have been pipetted with the highest concentrations of diazepam reference standard solutions i.e., diazepam pipetted on paper at 30, 20, 15 mg/mL, characteristics peaks of diazepam reference standard at ~1594 (red line), ~1315 (green line), ~1169 (light blue line) and ~1000 cm^{-1} (purple line) are visible [138]. While the intensity of the characteristic peak of BP at ~1088 (black line) cm^{-1} decreases [140], remaining visible though when the concentration of diazepam reference standard increases on the simulated paper samples.

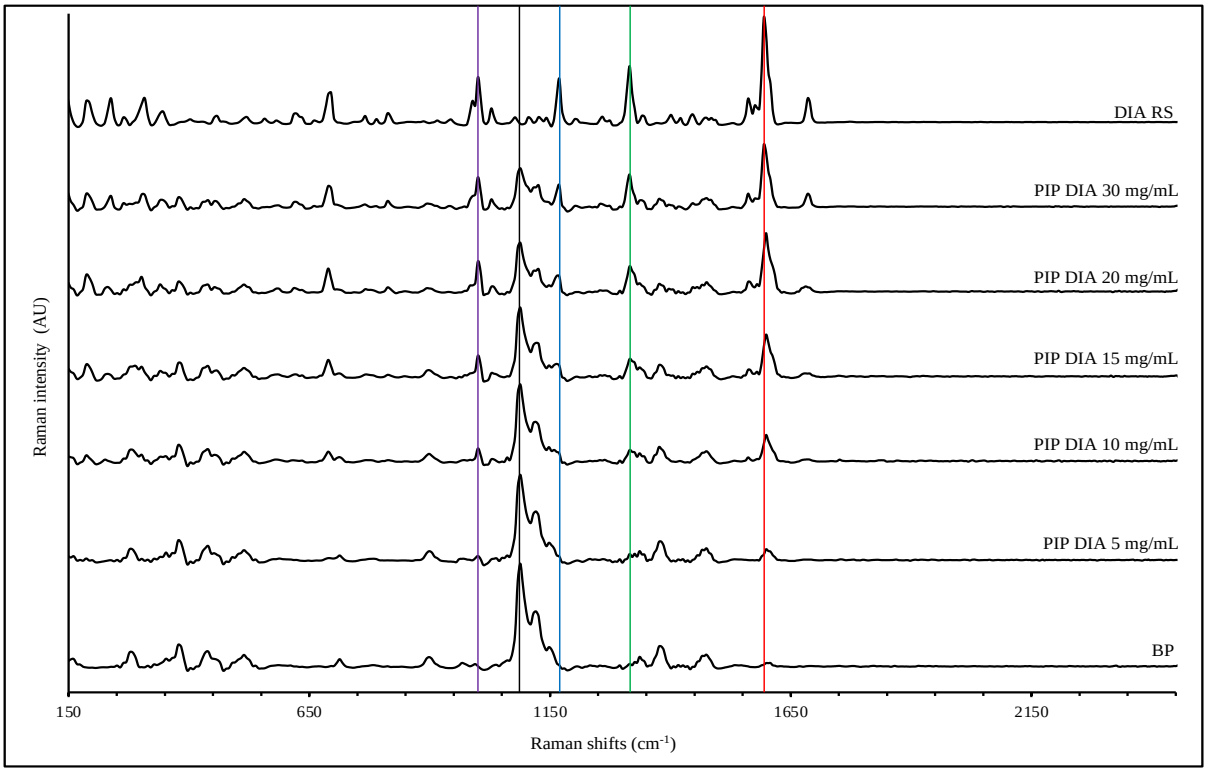

Figure 5.32. Raman Rigaku spectra of diazepam reference standard, diazepam pipetted on paper at 30, 20, 15, 10 and 5 mg/mL and BP (from top to bottom).

The line plots presented in Figures 5.29 to 5.32 show good promise for Raman analysis of reference standard pipetted on paper, while for the same psychoactive substances soaked on paper the concentration of the substances deposited on paper was so low that no characteristic peaks of the reference standard were visible.

The additional line plots of the spectra of the psychoactive substances (5F-PB-22, amphetamine, cocaine and diazepam) pipetted or soaked on simulated paper samples and collected using Raman Rigaku and Renishaw are reported in Appendices 4.23 and 4.24, respectively. While the full experimental and literature peaks assignment data are summarised in Appendix 4.9.

5.3.8.1. PCA classification of seven reference standards soaked on paper at five different concentrations and the seven neat reference standards spectra taken with Raman Renishaw (set 11) and Rigaku (set 12).

The set 11 PC-1 vs PC-2 2D scores plot (Figure 5.33) shows the two first PCs explaining 67% of the variance within the dataset. When the paper samples were prepared using the "soaking method" as opposed to the pipetting one, the 'mega cluster', in the left region of the scores plot, in the proximity of the BP samples, is more marked. This arises because of a higher dominance of the paper signal of the simulated paper samples due to the lower amount of substance deposited on them, and hence the reduced capabilities of the instrument to detect the substances. The samples that are projected away from the mega cluster on the scores plot but remain within the 95% ellipse CL are 5F-PB-22 R1 to R3 (CA-R1 to R3), amphetamine R1 to R3 (CB-R1 to R3), cocaine R1 to R3 (CE-R1 to R3), and paracetamol R1 to R3 (CG-R1 to R3). However, benzocaine R1 to R3 (CC-R1 to R3) and diazepam R1 to R3 (CF-R1 to R3) samples, fall outside the 95% ellipse CL. Substances that are outside of the 95% ellipse CL are strong scatters which have peaks with intensities like or greater than the blank paper peak, but at different wavenumbers, which is why they are separated so starkly from the 'mega cluster'.

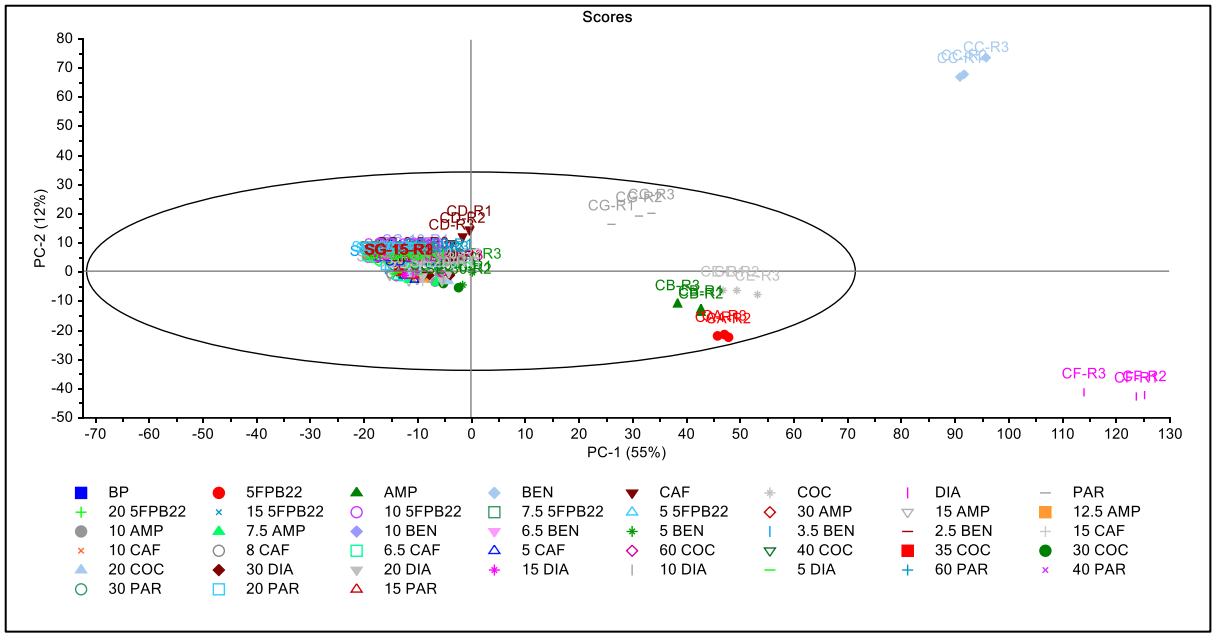

Figure 5.33. Set 11 PC-1 vs PC-2 2D scores plot.

All the samples falling outside the 95% ellipse CL, are also outliers which do not fit the model well and have high leverage. benzocaine R1 to R3 (CC-R1 to R3) and diazepam R1 to R3 (CF-R1 to R3) samples are outliers for the PC-1 (Figure 5.34 a), while only diazepam R3 (CF-R3) is an outlier for PC-2 (Figure 5.34 b), as it has a slightly higher intensity compared to the other two replicates (CF-R1 and R2).

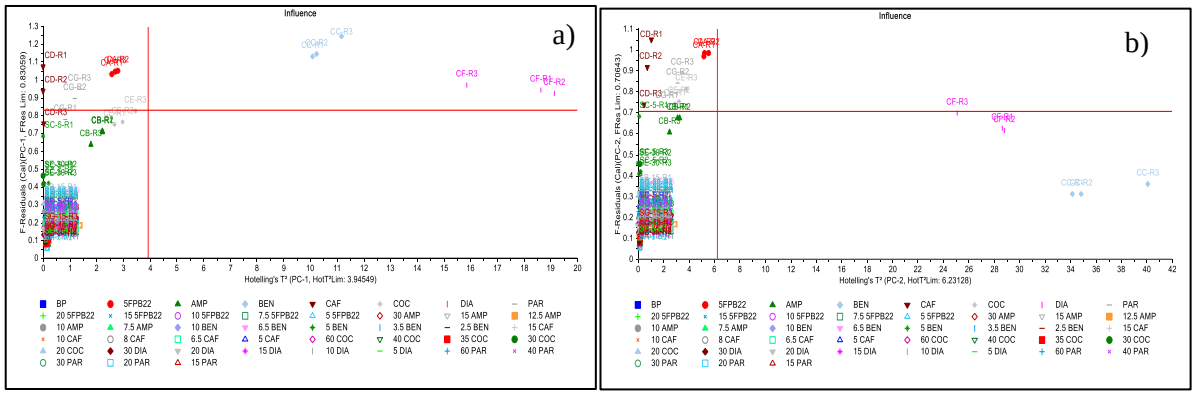

Figure 5.34. Set 11 F-residuals vs Hotelling T2 influence plots for a) PC-1 and b) PC-2.

The set 11 PC-1 loadings plot (Appendix 4.25- Figure A1) showed positive heavily loaded wavenumbers at 1604.32, 1594.09 and 105.77 cm^{-1}. While the PC-2 loadings plot (Appendix

4.25- Figure A2) showed positive heavily loaded wavenumbers at 1605.18, 1281.39 and 861.76 cm^{-1}, and negative heavily loaded wavenumber at 104.65 cm^{-1}. Consistent with the outliers highlighted in the influence plots, wavenumbers 1604.32, 1605.18, 1281.39 and 861 cm^{-1} are all related to benzocaine while 1594.09 cm^{-1} is related to diazepam. Wavenumbers 105.77 and 104.65 cm^{-1} as previously mentioned are associated with wavenumbers outside the fingerprint region, most likely to be noise, which is common to all the samples analysed. These wavenumbers are only found in Raman Renishaw dataset due to the shorter spectral range of Raman Rigaku which does not capture anything below the wavenumber 141 cm^{-1}.

The additional Raman Renishaw PCA plots of set 11 are available in Appendix 4.25.

The most concerning outliers benzocaine R1 to R3 (CC-R1 to R3) and diazepam R1 to R3 (CF-R1 to R3) were removed from the dataset, and the PCA recalculated. The newly generated PC-1 vs PC-2 2D scores plot (Appendix 4.26-Figure A1) of set 11 explained lower variance within the new dataset (60% vs 67%). Other samples are now becoming concerning outliers, namely 5F-PB-22 R1 to R3 (CA-R1 and R3), caffeine R3 (CE-R3) and paracetamol R2 and R3 (CG-R2 and R3) for PC-1 and 5F-PB-22 R1 to R3 (CA-R1 and R3), amphetamine R1 and R2 (CB-R1 and R2), benzocaine R1 and R2 (CC-R1 and R2) caffeine R1 to R3 (CE-R1 to R3), and paracetamol R2 and R3 (CG-R2 and R3) for PC-2. These samples have high leverage and do not fit the model.

The additional Raman Renishaw PCA plots of set 11 recalculated without outliers are available in Appendix 4.26.

The set 12 PC-1 vs PC-2 2D scores plot (Figure 5.35) shows the two first PCs explaining 66% of the variance within the dataset, which is similar to the results obtained with the Raman Renishaw set 11 (67%). Also, the way the samples cluster in the scores plot is similar to set 11, even though more samples are projected away from the BP samples, which are in the left region of the scores plot.

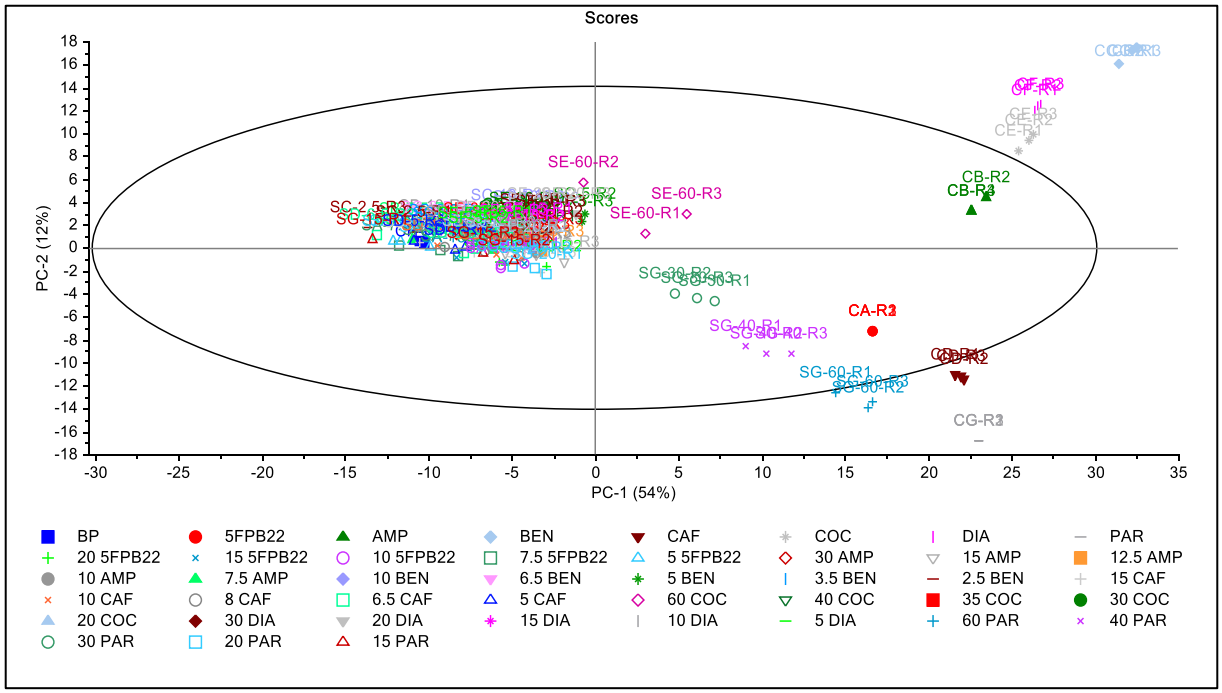

Figure 5.35. Set 12 PC-1 vs PC-2 2D scores plot.

Of all these samples falling out of the 95% ellipse CL, the most concerning outliers are benzocaine R1 to R3 (CC- R1 to R3), cocaine R1 to R3 (CE-R1 to R3), and diazepam R1 to R3 (CF- R1 to R3) for PC-1 (Figure 5.36 a) and benzocaine R1 to R3 (CC- R1 to R3), caffeine R1 to R3 (CD-R1 to R3), cocaine R1 to R3 (CE-R1 to R3), and diazepam R1 to R3 (CF- R1 to R3) for PC-2 (Figure 5.36 b), as these have high leverage and do not fit the model well.

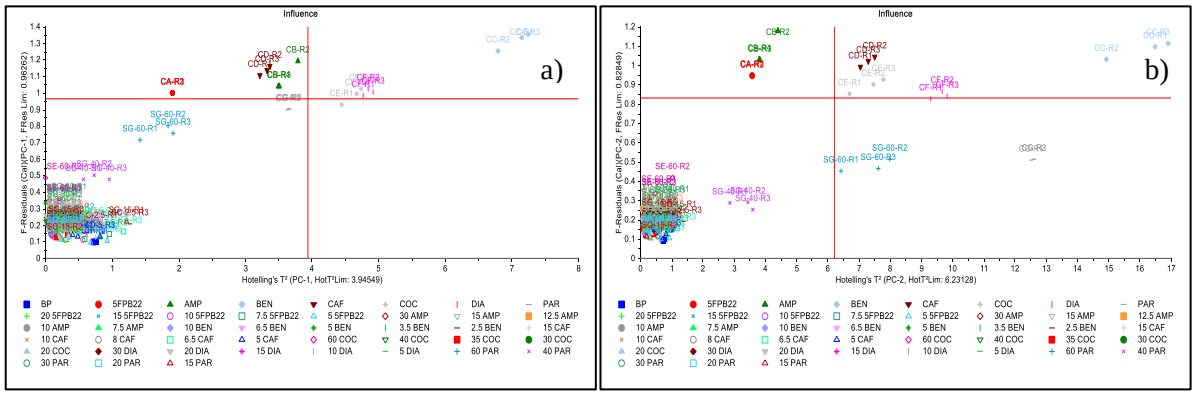

Figure 5.36. Set 12 F-residuals vs Hotelling T2 influence plots for a) PC-1 and b) PC-2.

The set 12 PC-1 loadings plot (Appendix 4.27- Figure A1) showed a positive heavily loaded region between 1603.35-1607.98 cm^{-1}, and a negative heavily loaded wavenumber at 1088.35

cm^{-1}. While the PC-2 loadings plot (Appendix 4.27- Figure A2) showed positive heavily loaded wavenumbers at 1000.24, 1598.71-1603.35, 1685.35 cm^{-1}, and negative heavily loaded wavenumber at 1325.77 and 1237.91 cm^{-1}. Consistently with the outliers highlighted in the influence plots, the region between 1603.35-1607.98 cm^{-1} is a region with peaks related to caffeine (~1604 cm^{-1}) and both amphetamine and benzocaine (~1608 cm^{-1}), wavenumbers at 1685.35, 1088.35 cm^{-1} are related to benzocaine, BP respectively. While wavenumber at 1000.24 is related to both cocaine and diazepam. The wavenumbers at 1237.91 and 1325.77 cm^{-1} do not seem to be related to any characteristic peak of the samples.

The additional Raman Rigaku PCA plots of set 12 are available in Appendix 4.27.

The most concerning outliers benzocaine R1 to R3 (CC- R1 to R3), caffeine R1 to R3 (CD-R1 to R3), cocaine R1 to R3 (CE-R1 to R3), and diazepam R1 to R3 (CF- R1 to R3) were removed from the dataset, and the PCA recalculated. The newly generated PC-1 vs PC-2 2D scores plot (Appendix 4.28- Figure A1) of set 12 explained higher variance within the new dataset (78% vs 66%). Other samples are now becoming concerning outliers, namely 5F-PB-22 R1 and R2 (CA-R1 and R2), amphetamine R1 to R3 (CB-R1 to R3) for PC-1 and amphetamine R2 (CB-R2) for PC-2, as they have high leverage and do not fit the model.

The additional Raman Rigaku PCA plots of set 12 recalculated without outliers are available in Appendix 4.28.

Looking at the result obtained with the Raman Rigaku using the in-built RMA only 9% (9/105) identification for any of the psychoactive substances and adulterants/cutting agents was achieved for set 12 (Appendix 4.14- Table A3), with a CC ranging between 0.99-0.59. The results were marked as positive using the same criteria described for set 10 in Section 5.3.5.1. The nine samples identified were all the paracetamol replicates soaked on paper at 60, 40 and 30 mg/mL samples. Interestingly paracetamol which is the only substance identified pipetted on paper at the three highest concentrations is not one of the top four substances with the higher Raman scattering activity. This could be since paracetamol solutions were made at higher concentrations compared to the other substances evaluated. While the remaining results of the simulated paper samples were matched to microcrystalline cellulose (MC) and calcium carbonate ($CaCO_3$) or a mixture of them, which as previously mentioned, could be interpreted as a positive match to BP.

5.3.8.2. PCA classification of the spectra of seven reference standards pipetted and soaked on paper at five different concentrations taken with Raman Renishaw (set 13) and Rigaku (set 14).

The set 13 PC-1 vs PC-2 2D scores plot (Figure 5.37) shows the two first PCs explaining 61% of the variance within the dataset. No pure reference standards were included in this dataset, the samples that are projected away from the 95% ellipse CL are the amphetamine 30 mg/mL R1 to R3 and (PB-30-R1 to R3), benzocaine 10 mg/mL R2 (PC-10-R2), benzocaine 6.5 mg/mL R1 (PC-6.5-R1) and diazepam 30 mg/mL R1 to R3 (PF-30-R1 to R3) pipetted on paper. benzocaine and diazepam samples outside of the 95% ellipse CL are strong scatters, while amphetamine is not well understood why is outside the ellipse.

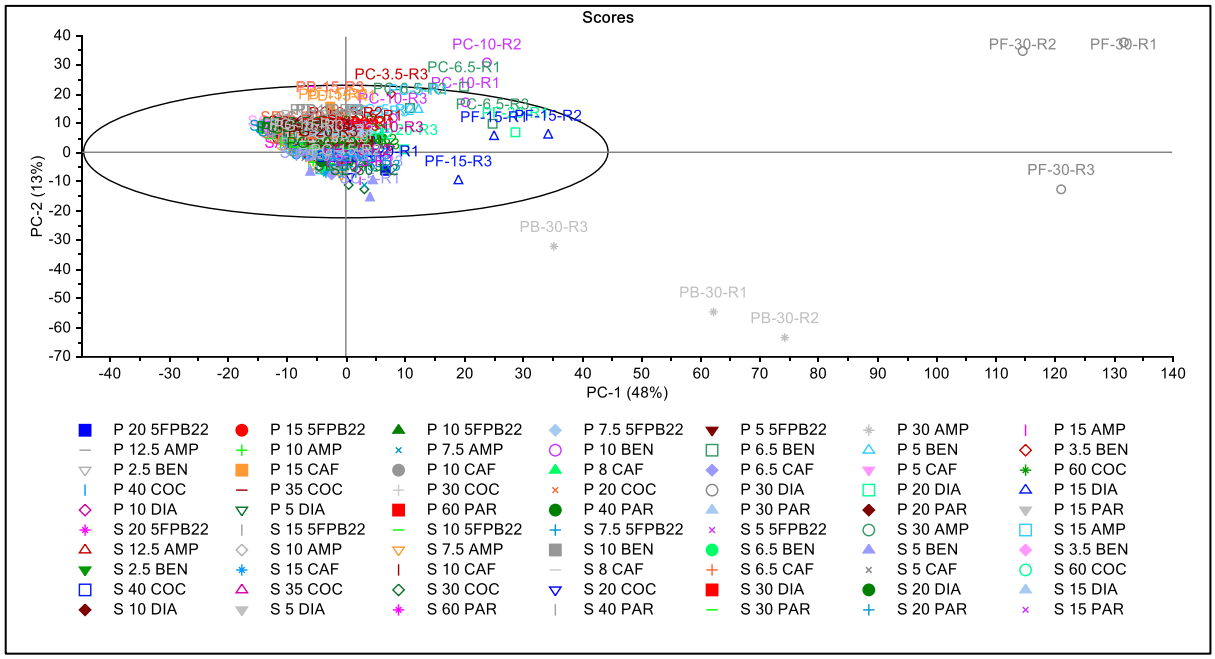

Figure 5.37. Set 13 PC-1 vs PC-2 2D scores plot.

Of all these samples falling out of the 95% ellipse CL, the most concerning outliers are amphetamine 30 mg/mL R1 and R2 and (PB-30-R1 and R2) and diazepam 30 mg/mL R1 to R3 (PF-30-R1 to R3) pipetted on paper for both PC-1 and PC-2 (Figure 5.38 a and b). Additionally, benzocaine 10 mg/mL R2 (PC-10-R2) and benzocaine 6.5 mg/mL R1 (PC-6.5-R1) are also concerning outliers only for PC-2 (Figure 5.38 b) as all of these have high leverage and do not fit the model well.

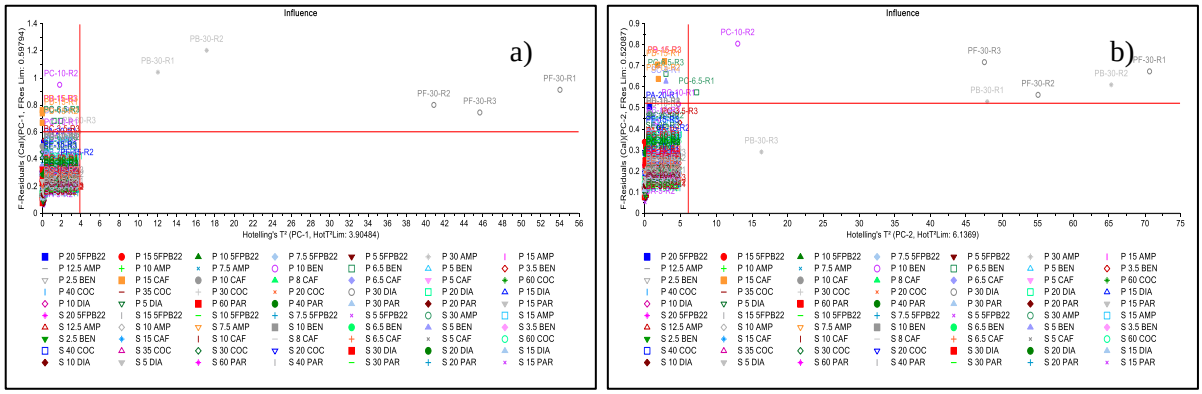

Figure 5.38. Set 13 F-residuals vs Hotelling T2 influence plots for a) PC-1 and b) PC-2.

The set 13 PC-1 loadings plot (Appendix 4.29- Figure A1) showed a positive heavily loaded region between1593.23-1592.38 and 104.65 cm^{-1}. While the PC-2 loadings plot (Appendix 4.29- Figure A2) showed positive heavily loaded wavenumbers at 1603.47 and between 1593.38-1592.38 cm^{-1}, and negative heavily loaded wavenumber at 1001.52 and between 976.55-975.59 cm^{-1}. Consistent with the outliers highlighted in the influence plots, wavenumbers 1593.23-1592.38 cm^{-1} are related to diazepam, 1603.47 cm^{-1} is related to benzocaine while 1001.52 and between 976.55-975.59 cm^{-1} are related to amphetamine. Wavenumbers 104.65 cm^{-1} as previously mentioned are associated with wavenumbers outside the fingerprint region, most likely to be noise, which is common to all the samples analysed.

The additional Raman Renishaw PCA plots of set 17 are available in Appendix 4.29.

The most concerning outliers amphetamine 30 mg/mL R1 and R2, (PB-30-R1 and R2), benzocaine 10 mg/mL R2 (PC-10-R2), benzocaine 6.5 mg/mL R2 (PC-6.5-R2) and diazepam 30 mg/mL R1 to R3 (PF-30-R1 to R3) pipetted on paper were removed from the dataset. Additionally, amphetamine 30 mg/mL R3 (PB-30-R3) was also removed as R3 of the amphetamine 30 mg/mL R1 and R2, (PB-30-R1 and R2) were having high leverage on the model The PCA was then recalculated. The newly generated PC-1 vs PC-2 2D scores plot of set 13 explained lower variance within the new dataset (51% vs 61%). The PC-1 vs PC-2 2D scores plot is presented in Figure 5.39, without labels, to give a better understanding of the spread of the samples.

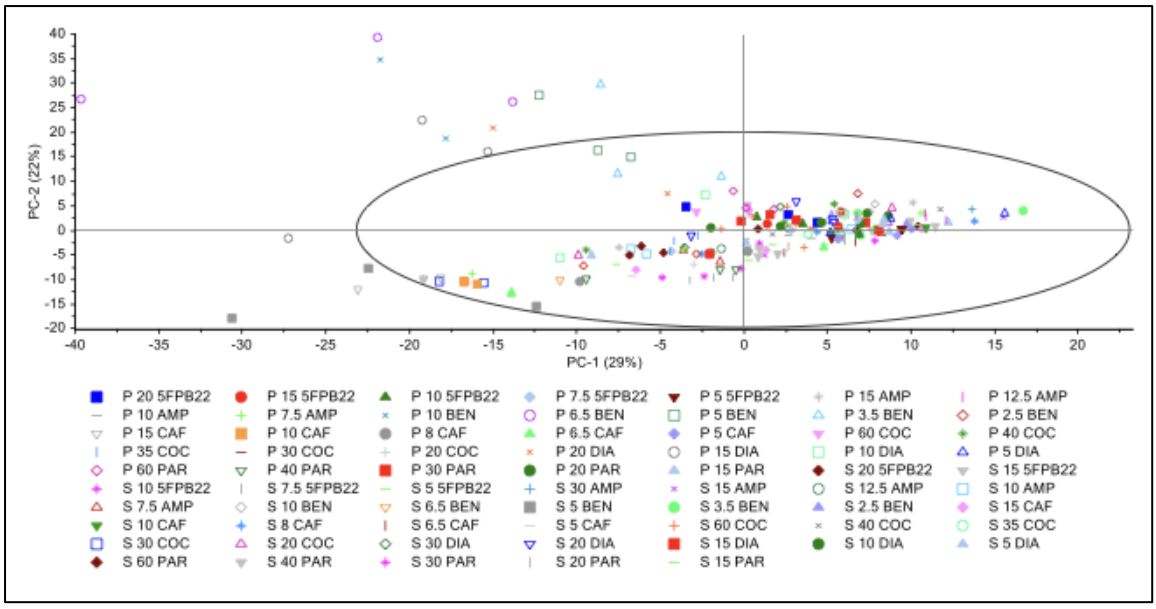

Figure 5.39. Set 13 PC-1 vs PC-2 2D scores plot recalculated without outliers.

Other samples are now becoming concerning outliers either for PC-1 or PC-2, namely benzocaine 10 mg/mL R1 (PC-10-R1), benzocaine 6.5 mg/mL R1 and R3 (PC-6.5-R1 and R3), caffeine 15 mg/mL R1 and R2 (PD-15-R1 and R2), diazepam 20 mg/mL R1 (PF-20-R1) and diazepam 15mg/ml R2 (PF-15-R2) pipetted on paper and benzocaine 5 mg/mL R1 (SC-5-R1) soaked on paper as they have high leverage and do not fit the model. However, removing the first layer of outliers which were dominating the PCA classification (Figure 5.37), the remainder samples spread out more showing potential for differentiation, which should be further investigated in future. out after removing the first set of outliers.

The full breakdown of the Figures is only shown here the first time these are mentioned unless a Figure is critical to the discussion.

The additional Raman Renishaw PCA plots of set 13 recalculated without outliers are available in Appendix 4.30.

The set 14 PC-1 vs PC-2 2D scores plot (Figure 5.40) shows the two first PCs explaining 61% of the variance within the dataset. Like set 13 no pure reference standards were included in this dataset. The samples that are projected outside the 95% ellipse CL are amphetamine 30mg/mL R3 (PB-30-R3), amphetamine 15 mg/mL R2 (PB-15-R2), benzocaine 10 mg/mL R1 and R3 (PC-10-R1 and R3), benzocaine 6.5 mg/mL R1 (PC-6.5-R1), diazepam 30 mg/mL R1 and R3

(PF-30-R1 and R3), diazepam 20 mg/mL R3 (PF-20-R1), paracetamol 60 mg/mL R1 to R3 (PG-60-R1 to R3), paracetamol 30 mg/mL R1 to R3 (PG-30-R1 to R3), pipetted on paper and paracetamol 60 mg/mL R1 to R3 (SG-60-R1 to R3) paracetamol 30 mg/mL R1 and R2 (SG-30-R1 and R2) soaked on paper.

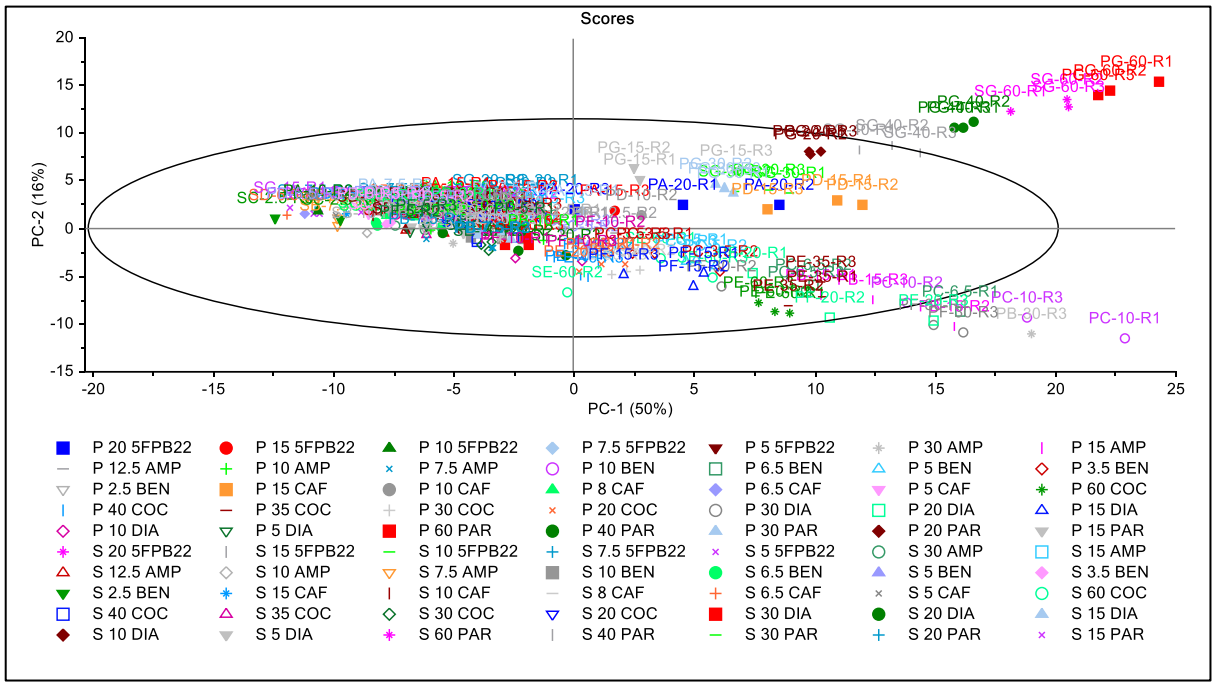

Figure 5.40. Set 14 PC-1 vs PC-2 2D Scores plot.

Of all these samples falling out of the 95% ellipse CL, the most concerning outliers for PC-1 and PC-2 are amphetamine 30mg/mL R3 (PB-30-R3), benzocaine 10 mg/mL R1 and R3 (PC-10-R1 and R3), benzocaine 6.5 mg/mL R1 (PC-6.5-R1), diazepam 30 mg/mL R3 (PF-30-R3) pipetted on paper (Figure 5.41 a and b). Additionally, paracetamol 60 mg/mL R1 (PG-60-R1) only for PC-1 and amphetamine 15 mg/mL R2 (PB-15-R2) only for PC-2 (Figure 5.41 b) are also concerning outliers as all of these have high leverage and do not fit the model well.

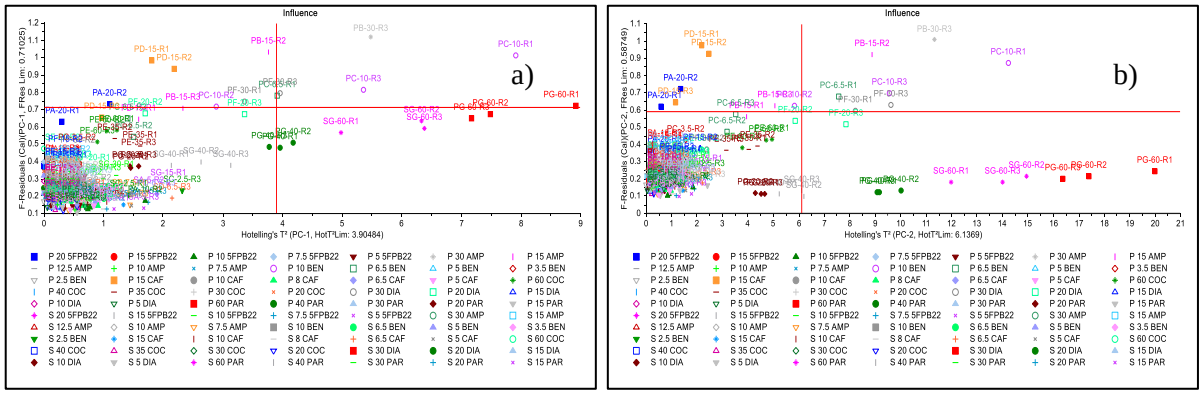

Figure 5.41. Set 14 F-residuals vs Hotelling T2 influence plots for a) PC-1 and b) PC-2.

The set 14 PC-1 loadings plot (Appendix 4.31- Figure A1) showed positive heavily loaded wavenumbers at 858.85, and 1607.98 cm^{-1}, and negative heavily loaded wavenumbers at 1088.35 and 1120.90 cm^{-1}. While the PC-2 loadings plot (Appendix 4.31- Figure A2) showed positive heavily loaded wavenumbers at 858.85, 1237.91 and 1325.77 cm^{-1}, and the negative heavily loaded region between 1603.35-1598.71 and at 1000.24 cm^{-1}. Consistent with the outliers highlighted in the influence plots, the region between 1603.35-1598.71 cm^{-1} is a region with peaks related to caffeine (~1604 cm^{-1}), and wavenumber at 1607.98 cm^{-1} is related to both amphetamine and benzocaine (~1608 cm^{-1}), wavenumber at 1000.24 is related to both cocaine and diazepam, wavenumbers at 858.85 and1088.35 cm^{-1} are related to both paracetamol and BP. The wavenumbers at 1237.91 and 1325.77 cm^{-1} do not seem to be related to any characteristic peak of the samples.

The additional Raman Rigaku PCA plots of set 14 are available in Appendix 4.31.

The most concerning outliers amphetamine 30 mg/mL R3 (PB-30-R3), amphetamine 15 mg/mL R2 (PB-15-R2), benzocaine 10 mg/mL R1 and R3 (PC-10-R1 and R3), benzocaine 6.5 mg/mL R1 (PC-6.5-R1), diazepam 30 mg/mL R3 (PF-30-R3) and paracetamol 60 mg/mL R1 (PG-60-R1) pipetted on paper were removed from the dataset. Additionally, benzocaine 10 mg/mL R2 (PC-10-R2), was removed due to having high leverage on the model. The PCA was then recalculated. The newly generated PC-1 vs PC-2 2D scores plot (Appendix 4.32-Figure A1) of set 14 explained higher variance within the new dataset (66% vs 61%). Other samples are now becoming concerning outliers either for PC-1 or PC-2, namely caffeine 15 mg/mL R2 (PD-15-R2), diazepam 20 mg/mL R2 and R3 (PF-20-R2 and R3) pipetted on paper, as they have high leverage and do not fit the model.

The additional Raman Rigaku PCA plots of set 14 recalculated without outliers are available in Appendix 4.32.

5.3.9. PCA classification of the Raman spectra of six reference standards binary mixture pipetted or soaked paper.

The pre-processing protocol [125] was also applied to i) the spectra of six reference standards binary mixtures pipetted on paper taken with Raman Renishaw (set 16) and Rigaku (set 17) ii) the spectra of six reference standards binary mixtures soaked on paper taken with Raman Renishaw (set 18) and Rigaku (set 19). Analysing paper impregnated with binary mixtures vs a single substance meant the addition of another layer of complexity to the analysis. Moreover, the solution concentrations used to prepare the simulated paper samples i.e., 20 mg/mL, were below the ones detectable for the single solution's substances simulated paper samples. Given the limitations identified in trying to determine a single PCA model for simulated paper samples and binary mixtures which contain both strong and weak Raman scatterers the data are not presented in the Chapter, however, are made available in the Appendices 4.33 to 4.36.

5.4. Conclusions

The optimal combined pre-processing protocol employed for this study [125] , consisted of two consecutive steps, namely baseline offset followed by mean normalisation. The pre-processing protocol selected was successfully validated by comparing calibration to validation sets, to ascertain whether the same substances were clustering together. The application of the pre-processing protocol successfully improved the classification and clustering of the pure substances of known composition in the scores, with replicates samples clustering close together. While the explained validated and calibrated variance plot remained almost invariant for both Raman Renishaw and Rigaku datasets.

Identification and classification of Raman spectra of reference standards mixtures have proved challenging with both instruments. Due to the inhomogeneous distribution of the two compounds in the mixtures (intra samples) and the impact of the orientation of oscillations (state of polarisation) of light waves of the excitation laser irradiating the molecules in the mixtures [141], replicates did not cluster together. benzocaine is a known strong Raman scattering substance due to the presence of high-intensity peaks related to functional groups found in its

structure. Therefore, often benzocaine signal swamped the signal from other reference standards, resulting in most mixtures containing benzocaine clustering together and making the identification of weaker scatterers in the mixtures challenging. Unsurprisingly, the most recurring wavenumbers e.g., 861.76, 1281.39, 1604.32 and 1682.13 cm^{-1} for Raman Renishaw and 864.59, 1279.54, 1607.98, 1685.35 cm^{-1} for Raman Rigaku, responsible for most of the variance in the first two PCs belonged to benzocaine reference standard or its mixtures. When the RMA was used, both components of the mixture were correctly identified in 86% (54/63) of the cases, which is a promising outcome.

The key factor playing a role in the identification of substances on paper are the i) strong/weak Raman activity displayed by the reference standards used to prepare the solutions; ii) initial reference standards concentration used to prepare the simulated paper sample; iii) simulated paper samples preparation's method e.g., soaking or pipetting; iv) intra and inter-sample variability due to the spread of the solution on paper (variable matrix) and, v) orientation of oscillations (state of polarisation) of light waves of the excitation laser irradiating the molecules [141]. Most of the simulated paper samples in the scores plot formed a 'mega cluster' in the proximity of BP samples, due to their Raman spectra being similar/almost identical to each other's especially when simulated paper samples were prepared at low concentration, highlighting the low capabilities of the instruments to detect such samples. When the simulated paper samples were prepared using the "soaking method" as opposed to the pipetting one, the 'mega cluster', was even more marked. This arose because of a higher dominance of the paper signal of the simulated paper samples prepared with the "soaking method" due to the lower amount of substance deposited on them. The final concentrations found on the simulated paper samples prepared using the "pipetting method" ranged between 0.125-3 mg/cm^2. For the simulated paper samples prepared using the "soaking method", the final concentration was not determinable unless using HPLC-UV or MS, which was out of the scope of this study. The most recurring wavelengths were also related to benzocaine and the BP (1088.35 cm^{-1}), the latter only applies to the Raman Rigaku datasets. While for the Raman Renishaw recurring wavenumbers located outside the fingerprint region were related to noise found at the lower wavenumbers. e.g., 105.77, 104.65 cm^{-1}. When the RMA was evaluated, samples prepared using the "pipetting method" resulted in a 42% (40/105) positive rate of identification of psychoactive substances and adulterants/cutting agents with the same range of solutions' concentrations, compared to only 9% (9/105) of positive rate for simulated paper samples

prepared using the “soaking method”. Most of the samples identified by the RMA were at the highest concentration evaluated e.g., 5F-PB-22 at 20 and 15 mg/mL, amphetamine at 15 mg/mL, benzocaine at 10mg/mL, caffeine at 15 mg/mL, cocaine at 60 and 35 (only R2) mg/mL, diazepam mg/mL at 30, 20 (only R1 and R2),15 and 10 (only R1 and R2) and paracetamol at 60, 40, 30 and 20 mg/mL replicate samples pipetted on paper, and paracetamol replicates soaked on paper at 60, 40 and 30 mg/mL replicate samples. Concerning outliers which did not fit the model and had high leverage, were found only when the PCA model was applied to simulated paper samples. When the concerning outliers were removed and a new PCA was generated, more outliers were found, meaning that the PCA model was not efficient anymore. However, when the first layer of outliers was removed from set 13, the remainder samples started spreading out, showing potential for differentiation which should be further investigated in future work. The line plots of the psychoactive substances i.e., 5F-PB-22, amphetamine, cocaine and diazepam reference standards pipetted on the simulated paper samples at five concentrations and collected using Raman Rigaku showed good promise for Raman analysis of such samples. Characteristic peaks were visible at the highest concentration of psychoactive substances reference standards pipetted on paper e.g., 5F-PB-22 pipetted on paper at 20 and 15 mg/mL; cocaine pipetted on paper at 60, 40, 35 and 30 mg/mL.

Raman Renishaw and Rigaku instruments showed different capabilities in the classification of the substances which could be attributed to the different spectral ranges and spectral resolution covered by the different instruments. Other factors contributing to the different performance of the instrument are laser spot diameter, laser power, laser wavelength and inbuilt pre-processing methods. Due to the different specifications of the instruments, cautions should be used when the comparison between the instrument is made. In this study cautions should be taken in generalising results as only seven psychoactive substances and adulterants/cutting agents have been evaluated. Knowing that synthetic cannabinoid is the most smuggled Npsychoactive substances class in prison future work should aim to include models containing more reference standards from the synthetic cannabinoid group.

Based on this chapter's findings it would be interesting to truncate the region where the most predominant peak of BP is present (*ca.* 1088 cm^{-1}) to see if a better PCA model for the classification of such samples could be achieved. However, in this study only one type of paper has been evaluated for detection of analytes on simulated samples, since using different paper

could potentially lead to different background spectra, it could be useful to simplify the analysis by removing the paper background. Therefore, analytes must be extracted from paper samples using a minimally invasive extraction method. Ideally, in the case of juridical samples, the extraction method should not damage the sample itself and should leave analytes in other areas of the samples for future analysis. Thus, in the next Chapter, a minimally invasive extraction method using agar gel was optimised using simulated samples and validated using a prison sample. The minimally invasive extraction method could be coupled in future with SERS, aimed to enhance the Raman signal and detect analytes in low concentrations [145,146] from such samples.

6. Optimisation of minimally invasive agar gel extraction of 5F-PB-22 from simulated paper samples using Design of Experiment.

To overcome the limitations of Raman coupled with PCA in detecting psychoactive substances and adulterants/cutting agents found on seized paper samples (Chapter 5), a minimally invasive extraction method using agar gel, was explored. Firstly, a reproducibility study was carried out to inform the Design of Experiment (DoE). Then the extraction of the model synthetic cannabinoid 5F-PB-22 from paper using agar gel was optimised. The optimisation of the extraction was carried out using the statistical approach DoE, which was divided into two phases: screening and optimisation. The model was then validated using the DoE optimised parameters employing simulated paper samples and further tested on the seized paper sample from prison analysed in Chapter 4. Therefore, work presented in this chapter aims to develop a minimally invasive extraction method suitable for seized paper samples, which could be needed as evidence in court after preliminary analysis.

6.1. Introduction

In UK prisons when paper matrices suspected of being impregnated with synthetic cannabinoids are found, these are screened by Ion Mobility Spectrometry (IMS). IMS is a non-destructive analytical technique, well suited for in-field analysis by non-expert users. However, this presents limitations such as reduced selectivity for substances that exhibit similar K_0 values (a difference < 0.025 $cm^2 V^{-1} s^{-1}$) and difficulty in detecting more than one analyte in a mixture. These limitations are overcome using gold standard analytical techniques such as Gas Chromatography-Mass Spectrometry (GC-MS) or High-Pressure Liquid Chromatography-Mass Spectrometry (HPLC-MS). However, it is important to preserve the integrity of such samples during analysis, as these may be needed in court, as juridical evidence. To this end, the optimisation of a minimally invasive extraction of a synthetic cannabinoid from paper using agar gel is investigated, in this chapter. The agar is made of a complex mixture of the polysaccharide agarose and agaropectin which, when associated with water, produces a thermo-reversible gel [147]. Agar is widely available, low cost and characterised by high biocompatibility and biodegradability. In prior studies, the use of agar gel was successful for the non-destructive microextraction of organic dyes from wool, silk, printed cotton and a panel painting mock [148]. Moreover, agar embedded with silver nanoparticles was found to be

extremely efficient for extraction and subsequent Raman analysis of organic dyes in works of art [149,150].

The optimisation of the agar extraction process was achieved using DoE, a multifactorial systematic approach, based on applied statistics aimed at understanding how process and product parameters affect response variables such as processability, physical properties, or product performance [151]. DoE evaluates different variables at the same time thus providing a large amount of information with the minimum number of experiments and identifying the relations or the interactions between the selected factors [152]. When compared to the traditional One-Factor-At-Time (OFAT) procedure, DoE provides the same result with fewer runs. With DoE, it is also possible to estimate factors' interactions and to allow multiple response optimisation, which is not achievable using OFAT.

DoE usually includes two different steps, namely screening and optimisation. For the screening step, Full Factorial Design (FFD), Plackett-Burman Design (PBD) and Fractional Factorial Design (FrFD) are the main designs available. A design is defined as a trial set-up which evaluates several factors at a given number of levels in a predefined number of experiments for the optimisation of the process [152]. The number of experiments (N) of the FFD can be expressed using Equation (6.1) below.

$$N = 2^k + C_p \qquad Equation\ (6.1)$$

Where 2 represents the number of levels; k is the number of factors and C_p is the number of centred points [153].

In the regular FFD, two levels are analysed for each of the factors, however, this can be customisable. One of the major advantages is the evaluation of the main factors and their interactions in a precise way. The PBD is used for robustness evaluation during method development, in which some interactions can be overlooked thus reducing the number of experiments. The maximum number of factors (k) that can be evaluated is expressed using Equation (6.2) below.

$$k = N - 1 \qquad Equation\ (6.2)$$

Where N is the number of experiments and is a multiple of four.

FrFD is a variation of the basic factorial design in which only a subset of the runs is used (Montgomery, 2005). In this case, the number of experiments (N) can be expressed using Equation (6.3) below.

$$\mathrm{N} = 2^{\mathrm{k-p}} + \mathrm{C_p} \qquad Equation\ (6.3)$$

Where 2 represents the number of levels; k is the number of factors, p is the number of independent design generators and $\mathrm{C_p}$ is the number of centred points. The FrFD takes into account only a low number of main effects and lower order of interactions [153]. Despite DoE wide use, it is not possible to discern the impact of each of the employed factors and their relations, as some of the factors are evaluated together (in this case it is said that factors are confounded). In addition to the number of runs set by the experimental design, centre points can be added. These are points at the centred value of all factor ranges which provide a measure of the reproducibility of the process and check for curvature.

The second step, that is the optimisation step is advantageous to determine the region in which the important factors lead to the best possible response [153]. The Response Surface Methodology (RSM) is the technique employed for this purpose. Based on statistical knowledge, RSM is useful to make predictions about the behaviour of a group of observations. In analytical chemistry, three different RSM designs are the most often employed: Central Composite Design (CCD), Box-Behnken Design (BBD) and Doehlert Design. CCD is one of the most common methods used for the optimisation of DoE. The CCD includes a two-level factorial design, a star design, and a centred point. The number of experiments (N) can be expressed using the Equation (6.4) below.

$$\mathrm{N} = K^2 + 2\mathrm{k} + \mathrm{C_p} \qquad Equation\ (6.4)$$

Where k is the factors numbers, 2 represents the number of levels; k is the number of factors and $\mathrm{C_p}$ is the number of centred points.

This study aims to optimise a minimally invasive gel-solid extraction method capable of yielding high recovery rates of psychoactive substances from paper, using the statistical approach DoE. The DoE was divided into two phases: screening and optimisation. The objectives are to i) carry out a reproducibility study to inform the DoE ii) screen 5 factors which

potentially can influence the extraction of 5F-PB-22 from paper using agar gel using 2^5 FFD; ii) optimise the factors, previously identified as significantly influencing the extraction process in the FFD, using a 2-factors CCD; iii) validate the model testing the optimum parameters identified by the DoE, on five simulated paper samples replicate containing 5F-PB-22 and on a seized paper sample from prison known to contain 5F-ADB (Chapter 4).

6.2. Material and methods

6.2.1. Chemicals and reagents

5F-PB-22 reference standard (> 99% purity) was obtained from CHIRON AS (Trondheim, Norway) while the 5F-PB-22 purified product (UHSOP/2020/P003, > 99% purity) was used for the preparation of the simulated paper sample. Ethyl acetate (EtOAc) laboratory reagent grade orthophosphoric acid, HPLC grade methanol (MeOH) and acetonitrile (all > 99% purity) were obtained by Fisher Scientific (Loughborough, UK). Common grade agar flakes (Clearspring, UK) were purchased online. A common A4 printing 80 g/m^2 density paper sheet (Envirocopy A4 500 sheet; ECF; 100% Recyclable paper; ISO 9706 Long Life paper) was employed to cut 55 x 1 cm^2 pieces of paper to prepare the simulated paper samples.

6.2.2. Seized paper samples

The A5 paper sheet from the evidence bag labelled UHSOP/2018/PR025 Chapter 4, Section 4.2.3.2., was used to validate the optimized method.

6.2.3. Instrumentation

6.2.3.1. High-Performance Liquid Chromatography-Ultraviolet-Visible

For instrument and parameter employed see Chapter 5 Section 5.2.2.2.

6.2.3.2. Ultra-Performance Liquid Chromatography-Photodiode Array Detector-Quadrupole Dalton-Mass Spectrometry

For instrument and parameter employed see Chapter 4 Section 4.2.2.1.

6.2.4. Sample preparation

6.2.4.1. Agar gel preparation

The agar gel was prepared by mixing agar flakes with water at three concentrations of 2, 3 and 4% w/v for the FFD screening phase and at five concentrations of 1.6, 1.7, 1.95, 2.2. and 2.3% w/v for the CCD optimisation phase. The weighed amount of agar flakes was transferred into a conical flask and placed on a hotplate stirrer at ~200 ºC and 200 rpm. The agar gel was left to boil for 12-15 minutes, poured into a petri dish, allowed to cool down to room temperature and then stored in a sealed box in the fridge (~ 4 ºC). The same procedure was repeated for all the different concentrations.

6.2.4.2. 5F-PB-22 simulated paper samples preparation and extraction

Around 100 mg 5F-PB-22 were weighed and dissolved in MeOH to obtain a 20 mg/mL solution. Sixty pieces of paper of 1 cm^2 were cut from common printing A4 80 g/m^2 density paper sheets with the help of a stencil. Five µL of the 5F-PB-22 solution was pipetted onto the 1 cm^2 piece of paper. The piece of paper was allowed to dry, held carefully in a corner by tweezers. Once dried, the simulated paper sample was laid onto a glass slide to avoid any loss of solution containing 5F-PB-22 by contact with surfaces, which would lead to irreproducibility. The procedure was repeated for each simulated paper sample.

The agar gels prepared at different w/v concentrations (2, 3 and 4% w/v for the FFD screening phase or 1.6, 1.7, 1.95, 2.2. and 2.3% w/v for the CCD optimisation phase) were cut into circles with an area of 0.385 cm^2 and thickness 0.4 cm, with the help of a stencil. Prior to application of the gels to the simulated paper samples for extraction, 10 µl of MeOH was applied to the agar gel bead. Then the agar gel bead was placed onto the 1 cm^2 simulated paper sample and a glass microscope slide with a variable weight set on (28.3, 56.7 or 85 grams) laid on it for a variable amount of time (30, 75 or 120 sec). Following the extraction, the agar gel bead was placed in a screw cap vial, with one mL of HPLC grade MeOH, to avoid any evaporation of the solvent. The vial was placed in a sonicator, and extraction was performed. The vials were sonicated for a variable amount of time (5, 7.5 or 10 min for the FFD screening phase or 7.5, 8, 19, 12 or 12.8 min for the CCD optimisation phase) and the extraction procedure consecutively repeated up to four times. The solution was filtered through a 0.2 µm pore size

PTFE hydrophobic filter (Thermo-Fisher, UK) and transferred to an HPLC vial for analysis. A MeOH blank was analysed at the beginning and the end of the experimental runs. Moreover, positive and negative controls were prepared and submitted for analysis. The negative control consisted of a blank paper sample (without 5F-PB-22) extracted using agar with the same parameters used for the centred points. The positive control consisted of a 5F-PB-22 simulated paper sample extracted with 0.5 mL of MeOH. Three repeated injections were performed for each sample.

6.2.5. Reproducibility study

A reproducibility study was carried out to estimate the reproducibility of the extraction process of 5F-PB-22 from simulated paper samples using agar gel which was then employed to perform the DoE. The reproducibility was evaluated over five replicate simulated paper samples and two consecutive extractions. The simulated paper samples were prepared and extracted according to Section 6.2.4.2. The parameters employed to evaluate the extraction were the ones used for the centred point (Table 6.1). The extracts were filtered through a 0.2 µm pore size PTFE hydrophobic filter (Thermo-Fisher, UK) and transferred to an HPLC vial for analysis. A MeOH blank was analysed at the beginning and the end of the experimental runs. Moreover, positive and negative control were prepared and submitted for analysis. The negative control consisted of a blank paper sample (without 5F-PB-22) extracted using agar. While the positive consisted of a 5F-PB-22 simulated paper sample extracted with 0.5 mL of MeOH. Three repeated injections were performed for each sample.

6.2.6. Statistical design of experiment

6.2.6.1. Screening phase: Full Factorial Design

No previous studies exploring minimally invasive agar gel extraction of analytes from paper samples were carried out, therefore the choice of factors to screen was based on similar available literature and scientific experience. Five factors (A-E) with two levels each (Table 6.1), were selected as potentially influencing the process.

Table 6.1. Factors and levels screened in the 2^5 FFD.

Factors evaluated		Units	Low levels	Centred points	High levels
A	Agar concentration	% w/v	2	3	4
B	Extraction time	sec	30	75	120
C	Weight applied	grams	28.3	56.7	85
D	Sonication time	min	5	7.5	10
E	Extraction number	N.A.	2	3	4

The first factor evaluated was the concentration of the agar flakes (A) used to prepare the gel, which influences the texture of the agar gel. To this end, two levels of Factor A at 2 and 4% w/v were evaluated. The choice of the concentration of the agar was based on published studies in which agar gel was used to micro-extract organic dyes from artworks without damaging them (Platania, 2013). The extraction time (B) e.g., the time agar bead has been applied onto the simulated paper sample impregnated with 5F-PB-22 and the weight applied (C) during this time, all of which were thought to affect the interactions between the agar gel pipetted with MeOH and the 5F-PB-22 on the simulated paper sample. The pressure applied by 28.3 and, 85 g weights and the extraction time of 30 and 120 sec were evaluated. Additionally, the sonication time (D) was evaluated, as it could affect the re-extraction process of the 5F-PB-22 from the agar to the MeOH. The samples were sonicated from 5 to 10 min depending upon the parameter selected for the run. The number of consecutive extractions (E) of the 5F-PB-22 from the agar gel bead evaluated were 2 and 4. The values were selected according to a previous study on percentage recovery over 5 consecutive extractions of a synthetic cannabinoid on simulated paper samples (Chapter 4).

The screening phase of the study involved the use of an FFD consisting of a 2^5 factorial design and eight-centred points, for a total of 40 experimental runs. Note that the centre points are required to i) assess the repeatability of the process and ii) check for a possible curvature in the resulting regression model. The FFD experimental matrix design is presented in Table 2. To determine the relationship between the measured response and the statistically significant variables, Analysis of Variance (ANOVA) was performed. The analyses were performed using Fisher's 'F-test',

The behaviour of the system was explained by the five-factor first-order polynomial Equation (6.5) below.

$$Y = \beta_0 + \sum_{i=1}^{n} \beta_i x_i + \sum_{i=1;\, j=1;\, i \neq j}^{n} \beta_{ij} x_{ij} + \sum_{i=1;\, j=1;\, k=1;\, i \neq j \neq k}^{n} \beta_{ijk} x_{ijk} + \sum_{i=1;\, j=1;\, k=1; l=;\, i \neq j \neq k \neq l}^{n} \beta_{ijkl} x_{ijkl} + \beta_n x_n \qquad Equation\ (6.5)$$

Where Y is the predicted response; β_0 is the constant process effect; β_i is the linear effect of factor X_i; β_{ij}, β_{ijk}, β_{ijkl} and β_n are the interactions of the first order of the factors X_{ij}, X_{ijk}, X_{ijkl}, and X_n, respectively. Since the factor evaluated were 5, n=5.

Stat-Ease Design-Expert (DE) v11 was used to design the FFD and analyse the data. The runs were executed randomly according to the DE software, to ensure the conditions in one run do not depend on the conditions of the previous one and do not predict the condition in the subsequent ones (Carroll & Tobias, 2012). The simulated paper samples were prepared using the method described in Section 6.2.4.2. and each sample was treated using a different combination of factors and levels. The FFD experimental matrix design is presented in Table 6.2.

Table 6.2. Level and Factors employed for the FFD experimental runs.

Experimental runs	Factor A: Agar concentration (% w/v)	Factor B: Extraction time (sec)	Factor C: Weight applied (grams)	Factor D: Sonication time (min)	Factor E: Extraction number
18	4	30	28.3	5	4
22	4	30	85	5	4
2	4	30	28.3	5	2
32	4	120	85	10	4
23	2	120	85	5	4
19	2	120	28.3	5	4
4	4	120	28.3	5	2
21	2	30	85	5	4
10	4	30	28.3	10	2
34	3	75	56.7	7.5	3
28	4	120	28.3	10	4
27	2	120	28.3	10	4
11	2	120	28.3	10	2
8	4	120	85	5	2
25	2	30	28.3	10	4
7	2	120	85	5	2
24	4	120	85	5	4
37	3	75	56.7	7.5	3
14	4	30	85	10	2
12	4	120	28.3	10	2
29	2	30	85	10	4
1	2	30	28.3	5	2
5	2	30	85	5	2
16	4	120	85	10	2
38	3	75	56.7	7.5	3
15	2	120	85	10	2
31	2	120	85	10	4
3	2	120	28.3	5	2

40	3	75	56.7	7.5	3
36	3	75	56.7	7.5	3
6	4	30	85	5	2
13	2	30	85	10	2
17	2	30	28.3	5	4
35	3	75	56.7	7.5	3
39	3	75	56.7	7.5	3
9	2	30	28.3	10	2
30	4	30	85	10	4
26	4	30	28.3	10	4
20	4	120	28.3	5	4
33	3	75	56.7	7.5	3

6.2.6.2. Screening phase: Central Composite Design

Once the results from the FFD were obtained, factor reduction was performed. A Central Composite Design (CCD) was carried out, with only two factors agar concentration (A) and sonication time (B). Star points were chosen with a rotatable alpha of 1.41421, set by the software as evaluating a number of factors k < 6.

Table 6.3. Factors and levels optimised in the 2 factors CCD.

Factors evaluated		Units	α -	Low levels	Centred points	High levels	α +
A	Agar concentration	% w/v	1.6	1.7	1.95	2.2	2.3
B	Sonication time	min	7.5	8	10	12	12.8

To note that after the FFD, the following factors were fixed: extraction time (120 sec), weight applied (85 grams), and extraction number (2). Once again, to determine the relationship between the measured response and the statistically significant variables ANOVA at a 95% confidence interval was performed.

The behaviour of the system was explained by the two-factor second-order polynomial Equation (6.6) below.

$$Y = b_0 + \sum_{i=1}^{n} b_i x_i + \sum_{i<j}^{n} b_{ij} x_i x_j + \sum_{i=1}^{n} b_{ii} x_i^n \qquad Equation\ (6.6)$$

Where Y is the predicted response, β_0 is the constant process effect, β_i is the linear effect of the factor X_i, β_{ij} are the interactions of the first order of the factors X_{ij}, and β_{ii} are the quadratic effects of X_i.

Stat-Ease DE v11 was used to design the CCD and analyse the data. The runs were executed randomly according to the DE software. The simulated paper samples were prepared using the method described in Section 6.2.4.2. and each sample was treated using a different combination of factors and levels. The CCD experimental matrix design is presented in Table 6.4.

Table 6.4. Level and Factors employed for the CCD experimental runs.

Experimental runs	Factor A: Agar concentration (% w/v)	Factor B: Sonication time (min)
11	1.95	10
4	2.2	12
7	1.95	7.17
1	1.7	8
8	1.95	12.8
12	1.95	10
6	2.3	10
13	1.95	10
9	1.95	10
10	1.95	10
3	1.7	12
2	2.2	8
5	1.6	10

6.2.6.3. Validation of the model

The model was validated by running five confirmation runs on simulated paper samples using the same parameters as the optimised conditions, being 2% agar concentration, and 10.95 min sonication time, whilst the extraction time, weight applied and extraction number were fixed at 120 sec, 85 grams and 2, respectively. The Confidence Interval (CI) at 95% was calculated using Equation (6.7).

$$CI = \bar{x} \pm Z\frac{s}{\sqrt{n}} \qquad Equation\ (6.7)$$

Where $\bar{x}$ represents the sample mean, Z is the Z-score at 95% confidence level (1.959964 σ), s is the standard deviation and n is the sample size.

The percentage extraction was calculated, and the results obtained were then compared to the ones obtained in Section 6.3.2. Moreover, the application of the optimised extraction method was tested on the seized paper sample from prison UHSOP/2018/P025, which content was already established in Chapter 4. The sampling was executed on the subunit A18 of the sample (Chapter 4- Section 4.4), as the adjacent subunit A17 was known to contain the highest concentration of the synthetic cannabinoid 5F-ADB of 0.055 mg/cm^2.

6.3. Results and discussion

6.3.1. Reproducibility study

The reproducibility of the extraction process of 5F-PB-22 from simulated paper samples using agar gel was carried out to gain some preliminary knowledge before running the DoE. The average of the AUC resulting from the two consecutive extractions over five replicates was 81.05 ± 6.07 AU. The Relative Standards Deviation (RSD) was also calculated and found to be 7.49%. Considering the complexity of the several steps involved in both the simulated sample preparation and their extraction using agar gel, the overall reproducibility of the process was deemed acceptable. Moreover, the quantity of 5F-PB-22 extracted from the simulated samples was found to be 0.91 ± 7.32 µg/mL, corresponding to 1.20 ± 0.09% of the total 5F-PB-22 recovered. The quantity of analyte extracted from simulated paper samples using this process was lower in comparison to the traditional solvent extraction performed in Chapters 4 and 5. However, this was expected as the process can be considered a micro-extraction, aimed to take out only a fraction of the analyte. The extracts resulting from paper samples are envisioned to be analysed only qualitatively for screening analysis, with techniques with a LOD in the order of the µg/mL.

6.3.2. Screening phase using Full Factorial Design

Once the experimental data were collected, the AUC values related to the quantity of 5F-PB-22 extracted from the agar gel bead, were input into the DE software for analysis. The half-normal plot is the primary model selection tool for factorial designs displaying the absolute

value of all effects, which are plotted as squares. The colour coding will provide details on the effects i.e., orange is positive, blue is negative. To note that no transformation was applied to the data. Firstly, starting from the factor with the largest effect: sonication time (D), all the terms that fell below or to the right of the red line i.e. A, AE, CDE, AD, CD, AB, ADE, BE, BC, E, ABC, C, BD, ABD, DE, ABE, B and ABCD, were selected (Figure 6.1). These are the statistically significant ones. There are however factors that have been kept despite their lack of statistical significance: CE, ACD, and BCD; these are needed to ensure hierarchy within the model as they feature in other interactions.

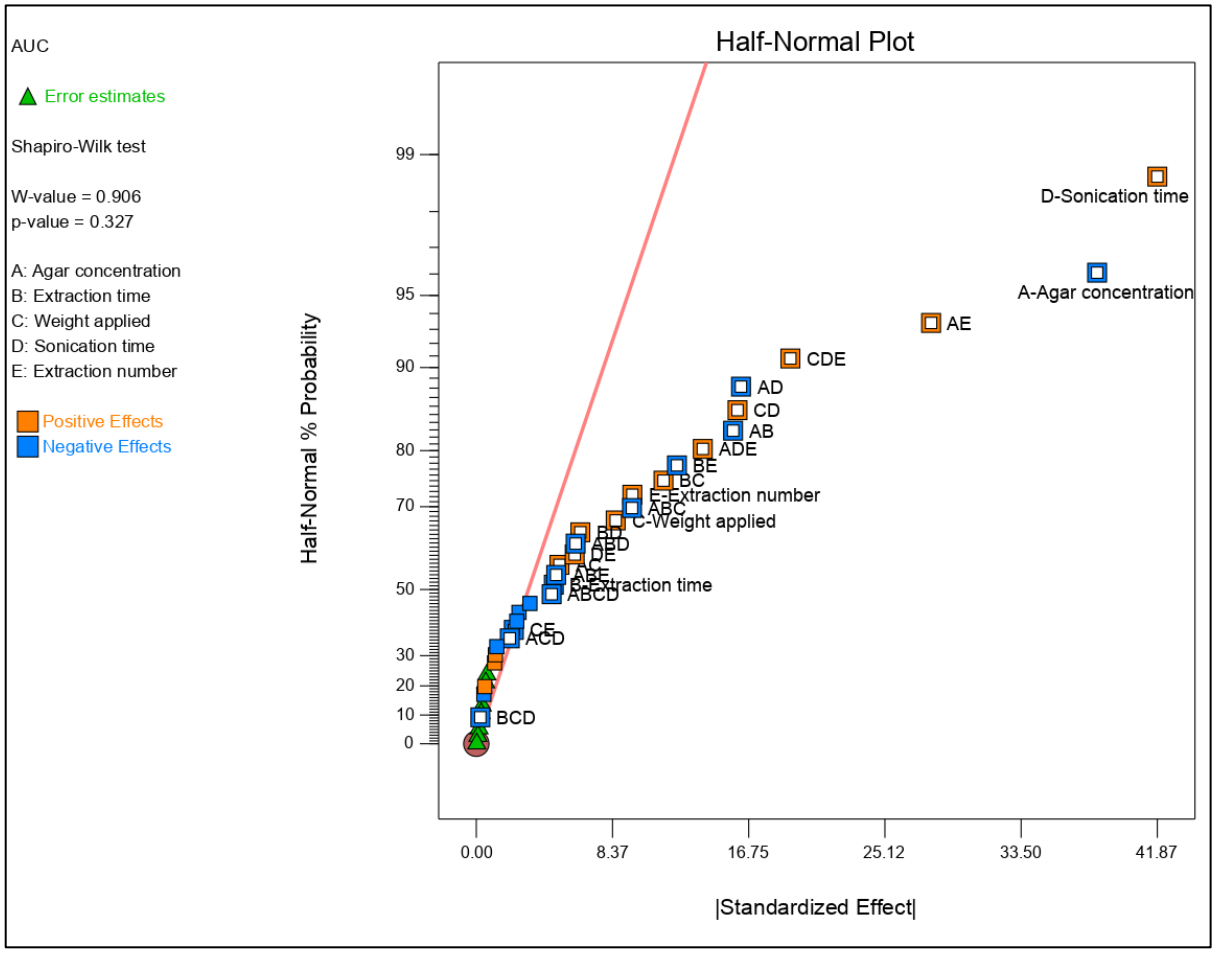

Figure 6.1. Half-Normal Plot of the 2^5 FFD model.

The full ANOVA results of the 2^5 FFD are shown in Table 6.5.

Table 6.5. Summary of the ANOVA results of the 2^5 FFD

Source	Sum of Squares	df	Mean Square	F-value	p-value	Note
Model	48750.98	23	2119.61	68.17	< 0.0001	Significant
A-Agar concentration	11658.21	1	11658.21	374.96	< 0.0001	Significant
B-Extraction time	181.83	1	181.83	5.85	0.0288	Significant
C-Weight applied	588.01	1	588.01	18.91	0.0006	Significant
D-Sonication time	14028.07	1	14028.07	451.18	< 0.0001	Significant
E-Extraction number	737.12	1	737.12	23.71	0.0002	Significant
AB	1994.7	1	1994.7	64.16	< 0.0001	Significant
AC	209.32	1	209.32	6.73	0.0203	Significant
AD	2119.43	1	2119.43	68.17	< 0.0001	Significant
AE	6256.49	1	6256.49	201.23	< 0.0001	Significant
BC	1060.86	1	1060.86	34.12	< 0.0001	Significant
BD	327.64	1	327.64	10.54	0.0054	Significant
BE	1218.03	1	1218.03	39.18	< 0.0001	Significant
CD	2065.26	1	2065.26	66.42	< 0.0001	Significant
CE	42.79	1	42.79	1.38	0.2591	Kept for hierarchy
DE	293.37	1	293.37	9.44	0.0078	Significant
ABC	733.9	1	733.9	23.6	0.0002	Significant
ABD	298.92	1	298.92	9.61	0.0073	Significant
ABE	193.19	1	193.19	6.21	0.0249	Significant
ACD	33.93	1	33.93	1.09	0.3127	Kept for hierarchy
ADE	1552.64	1	1552.64	49.94	< 0.0001	Significant
BCD	0.4997	1	0.4997	0.0161	0.9008	Kept for hierarchy
CDE	2984.77	1	2984.77	96	< 0.0001	Significant
ABCD	172.03	1	172.03	5.53	0.0327	Significant

Curvature	30.03	1	30.03	0.9657	0.3413	Not significant
Residual	466.38	15	31.09			
Lack of Fit	229.93	8	28.74	0.8509	0.591	Not significant
Pure Error	236.45	7	33.78			
Cor Total	49247.38	39				

Table 6.5 highlights the factors whose p-value was above 0.05 at 95% confidence level: ACE, BCE, ABCE, ABDE, ACDE, BCDE, ABCDE. Their effect on the model's response is not statistically significant, and they can be removed to simplify the model. By far, the factors with the largest statistical significance are the agar concentration (A) and the sonication time (D), followed by the interaction between the agar concentration and the extraction number (AE).

To note that the F-value of 68.17 implies the model is significant. In fact, the model's p-value is < 0.0001. There is only a 0.01% chance that an F-value this large could occur due to noise. Both the curvature and the lack of fit are insignificant. In terms of Fit statistics, the r^2 is equal to 0.9905; the Adjusted r^2 is equal to 0.9760; the Predicted r^2 is equal to 0.9190 and finally, the Adequate precision is equal to 33.6492. These are particularly good values. Specifically, the Predicted r^2 and the Adjusted r^2 are in reasonable agreement i.e., the difference is less than 0.3; and the Adequate precision, which measures the signal-to-noise ratio, is much larger than 4, the minimum desirable, indicating an adequate signal. This model can be used to navigate the design space.

The following diagnostic plots were analysed: normal plot of residual (or normal probability plot); predicted vs. actual; residuals vs. run. To note that externally studentized residuals are set as default, which improves the detection of abnormalities in the analysis.

The normal plot of residuals is used to determine whether the residuals follow a normal distribution. Ideally, the normal plot of residuals should follow a straight line, indicating no abnormalities, however, some scatter can be expected even within normal data. In Figure 6.2 the normal plot of residuals of the FFD model shows a random distribution of residuals which indicates a good fit of the data.

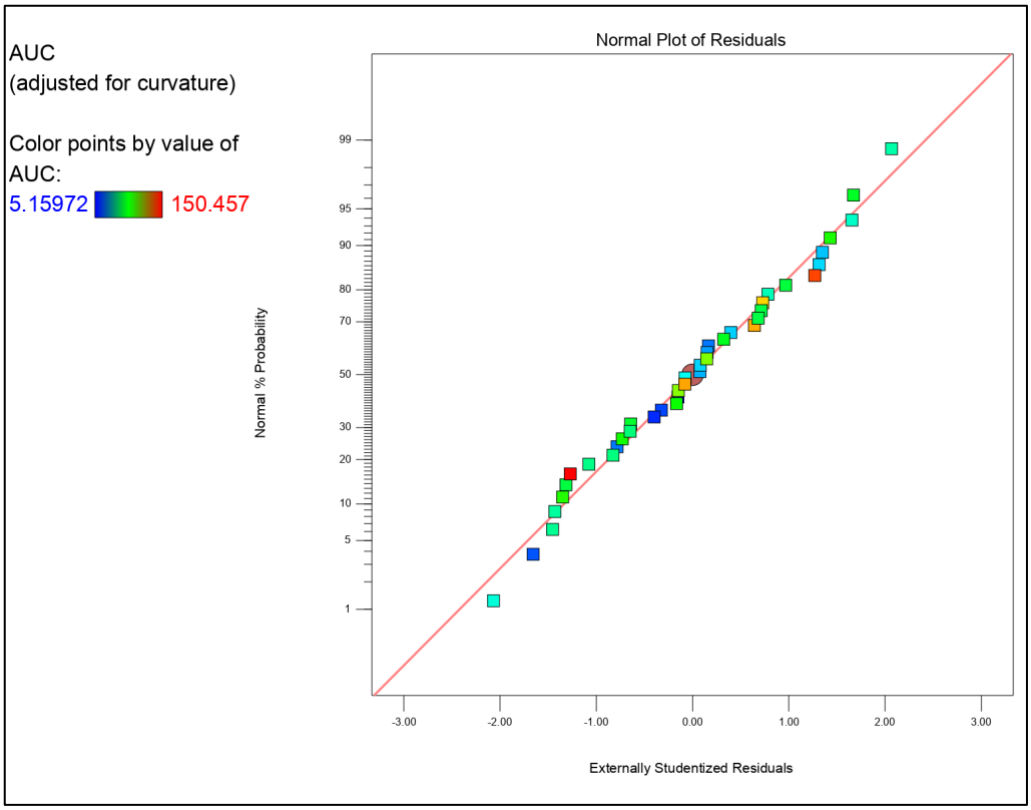

Figure 6.2. Normal plot of residual of the FFD model.

The predicted vs actual errors plot predicts the response values versus the actual response values. This plot is used to detect a value, or group of values, that are not easily predicted by the model. In Figure 6.3 The predicted vs actual errors plot of the FFD model shows a random distribution of residuals which indicates a good fit of the data.

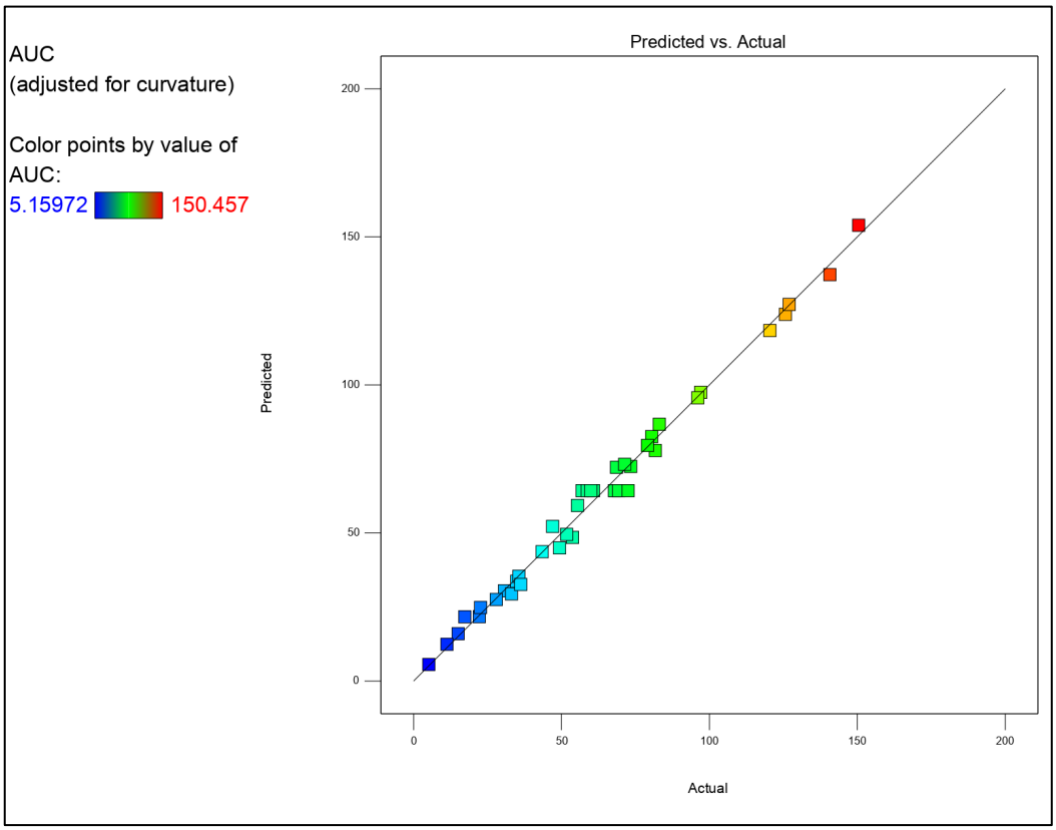

Figure 6.3. Predicted vs actual errors plot of the FFD model.

In the residuals vs. the experimental run order plot, the DE software provides upper and lower red lines that are similar to 95% confidence control limits. It checks for hidden variables (outliers) that may have influenced the response during the experiment. The plot should follow a random scatter distribution of the residuals as shown in Figure 6.4, indicating no external events impacted the execution of the experiment and no shift in the process behaviour could be detected.

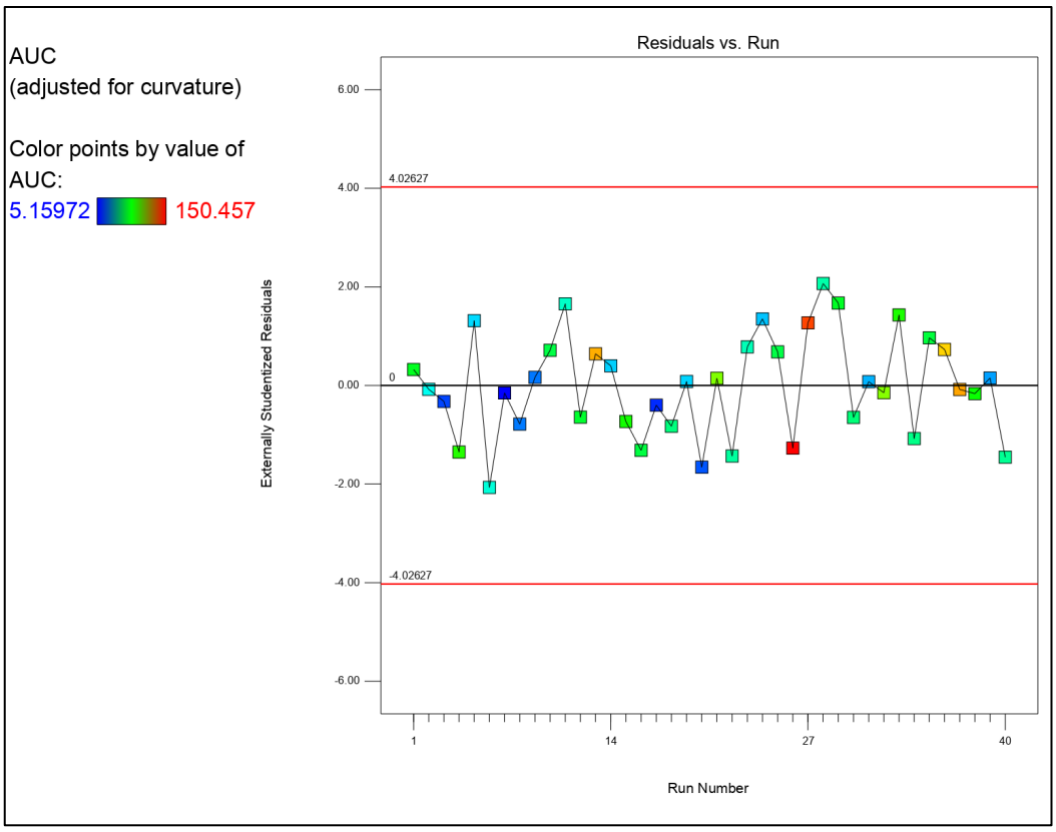

Figure 6.4. Residual vs run plot of the FFD model.

The final equation with actual factors is shown in Table 6.6. This can be used to make predictions about the response for given levels of each factor. Here, the levels should be specified in the original units for each factor. This equation should not be used to determine the relative impact of each factor because the coefficients are scaled to accommodate the units of each factor and the intercept is not at the centre of the design space. However, this will not be the last equation to be considered, as this experiment was followed by the optimisation phase carried out using a CCD.

Table 6.6. Final equation of the FFD model.

AUC	**=**
-142.18471	
7.59092	Agar concentration
-0.414986	Extraction time
54.24738	Weight applied
54.72622	Sonication time
74.71552	Extraction number
0.095813	Agar concentration * Extraction time
2.03559	Agar concentration * Weight applied
-11.84417	Agar concentration * Sonication time
-2.81909	Agar concentration * Extraction number
-0.008168	Extraction time * Weight applied
-0.011491	Extraction time * Sonication time
0.026704	Extraction time * Extraction number
-11.69411	Weight applied * Sonication time
-30.12983	Weight applied * Extraction number
-14.87391	Sonication time * Extraction number
0.04815	Agar concentration * Extraction time * Weight applied
0.014052	Agar concentration * Extraction time * Sonication time
-0.054602	Agar concentration * Extraction time * Extraction number
1.13382	Agar concentration * Weight applied * Sonication time
2.78626	Agar concentration * Sonication time * Extraction number
0.060718	Extraction time * Weight applied * Sonication time
3.86314	Weight applied * Sonication time * Extraction number
-0.02061	Agar concentration * Extraction time * Weight applied * Sonication time

An illustrative example of a 3D surface plot of the interactions between the factors (A) agar concentration and (D) sonication time is shown in Figure 6.5. The 3D plot shows that as the sonication time (D) increases the response (AUC) increases too, while as the concentration of agar (A) increases the response (AUC) decreases.

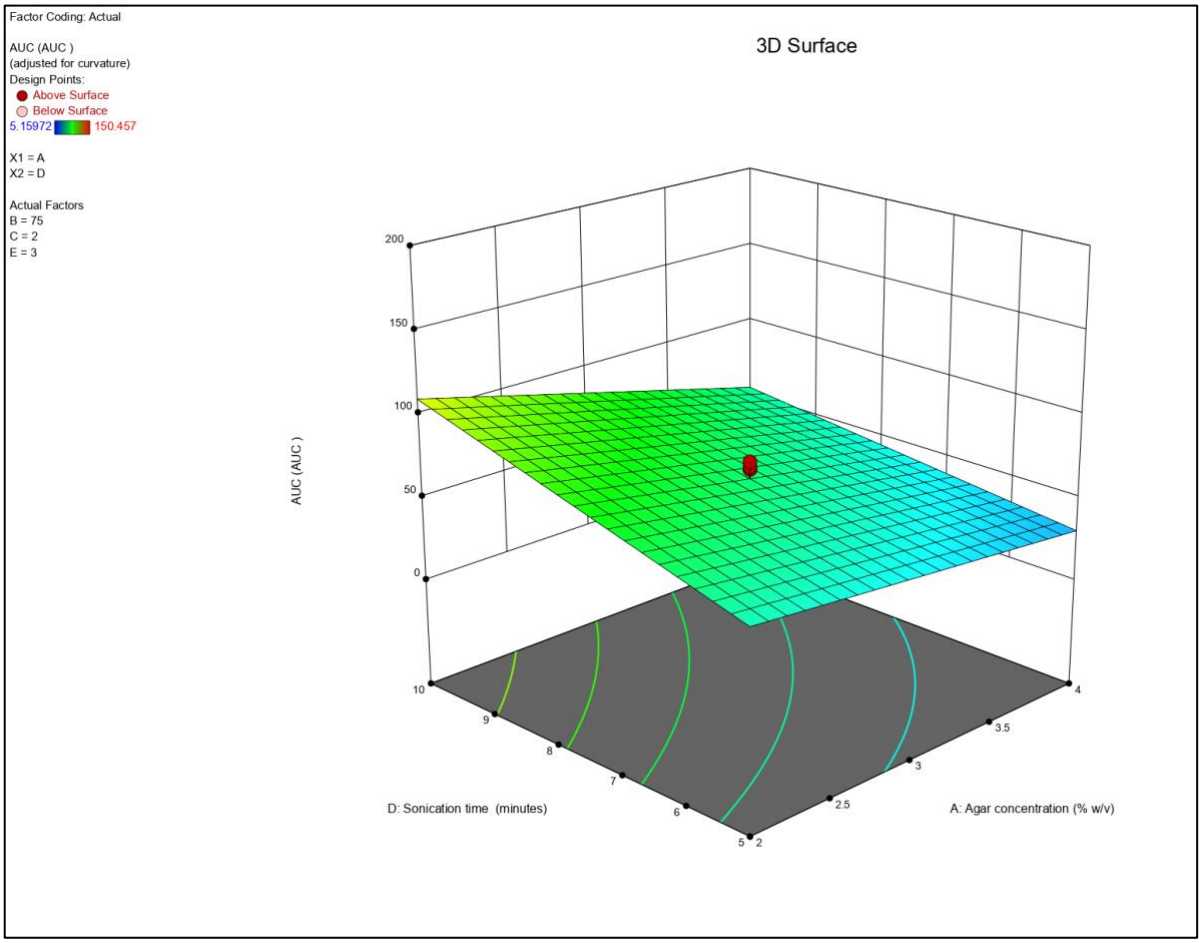

Figure 6.5. 3D surface plot of the interactions between the factors (A) agar concentration and (D) sonication time.

Additional 3D surface plots showing the interaction between (A) agar concentration and (B) extraction time, C) weight applied and (B) sonication are presented in Appendix 5.1 (Figure A1 to A3).

Factors were reduced by removing the least significant ones before optimising the extraction method using the CCD. The factors that were dropped were the extraction time (B), the weight applied (C), and the extraction number (E).

6.3.3. Optimisation phase using Central Composite Design

Once the experimental data were collected, the AUC values related to the quantity of 5F-PB-22 extracted from the agar gel bead were input into the Desing-Expert software for analysis. The ANOVA results at a 95% confidence interval of the 2 factors CCD model are shown in Table 6.7.

Table 6.7. Summary of the ANOVA results of the 2 factors CCD.

Source	Sum of Squares	df	Mean Square	F-value	p-value	Note
Model	3723.49	5	744.7	35.19	< 0.0001	Significant
A- Agar concentration	60.64	1	60.64	2.87	0.1343	Not significant
B- Sonication time	1061.01	1	1061.01	50.14	0.0002	Significant
AB	210.83	1	210.83	9.96	0.016	Significant
A^2	1386.76	1	1386.76	65.53	< 0.0001	Significant
B^2	1315.98	1	1315.98	62.18	< 0.0001	Significant
Residual	148.14	7	21.16			
Lack of Fit	70.5	3	23.5	1.21	0.4136	Not significant
Pure Error	77.64	4	19.41			
Cor Total	3871.63	12				

Table 6.7 highlights the factors whose p-value are below 0.05 (95% confidence interval): B, AB, A^2, B^2. Interestingly the effect of the agar concentration (A) on the response (AUC) is not significant. This is possibly because the range of the factor (from 1.95% to 2.2%) is too narrow to capture any measurable effect. However, its quadratic effect (A^2) is significant, with a p-value < 0.001. The agar concentration (A) was kept in the model to preserve the hierarchy.

To note that the F-value of 68.17 implies the whole model is significant. There is only a 0.01% chance that an F-value this large could occur due to noise. The lack-of-fit of 1.21 is non-significant relative to the pure error. In terms of Fit statistics, the r^2 is equal to 0.9617; the Adjusted r^2 is equal to 0.9344; the Predicted r^2 is equal to 0.8392 and finally, the Adequate precision is equal to 14.04. These are particularly good values. Specifically, the Predicted r^2 and the Adjusted r^2 are in reasonable agreement; and the Adequate precision, which measures

the signal-to-noise ratio, is much larger than 4, the minimum desirable, indicating an adequate signal. This model can be used to navigate the design space.

The following diagnostic plots were analysed: normal plot of residual (or normal probability plot); predicted vs. actual; residuals vs. run.

Some scatter in the normal plot of residuals can be expected also with normal data. Specific patterns e.g., an "S-shaped" curve would be concerning and would usually indicate that a transformation of the response is needed. In this case, the normal plot of residuals of the CCD model in Figure 6.6 shows random distribution which indicates a good fit, and no need for transformation.

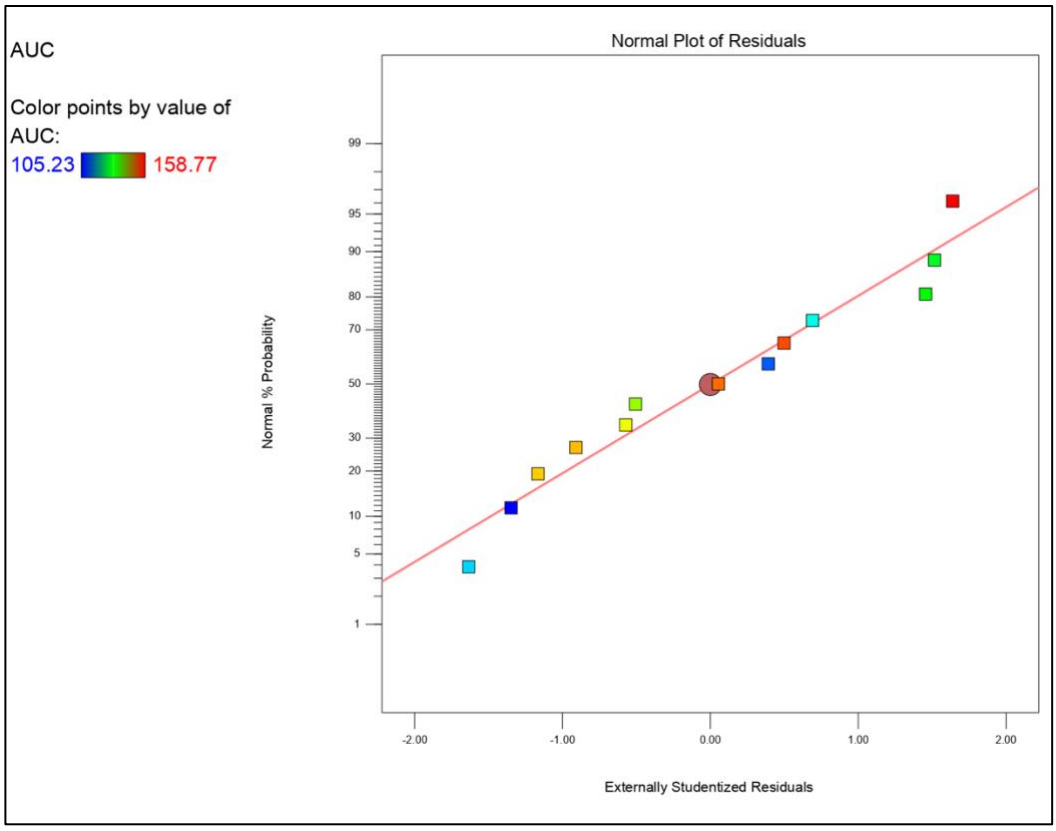

Figure 6.6. The normal plot of residual of the CCD model.

The predicted vs actual errors plot (Figure 6.7) of the CCD model also shows a random distribution of residuals which indicates a good fit.

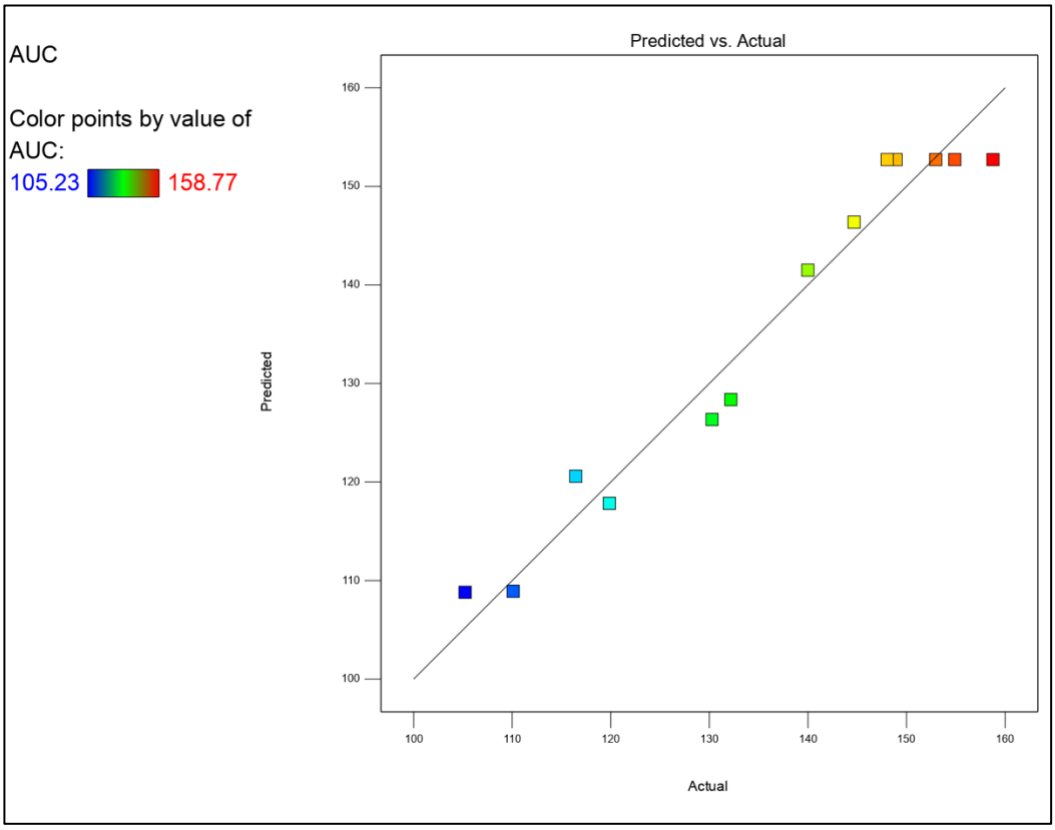

Figure 6.7. Predicted vs actual errors plot of the CCD model.

Finally, with regards to the residual vs run plot (Figure 6.8) of the CCD model, the random distribution of residuals indicates no external events impacted the execution of the experiment and no shift in the process behaviour could be detected.

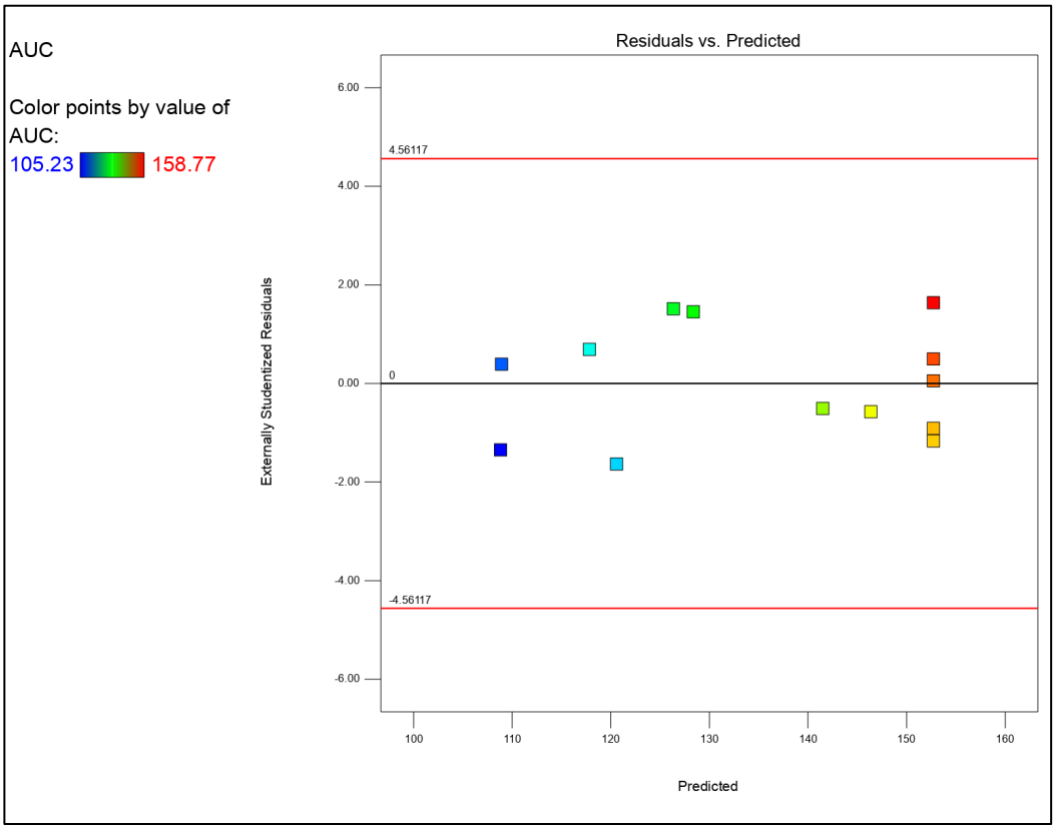

Figure 6.8. Residual vs run plot of the CCD model.

The final equation of actual factors is shown in Table 6.8. This can be used to make predictions about the response for given levels of each factor. Here, the levels should be specified in the original units for each factor. This equation should not be used to determine the relative impact of each factor because the coefficients are scaled to accommodate the units of each factor and the intercept is not at the centre of the design space.

Table 6.8. Final equation of the CCD model.

AUC	**=**
-846.04868	
746.83839	Agar concentration
46.21418	Sonication time
14.52	Agar concentration * Sonication time
-225.904	Agar concentration^2
-3.4385	Sonication time^2

The equation shown in table 6.8 was optimised numerically to identify the parameters set that would yield the maximum predicted AUC value of 155.77. This would be agar concentration A= 2%, and sonication time B= 10.95 min, whilst the extraction time, weight applied and extraction number were fixed at 120 sec, 85 grams, and 2 extractions, respectively. The 3D surface plot of the response of the interactions between the factors (A) agar concentration and (B) sonication time is shown in Figure 6.9.

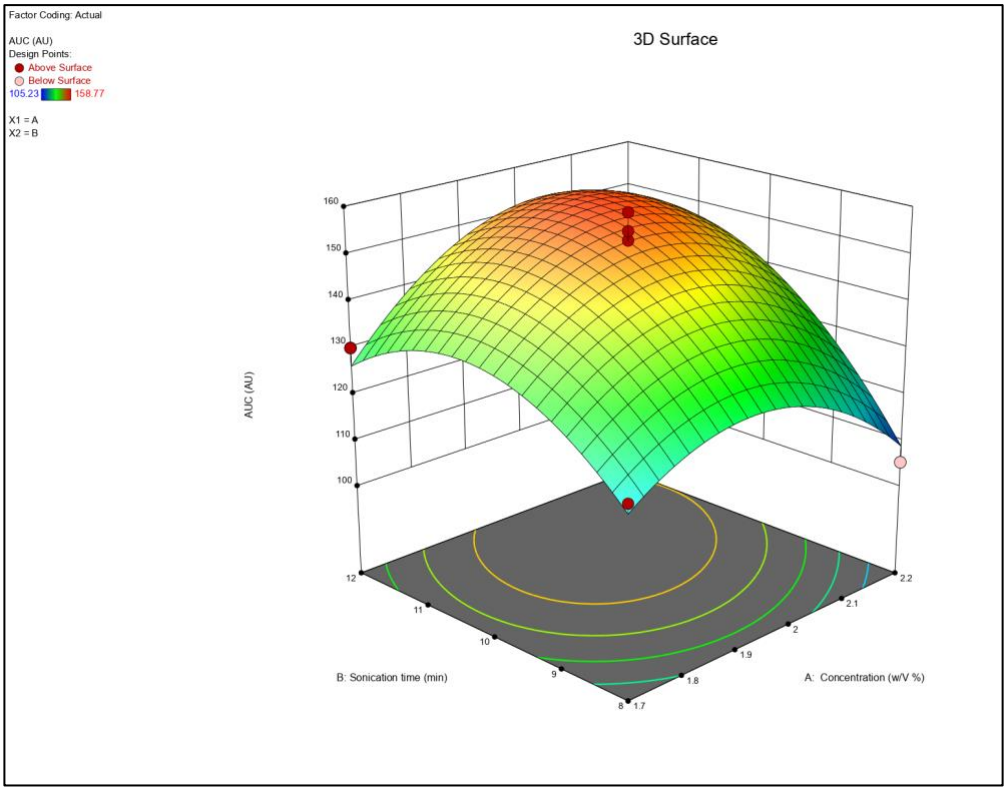

Figure 6.9. 3D surface plot of the response of the interactions between the factors (A) agar concentration and (B) sonication.

The contour plot of the response of the interactions between the factors (A) agar concentration and (B) sonication is presented in Appendix 5.2.

6.3.4. Validation of the model

The model was validated by running five confirmation runs on simulated paper samples using the same parameters as the optimised conditions (2% agar concentration, 10.95 min sonication time, 120 sec extraction time, 85 grams weight applied, and two extractions). The CI calculated accordingly to Equation 6.7 was found to be 152.19 ± 10.51 AU, where the lower bound value is 141.7 AU and the upper bound value is 162.7 AU. The average of the AUC resulting from the two consecutive extractions over five replicates was 152.19 ± 11.99 AU, which falls within our CI. However, some of the AUCs resulting from the validation runs do not fall in this range e.g., 164.91, 140.94, and 138.01 AU.

The RSD between the validation runs was also calculated and found to be 7.88%, in line with the previous results obtained. Moreover, the quantity of 5F-PB-22 extracted from the validation runs was found to be 1.78 ± 0.15 µg/mL, corresponding to the 2.36 ± 0.19% of the total 5F-PB-22 recovered from the simulated samples. This compared to the percentage recovery calculated in Section 6.3.2. (1.20 ± 0.09%) showed a 99.67% percent increase of the 5F-PB-22 extraction from the simulated paper samples using agar gel. Despite the extraction, optimisation performed the quantity of analyte extracted is still quite low. However, this type of extract can still be analysed by analytical techniques with a LOD in the order of the µg/mL or lower e.g., LC-MS or Surface Enhanced Raman Spectroscopy (SERS).

Moreover, the application of the optimised extraction method was tested on the seized paper sample from prison UHSOP/2018/P025, containing the synthetic cannabinoid 5F-ADB and previously tested in Chapter 4, was investigated. 5F-ADB was detected in the agar gel extract of the subunit A18 of the seized prison sample, and its chromatogram is presented in Figure 6.10.

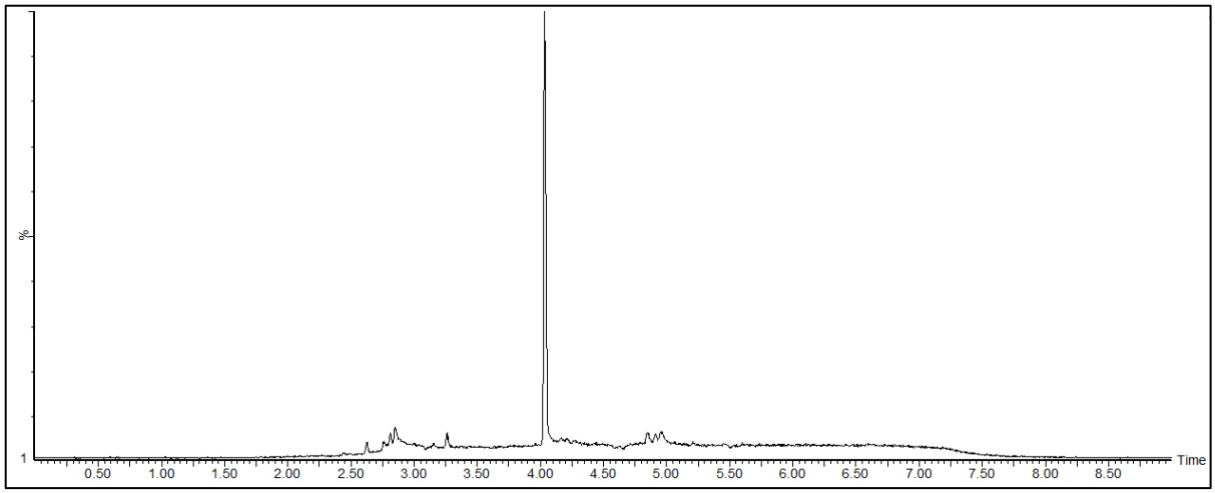

Figure 6.10. Chromatogram showing the detection of 5F-ADB from the agar gel extract of the subunit A18 of the seized prison sample.

The results obtained by these experiments confirmed the validation of the DoE model and the feasibility of the application of the extraction method on seized paper samples from prison.

6.4. Conclusions

The reproducibility of the extraction process of 5F-PB-22 from simulated paper samples using agar gel was calculated as the RSD of the AUC resulting from the two consecutive extractions over five replicates and found to be 7.49%. Considering the complexity of the process where several steps are involved in both the simulated sample preparation and in their extraction using agar gel, it was deemed acceptable. The quantity of 5F-PB-22 extracted from the simulated samples was as low as 0.91 ± 7.32 µg/mL, corresponding to 1.20 ± 0.09% of the total 5F-PB-22 recovered. The screening phase of the DoE performed using a 2^5 FFD lead to the identification of two statistically significant factors namely agar concentration (A) and the sonication time (D), involved in the extraction process of 5F-PB-22 from simulated paper samples using agar gel. An optimisation phase was then carried out using the two statistically significant factors, identifying the optimum agar concentration at 2%, and optimum sonication time at 10.95 min, whilst the other factors, namely extraction time, weight applied and extraction number were fixed at 120 sec, 85 grams, and 2 extractions, respectively. The DoE model was successfully validated by running five confirmation experiments on simulated paper samples using the same parameters as the optimised conditions (2% agar concentration, 10.95 min sonication time, 120 sec extraction time, 85 grams weight applied, and two extractions) as

the average of the AUC resulting from the two consecutive extractions over five replicates was 152.19, which falls within the CI calculated. However, some of the AUC resulting from the validation runs do not fall in this range e.g., 164.91, 140.94, and 138.01 AU. The RSD calculated between the validation runs of 7.88%, was in line with the previous results obtained. The quantity of 5F-PB-22 extracted from the validation runs was found to be 1.78 ± 0.15 µg/mL, corresponding to the 2.36 ± 0.19% of the total 5F-PB-22 recovered from the simulated samples. This compared to the percentage recovery calculated in Section 6.3.2. (1.20 ± 0.09%) showed a 99.67% percent increase in the extraction of 5F-PB-22.

The minimally invasive extraction method that was optimised and validated has the advantage to preserve the integrity of samples analysed that might be needed as evidence in court after the analysis. Moreover, the extraction of analytes from paper removes the paper background which has been proved to hinder the Raman signal of substances on simulated samples (Chapter 5). Since the quantity of analyte extracted using the optimised extraction method is still small this type of extract can be only analysed by analytical techniques with a LOD in the order of µg/mL or lower. The rationale for this study is to facilitate the development of a minimally invasive, highly sensitive, in-field NPS detection technique such as SERS, which is a method to enhance the Raman signal of low concentration analyte.

7. Conclusions, Future Work, and Limitations

From the systematic literature review on the detection of NPS in prison (Chapter 2), it was found that the synthetic cannabinoids were the most predominant NPS class, smuggled into prison on paper matrices. Laboratory techniques such as LC-HRMS/MSGC-MS were found to be used for the characterisation of such samples. A gap in knowledge for specific and selective in-field analytical techniques suitable for the detection of psychoactive substances on paper samples was highlighted. The systematic literature review helped identify the thesis's aim and objectives.

The thesis aimed to develop a minimally invasive extraction method of psychoactive substances from paper samples applicable in conjunction with a highly sensitive in-field detection technique, through the following objectives: i) characterisation the extraction process of psychoactive substances and adulterants/cutting agents and their ternary mixtures from simulated paper samples; ii) qualitative and quantitative analysis of a seized paper sample from prison; iii) evaluation of Raman instruments' capabilities coupled with PCA in identifying psychoactive substances, cutting agents/adulterants and their mixtures on simulated paper samples; iv) optimisation of the agar-gel extraction of the model synthetic cannabinoid 5F-PB-22 from simulated paper samples using DoE. At the end of the project, the aim and objectives were mostly met.

In this thesis, the extraction process of psychoactive substances and adulterants/cutting agents and their ternary mixtures from simulated paper samples was investigated to gain knowledge on the percentage extraction that could be achieved. Sonication and extraction time were evaluated using an HPLV-UV-Vis validated method and were not found to have an impact on the quantity of paracetamol extracted from paper. When the percentage recovery was firstly evaluated (Chapter 3), it was found to be consistent, with *ca.* 75% of the psychoactive substances and adulterants/cutting extracted i.e., paracetamol, caffeine, cocaine and THJ-018, extracted after the first extraction. When two consecutive extractions were employed *ca.* 80% of paracetamol was extracted from the simulated paper samples. The method developed was unable to extract 100% of the analytes. However, when the preparation method of the simulated samples was optimised by changing the way the solution was pipetted on the simulated paper samples, a higher percentage recovery was achieved. The percentage recovery evaluated on

simulated paper samples (n=15) impregnated with the synthetic cannabinoid 5F-ADB at three different concentrations, increased to 98.7 ± 0.8% (Chapter 4). A single extraction would be suitable for qualitative analysis as it takes the majority of the analytes out while three consecutive extractions should be used for accurate quantification of the analytes (Chapter 4). No studies investigating the impact of paper matrices during the quantification of analytes extracts from the paper were available in the literature. It was found that the five paper matrices evaluated did not affect the extraction and quantification of the 5F-ADB, based on the low RSD calculated between the AUC which was 2.25% (Chapter 4).

A UPLC-PdA-QToF-MS and UPLC-PdA-QDa-MS methods were employed to screen and quantify a seized paper sample from prison, respectively. The synthetic cannabinoid 5F-ADB was identified by comparison of the RT, parent ion, and fragmentation pattern with the 5F-ADB reference standard. The content of 5F-ADB found in the 39 units of the sample after three consecutive extractions ranged between 0.00026-0.055 mg/cm^2 (Chapter 4). While a study in the literature by McKenzie and co-workers found higher synthetic cannabinoids concentrations ranging between 0.05-1.17 mg/cm^2, across prison samples (n=154). Both data showed high variability of the synthetic cannabinoids concentration inter and intra-seized paper samples impacting in-field detection. Thus, when developing new detection methods, this must be taken into account, and values at the lower end should be used to develop such methods.

The capabilities and limitations of Raman spectroscopy when coupled with PCA in identifying psychoactive substances, cutting agents/adulterants and their mixtures on paper, and simulating prison samples, were investigated. A Raman benchtop (785 nm) and a Raman handheld (1064 nm) were used to collect data while 'The Unscrambler' PCA software was used for the pre-processing and to perform PCA on the data. Firstly, eight pre-processing protocols from the literature were evaluated, and a pre-processing protocol consisting of baseline offset followed by mean normalisation, which was used throughout this study was selected and validated. Raman spectroscopy coupled with PCA showed good discrimination between the spectra of neat psychoactive substances and related adulterant/cutting agent reference standards analysed. PCA discrimination of the Raman spectra of mixtures of psychoactive substances and related adulterant/cutting agent reference standards has been proved challenging due to the impact of the orientation of oscillations (state of polarisation) of light waves of the excitation laser irradiating the molecules [141] and the different Raman scattering properties of the compounds

in the mixtures. While most paper samples impregnated with psychoactive substances and related adulterant/cutting agents formed a 'mega cluster' in the scores plot near the BP samples, due to the paper background present in the spectra. However, observation of Raman spectra of such samples showed potential for their discrimination. For instance, when the line plot of the psychoactive substances i.e., 5F-PB-22, amphetamine, cocaine and diazepam reference standard pipetted on the simulated paper samples at five concentrations and collected using Raman Rigaku were examined characteristic peaks of the related reference standards were visible at the highest concentration e.g., 5F-PB-22 pipetted on paper at 20 and 15 mg/mL; cocaine pipetted on paper at 60, 40, 35 and 30 mg/mL. The key factor playing a role in the identification of substances on paper are the i) strong/weak Raman activity displayed by the reference standard used to prepare the solutions; ii) initial reference standard concentration used to prepare the simulated paper sample; iii) simulated paper samples preparation's method e.g., soaking or pipetting; iv) intra and inter-sample variability due to the spread of the solution on paper (variable matrix) and, v) orientation of oscillations (state of polarisation) of light waves of the excitation laser irradiating the molecules [141]. Multiple measurements are advisable, as the way the paper has been impregnated with psychoactive substances is not uniform.

To overcome the limitations of Raman coupled with PCA in detecting psychoactive substances and adulterants/cutting agents found on seized paper samples (Chapter 5), a minimally invasive extraction method was optimised using the DoE. An HPLC_UV-Vis validated method was employed to perform the DoE. The screening phase of the DoE, performed using a 2^5 FFD, led to the identification of two statistically significant factors, agar concentration (A) and sonication time (D), involved in the extraction process of 5F-PB-22 from simulated paper samples using agar gel. The optimisation phase was then carried out using a 2-factor CCD on the two statistically significant factors, identified with the 2^5 FFD. The optimum agar concentration and sonication time were found to be 2% at 10.95 min, respectively, whilst the extraction time (B), weight applied (C) and extraction number (E) were fixed at 120 sec, 85 grams, and 2 extractions, respectively. The model was successfully validated by five confirmation runs using the same parameters as the optimised conditions (2% agar concentration, 10.95 min sonication time, 120 sec extraction time, 85 grams weight applied, and two extractions). The CI calculated was found to be 152.19 ± 10.51 AU, and the average

of the AUC (152.19 ± 11.99 AU) of the confirmation runs fell within the CI. The percentage of the analyte recovered was calculated and was 2.36 ± 0.19%, which compared to the percentage recovery previously calculated for the unoptimised extraction of 1.20 ± 0.09% showed a 99.7% increase in the extraction of 5F-PB-22. Finally, the optimised extraction model was successfully applied to a seized paper sample detecting 5F-ADB, using the previously UPLC-PdA-QDa-MS validated method (Chapter 4). The minimally invasive extraction method using agar gel that was optimised and validated has the advantage to preserve the integrity of samples analysed that might be needed as evidence in court after the analysis. Moreover, the extraction of analytes from paper removes the paper background which has been proved to hinder the Raman signal of substances on simulated samples (Chapter 5). The rationale for this study was to facilitate the development of a minimally invasive, highly sensitive, in-field NPS detection technique.

A limitation of the UPLC-PdA-QDa-MS method used for the quantification of 5F-ADB in seized prison sample (Chapter 4), was the lack of the use of the IS, which corrects for analyte loss during the extraction and quantification process, which should be addressed in future work. Future work should aim to evaluate the capabilities and limitations of Raman spectroscopy coupled with PCA in models containing more reference standards from the synthetic cannabinoids group since these were the most predominantly found in prison. Moreover, it would be interesting to evaluate PCA models for simulated paper samples in which the region where the most predominant peak of BP is present (*ca.* 1088 cm^{-1}) has been truncated, to see if a better classification of such samples could be achieved. Moreover, the use of SERS should be evaluated to analyse paper samples impregnated with psychoactive substances. SERS is a Raman application that involves the use of gold or silver nanoparticles to enhance the Raman signal, enabling the detection of analytes at lower concentrations and reducing fluorescence. However, SERS is a destructive technique as the metal nanoparticles must be mixed or in close contact with the analytes to be detected. Coupling the SERS with a minimally invasive micro-extraction technique, like the one optimised in this thesis, would allow the extraction of analytes from the sample and the analysis without destroying the sample itself. Alternatively, the metal nanoparticles could be embedded in the agar gel, which could then be analysed using a Raman handheld instrument.

8. References

1. User Voice. Spice: The Bird Killer. What Prisoners Think About the Use of Spice and Other Legal Highs in Prison. Published 2016. https://www.uservoice.org/wp-content/uploads/2020/07/User-Voice-Spice-The-Bird-Killer-Report-compressed.pdf

2. Ralphs R, Williams L, Askew R, Norton A. Adding Spice to the Porridge: The development of a synthetic cannabinoid market in an English prison. International Journal of Drug Policy. 2016;1854(December 2016):1-13. doi:10.1016/j.drugpo.2016.10.003

3. Norman C, Walker G, McKirdy B, et al. Detection and quantitation of synthetic cannabinoid receptor agonists in infused papers from prisons in a constantly evolving illicit market. Drug Testing and Analysis. 2020;12:538-554. doi:10.1002/dta.2767

4. Vaccaro G, Massariol A, Guirguis A, Kirton SB, Stair JL. NPS detection in prison: A systematic literature review of use, drug form, and analytical approaches. Drug Testing and Analysis. Published online 2022. doi:10.1002/dta.3263

5. Ford LT, Berg JD. Analytical evidence to show letters impregnated with novel psychoactive substances are a means of getting drugs to inmates within the UK prison service. Annals of Clinical Biochemistry. 2018;55(6):673-678. doi:10.1177/0004563218767462

6. European Monitoring Centre for Drugs and Drug Addiction (EMCDDA). EMCDDA Operating Guidelines for the European Union Early Warning System on New Psychoactive Substances.; 2019. doi:10.2810/027404

7. United Nations Office on Drugs and Crime (UNODC). The challenge of new psychoactive substances: A Report from the Global SMART Programme March 2013. Global SMART Programe. Published 2013. Accessed October 14, 2020. https://www.unodc.org/documents/scientific/NPS_Report.pdf

8. Peacock A, Bruno R, Gisev N, et al. New psychoactive substances: challenges for drug surveillance, control, and public health responses. The Lancet. 2019;4:1-17. doi:10.1016/S0140-6736(19)32231-7

9. Hvozdovich JA, Chronister CW, Logan BK, Goldberger BA. Case Report: Synthetic Cannabinoid Deaths in State of Florida Prisoners. Journal of Analytical Toxicology. 2019;44:298-300. doi:10.1093/jat/bkz092

10. Caterino J, Clark J, Yohannan JC. Analysis of synthetic cannabinoids on paper before and after processing for latent print using DFO and ninhydrin. Forensic Science International. 2019;305(110000):1-5. doi:10.1016/j.forsciint.2019.110000

11. HM Chief Inspector of Prisons for England and Wales. Annual Report 2018-19.; 2019.

12. HM Inspectorate of Prisons. Thematic report by HM Inspectorate of Prisons Changing patterns of substance misuse in adult prisons and service responses. Published 2015. Accessed July 20, 2020. https://www.justiceinspectorates.gov.uk/hmiprisons/wp-content/uploads/sites/4/2015/12/Substance-misuse-web-2015.pdf

13. European Monitoring Centre for Drugs and Drug Addiction (EMCDDA). 1 New Psychoactive Substances in Prison - Results from an EMCDDA Trendspotter Study.; 2018. doi:10.2810/7247

14. HM Chief Inspector of Prisons. HM Chief Inspector of Prisons for England and Wales Annual report 2019-20. Published 2020. Accessed July 16, 2020. https://assets.publishing.service.gov.uk/government/uploads/system/uploads/attachment_data/file/927361/hmi-prisons-annual-report-accounts-201920.pdf

15. European Monitoring Centre for Drugs and Drug Addiction (EMCDDA). High-risk drug use and new psychoactive substances Results from an EMCDDA trendspotter study. doi:10.2810/807363

16. Her Majesty's Prison and Probation Service. Psychoactive substances in prisons - A summary of evidence relating to the use of psychoactive substances in prisons. Published 2019. Accessed July 6, 2020. https://www.gov.uk/guidance/psychoactive-substances-in-prisons

17. United Nations Office on Drugs and Crime (UNODC). World drug report 2020 Cross-cutting issues: Evolving trends and new challenges. Published 2020. Accessed July 20, 2020. https://wdr.unodc.org/wdr2020/field/WDR20_BOOKLET_4.pdf

18. HM Prison & Probation Service. HMPPS Annual Digest, April 2020 to March 2021. Published 2021. https://www.gov.uk/government/statistics/hmpps-annual-digest-april-2020-to-march-2021

19. United Nations Office on Drugs and Crime (UNODC). World Drug Report 2020 Drug use and health consequences. Published 2020. Accessed July 20, 2020. https://wdr.unodc.org/wdr2020/field/WDR20_Booklet_2.pdf

20. HM Inspectorate of Prisons. HM Chief Inspector of Prisons for England and Wales Annual Report 2013–14.; 2014.

21. Public Health England. New Psychoactive Substances (NPS) in prisons: A toolkit for prison staff. Published 2017. Accessed September 9, 2020. https://assets.publishing.service.gov.uk/government/uploads/system/uploads/attachment_data/file/669541/9011-phe-nps-toolkit-update-final.pdf

22. Antonides LH, Cannaert A, Norman C, et al. Shape Matters: The Application of Activity-Based In Vitro Bioassays and Chiral Profiling to the Pharmacological Evaluation of Synthetic Cannabinoid Receptor Agonists in Drug-Infused Papers Seized in Prisons. Drug Testing and Analysis. 2020;13(3):628-643. doi:10.1002/dta.2965

23. Norman C, Halter S, Haschimi B, et al. A transnational perspective on the evolution of the synthetic cannabinoid receptor agonists market: Comparing prison and general populations. Drug Testing and Analysis. 2021;13(4):841-852. doi:10.1002/dta.3002

24. United Nations Office on Drugs and Crime. Current NPS Threats. Vol II.; 2020.

25. Arillotta D, Schifano F, Napoletano F, et al. Novel Opioids: Systematic Web Crawling Within the e-Psychonauts' Scenario. Frontiers in Neuroscience. 2020;14:1-10. doi:10.3389/fnins.2020.00149

26. European Monitoring Centre for Drugs and Drug Addiction (EMCDDA). European Drug Report 2019: Trends and Developments. doi:10.2810/191370

27. Apirakkan O, Frinculescu A, Denton H, et al. Isolation, detection and identification of synthetic cannabinoids in alternative formulations or dosage forms. Forensic Chemistry. 2020;18(100227):1-10. doi:10.1016/j.forc.2020.100227

28. O'Hagan A, Hardwick R. Behind Bars: The Truth about Drugs in Prisons. Forensic Research & Criminology International Journal. 2017;52(August 2015):1-12. doi:10.15406/frcij.2017.05.00158

29. Metternich S, Zörntlein S, Schönberger T, Huhn C. Ion mobility spectrometry as a fast screening tool for synthetic cannabinoids to uncover drug trafficking in jail via herbal mixtures. Drug Testing and Analysis. 2019;11:833-846. doi:10.1002/dta.2565

30. Harper L, Powell J, Pijl EM. An overview of forensic drug testing methods and their suitability for harm reduction point-of-care services. Harm Reduction Journal. 2017;14(1). doi:10.1186/s12954-017-0179-5

31. Rethlefsen ML, Kirtley S, Waffenschmidt S, et al. PRISMA-S: An Extension to the PRISMA Statement for Reporting Literature Searches in Systematic Reviews. Syst Rev. 2021;10(39):1-19. doi:10.1186/s13643-020-01542-z

32. Bonds C, Hudson S. North West 'Through the Gate Substance Misuse Services' Drug Testing Project. Published 2015. Accessed July 31, 2020. https://www.lgcgroup.com/media/1795/noms-final-phm-report-version-5.pdf

33. Giorgetti A, Mogler L, Halter S, et al. Four cases of death involving the novel synthetic cannabinoid 5F-Cumyl-PEGACLONE. Forensic Toxicology. Published online 2019. doi:10.1007/s11419-019-00514-w

34. Welsh Emerging Drugs & Identification of Novel Substances (WEDINOS). Annual Report 1st October 2015 - 30th september 2016. Published 2016. http://www.wales.nhs.uk/sitesplus/documents/888/WEDINOS Annual Report 2015-16 %28FINAL%29.pdf

35. Norman C, McKirdy B, Walker G, Dugard P, NicDaéid N, McKenzie C. Large-scale evaluation of ion mobility spectrometry for the rapid detection of synthetic cannabinoid

receptor agonists in infused papers in prisons. Drug Testing and Analysis. 2021;13(3):644-663. doi:10.1002/dta.2945

36. Rook W, Ford L, Vale A. Four analytically confirmed cases of use of third-generation synthetic cannabinoid receptor agonists incorporating an adamantyl group. Clinical Toxicology. 2016;54(6):533-534. doi:10.1080/15563650.2016.1175005

37. European Monitoring Centre for Drugs and Drug Addiction (EMCDDA) and Europol. EMCDDA technical report on the new psychoactive substance methyl 2-{[1-(4-fluorobutyl)-1H-indole-3- carbonyl]amino}-3,3-dimethylbutanoate (4F-MDMB-BICA). Published 2020. https://www.emcdda.europa.eu/system/files/publications/13477/TR-4F-MDMB-BICA_Advanced-release.pdf

38. European Monitoring Centre for Drugs and Drug Addiction and Europol (EMCDDA), European Monitoring Centre for Drugs and Drug Adiction. EMCDDA Technical Report on the New Psychoactive Substance Methyl 3,3-Dimethyl-2-{[1-(Pent-4-En-1-Yl)-1H-Indazole-3- Carbonyl]Amino}butanoate (MDMB-4en-PINACA).; 2020.

39. Halter S, Haschimi B, Mogler L, Auwärter V. Impact of legislation on NPS markets in Germany – The rise and fall of 5F-ADB. Drug Testing and Analysis. 2020;12(6):853-856. doi:10.1002/dta.2786

40. Haschimi B, Mogler L, Halter S, et al. Detection of the recently emerged synthetic cannabinoid 4F-MDMB-BINACA in “legal high” products and human urine specimens. Drug Testing and Analysis. 2019;11(9):1377-1386. doi:10.1002/dta.2666

41. Kleis J, Germerott T, Halter S, et al. The synthetic cannabinoid 5F-MDMB-PICA: A case series. Forensic Science International. 2020;314(110410):1-9. doi:10.1016/j.forsciint.2020.110410

42. European Monitoring Centre for Drugs and Drug Addiction (EMCDDA)- EUROPOL. EMCDDA-Europol Joint Report on a new psychoactive substance: methyl 2-[[1-(cyclohexylmethyl)ondole-3-carbonyl]amino]-3,3-dimethylbutanoate (MDMB-CHIMICA). doi:10.2810/08132

43. Meyyappan C, Ford L, Vale A. Poisoning due to MDMB-CHMICA, a synthetic cannabinoid receptor agonist. Clinical Toxicology. Published online 2016. doi:10.1080/15563650.2016.1227832

44. European Monitoring Centre for Drugs and Drug Adiction (EMCDDA). Report on the risk assessment of 1-(4-Cyanobutyl)-N-(2-phenylpropan-2-yl)-1H-indazole-3-carboxamide (CUMYL-4CN-BINACA) in the framework of the Council Decision on new psychoactive substances. Publications Office of the European Union, Luxembourg. doi:10.2810/408735

45. European Monitoring Centre for Drugs and Drug Addiction (EMCDDA). Report on the risk assessment of methyl 2-{[1-(5-fluoropentyl)-1H-indazole-3-carbonyl]amino}-3,3-dimethylbutanoate (5F-MDMB-PINACA) in the framework of the Council Decision on new psychoactive substances. Publications Office of the European Union, Luxembourg. doi:10.2810/868403

46. Nacca N, Schult R, Loflin R, et al. Coma, Seizures, Atrioventricular Block, and Hypoglycemia in an ADB-FUBINACA Body-Packer. Journal of Emergency Medicine. 2018;55(6):788-791. doi:10.1016/j.jemermed.2018.09.012

47. European Monitoring Centre for Drugs and Drug Adiction. EMCDDA Technical Report on the New Psychoactive Substance Methyl 3,3-Dimethyl-2-{[1-(Pent-4-En-1-Yl)-1H-Indazole-3- Carbonyl]Amino}butanoate (MDMB-4en-PINACA).; 2020.

48. Krotulski AJ, Cannaert A, Stove C, Logan BK. The next generation of synthetic cannabinoids: Detection, activity, and potential toxicity of pent-4en and but-3en analogues including MDMB-4en-PINACA. Drug Testing and Analysis. Published online 2020:1-12. doi:10.1002/dta.2935

49. Øiestad EL, Johansen U, Christophersen AS, Karinen R. Screening of synthetic cannabinoids in preserved oral fluid by UPLC-MS/MS. Bioanalysis. 2013;5(18):2257-2268. doi:10.4155/bio.13.182

50. Grace S, Lloyd C, Perry A. The spice trail: transitions in synthetic cannabis receptor agonists (SCRAs) use in English prisons and on release. Drugs: Education, Prevention and Policy. 2019;27(4):271-278. doi:10.1080/09687637.2019.1684878

51. Prisons and Probation Ombudsman indipendent investigation. Prisons and Probation Ombudsman Annual Report 2016-17. Published 2017. Accessed December 13, 2020. http://www.ppo.gov.uk/app/uploads/2017/07/PPO_Annual-Report-201617_Interactive.pdf

52. HM Chief Inspector of Prisons for England and Wales. HM Chief Inspector of Prisons for England and Wales Annual Report 2016–17. Published 2017. Accessed August 16, 2020. https://assets.publishing.service.gov.uk/government/uploads/system/uploads/attachment_data/file/629719/hmip-annual-report-2016-17.pdf

53. Prisons and Probation Ombudsman indipendent investigation. Prisons and Probation Ombudsman Annual Report 2015-16. Published 2016. Accessed August 19, 2020. http://www.ppo.gov.uk/app/uploads/2016/09/PPO_Annual-Report-201516_WEB_Final.pdf

54. Prisons and Probation Ombudsman indipendent investigation. Prisons and Probation Ombudsman Annual Report 2014-15. Published 2015. Accessed September 21, 2020. http://www.ppo.gov.uk/app/uploads/2015/09/PPO_Annual-Report-2014-15_Web-Final.pdf

55. HM Chief Inspector of Prisons for England and Wales. HM Chief Inspector of Prisons for England and Wales Annual Report 2014–15. Published 2015. Accessed September 9, 2020. https://assets.publishing.service.gov.uk/government/uploads/system/uploads/attachment_data/file/444785/hmip-2014-15.pdf

56. Lloyd C, Page G, McKeganey N, Russell C. Capital depreciation: The lack of recovery capital and post-release support for prisoners leaving the Drug Recovery Wings in England and Wales. International Journal of Drug Policy. 2019;70:107-116. doi:10.1016/j.drugpo.2019.06.012

57. HM Chief Inspector of Prisons for England and Wales. HM Chief Inspector of Prisons for England and Wales Annual Report 2017-18. Published 2018. Accessed November 3, 2020. https://assets.publishing.service.gov.uk/government/uploads/system/uploads/attachment_data/file/761589/hmi-prisons-annual-report-2017-18-revised-web.pdf

58. European Monitoring Centre for Drugs and Drug Addiction (EMCDDA). New psychoactive substances : global markets, glocal threats and the COVID-19 pandemic An update from the EU Early Warning System.), Publications Office of the European Union,

Luxembourg. Published 2020. https://www.emcdda.europa.eu/system/files/publications/13464/20205648_TD0320796ENN_PDF_rev.pdf

59. Corazza O, Coloccini S, Marrinan S, et al. Novel Psychoactive Substances in Custodial Settings: A Mixed Method Investigation on the Experiences of People in Prison and Professionals Working With Them. Frontiers in Psychiatry. 2020;11:1-10. doi:10.3389/fpsyt.2020.00460

60. Prisons & Probation Ombudsman. Annual Report 2018-19.; 2019.

61. Blackman S, Bradley R. From niche to stigma—Headshops to prison: Exploring the rise and fall of synthetic cannabinoid use among young adults. International Journal of Drug Policy. 2017;40:70-77. doi:10.1016/j.drugpo.2016.10.015

62. HM Inspectorate of Prisons. HM Chief Inspector of Prisons for England and Wales Annual Report 2015-16.; 2016.

63. Ford LT, Berg JD. Analysis of legal high materials by ultra-performance liquid chromatography with time of flight mass spectrometry as part of a toxicology vigilance system: what are the most popular novel psychoactive substances in the UK? Annals of Clinical Biochemistry. 2016;54(2):219-229. doi:10.1177/0004563216651646

64. Van Dyken E, Lai FY, Thai PK, et al. Challenges and opportunities in using wastewater analysis to measure drug use in a small prison facility. Drug and Alcohol Review. 2016;35(2):138-147. doi:10.1111/dar.12156

65. European Monitoring Centre for Drugs and Drug Adiction (EMCDDA). Report on the risk assessment of N-(1-phenethylpiperidin-4-yl)-N- phenylacrylamide (acryloylfentanyl) in the framework of the Council Decision on new psychoactive substances. Publications Office of the European Union, Luxembourg. doi:10.2810/16112

66. European Monitoring Centre for Drugs and Drug Addiction (EMCDDA). Report on the risk assessment of methyl 1-(2-phenylethyl)-4-[phenyl(propanoyl)amino]piperidine-4-

carboxylate (carfentanil) in the framework of the Council Decision on new psychoactive substances. Publications Office of the European Union, Luxembourg. doi:10.2810/411341

67. European Monitoring Centre for Drugs and Drug Addiction (EMCDDA). Report on the risk assessment of N-phenyl-N-[1-(2-phenylethyl)piperidin-4-yl] cyclopropanecarboxamide (cyclopropylfentanyl)in the framework of the Council Decision on new psychoactive substances. Publications Office of the European Union, Luxembourg. doi:10.2810/895612

68. Wikström M, Holmgren P, Ahlner J. A2 (N-Benzylpiperazine) a New Drug of Abuse in Sweden. Journal of Analytical Toxicology. 2004;28(1):67-70. doi:10.1093/jat/28.1.67

69. Abbate V, Schwenk M, Presley BC, Uchiyama N. The ongoing challenge of novel psychoactive drugs of abuse. Part I. Synthetic cannabinoids (IUPAC Technical Report). Pure and Applied Chemistry. 2018;90(8):1255-1282. doi:10.1515/pac-2017-0605

70. European Monitoring Centre for Drugs and Drug Addiction (EMCDDA). 2 New Psychoactive Substances in Prison - Results from an EMCDDA Trendspotter Study.; 2018. doi:10.2810/7247

71. European Monitoring Centre for Drugs and Drug Addiction (EMCDDA). Report on the risk assessment of methyl 2-{[1-(5-fluoropentyl)-1H-indazole-3-carbonyl]amino}-3,3-dimethylbutanoate (5F-MDMB-PINACA) in the framework of the Council Decision on new psychoactive substances. Publications Office of the European Union, Luxembourg. doi:10.2810/868403

72. European Monitoring Centre for Drugs and Drug Addiction (EMCDDA). Report on the risk assessment of N-(1-amino-3-methyl-1-oxobutan-2-yl)-1-(cyclohexylmethyl)-1H-indazole-3-carboxamide (AB-CHMINACA) in the framework of the Council Decision on new psychoactive substances. Publications Office of the European Union, Luxembourg. doi:10.2810/565855

73. Expert Committee on Drug Dependence-World Health Organisation. 5F-PB-22 Critical Review Report.; 2017.

74. Winstock AR, Maier LG, Zhuparris A, et al. GLOBAL DRUG SURVEY (GDS) 2021 Key Findings Report.; 2021.

75. Penfold C, Turnbull P, Webster R. Tackling prison drug markets: an exploratory qualitative study. Home Office. Published 2016. https://www.researchgate.net/publication/237776662_Tackling_Prison_Drug_Markets_An_Exploratory_Qualitative_Study

76. European Monitoring Centre for Drugs and Drug Addiction (EMCDDA). 2 New Psychoactive Substances in Prison - Results from an EMCDDA Trendspotter Study.; 2018. doi:10.2810/7247

77. European Monitoring Centre for Drugs and Drug Addiction. EMCDDA Technical Report on the New Psychoactive Substance Methyl 2-{[1-(4-Fluorobutyl)-1H-Indole-3-Carbonyl]Amino}-3,3- Dimethylbutanoate (4F-MDMB-BICA).; 2020.

78. Bell V, Leese M. . . A Mixed Methods Study of Increased Security Measures in a Drug Recovery Prison: Final Report May 2019.; 2019.

79. Scotland Goverment. The Prisons and Young Offenders Institutions (Scotland) Rules 2011.

80. Legislation.gov.uk. The Prison Rules. Published online 1999.

81. Antonides LH, Cannaert A, Norman C, et al. Shape Matters: The Application of Activity-Based in Vitro Bioassays and Chiral Profiling to the Pharmacological Evaluation of Synthetic Cannabinoid Receptor Agonists in Drug-Infused Papers Seized in Prisons. Vol 13.; 2021. doi:10.1002/dta.2965

82. European Monitoring Centre for Drugs and Drug Adiction (EMCDDA). Perspectives on drugs. Synthetic cannabinoids in Europe. Published 2017. https://www.emcdda.europa.eu/publications/pods/synthetic-cannabinoids_en

83. SWGDRUG. Scientific Working Group for the Analysis of Seized Drugs Reccomendations. Published online 2016.

84. United Nations Office on Drugs and Crime (UNODC). Recommended methods for the Identification and Analysis of Synthetic Cannabinoid Receptor Agonists in Seized Materials. Published online 2013:26.

85. Kerrigan S. Sampling, storage and stability. In: Clarke´s Analysis of Drug and Poisons. 4th editio. Pharmaceutical Press; 2011:335-356.

86. Yu B, Ge M, Li P, Xie Q, Yang L. Development of surface-enhanced Raman spectroscopy application for determination of illicit drugs: Towards a practical sensor. Talanta. 2019;191(January 2018):1-10. doi:10.1016/j.talanta.2018.08.032

87. Lee WWY, Silverson VAD, Jones LE, et al. Surface-enhanced Raman spectroscopy of novel psychoactive substances using polymer-stabilized Ag nanoparticle aggregates. Chemical Communications. 2016;52(3):493-496. doi:10.1039/c5cc06745f

88. Yu WW, White IM. Inkjet-printed paper-based SERS dipsticks and swabs for trace chemical detection. Analyst. 2013;138(4):1020-1025. doi:10.1039/c2an36116g

89. Mercer J, Shakleya D, Bell S. Applications of ion mobility spectrometry (IMS) to the analysis of gamma-hydroxybutyrate and gamma-hydroxyvalerate in toxicological matrices. Journal of Analytical Toxicology. 2006;30(8):539-544. doi:10.1093/jat/30.8.539

90. Sorribes-Soriano A, Herrero-Martínez JM, Esteve-Turrillas FA, Armenta S. Molecularly imprinted polymer-based device for field collection of oral fluid samples for cocaine identification. Journal of Chromatography A. 2020;1633:461629. doi:10.1016/j.chroma.2020.461629

91. May B, Naqi HA, Tipping M, et al. Synthetic Cannabinoid Receptor Agonists Detection Using Fluorescence Spectral Fingerprinting. Analytical Chemistry. 2019;91(20):12971-12979. doi:10.1021/acs.analchem.9b03037

92. Gent L, Paul R. Air monitoring for illegal drugs including new psychoactive substances: A review of trends, techniques and thermal degradation products. Drug Testing and Analysis. 2021;13(6):1078-1094. doi:10.1002/dta.3051

93. Paul R, Smith S, Gent L, Sutherill R. Air monitoring for synthetic cannabinoids in a UK prison: Application of personal air sampling and fixed sequential sampling with thermal desorption two-dimensional gas chromatography coupled to time-of-flight mass spectrometry. Drug Testing and Analysis. 2021;13(9):1678-1685. doi:10.1002/dta.3101

94. Ford LT, Berg JD. Analytical evidence to show letters impregnated with novel psychoactive substances (NPS) are a means of getting drugs to inmates within the UK prison service. Annals of Clinical Biochemistry. Published online 2018:1-6. doi:10.1177/0004563218767462

95. United Nations Office On Drugs and Crime (UNODC). Recommended methods for the Identification and Analysis of Synthetic Cannabinoid Receptor Agonists in Seized Materials. Published online 2020:1-99.

96. WEDINOS-Welsh Emerging Drugs & Identification of Novel Substances. Annual Report 2018-19.; 2019. https://www.wedinos.org/resources/downloads/Annual_Report_201819.pdf

97. ICH Harmonised tripartite Guideline. Validation of Analytical Procedures: Methodology.; 1996.

98. ICH Harmonised tripartite Guideline. Text on Validation of Analytical Procedures.; 1994.

99. Centre for drugs evaluation and research. Reviewer Guidance: Validation of Chromatographic Methods.; 1994.

100. Assi S, Guirguis A, Halsey S, Fergus S, Stair JL. Analysis of “legal high” substances and common adulterants using handheld spectroscopic techniques. Analytical Methods. 2015;7(2):736-746. doi:10.1039/c4ay02169j

101. LGC group. Class A- National drugs intelligence bulletin- Q2 2017. Published online 2017:1-15.

102. Field A. Discovering Statistics Using IBM SPSS Statistics.; 2013.

103. Dybowski MP, Typek R, Dawidowicz AL, Holowinski P. On practical problems in precise estimation of 5F-ADB in urine samples. Forensic Toxicology. 2021;39(1):213-221. doi:10.1007/s11419-020-00542-x

104. McLaughlin G, Morris N, Kavanagh P v., et al. The synthesis and characterization of the "research chemical" N-(1-amino-3-methyl-1-oxobutan-2-yl)-1-(cyclohexylmethyl)-3-(4-fluorophenyl)-1H-pyrazole-5-carboxamide (3,5-AB-CHMFUPPYCA) and differentiation from its 5,3-regioisomer. Drug Test Anal. 2016;8(9):920-929. doi:10.1002/dta.1864

105. Naqi HA, Woodman TJ, Husbands SM, Blagbrough IS. 19F and 1H quantitative-NMR spectroscopic analysis of fluorinated third-generation synthetic cannabinoids. Analytical Methods. 2019;11(24):3090-3100. doi:10.1039/c9ay00814d

106. Cambridge Isotope Laboratories. 1H NMR and 13C NMR chemical shifts of some common solvents. http://www.users.csbsju.edu/~kgraham/nmrshift.html

107. World Health Organisation- WHO. 5F-ADB Critical Review Report.; 2017.

108. von Cüpper M, Dalsgaard PW, Linnet K. Identification of New Psychoactive Substances in Seized material Using UHPLC–QTOF-MS and An Online Mass Spectral Database. Journal of Analytical Toxicology. 2021;44(9):1047-1051. doi:10.1093/jat/bkaa028

109. United Nations Office on Drugs and Crime. Laboratory and Scientific Section. Guidance for the Validation of Analytical Methodology and Calibration of Equipment Used for Testing of Illicit Drugs in Seized Materials and Biological Specimens : A Commitment to Quality and Continuous Improvement. United Nations; 2009.

110. United Nations Office on Drugs and Crime. Laboratory and Scientific Section., European Network of Forensic Science Institutes. Drugs Working Group. Guidelines on Representative Drug Sampling. United Nations; 2009.

111. Hansen MJ, Douglas Beard T, Hayes DB. Sampling and Experimental Design.

112. Ferraro JR, Nakamoto K, Brown CW. Introductory Raman Spectroscopy.; 2003. doi:10.1002/jrs.1407

113. Bumbrah GS, Sharma RM. Raman spectroscopy – Basic principle , instrumentation and selected applications for the characterization of drugs of abuse. Egyptian Journal of Forensic Sciences. 2016;6(3):209-215. doi:10.1016/j.ejfs.2015.06.001

114. Buttingsrud B. Multivariate Data Analysis- Level 1. Camo; 2015.

115. Kumar K. Principal component analysis: Most favourite tool in chemometrics. Resonance. 2017;22(8):747-759. doi:10.1007/s12045-017-0523-9

116. Noonan KY, Tonge LA, Fenton OS, Damiano DB, Frederick KA. Rapid Classification of Simulated Street Drug Mixtures Using Raman Spectroscopy and Principal Component Analysis. 2009;63(7):742-747.

117. Kumar N, Bansal A, Sarma GS, Rawal RK. Chemometrics tools used in analytical chemistry: An overview. Talanta. 2014;123:186-199. doi:10.1016/j.talanta.2014.02.003

118. Swarbrick B, Westad F. An overview of Chemometrics for the Engineering and Measurement Science. Published online 2016.

119. O'Connell M louise, Howley T, Ryder AG, Leger MN, Madden MG. Classification of a target analyte in solid mixtures using principal component analysis , support vector machines and Raman. Published online 2005.

120. O'Connell M louise, Ryder AG, Leger MN, Howley TOM. Qualitative Analysis Using Raman Spectroscopy and Chemometrics : A Comprehensive Model System for Narcotics Analysis. 2010;64(10):1109-1121.

121. Ryder, Alan G.; O'Connor, Gerard M.; Thomas J. G. Quantitative analysis of cocaine in solid mixtures using Raman spectroscopy and chemometric methods. Journal of Raman Spectroscopy. 2000;31(3):221-227. doi:10.1002/(SICI)1097

122. Omar J, Slowikowski B, Guillou C, Reniero F, Holland M, Boix A. Identification of new psychoactive substances (NPS) by Raman spectroscopy. Journal of Raman Spectroscopy. 2019;50(1):41-51. doi:10.1002/jrs.5496

123. Bedward TM, Xiao L, Fu S. Application of Raman spectroscopy in the detection of cocaine in food matrices. Australian Journal of Forensic Sciences. 2017;51(2):209-219. doi:10.1080/00450618.2017.1356867

124. Calvo-Castro J, Guirguis A, Samaras EG, Zloh M, Kirton SB, Stair JL. Detection of newly emerging psychoactive substances using Raman spectroscopy and chemometrics. RSC Advances. Published online 2018:31924-31933. doi:2018/RA/C8RA05847D

125. Guirguis A. Identification and Classification of New Psychoactive Substances Using Raman Spectroscopy and Chemometrics. PhD Dissertation. University of Hertfordshire; 2017.

126. Hargreaves MD, Burnett AD, Munshi T, et al. Comparison of near infrared laser excitation wavelengths and its influence on the interrogation of seized drugs-of-abuse by Raman spectroscopy. Journal of Raman Spectroscopy. 2009;40(12):1974-1983. doi:10.1002/jrs.2352

127. World Health Organisation. Drugs (psychoactive) Drugs (psychoactive).

128. Batrick EG. Technical Evaluation: Rigaku Analytical Devices ProgenyTM ResQTM Application: Illegal Drug Screening.; 2015.

129. Bakeev KA, Chimenti R v. Pros and cons of using correlation versus multivariate algorithms for material identification via handheld spectroscopy. american pharmaceutical review. Published online 2013:1-5.

130. Harwood LM, Moody CJ. Experimental Organic Chemistry: Principles and Practise. (Publications BS, ed.).; 1989.

131. O'Connell ML, Howley T, Ryder AG, Leger MN, Madden MG. Classification of a target analyte in solid mixtures using principal component analysis, support vector machines, and Raman spectroscopy. In: Opto-Ireland 2005: Optical Sensing and Spectroscopy. Vol 5826. SPIE; 2005:340. doi:10.1117/12.605156

132. Hargreaves MD, Burnett AD, Munshi T, et al. Comparison of near infrared laser excitation wavelengths and its influence on the interrogation of seized drugs-of-abuse by

Raman spectroscopy. Journal of Raman Spectroscopy. 2009;40(12):1974-1983. doi:10.1002/jrs.2352

133. Omar J, Slowikowski B, Guillou C, Reniero F, Holland M, Boix A. Identification of new psychoactive substances (NPS) by Raman spectroscopy. Journal of Raman Spectroscopy. 2019;50(1):41-51. doi:10.1002/jrs.5496

134. Westad F, Esbensen KH, Houmoller LP 1. Multivariate Data Analysis: In Practice : An Introduction to Multivariate Data Analysis and Experimental Design. Vol 5. 6th ed.; 2001.

135. CAMO. The Unscrambler® X V10.3 User Manual.; 2014. www.camo.com

136. Heraud P, Wood BR, Beardall J, McNaughton D. Effects of pre-processing of Raman spectra onin vivo classification of nutrient status of microalgal cells. Journal of Chemometrics. 2006;20(5):193-197. doi:10.1002/cem.990

137. Edwards HGM, Munshi T, Anstis M. Raman spectroscopic characterisations and analytical discrimination between caffeine and demethylated analogues of pharmaceutical relevance. Spectrochimica Acta - Part A: Molecular and Biomolecular Spectroscopy. 2005;61(7):1453-1459. doi:10.1016/j.saa.2004.10.022

138. Gunasekaran S, Sankari G, Ponnusamy S. Vibrational spectral investigation on xanthine and its derivatives - Theophylline, caffeine and theobromine. Spectrochimica Acta - Part A: Molecular and Biomolecular Spectroscopy. 2005;61(1-2):117-127. doi:10.1016/j.saa.2004.03.030

139. Palafox MA. Raman Spectra and Vibrational Analysis for Benzocaine. Vol 20.; 1989.

140. Udritioiu FM, Tnase IG, Bunaciu AA, Aboul-Enein HY. Paper analysis: Nondestructive and destructive analytical methods. Applied Spectroscopy Reviews. 2012;47(7):550-570. doi:10.1080/05704928.2012.682285

141. British Pharmacopoeia. Appendix II H. Raman Spectrometry. In: The Stationery Office; 2014.

142. de Oliveira Penido caffeine, Pacheco MTT, Lednev IK, Silveira L. Raman spectroscopy in forensic analysis: Identification of cocaine and other illegal drugs of abuse. Journal of Raman Spectroscopy. 2016;47(1):28-38. doi:10.1002/jrs.4864

143. Alkaseem M, Baron M. SERS and DFT study of 5F-PB-22. Journal of Raman Spectroscopy. 2018;49(10):1594-1606. doi:10.1002/jrs.5444

144. Berg RW, Nrbygaard T, White PC, Abdali S. Ab initio calculations and raman and sers spectral analyses of amphetamine species. Applied Spectroscopy Reviews. 2011;46(2):107-131. doi:10.1080/05704928.2010.520180

145. Chalmers JM, Edwards HGM, Hargreaves MD. Vibrational Spectroscopy Techniques: Basics and Instrumentation. Infrared and Raman Spectroscopy in Forensic Science. Published online 2012:9-44. doi:10.1002/9781119962328.ch2

146. Sharma B, Frontiera RR, Henry AI, Ringe E, van Duyne RP. SERS: Materials, applications, and the future. Materials Today. 2012;15(1-2):16-25. doi:10.1016/S1369-7021(12)70017-2

147. Davies E, Huang Y, Harper JB, et al. Dynamics of water in agar gels studied using low and high resolution 1H NMR spectroscopy. International Journal of Food Science and Technology. 2010;45(12):2502-2507. doi:10.1111/j.1365-2621.2010.02448.x

148. Platania E, Lombardi JR, Leona M, et al. Suitability of Ag-agar gel for the microextraction of organic dyes on different substrates: The case study of wool, silk, printed cotton and a panel painting mock-up. Journal of Raman Spectroscopy. 2014;45(11-12):1133-1139. doi:10.1002/jrs.4531

149. Platania E. Synthesis and Application of Ag-agar gel SERS substrates for the non-destructive detection of organic dyes in works of art. Published online 2013:1-104.

150. Lofrumento C, Ricci M, Platania E, Becucci M, Castellucci E. SERS detection of red organic dyes in Ag-agar gel. Journal of Raman Spectroscopy. 2013;44(1):47-54. doi:10.1002/jrs.4162

151. Müller ALH, de Oliveira JA, Prestes OD, Adaime MB, Zanella R. Design of experiments and method development. In: Solid-Phase Extraction. Elsevier; 2019:589-608. doi:10.1016/B978-0-12-816906-3.00022-4

152. Narenderan ST, Meyyanathan SN, Venkata V, Reddy S. Experimental design in pesticide extraction methods : A reviewidentifying. Food Chemistry. 2019;289(November 2018):384-395. doi:10.1016/j.foodchem.2019.03.045

153. Durakovic B. Design of experiments application, concepts, examples: State of the art. Periodicals of Engineering and Natural Sciences. 2017;5(3):421-439. doi:10.21533/pen.v5i3.145

9. Appendices

Appendix 1. (Chapter 2)

Appendix 1.1. Full methodology strategy

Database search

The databases search (KEY WORDS- TITLE -ABSTRACT) was conducted on Scopus (http://www.scopus.com) between May 2020 and January 2021. While MEDLINE (https://www.ebsco.com/products/research-databases/medline-complete), PubMed (https://pubmed.ncbi.nlm.nih.gov/) Web of Science (https://access.clarivate.com/login?app=wos&alternative=true&shibShireURL=https:%2F%2Fwww.webofknowledge.com%2F%3Fauth%3DShibboleth&shibReturnURL=https:%2F%2Fwww.webofknowledge.com%2F%3Fmode%3DNextgen%26action%3Dtransfer%26path%3D%252Fwos%252Fwoscc%252Fbasic-search%26DestApp%3DUA&referrer=mode%3DNextgen%26path%3D%252Fwos%252Fwoscc%252Fbasic-search%26DestApp%3DUA%26action%3Dtransfer&roaming=true) were searched between August 2021 and December 2021. The search was performed using the two-word groups (Table A1) to give a search string. To note that for the databases Scopus and PubMed the string was split in three parts as only a limited number of digits in the search bar were allowed. Boolean operators 1) OR was used to combine words within groups while 2) AND was used to combine words between groups. Double quotation was used to search for a two or more words near each other. While the wildcard * represented any number of characters, e.g., prison* is equal to prison, prisons, prisoner and prisoners.

Table A1. Key words related to the systematic literature review.

Word group 1	**Word group 2**
"psychoactive substance"	prison*
"legal high"	jail
"designer drug"	penitentiary
NPS	“correctional service”
"synthetic cannabinoid"	“correctional institution”
SCRA	
"NPS opi*"	
"NPS benzodiazepine"	
"phencyclidine-type"	
"ketamine-type"	
"plant-based NPS"	
aminoindane	
tryptamine	
piperazine	
phenethylamine	
"synthetic cathinone"	
Notes: Boolean operators 1) OR combined with words within groups 2) AND combined between groups. Double quotation is used to search for a phrase, while the wildcard * represents any number of characters, even zero.	

The full search strings strategy performed on **MEDLINE**, lead to n= **203** results (updated on the 31/04/21) and is detailed below:

One unique string: "NPS" OR "synthetic cannabinoid" OR "SCRA" OR "designer drug" OR "psychoactive substance" OR "legal high" OR "NPS opi*" OR "NPS benzodiazepine" OR "Phencyclidine-type" OR "Plant-based NPS" OR "Aminoindane" OR "Tryptamine" OR "Piperazine" OR "Phenethylamine" OR "Synthetic cathinone" AND prison* OR jail OR penitentiary OR "correctional services" OR "correctional institution" (203 results).

The full search strings strategy performed on **PubMed**, lead to n= **62** results and is described below:

1A-part 1) "NPS" OR "synthetic cannabinoid" OR "SCRA" OR "designer drug" OR "psychoactive substance" OR "legal high" AND prison* OR jail OR penitentiary OR "correctional service" OR "correctional institution" (59 results)

1A-part 2) "NPS opi*" OR "NPS benzodiazepine" OR "phencyclidine-type" OR "plant-based NPS" OR "aminoindane" OR "tryptamine" OR "piperazine" OR "phenethylamine" AND prison* OR jail OR penitentiary OR "correctional service" OR "correctional institution" (3 results)

1A-part 3) "synthetic cathinone" AND prison* OR jail OR penitentiary OR "correctional services" OR "correctional institution" (0 results)

The full search strings strategy performed on **Scopus**, lead to n= **175** results (updated on the 31/04/21 through alerts) and is described below:

1A-part 1) "NPS" OR "synthetic cannabinoid" OR "SCRA" OR "designer drug" OR "psychoactive substance" OR "legal high" AND prison* OR jail OR penitentiary OR "correctional service" OR "correctional institution" (162 results)

1A-part 2) "NPS opi*" OR "NPS benzodiazepine" OR "phencyclidine-type" OR "plant-based NPS" OR "aminoindane" OR "tryptamine" OR "piperazine" OR "phenethylamine" AND prison* OR jail OR penitentiary OR "correctional service" OR "correctional institution" (13 results)

1A-part 3) "synthetic cathinone" AND prison* OR jail OR penitentiary OR "correctional services" OR "correctional institution" (0 results)

The full search strings strategy performed on **Web of Science**, lead to n= **53** results and is described below:

One unique string: ("NPS" OR "synthetic cannabinoid" OR "SCRA" OR "designer drug" OR "psychoactive substance" OR "legal high" OR "NPS opi*" OR "NPS benzodiazepine" OR "Phencyclidine-type" OR "Plant-based NPS" OR "aminoindane" OR "Tryptamine" OR "Piperazine" OR "Phenethylamine" OR "Synthetic cathinone") AND (prison* OR jail OR penitentiary OR "correctional services" OR "correctional institution") (53 results).

The search was not associated with any time or geographical restrictions; all languages were included in the search results; however non-English results were removed during the review process. All the document type available were searched on the databases.

After the second update on the Scopus search done on the 31/01/21 the alert for each string was set up to provide updates of the literature in the form of weekly e-mails, until the end of April 2021. This led to an additional 6 articles, of which 1 met the systematic literature review inclusion criteria and it was accepted. While the other databases were added at a later date, however, the time limit was set to April 2021 for consistency.

The full databases literature search led to a total n= **493** documents.

Grey literature search

The grey literature search was conducted between May 2020 and January 2021 (31/01/21) and included targeted hand searching of websites listed below. A particular focus was put on UK government and/or research organization websites (from 1 to 4), while also European (5) and global (6) agencies websites were consulted.

1) HM Inspectorate of Prisons (https://www.justiceinspectorates.gov.uk/hmiprisons/), which was searched in the section "Our reports" for the following report type: "Annual report" and "Thematic reports and research" selecting only reports from 2010 to 2020 without any location restriction ("Annual report" 23/05/20 n=12; "Thematic reports and research" 10/06/20 n=59).
2) Prisons & Probations Ombudsman (https://www.ppo.gov.uk), which was searched in the section "Reports and Publications" for the following report type: "Annual reports" and "Learning lesson reports" selecting only reports from 2010 to 2020 without any other restriction ("Annual report" 22/05/20 n=11).
3) UK Focal Point on Drugs (https://www.gov.uk/government/publications/united-kingdom-drug-situation-focal-point-annual-report) which was searched in the section "Annual Reports" selecting only reports from 2010 to 2020 without any other restriction (10/05/20 n=8). Additionally, the organisation was e-mailed on date 18/05/20 to enquire about the reports for the years 2018 and 2019, which has not been yet published.

4) WEDINOS (https://www.wedinos.org/) which was searched in the section "Newsletter" selecting only annual reports from 2013 to 2020 (as before 2013 the service/organisation was not active hence no reports were produced) without any other restriction (04/06/20 n=7).
5) EMCDDA (https://www.emcdda.europa.eu/), which was searched in the section "Publications" categorised by "keyword(s)" for "NPS" ("NPS" 09/06/20 n=109)
6) UNODC (https://www.unodc.org/), which was searched in the section "What do we do?" then "Research" by selecting "Synthetic drugs" and then clicking on "SMART Publications" icon selecting only reports from 2010 to 2021 and excluding poster and leaflets as not an acceptable academic source (09/06/20 n=66)

The grey literature search led to an additional total n=**272** documents.

Also, EMCDDA newsletter for new publications on the topic was subscribed. While where setting an alert was not possible, the search was rerun the date prior the paper submission (31/01/21) to ensure everything was kept up to date.

Some of the grey literature searches were associated with some time restrictions (specified above for each organisation website/database) as from preliminary searches we found that prior the 2010 the use of NPS was not spread in the prison setting. Only research document, annual reports and thematic paper were searched on government and/or research organisation websites. Some organisations were also contacted to enquiry about the latest reports and/or additional unpublished data (e.g., UK FOCAL POINT ON DRUGS, WEDINOS, Office for National Statistics UK and EMCDDA). None of the above led to additional record.

Inclusion/exclusion criteria

inclusion criteria for this systematic literature review will be peer reviewed empirical research studies (quantitative/qualitative self-reporting studies; analytical studies of biological/non-biological samples; organisational reports and generic publications) and organisational reports and publications, which explore, evaluate or relate to 1) the use and 2) the forms and ways in which NPS are smuggled in prison setting. The search was limited to studies published in the English language.

Studies that considered the following were excluded:

- NPS use related to community settings (e.g., offenders on conditional release, detainees in police custody, any testing done on admission to prison).
- Opinion/discussion papers, letters to editor which were not peer reviewed, press release/magazines/websites articles, published conference abstracts, leaflets, posters, thesis, protocols and patents.
- Systematic Literature reviews, as categorised as a secondary source of information (however these were cross referenced to find primary pieces of information otherwise not accessible)
- Studies where due to the lack breakdown by specific class, it was not possible to extract data correctly.

Study selection

The abstracts of identified papers were assessed against the inclusion and exclusion criteria by GV and AM. Discrepancies were resolved through meetings between GV, AM, JS and AG. Following this process, full papers were retrieved for review by GV or AM.

Deduplication of results

A total of n=765 of results were retrieved from the database search the grey literature and the Scopus alert. The duplicates were removed using the Excel function to find and remove duplicated. After deduplication the total number of results dropped to n= 608, as n=157 of duplicates was found.

Additional studies

A n=1 (Van Dyken et al.) additional study was found through expert's advice/consultation.

Cross referencing

The reference list of the included articles (n=44) found through the search string, grey literature search and expert's advice/consultation, was cross referenced. Additionally, also the articles added to the review from the cross-referencing search (n=5) were cross referenced. This process led to a total of n=1937 additional citations which were manually searched to identify additional pertinent studies.

Appendix 1.2. SC seizures reported in non-biological samples by country and year

Table A2. SC seizures reported in non-biological samples by country and year.

Scotland	**2018**	**2019**	**2020**	**Tot.**	**Reference**
Cumyl-4CN-BINACA	1	0	0	1	Norman et *al.*, 2021
4F-MDMB-BINACA	0	94	61	155	Norman et *al.*, 2021
5F-MDMB-PINACA	22	23	3	48	Norman et *al.*, 2021
AMB-FUBINACA	4	2	0	6	Norman et *al.*, 2021
EMB-FUBINACA	2	2	0	4	Norman et *al.*, 2021
MDMB-4en-PINACA	0	63	109	172	Norman et *al.*, 2021
4F-MDMB-BICA	0	0	8	8	Norman et *al.*, 2021
5F-EMB-PICA	0	0	11	11	Norman et *al.*, 2021
5F-MDMB-PICA	2	80	46	128	Norman et *al.*, 2021
5F-MPP-PICA	0	0	1	1	Norman et *al.*, 2021
AMB-CHMICA	0	2	0	2	Norman et *al.*, 2021
Wales	**2018**	**2019**	**2020**	**Tot.**	**Reference**
5F-PB-22	0	4	0	4	Norman et *al.*, 2021
4F-MDMB-BINACA	0	77	12	89	Norman et *al.*, 2021
5F-APINACA	0	4	0	4	Norman et *al.*, 2021
5F-MDMB-PINACA	28	103	0	131	Norman et *al.*, 2021
AMB-FUBINACA	16	33	0	49	Norman et *al.*, 2021
MDMB-4en-PINACA	0	26	11	37	Norman et *al.*, 2021
MDMB-CHMICA	0	1	0	1	Norman et *al.*, 2021
England	**2015**			**Tot.**	**Reference**
5F AKB-48	317	N.A.	N.A.	317	Bond and Hudson, 2015
5F AMB	12	N.A.	N.A.	12	Bond and Hudson, 2015
5F PB-22	258	N.A.	N.A.	258	Bond and Hudson, 2015
5F UR-144	7	N.A.	N.A.	7	Bond and Hudson, 2015
AB-CHMINACA	11	N.A.	N.A.	11	Bond and Hudson, 2015
AB-FUBINACA	11	N.A.	N.A.	11	Bond and Hudson, 2015
AKB-48	6	N.A.	N.A.	6	Bond and Hudson, 2015
AM-2201	16	N.A.	N.A.	16	Bond and Hudson, 2015
FUB-PB-22	1	N.A.	N.A.	1	Bond and Hudson, 2015
MAM-2201	4	N.A.	N.A.	4	Bond and Hudson, 2015
MDMB-CHMICA	59	N.A.	N.A.	59	Bond and Hudson, 2015
PB-22	1	N.A.	N.A.	1	Bond and Hudson, 2015
QUICHIC	69	N.A.	N.A.	69	Bond and Hudson, 2015
STS-135	3	N.A.	N.A.	3	Bond and Hudson, 2015
UR-144	1	N.A.	N.A.	1	Bond and Hudson, 2015
England	**2016**			**Tot.**	**Reference**

5F-APINACA (aka **5F-AKB-48**)	5	N.A.	N.A.	5	Ford & Berg, 2018
AB-FUBINACA	3	N.A.	N.A.	3	Ford & Berg, 2018
MDMB-CHMICA	4	N.A.	N.A.	4	Ford & Berg, 2018
England	**2014/ 2015**			**Tot.**	**Reference**
5F-APINACA (aka 5F-AKB-48)	10	N.A.	N.A.	10	Ford & Berg, 2016
5F-PB-22	11	N.A.	N.A.	11	Ford & Berg, 2016
AB-FUBINACA	2	N.A.	N.A.	2	Ford & Berg, 2016
AM-2201	1	N.A.	N.A.	1	Ford & Berg, 2016
APINACA (aka AKB-48)	1	N.A.	N.A.	1	Ford & Berg, 2016
PB-22 (aka QUPIC)	1	N.A.	N.A.	1	Ford & Berg, 2016
STS-135 (aka 5F-APICA)	1	N.A.	N.A.	1	Ford & Berg, 2016
England	**N\A**			**Tot.**	**Reference**
AMB-FUBINACA (aka FUB-AMB)	1	N.A.	N.A.	1	Apikkaran et al. 2020
MMB-CHMICA (aka AMB-CHMICA)	1	N.A.	N.A.	1	Apikkaran et al. 2020
Germany	**N\A**			**Tot.**	**Reference**
5F-ADB (aka 5F-MDMB-PINACA)	6	N.A.	N.A.	6	Metternich *et al.*, 2018
AB-CHMINACA	1	N.A.	N.A.	1	Metternich *et al.*, 2018
AMB-FUBINACA (aka FUB-AMB)	5	N.A.	N.A.	5	Metternich *et al.*, 2018
APINACA (aka AKB-48)	3	N.A.	N.A.	3	Metternich *et al.*, 2018
Cumyl-PeGaClone	3	N.A.	N.A.	3	Metternich *et al.*, 2018
MMB-2201	1	N.A.	N.A.	1	Metternich *et al.*, 2018
PB-22 (aka QUPIC)	1	N.A.	N.A.	1	Metternich *et al.*, 2018
Germany		**2019**		**Tot.**	**Reference**
4F-MDMB-BINACA (aka 4F-MDMB-BUTINACA)	N.A.	1	N.A.	1	Hascimi et *al.*, 2020
5F-MDMB-PICA	N.A.	1	N.A.	1	Hascimi et *al.*, 2020
US		**2019**		**Tot.**	**Reference**
4F-MDMB-BINACA (aka 4F-MDMB-BUTINACA)	N.A.	1	N.A.	1	Caterino *et al.*, 2019
4F-MDMB-BINACA 2'-indazole isomer	N.A.	1	N.A.	1	Caterino *et al.*, 2019
5F-ADB (aka 5F-MDMB-PINACA)	N.A.	1	N.A.	1	Caterino *et al.*, 2019
5F-MDMB-PICA	N.A.	1	N.A.	1	Caterino *et al.*, 2019

Table 3. SC reported in biological samples by country and year.

Germany	**2018**	**2019**	**2020**	**Tot.**	**Reference**
JWH-081	0	1	1	2	Norman *et al.*, 2021
JWH-122	0	0	1	1	Norman *et al.*, 2021
FUB-144	0	0	1	1	Norman *et al.*, 2021
EG-018	0	1	0	1	Norman *et al.*, 2021
5F-Cumyl-PEGACLONE	28	32	1	61	Norman *et al.*, 2021
Cumyl-CBMEGACLONE	0	0	4	4	Norman *et al.*, 2021
Cumyl-CHMEGALONE	0	1	0	1	Norman *et al.*, 2021
Cumyl-PEGACLONE	5	2	0	7	Norman *et al.*, 2021
Cumyl-4CN-BINACA	1	0	0	1	Norman *et al.*, 2021
Cumyl-CBMINACA	0	0	6	6	Norman *et al.*, 2021
5F-Cumyl-PICA	0	1	0	1	Norman *et al.*, 2021
Cumyl-CBMICA	0	5	11	16	Norman *et al.*, 2021
Cumyl-4CN-B7AICA	2	1	0	3	Norman *et al.*, 2021
5F-MDMB-P7AICA	4	4	2	10	Norman *et al.*, 2021
4F-MDMB-BINACA	0	200	97	297	Norman *et al.*, 2021
5F-AB-PINACA	10	0	4	14	Norman *et al.*, 2021
5F-ADB-PINACA	4	0	0	4	Norman *et al.*, 2021
5F-MDMB-PINACA	79	15	4	98	Norman *et al.*, 2021
ADB-BINACA	0	0	22	22	Norman *et al.*, 2021
AB-CHMINACA	3	0	1	4	Norman *et al.*, 2021
ADB-CHMINACA	3	0	0	3	Norman *et al.*, 2021
MDMB-CHMINACA	2	0	0	2	Norman *et al.*, 2021
FUB-APINACA	3	0	0	3	Norman *et al.*, 2021
AB-FUBINACA amide hydrolysis metabolite	84	35	2	121	Norman *et al.*, 2021
ADB-FUBINACA	7	0	0	7	Norman *et al.*, 2021
MDMB-4en-PINACA	0	23	142	165	Norman *et al.*, 2021
4F-MDMB-BICA	0	0	17	17	Norman *et al.*, 2021
5F-ABICA amide hydrolysis metabolite	0	1	21	22	Norman *et al.*, 2021
5F-MDMB-PICA	28	168	180	376	Norman *et al.*, 2021
AMB-CHMICA	1	0	0	1	Norman *et al.*, 2021
AMB-FUBICA	0	1	0	1	Norman *et al.*, 2021
AMB-4en-PICA	0	0	1	1	Norman *et al.*, 2021
Germany	**2019**			**Tot**	**Reference**
5F-Cumyl-PEGACLONE and metabolites	1	N.A.	N.A.	1	Giorgetti *et al., 2019*

England	**2014/2015**	**2015**		**Tot**	**Reference**
5F-AB-PINACA	1	0	N.A.	1	Bond and Hudson, 2015
5F-ADB-PINACA	1	1	N.A.	2	Bond and Hudson, 2015
5F-AKB-48	1177	272	N.A.	1449	Bond and Hudson, 2015
5F-PB-22	24	7	N.A.	31	Bond and Hudson, 2015
5F-UR-144	80	6	N.A.	86	Bond and Hudson, 2015
AB-FUBINACA	3	0	N.A.	3	Bond and Hudson, 2015
AKB-48	3	3	N.A.	6	Bond and Hudson, 2015
AM-2201	87	13	N.A.	100	Bond and Hudson, 2015
AM-694	18	0	N.A.	18	Bond and Hudson, 2015
Cumyl-5F-PINACA	13	9	N.A.	22	Bond and Hudson, 2015
MAM-2201	42	1	N.A.	43	Bond and Hudson, 2015
MDMB-CHMICA	371	210	N.A.	581	Bond and Hudson, 2015
STS-135	9	0	N.A.	9	Bond and Hudson, 2015
THJ-018	3	0	N.A.	3	Bond and Hudson, 2015
THJ-2201	9	0	N.A.	9	Bond and Hudson, 2015
UR-144	72	1	N.A.	73	Bond and Hudson, 2015
England	**N/A**			**Tot**	**Reference**
MDMB-CHMICA	3	N.A.	N.A.	3	Meyappan *et al.*, 2016
Norway	**N/A**			**Tot**	**Reference**
AM-2201	9	N.A.	N.A.	9	Øiestad *et al., 2013*
JWH-018	9	N.A.	N.A.	9	Øiestad *et al., 2013*
USA	**2019**			**Tot**	**Reference**
4F-MDMB-BINACA 3,3-dimethylbutanoic acid	3	N.A.	N.A.	3	Norman *et al.*, 2021
5F-MDMB-PICA 3,3-dimethylbutanoic acid	11	N.A.	N.A.	11	Norman *et al.*, 2021
USA	**2019**			**Tot**	**Reference**
MDMB-4en-PINACA 3,3-dimethylbutanoic acid	1	N.A.	N.A.	1	Kroutulski *et al. 2020*
USA	**2018/2019**			**Tot**	**Reference**
5F-AMB butanoic acid conjugated metabolite	2	N.A.	N.A.	2	Hvozdovich *et al., 2019*
5F-MDMB-PINACA aka 5F-ADB butanoic acid conjugated metabolite	52	N.A.	N.A.	52	Hvozdovich *et al., 2019*
AB-CHMINACA butanoic acid conjugated metabolite	1	N.A.	N.A.	1	Hvozdovich *et al., 2019*

FUB-AMB butanoic acid conjugated metabolite	21	N.A.	N.A.	21	Hvozdovich *et al., 2019*
MDMB-FUBINACA butanoic acid conjugated metabolite	2	N.A.	N.A.	2	Hvozdovich *et al., 2019*
USA	**N/A**			**Tot**	**Reference**
4F-MDMB-BINACA	1	N.A.	N.A.	1	Kleis *et. al.,* 2020
5F-MDMB-PICA	1	N.A.	N.A.	1	Kleis *et. al.,* 2020
USA	**N/A**			**Tot**	**Reference**
ADB-FUBINACA	1	N.A.	N.A.	1	Nacca *et al., 2018*

Table 4. Common, street and IUPAC names of NPS mentioned in the review

Common name	**Street name**	**Systematic name**
1-benzylpiperazine	BZP and A2	1-benzylpiperazine
4-methyl-methamphetamine	4-MMA	*N*-methyl-1-(4-methylphenyl)propan-2-amine
4F-MDMB-BICA (aka 4F-MDMB-BUTICA)	Spice and black mamba	Methyl (S)-2-(1-(4-fluorobutyl)- 1H-indole-3-carboxamido)-3,3- dimethylbutanoate
4F-MDMB-BINACA (aka 4F-MDMB-BUTINACA)	Spice and black mamba	Methyl (2R)-2-{[1-(4- fluorobutyl)-1H-indazole-3-carbonyl]amino}-3,3-dimethylbutanoate
4F-PHP	Bath salts	1-(4-fluorophenyl)-2-(pyrrolidin-1-yl)hexan-1-one, monohydrochloride
5F-AB-PINACA	Spice and black mamba	*N*-[(1S)-1-(aminocarbonyl)-2-methylpropyl]-1-(5-fluoro)pentyl-1H-indazole-3-carboxamide
5F-ADB (aka 5F-MDMB-PINACA)	Spice and black mamba	Methyl-[2-(1-(5-fluoropentyl)-1H-indazole-3-carboxamido)-3,3-dimethylbutanoate]
5F-ADB-PINACA	Spice and black mamba	*N*-(1-amino-3,3-dimethyl-1-oxobutan-2-yl)-1-(5-fluoropentyl)-1H-indazole-3-carboxamide
5F-AMB (aka 5F-MMB-PINACA aka 5F-AMB-PINACA)	Spice and black mamba	Methyl 2-({[1-(5-fluoropentyl)-1H-indazol-3-yl]carbonyl}amino)-3-methylbutanoate
5F-APINACA (aka 5F-AKB-48)	Spice and black mamba	*N*-(1-adamantyl)-1-(5-fluoropentyl)-1H-indazole-3 -carboxamide
5F-Cumyl-PEGACLONE	Spice and black mamba	5-(5-fluoropentyl)-2-(1-methyl-1-phenylethyl)-pyrido[4,3-b]indol-1-one
5F-Cumyl-PICA	Spice and black mamba	1-(5-fluoropentyl)-N-(1-methyl-1-phenylethyl)-1H-indole-3-carboxamide
5F-Cumyl-PINACA	Spice and black mamba	1-(5-fluoropentyl)-N-(1-methyl-1-phenylethyl)-1H-indazole-3-carboxamide
5F-EMB-PICA (aka EMB-2201)	Spice and black mamba	Ethyl (1-(5-fluoropentyl)-1H-indole-3-carbonyl)-L-valinate

5F-MDMB-P7AICA	Spice and black mamba	Methyl 2-{[1-(5-fluoropentyl)-1H-pyrrolo[2,3-b]pyridin-3-yl]formamido}-3,3-dimethylbutanoate
5F-MDMB-PICA	Spice and black mamba	Methyl 2-[[1-(5-fluoropentyl)indole-3-carbonyl]amino]-3,3-dimethyl-butanoate
5F-MPP-PICA (aka MPHP-2201)	Spice and black mamba	Methyl (1-(5-fluoropentyl)- 1H-indole-3-carbonyl)-L-phenylalaninate
5F-PB-22	Spice and black mamba	Quinolin-8-yl 1-(5-fluoropentyl)-1H-indole-3-carboxylate
5F-UR-144 (aka XLR-11)	Spice and black mamba	(1-(5-fluoropentyl)-1H-indol-3-yl)(2,2,3,3-tetramethylcyclopropyl)methanone
AB-CHMINACA	Spice and black mamba	*N*-[(1S)-1-(aminocarbonyl)-2-methylpropyl]-1-(cyclohexylmethyl)-1H-indazole-3-carboxamide
AB-FUBINACA	Spice and black mamba	*N*-(1-amino-3-methyl-1-oxobutan-2-yl)-1-(4-fluorobenzyl)-1H-indazole-3-carboxamide
Acryloylfentanyl	N/A	*N*-(1-phenethylpiperidin-4-yl)-N-phenylacrylamide
ADB-BINACA	Spice and black mamba	*N*-(1-amino-3,3-dimethyl-1-oxobutan-2-yl)-1-benzyl-1H-indazole-3-carboxamide
ADB-CHMINACA (aka MAB-CHMINACA)	Spice and black mamba	*N*-[1-(aminocarbonyl)-2,2-dimethylpropyl]-1-(cyclohexylmethyl)-1H-indazole-3-carboxamide
ADB-FUBINACA	Spice and black mamba	*N*-[(1S)-1-(aminocarbonyl)-2,2-dimethylpropyl]-1-[(4-fluorophenyl)methyl]-1H-indazole-3-carboxamide
AM-2201	Spice and black mamba	1-[(5-fluoropentyl)-1H-indol-3-yl]-(naphthalen-1-yl)methanone
AM-694	Spice and black mamba	1-[(5-fluoropentyl)-1H-indol-3-yl]-(2-iodophenyl)methanone
AMB-4en-PICA (aka MMB-4en-PICA, MMB022)	Spice and black mamba	Methyl (1-(pent-4-en-1-yl)-1H-indole-3-carbonyl)-L-valinate
AMB-FUBICA	Spice and black mamba	Methyl 2-[[1-[(4-fluorophenyl)methyl]indole-3-carbonyl]amino]-3-methyl-butanoate
AMB-FUBINACA (aka FUB-AMB)	Spice and black mamba	Methyl-2-(1-(4-fluorobenzyl)-1H-indazole-3-carboxamide)-3-methylbutanoate
APINACA (aka AKB-48)	Spice and black mamba	*N*-(1-adamantyl)-1-pentyl-1H-indazole-3-carboxamide
Carfentanil	N/A	Methyl 1-phenethyl-4-(*N*-phenylpropionamido)piperidine-4-carboxylate
Cumyl-4CN-B7AICA	Spice and black mamba	1-(4-cyanobutyl)-N-(2-phenylpropan-2-yl)-1H-pyrrolo[2,3-b]pyridin-3-carboxamide
Cumyl-4CN-BINACA (aka Cumyl-CYBINACA aka SGT-78)	Spice and black mamba	1-(4-cyanobutyl)-N-(1-methyl-1-phenyl-ethyl)indazole-3-carboxamide
Cumyl-5F-PINACA (aka SGT-25)	Spice and black mamba	1-(5-fluoropentyl)-N-(1-methyl-1-phenylethyl)-1H-indazole-3-carboxamide
Cumyl-CB-MeGACLONE	Spice and black mamba	5-(cyclobutylmethyl)-2-(2-phenylpropan-2-yl)-2,5-dihydro-1H-pyrido[4,3-b]indol-1-one

Cumyl-CBMICA	Spice and black mamba	1-(cyclobutylmethyl)-N-(2-phenylpropan-2-yl)-1H-indole-3-carboxamide
Cumyl-CBMINACA	Spice and black mamba	1-(cyclobutylmethyl)-N-(2-phenylpropan-2-yl)-1H-indazole-3-carboxamide
CUMYL-PEGACLONE (aka SGT-151)	Spice and black mamba	5-pentyl-2-(2-phenylpropan-2-yl)pyrido[4,3-b]indol-1-one
Cumyl-PeGACLONE (aka SGT-151)	Spice and black mamba	5-(5-fluoropentyl)-2-(1-methyl-1-phenylethyl)-pyrido[4,3-b]indol-1-one
Cyclopropylfentanyl	N/A	*N*-phenyl-N-[1-(2-phenylethyl)piperidin-4-yl]cyclopropanecarboxamide
EG-018	Spice and black mamba	Naphthalen-1-yl(9-pentyl-9H-carbazol-3-yl)methanone
Ethylphenidate	Nopaine and Fake cocaine	Ethyl 2-phenyl-2-piperidin-2-ylacetate
Etizolam	Street Valium	4-(2-chlorophenyl)-2-ethyl-9-methyl-6H-thieno[3,2-f][1,2,4]triazolo[4,3-a][1,4]diazepine
FUB-144 (aka FUB-UR-144)	Spice and black mamba	[1-[(4-fluorophenyl)methyl]indol-3-yl]-(2,2,3,3-tetramethylcyclopropyl)methanone
FUB-APINACA (aka FUB-AKB48, AFB-48, AFUBINACA, FUB-APINACA)	Spice and black mamba	*N*-((3s,5s,7s)-adamantan-1-yl)-1-(4-fluorobenzyl)-1H-indazole-3-carboxamide
FUB-PB-22 (aka QUFUBIC)	Spice and black mamba	Quinolin-8-yl-1-(4-fluorobensyl)-1H-indole-3-carboxylate
JWH-018	Spice and black mamba	Naphthalen-1-yl-(1-pentylindol-3-yl)methanon
JWH-081	Spice and black mamba	(1-pentyl-3-(4-methoxy-1-naphthoyl)indole)
JWH-122	Spice and black mamba	1-pentyl-3-(4-methyl-1-naphthoyl)indole
JWH-210	Spice and black mamba	1-pentyl-3-(4-ethyl-1-naphthoyl)indole
Kava	Kava kava and kawa	Piper methysticum
MAM-2201	Spice and black mamba	1-(5-fluoropentyl)-3-(4-methyl-naphthoyl)indole
MDMB-4en-PINACA	Spice and black mamba	Methyl (S)-3,3-dimethyl-2-(1-(pent-4-en-1-yl)-1H-indazole-3-carboxamido)butanoate
MDMB-CHMICA (aka MDMB-CHMINACA)	Spice and black mamba	*N*-[[1-(cyclohexylmethyl)-1H-indol-3-yl]carbonyl]-3-methyl-valine, methyl ester
MDMB-FUBINACA (aka FUB-MDMB aka MDMB-Bz-F)	Spice and black mamba	2-[[1-[(4-fluorophenyl) methyl] indazole-3-carbonyl] amino]-3,3-dimethyl-butanoate

Mephedrone (aka 4-methyl methcathinone)	Bath salts, M-CAT and Meow Meow	(RS)-2-methylamino-1-(4-methylphenyl)propan-1-one
Methiopropamine	MPA	*N*-Methyl-1-(thiophen-2-yl)propan-2-amine
Methoxphenidine	MXP	1-(1-(2-methoxyphenyl)-2-phenylethyl)piperidine, monohydrochloride
Methylethcathinone	Bath salts and 2-MEC	2-(ethylamino)-1-(2-methylphenyl)propan-1-one
Methylhexaneamine	DMMA	4-methylhexan-2-amine
Methylone	Bath salts and MDM-CAT	1-(1,3-Benzodioxol-5-yl)-2-(methylamino)propan-1-one
Methylphenidate	Nopaine and fake cocaine	Methyl 2-phenyl-2-piperidin-2-ylacetate
MMB-CHMICA (aka AMB-CHMICA)	Spice and black mamba	Methyl 2-(1-(cyclohexylmethyl)-1H-indazole-3-carboxamide)-3-methylbutanoate
MMB-2201	Spice and black mamba	Methyl (1-(5-fluoropentyl)-1H-indole-3-carbonyl)valinate
PB-22 (aka QUPIC)	Spice and black mamba	1-Pentyl-1*H*-indole-3-carboxylic acid 8-quinolinyl ester
QUCHIC (aka BB-22)	Spice and black mamba	Quinolin-8-yl 1-(cyclohexylmethyl)-1H-indole-3-carboxylate
(R)-4F-MDMB-BINACA	Spice and black mamba	Methyl (2R)-2-{[1-(4-fluorobutyl)-1H-indazole-3-carbonyl]amino}-3,3-dimethylbutanoate
(R)-5F-ADB (aka (R)-5F-MDMB-PINACA)	Spice and black mamba	Methyl-[2R-(1-(5-fluoropentyl)-1H-indazole-3-carboxamido)-3,3-dimethylbutanoate]
(R)-5F-MDMB-PICA	Spice and black mamba	Methyl-(2R)-[[1-(5-fluoropentyl)indole-3-carbonyl]amino]-3,3-dimethyl-butanoate
(R)-MDMB-4en-PINACA	Spice and black mamba	Methyl (R)-3,3-dimethyl-2-(1-(pent-4-en-1-yl)-1H-indazole-3-carboxamido)butanoate
STS-135 (aka 5F-APICA)	Spice and black mamba	1-(5-fluoropentyl)-N-tricyclo[3.3.1.13,7]dec-1-yl-1H-indole-3-carboxamide
THJ-018	Spice and black mamba	Naphthalen-1-yl(1-pentyl-1H-indazol-3-yl)methanone
THJ-2201	Spice and black mamba	(1-(5-fluoropentyl)-1H-indazol-3-yl)(naphthalen-1-yl)methanone
UR-144	Spice and black mamba	(1-pentyl-1H-indol-3-yl)(2,2,3,3-tetramethylcyclopropyl)methanone

Appendix 1.3. Trends of scientific publications of NPS reported in prison settings

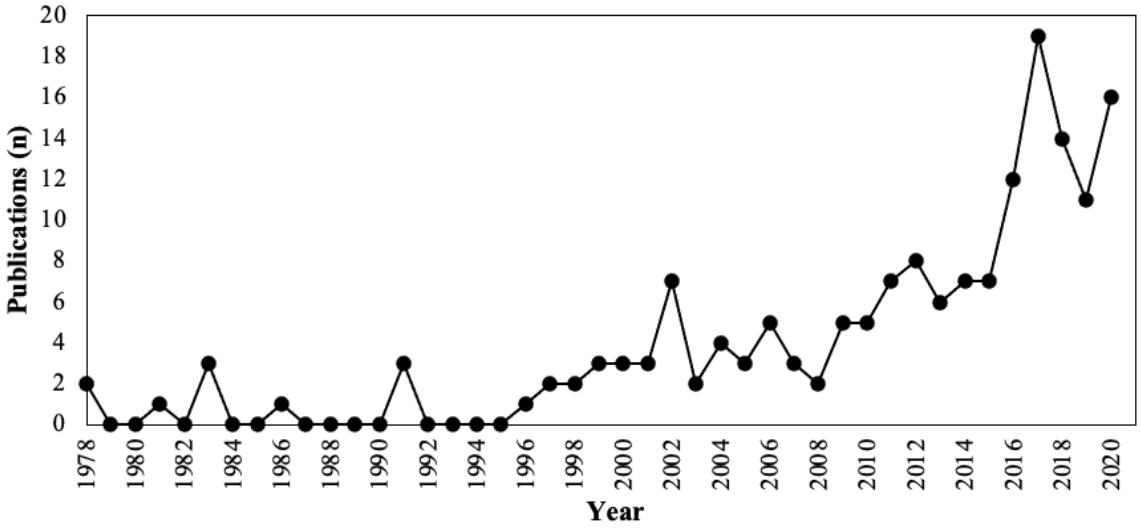

Figure A1. Trends of scientific publications of NPS reported in prison settings from 1978-2020.

Appendix 1.4. Routes and forms in which NPS are smuggled into prison

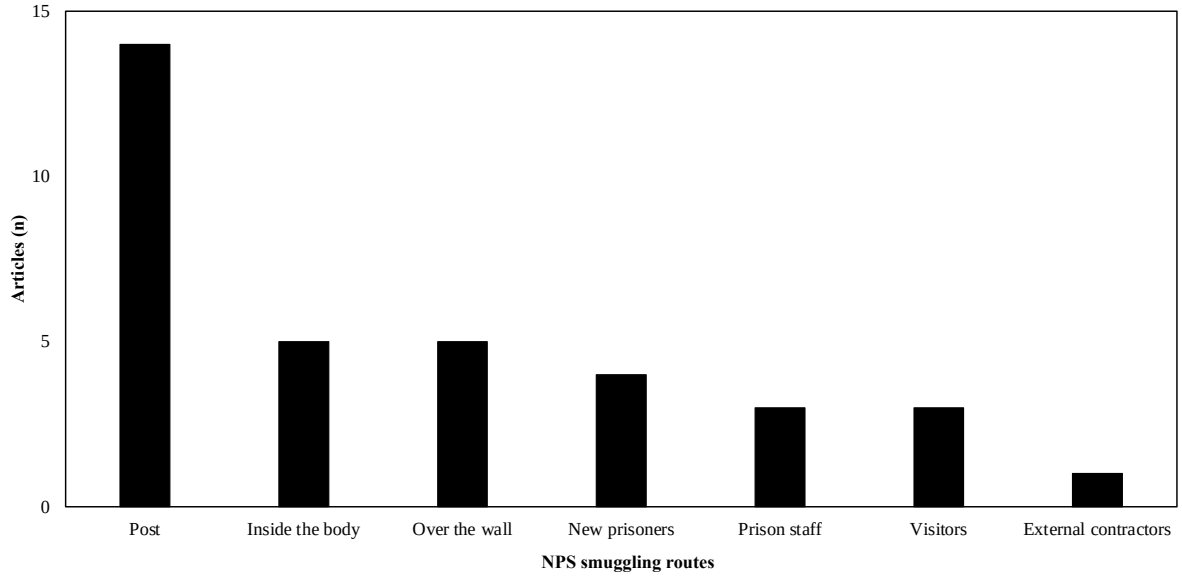

Figure A1. Routes in which NPS are smuggled into prison.

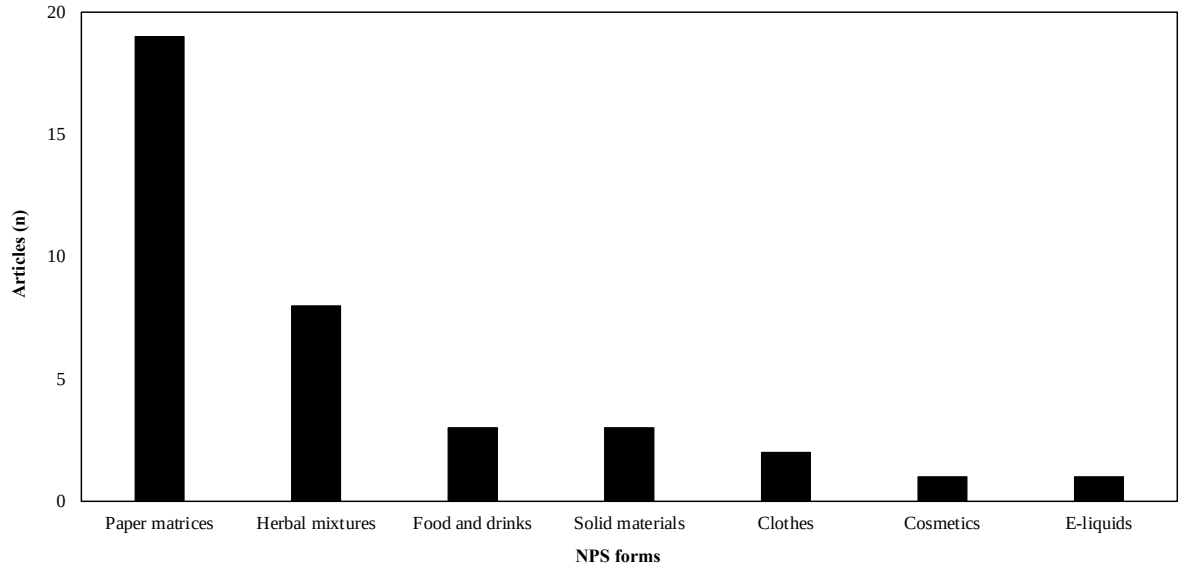

Figure A2. Forms in which NPS are smuggled into prison.

Appendix 2. (Chapter 3)

Appendix 2.1. Example of HPLC-UV-Vis paracetamol reference standard chromatogram

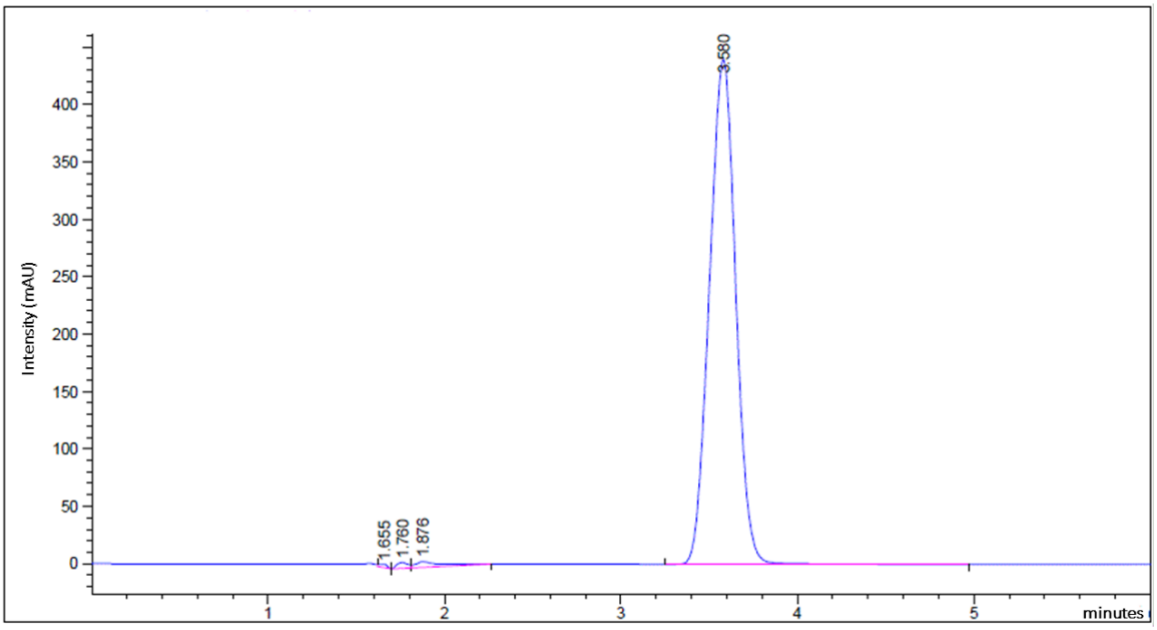

Figure A1 HPLC-UV-Vis paracetamol reference standard (100 ppm) chromatogram.

Appendix 2.2. Summary of HPLC-UV and UPLC-PdA-MS validation data results

Table A1. Summary of the results of the paracetamol HPLC-UV method validation.

	1st calibration curve	**2nd calibration curve**	**3rd calibration curve**	**Acceptance criteria**
Theoretical plate number (N)	2517	2883	2113	N > 2000
Tailing Factor (T)	1.04	1.02	1.08	T < 2
Linearity (R^2)	0.9999	0.9994	0.9999	R^2 > 0.9990
LOD (mg/ml)	0.00099	0.00232	0.00061	-
LOQ (mg/ml)	0.00301	0.00705	0.00181	-
	1st calibration curve	**2nd calibration curve**	**3rd calibration curve**	**Acceptance criteria**
Precision- Repeatability				
%RSD at low concentration	0.89	0.77	0.28	
%RSD at medium concentration	1.05	0.99	0.56	%RSD< 2%
%RSD at high concentration	0.55	1.23	0.65	
Intermediate Precision				
%RSD at low concentration	1.13	0.36	0.27	
%RSD at medium concentration	0.98	0.38	1.09	%RSD< 2%
%RSD at high concentration	1.64	1.21	0.51	
Accuracy				
%Accuracy at low concentration	98.8	99.0	98.2	
%Accuracy at medium concentration	98.1	98.5	98.6	100 ± 2%
%Accuracy at high concentration	98.8	98.6	99.7	

Table A2. Summary of the results of the cocaine UPLC-PdA-MS method validation.

	1st calibration curve	**2nd calibration curve**	**3rd calibration curve**	**Acceptance criteria**
Injection Repeatability (%RSD)	0.70	0.26	0.51	%RSD< 2%
Linearity (R^2)	1.0000	0.9998	1.0000	R^2>0.9990
Limit of Detection(mg/ml)	0.00042	0.00137	0.00052	-
Limit of Quantification(mg/ml)	0.00127	0.00417	0.00158	-
	1st calibration curve	**2nd calibration curve**	**3rd calibration curve**	**Acceptance criteria**
Precision- Repeatability				
%RSD at low concentration	1.07	0.37	0.72	
%RSD at medium concentration	0.47	0.21	0.45	%RSD< 2%
%RSD at high concentration	0.68	0.10	0.54	
Intermediate Precision				
%RSD at low concentration	0.21	0.47	0.58	
%RSD at medium concentration	0.04	0.06	0.06	%RSD< 2%
%RSD at high concentration	0.13	0.04	0.11	
Accuracy				
%Accuracy at low concentration	100.0	100.4	99.7	
%Accuracy at medium concentration	101.5	99.1	99.7	100 ± 2%
%Accuracy at high concentration	100.1	99.4	100.5	

Table A3. Summary of the results of the caffeine UPLC-PdA-MS method validation

	1st calibration curve	**2nd calibration curve**	**3rd calibration curve**	**Acceptance criteria**
Injection Repeatability (%RSD)	0.49	0.21	0.22	%RSD< 2%
Linearity (R^2)	1.0000	0.9999	1.0000	R^2>0.9990
Limit of Detection(mg/ml)	0.00046	0.00070	0.00082	-
Limit of Quantification(mg/ml)	0.00141	0.00213	0.00249	-
	1st calibration curve	**2nd calibration curve**	**3rd calibration curve**	**Acceptance criteria**
Precision- Repeatability				
%RSD at low concentration	0.69	0.31	0.44	
%RSD at medium concentration	0.47	0.28	0.12	%RSD< 2%
%RSD at high concentration	0.24	0.32	0.38	
Intermediate Precision				
%RSD at low concentration	0.16	0.32	0.09	
%RSD at medium concentration	0.09	0.08	0.08	%RSD< 2%
%RSD at high concentration	0.07	0.03	0.25	
Accuracy				
%Accuracy at low concentration	99.4	99.0	100.2	
%Accuracy at medium concentration	99.1	100.5	100.1	100 ± 2%
%Accuracy at high concentration	101.6	100.1	1009	

Table A4. Summary of UPLC-PdA-MS method validation results for THJ-018.

	1st calibration curve	2nd calibration curve	3rd calibration curve	Acceptance criteria
Injection Repeatability (%RSD)	0.14	0.02	0.22	%RSD< 2%
Linearity (R^2)	0.9999	0.9991	0.9990	R^2>0.9990
Limit of Detection(mg/ml)	0.01969	0.05846	0.06105	-
Limit of Quantification(mg/ml)	0.05966	0.17717	0.18500	-
	1st calibration curve	**2nd calibration curve**	**3rd calibration curve**	**Acceptance criteria**
Precision- Repeatability				
%RSD at low concentration	0.39	0.38	0.17	
%RSD at medium concentration	0.08	0.09	0.06	%RSD< 2%
%RSD at high concentration	0.04	0.04	0.34	
Intermediate Precision				
%RSD at low concentration	0.24	0.52	0.22	
%RSD at medium concentration	0.63	0.30	0.54	%RSD< 2%
%RSD at high concentration	0.27	0.28	0.25	
Accuracy				
%Accuracy at low concentration	98.9	99.0	98.4	
%Accuracy at medium concentration	99.1	101.5	100.1	100 ± 2%
%Accuracy at high concentration	101.0	101.9	101.0	

Appendix 2.3. Summary of caffeine, cocaine and THJ-018 % recovery

Table A1. Recovery % of caffeine, cocaine and THJ-018 from simulated paper samples

	Replicates samples	Recovery % CAF	Recovery % CAF+COC	Recovery % CAF+COC+THJ-018
CAF	**A**	72.24	72.15	72.73
	B	72.57	71.64	73.03
	C	71.83	73.73	73.23
COC	**A**		71.49	71.91
	B		72.17	73.66
	C		74.63	73.72
THJ-018	**A**			71.97
	B			74.51
	C			74.73

Appendix 2.4. Example of UPLC-PdA-QDa-MS chromatogram of MeOH

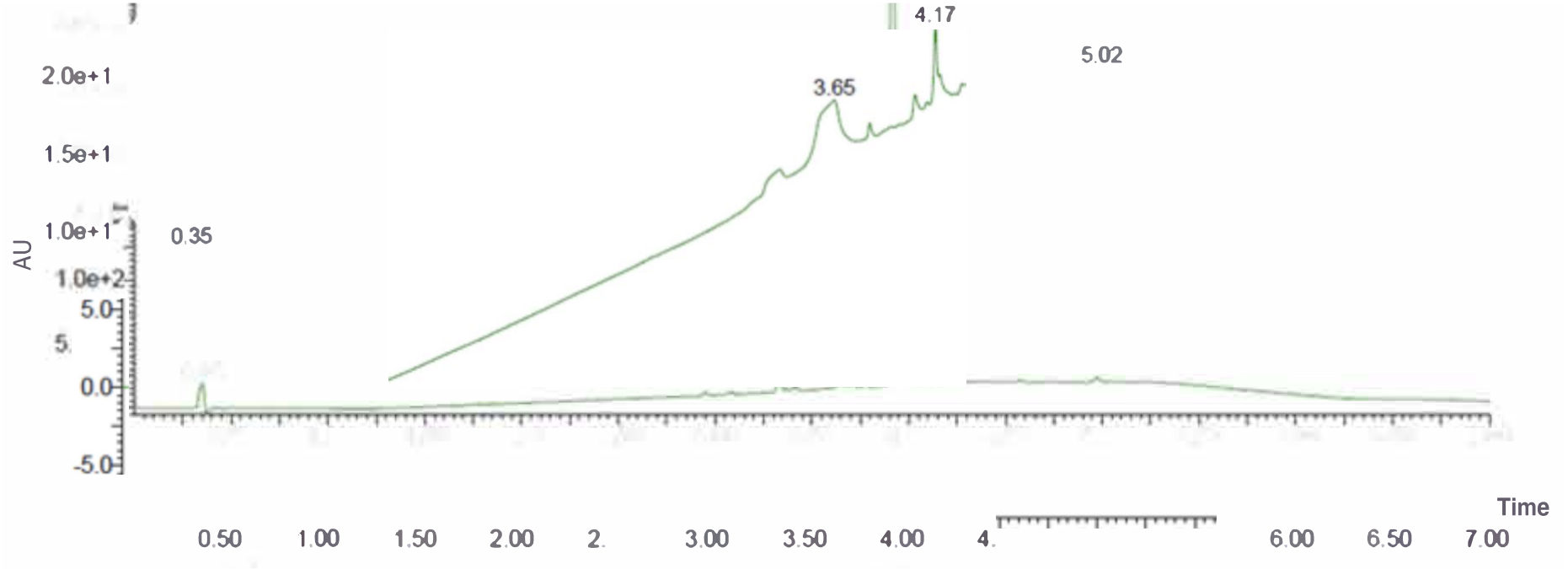

Figure A1. PdA chromatogram of MeOH.

Appendix 3. (Chapter 4)

Appendix 3.1. UPLC-PdA-QDa-MS method validation data summary

Table A1. UPLC-PdA-QDa-MS method validation results for 5F-ADB.

	1st calibration curve	**2nd calibration curve**	**3rd calibration curve**	**4th calibration curve**	**5th calibration curve**	**6th calibration curve**	**Acceptance criteria**
Theoretical plate number (N)	2314	29744	2437	29977	2256	2897	N > 2000
Tailing Factor (T)	1.03	1.01	1.06	1.01	1.02	1.05	T < 2
Linearity (R^2)	0.9958	0.9989	0.9988	0.9997	0.9985	0.9995	R^2 > 0.99
Limit of Detection (ng/ml)	0.11	0.06	0.06	0.03	0.06	0.04	-
Limit of Quantification (ng/ml)	0.33	0.18	0.17	0.09	0.19	0.11	-
	1st calibration curve	**2nd calibration curve**	**3rd calibration curve**	**4th calibration curve**	**5th calibration curve**	**6th calibration curve**	**Acceptance criteria**
Precision under repeatability & reproducibility condition							
RSD % at concentration 1 (highest)	0.85	0.51	0.16	0.23	0.59	0.47	% RSD < 15%
RSD % at concentration 2	0.69	0.53	0.55	0.99	0.50	0.42	% RSD < 15%
RSD % at concentration 3	0.42	0.51	0.33	0.65	0.46	0.73	% RSD < 15%
RSD % at concentration 4	1.09	1.37	0.99	0.29	0.36	0.37	% RSD < 20%

RSD % at concentration 5	3.57	3.68	2.56	1.29	3.64	2.81	% RSD < 20%
RSD % at concentration 6 (lowest)	4.63	2.92	2.16	1.33	4.93	4.31	% RSD < 20%
Accuracy							
Accuracy % at high concentration	109.3	89.6	109.4	90.0	86.6	102.1	% Error < 15%
Accuracy % at medium concentration	107.1	104.9	104.3	100.8	88.4	104.9	% Error < 15%
Accuracy % at low concentration	81.2	99.0	85.8	80.6	104.7	87.2	% Error < 20%

Appendix 3.2. UPLC-PdA-QToF-MS TIC of 11A, 11E and 11M subunits of the seized prison sample

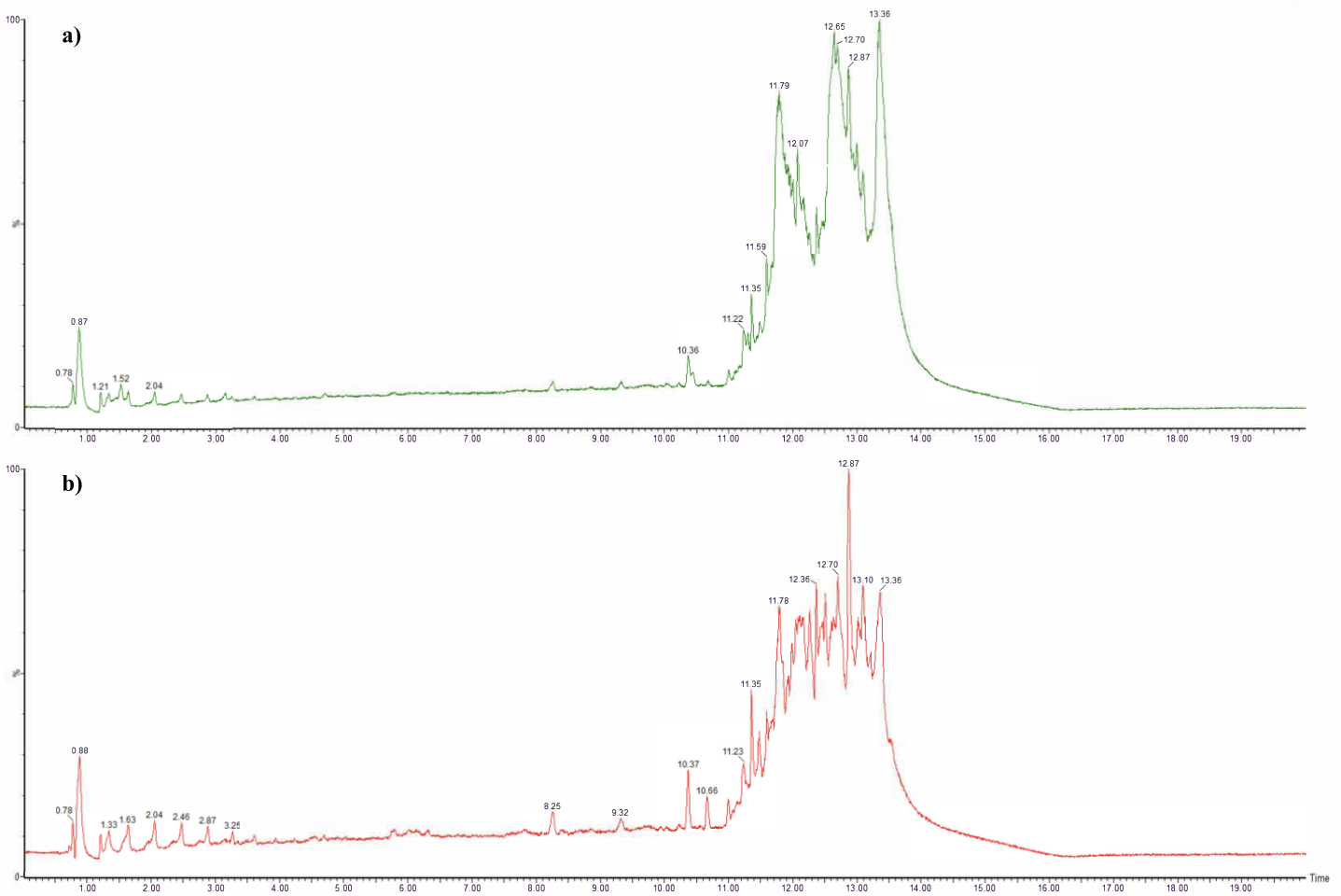

Figure A1. TIC in resolution mode of samples a) BP extract vs b) 11A replicate

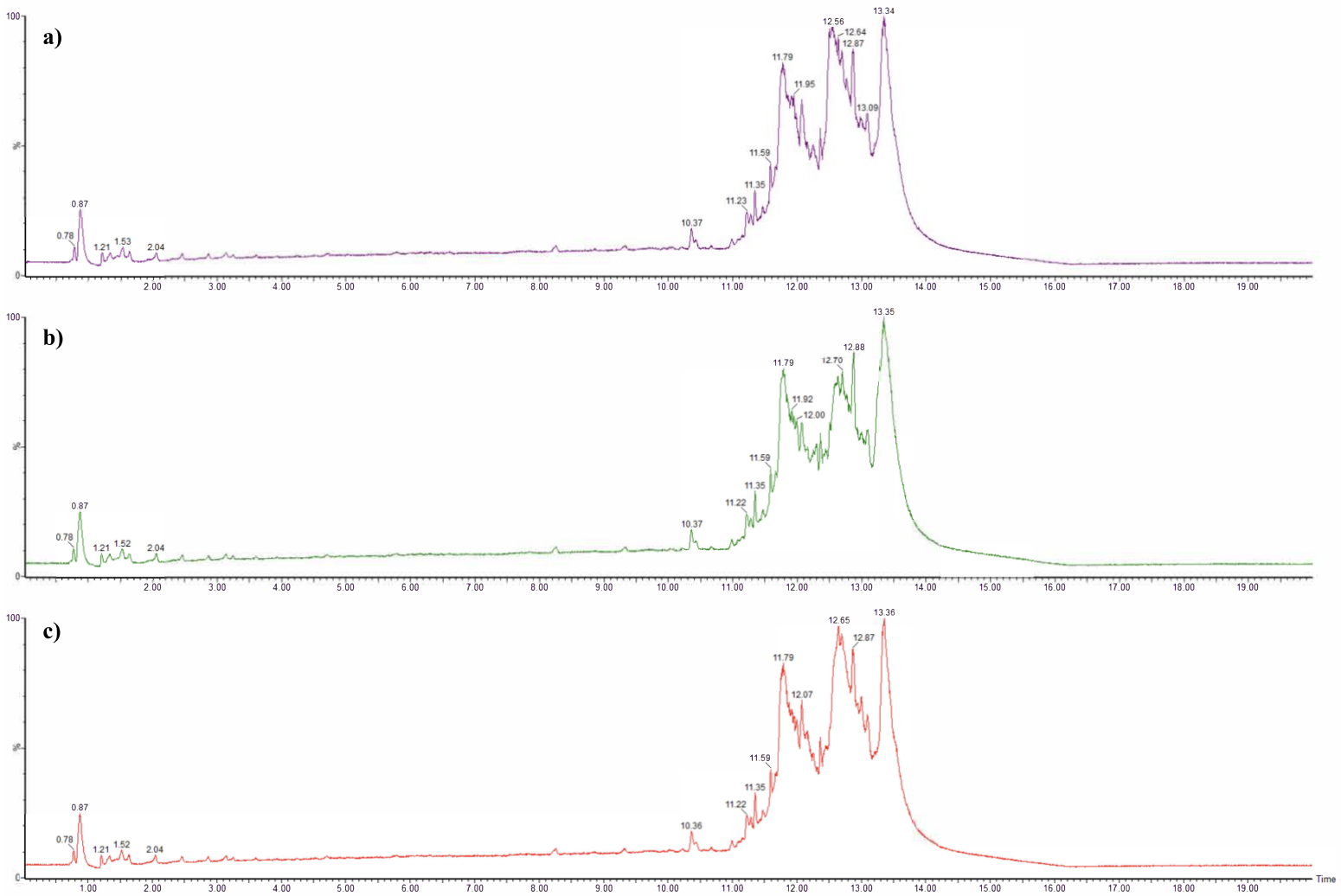

Figure A2. TIC in resolution mode of samples a) 11A replicate 3 vs. b) replicate 2 and c) replicate

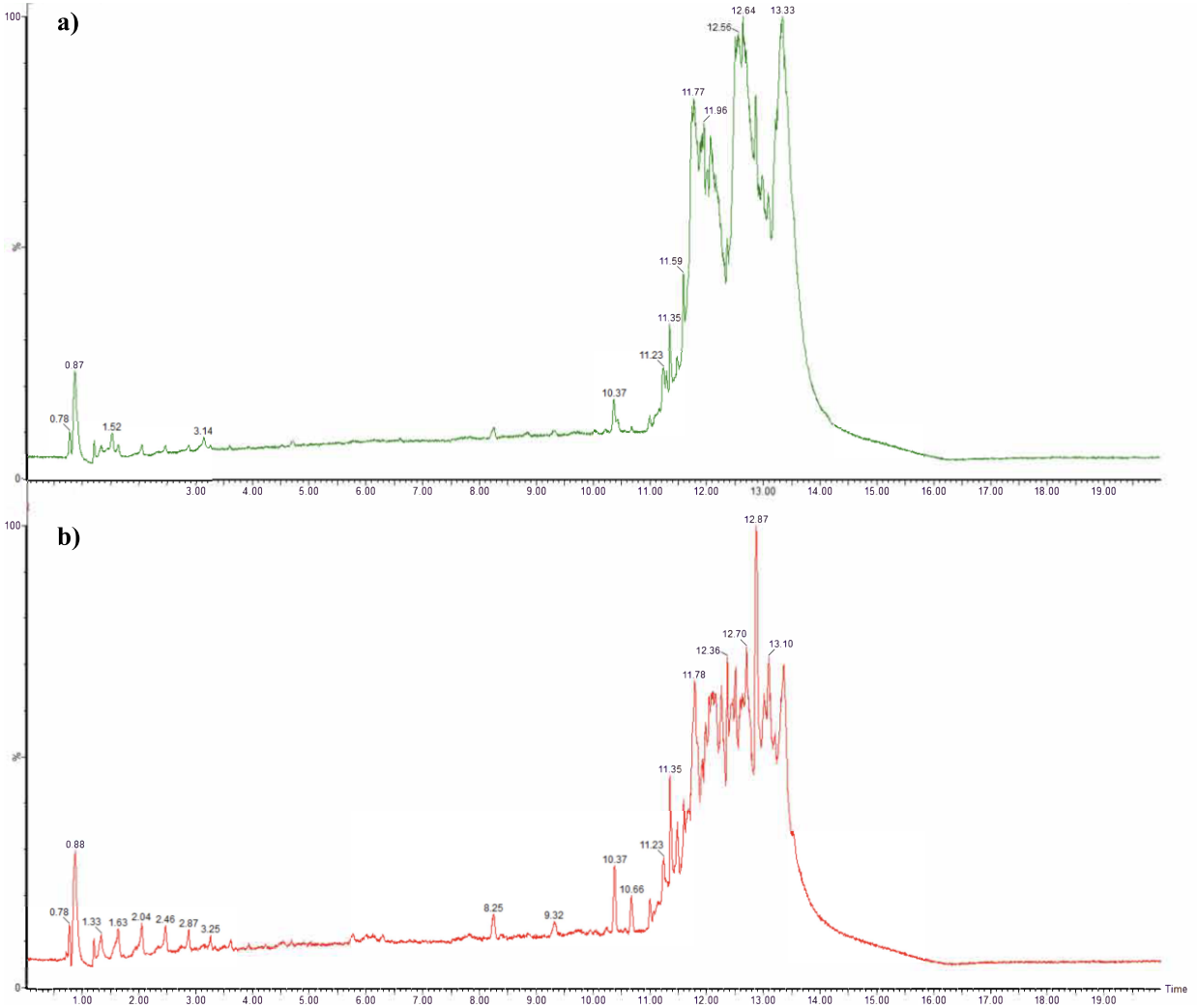

Figure A3. TIC in resolution mode of samples a) 11E replicate 1 vs. b) BP extract.

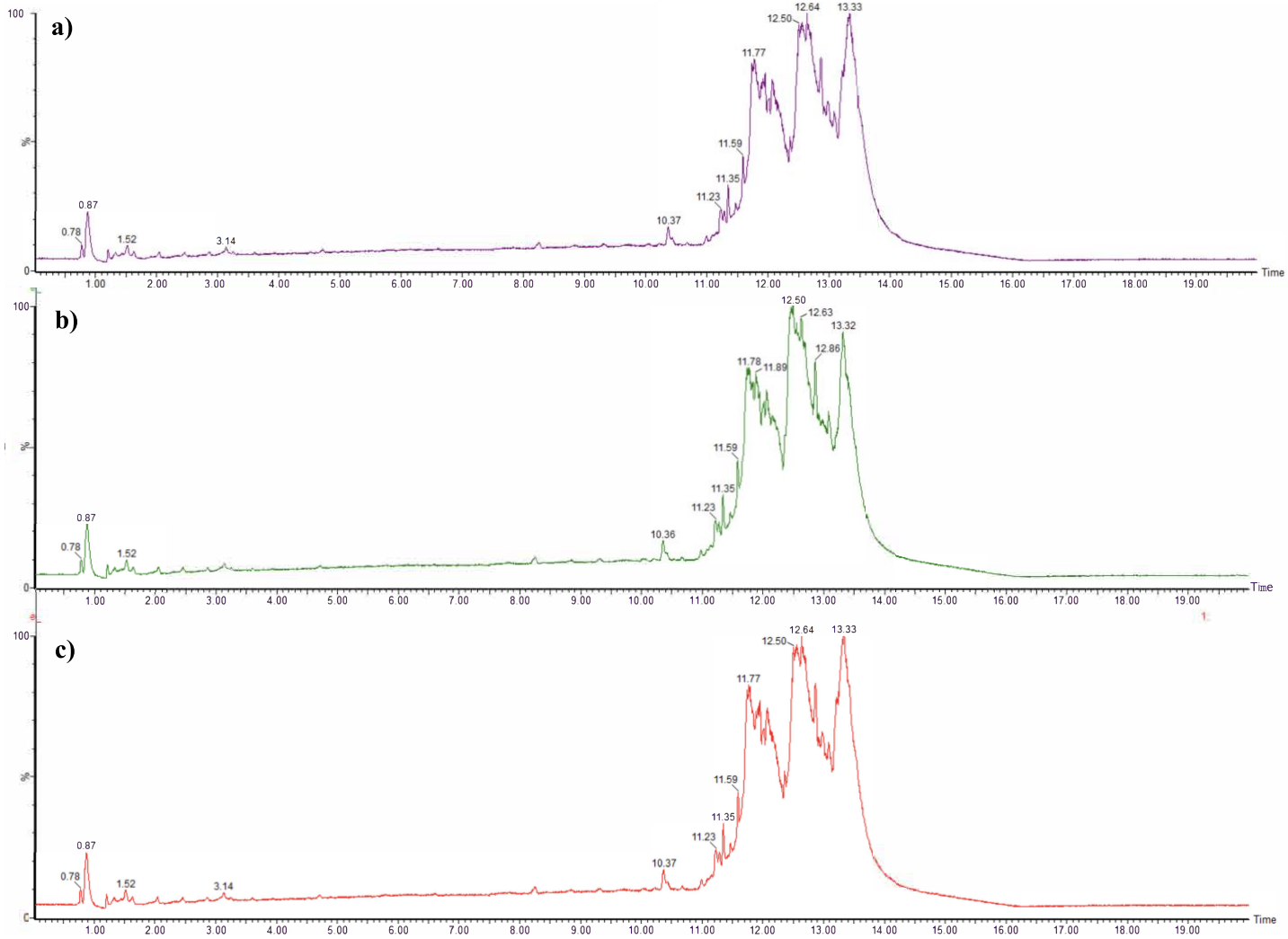

Figure A4. TIC in resolution mode of samples a) 11E replicate 3 vs. b) replicate 2 and c) replicate 1.

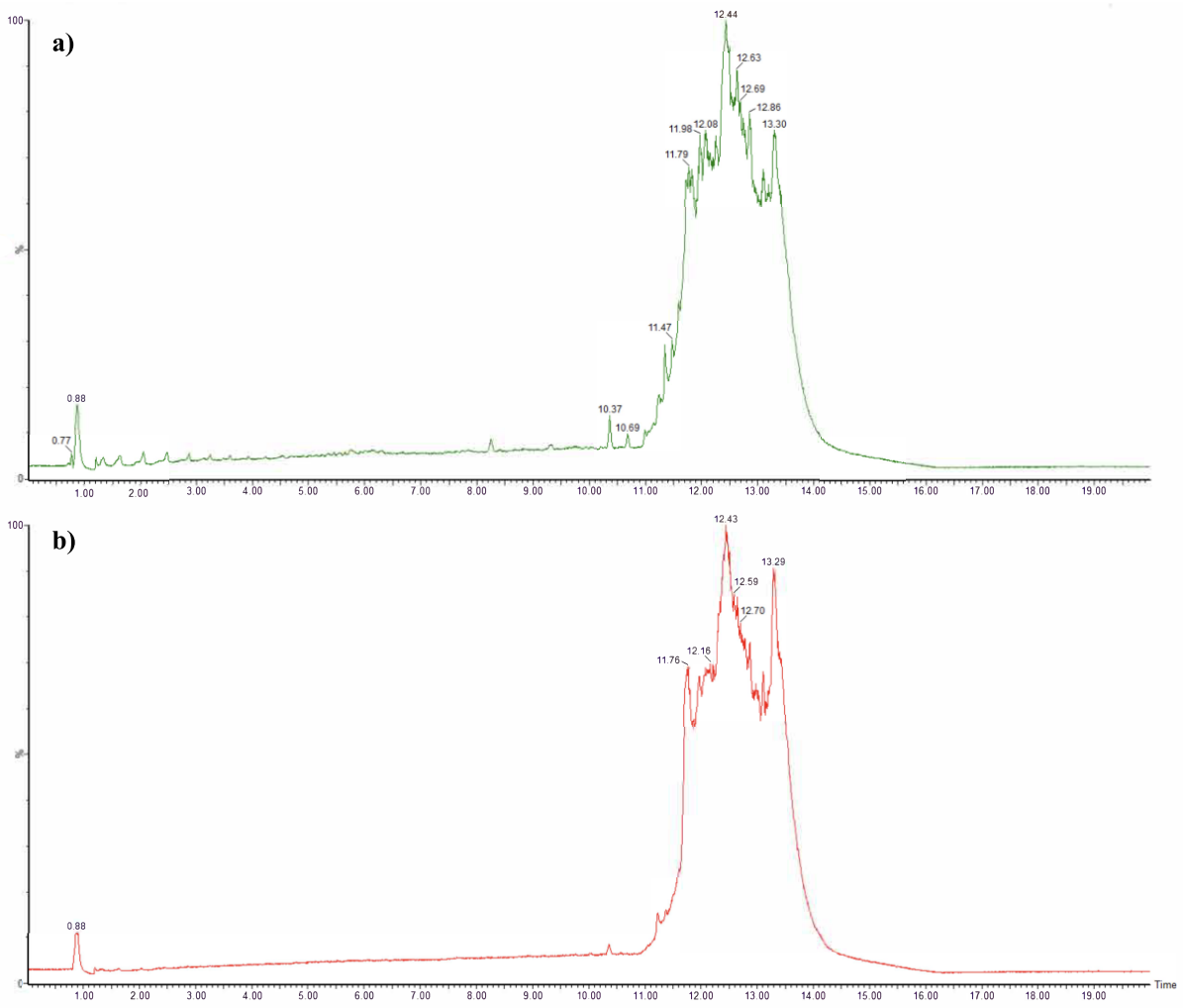

Figure A5. TIC in sensitivity mode of samples a) BP extract vs. b) MeOH blank.

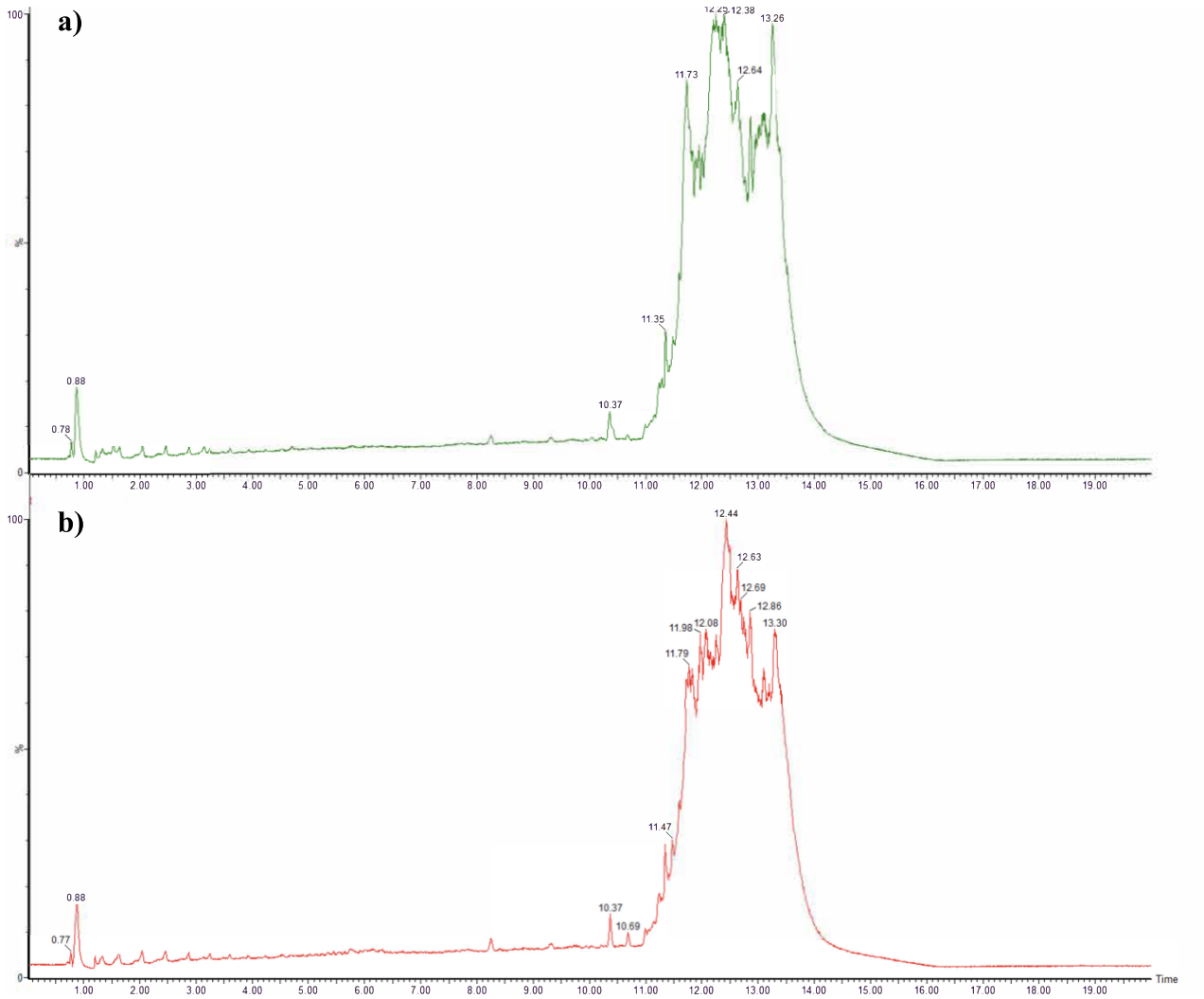

Figure A6. TIC in sensitivity mode of samples a) 11A replicate 1 vs. b) BP extract.

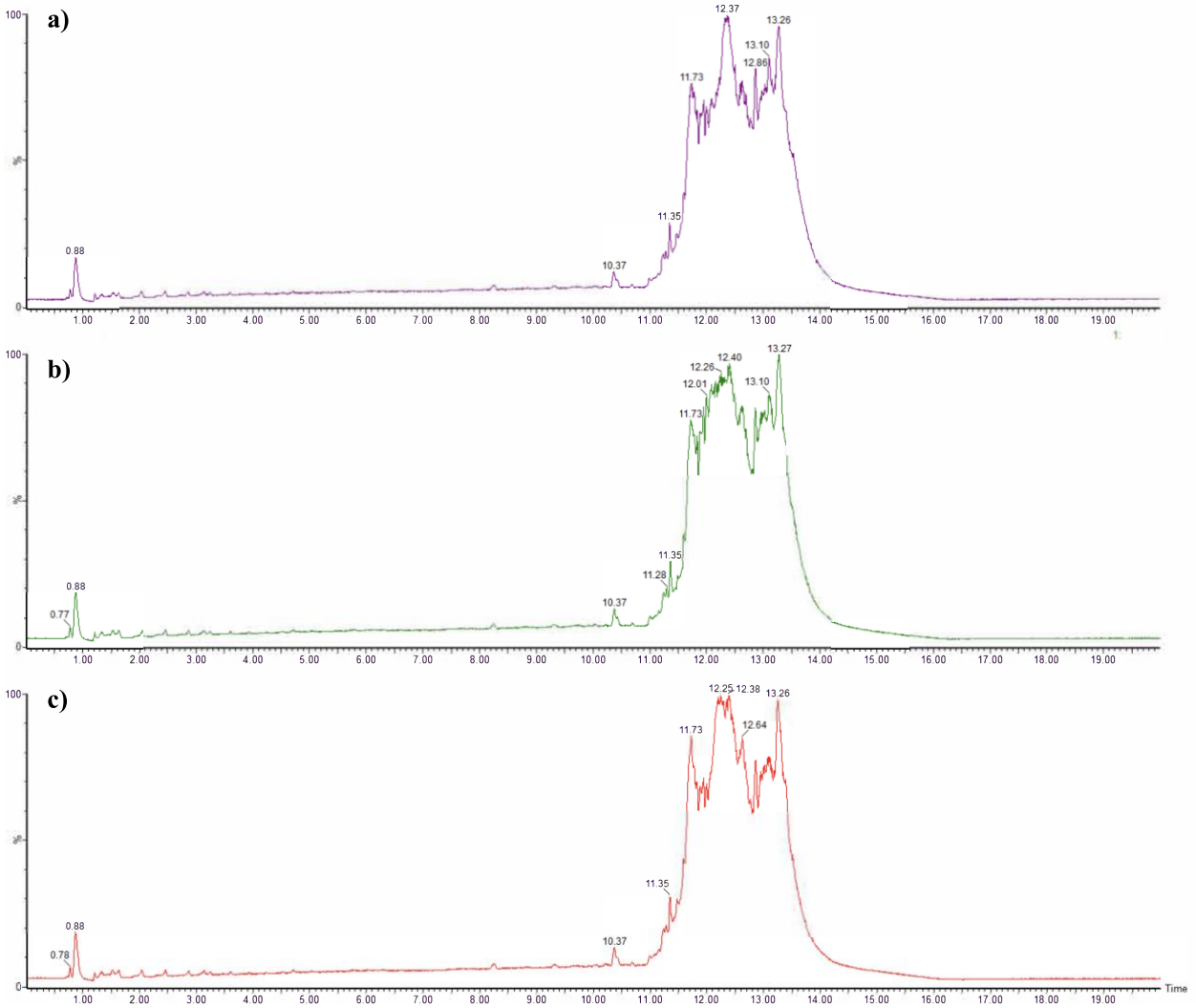

Figure A7. TIC in sensitivity mode of samples a) 11A replicate 3 vs. b) replicate 2 and c) replicate 1.

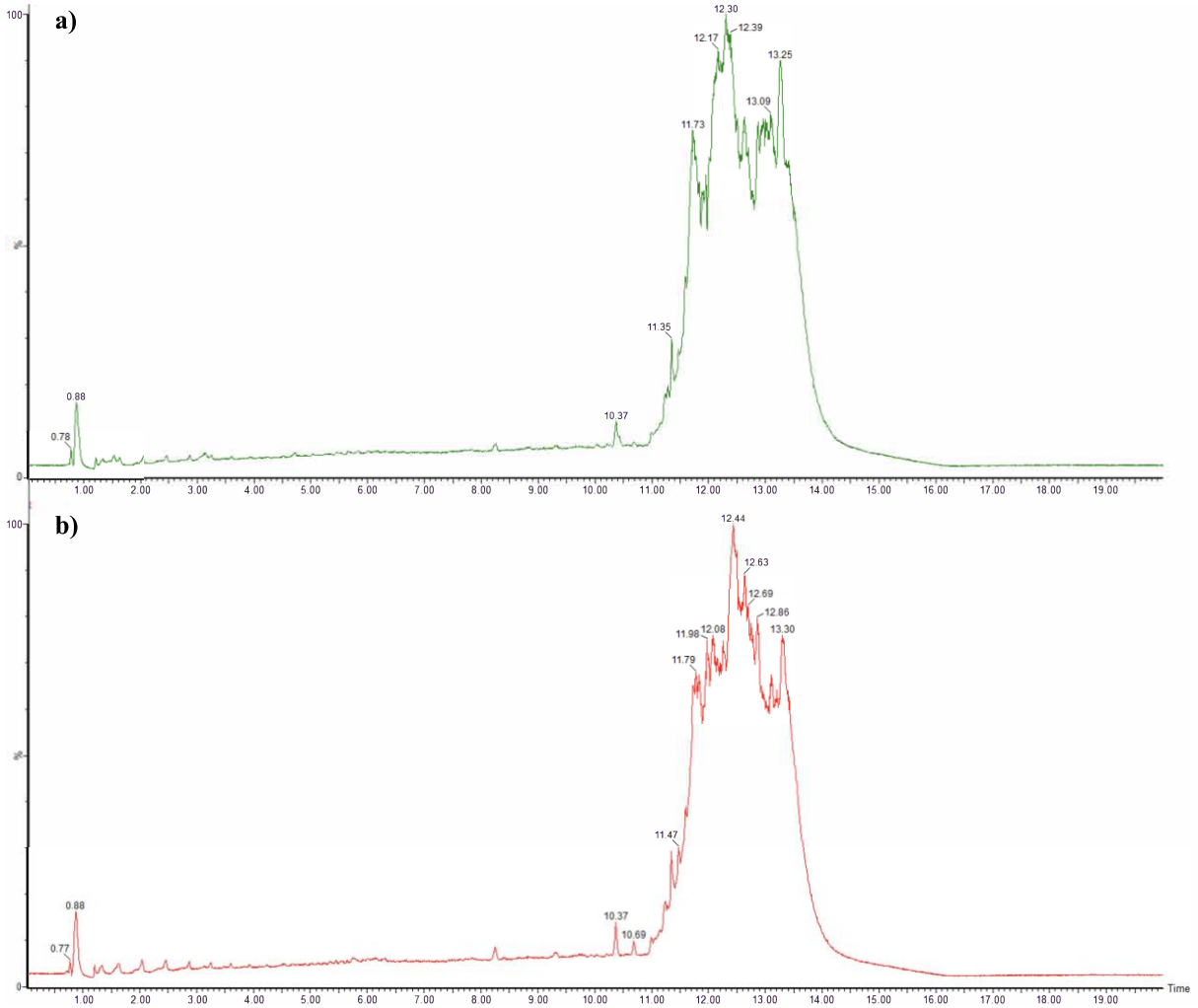

Figure A8. TIC in sensitivity mode of samples a) 11E replicate 1 vs. b) BP extract.

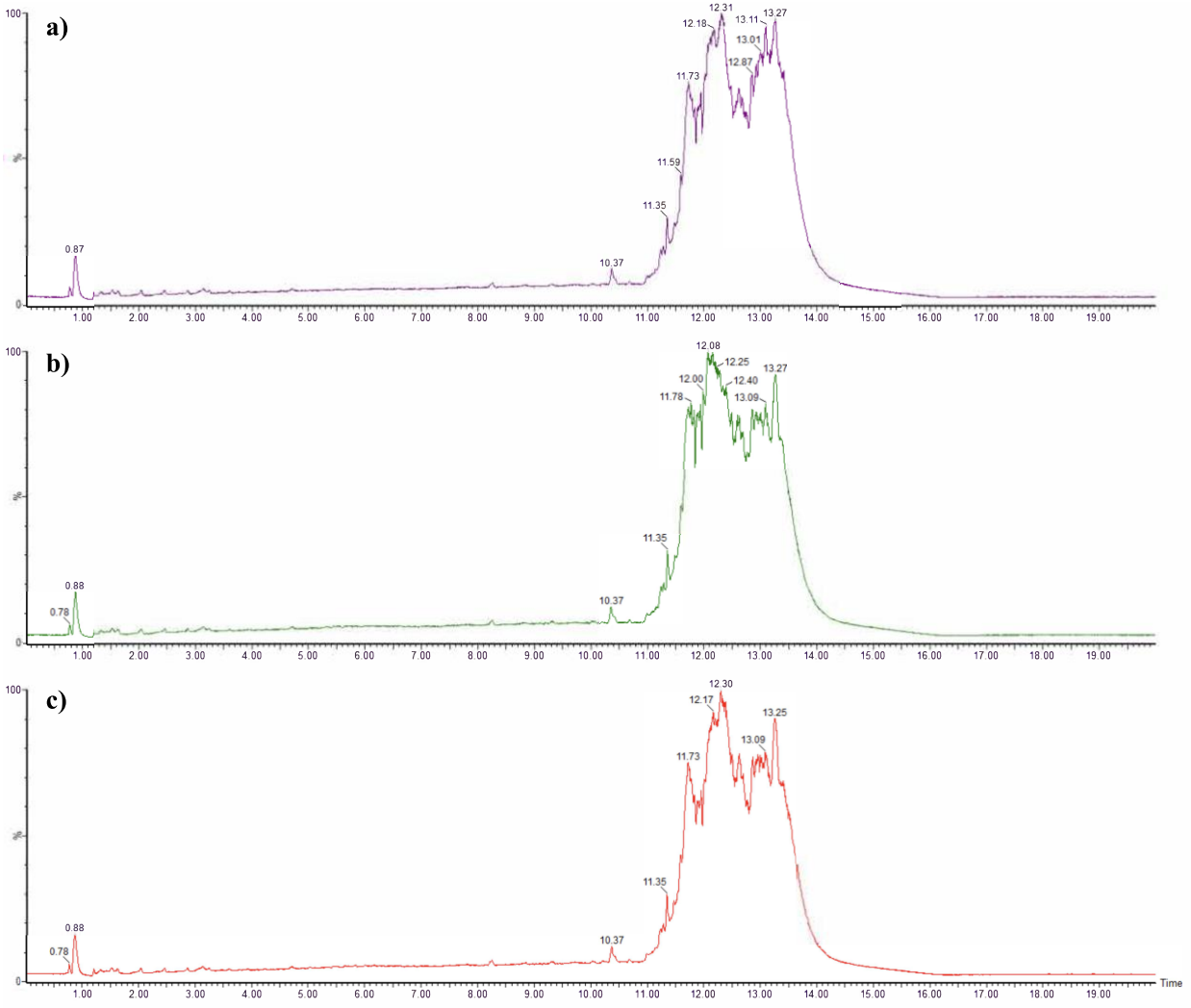

Figure A9. TIC in sensitivity mode of samples a) 11E replicate 3 vs. b) replicate 2 and c) replicate 1.

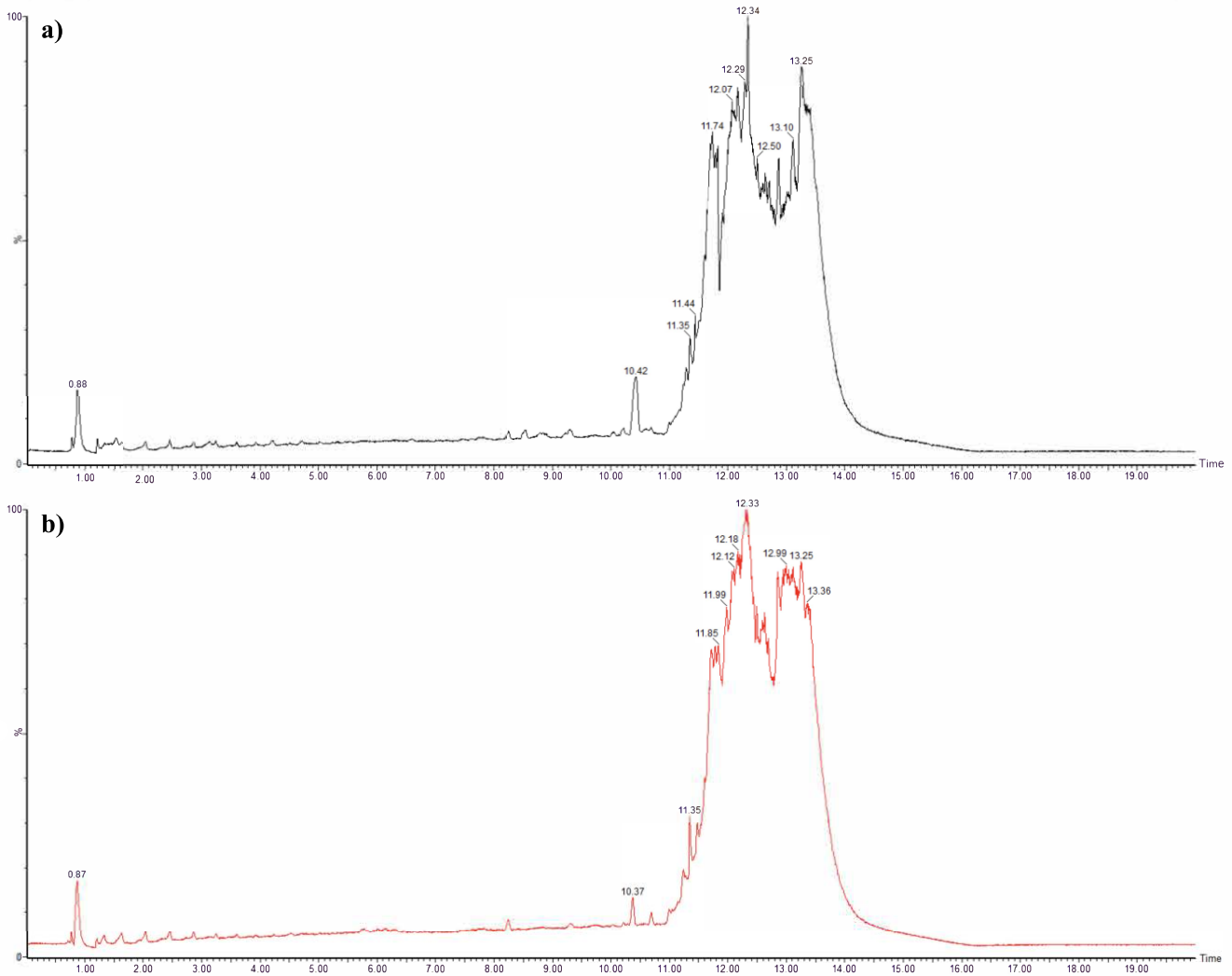

Figure A10. TIC in sensitivity mode of samples a) 11M replicate 1 vs. b) BP extract.

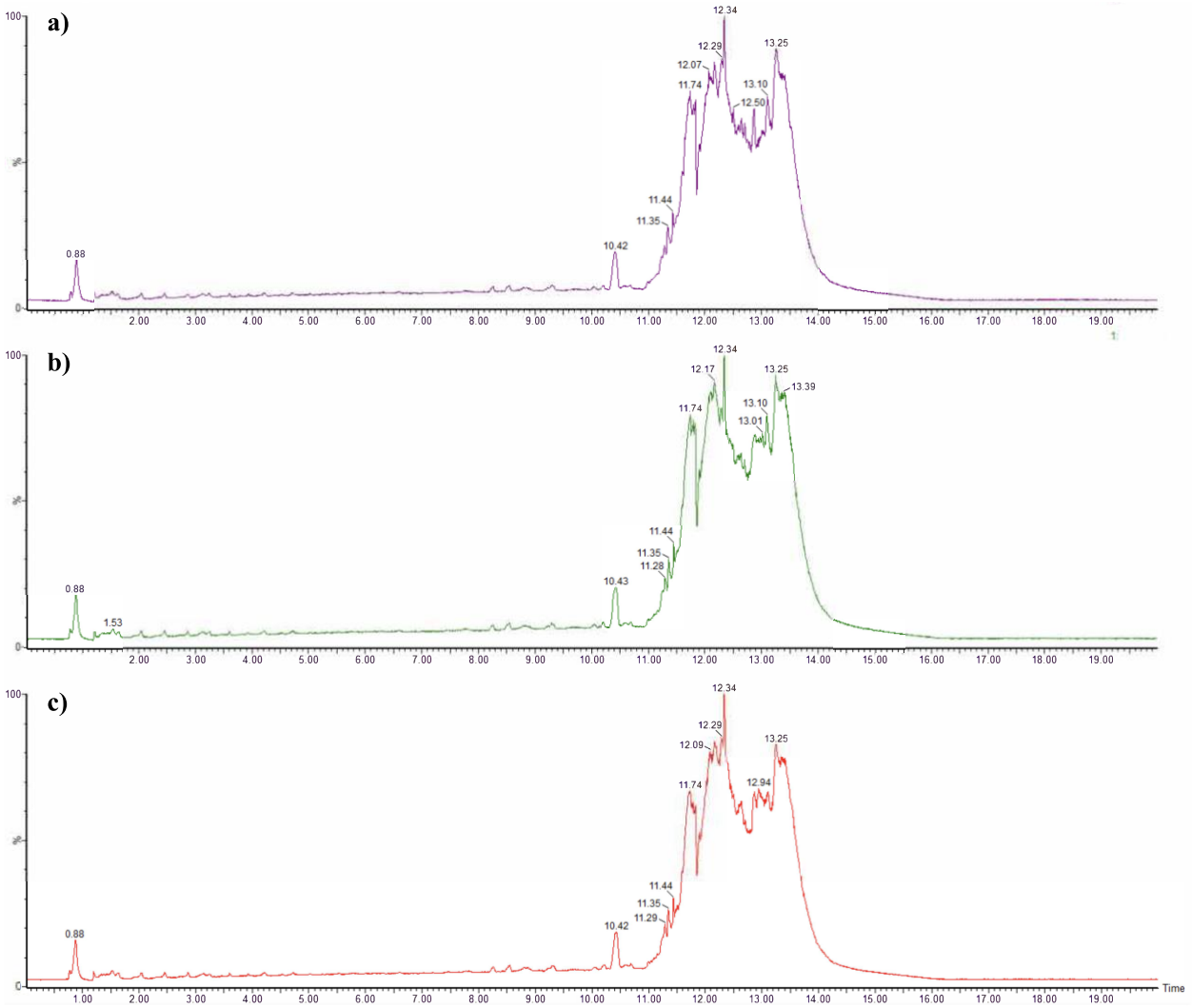

Figure A11. TIC in sensitivity mode of samples a) 11M replicate 3 vs. b) replicate 2 and c) replicate 1.

Appendix 4 (Chapter 5)

Appendix 4.1. Summary of data sets

Table A1. Summary of samples included in the calibration datasets 1-2.

Sample name	No. of samples	No. of analysis measurements/samples	Sample weight (mg)	Sample label	Batch No.
5F-PB-22	1	3	5	CA-R1 to R3	15494
AMP	1	3	5	CB-R1 to R3	46H1367
BEN	1	3	5	CC-R1 to R3	SLBB1067V
CAF	1	3	5	CD-R1 to R3	BCB8699V
COC	1	3	5	CE-R1 to R3	1050451F
DIA	1	3	5	CF-R1 to R3	50K1124
PAR	1	3	5	CG-R1 to R3	SLBB2780V
BP	1	3	N/A	CH-R1 to R3	N/A

Table A2. Summary of samples included in validation datasets 3-4.

Sample name	No. of samples	No. of analysis measurements	Sample weight (mg)	Sample label	Batch No.
5F-PB-22	1	3	5	CA-R1 to R3	15494
AMP	1	3	5	CB-R1 to R3	46H1367
BEN	1	3	5	CC-R1 to R3	SLBB1067V
CAF	1	3	5	CD-R1 to R3	BCB8699V
COC	1	3	5	CE-R1 to R3	1050451F
DIA	1	3	5	CF-R1 to R3	50K1124
PAR	1	3	5	CG-R1 to R3	SLBB2780V
BP	1	3	N/A	CH-R1 to R3	N/A
5F-PB-22	1	3	5	VA-R1 to R3	N/A
AMP	1	3	5	VB-R1 to R3	46H1367
BEN	1	3	5	VC-R1 to R3	SLBB1067V
CAF	1	3	5	VD-R1 to R3	BCB8699V
COC	1	3	5	VE-R1 to R3	1050451F
DIA	1	3	5	VF-R1 to R3	50K1124
PAR	1	3	5	VG-R1 to R3	SLBB2780V
BP	1	3	N/A	VH-R1 to R3	N/A

Table A3. Summary of samples included in mixture test datasets 5-6 & 7-8 (includes*).

Sample name	No. of samples	No. of analysis measurements	Sample weight (mg)	Sample label
5F-PB-22*	1	3	5	CA-R1 to R3
AMP*	1	3	5	CB-R1 to R3
BEN*	1	3	5	CC-R1 to R3
CAF*	1	3	5	CD-R1 to R3
COC*	1	3	5	CE-R1 to R3
DIA*	1	3	5	CF-R1 to R3
PAR*	1	3	5	CG-R1 to R3
BP*	1	3	N/A	CH-R1 to R3
5F-PB-22/AMP	1	3	5	M1-R1 to R3
5F-PB-22/BEN	1	3	5	M2-R1 to R3
5F-PB-22/CAF	1	3	5	M3-R1 to R3
5F-PB-22/COC	1	3	5	M4-R1 to R3
5F-PB-22/DIA	1	3	5	M5-R1 to R3
5F-PB-22/PAR	1	3	5	M6-R1 to R3
AMP/BEN	1	3	5	M7-R1 to R3
AMP/CAF	1	3	5	M8-R1 to R3
AMP/COC	1	3	5	M9-R1 to R3
AMP/DIA	1	3	5	M10-R1 to R3
AMP/PAR	1	3	5	M11-R1 to R3
BEN/CAF	1	3	5	M12-R1 to R3
BEN/COC	1	3	5	M13-R1 to R3
BEN/DIA	1	3	5	M14-R1 to R3
BEN/PAR	1	3	5	M15-R1 to R3
CAF/COC	1	3	5	M16-R1 to R3
CAF/DIA	1	3	5	M17-R1 to R3
CAF/PAR	1	3	5	M18-R1 to R3
COC/DIA	1	3	5	M19-R1 to R3
COC/PAR	1	3	5	M20-R1 to R3
DIA/PAR	1	3	5	M21-R1 to R3

Table A4. Summary of simulated single substance paper samples pipetted (set 9-10),

soaked (sets 11-12) & pipetted or soaked (set 13-14).

Sample name	Concentration (mg/mL)	No. of samples	No. of analysis measurements	Sample label pipetting	Sample label soaking
5F-PB-22	20	1	3	PA-20-R1 to R3	SA-20-R1 to R3
5F-PB-22	15	1	3	PA-15-R1 to R3	SA-15-R1 to R3
5F-PB-22	10	1	3	PA-10-R1 to R3	SA-10-R1 to R3
5F-PB-22	7.5	1	3	PA-7.5-R1 to R3	SA-7.5-R1 to R3
5F-PB-22	5	1	3	PA-5-R1 to R3	SA-5-R1 to R3
AMP	30	1	3	PB-30-R1 to R3	SB-30-R1 to R3
AMP	15	1	3	PB-15-R1 to R3	SB-15-R1 to R3
AMP	12.5	1	3	PB-12.5-R1 to R3	SB-12.5-R1 to R3
AMP	10	1	3	PB-10-R1 to R3	SB-10-R1 to R3
AMP	7.5	1	3	PB-7.5-R1 to R3	SB-7.5-R1 to R3
BEN	10	1	3	PC-10-R1 to R3	SC-10-R1 to R3
BEN	6.5	1	3	PC-6.5-R1 to R3	SC-6.5-R1 to R3
BEN	5	1	3	PC-5-R1 to R3	SC-5-R1 to R3
BEN	3.5	1	3	PC-3.5-R1 to R3	SC-3.5-R1 to R3
BEN	2.5	1	3	PC-2.5-R1 to R3	SC-2.5-R1 to R3
CAF	15	1	3	PD-15-R1 to R3	SD-15-R1 to R3
CAF	10	1	3	PD-10-R1 to R3	SD-10-R1 to R3
CAF	8	1	3	PD-8-R1 to R3	SD-8-R1 to R3
CAF	6.5	1	3	PD6.5-R1 to R3	SD-6.5-R1 to R3
CAF	5	1	3	PD-5-R1 to R3	SD-5-R1 to R3
COC	60	1	3	PE-60-R1 to R3	SE-60-R1 to R3
COC	40	1	3	PE-40-R1 to R3	SE-40-R1 to R3
COC	35	1	3	PE-35-R1 to R3	SE-35-R1 to R3
COC	30	1	3	PE-30-R1 to R3	SE-30-R1 to R3
COC	20	1	3	PE-20-R1 to R3	SE-20-R1 to R3
DIA	30	1	3	PF-30-R1 to R3	SF-30-R1 to R3
DIA	20	1	3	PF-20-R1 to R3	SF-20-R1 to R3
DIA	15	1	3	PF-15-R1 to R3	SF-15-R1 to R3
DIA	10	1	3	PF-10-R1 to R3	SF-10-R1 to R3
DIA	5	1	3	PF-5-R1 to R3	SF-5-R1 to R3
PAR	60	1	3	PG-60-R1 to R3	SG-60-R1 to R3

PAR	30	1	3	PG-30-R1 to R3	SG-30-R1 to R3
PAR	20	1	3	PG-20-R1 to R3	SG-20-R1 to R3
PAR	15	1	3	PG-15-R1 to R3	SG-15-R1 to R3
PAR	10	1	3	PG-10-R1 to R3	SG-10-R1 to R3

Table A5. Summary of samples included in pipetting & soaking binary mixture simulated paper sample sets (sets 15-18).

Sample name	Concentration (mg/mL)	No. of samples	No. of analysis measurements	Sample label pipetting	Sample label soaking
5F-PB-22/AMP	20:20	1	3	PM1-R1 to R3	SM1-R1 to R3
5F-PB-22/BEN	20:20	1	3	PM2-R1 to R3	SM2-R1 to R3
5F-PB-22/CAF	20:20	1	3	PM3-R1 to R3	SM3-R1 to R3
5F-PB-22/COC	20:20	1	3	PM4-R1 to R3	SM4-R1 to R3
5F-PB-22/DIA	20:20	1	3	PM5-R1 to R3	SM5-R1 to R3
5F-PB-22/PAR	20:20	1	3	PM6-R1 to R3	SM6-R1 to R3

Appendix 4.2. Results of the 5F-PB-22 HPLC-UV method validation

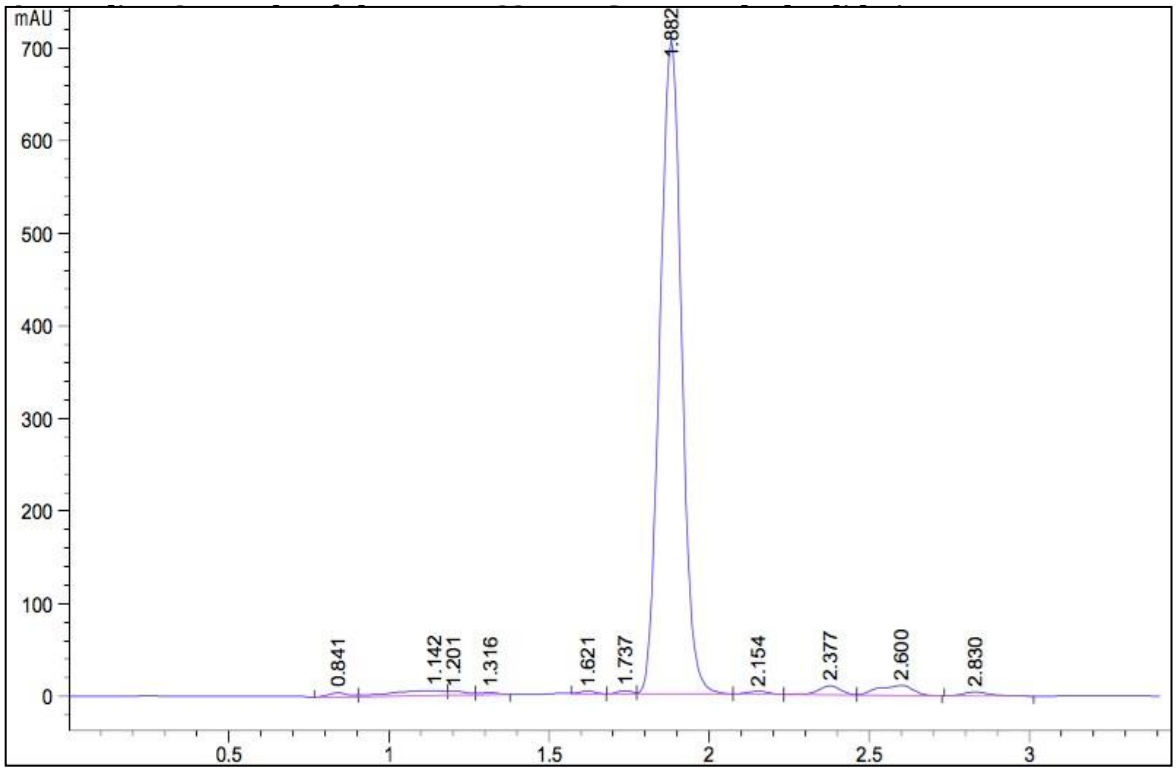

Figure A1. HPLC-UV-Vis 5F-PB-22 reference standard (0.04 mg/ml) chromatogram.

Table A1. Summary of the results of the 5F-PB-22 HPLC-UV method validation.

	1st calibration curve	**2nd calibration curve**	**3rd calibration curve**	**Acceptance criteria**
Theoretical plate number (N)	3475.65	3182.06	3498.21	N > 2000
Tailing Factor (T)	1.13	1.11	1.11	T < 2
Linearity (R^2)	0.9999	1	1	R^2 > 0.9990
Limit of Detection (mg/ml)	0.0004	0.0001	0.00017307	-
Limit of Quantification (mg/ml)	0.0014	0.0003	0.0005	-
	1st calibration curve	**2nd calibration curve**	**3rd calibration curve**	**Acceptance criteria**
Precision- Repeatability				
%RSD at low concentration	1.01	0.74	1.63	
%RSD at medium concentration	2.13	0.23	0.21	%RSD < 2%
%RSD at high concentration	0.09	0.1	0.23	
Intermediate Precision				
%RSD at low concentration	0.12	0.2	0.17	
%RSD at medium concentration	0.09	0.09	0.19	%RSD < 2%
%RSD at high concentration	0.12	0.1	0.16	
Accuracy				
%Accuracy at low concentration	101.27	101.46	98.76	
%Accuracy at medium concentration	99.62	99.04	79.55	100 ± 2%
%Accuracy at high concentration	100.93	100.61	99.58	

Appendix 4.3. Evaluation of the eight pre-processing protocols on Raman Renishaw set 1

1) Quantitative analysis of cocaine in solid mixtures using Raman spectroscopy and chemometric methods (Ryder et al. 2000)

Below are shown the final PCA plots resulting from the application of the pre-processing sequence, consisting of i) spectral data truncation in the range of 450-1100 cm^{-1} and ii) multiplicative scatter correction (MSC) for common offset, on our raw Raman Renishaw set 1.

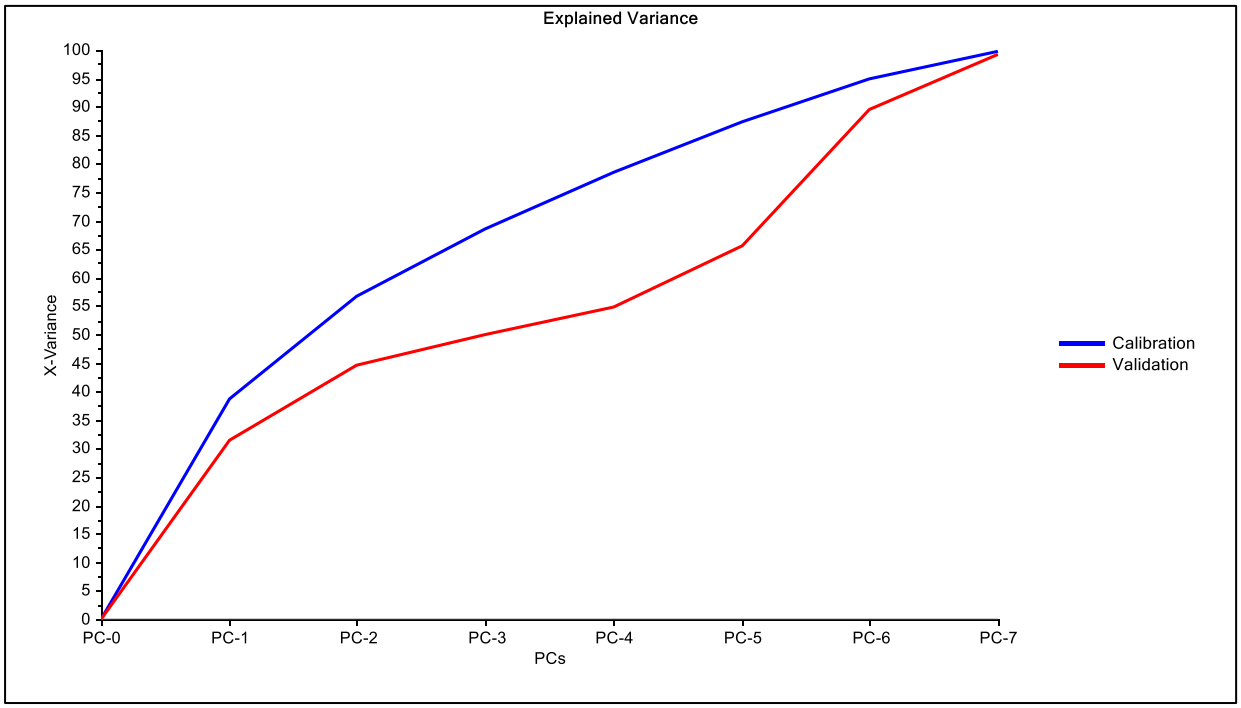

Figure A1. Explained variance plot of set 1 after application of pre-processing protocol 1.

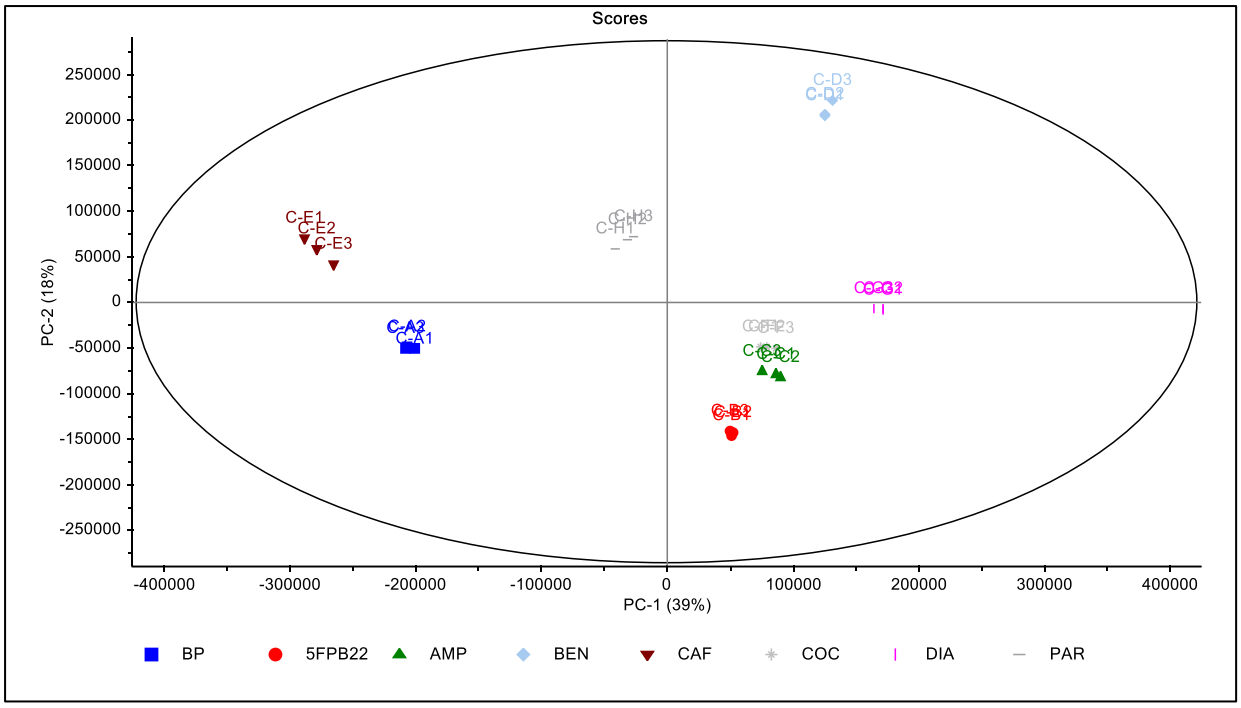

Figure A2. PC-1 vs PC-2 2D scores plot of set 1 after application of pre-processing protocol 1.

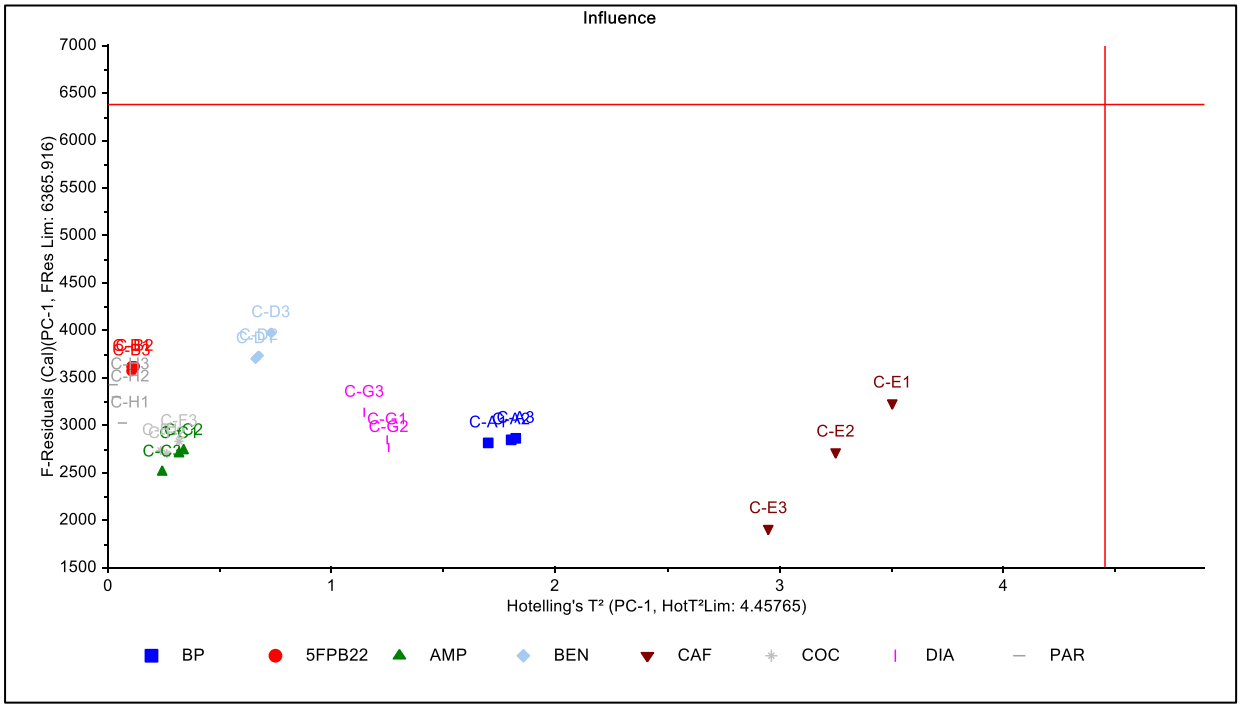

Figure A3. PC-1 F-residuals vs Hotelling T^2 influence plot of set 1 after application of pre-processing protocol 1.

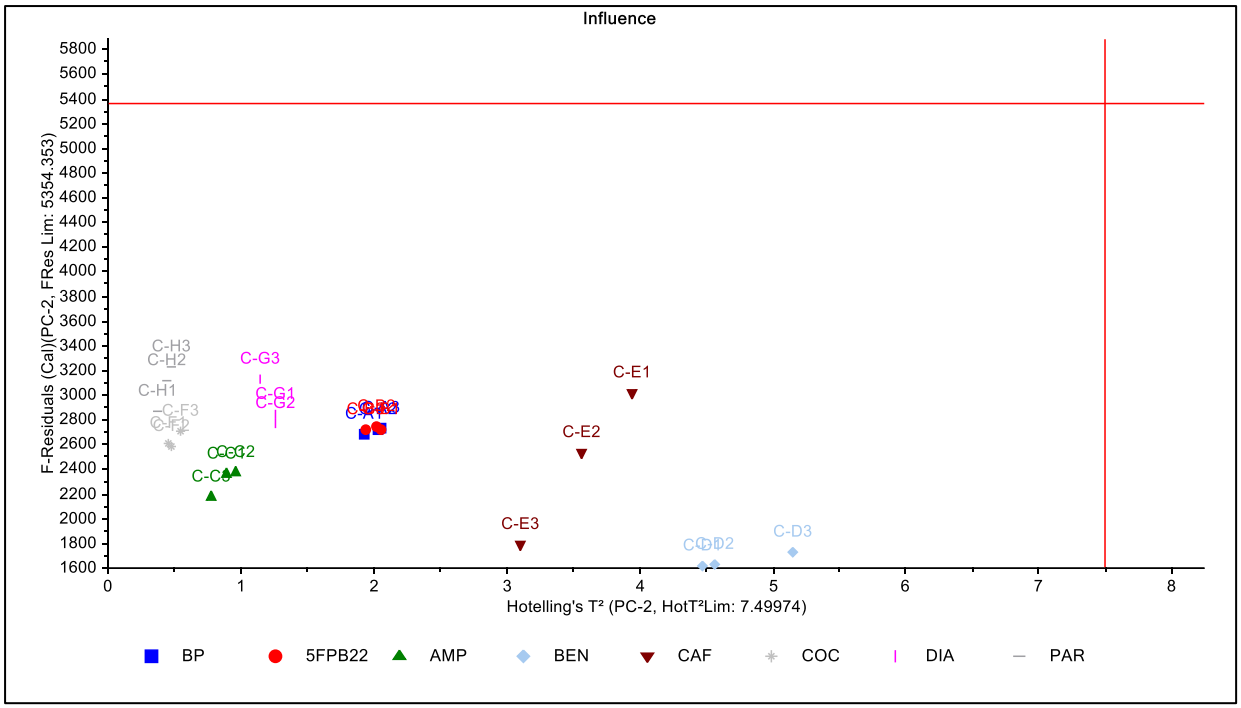

Figure A4. PC-2 F-residuals vs Hotelling T^2 influence plot of set 1 after application of pre-processing protocol 1.

2) Classification of a target analyte in solid mixtures using principal component analysis, support vector machines and Raman spectroscopy (O'Connell et al. 2005)

Below are shown the final PCA plots resulting from the application of the pre-processing sequence, consisting of i) Savitzky-Golay first derivative, seven-point averaging algorithm and ii) maximum normalisation to reduce the large intensity difference between the spectra, on our raw Raman Renishaw set 1.

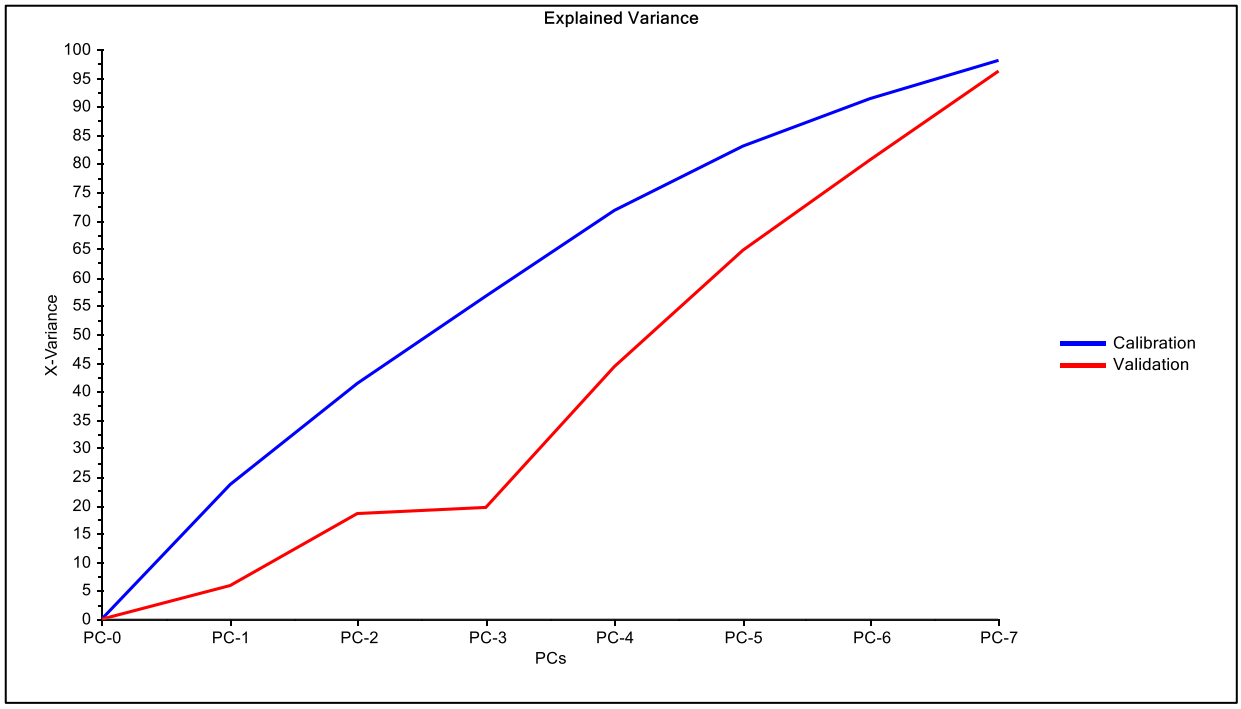

Figure A5. Explained variance plot of set 1 after application of pre-processing protocol 2.

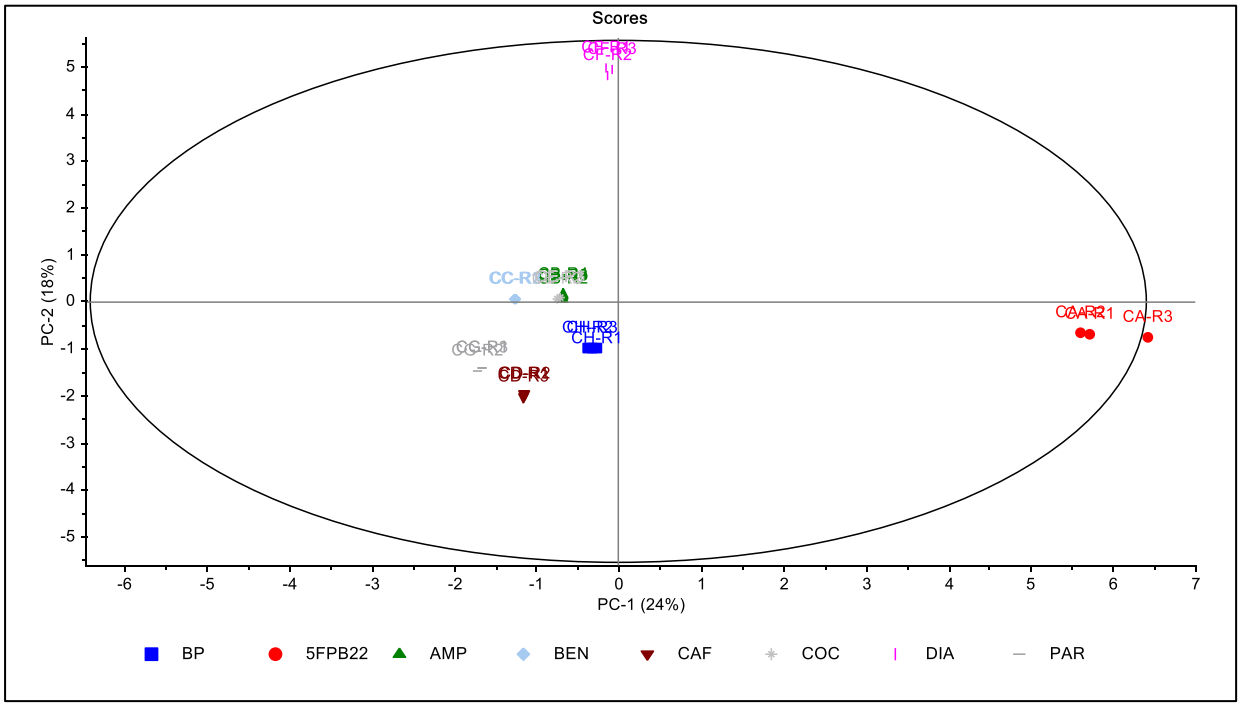

Figure A6. PC-1 vs PC-2 2D scores plot of set 1 after application of pre-processing protocol 2.

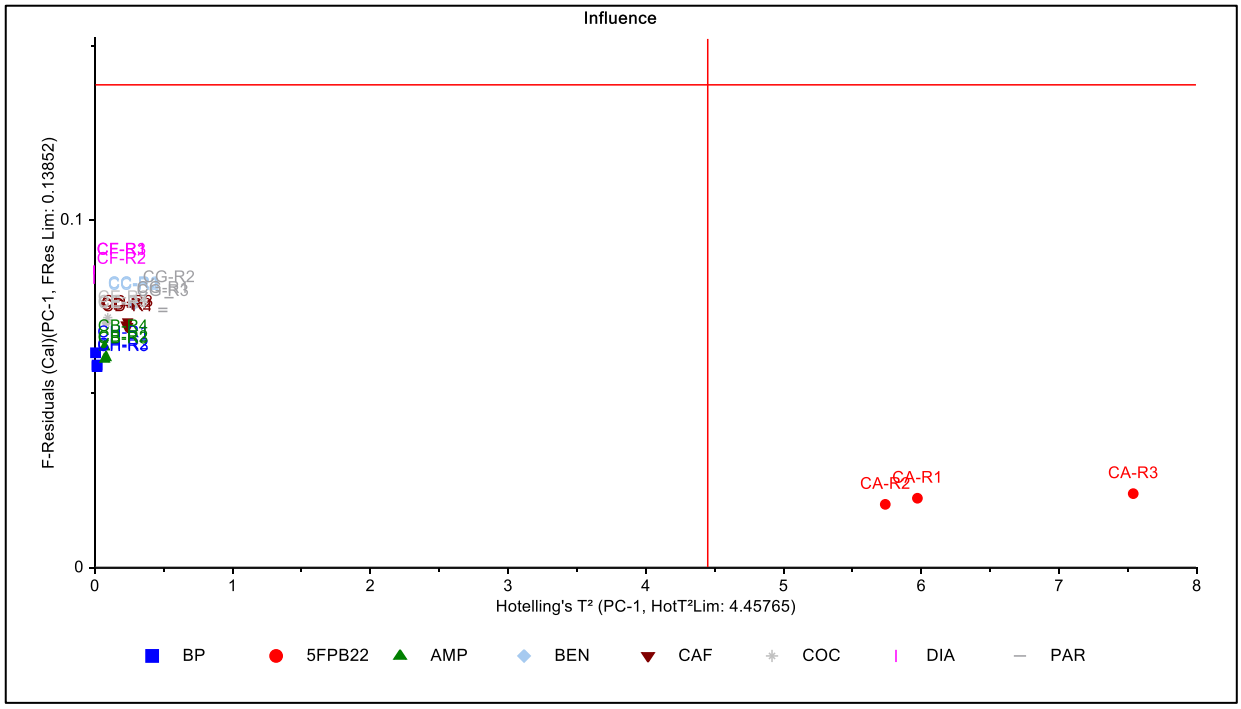

Figure A7. PC-1 F-residuals vs Hotelling T^2 influence plot of set 1 after application of pre-processing protocol 2.

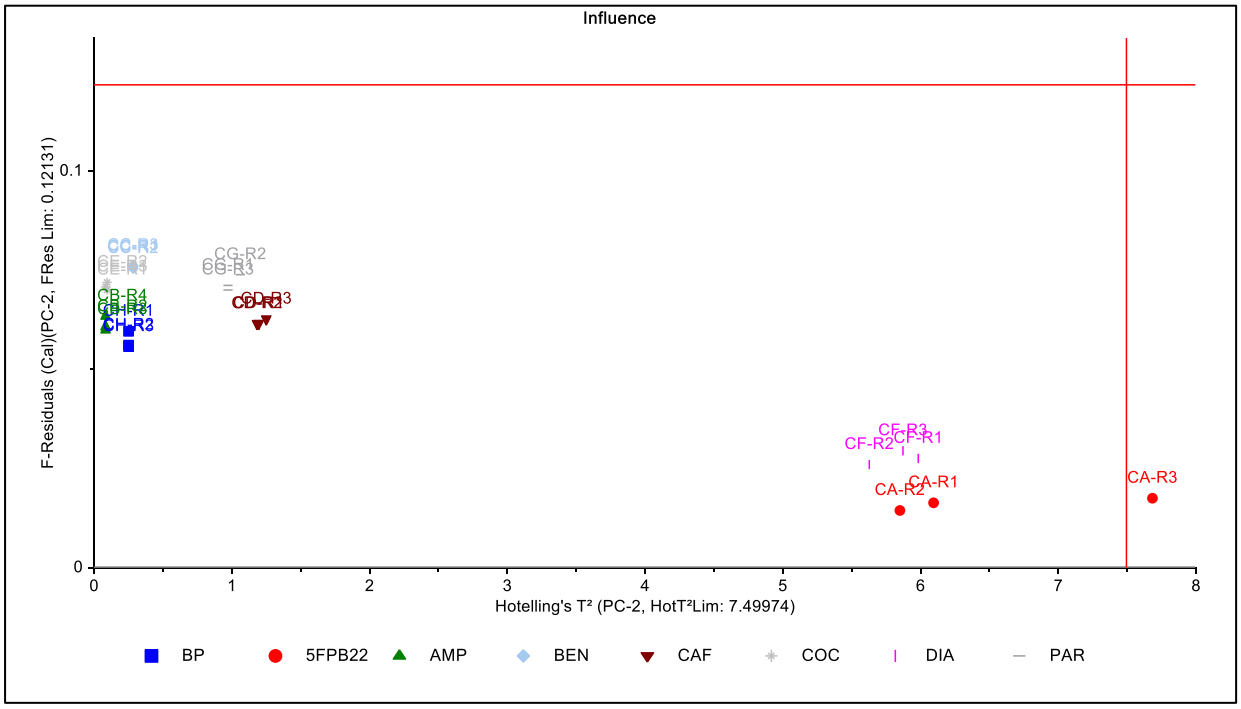

Figure A8. PC-2 F-residuals vs Hotelling T^2 influence plot of set 1 after application of pre-processing protocol 2.

3) Comparison of near infrared laser excitation wavelengths and its influence on the interrogation of seized drugs-of-abuse by Raman spectroscopy (Hargreaves et al. 2009)

Below are shown the final PCA plots resulting from the application of the pre-processing sequence, consisting of i) Savitsky–Golay smoothing algorithm using a 15-point smoothing window and a second-order deconvolution and ii) Standard Normal Variate (SNV), on our raw Raman Renishaw set 1.

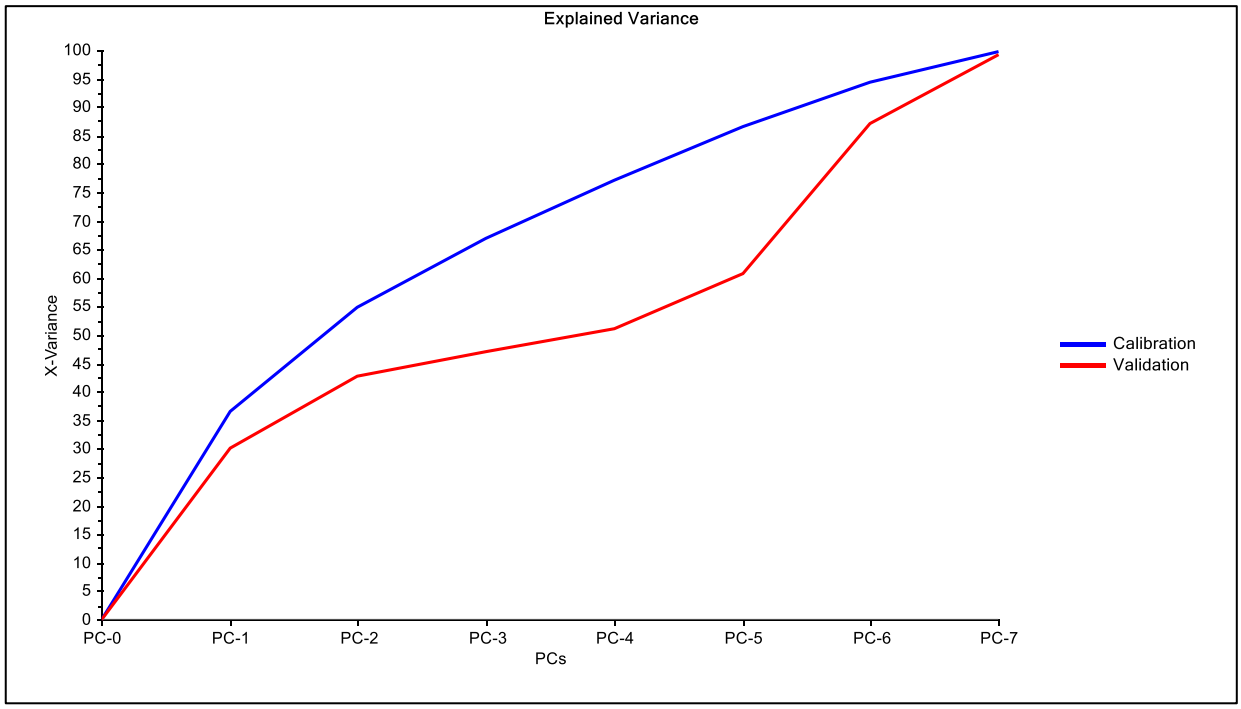

Figure A9. Explained variance plot of set 1 after application of pre-processing protocol 3.

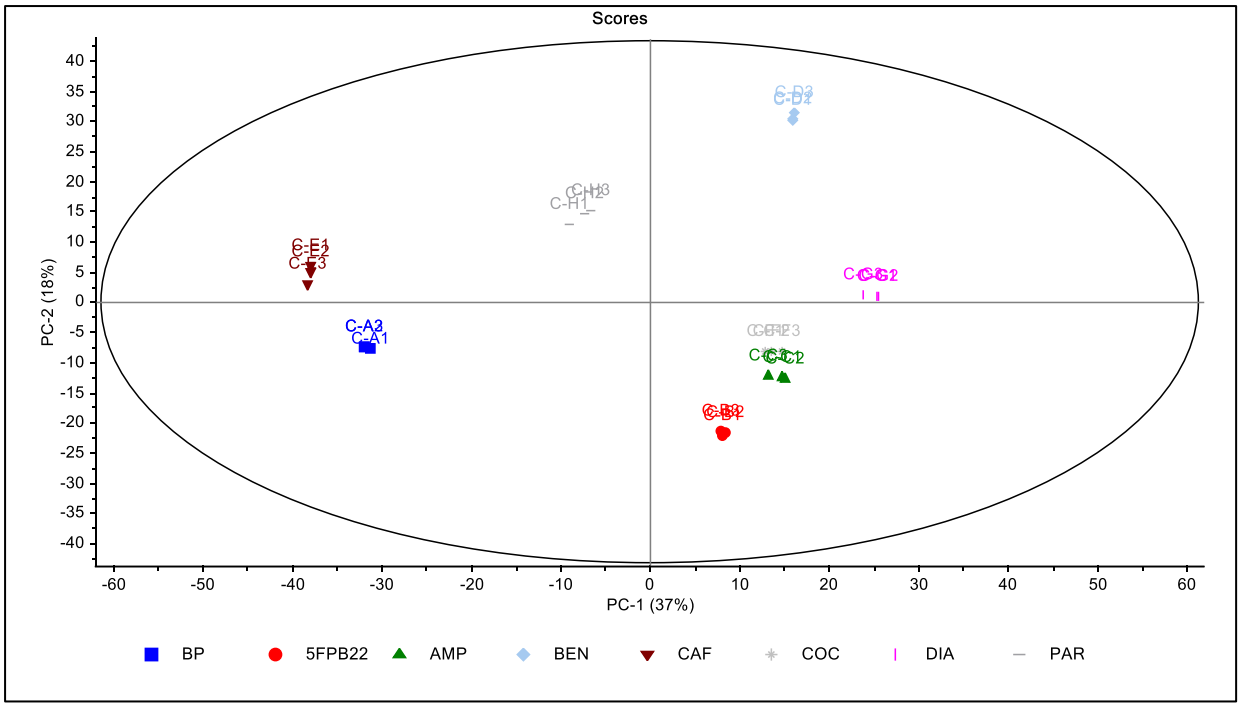

Figure A10. PC-1 vs PC-2 2D scores plot of set 1 after application of pre-processing protocol 3.

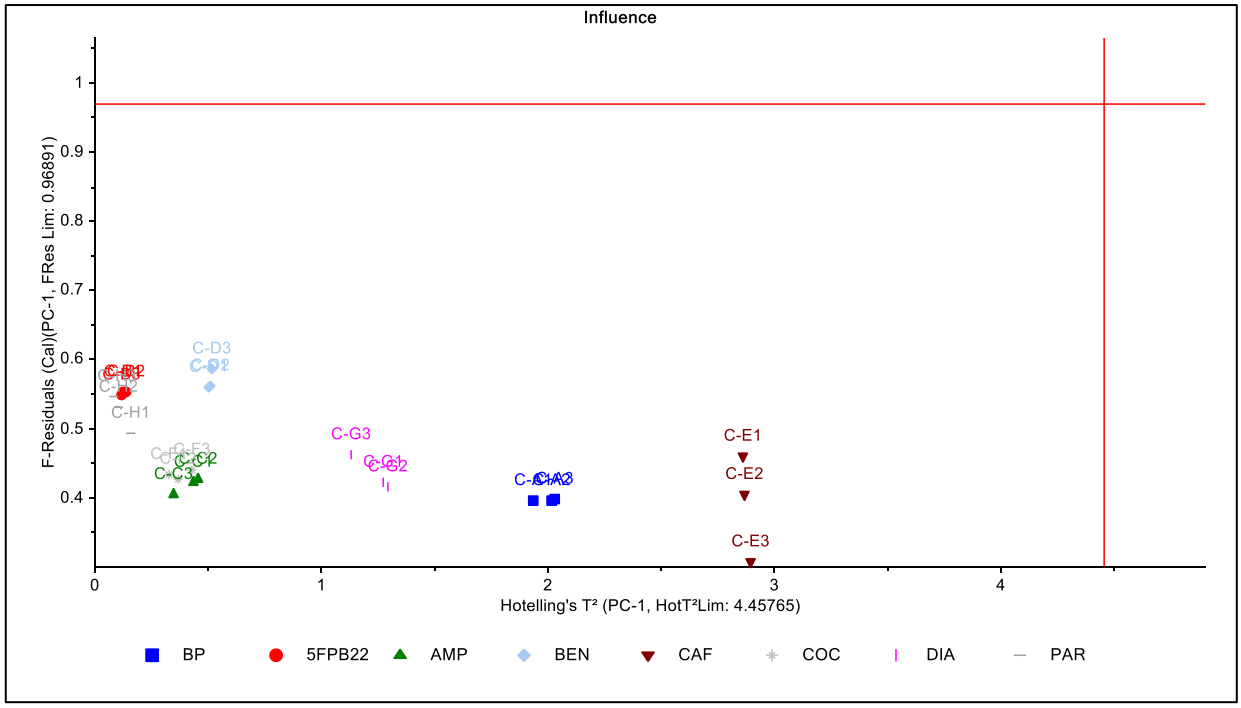

Figure A11. PC-1 F-residuals vs Hotelling T^2 influence plot of set 1 after application of pre-processing protocol 3.

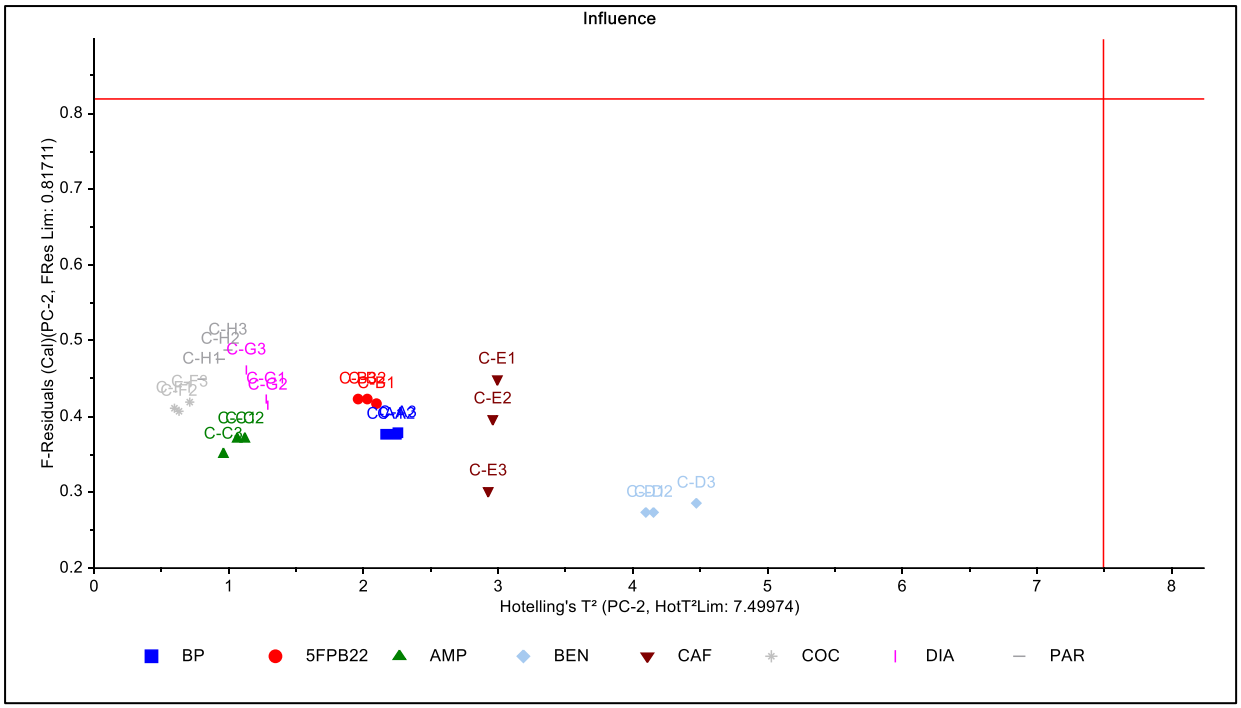

Figure A12. PC-2 F-residuals vs Hotelling T^2 influence plot of set 1 after application of pre-processing protocol 3.

4) Qualitative Analysis Using Raman Spectroscopy and Chemometrics: A Comprehensive Model System for Narcotics Analysis (O'Connell et al. 2010)

Below are shown the final PCA plots resulting from the application of the pre-processing sequence, consisting of i) Data truncation 750-1900 cm^{-1} and ii) Savitzky–Golay first-derivative, nine-point averaging (removing both linear and sloping backgrounds from spectra), on our raw Raman Renishaw set 1.

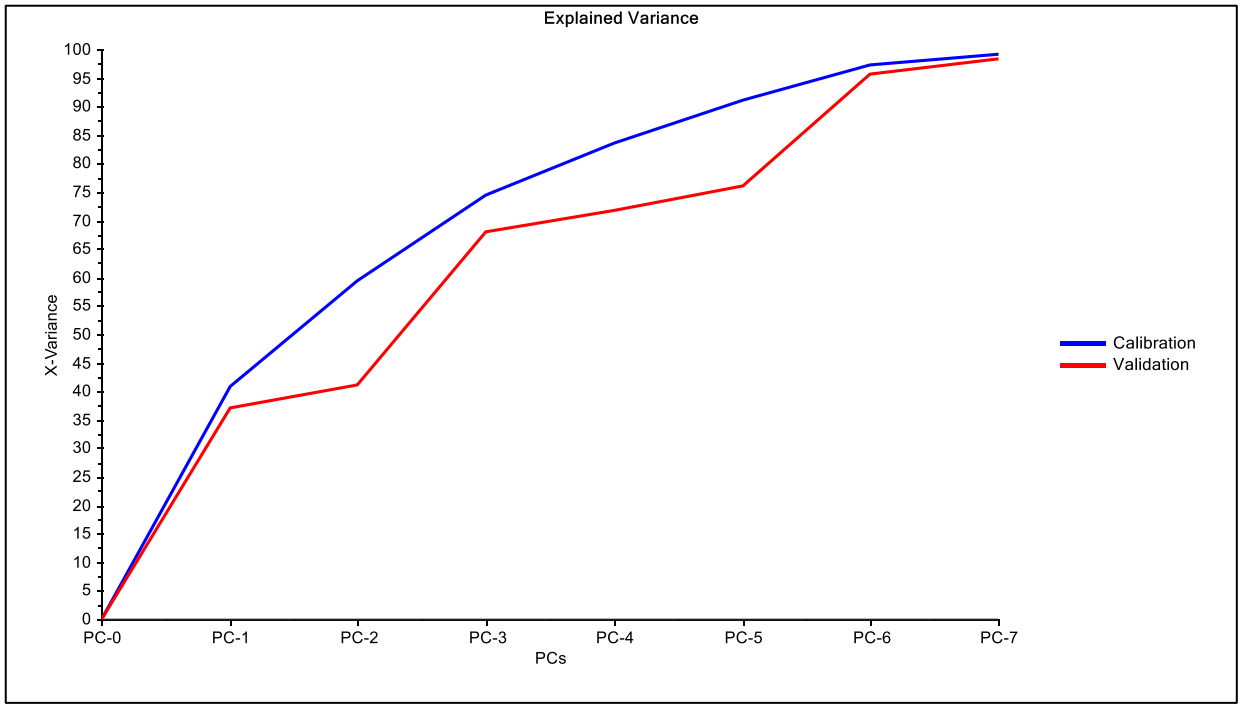

Figure A13. Explained variance plot of set 1 after application of pre-processing protocol 4.

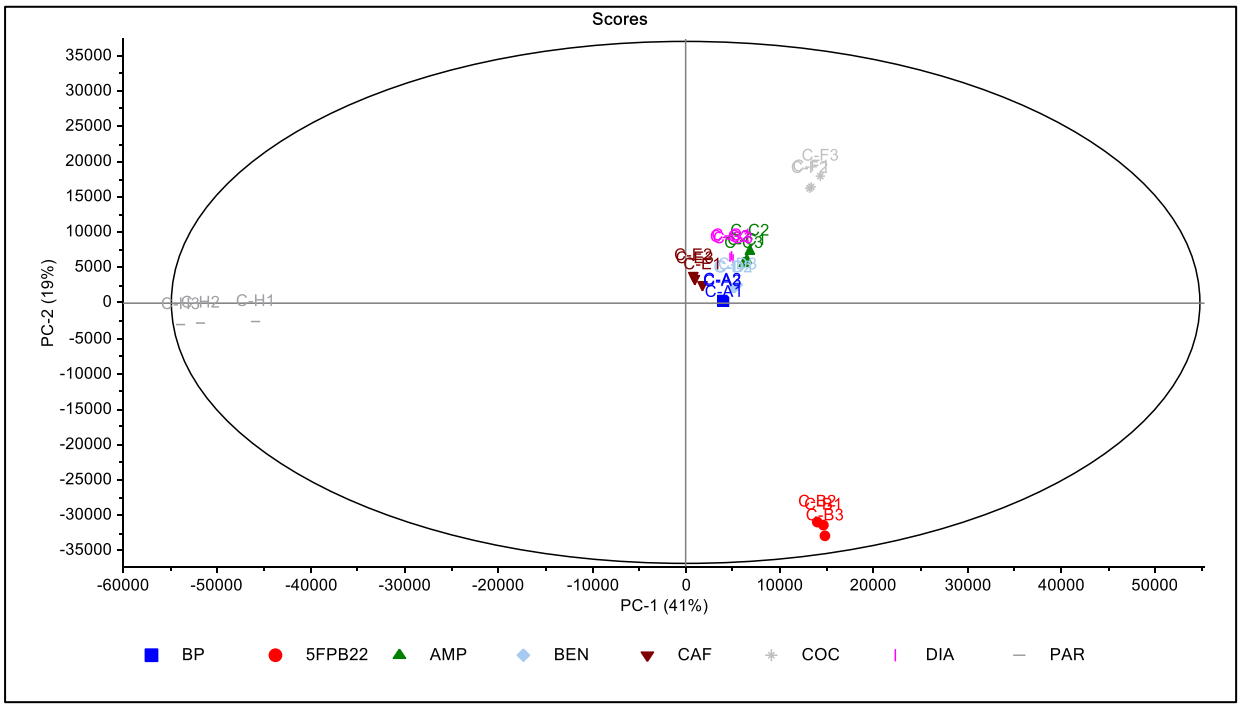

Figure A14. PC-1 vs PC-2 2D scores plot of set 1 after application of pre-processing protocol 4.

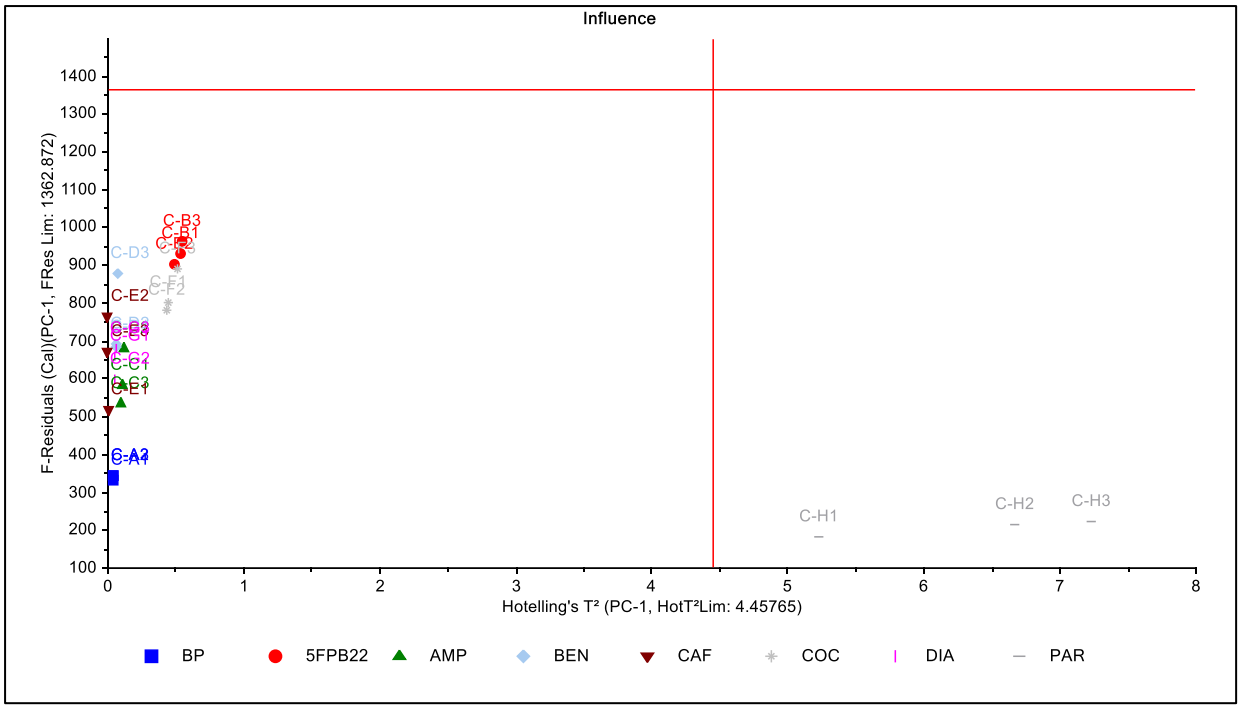

Figure A15. PC-1 F-residuals vs Hotelling T^2 influence plot of set 1 after application of pre-processing protocol 4.

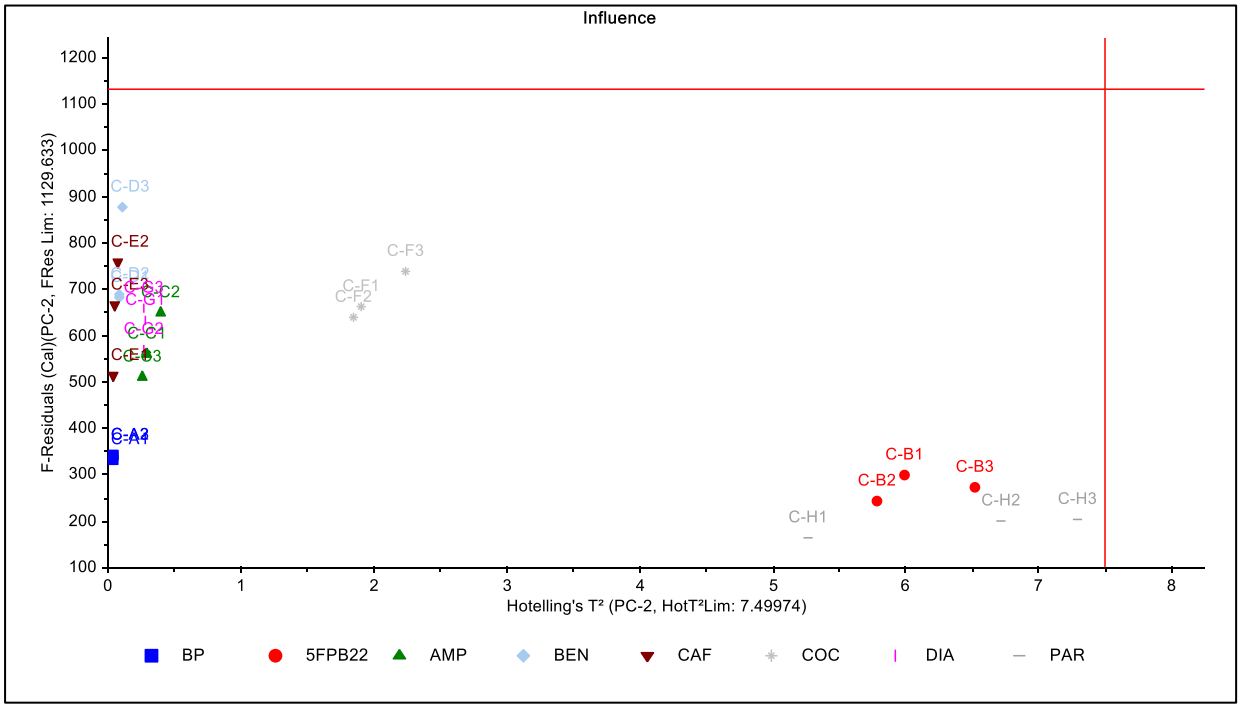

Figure A16. PC-2 F-residuals vs Hotelling T^2 influence plot of set 1 after application of pre-processing protocol 4.

5) Application of Raman spectroscopy in the detection of cocaine in food matrices (Bedward et al., 2017)
Equation (1)

Below are shown the final PCA plots resulting from the application of the pre-processing sequence, consisting of i) spectra truncation 200-1800 cm^{-1}, ii) unit normalization and iii) linear baseline correction, on our raw Raman Renishaw set 1.

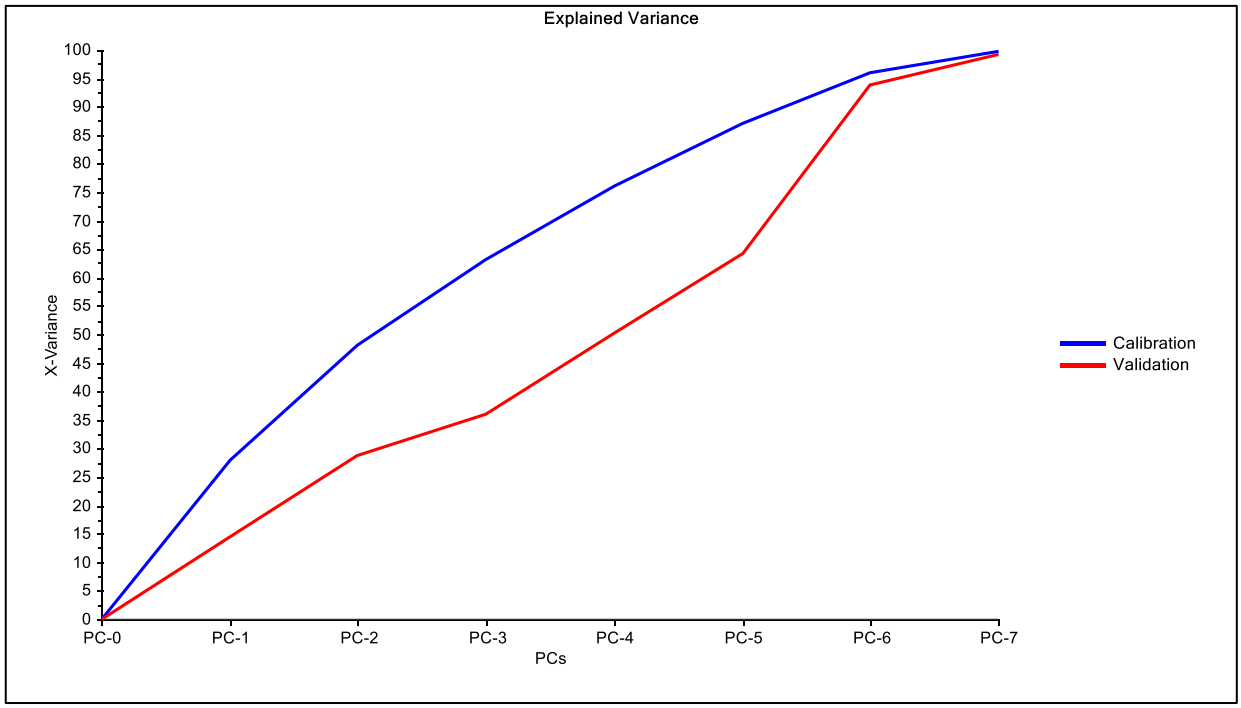

Figure A17. Explained variance plot of set 1 after application of pre-processing protocol 5.

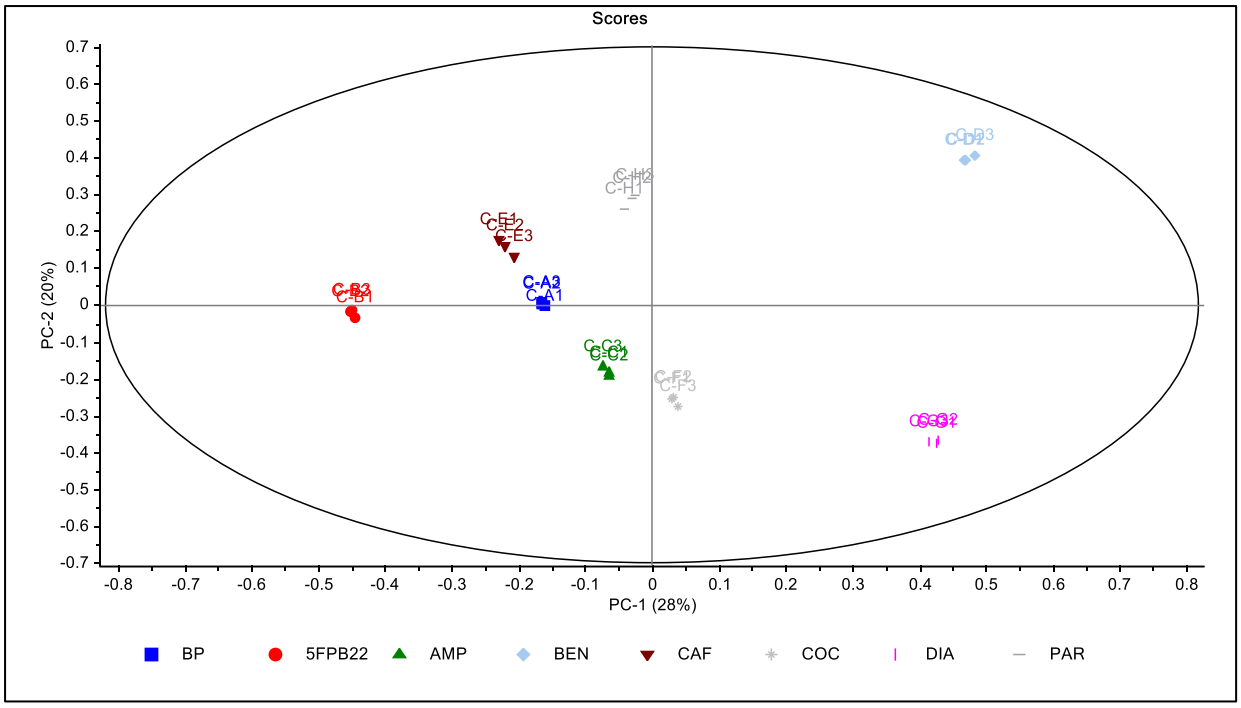

Figure A18. PC-1 vs PC-2 2D scores plot of set 1 after application of pre-processing protocol 5.

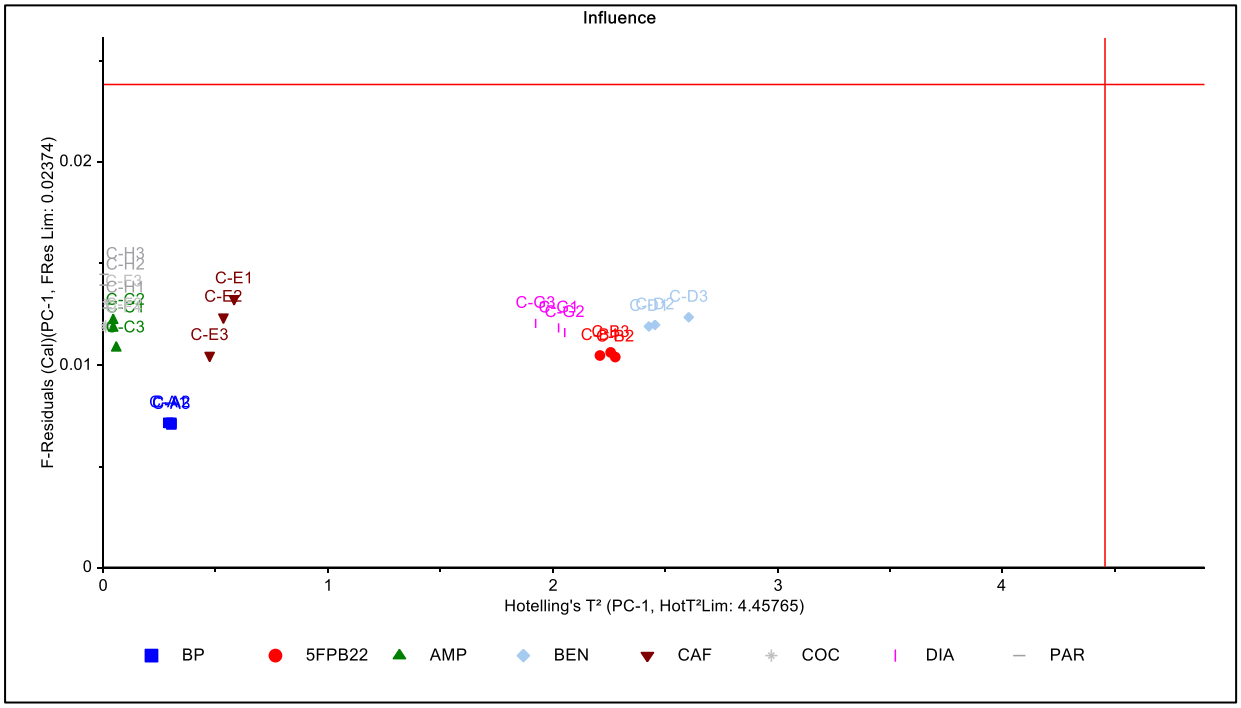

Figure A19. PC-1 F-residuals vs Hotelling T^2 influence plot of set 1 after application of pre-processing protocol 5.

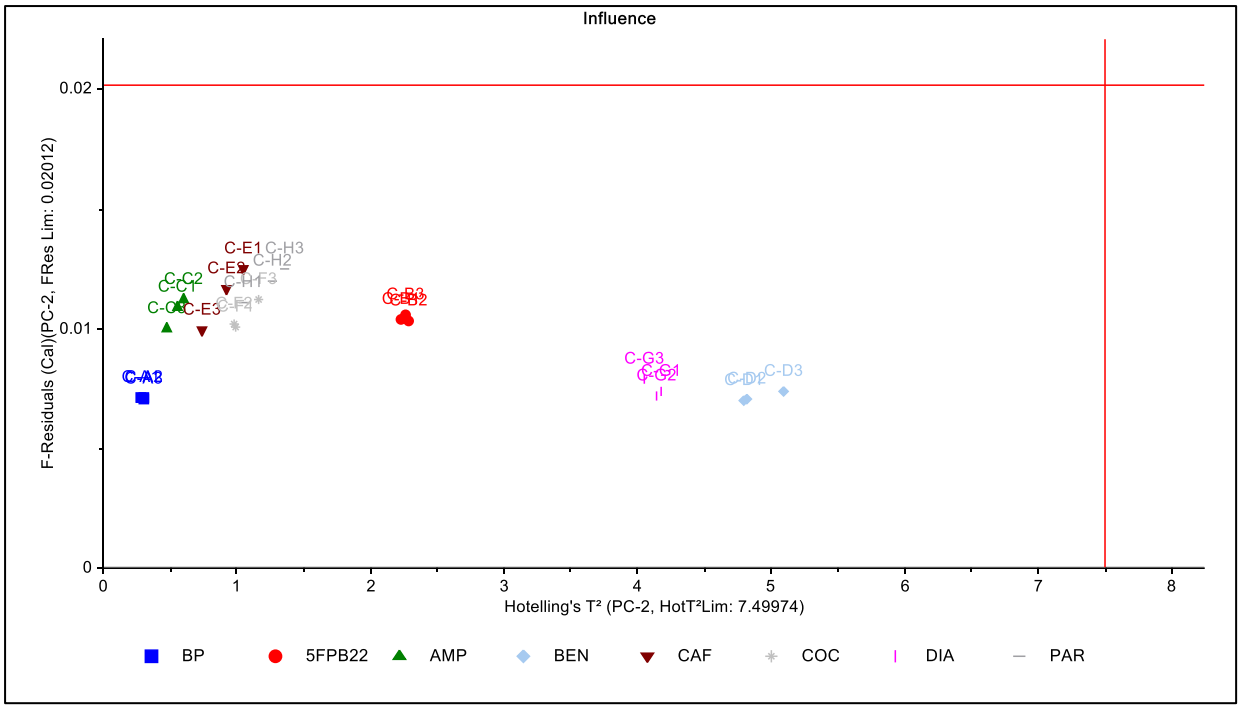

Figure A20. PC-2 F-residuals vs Hotelling T^2 influence plot of set 1 after application of pre-processing protocol 5.

6) Development of a pre-processing protocol for Raman spectra of NPS related powders (Gurguis, 2017. Unpublished)

Below are shown the final PCA plots resulting from the application of the pre-processing sequence, consisting of i) baseline offset and ii) mean normalisation, on our raw Raman Renishaw set 1.

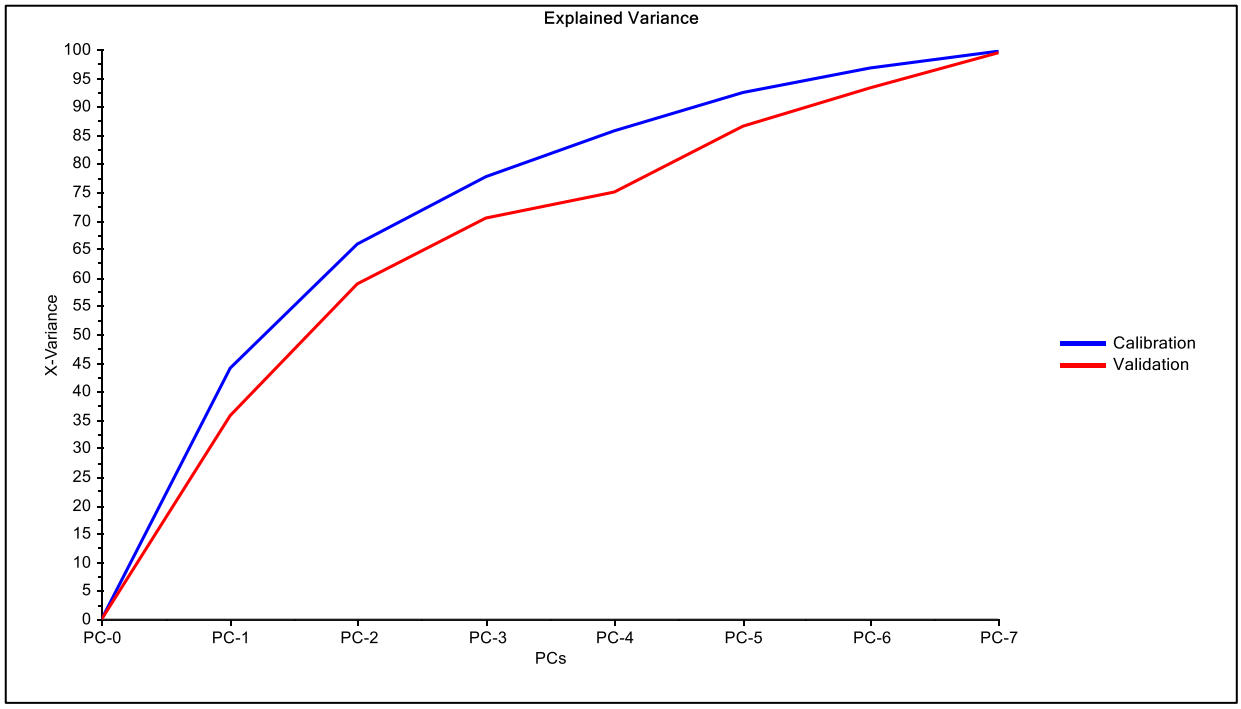

Figure A21. Explained variance plot of set 1 after application of pre-processing protocol 6.

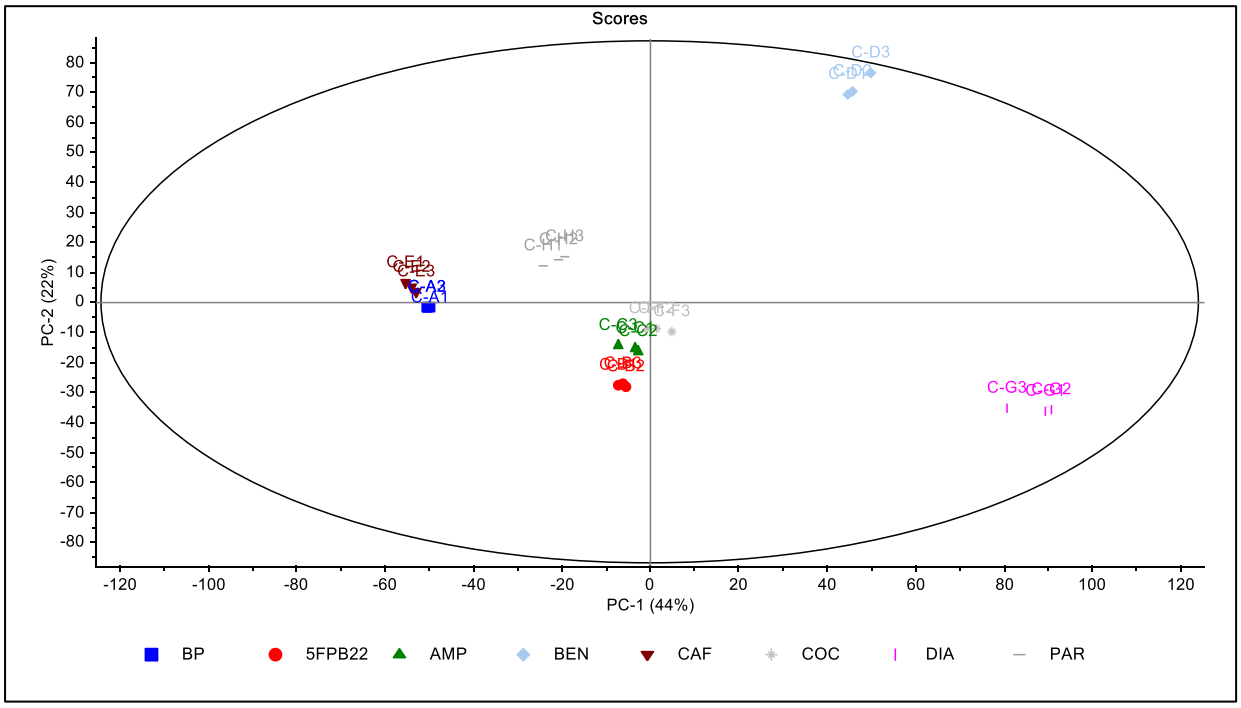

Figure A22. PC-1 vs PC-2 2D scores plot of set 1 after application of pre-processing protocol 6.

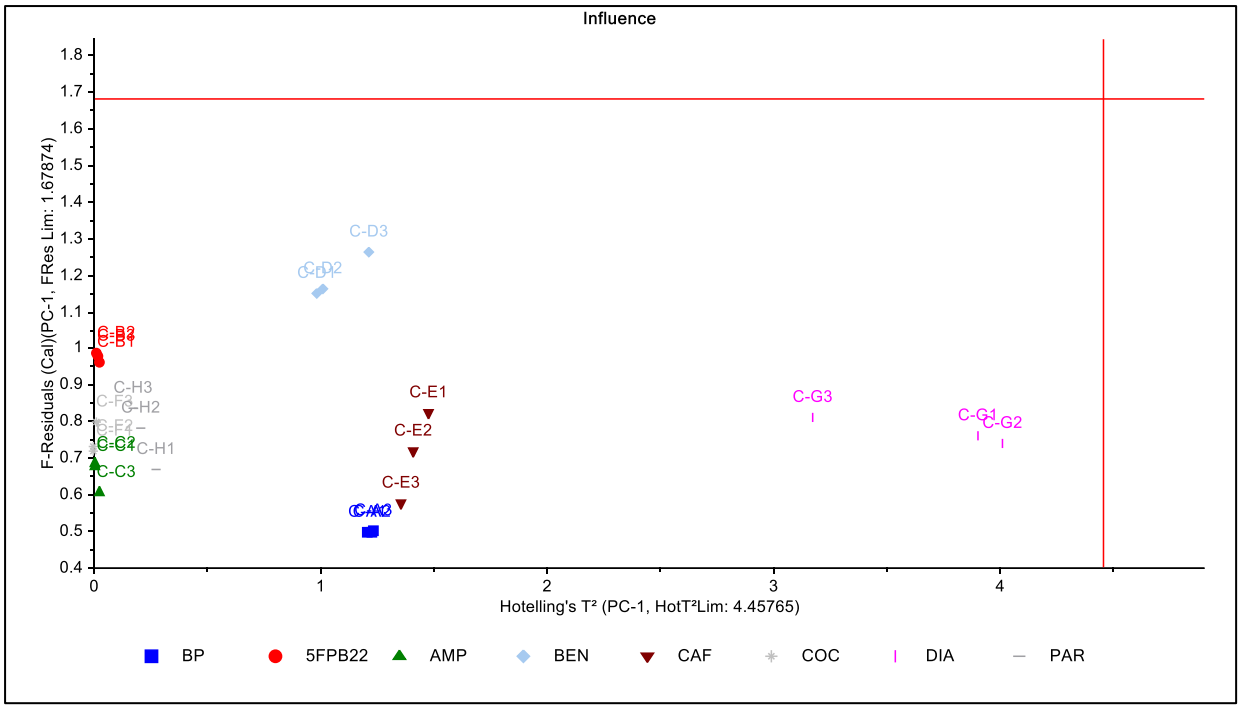

Figure A23. PC-1 F-residuals vs Hotelling T^2 influence plot of set 1 after application of pre-processing protocol 6.

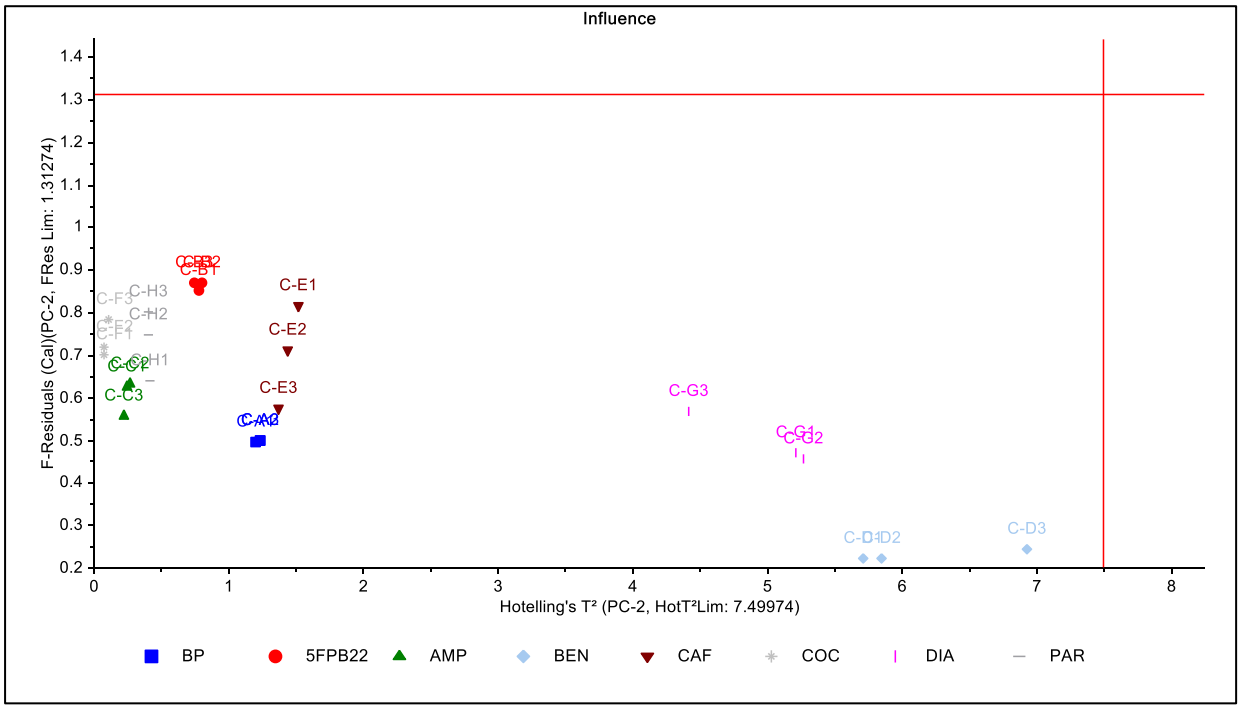

Figure A24. PC-2 F-residuals vs Hotelling T^2 influence plot of set 1 after application of pre-processing protocol 6.

7) Classification of NPS reference standards using Raman spectroscopy (Calvo-Castro et al, 2018)

Below are shown the final PCA plots resulting from the application of the pre-processing sequence, consisting of i) smoothing SG 21 smoothing points 4 order derivative, ii) baseline subtraction 2nd derivative, iii) zero negative points and iv) max normalisation, on our raw Raman Renishaw set 1.

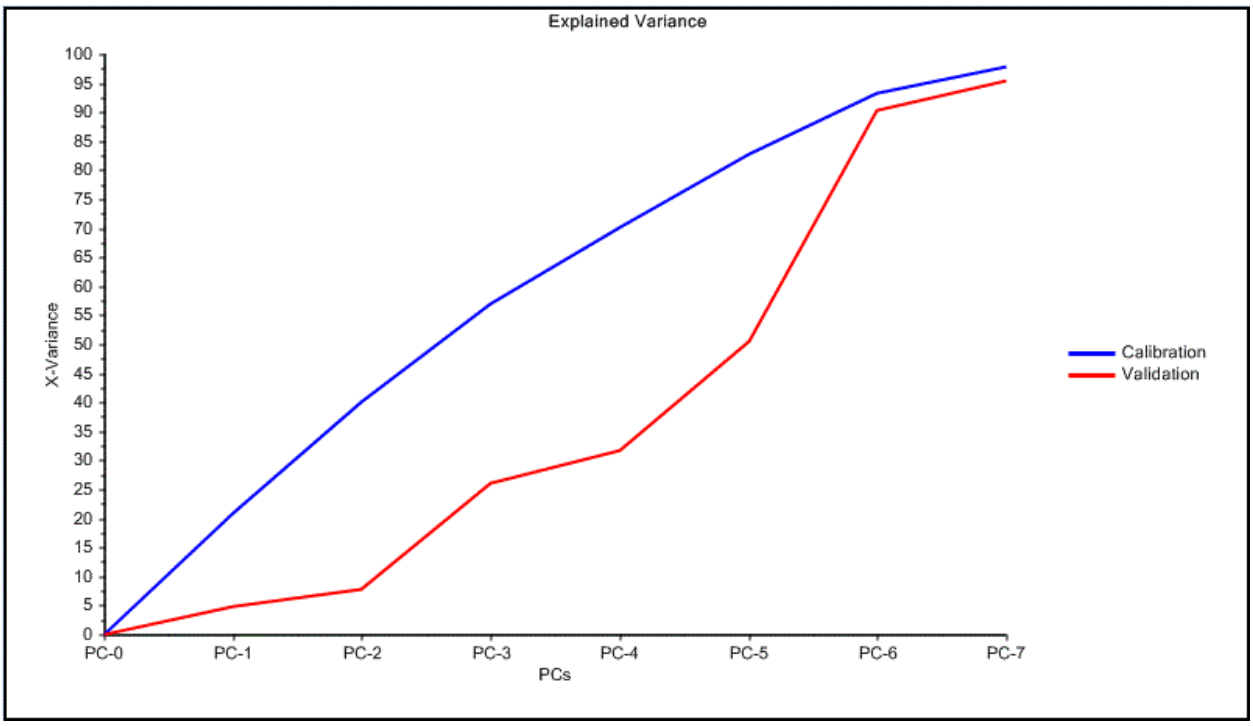

Figure A25. Explained variance plot of set 1 after application of pre-processing protocol 7.

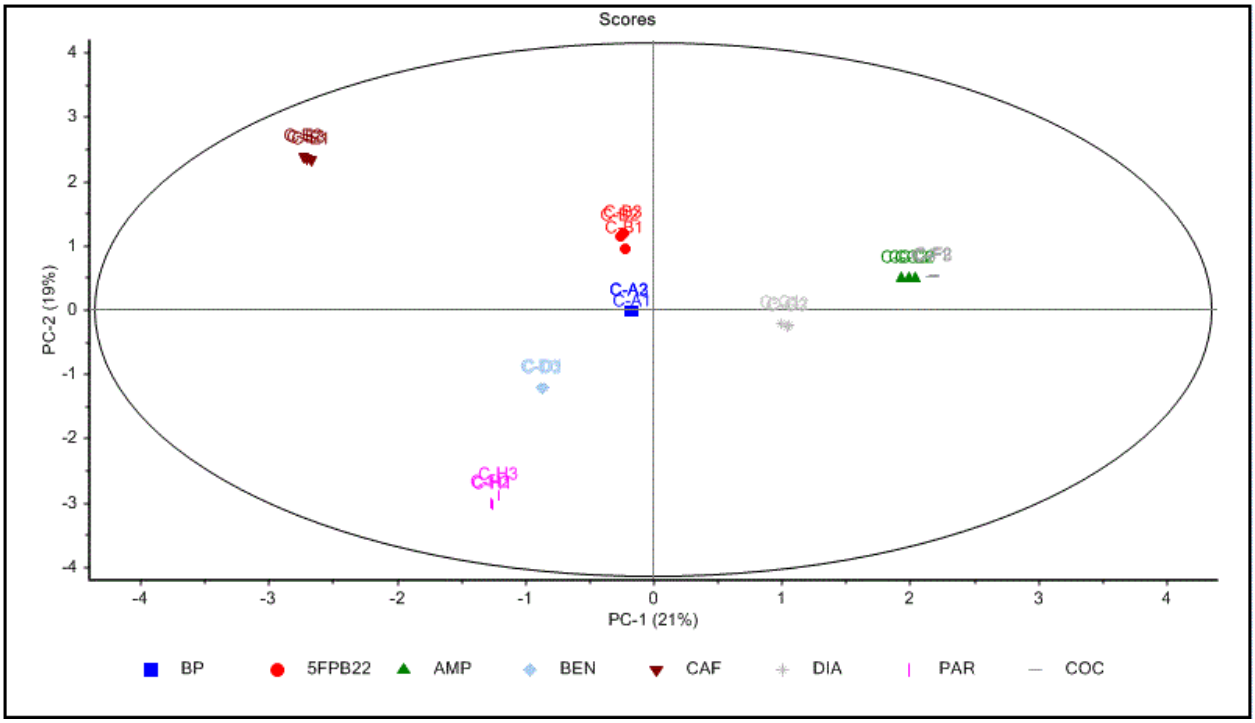

Figure A26. PC-1 vs PC-2 2D scores plot of set 1 after application of pre-processing protocol 7.

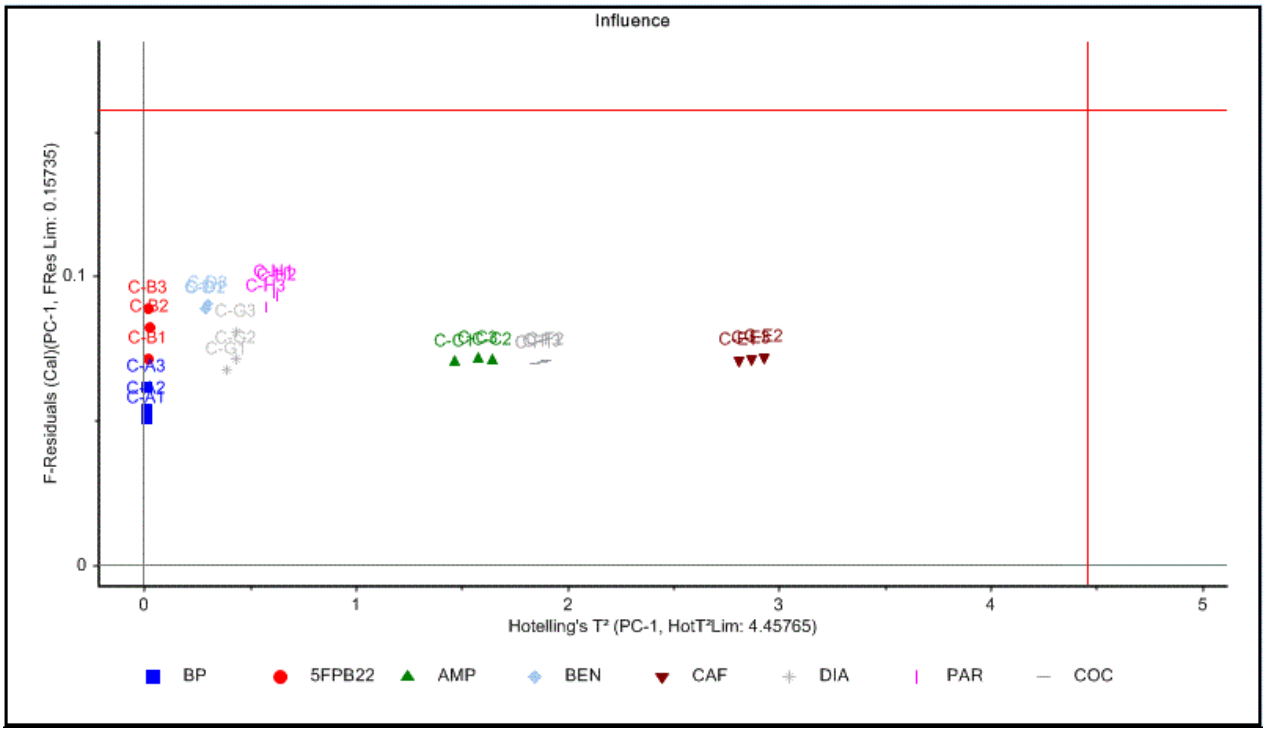

Figure A27. PC-1 F-residuals vs Hotelling T^2 influence plot of set 1 after application of pre-processing protocol 7.

8) Identification of new NPS by Raman spectroscopy (Omar et al, 2019)

Below are shown the final PCA plots resulting from the application of the pre-processing sequence, consisting of i) spectra truncation 250-1750 cm^{-1}, ii) replicate were averaged (big dataset) and iii) SNV, on our raw Raman Renishaw set 1.

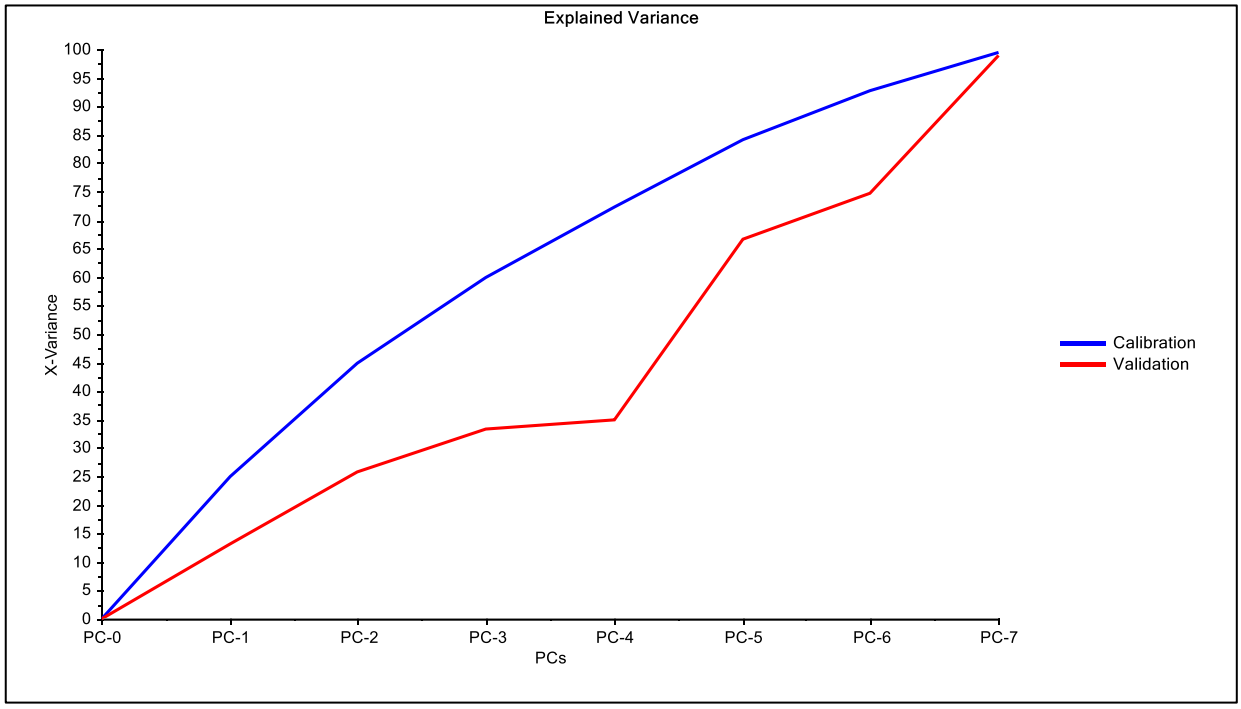

Figure A28. Explained variance plot of set 1 after application of pre-processing protocol 8.

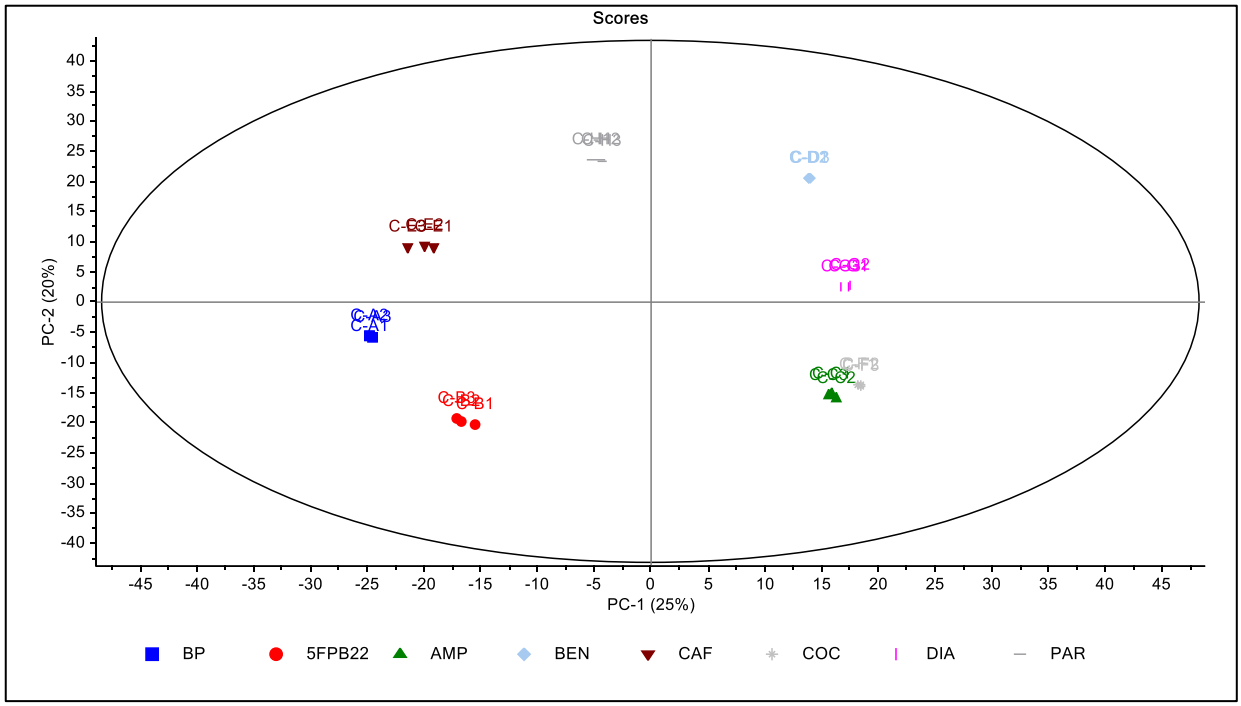

Figure A29. PC-1 vs PC-2 2D scores plot of set 1 after application of pre-processing protocol 8.

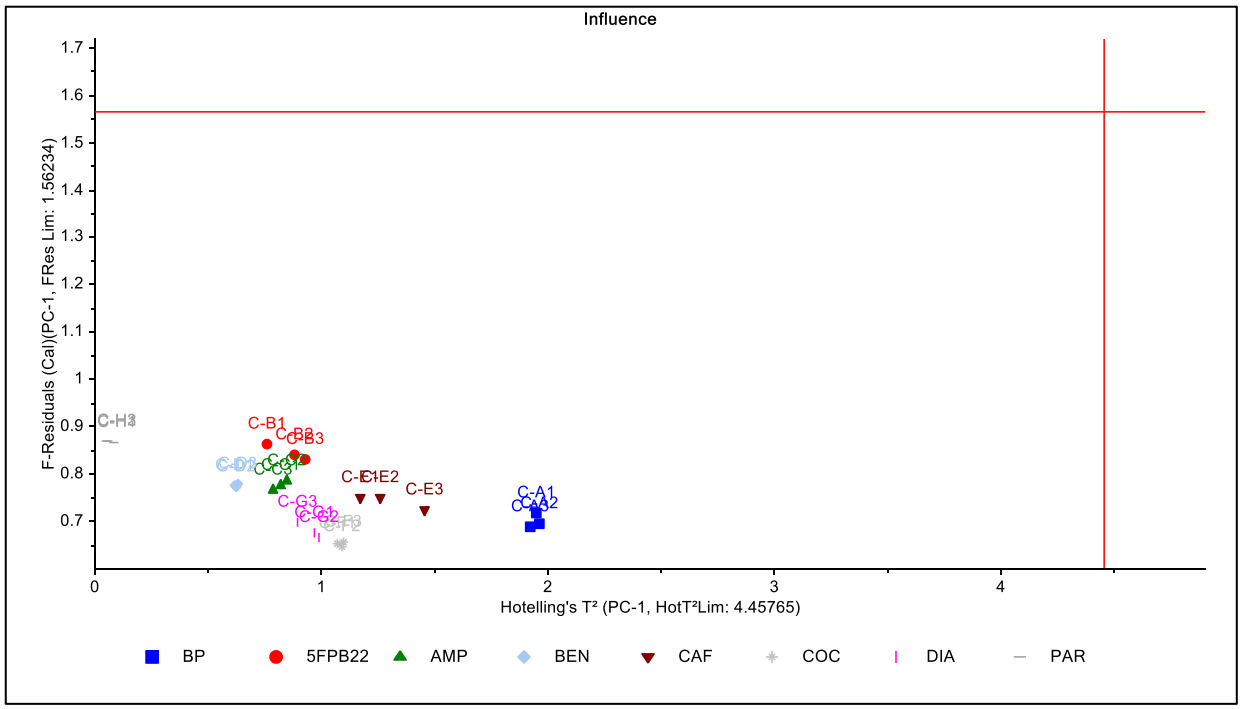

Figure A30. PC-1 F-residuals vs Hotelling T^2 influence plot of set 1 after application of pre-processing protocol 8.

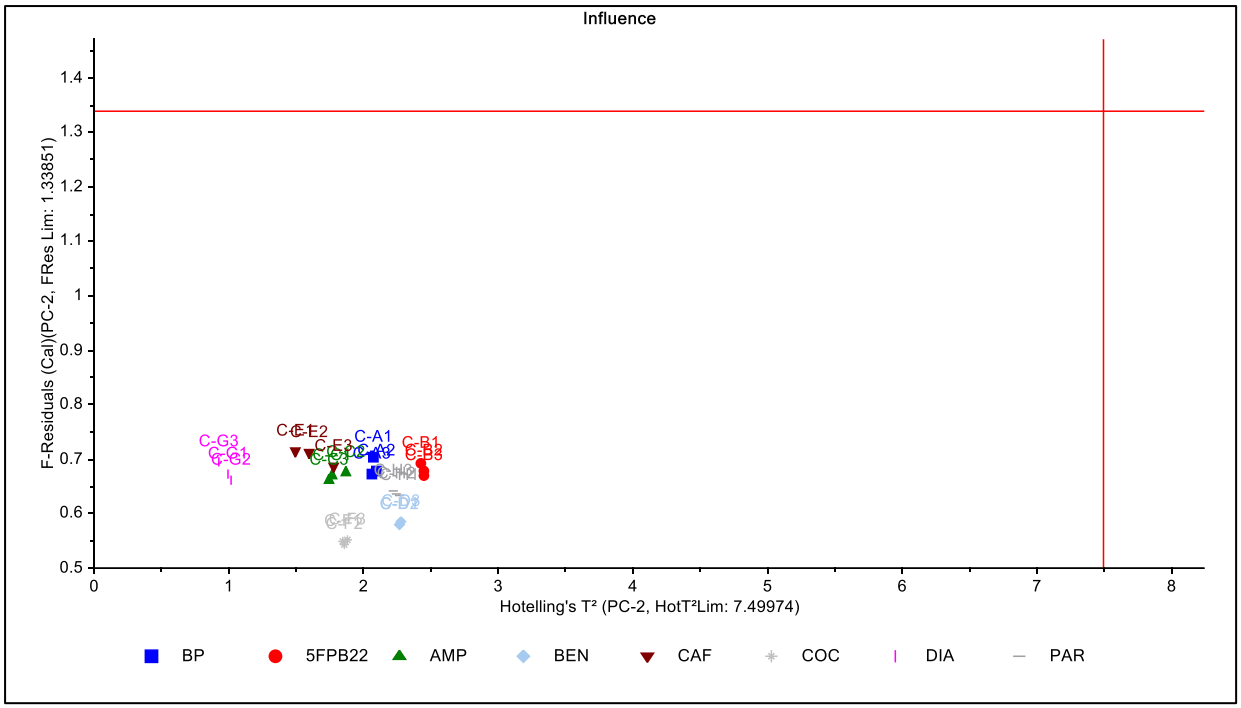

Figure A31. PC-2 F-residuals vs Hotelling T^2 influence plot of set 1 after application of pre-processing protocol 8.

Appendix 4.4. Validation of Raman Renishaw pre-processing protocol

Validation of the optimal pre-processing protocol (Guirguis 2017) was performed using a new set of independent samples to ensure that the model is not over fitted to the data. The data set was inspected the same way described in section 5.2.4.1. The optimal pre-processing protocol was applied to both the training (calibration) and test sets (validation) and was successful in classifying the test set. A 2-PC model explained 64% and 60% of the cumulative calibration and validation variance, respectively. The scores plot (Figure A1) showed that all benzocaine calibration and validation data sets have a higher-than-average values for positive loadings (PC-1).

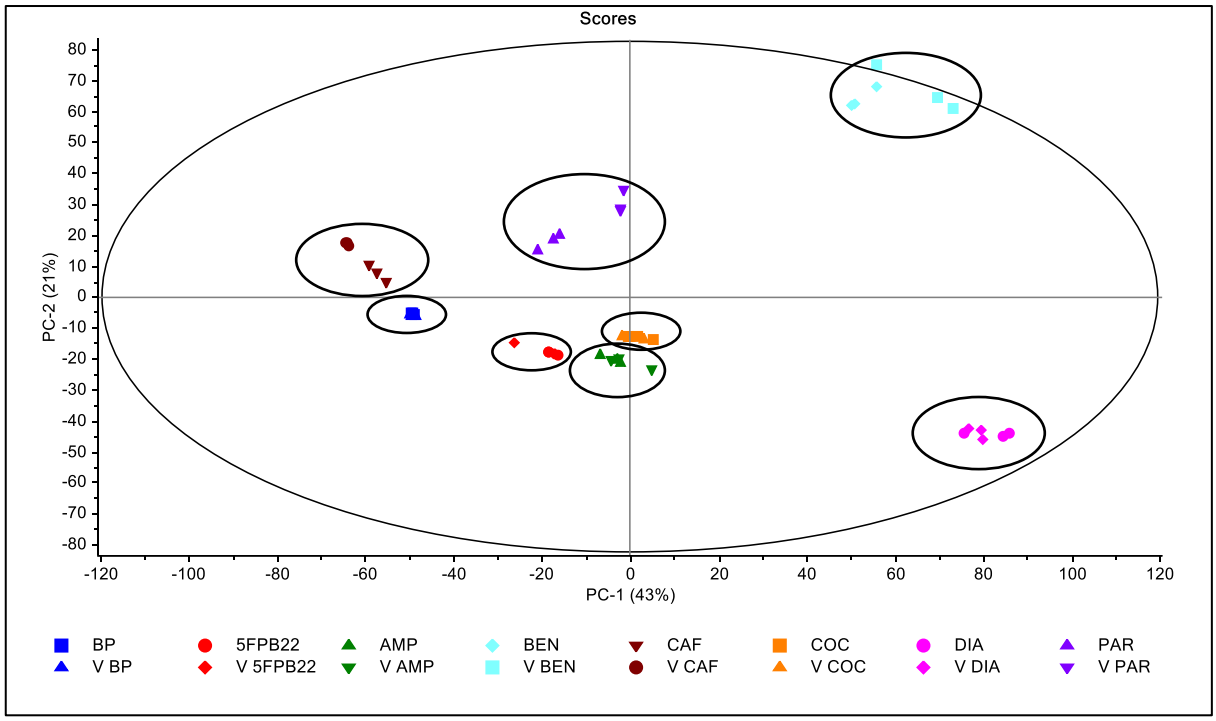

Figure A1. PC-1 vs PC-2 2D scores plot of set 3.

All samples are fitted in the 95% confidence interval ellipse except benzocaine VC replicate 3, which was further investigated. The visual inspection of the benzocaine replicate samples, showed that the sample benzocaine VC-R3 had a lower intensity when compared to the other replicates. This was investigated further through the F-residuals vs Hotelling T^2 influence plots (Figure A2 and A3), which showed that this sample fits in the model, but has a high leverage for PC-2.

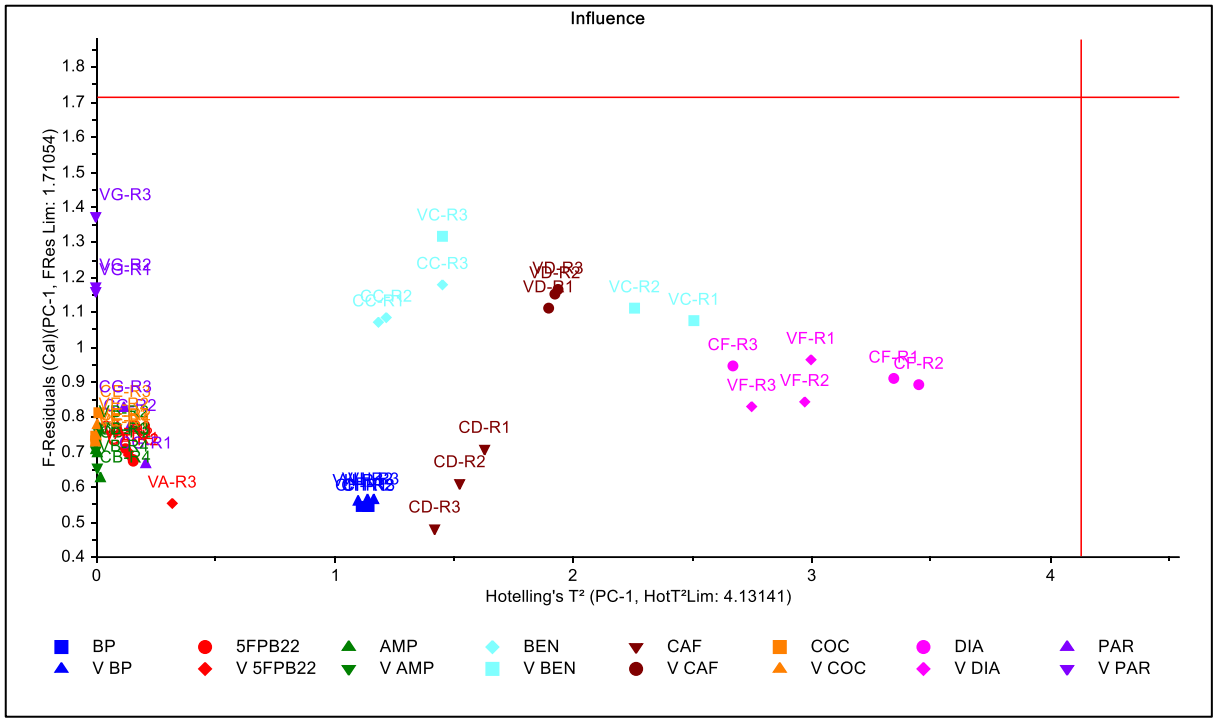

Figure A2. PC-1 F-residuals vs Hotelling T^2 influence plot of set 3.

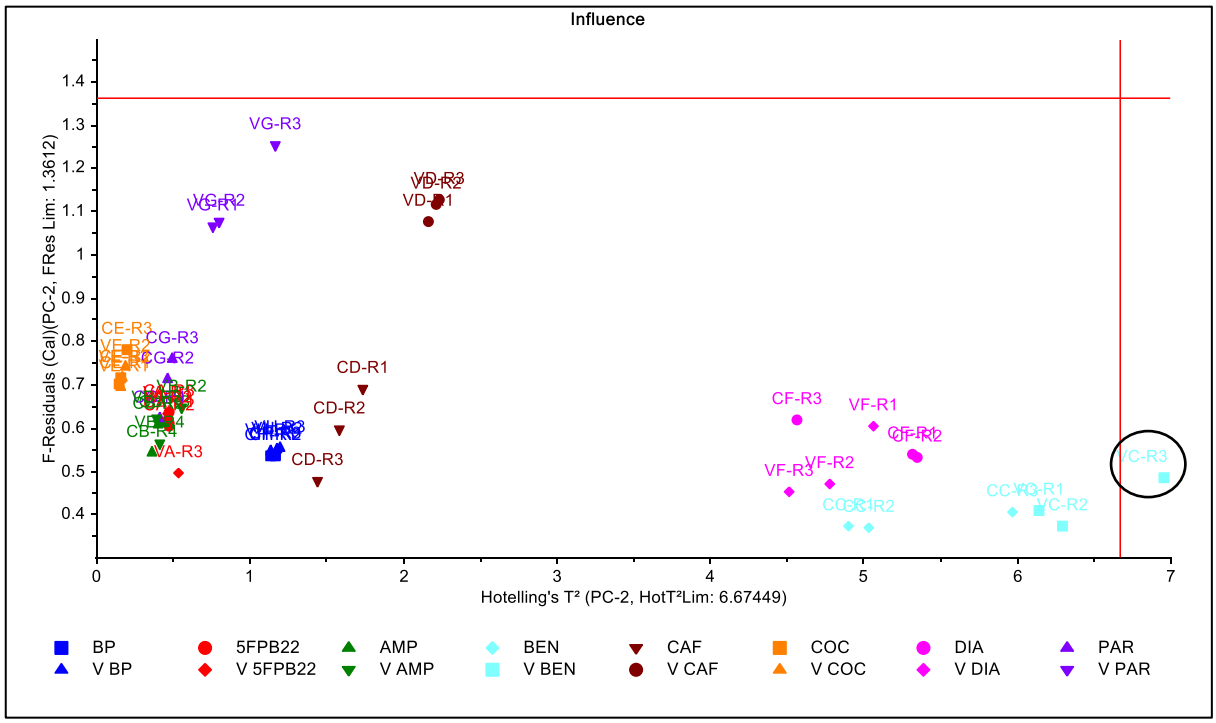

Figure A3. PC-2 F-residuals vs Hotelling T^2 influence plot of set 3.

Appendix 4.5 Validation of Raman Rigaku pre-processing protocol

Validation of the optimal pre-processing protocol (Guirguis 2017) was performed using a new set of independent samples to ensure that the model is not over fitted to the data. The data set was inspected the same way described in section 3.2.1. The optimal pre-processing protocol was applied to both the training (calibration) and test sets (validation) and was successful in classifying the test set. A 2-PC model explained 48% and 40% of the cumulative calibration and validation variance, respectively. All samples are fitted in the 95% confidence interval ellipse (Figure A1).

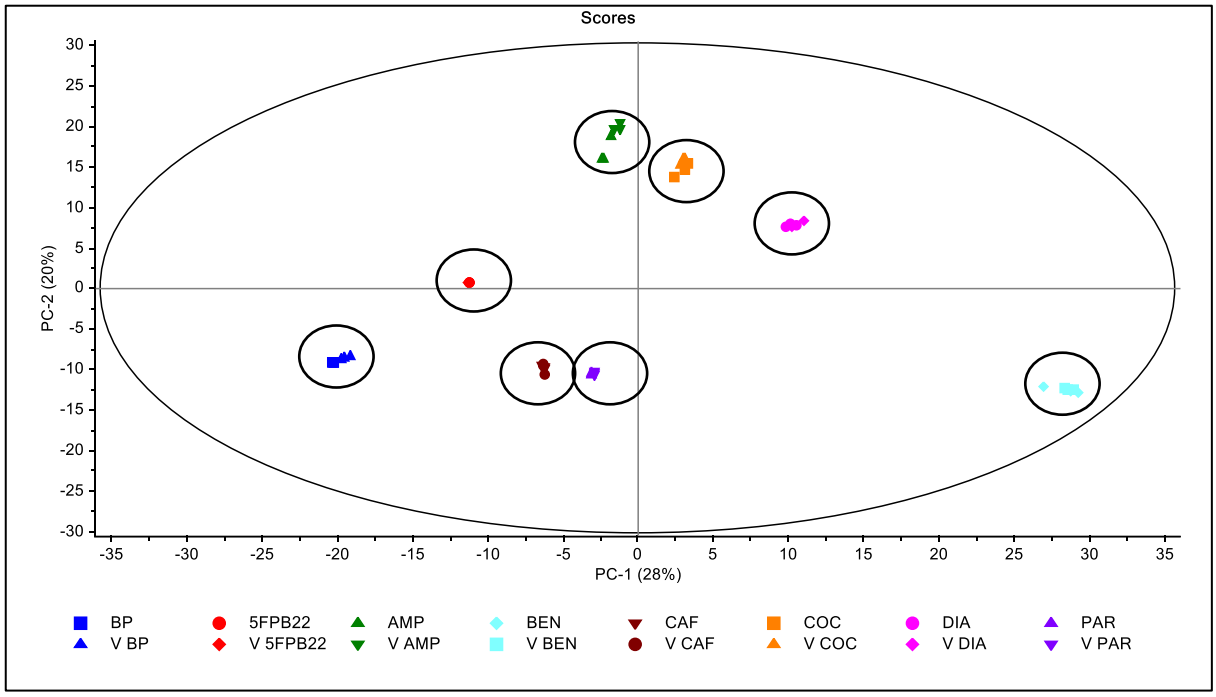

Figure A1. PC-1 vs PC-2 2D scores plot of set 4.

F-residuals vs Hotelling T^2 influence plots (Figure A2 and A3) were also investigated, showing that benzocaine sample fits in the model, but these have a high leverage for PC-.1

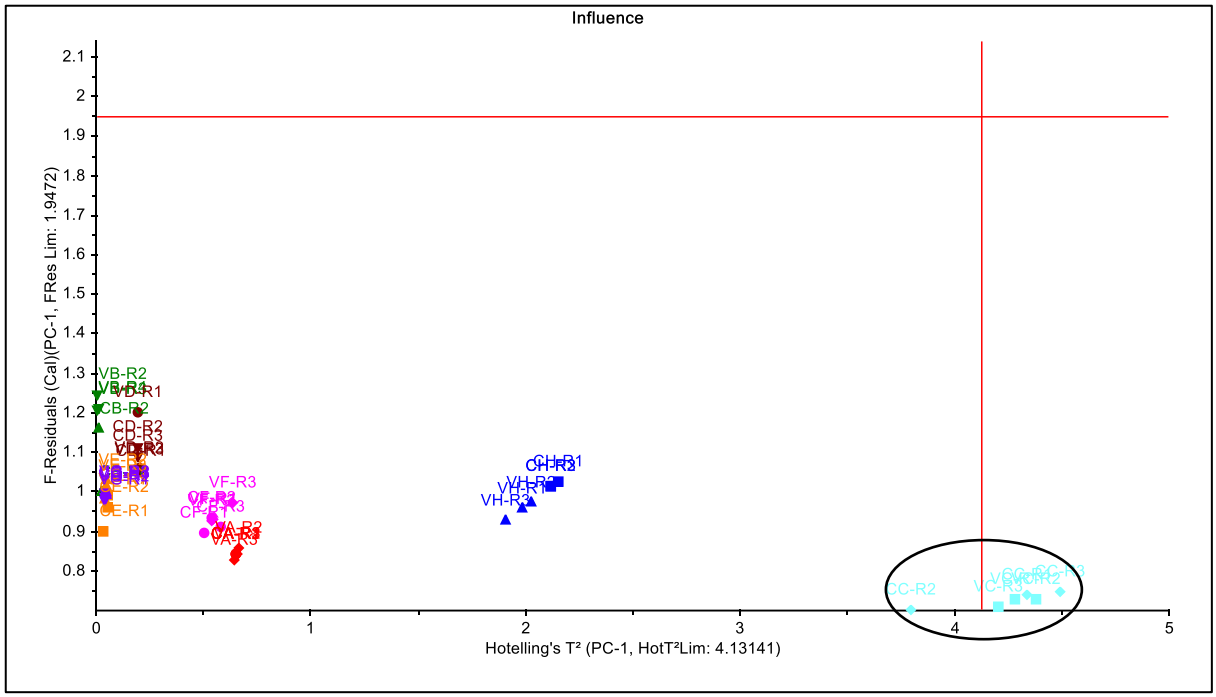

Figure A2. PC-1 F-residuals vs Hotelling T^2 influence plot of set 4.

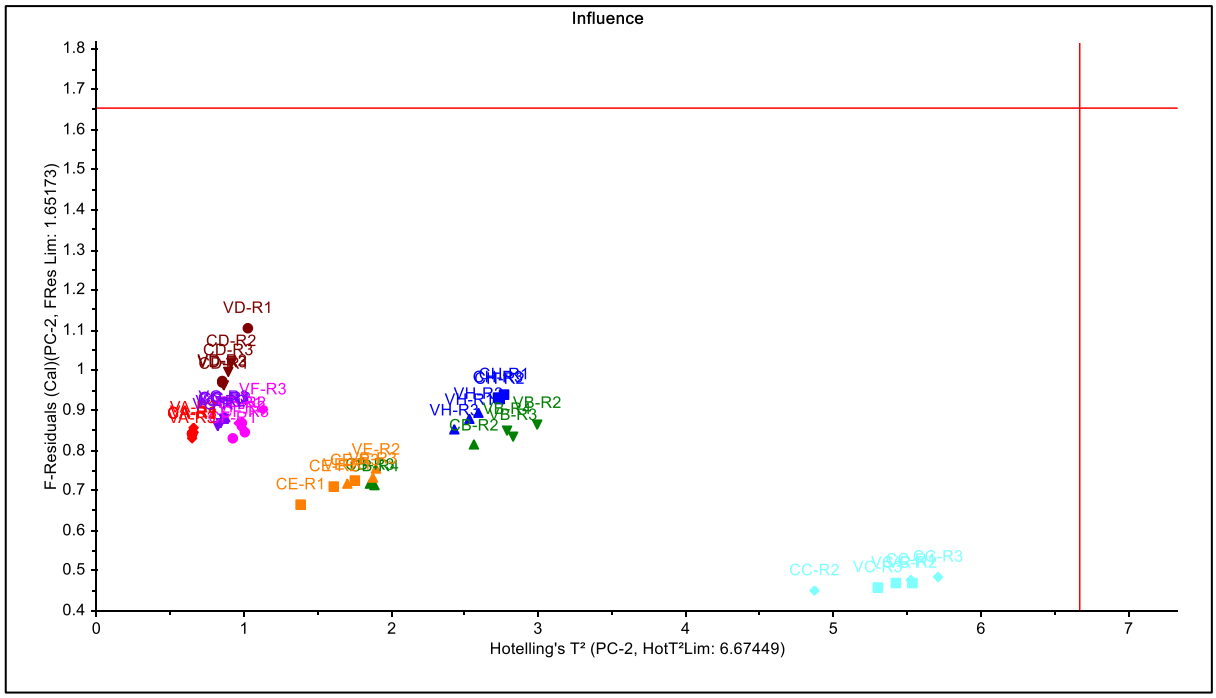

Figure A3. PC-2 F-residuals vs Hotelling T^2 influence plot of set 4.

Appendix 4.5. Coefficient correlation matrix of Raman Renishaw raw data

Table A1. Coefficient correlation matrix.

	BP			5F-PB-22			AMP			BEN			CAF			COC			DIA			PAR		
	C-H1	C-H2	C-H3	C-A1	C-A2	C-A3	C-B1	C-B2	C-B3	C-C1	C-C2	C-C3	C-D1	C-D2	C-D3	C-E1	C-E2	C-E3	C-F1	C-F2	C-F3	C-G1	C-G2	C-G3
C-H1	1																							
C-H2	0.998	1	0	0	0	0	0	0	0	0	0	0	0	0	0	0	0	0	0	0	0	0	0	0
C-H3	0.9967	0.9992	1	0	0	0	0	0	0	0	0	0	0	0	0	0	0	0	0	0	0	0	0	0
C-A1	0.5527	0.5497	0.5498	1	0	0	0	0	0	0	0	0	0	0	0	0	0	0	0	0	0	0	0	0
C-A2	0.5464	0.5438	0.5442	0.9952	1	0	0	0	0	0	0	0	0	0	0	0	0	0	0	0	0	0	0	0
C-A3	0.557	0.5541	0.5547	0.9905	0.9971	1	0	0	0	0	0	0	0	0	0	0	0	0	0	0	0	0	0	0
C-B1	0.5737	0.5644	0.5634	0.7335	0.7369	0.7394	1	0	0	0	0	0	0	0	0	0	0	0	0	0	0	0	0	0
C-B2	0.5708	0.5601	0.5587	0.7309	0.7344	0.7369	0.9985	1	0	0	0	0	0	0	0	0	0	0	0	0	0	0	0	0

C-B3	0.6046	0.5954	0.5943	0.7463	0.7495	0.7522	0.9984	0.9979	1	0	0	0	0	0	0	0	0	0	0	0	0	0	0	0	0
C-C1	0.4328	0.4274	0.4266	0.5479	0.5502	0.554	0.6415	0.6364	0.6501	1	0	0	0	0	0	0	0	0	0	0	0	0	0	0	0
C-C2	0.4295	0.4242	0.4235	0.5455	0.5479	0.5516	0.6383	0.6331	0.6468	0.9998	1	0	0	0	0	0	0	0	0	0	0	0	0	0	0
C-C3	0.4127	0.4075	0.4069	0.5258	0.5283	0.5317	0.6201	0.615	0.6282	0.9991	0.9993	1	0	0	0	0	0	0	0	0	0	0	0	0	0
C-D1	0.6596	0.6639	0.6648	0.4342	0.4346	0.4361	0.4057	0.3962	0.4284	0.3862	0.3845	0.3719	1	0	0	0	0	0	0	0	0	0	0	0	0
C-D2	0.7072	0.708	0.7068	0.4516	0.4508	0.4529	0.4328	0.4253	0.4566	0.4006	0.3985	0.3851	0.9949	1	0	0	0	0	0	0	0	0	0	0	0
C-D3	0.7878	0.786	0.783	0.4813	0.4792	0.4827	0.4723	0.4662	0.4983	0.4197	0.4173	0.4027	0.9735	0.9902	1	0	0	0	0	0	0	0	0	0	0
C-E1	0.5807	0.5693	0.5654	0.729	0.7142	0.7155	0.816	0.8165	0.8248	0.6767	0.6743	0.6567	0.4466	0.4772	0.5157	1	0	0	0	0	0	0	0	0	0
C-E2	0.5718	0.5602	0.5562	0.7315	0.7172	0.7188	0.8213	0.8219	0.8296	0.6811	0.6787	0.661	0.4408	0.471	0.5088	0.9995	1	0	0	0	0	0	0	0	0
C-E3	0.5486	0.5367	0.5327	0.7256	0.7108	0.7116	0.8119	0.8128	0.8193	0.6738	0.6714	0.654	0.4256	0.4552	0.4912	0.9988	0.9999	1	0	0	0	0	0	0	0
C-F1	0.4045	0.3943	0.3908	0.6539	0.661	0.6565	0.768	0.7705	0.7725	0.6826	0.6815	0.6681	0.3245	0.3481	0.3741	0.7274	0.7311	0.7303	1	0	0	0	0	0	0

C-F2	0.4045	0.3942	0.3908	0.6577	0.6649	0.6603	0.7732	0.7756	0.7777	0.6887	0.6875	0.6741	0.3262	0.3499	0.3756	0.7315	0.7354	0.7345	0.9995	1	0	0	0	0
C-F3	0.4152	0.4064	0.4033	0.6381	0.6453	0.6403	0.7495	0.7511	0.7549	0.6697	0.6688	0.6559	0.3332	0.3559	0.3824	0.7082	0.7108	0.7096	0.9961	0.9951	1	0	0	0
C-G1	0.6922	0.6855	0.6825	0.6266	0.6295	0.6382	0.6748	0.6708	0.6944	0.6634	0.6614	0.6452	0.5736	0.6005	0.6447	0.6526	0.6528	0.6366	0.5946	0.5985	0.5872	1	0	0
C-G2	0.6467	0.6408	0.6384	0.612	0.6159	0.6245	0.6605	0.6559	0.6786	0.6629	0.661	0.6455	0.5526	0.5751	0.6136	0.6359	0.6368	0.6215	0.5888	0.5929	0.5805	0.9974	1	0
C-G3	0.626	0.6205	0.6183	0.6059	0.6101	0.6185	0.6536	0.6488	0.671	0.6608	0.659	0.6438	0.5421	0.5628	0.5988	0.6279	0.6291	0.6143	0.5861	0.5903	0.5774	0.9952	0.9994	1

Appendix 4.6. caffeine raw & pre-processed Renishaw spectral data

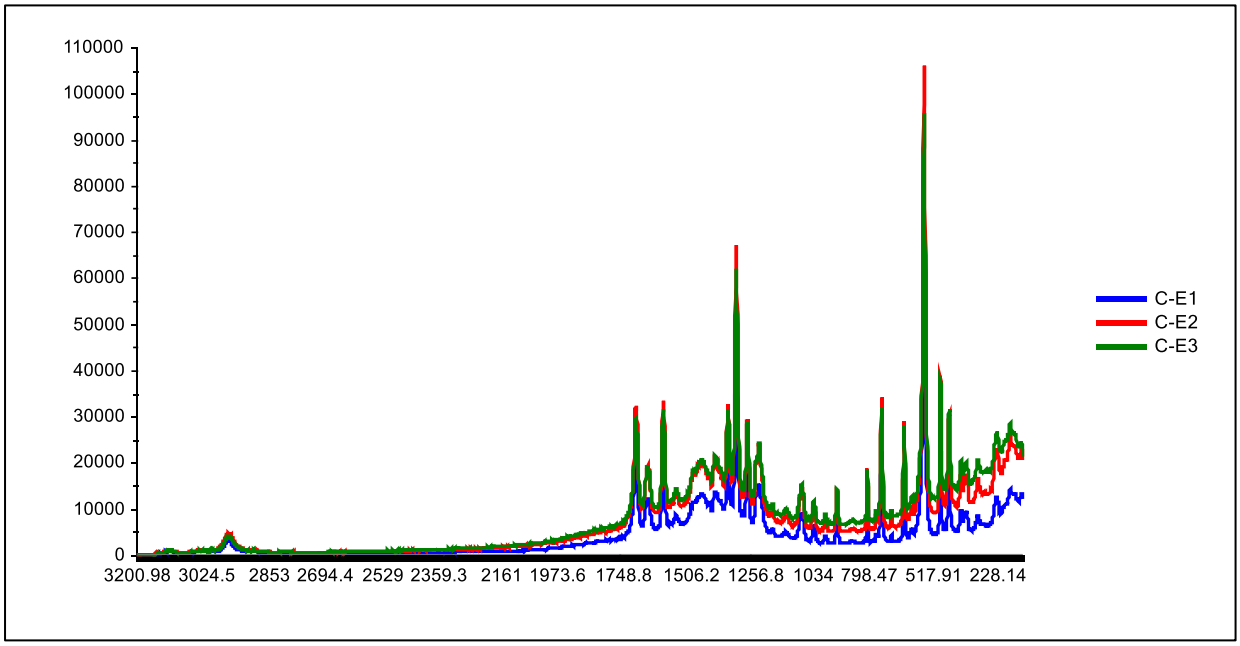

Figure A1. caffeine triplicate raw Raman Renishaw spectral data.

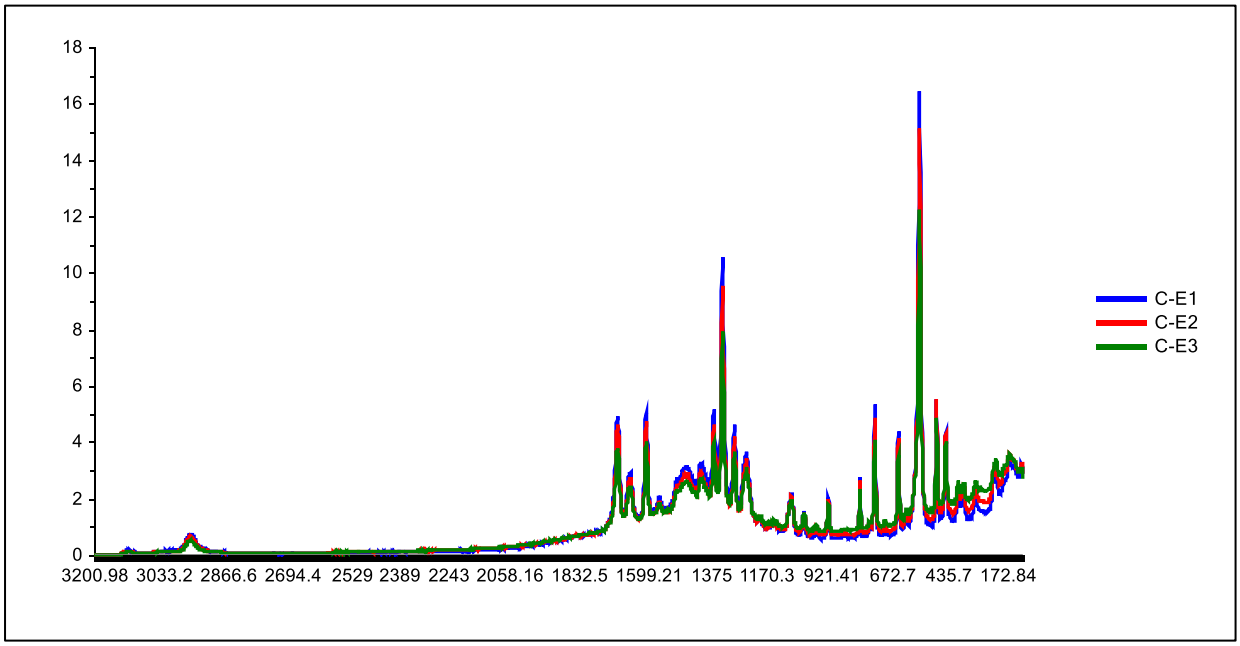

Figure A2. caffeine triplicate**)** pre-processed Raman Renishaw spectral data.

Appendix 4.7. S/N calculation & values

The signal value was calculated by manually fitting a linear baseline tangentially at the base of the maximum peak from the high wavenumber shift end towards the region of low wavenumber shift end of the fingerprint region (1750-250 cm^{-1}) of chemical information (Figure A1). The signal was then calculated by subtracting the absolute intensity value of the linear baseline from the absolute intensity value of the maximum peak in each spectrum [49]. This was performed for all the samples replicates.

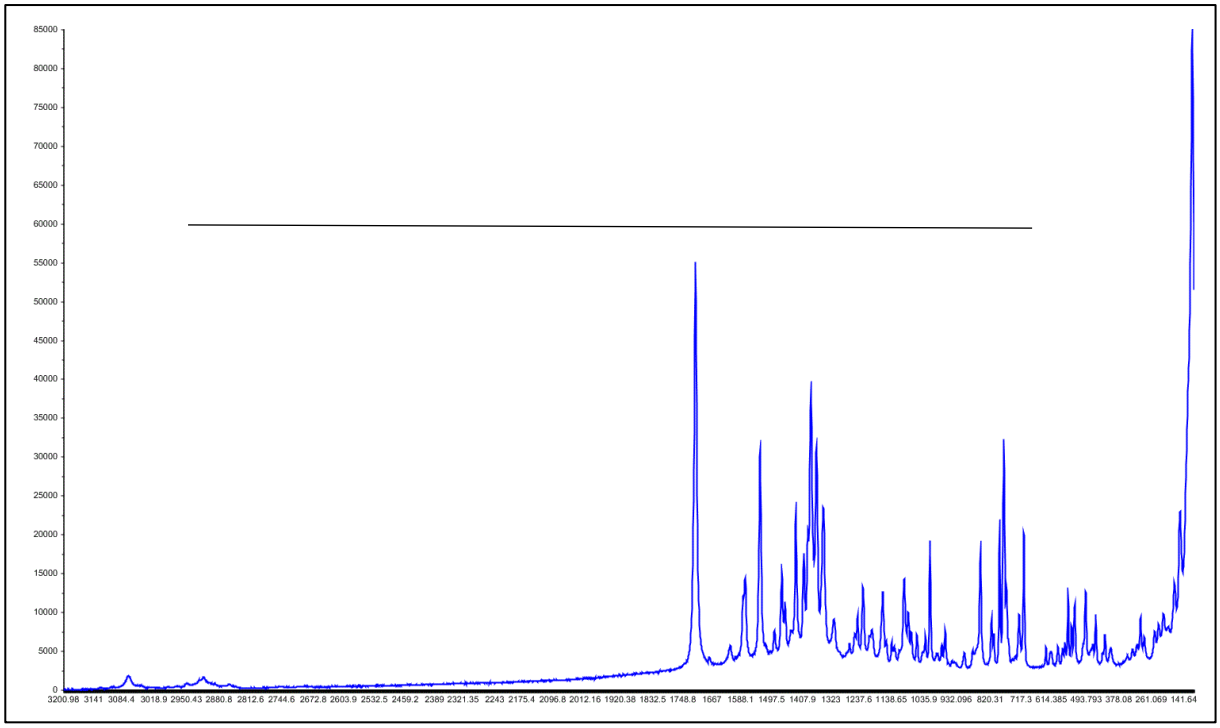

Figure A1. Manual calculation of the signal at 1713 cm^{-1} for 5F-PB-22 R1 (The Unscramble X).

In contrast, the noise value was estimated by measuring the peak-to-peak distance between two parallel lines, which is estimated to contain about 80% of peaks in the region 2700-2500 cm^{-1} in all spectra (Figure A2).

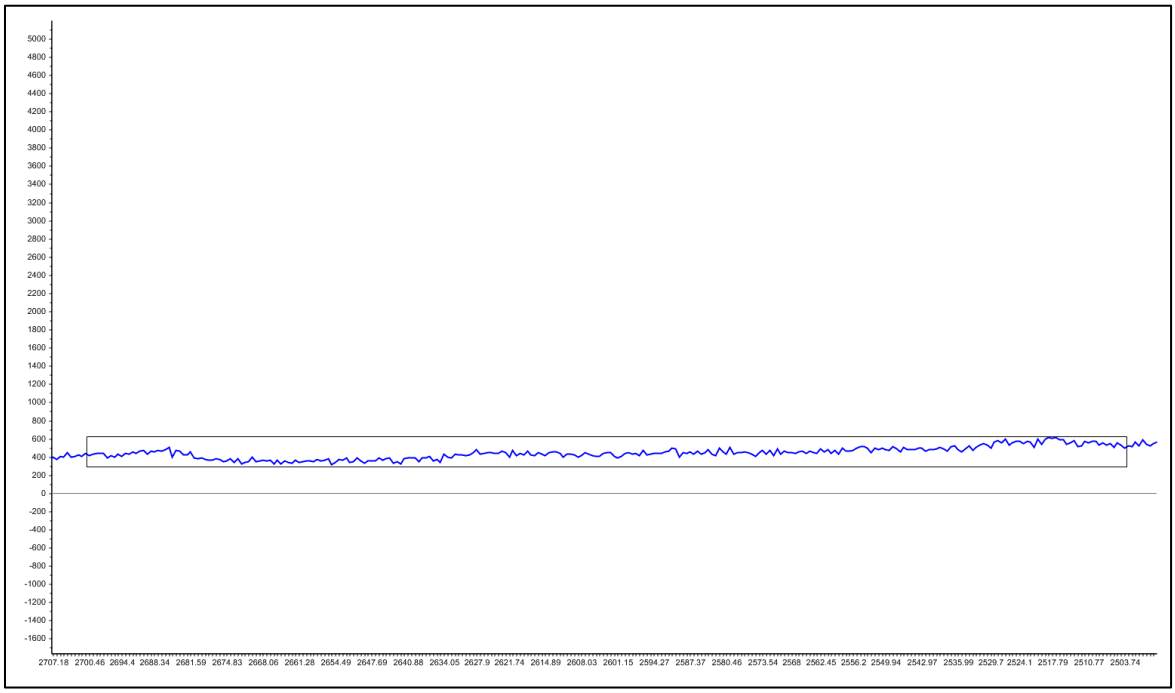

Figure A2. Manual calculation of the baseline noise of a 5F-PB-22 R1 spectrum (2500-2700 cm^{-1}) (The Unscramble X).

In Table A1 are summarised the S/N values calculated for the three replicates of the seven reference standards & BP.

Table A1: The S/N of Raman Rigaku spectra.

Samples	Labels	Maximum Peak (cm^{-1})	Signal (S)	Noise (N)	S/N
BP	C-A1	1085	16751	650	25.77076923
	C-A2	1085	19790	540	36.64814815
	C-A3	1085	19307	490	39.40204082
5F-PB-22	C-B1	1713	55070	390	141.2051282
	C-B2	1713	46122	380	121.3736842
	C-B3	1713	42468	385	110.3064935
AMP	C-C1	1001	37997	320	118.740625
	C-C2	1001	46532	340	136.8588235
	C-C3	1001	36255	300	120.85
BEN	C-D1	1605	42897	135	317.7555556
	C-D2	1605	42704	95	449.5157895

	C-D3	1605	54156	105	515.7714286
CAF	C-E1	555	67904	295	230.1830508
	C-E2	555	95815	485	197.556701
	C-E3	555	106103	490	216.5367347
COC	C-F1	999	46487	460	101.0586957
	C-F2	999	46043	400	115.1075
	C-F3	999	50889	350	145.3971429
DIA	C-G1	1593	44243	330	134.069697
	C-G2	1593	42304	280	151.0857143
	C-G3	1593	48269	300	160.8966667
PAR	C-H1	856	73899	520	142.1134615
	C-H2	856	81432	430	189.3767442
	C-H3	857	81941	425	192.8023529

Appendix 4.8. Raman Renishaw set 1 additional PCA plots

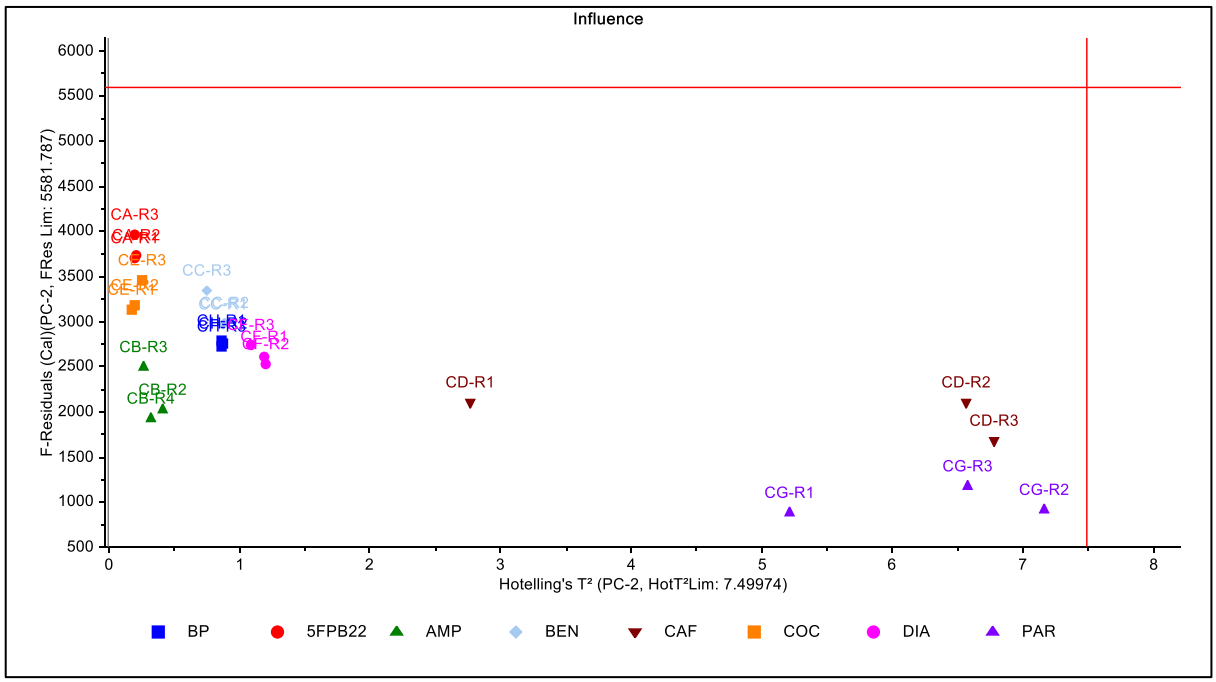

Figure A1. PC-2 F-residuals vs Hotelling T^2 influence plot of the unprocessed set 1.

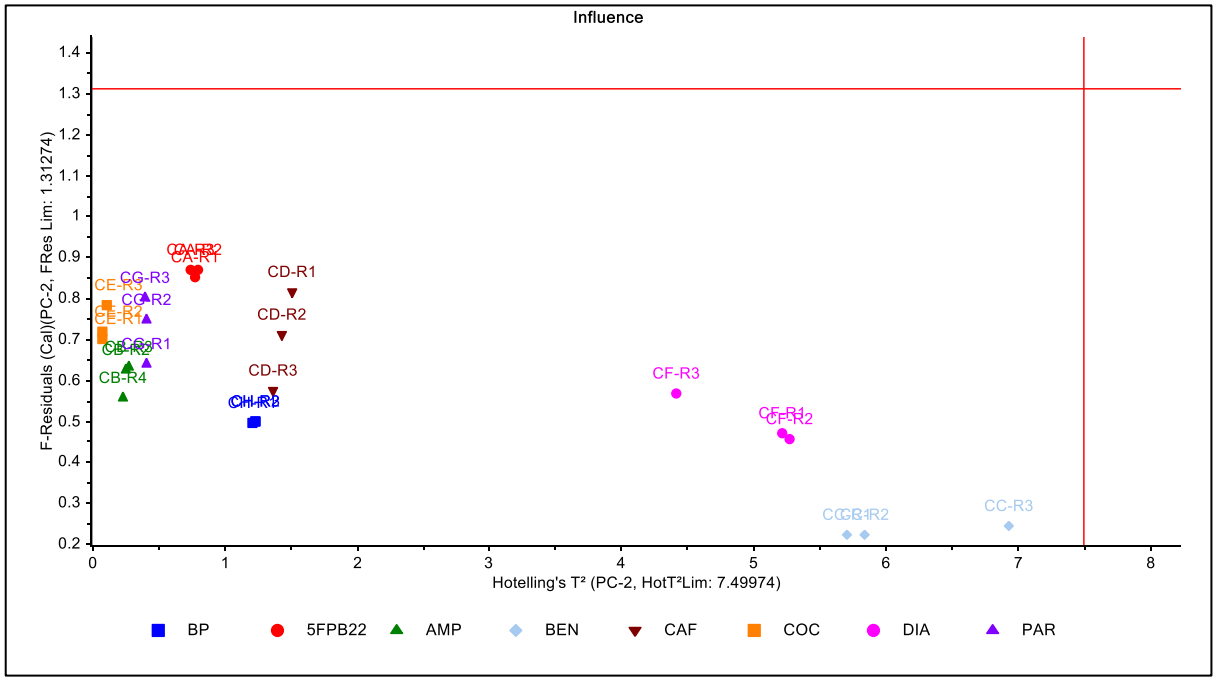

Figure A2. PC-2 F-residuals vs Hotelling T^2 influence plot pre-processed set 1.

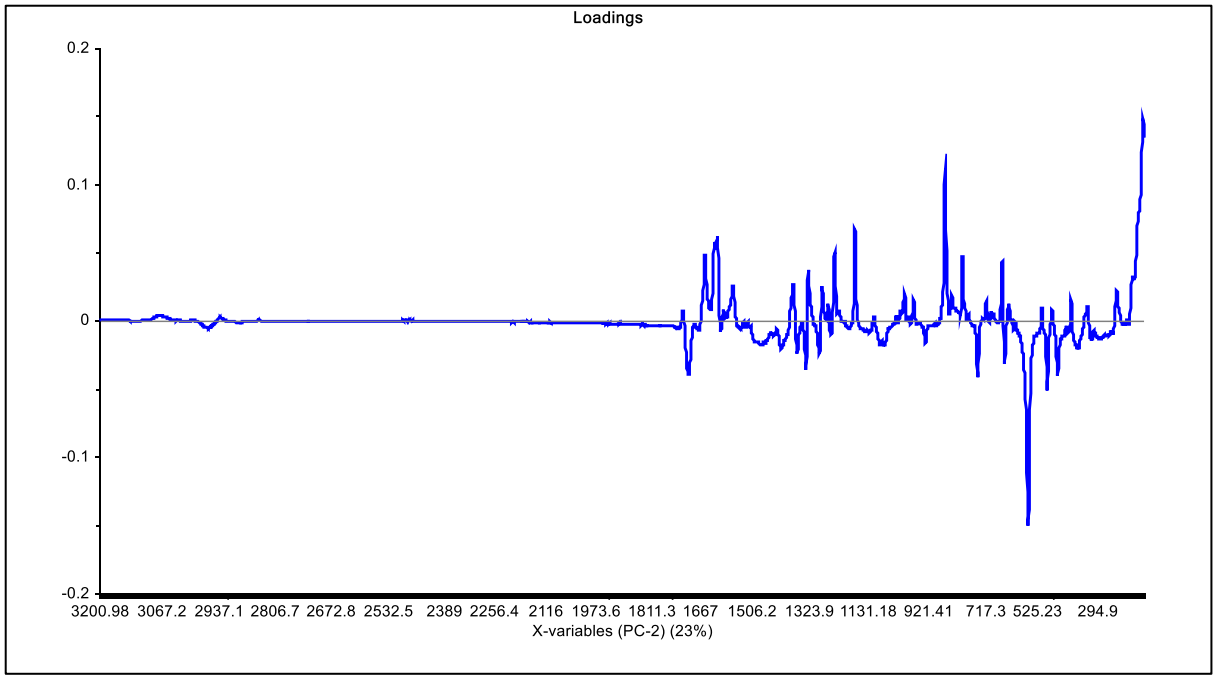

Figure A3. PC-2 loadings plot of the unprocessed set 1.

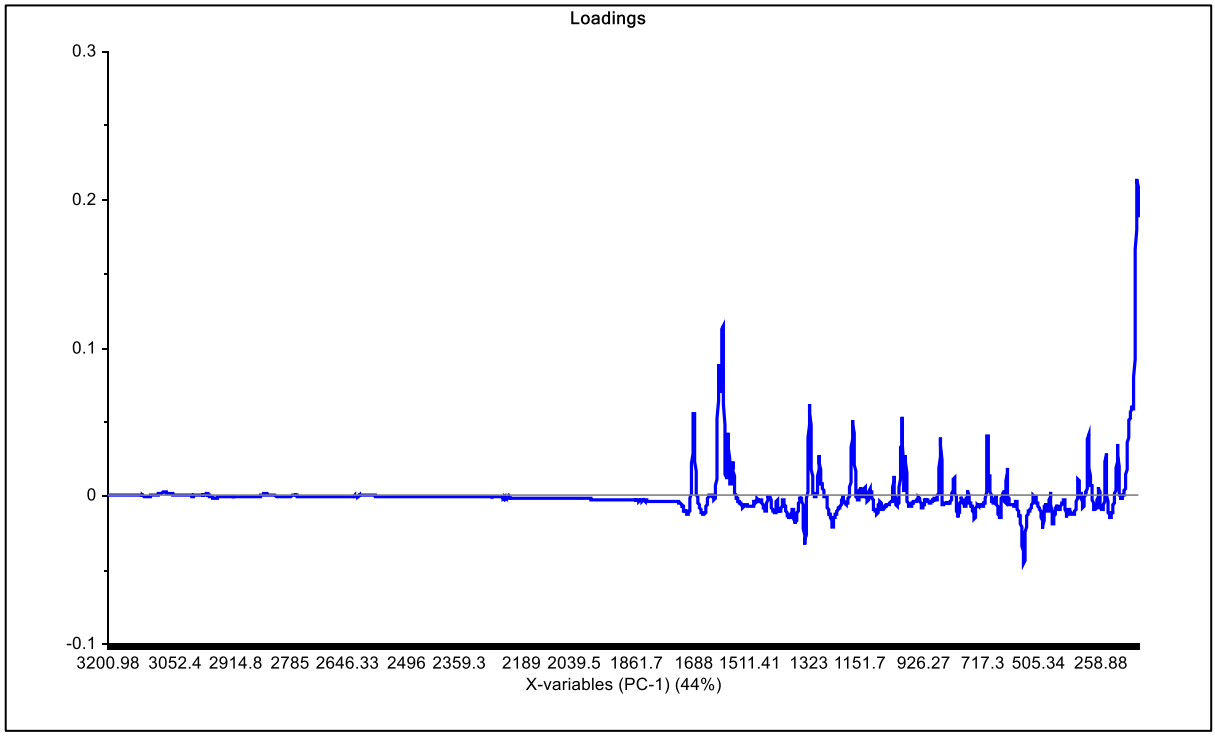

Figure A4. PC-2 loadings plot of the pre-processed set 1.

Appendix 4.9. Rigaku Raman spectra and related peak assignments

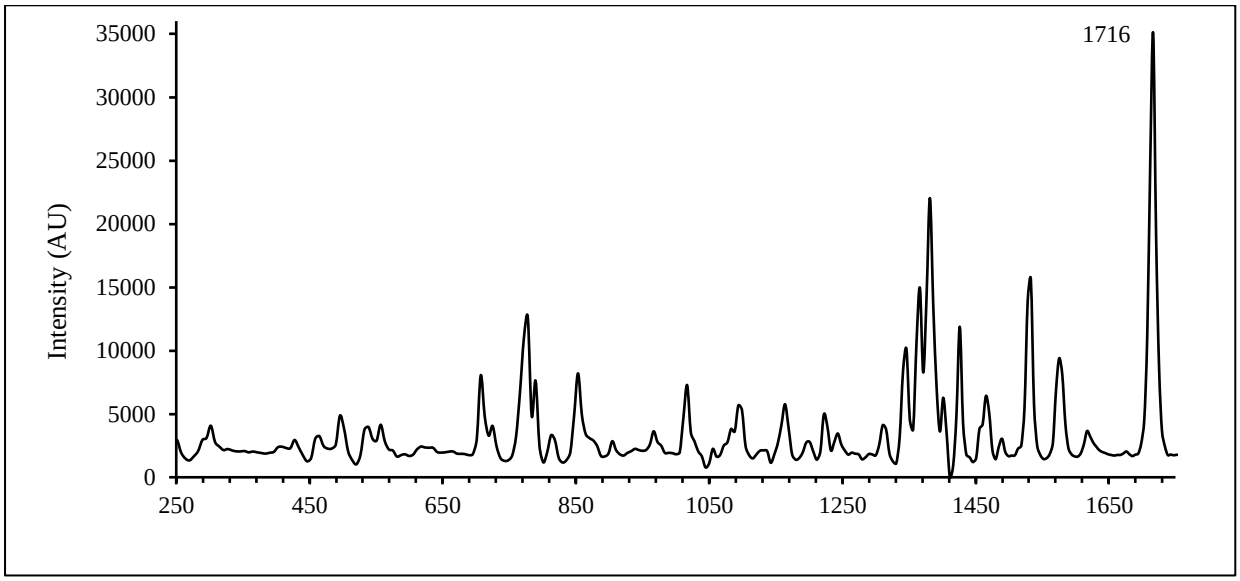

Figure A1. 5F-PB-22 Raman Rigaku spectrum (Excel version 2015, build 14026.20308).

Table A1. 5F-PB-22 Raman peaks assignments (Alkaseem et al., 2018).

5F-PB-22				
Functional groups	**Mode**	**Literature peaks (cm^{-1})**	**Rigaku peaks (cm^{-1})**	**Renishaw peaks (cm^{-1})**
$C_{24}C_{25}C_{27}$ & $C_{17}O_{15}O_{16}$	Torsion & bending	~706	~707 w	~706 m/w
$H_{45}C_{21}C_{23}C_{22}$ + HCCF	Torsion	~773	~778 m/w	~773 m
H28C5C1C2 & C49F10	Torsion & stretching	~850	~853 w	~850 m/w
C23C21C19 & C18C20	Bending & stretching	~1334 w	~1341 w	~1343 w
N4C3	Stretching	~1363	~1366 m/w	~1364 m
48C27N26 + C26C27	Bending	~1381	~1381 m/s	~1380 s
H48C27N26	Bending	~1425	~1426 m	~1426 m
N26C27 + C19–C20 & H38C10H37	Stretching & bending	~1529	~1533 m	~1529 m
C2C4 + C12C13	Stretching	~1570	~1580 m/w	~1573 w
$O_{17}C_{15}$	Stretching	~1712	~1716 vs	~1712 vs

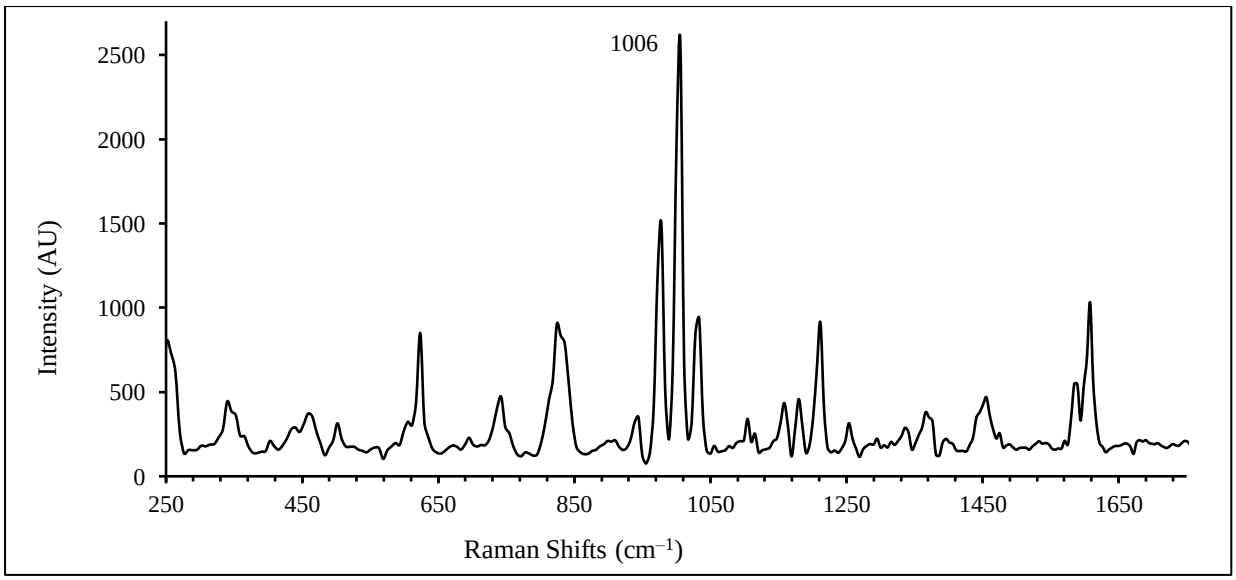

Figure A2. D-amphetamine sulphate Raman Rigaku spectrum (Excel version 2015, build 14026.20308).

Table A2. D-amphetamine sulphate Raman peaks assignments (Berg et al., 2011).

D-amphetamine				
Functional groups	**Mode**	**Literature peaks (cm^{-1})**	**Rigaku peaks (cm^{-1})**	**Renishaw peaks (cm^{-1})**
Chain CH + ring CH	Deformation oopl	~623 m	~623 m	~621 m
Ring CC & CH	Stretching & deformation ipl	~838 m	~830 m	~836 m
Sulphate	Symmetric stretching	~977 s	~978 s	~976 s
Ring + chain CC & CH	Stretching & angle deformation	~1002 vs	~1006 vs	~1002 vs
Ring & chain CC + CH	Stretching & angle deformation	~1033 m	~1033 m	~1033 m
$CH2 + CH_3$	Deformation	~1210 m	~1212 m	~1210 m
Ring CC & ring	Stretching &bending ipl	~1605 m	~1608 m	~1608 m/w

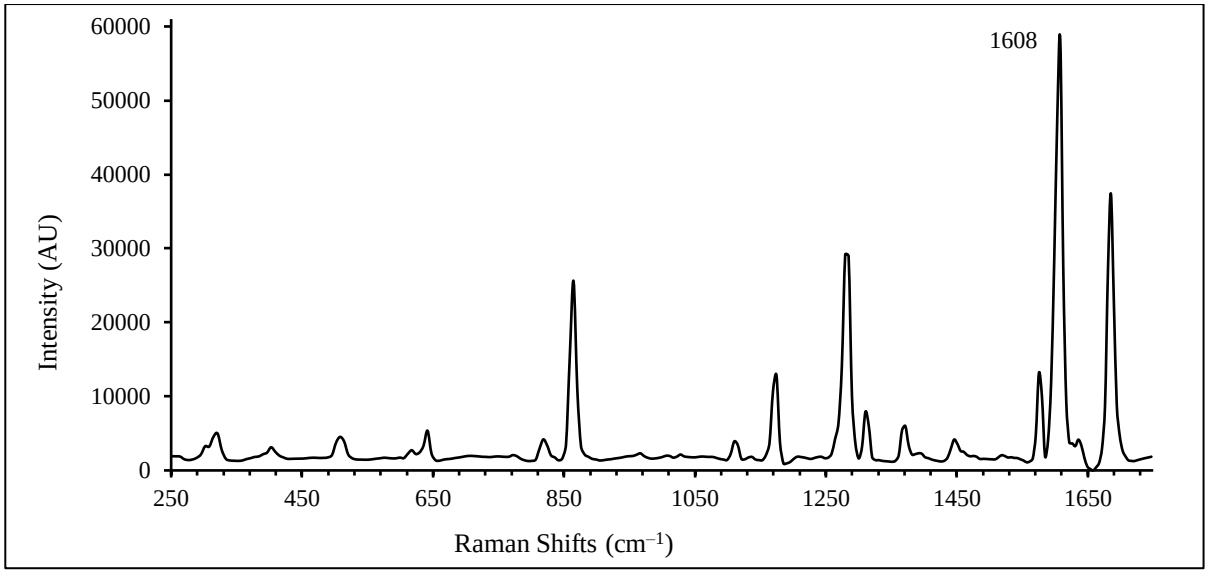

Figure A3. Benzocaine Raman Rigaku spectrum (Excel version 2015, build 14026.20308).

Table A3 Benzocaine Raman Rigaku peaks assignments (Palafox et al., 1989).

Benzocaine				
Functional groups	**Mode**	**Literature peaks (cm^{-1})**	**Rigaku peaks (cm^{-1})**	**Renishaw peaks (cm^{-1})**
Ring C-H	Stretching oop	~864 vs	~864 s/m	~862 m
Ring C-H	Bending ipl	~1173 vs	~1174 w/m	~1172 m
C-N & C-O-C	Stretching	~1283 vs	~1285 s	~1281 vs
Ring C=C	Stretching	~1570 s	~1576 w/m	~1574 w
Ring C=C	Stretching	~1608 vs	~1608 vs	~1604 vs
C=O	Stretching	~1683 vs	~1685 s	~1682 vs

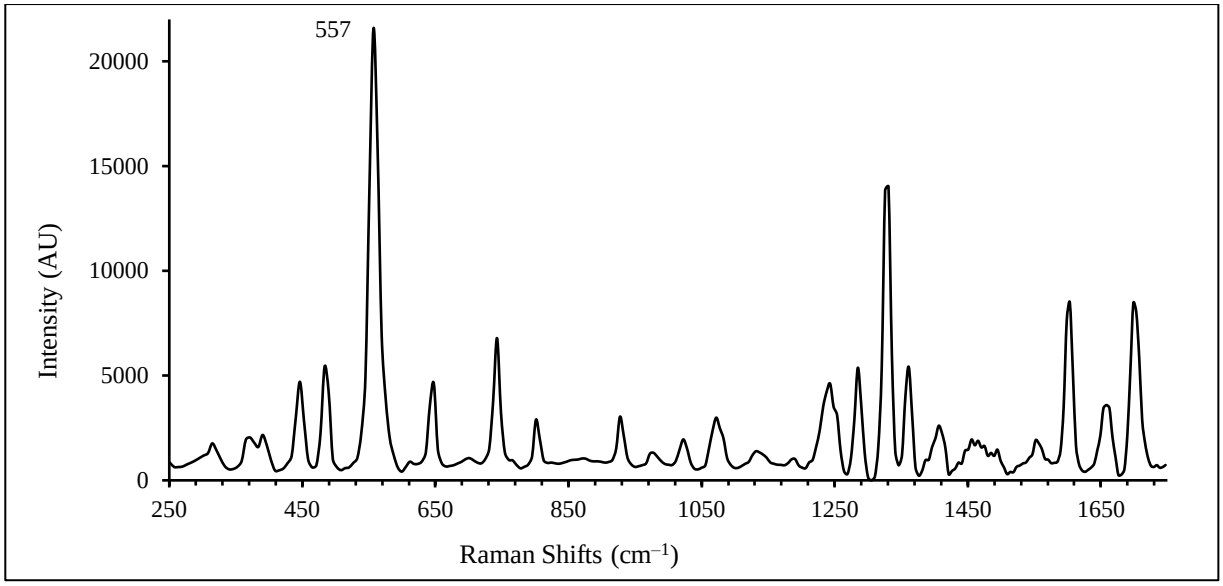

Figure A4. Caffeine Raman Rigaku spectrum (Excel version 2015, build 14026.20308).

Table A4. Caffeine Raman peaks assignments literature (Edwards et al., 2004).

Caffeine				
Functional groups	**Mode**	**Literature peaks (cm^{-1})**	**Rigaku peaks (cm^{-1})**	**Renishaw peaks (cm^{-1})**
Pyrimidine ring + CNO + CH	Bending	~483 w	~483 m	~482 m
Pyrimidine ring (C–N–CH_3) & CH_3	Bending & rocking	~556 s	~557 vs	~554 vs
Pyrimidine, imidazole ring	Bending	~741 m	~742 w/m	~741 w/m
C–N & CH_3	Stretching & rocking	~1284 m	~1285 w/m	~1286 w/m
Imidazole ring	Stretching	~1328 s	~1326 s	~1329 s
C=N + C-N	Stretching	~1361 w/m	~1361 m	~1361 w/m
C=C + C–N & CH_3	Stretching & bending	~1600 ms	~1604 m	~1601 ms
C=O	Stretching ipl	~1698 ms	~1703 m	~1701 m

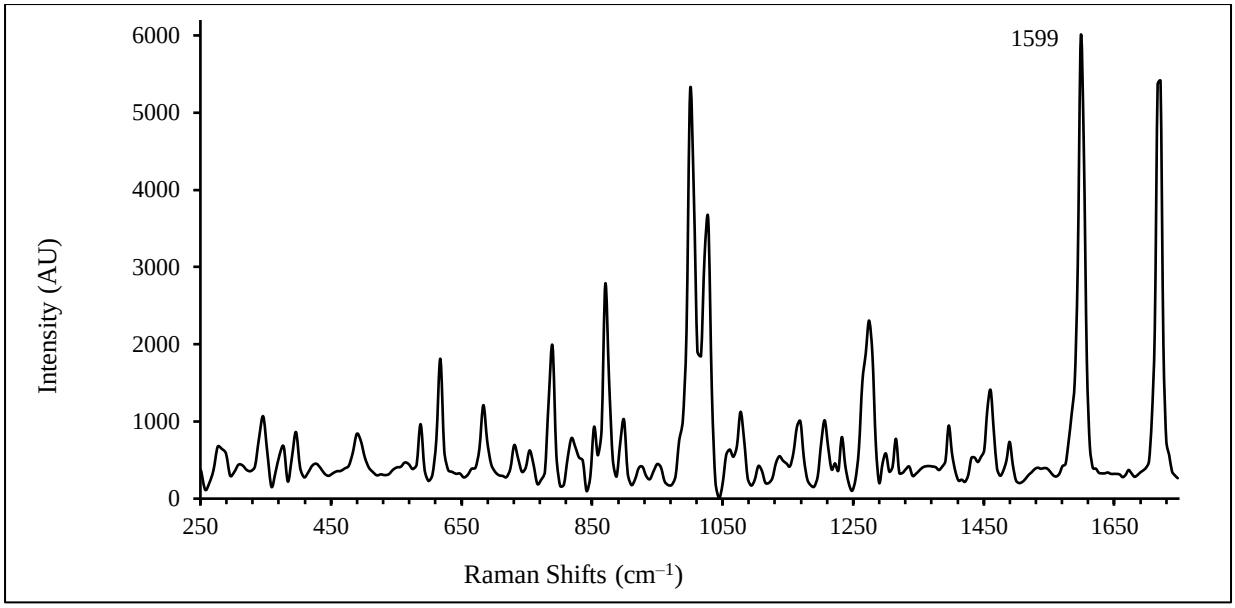

Figure A5. Cocaine hydrochloride Raman Rigaku spectrum (Excel version 2015, build 14026.20308).

Table A5. Cocaine hydrochloride Raman peaks assignments (Penido et al., 2016).

Cocaine				
Functional groups	**Mode**	**Literature peaks (cm^{-1})**	**Rigaku peaks (cm^{-1})**	**Renishaw peaks (cm^{-1})**
C–C tropane ring	Stretching	~898	~899 w	~870 m
C–C tropane ring	Stretching	~874	~870 m	~896 w
Aromatic ring	Symmetric stretching –breathing	~1004	~1000 s	~1000 s
Aromatic ring	Asymmetric stretching	~1026	~1028 m	~1026 m
C–N	Stretching	~1279	~1274 m/w	~1278 m/w
CH3	Asymmetric deformation	~1462	~1460 w	~1459 w
C=C	Ring stretching	~1601	~1596 vs	~1598 s
C=O	Symmetric stretching	~1716	~1716 s	~1716 s

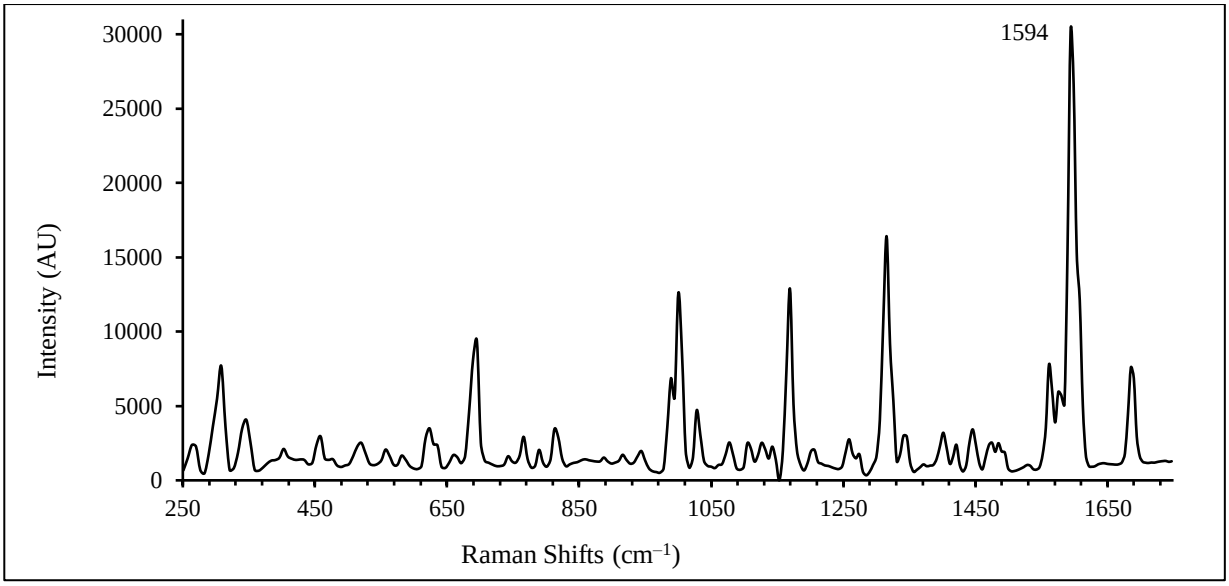

Figure A6. Diazepam Raman Rigaku spectrum (Excel version 2015, build 14026.20308).

Table A6. Diazepam Raman peaks assignments (Gunaserakan et al., 2006).

Diazepam				
Functional groups	**Mode**	**Literature peaks (cm^{-1})**	**Rigaku peaks (cm^{-1})**	**Renishaw peaks (cm^{-1})**
C–N–C	Asymmetric bending	~698 vw	~695 m/w	~690 m
–	–	–	~1000 m	~998 w/m
C–C	Stretching	~1321 vw	~1315 s	~1312 s
C–N	Symmetric stretching	~1174 vw	~1169 m	~1168 m
C-C aromatic ring	Asymmetric stretching	~1561 m/w	~1567 w	~1562 w
C=N	Stretching	~1599 vs	~1594 vs	~1593 vs
C=O	Stretching	~1690 w	~1689 m/w	~1685 m/w

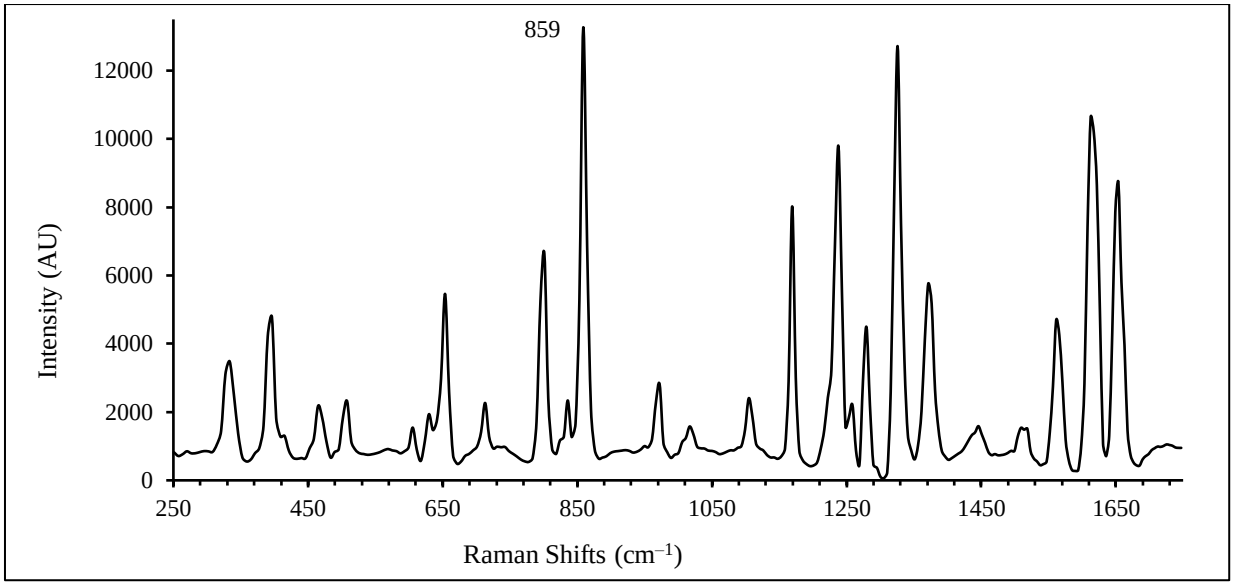

Figure A7. Paracetamol Raman Rigaku spectrum (Excel version 2015, build 14026.20308).

Table A7. Paracetamol Raman peaks assignments (Shende et al., 2014).

Paracetamol				
Functional groups	**Modes**	**Literature peaks (cm^{-1})**	**Rigaku peaks (cm^{-1})**	**Renishaw peaks (cm^{-1})**
C-N-C	Ring stretching	~797	~801 m	~797 m
C-N-C	Ring breathing	~859	~858 vs	~857 vs
C-C	Ring stretching	~1238	~1236 s	~1237 s
RCNR'R"	Amide III mode	~1326	~1324 vs	~1326 vs
RCNR'R"	Amide II mode	~1560	~1561 m	~1561 m/w
Ring	Stretching	~1611	~1612 s	~1611 s
RCNR'R"	Amide I mode	~1649	~1653 s	~1649 s

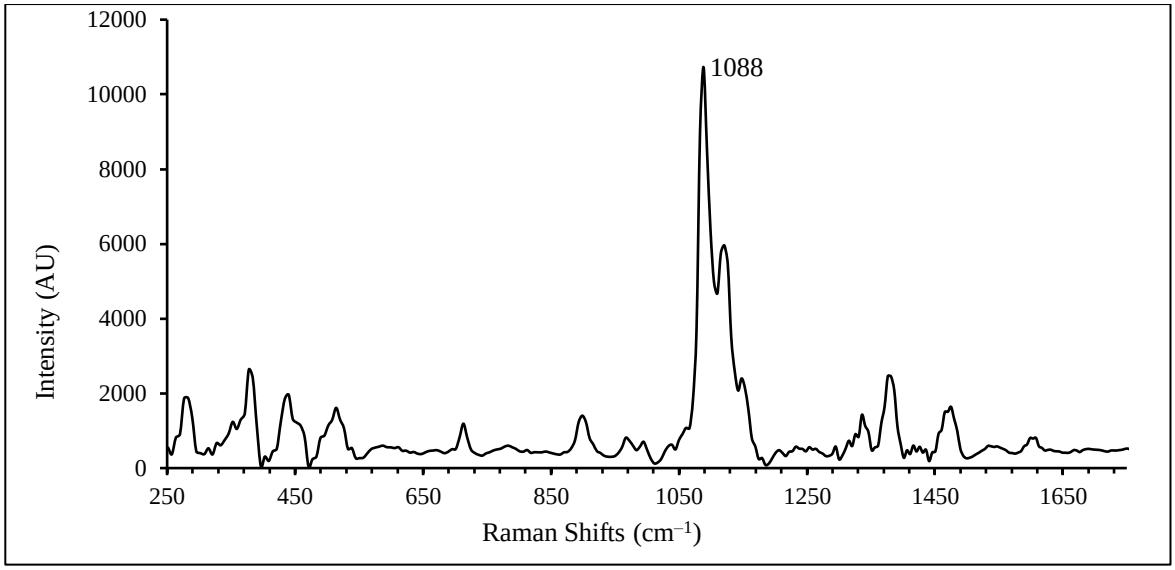

Figure A8. Negative control (BP) Raman Rigaku spectrum (Excel version 2015, build 14026.20308).

Table A8. Negative control (BP) Raman peaks assignments (Udristioiu et al.,2012).

BP				
Functional groups	**Mode**	**Literature peaks (cm^{-1})**	**Rigaku peaks (cm^{-1})**	**Renishaw peaks (cm^{-1})**
Cellulose		~434	~434 m/w	~278 m/w
CaCO3	Rotatory lattice vibration	~282	~283 w	~434 w
CaCO3 (C=O)	Bending	~712	~713 vw	~713 w
CaCO3 (C=O)	Symmetric stretching	~1086 vs	~1088 vs	~1086 s
Celllulose		~1378	~1381 m/w	~1382 w

Appendix 4.10. Raman Rigaku set 2 additional PCA plots

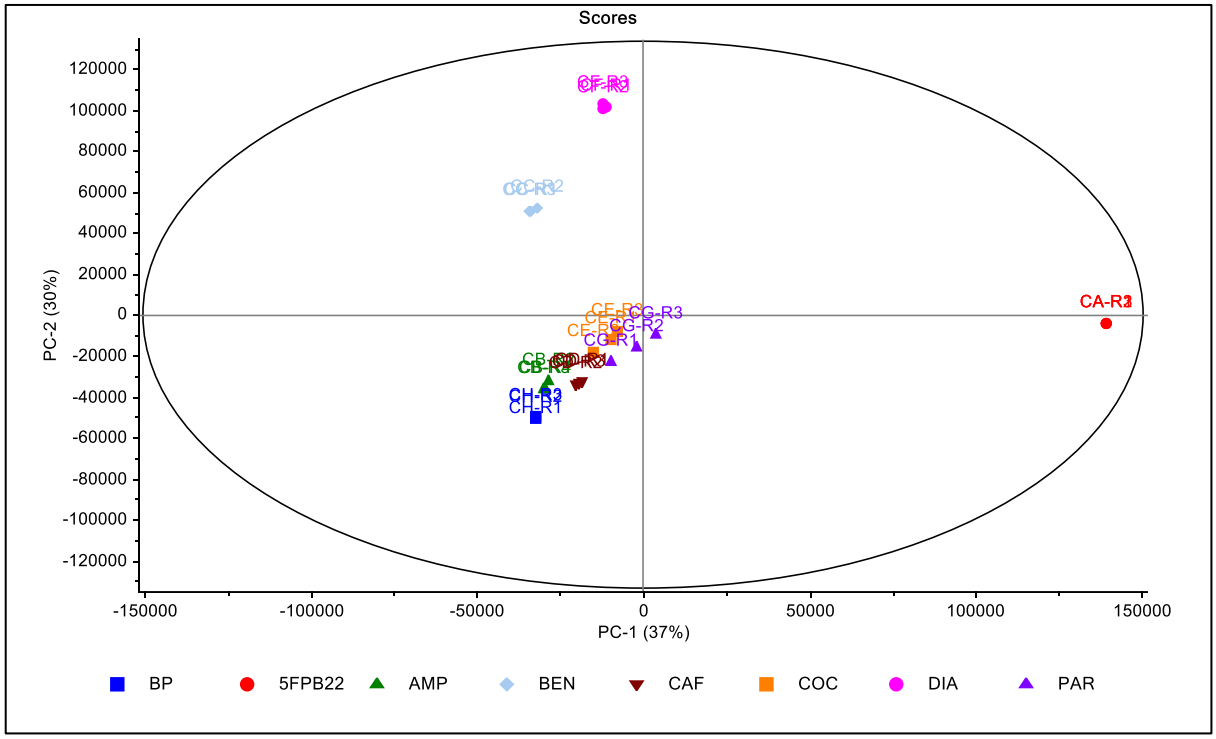

Figure A1. PC-1 vs PC-2 2D scores plot of the unprocessed set 2.

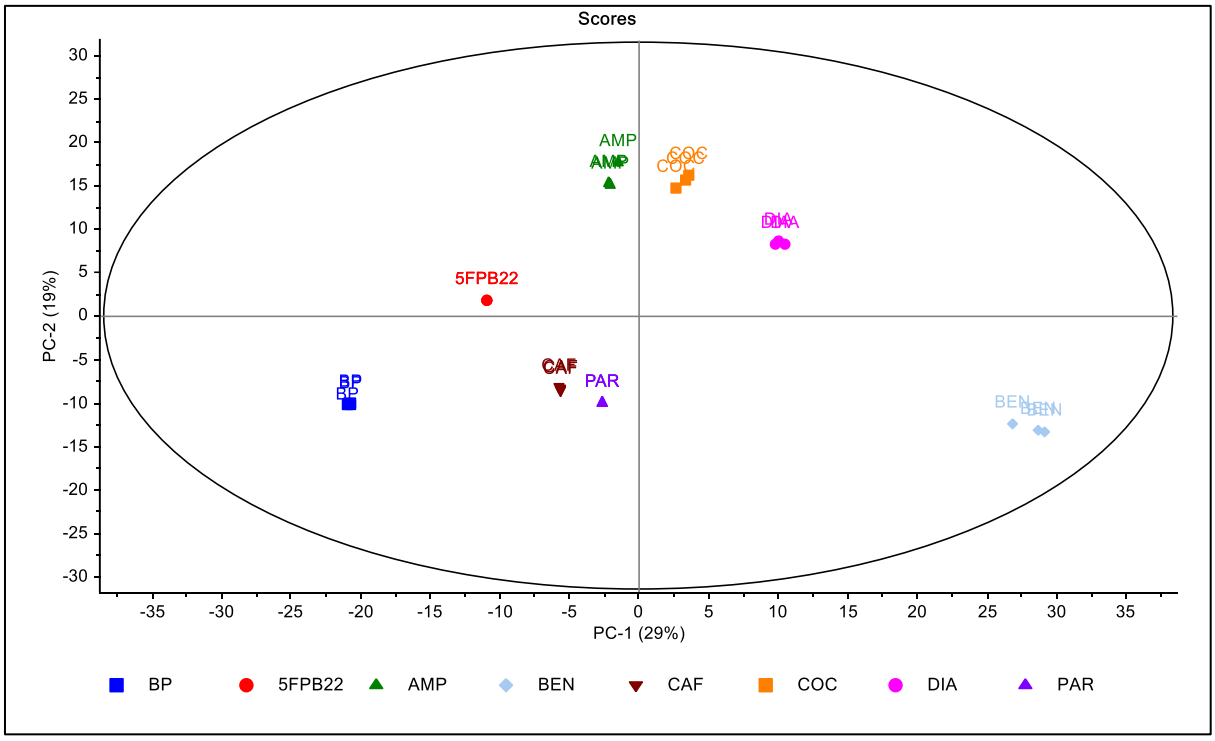

Figure A2. PC-1 vs PC-2 2D scores plot of the pre-processed set 2.

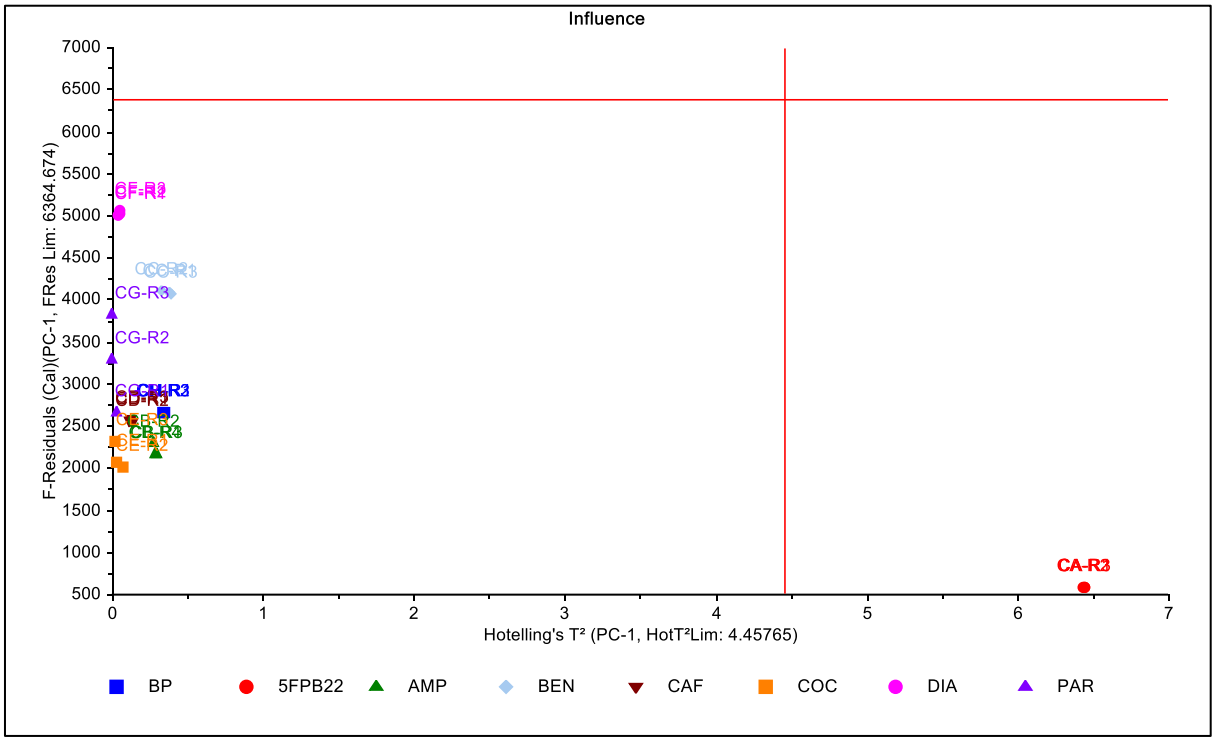

Figure A3. PC-1 F-residuals vs Hotelling T^2 influence plot of the unprocessed set 2.

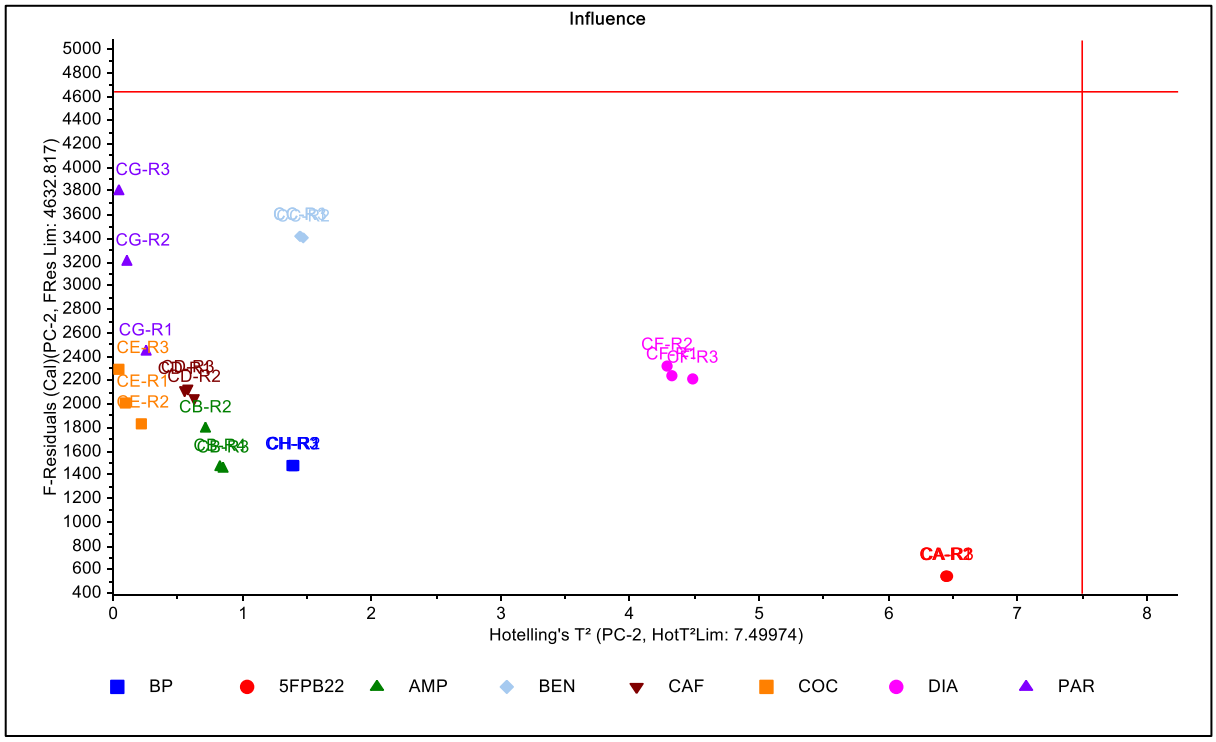

Figure A4. PC-2 F-residuals vs Hotelling T^2 influence plot of the unprocessed set 2.

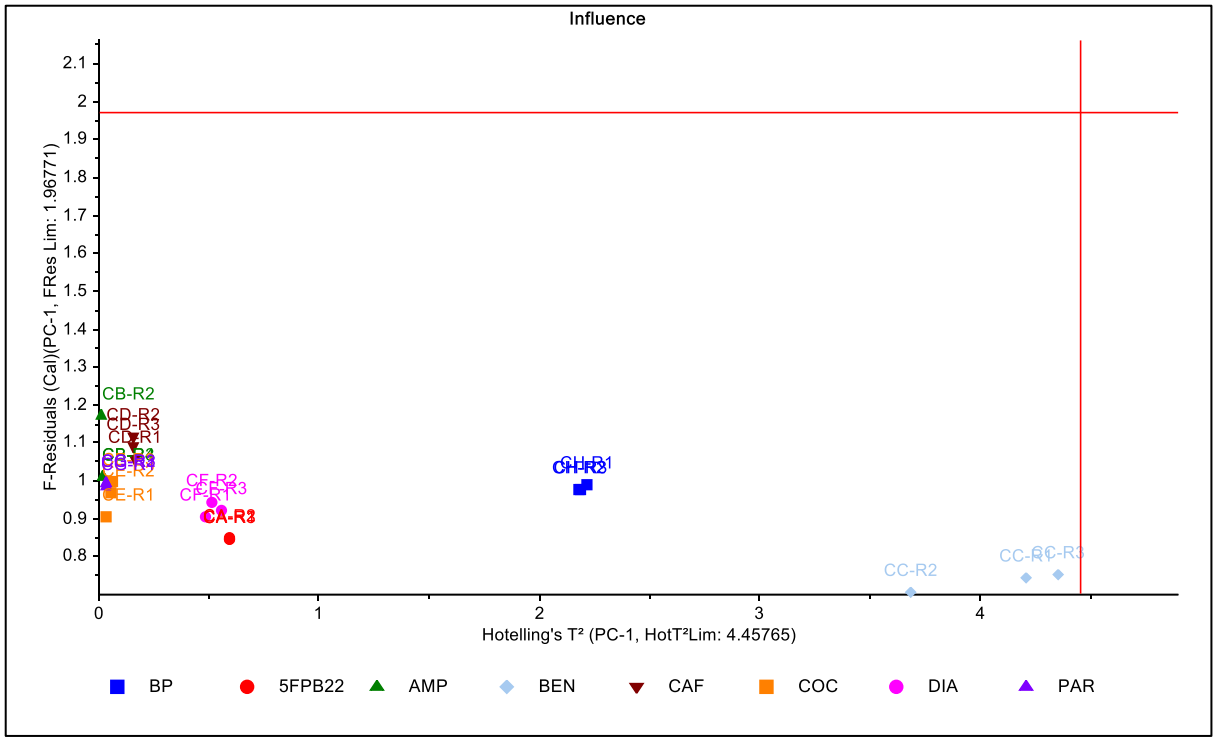

Figure A5. PC-1 F-residuals vs Hotelling T^2 influence plot of the pre-processed set 2.

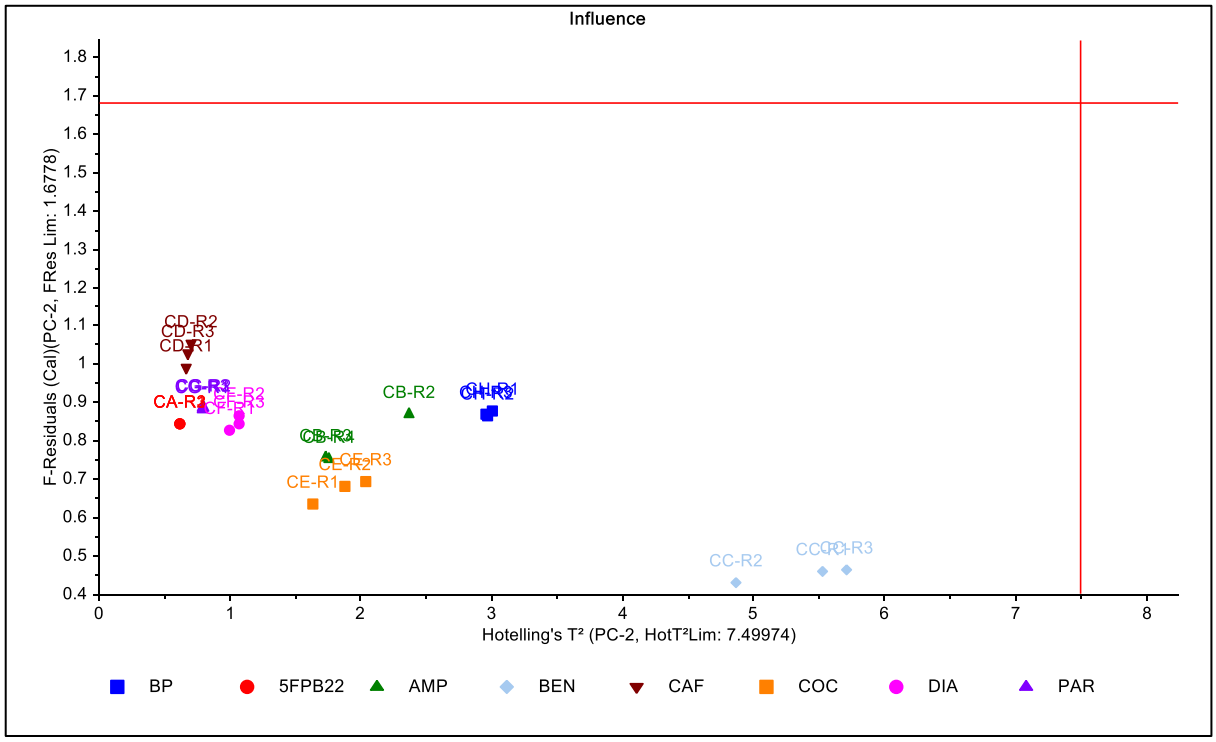

Figure A6. PC-2 F-residuals vs Hotelling T^2 influence plot of the pre-processed set 2.

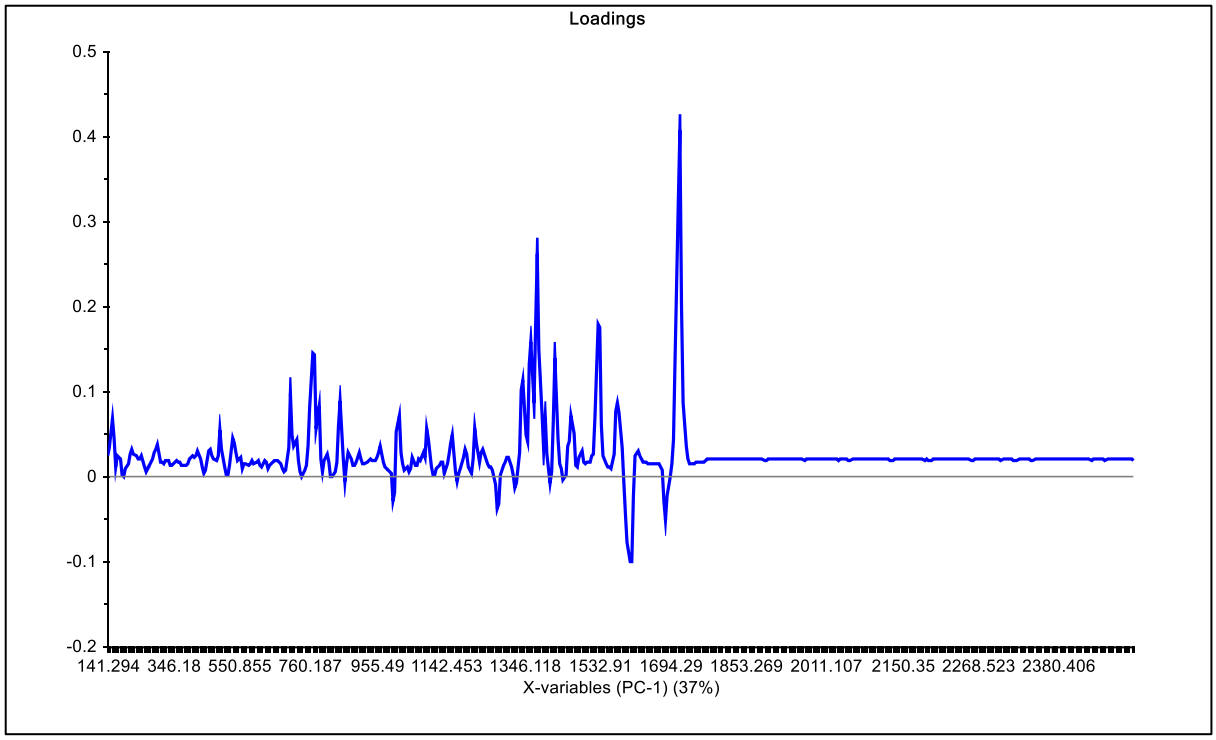

Figure A7. PC-1 loadings plot of the unprocessed set 2.

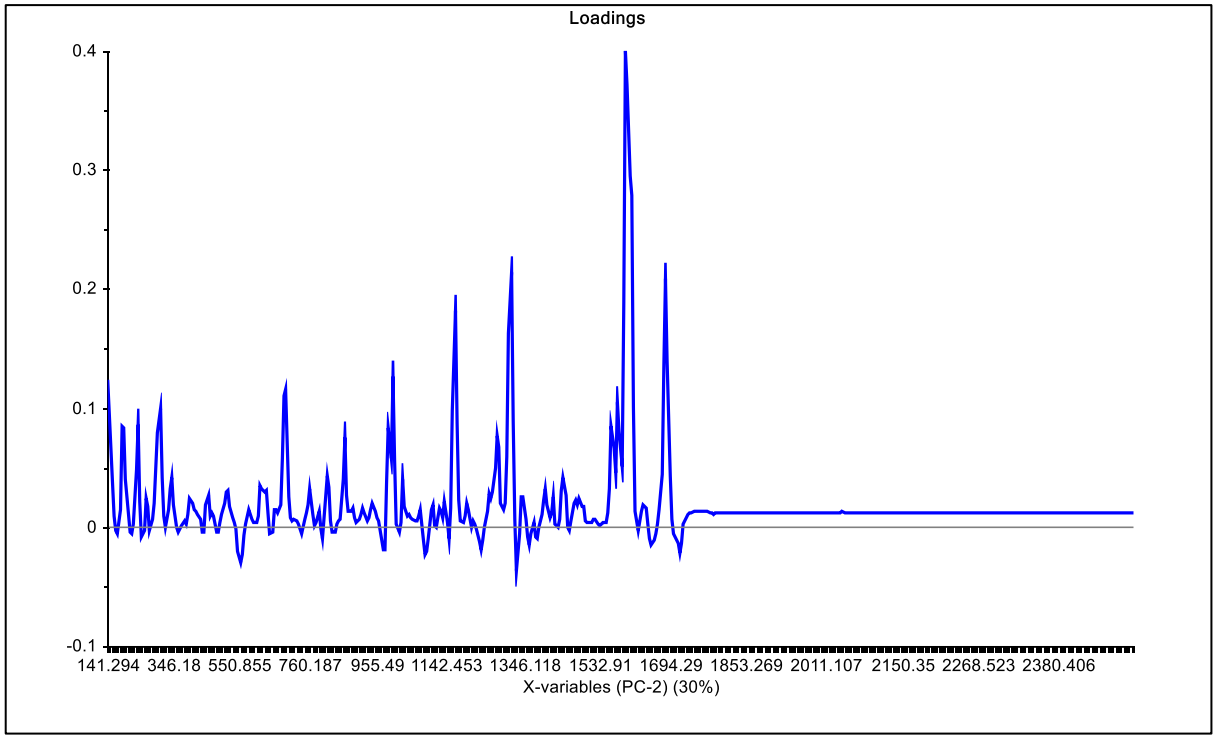

Figure A8. PC-2 loadings plot of the unprocessed set 2.

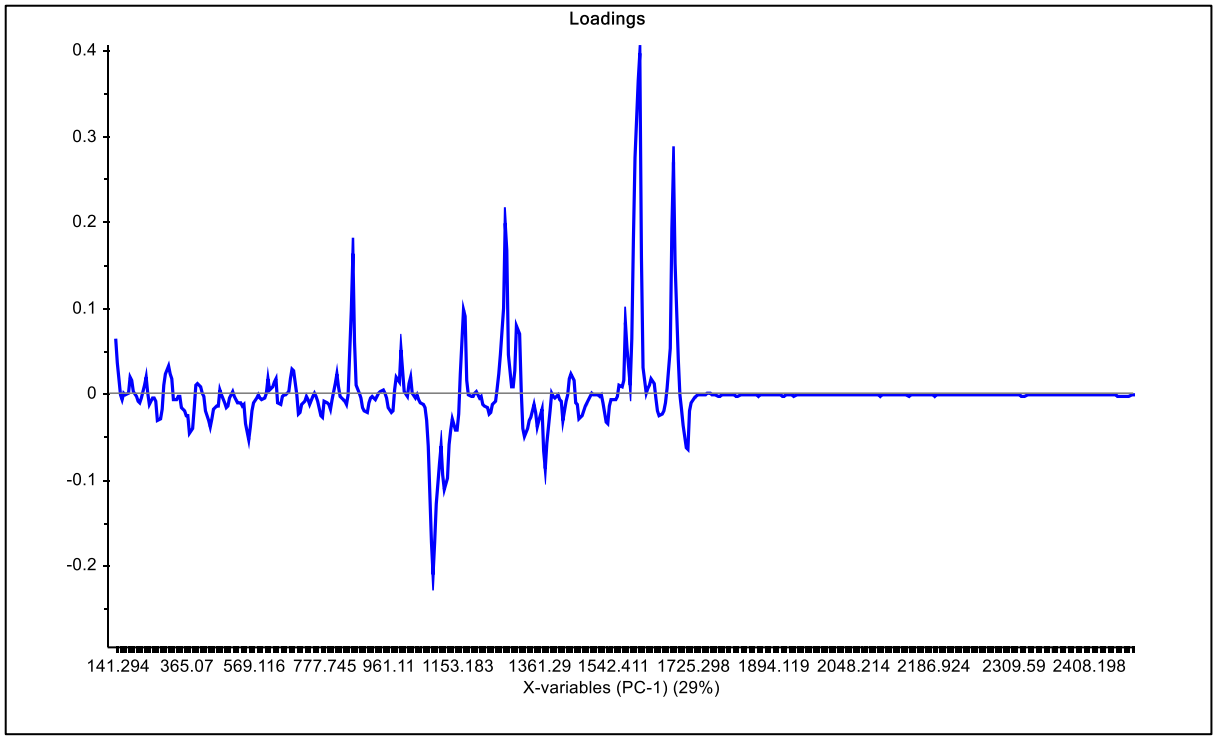

Figure A9. PC-1 loadings plot of the pre-processed set 2.

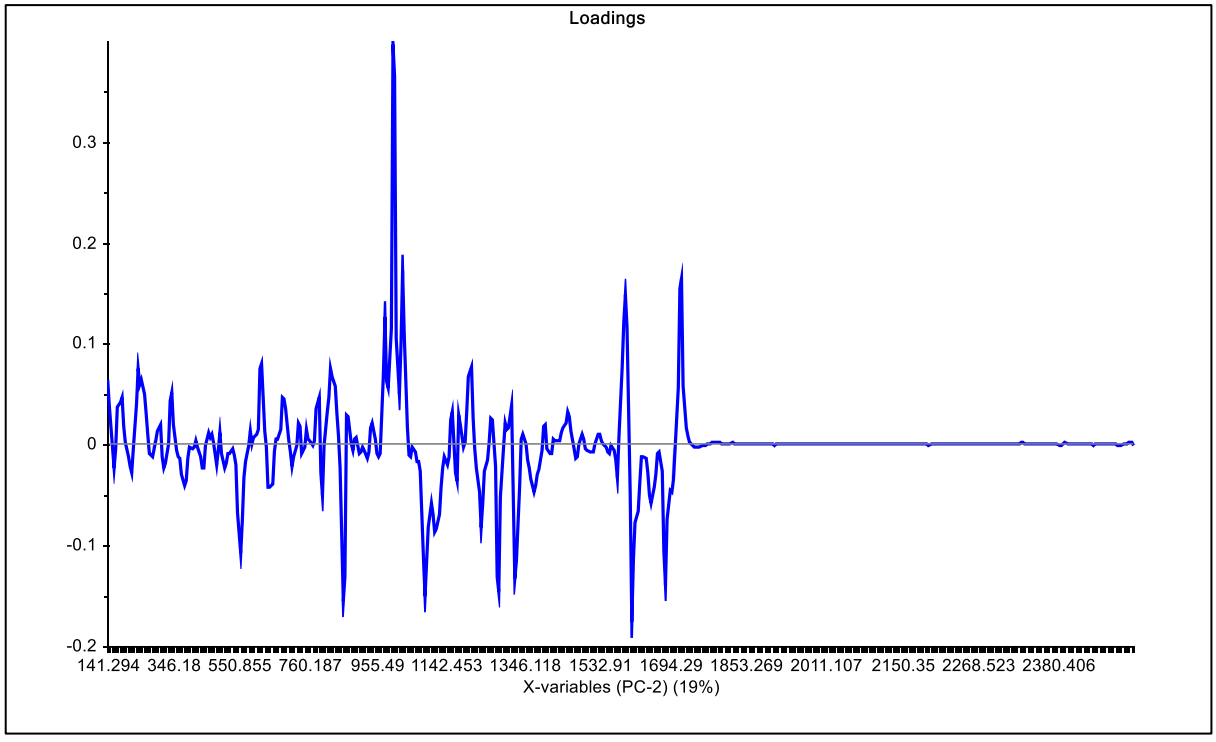

Figure A9. PC-2 loadings plot of the pre-processed set 2.

Appendix 4.11. Set 5 overlaid spectra of amphetamine/caffeine and benzocaine/diazepam.

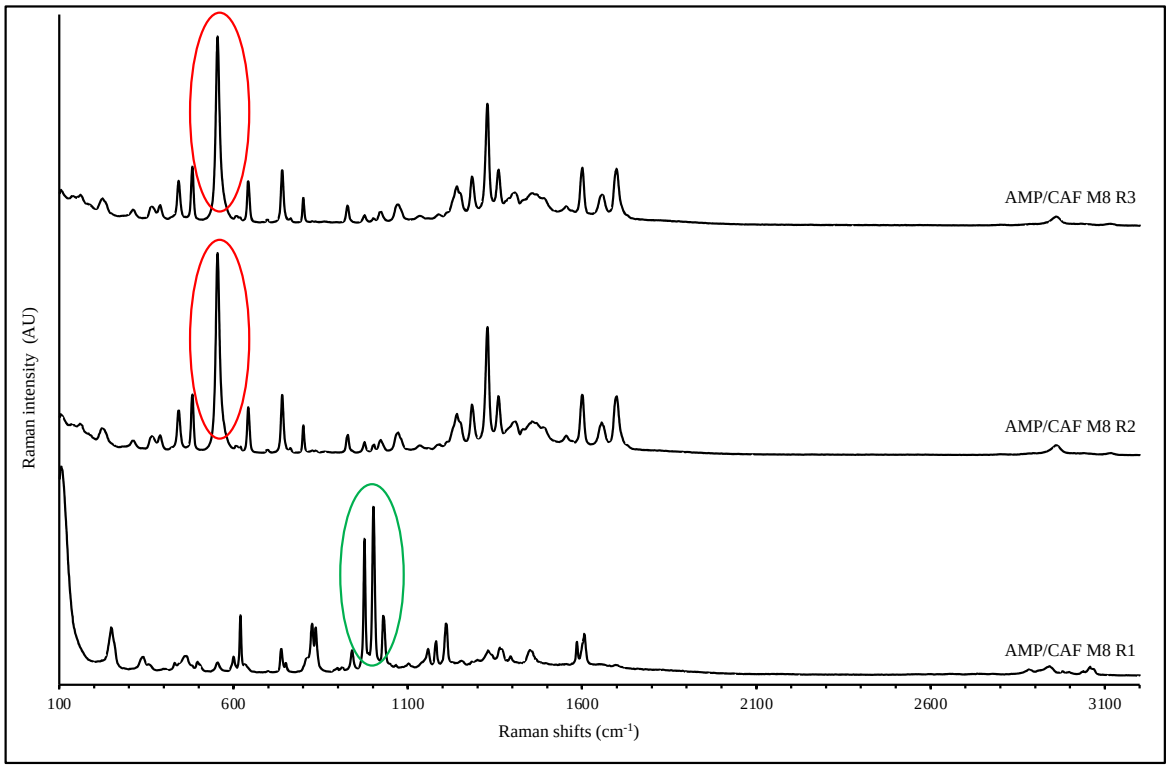

Figure 1A. Set 5 overlaid Raman spectra of amphetamine/caffeine (M8) replicate samples. Red circles show the caffeine characteristic very strong intensity peak at 557 cm^{-1}. Green circle shows amphetamine characteristic strong, very strong and medium intensities peaks at 976, 1002 and 1033 cm^{-1}, respectively.

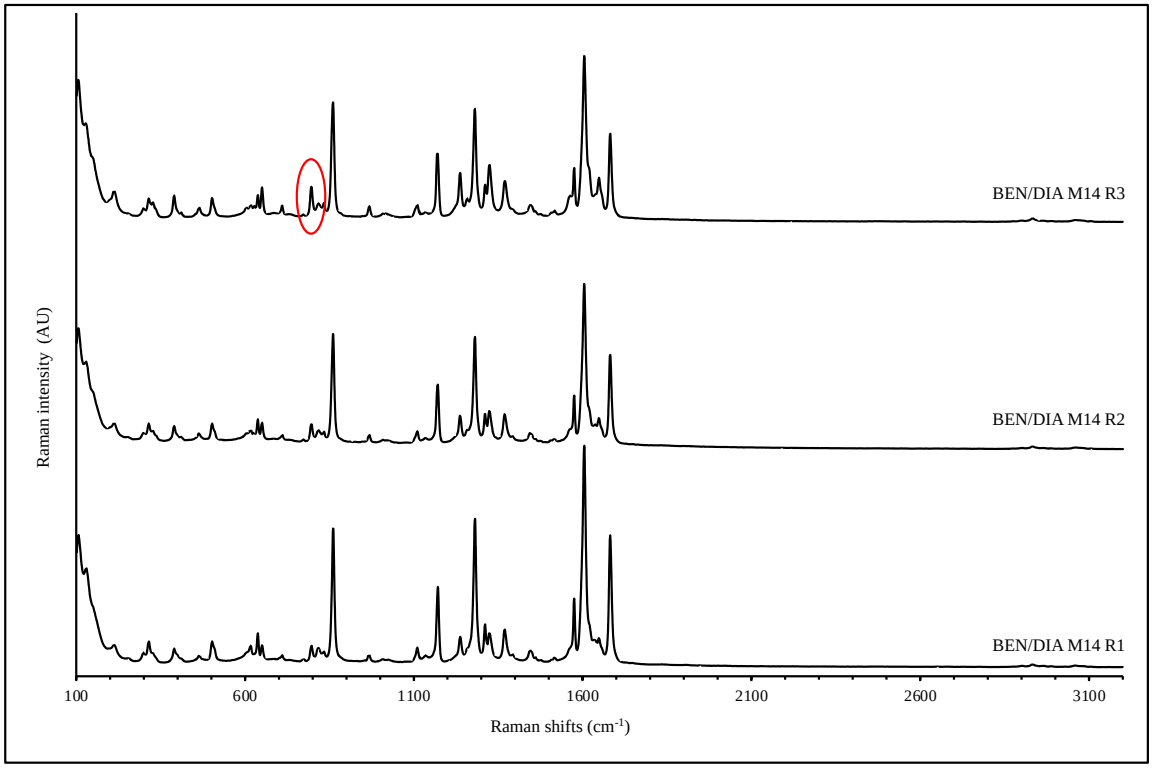

Figure 2A. Set 5 overlaid Raman spectra of benzocaine/diazepam (M14) replicates samples. Red circles the more marked peak at 800 cm^{-1} of replicate 3.

Appendix 12. Raman Renishaw set 5 additional PCA plots

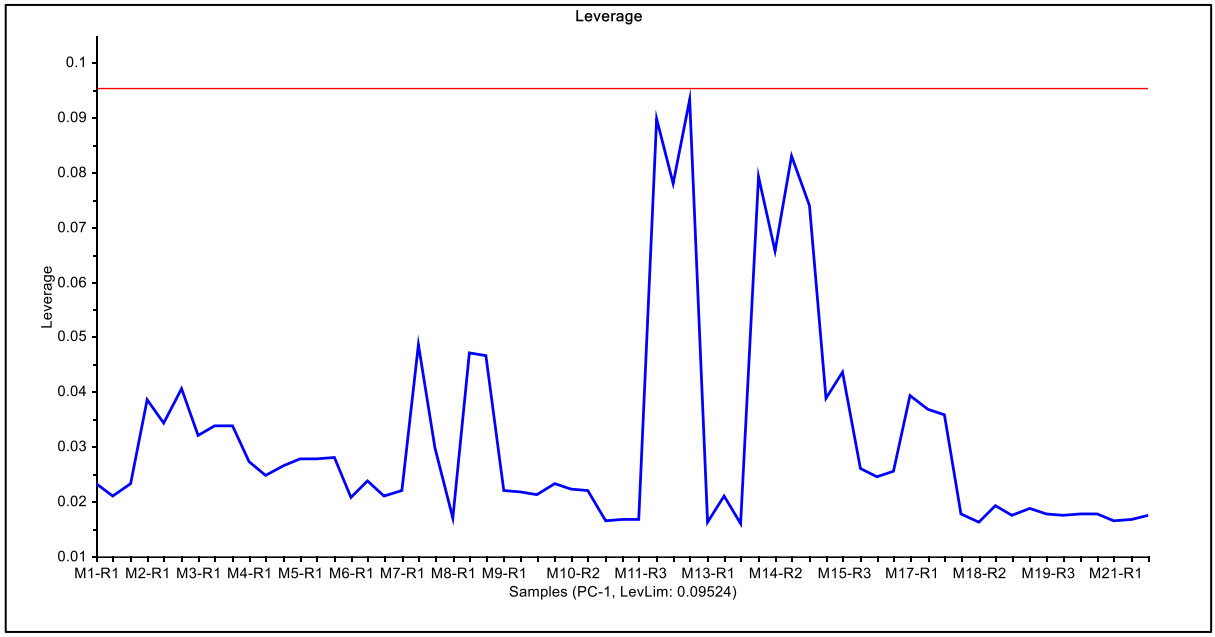

Figure A1. Set 5 PC-1 leverage plot.

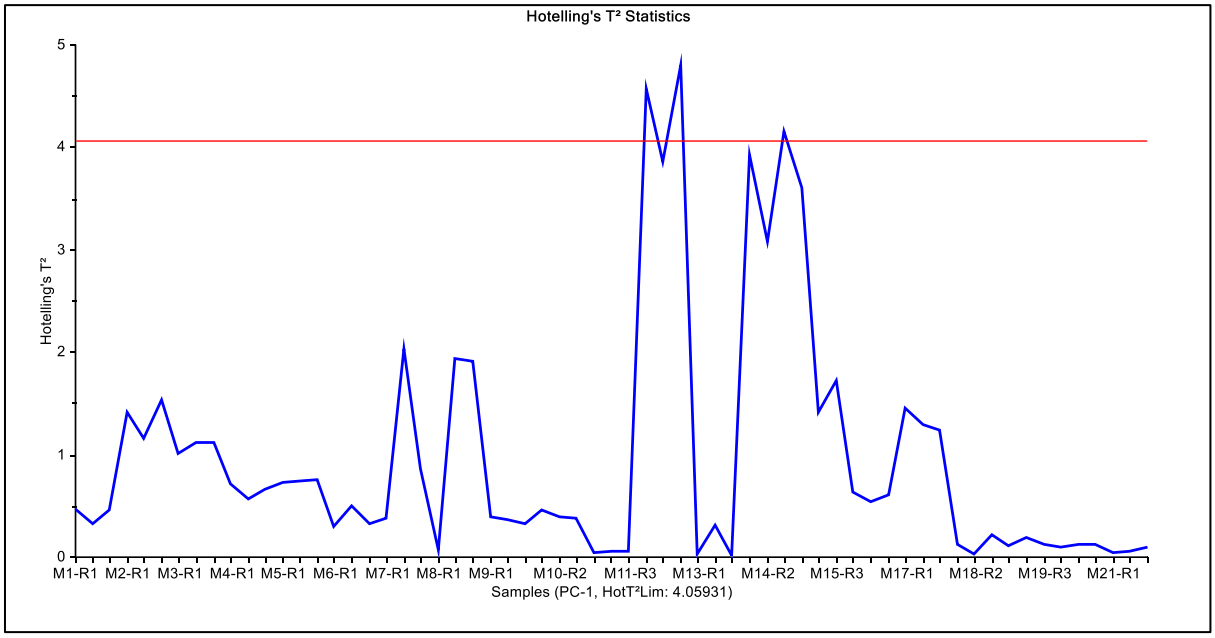

Figure A2. Set 5 PC-1 Hotelling T^2 plot.

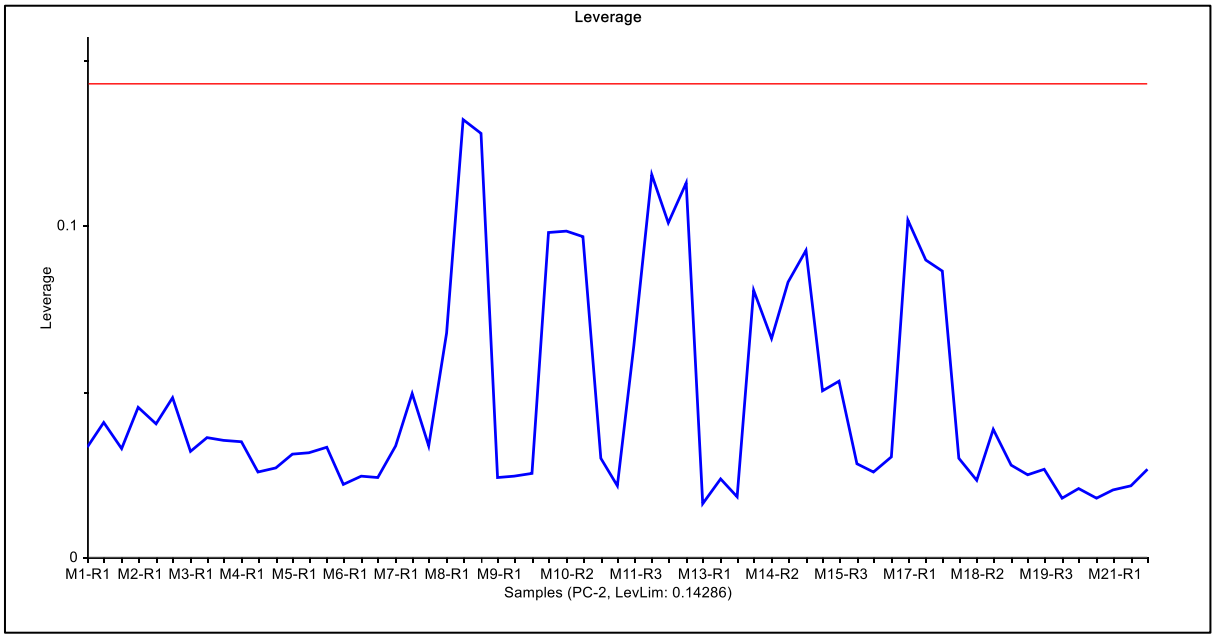

Figure A3. Set 5 PC-2 leverage plot.

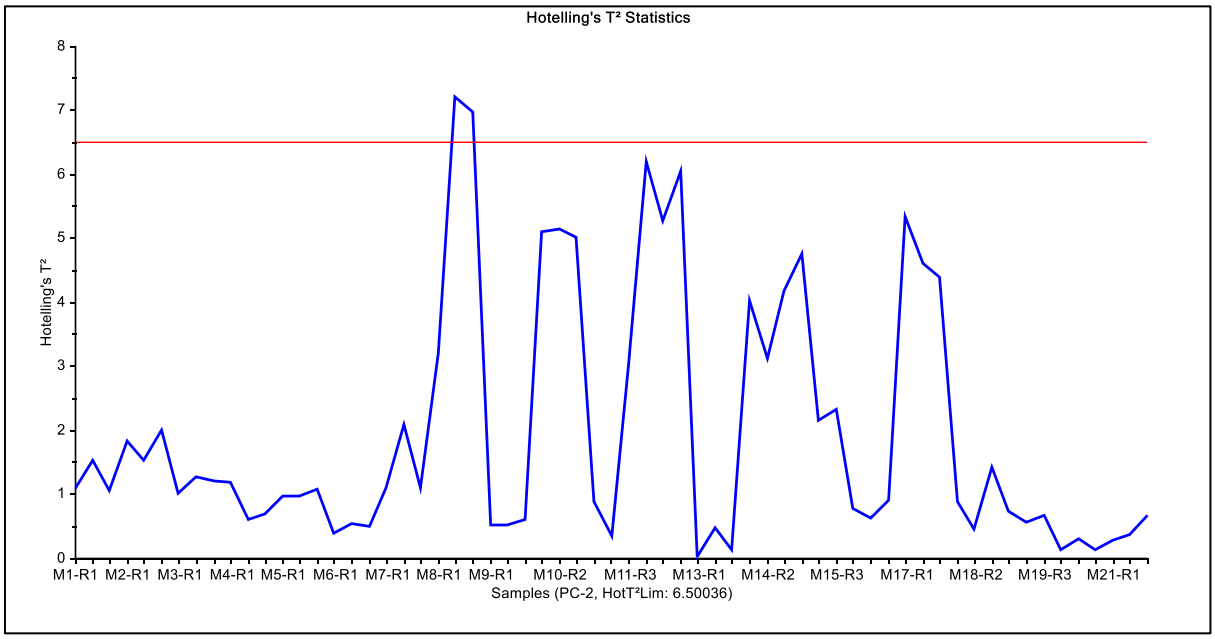

Figure A4. Set 5 PC-2 Hotelling T^2 plot.

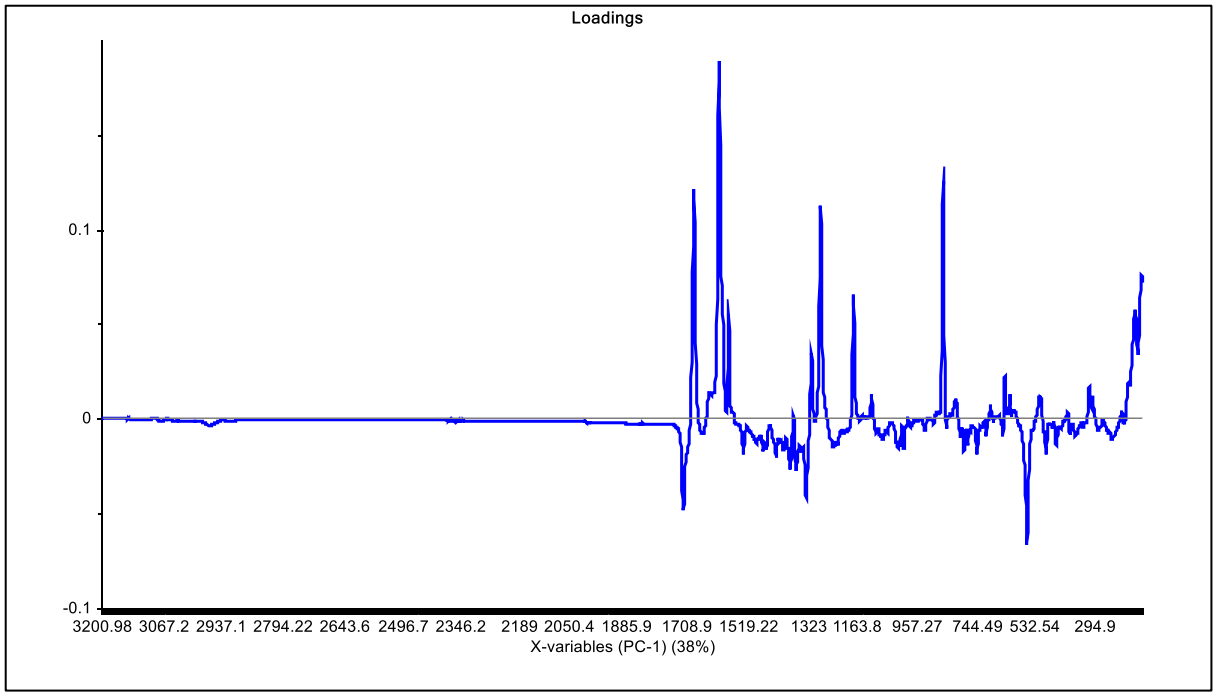

Figure A5. PC-1 loadings plot of set 5.

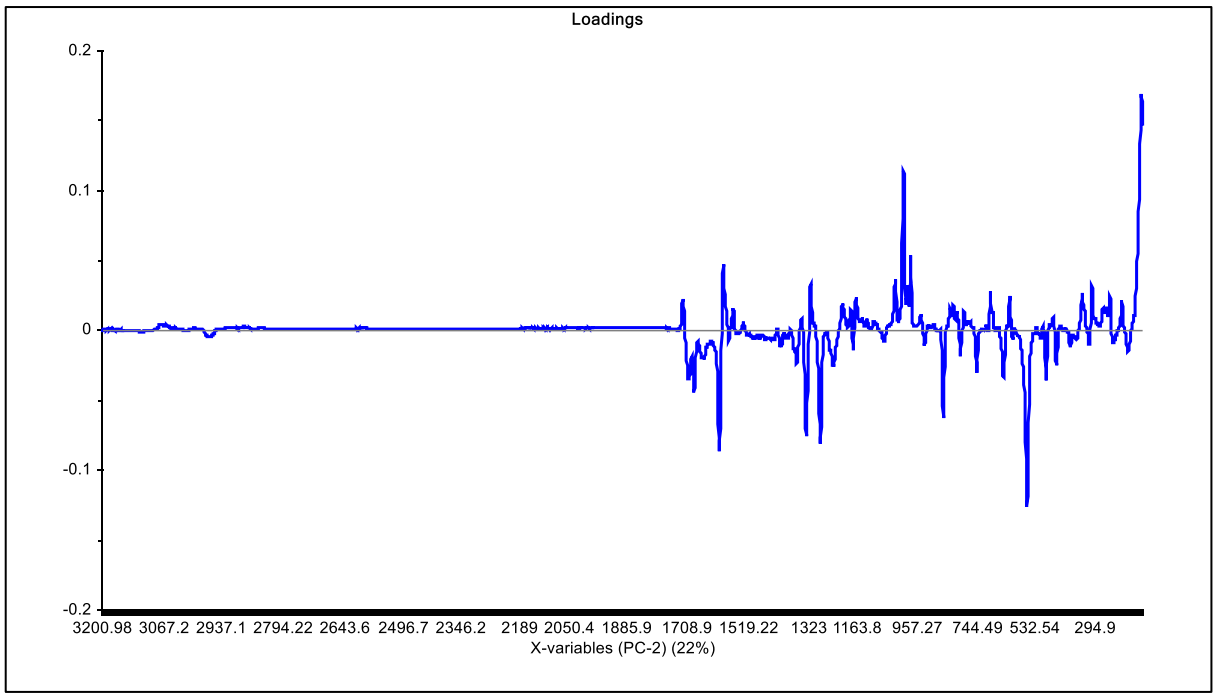

Figure A6. PC-2 loadings plot of set 5.

Appendix 4.13. Raman Rigaku set 6 additional PCA plots

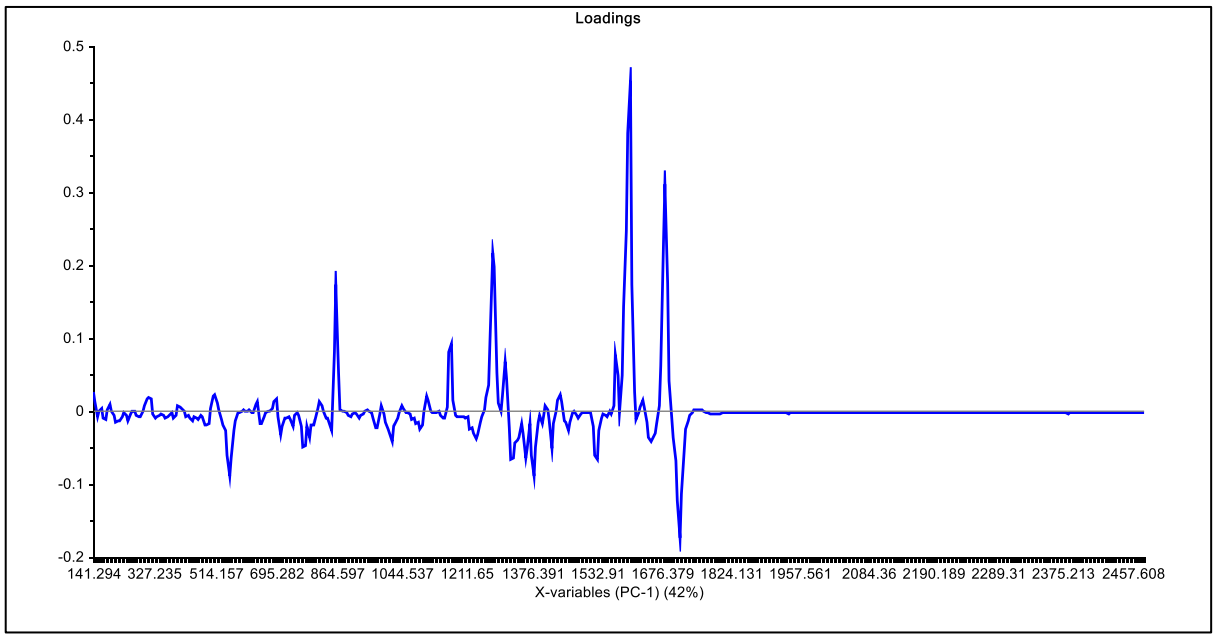

Figure A1. PC-1 loadings plot of set 6.

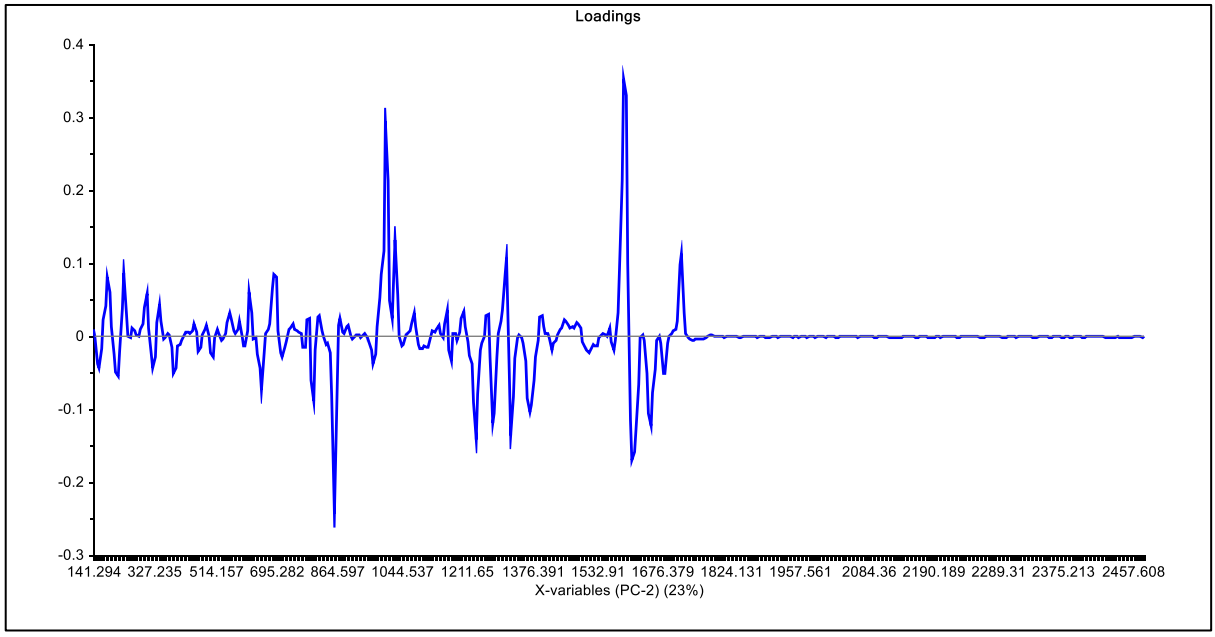

Figure A2. PC-2 loadings plot of set 6.

Appendix 4.14. Summary of RMA matches

Table A1. Summary of set 6 RMA matches

Binary mixture samples	Set 6					
	CC	**1st match**	**CC**	**2nd match**	**CC**	**3rd match**
5F-PB-22/AMP R1	0.93	5F-PB-22 & BB-22	0.91	BB-22 & AMP	0.88	5F-PB-22
5F-PB-22/AMP R2	0.94	5F-PB-22 & BB-22	0.92	5F-PB-22	0.91	BB-22 & NM-2201
5F-PB-22/AMP R3	0.96	5F-PB-22, BB-22 & N-ethylamphetamine	0.91	BB-22, NM-2201 & DL-acetyl-AMP	0.93	5F-PB-22 & BB-22
5F-PB-22/BEN R1	0.96	BEN & 5F-PB-22	0.91	Dimethocaine & 5F-PB-22	0.91	BEN
5F-PB-22/BEN R2	0.97	BEN & 5F-PB-22	0.94	Dimethocaine & 5F-PB-22	0.85	5F-PB-22 & mephedrone
5F-PB-22/BEN R3	0.97	BEN & 5F-PB-22	0.91	Dimethocaine & 5F-PB-22	0.87	BEN
5F-PB-22/CAF R1	0.95	CAF & 5F-PB-22	0.92	CAF	0.72	Theophylline
5F-PB-22/CAF R2	0.93	5F-PB-22 & CAF	0.89	BB-22 & CAF	0.88	5F-PB-22
5F-PB-22/CAF R3	0.95	5F-PB-22 & CAF	0.92	BB-22 & CAF	0.86	FDU-PB-22 & theophylline
5F-PB-22/COC R1	0.95	5F-PB-22 & COC	0.90	5F-PB-22	0.89	BB-22 & COC
5F-PB-22/COC R2	0.90	5F-PB-22	0.89	BB-22 & COC	0.84	BB-22
5F-PB-22/COC R3	0.93	5F-PB-22	0.89	BB-22 & NM-2201	0.89	FDU-PB-22 & BB-22
5F-PB-22/DIA R1	0.95	DIA & 5F-PB-22	0.83	5F-PB-22 & Phenazepam	0.83	COC & 5F-PB-22
5F-PB-22/DIA R2	0.95	DIA & 5F-PB-22	0.84	5F-PB-22 & Phenazepam	0.83	COC & 5F-PB-22
5F-PB-22/DIA R3	0.96	5F-PB-22, DIA & BB-22	0.93	BB-22, 5F-PB-22 & NM-22	0.92	5F-PB-22 & DIA

5F-PB-22/PAR R1	0.96	5F-PB-22 & BB-22	0.94	BB-22 & FDU-PB-22	0.91	5F-PB-22
5F-PB-22/PAR R2	0.96	5F-PB-22, PAR & BB-22	0.94	BB-22, PAR & NM-22	0.93	FDU-PB-22, PAR & BB-22
5F-PB-22/PAR R3	0.97	PAR & 5F-PB-22	0.90	PAR	0.86	Phenacetin & 5F-PB-22
AMP/BEN R1	0.98	BEN	0.94	BEN & AMP	0.79	BEN & N-ethylamphetamine
AMP/BEN R2	0.98	BEN	0.89	AMP	0.76	BEN & N-ethylamphetamine
AMP/BEN R3	0.99	BEN	0.87	BEN & AMP	0.77	AMP
AMP/CAF R1	0.99	CAF & AMP	0.82	CAF	0.72	AMP & theophylline
AMP/CAF R2	0.99	CAF & AMP	0.79	CAF	0.76	AMP & CAF
AMP/CAF R3	0.99	CAF & AMP	0.82	CAF	0.72	AMP & theophylline
AMP/COC R1	0.97	COC	0.75	COC & AMP	0.70	AMP
AMP/COC R2	0.97	COC	0.75	COC & AMP	0.70	AMP
AMP/COC R3	0.98	COC & AMP	0.94	COC	0.76	AMP
AMP/DIA R1	0.97	DIA	0.94	DIA & AMP	0.84	Phenazepam & AMP
AMP/DIA R2	0.99	DIA	0.95	DIA & AMP	0.82	AMP
AMP/DIA R3	0.97	DIA	0.94	DIA & AMP	0.84	Phenazepam & AMP
AMP/PAR R1	0.99	PAR & AMP	0.95	PAR	0.91	AMP
AMP/PAR R2	0.98	PAR	0.91	PAR & AMP	0.84	Phenacetin & AMP
AMP/PAR R3	0.98	PAR	0.91	PAR & AMP	0.84	Phenacetin & AMP
BEN/CAF R1	0.99	BEN	0.91	BEN & CAF	0.79	BEN & theophylline
BEN/CAF R2	0.98	BEN	0.93	BEN & CAF	0.76	BEN & theophylline
BEN/CAF R3	0.98	BEN	0.91	BEN & CAF	0.77	BEN & theophylline

BEN/COC R1	0.96	BEN	0.90	BEN & COC	0.78	Dimethocaine & COC
BEN/COC R2	0.98	BEN	0.89	BEN & COC	0.77	Dimethocaine & COC
BEN/COC R3	0.96	BEN & COC	0.92	BEN	0.70	Dimethocaine
BEN/DIA R1	0.96	BEN	0.89	BEN & DIA	0.70	BEN & Phenazepam
BEN/DIA R2	0.98	BEN & DIA	0.91	BEN	0.72	BEN & Phenazepam
BEN/DIA R3	0.98	BEN & DIA	0.93	BEN	0.70	BEN & Phenazepam
BEN/PAR R1	0.95	BEN	0.92	BEN & PAR	0.80	Dimethocaine & PAR
BEN/PAR R2	0.98	BEN	0.92	BEN & PAR	0.82	Dimethocaine & PAR
BEN/PAR R3	0.97	BEN	0.93	BEN & PAR	0.81	Dimethocaine & PAR
CAF/COC R1	0.97	COC & CAF	0.91	COC	0.86	CAF
CAF/COC R2	0.98	COC & CAF	0.88	COC	0.67	CAF
CAF/COC R3	0.99	COC & CAF	0.86	COC	0.69	CAF
CAF/DIA R1	0.94	DIA	0.84	CAF	0.72	DIA & theophylline
CAF/DIA R2	0.94	DIA	0.83	CAF	0.71	DIA & theophylline
CAF/DIA R3	0.97	DIA & CAF	0.85	DIA	0.75	CAF
CAF/PAR R1	0.97	PAR & CAF	0.93	PAR	0.75	CAF
CAF/PAR R2	0.99	PAR & CAF	0.94	PAR	0.72	Phenacetin & CAF
CAF/PAR R3	0.99	PAR & CAF	0.94	PAR	0.75	CAF
COC/DIA R1	0.98	COC & DIA	0.94	COC	0.89	DIA
COC/DIA R2	0.98	COC & DIA	0.91	COC	0.86	DIA
COC/DIA R3	0.96	COC	0.91	COC & DIA	0.78	DIA

COC/PAR R1	0.98	PAR & COC	0.94	PAR	0.76	COC
COC/PAR R2	0.98	PAR	0.94	PAR & COC	0.76	Phenacetin & COC
COC/PAR R3	0.97	PAR	0.92	PAR & COC	0.74	Phenacetin & COC
DIA/PAR R1	0.99	PAR & DIA	0.94	PAR	0.78	DIA
DIA/PAR R2	0.99	PAR & DIA	0.93	PAR	0.77	Phenacetin & DIA
DIA/PAR R3	0.99	PAR & DIA	0.94	PAR	0.78	Phenacetin & DIA

Table A2. Summary of set 10 RMA matches

Single simulated paper samples	**Set 10 (pipetting method)**					
	CC	**1st match**	**CC**	**2nd match**	**CC**	**3rd match**
5F-PB-22 20mg/mL R1	0.90	BB-22 & MC	0.86	FDU-PB-22 & MC	0.63	BB-22
5F-PB-22 20mg/mL R2	0.89	MC & 5F-PB-22	0.78	MC	0.76	FDU-PB-22 & CaCO3
5F-PB-22 20mg/mL R3	0.78	MC	0.66	FDU-PB-22	0.65	5F-PB-22
5F-PB-22 15mg/mL R1	0.91	5F-PB-22	0.89	BB-22 & MC	0.89	BB-22 & MC
5F-PB-22 15mg/mL R2	0.95	5F-PB-22 & MC	0.91	BB-22 & MC	0.90	5F-PB-22 & BB-22
5F-PB-22 15mg/mL R3	0.92	5F-PB-22 & MC	0.99	BB-22 & MC	0.89	FDU-PB-22 & MC
5F-PB-22 10mg/mL R1	0.94	MC & CaCO3	0.85	CaCO3	0.66	α-lactose monohydrate
5F-PB-22 10mg/mL R2	0.90	MC & PB-22	0.78	MC	0.77	FDU-PB-22 & CaCO3
5F-PB-22 10mg/mL R3	0.94	MC & CaCO3	0.85	MC	0.66	CaCO3
5F-PB-22 7.5mg/mL R1	0.95	MC & CaCO3	0.81	MC	0.73	CaCO3

5F-PB-22 7.5mg/mL R2	0.95	MC & CaCO3	0.82	MC	0.73	CaCO3
5F-PB-22 7.5mg/mL R3	0.84	MC	0.66	CaCO3	0.64	α-lactose monohydrate
5F-PB-22 5mg/mL R1	0.86	MC	0.66	CaCO3	0.66	α-lactose monohydrate
5F-PB-22 5mg/mL R2	0.94	MC & CaCO3	0.87	MC	0.66	CaCO3
5F-PB-22 5mg/mL R3	0.96	MC & CaCO3	0.86	MC	0.68	CaCO3
AMP 30mg/mL R1	0.96	MC & CaCO3	0.82	MC	0.73	CaCO3
AMP 30mg/mL R2	0.95	MC & CaCO3	0.85	MC	0.69	CaCO3
AMP 30mg/mL R3	0.93	MC & CaCO3	0.88	MC	0.67	CaCO3
AMP 15mg/mL R1	0.95	MC & AMP	0.87	MC	0.76	AMP
AMP 15mg/mL R2	0.96	MC & AMP	0.9	MC	0.66	AMP
AMP 15mg/mL R3	0.95	MC & AMP	0.91	MC	0.67	AMP
AMP 12.5mg/mL R1	0.86	MC	0.66	α-lactose monohydrate	0.63	CaCO3
AMP 12.5mg/mL R2	0.87	MC	0.66	α-lactose monohydrate	0.63	CaCO3
AMP 12.5mg/mL R3	0.85	MC	0.66	α-lactose monohydrate	0.66	CaCO3
AMP 10mg/mL R1	0.94	MC & CaCO3	0.9	MC	0.66	α-lactose monohydrate
AMP 10mg/mL R2	0.96	MC & CaCO3	0.91	MC	0.66	α-lactose monohydrate
AMP 10mg/mL R3	0.95	MC & CaCO3	0.89	MC	0.66	α-lactose monohydrate
AMP 7.5mg/mL R1	0.95	MC & CaCO3	0.88	MC	0.66	α-lactose monohydrate
AMP 7.5mg/mL R2	0.96	MC & CaCO3	0.89	MC	0.67	α-lactose monohydrate
AMP 7.5mg/mL R3	0.94	MC & CaCO3	0.88	MC	0.67	α-lactose monohydrate
BEN 10mg/mL R1	0.94	MC & BEN	0.88	MC	0.66	BEN

BEN 10mg/mL R2	0.93	MC & BEN	0.90	MC	0.73	BEN
BEN 10mg/mL R3	0.95	MC & BEN	0.82	MC	0.65	BEN
BEN 6.5mg/mL R1	0.93	MC & CaCO3	0.87	MC	0.65	α-lactose monohydrate
BEN 6.5mg/mL R2	0.94	MC & CaCO3	0.84	MC	0.66	CaCO3
BEN 6.5mg/mL R3	0.94	MC & CaCO3	0.84	MC	0.67	CaCO3
BEN 5mg/mL R1	0.94	MC & CaCO3	0.88	MC	0.67	α-lactose monohydrate
BEN 5mg/mL R2	0.95	MC & CaCO3	0.83	MC	0.72	α-lactose monohydrate
BEN 5mg/mL R3	0.93	MC & CaCO3	0.88	MC	0.66	α-lactose monohydrate
BEN 3.5mg/mL R1	0.93	MC & CaCO3	0.87	MC	0.65	α-lactose monohydrate
BEN 3.5mg/mL R2	0.94	MC & CaCO3	0.84	MC	0.67	CaCO3
BEN 3.5mg/mL R3	0.94	MC & CaCO3	0.84	MC	0.67	α-lactose monohydrate
BEN 2.5mg/mL R1	0.94	MC & CaCO3	0.88	MC	0.66	α-lactose monohydrate
BEN 2.5mg/mL R2	0.94	MC & CaCO3	0.82	MC	0.72	CaCO3
BEN 2.5mg/mL R3	0.95	MC & CaCO3	0.9	MC	0.65	α-lactose monohydrate
CAF 15mg/mL R1	0.92	CAF	0.66	theophillyne	0.50	α-lactose monohydrate
CAF 15mg/mL R2	0.88	MC & CAF	0.78	CAF & CaCO3	0.76	MC
CAF 15mg/mL R3	0.91	MC & CAF	0.79	MC	0.72	CAF & maize starch
CAF 10mg/mL R1	0.94	MC & CaCO3	0.90	MC	0.69	α-lactose monohydrate
CAF 10mg/mL R2	0.96	MC & CaCO3	0.89	MC	0.68	α-lactose monohydrate
CAF 10mg/mL R3	0.96	MC & CaCO3	0.89	MC	0.68	CaCO3
CAF 8mg/mL R1	0.96	MC & CaCO3	0.89	MC	0.68	CaCO3

CAF 8mg/mL R2	0.97	MC & CaCO3	0.91	MC	0.69	α-lactose monohydrate
CAF 8mg/mL R3	0.94	MC & CaCO3	0.89	MC	0.68	α-lactose monohydrate
CAF 6.5mg/mL R1	0.96	MC & CaCO3	0.91	MC	0.67	α-lactose monohydrate
CAF 6.5mg/mL R2	0.96	MC & CaCO3	0.92	MC	0.67	α-lactose monohydrate
CAF 6.5mg/mL R3	0.96	MC & CaCO3	0.91	MC	0.69	α-lactose monohydrate
CAF 5mg/mL R1	0.91	MC	0.68	α-lactose monohydrate	0.62	Alginic acid Na salt
CAF 5mg/mL R2	0.97	MC & CaCO3	0.90	MC	0.68	α-lactose monohydrate
CAF 5mg/mL R3	0.91	MC	0.68	α-lactose monohydrate	0.62	Alginic acid Na salt
COC 60mg/mL R1	0.83	MC & COC	0.78	URB-597, α-lactose monohydrate & methoxetamine	0.78	URB-597, α-lactose monohydrate & BB-22
COC 60mg/mL R2	0.85	MC & COC	0.77	URB-597, CaCO3 & maize starch	0.77	URB-597, CaCO3 & maize starch
COC 60mg/mL R3	0.84	MC & COC	0.79	URB-597, CaCO3 & dextrose	0.79	URB-597, CaCO3 & dextrose
COC 40mg/mL R1	0.76	MC	0.62	α-lactose monohydrate	0.62	URB-597 & maize starch
COC 40mg/mL R2	0.78	MC	0.62	α-lactose monohydrate	0.62	URB-597 & maize starch
COC 40mg/mL R3	0.84	MC & CaCO3	0.74	MC	0.63	CaCO3
COC 35mg/mL R1	0.78	URB-597, CaCO3 & dextrose	0.78	URB-597, CaCO3 & dextrose	0.78	URB-597, CaCO3 & dextrose
COC 35mg/mL R2	0.84	MC & COC	0.8	URB-597, CaCO3 & dextrose	0.79	URB-597, CaCO3 & dextrose
COC 35mg/mL R3	0.77	URB-597, α-lactose monohydrate & BB-22	0.77	URB-597, α-lactose monohydrate & BB-22	0.77	URB-597, α-lactose monohydrate & BB-22
COC 30mg/mL R1	0.9	MC & CaCO3	0.83	MC	0.65	α lactose monohydrate
COC 30mg/mL R2	0.84	MC	0.64	α-lactose monohydrate	0.61	Alginic acid Na salt

COC 30mg/mL R3	0.83	MC	0.65	α-lactose monohydrate	0.61	Alginic acid Na salt
COC 20mg/mL R1	0.86	MC	0.65	α-lactose monohydrate	0.61	Alginic acid Na salt
COC 20mg/mL R2	0.86	MC	0.65	α-lactose monohydrate	0.61	Alginic acid Na salt
COC 20mg/mL R3	0.83	MC	0.64	α-lactose monohydrate	0.60	Alginic acid Na salt
DIA 30mg/mL R1	0.95	DIA & MC	0.83	DIA	0.80	Phenazepam & MC
DIA 30mg/mL R2	0.99	DIA	0.72	Phenazepam	0.70	α-PVP HCl
DIA 30mg/mL R3	0.94	DIA & MC	0.81	Phenazepam & MC	0.81	DIA
DIA 20mg/mL R1	0.97	DIA	0.78	Phenazepam & 4-MeO-α-PVP HCl	0.73	Phenazepam
DIA 20mg/mL R2	0.97	DIA	0.78	Phenazepam & 4-MeO-α-PVP HCl	0.74	Phenazepam
DIA 20mg/mL R3	0.78	MC	0.61	α-lactose monohydrate	0.61	Alginic acid Na salt
DIA 15mg/mL R1	0.85	MC & DIA	0.76	MC	0.70	DIA & CaCO3
DIA 15mg/mL R2	0.86	MC & DIA	0.76	DIA & CaCO3	0.71	MC
DIA 15mg/mL R3	0.97	DIA & MC	0.91	DIA	0.70	Phenazepam
DIA 10mg/mL R1	0.77	MC	0.61	α-lactose monohydrate	0.60	Alginic acid Na salt
DIA 10mg/mL R2	0.85	MC & DIA	0.77	MC	0.70	DIA & CaCO3
DIA 10mg/mL R3	0.84	MC & DIA	0.77	DIA & CaCO3	0.72	MC
DIA 5mg/mL R1	0.96	MC & CaCO3	0.87	MC	0.68	CaCO3
DIA 5mg/mL R2	0.94	MC & CaCO3	0.86	MC	0.66	α-lactose monohydrate
DIA 5mg/mL R3	0.96	MC & CaCO3	0.86	MC	0.69	CaCO3
PAR 60mg/mL R1	0.92	PAR & MC	0.81	PAR	0.81	Phenacetin & MC
PAR 60mg/mL R2	0.95	PAR & MC	0.91	PAR	0.78	Phenacetin

PAR 60mg/mL R3	0.95	PAR & MC	0.89	PAR	0.81	Phenacetin
PAR 40mg/mL R1	0.91	PAR & MC	0.82	PAR	0.79	Phenacetin & MC
PAR 40mg/mL R2	0.93	PAR & MC	0.85	PAR	0.80	Phenacetin & MC
PAR 40mg/mL R3	0.92	PAR & MC	0.82	PAR	0.80	Phenacetin & MC
PAR 30mg/mL R1	0.91	PAR & MC	0.82	PAR	0.79	Phenacetin & MC
PAR 30mg/mL R2	0.90	PAR & MC	0.80	Phenacetin & MC	0.78	PAR
PAR 30mg/mL R3	0.90	PAR & MC	0.79	PAR	0.79	Phenacetin & MC
PAR 20mg/mL R1	0.73	MC	0.65	α-lactose monohydrate	0.62	PAR
PAR 20mg/mL R2	0.80	PAR & CaCO3	0.74	MC	0.70	Phenacetin & MC
PAR 20mg/mL R3	0.85	MC & PAR	0.75	MC	0.64	α-lactose monohydrate
PAR 15mg/mL R1	0.78	MC	0.66	α-lactose monohydrate	0.60	Alginic acid Na salt
PAR 15mg/mL R2	0.75	MC	0.63	α-lactose monohydrate	0.55	JWH-122
PAR 15mg/mL R3	0.70	MC	0.64	JWH-122 & CaCO3	0.60	α-lactose monohydrate

Table A3. Summary of set 12 RMA matches

Single simulated paper samples	Set 12 (soaking method)					
	CC	**1st match**	**CC**	**2nd match**	**CC**	**3rd match**
5F-PB-22 20mg/mL R1	0.95	MC & CaCO3	0.89	MC	0.67	α-lactose monohydrate
5F-PB-22 20mg/mL R2	0.94	MC & CaCO3	0.84	MC	0.67	CaCO3
5F-PB-22 20mg/mL R3	0.94	MC & CaCO3	0.88	MC	0.66	α-lactose monohydrate
5F-PB-22 15mg/mL R1	0.95	MC	0.81	MC & CaCO3	0.73	CaCO3
5F-PB-22 15mg/mL R2	0.95	MC & CaCO3	0.82	MC	0.72	CaCO3
5F-PB-22 15mg/mL R3	0.84	MC	0.66	CaCO3	0.64	α-lactose monohydrate
5F-PB-22 10mg/mL R1	0.86	MC & CaCO3	0.66	MC	0.65	α-lactose monohydrate
5F-PB-22 10mg/mL R2	0.93	MC	0.87	CaCO3	0.66	CaCO3
5F-PB-22 10mg/mL R3	0.96	MC & CaCO3	0.85	CaCO3	0.68	CaCO3
5F-PB-22 7.5mg/mL R1	0.95	MC & CaCO3	0.81	MC	0.73	CaCO3
5F-PB-22 7.5mg/mL R2	0.95	MC & CaCO3	0.82	MC	0.73	CaCO3
5F-PB-22 7.5mg/mL R3	0.84	MC	0.66	CaCO3	0.64	α-lactose monohydrate
5F-PB-22 5mg/mL R1	0.88	MC	0.66	CaCO3	0.66	CaCO3
5F-PB-22 5mg/mL R2	0.91	MC & CaCO3	0.87	MC	0.65	CaCO3
5F-PB-22 5mg/mL R3	0.94	MC & CaCO3	0.85	MC	0.68	α-lactose monohydrate
AMP 30mg/mL R1	0.95	MC & CaCO3	0.89	MC	0.66	α-lactose monohydrate
AMP 30mg/mL R2	0.96	MC & CaCO3	0.88	MC	0.67	α-lactose monohydrate
AMP 30mg/mL R3	0.96	MC & CaCO3	0.87	MC	0.67	α-lactose monohydrate

AMP 15mg/mL R1	0.95	MC & CaCO3	0.89	MC	0.66	α-lactose monohydrate
AMP 15mg/mL R2	0.96	MC & CaCO3	0.88	MC	0.67	α-lactose monohydrate
AMP 15mg/mL R3	0.94	MC & CaCO3	0.88	MC	0.67	α-lactose monohydrate
AMP 12.5mg/mL R1	0.86	MC	0.66	α-lactose monohydrate	0.66	CaCO3
AMP 12.5mg/mL R2	0.87	MC	0.66	α-lactose monohydrate	0.63	CaCO3
AMP 12.5mg/mL R3	0.85	MC	0.92	α-lactose monohydrate	0.66	CaCO3
AMP 10mg/mL R1	0.94	MC & CaCO3	0.90	MC	0.66	α-lactose monohydrate
AMP 10mg/mL R2	0.96	MC & CaCO3	0.91	MC	0.66	α-lactose monohydrate
AMP 10mg/mL R3	0.95	MC & CaCO3	0.89	MC	0.66	α-lactose monohydrate
AMP 7.5mg/mL R1	0.86	MC	0.66	α-lactose monohydrate	0.63	CaCO3
AMP 7.5mg/mL R2	0.87	MC	0.66	α-lactose monohydrate	0.63	CaCO3
AMP 7.5mg/mL R3	0.85	MC	0.66	α-lactose monohydrate	0.66	CaCO3
BEN 10mg/mL R1	0.93	MC & CaCO3	0.88	MC	0.66	α-lactose monohydrate
BEN 10mg/mL R2	0.96	MC & CaCO3	0.82	MC	0.73	CaCO3
BEN 10mg/mL R3	0.95	MC & CaCO3	0.9	MC	0.70	α-lactose monohydrate
BEN 6.5mg/mL R1	0.93	MC & CaCO3	0.88	MC	0.65	α-lactose monohydrate
BEN 6.5mg/mL R2	0.94	MC & CaCO3	0.84	MC	0.67	CaCO3
BEN 6.5mg/mL R3	0.95	MC & CaCO3	0.84	MC	0.67	α-lactose monohydrate
BEN 5mg/mL R1	0.94	MC & CaCO3	0.88	MC	0.66	CaCO3
BEN 5mg/mL R2	0.94	MC & CaCO3	0.82	MC	0.72	CaCO3
BEN 5mg/mL R3	0.95	MC & CaCO3	0.90	MC	0.65	α-lactose monohydrate

BEN 3.5mg/mL R1	0.93	MC & CaCO3	0.87	MC	0.65	α-lactose monohydrate
BEN 3.5mg/mL R2	0.94	MC & CaCO3	0.84	MC	0.66	CaCO3
BEN 3.5mg/mL R3	0.92	MC & CaCO3	0.84	MC	0.67	CaCO3
BEN 2.5mg/mL R1	0.94	MC & CaCO3	0.88	MC	0.66	α-lactose monohydrate
BEN 2.5mg/mL R2	0.95	MC & CaCO3	0.85	MC	0.72	α-lactose monohydrate
BEN 2.5mg/mL R3	0.92	MC & CaCO3	0.88	MC	0.66	α-lactose monohydrate
CAF 15mg/mL R1	0.94	MC & CaCO3	0.86	MC	0.72	Alginic acid Na salt
CAF 15mg/mL R2	0.93	MC & CaCO3	0.87	MC	0.68	CaCO3
CAF 15mg/mL R3	0.95	MC & CaCO3	0.81	MC	0.69	CaCO3
CAF 10mg/mL R1	0.97	MC & CaCO3	0.91	MC	0.67	α-lactose monohydrate
CAF 10mg/mL R2	0.90	MC & CaCO3	0.92	MC	0.67	CaCO3
CAF 10mg/mL R3	0.96	MC & CaCO3	0.93	MC	0.69	α-lactose monohydrate
CAF 8mg/mL R1	0.91	MC	0.68	α-lactose monohydrate	0.62	Alginic acid Na salt
CAF 8mg/mL R2	0.97	MC & CaCO3	0.90	MC	0.68	α-lactose monohydrate
CAF 8mg/mL R3	0.91	MC	0.68	α-lactose monohydrate	0.62	Alginic acid Na salt
CAF 6.5mg/mL R1	0.94	MC & CaCO3	0.9	MC	0.69	α-lactose monohydrate
CAF 6.5mg/mL R2	0.96	MC & CaCO3	0.9	MC	0.68	α-lactose monohydrate
CAF 6.5mg/mL R3	0.97	MC & CaCO3	0.89	MC	0.68	CaCO3
CAF 5mg/mL R1	0.96	MC & CaCO3	0.88	MC	0.68	Alginic acid Na salt
CAF 5mg/mL R2	0.97	MC & CaCO3	0.91	MC	0.69	α-lactose monohydrate
CAF 5mg/mL R3	0.95	MC & CaCO3	0.89	MC	0.68	CaCO3

COC 60mg/mL R1	0.79	MC	0.63	α-lactose monohydrate	0.59	CaCO3
COC 60mg/mL R2	0.83	MC	0.64	α-lactose monohydrate	0.60	Alginic acid Na salt
COC 60mg/mL R3	0.76	MC	0.62	α-lactose monohydrate	0.61	CaCO3
COC 40mg/mL R1	0.90	MC & CaCO3	0.83	MC	0.65	α-lactose monohydrate
COC 40mg/mL R2	0.84	MC	0.64	α-lactose monohydrate	0.61	Alginic acid Na salt
COC 40mg/mL R3	0.83	MC	0.65	α-lactose monohydrate	0.61	Alginic acid Na salt
COC 35mg/mL R1	0.86	MC	0.65	α-lactose monohydrate	0.61	Alginic acid Na salt
COC 35mg/mL R2	0.86	MC	0.65	α-lactose monohydrate	0.61	Alginic acid Na salt
COC 35mg/mL R3	0.83	MC	0.64	α-lactose monohydrate	0.60	Alginic acid Na salt
COC 30mg/mL R1	0.76	MC	0.62	α-lactose monohydrate	0.62	Alginic acid Na salt
COC 30mg/mL R2	0.78	MC	0.62	α-lactose monohydrate	0.62	Alginic acid Na salt
COC 30mg/mL R3	0.84	MC & CaCO3	0.74	α-lactose monohydrate	0.63	CaCO3
COC 20mg/mL R1	0.78	MC & CaCO3	0.78	URB-597, CaCO3 & dextrose	0.78	CaCO3
COC 20mg/mL R2	0.84	MC	0.80	URB-597, CaCO3 & dextrose	0.79	CaCO3 & dextrose
COC 20mg/mL R3	0.77	α-lactose monohydrate	0.77	URB-597, α-lactose monohydrate & BB-22	0.77	α-lactose monohydrate
DIA 30mg/mL R1	0.85	MC	0.65	α-lactose monohydrate	0.59	CaCO3
DIA 30mg/mL R2	0.91	MC & CaCO3	0.86	MC	0.64	α-lactose monohydrate
DIA 30mg/mL R3	0.86	MC	0.65	α-lactose monohydrate	0.63	Alginic acid Na salt
DIA 20mg/mL R1	0.97	MC & CaCO3	0.88	MC	0.68	Alginic acid Na salt
DIA 20mg/mL R2	0.97	MC & CaCO3	0.91	MC	0.69	α-lactose monohydrate

DIA 20mg/mL R3	0.78	MC & CaCO3	0.89	MC	0.68	CaCO3
DIA 15mg/mL R1	0.85	MC & CaCO3	0.87	MC	0.68	CaCO3
DIA 15mg/mL R2	0.86	MC & CaCO3	0.86	MC	0.66	α-lactose monohydrate
DIA 15mg/mL R3	0.97	MC & CaCO3	0.86	MC	0.69	CaCO3
DIA 10mg/mL R1	0.77	MC	0.61	α-lactose monohydrate	0.60	Alginic acid Na salt
DIA 10mg/mL R2	0.85	MC & CaCO3	0.77	MC	0.70	DIA & CaCO3
DIA 10mg/mL R3	0.84	MC & CaCO3	0.77	CaCO3	0.72	MC
DIA 5mg/mL R1	0.96	MC & CaCO3	0.87	MC	0.68	CaCO3
DIA 5mg/mL R2	0.94	MC & CaCO3	0.86	MC	0.66	α-lactose monohydrate
DIA 5mg/mL R3	0.96	MC & CaCO3	0.86	MC	0.69	CaCO3
PAR 60mg/mL R1	0.84	PAR	0.77	Phenacetin	0.68	URB-754
PAR 60mg/mL R2	0.84	PAR	0.76	Phenacetin	0.70	URB-754
PAR 60mg/mL R3	0.84	PAR	0.76	Phenacetin	0.69	URB-754
PAR 40mg/mL R1	0.93	PAR & MC	0.71	Phenacetin, MC & CaCO3	0.83	PAR
PAR 40mg/mL R2	0.91	PAR & MC	0.84	PAR	0.79	Phenacetin & MC
PAR 40mg/mL R3	0.91	PAR & MC	0.80	Phenacetin & MC	0.79	MC & URB-754
PAR 30mg/mL R1	0.87	MC & PAR	0.73	Phenacetin & α-lactose monohydrate	0.71	MC
PAR 30mg/mL R2	0.75	MC	0.64	α-lactose monohydrate	0.61	PAR
PAR 30mg/mL R3	0.86	MC & PAR	0.75	MC	0.66	α-lactose monohydrate
PAR 20mg/mL R1	0.85	MC	0.67	α-lactose monohydrate	0.62	Alginic acid Na salt
PAR 20mg/mL R2	0.86	MC	0.67	α-lactose monohydrate	0.63	Alginic acid Na salt

PAR 20mg/mL R3	0.92	MC & CaCO3	0.88	MC	0.67	α-lactose monohydrate
PAR 15mg/mL R1	0.91	MC	0.82	α-lactose monohydrate	0.79	Alginic acid Na salt
PAR 15mg/mL R2	0.90	MC & CaCO3	0.80	MC	0.78	α-lactose monohydrate
PAR 15mg/mL R3	0.90	MC	0.79	α-lactose monohydrate	0.63	Alginic acid Na salt

Table A4. Summary of set 16 RMA matches

Binary simulated paper samples	**Set 16 (pipetting method)**					
	CC	**1st match**	**CC**	**2nd match**	**CC**	**3rd match**
5F-PB-22/AMP R1	0.91	MC & 5F-PB-22	0.77	MC	0.71	5F-PB-22
5F-PB-22/AMP R2	0.89	MC & 5F-PB-22	0.76	MC	0.68	5F-PB-22
5F-PB-22/AMP R3	0.87	MC & CaCO3	0.77	MC	0.64	α-lactose monohydrate
5F-PB-22/BEN R1	0.98	BEN	0.91	Dimethocaine	0.79	mephedrone
5F-PB-22/BEN R2	0.98	BEN	0.92	Dimethocaine	0.79	mephedrone
5F-PB-22/BEN R3	0.89	BEN & MC	0.86	Dimethocaine & MC	0.79	BEN
5F-PB-22/CAF R1	0.89	MC & CaCO3	0.82	MC	0.66	α-lactose monohydrate
5F-PB-22/CAF R2	0.91	MC & BB-22	0.74	MC	0.73	FDU-PB-22
5F-PB-22/CAF R3	0.92	BB-22 & MC	0.88	FDU-PB-22 & MC	0.86	MC & 5F-PB-22
5F-PB-22/COC R1	0.9	MC & BB-22	0.75	MC	0.71	BB-22
5F-PB-22/COC R2	0.93	MC & BB-22	0.88	FDU-PB-22 & MC	0.85	NM-22 & MC
5F-PB-22/COC R3	0.87	MC & BB-22	0.8	BB-22 & CaCO3	0.78	FDU-PB-22 & CaCO3

5F-PB-22/DIA R1	0.87	MC & DIA	0.8	MC	0.67	CaCO3 & MC
5F-PB-22/DIA R2	0.83	MC & BB-22	0.73	MC	0.64	FDU-PB-22
5F-PB-22/DIA R3	0.88	MC & CaCO3	0.8	MC	0.62	α-lactose monohydrate
5F-PB-22/PAR R1	0.88	PAR & BB-22	0.86	FDU-PB-22 & PAR	0.85	BB-22, Phenacetin & NM-22
5F-PB-22/PAR R2	0.79	MC	0.65	α-lactose monohydrate	0.6	Alginic acid Na salt
5F-PB-22/PAR R3	0.89	BB-22 & MC	0.86	FDU-PB-22 & MC	0.53	NM-22 & MC

Table A5. Summary of set 18 RMA matches

Binary simulated paper samples	**Set 18 (soaking method)**					
	CC	**1st match**	**CC**	**2nd match**	**CC**	**3rd match**
5F-PB-22/AMP R1	0.91	BB-22 & MC	0.89	FDU-PB-22 & MC	0.86	BB-22
5F-PB-22/AMP R2	0.89	MC	0.66	α-lactose monohydrate	0.61	Alginic acid Na salt
5F-PB-22/AMP R3	0.87	MC & BB-22	0.83	MC	0.63	α-lactose monohydrate
5F-PB-22/BEN R1	0.91	MC & CaCO3	0.62	MC	0.65	α-lactose monohydrate
5F-PB-22/BEN R2	0.95	MC & CaCO3	0.86	MC	0.66	α-lactose monohydrate
5F-PB-22/BEN R3	0.94	MC & CaCO3	0.87	MC	0.67	α-lactose monohydrate
5F-PB-22/CAF R1	0.95	MC & CaCO3	0.87	MC	0.68	α-lactose monohydrate
5F-PB-22/CAF R2	0.95	MC & CaCO3	0.86	MC	0.67	α-lactose monohydrate
5F-PB-22/CAF R3	0.88	MC	0.67	α-lactose monohydrate	0.62	CaCO3
5F-PB-22/COC R1	0.83	MC	0.68	CaCO3	0.66	α-lactose monohydrate
5F-PB-22/COC R2	0.83	MC	0.65	α-lactose monohydrate	0.6	CaCO3

5F-PB-22/COC R3	0.92	MC & CaCO3	0.84	MC	0.66	α-lactose monohydrate
5F-PB-22/DIA R1	0.92	MC & CaCO3	0.83	MC	0.65	α-lactose monohydrate
5F-PB-22/DIA R2	0.81	MC	0.67	CaCO3	0.65	α-lactose monohydrate
5F-PB-22/DIA R3	0.82	MC	0.65	CaCO3	0.65	α-lactose monohydrate
5F-PB-22/PAR R1	0.94	MC & CaCO3	0.84	MC	0.68	CaCO3
5F-PB-22/PAR R2	0.91	MC & CaCO3	0.82	MC	0.66	CaCO3
5F-PB-22/PAR R3	0.88	MC	0.68	α-lactose monohydrate	0.62	Alginic acid Na salt

Appendix 4.15. Set 7 overlaid Raman spectra of averaged replicates of amphetamine/diazepam (M10) and diazepam (CF).

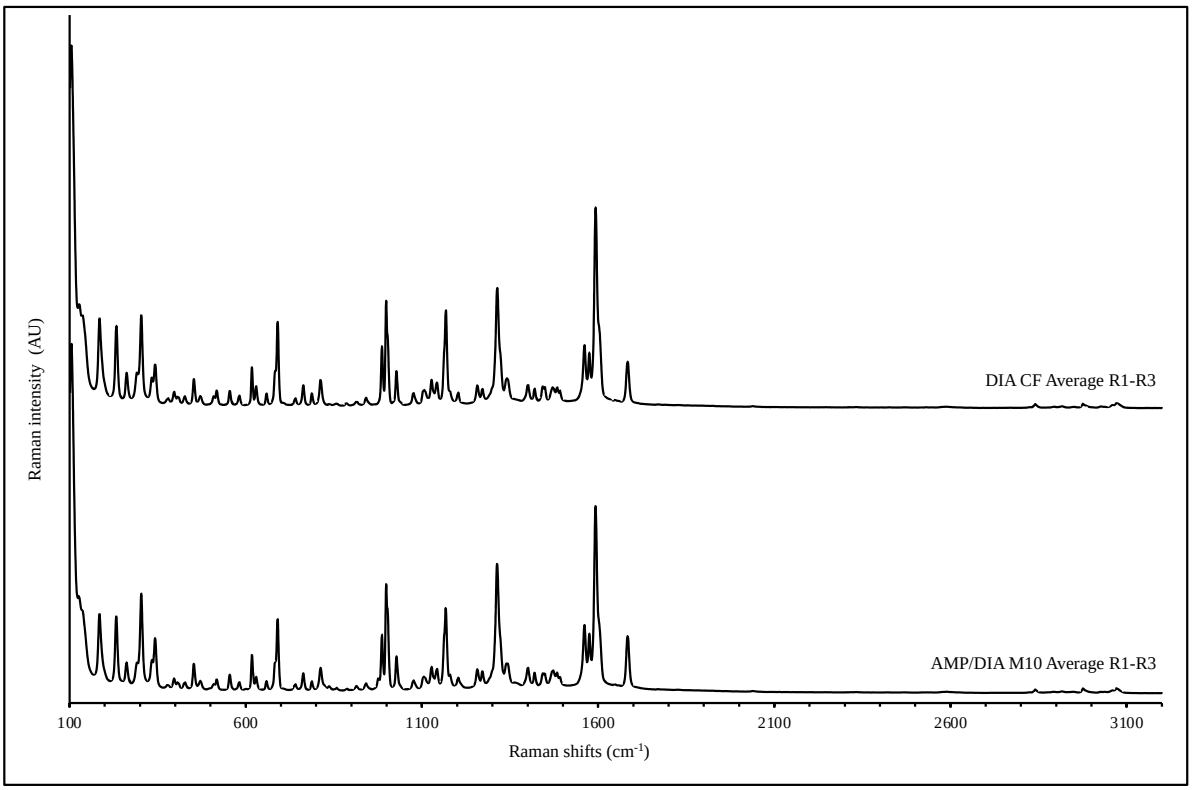

Figure 1A. Set 7 overlaid Raman spectra of averaged replicates of amphetamine/diazepam (M10) and diazepam (CF).

Appendix 4.16. Raman Renishaw set 7 additional PCA plots

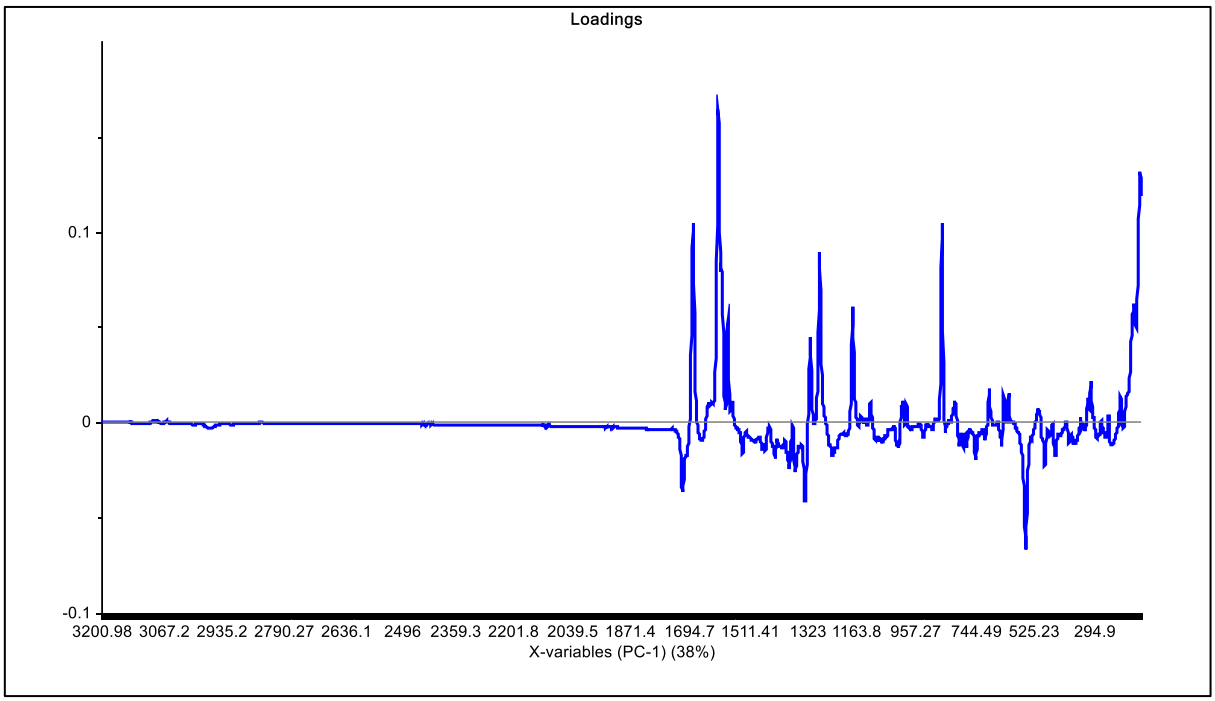

Figure A1. PC-1 loadings plot of set 7.

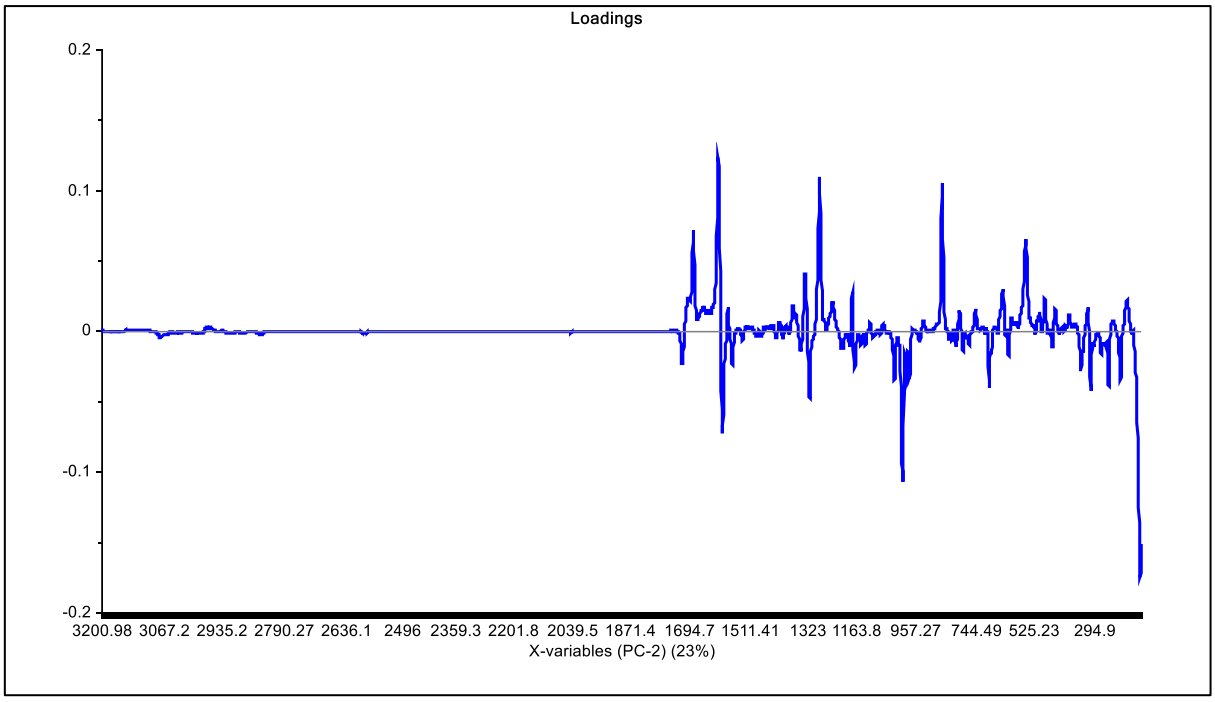

Figure A2. PC-2 loadings plot of set 7.

Appendix 4.17. Raman Rigaku set 8 additional PCA plots

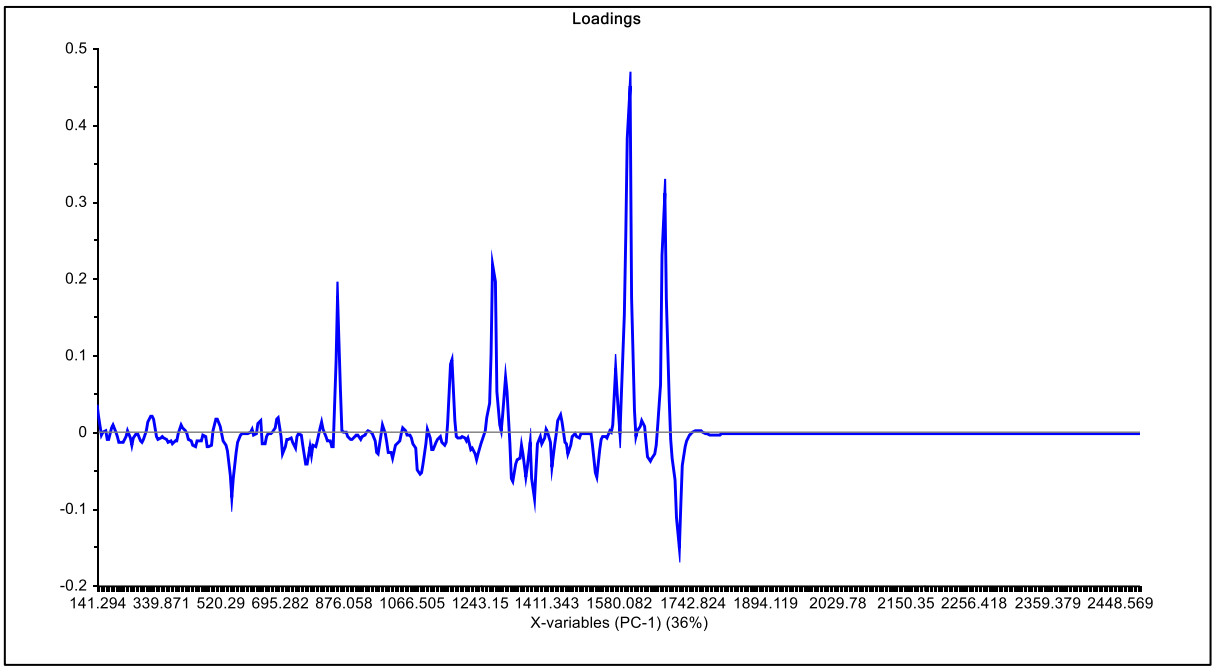

Figure A1. PC-1 loadings plot of set 8.

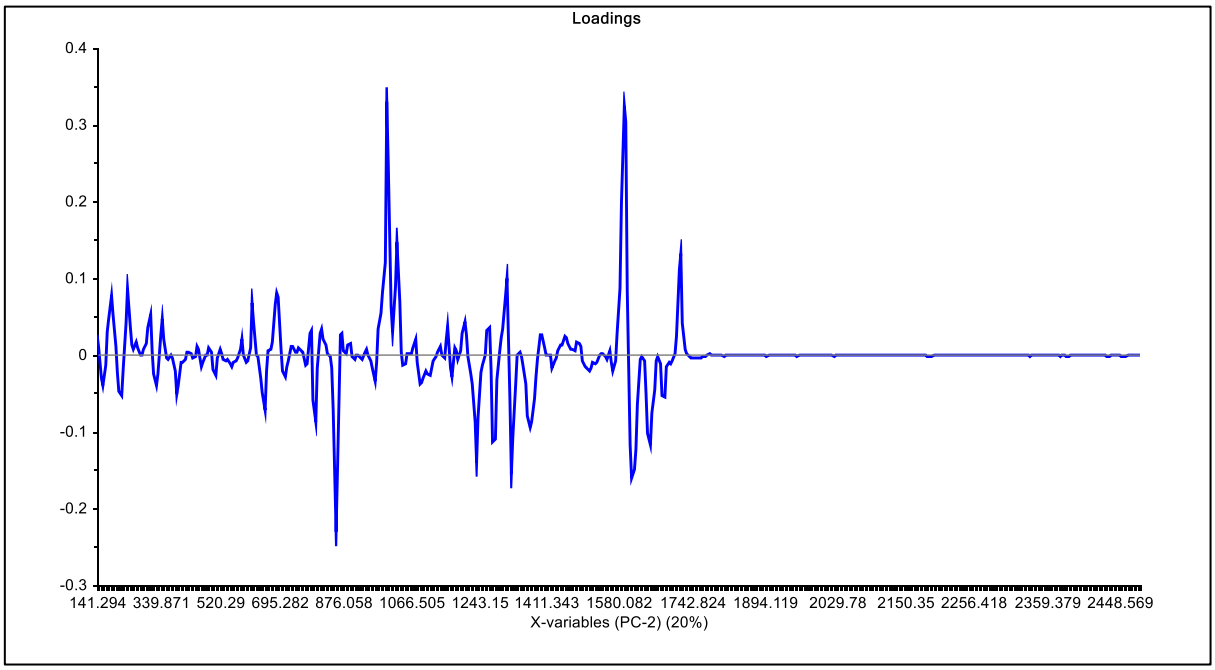

Figure A2. PC-2 loadings plot of set 8.

Appendix 4.18. Raman Renishaw set 9 additional PCA plots

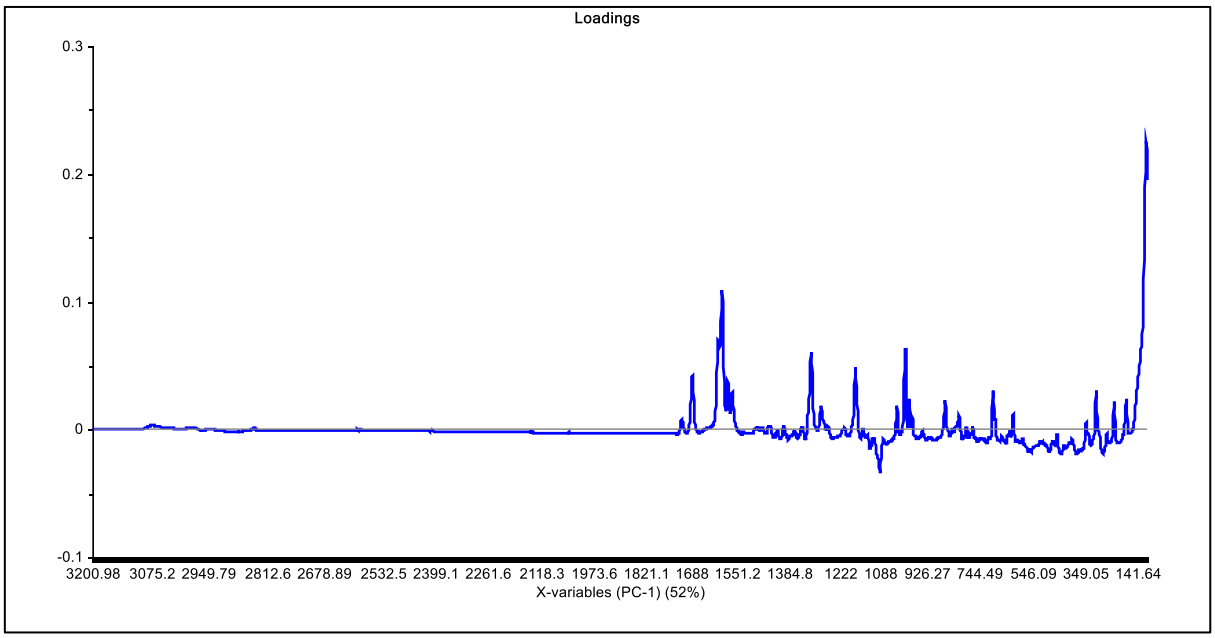

Figure A1. PC-1 loadings plot of set 9.

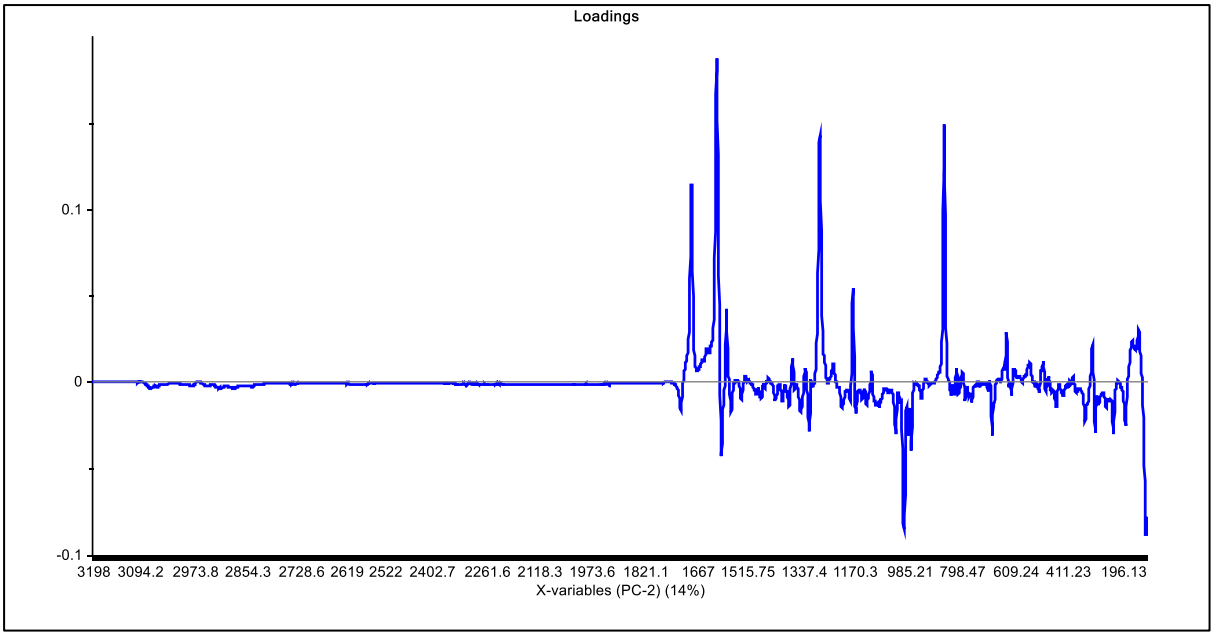

Figure A2. PC-2 loadings plot of set 9.

Appendix 4.19. Raman Renishaw additional PCA plots of set 9 recalculated without outliers

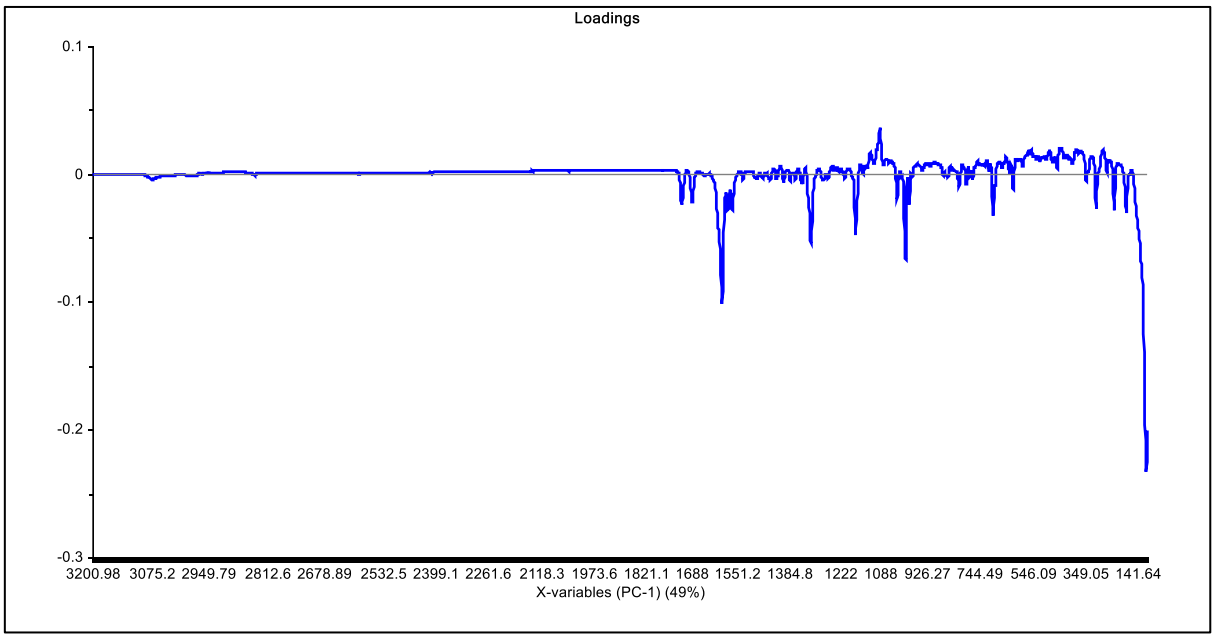

Figure A1. PC-1 loadings plot of set 9 recalculated without outliers.

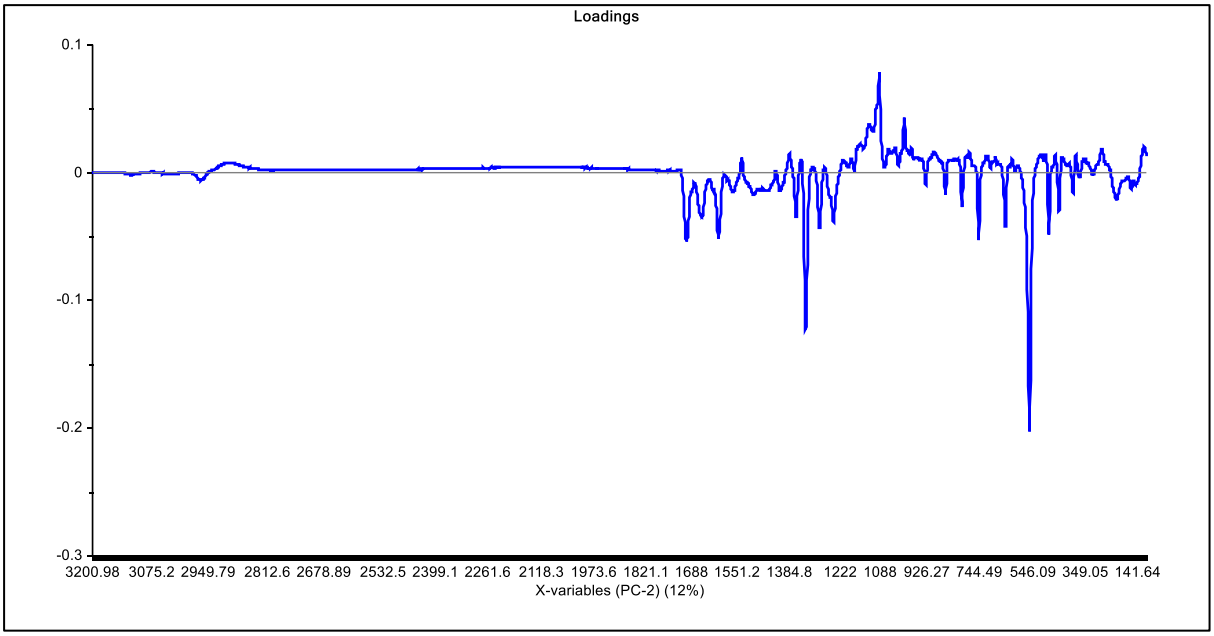

Figure A2. PC-2 loadings plot of set 9 recalculated without outliers.

Appendix 4.20. Overlaid spectra of set 10 benzocaine 10 mg/mL pipetted on paper and benzocaine replicate samples.

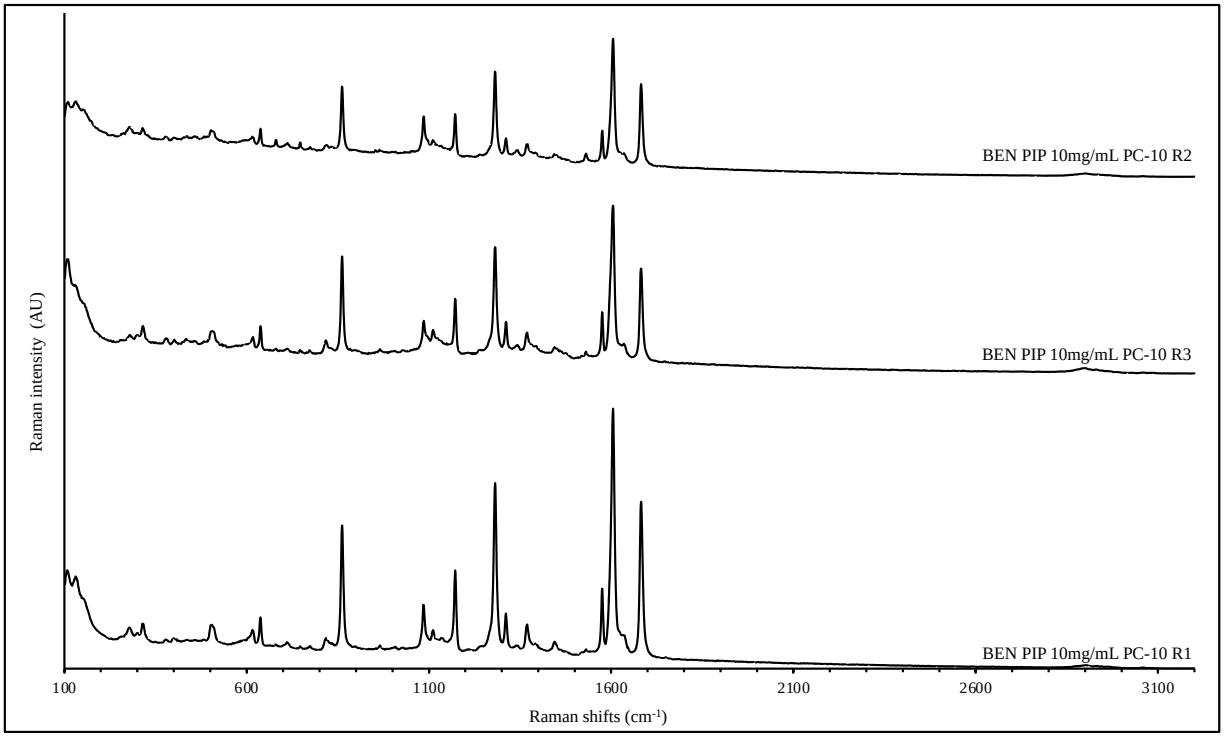

Figure A1. Overlaid Raman spectra benzocaine 10 mg/mL pipetted on paper replicate samples.

Appendix 4.21. Raman Rigaku set 10 additional PCA plots

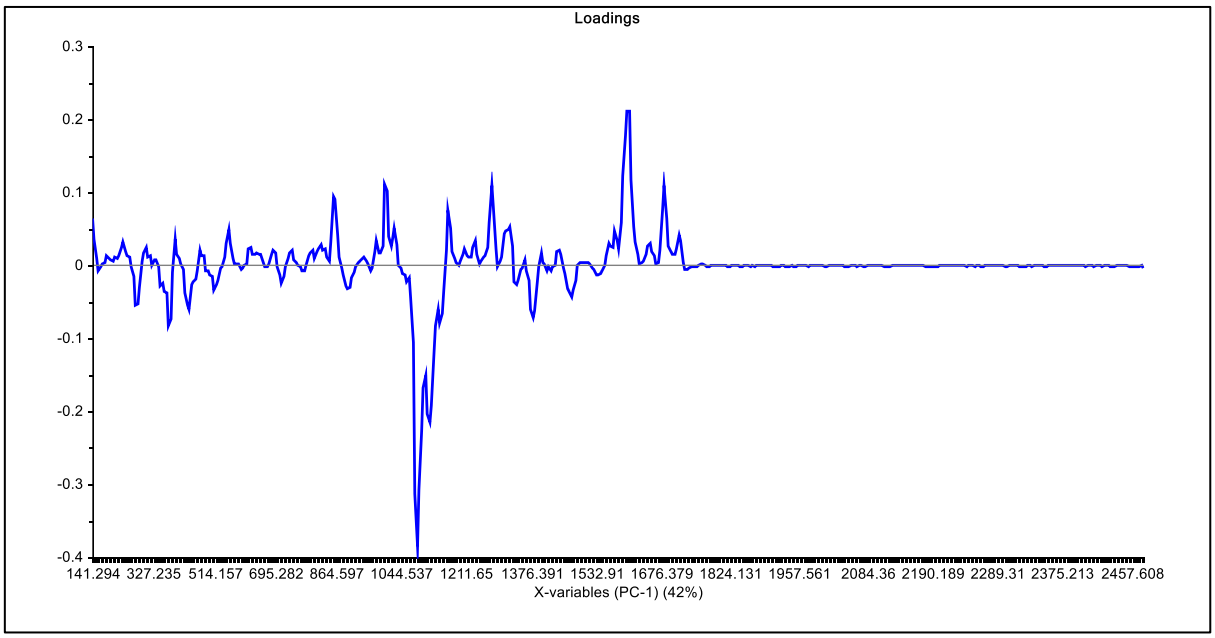

Figure A1. PC-1 loadings plot of set 10.

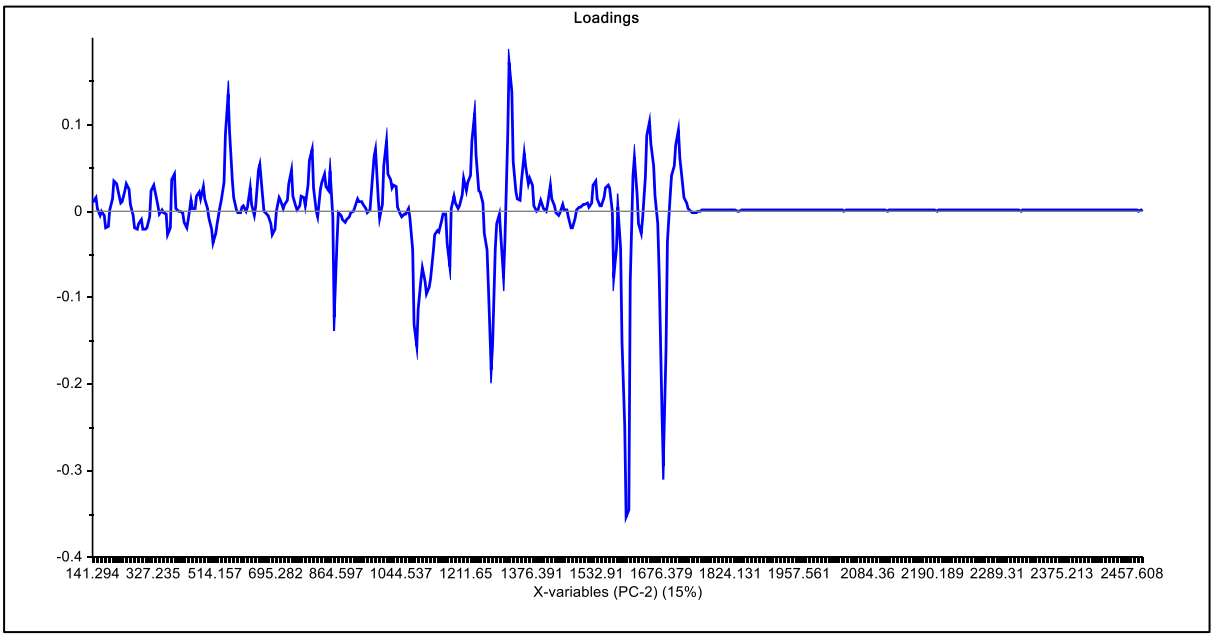

Figure A2. PC-2 loadings plot of set 10.

Appendix 4.22. Raman Rigaku additional PCA plots of set 10 recalculated without outliers

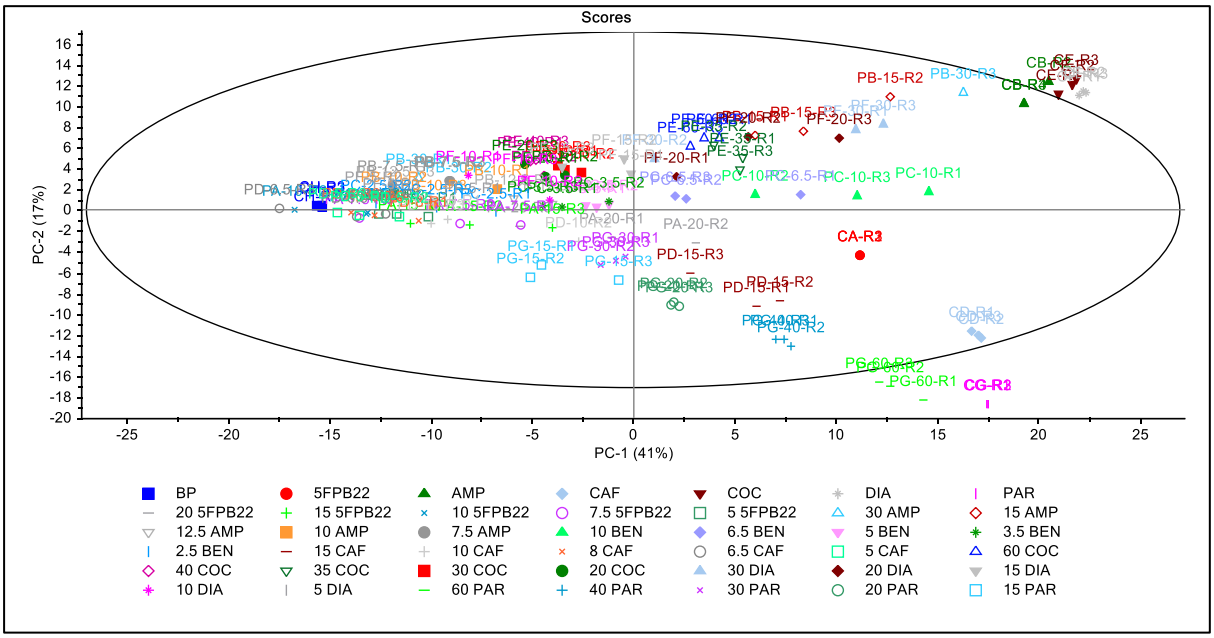

Figure A1. PC-1 vs PC-2 2D scores plot of set 10 recalculated without outliers

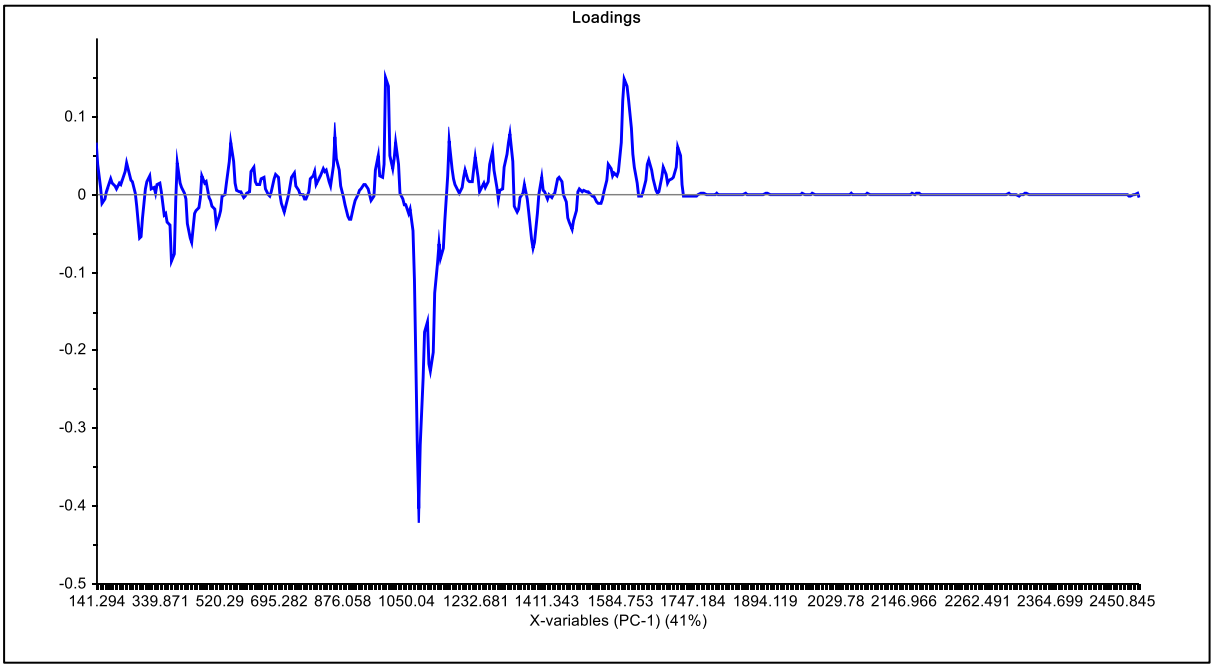

Figure A2. PC-1 loadings plot of set 10 recalculated without outliers.

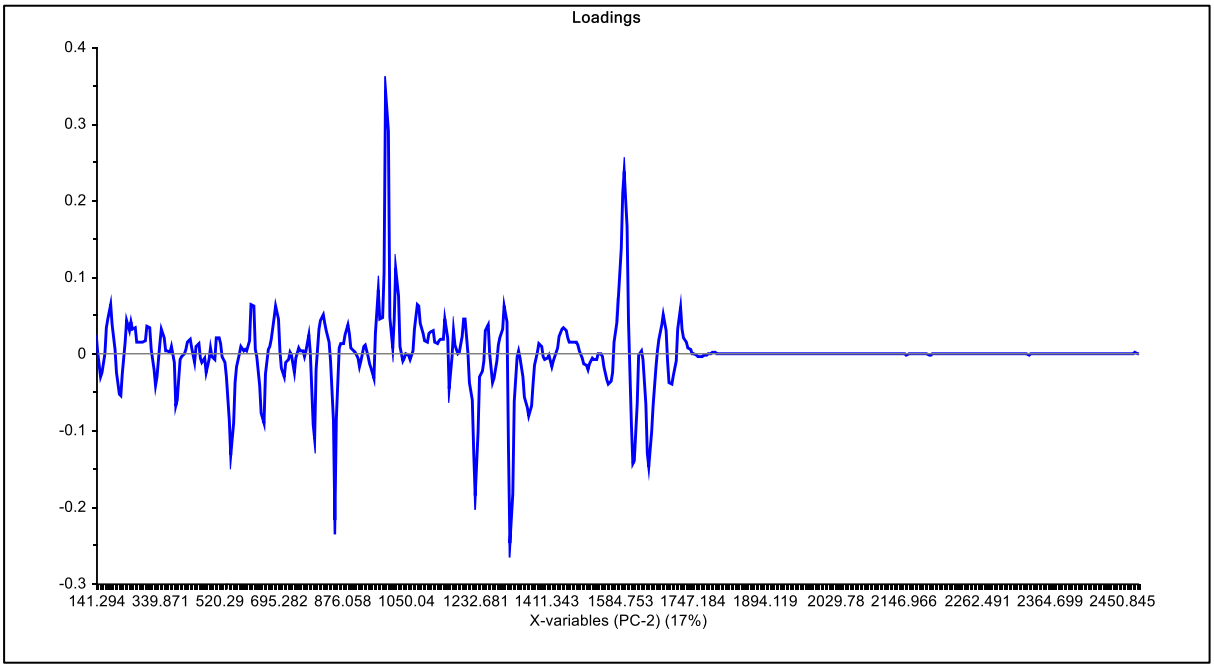

Figure A3. PC-2 loadings plot of set 10 recalculated without outliers.

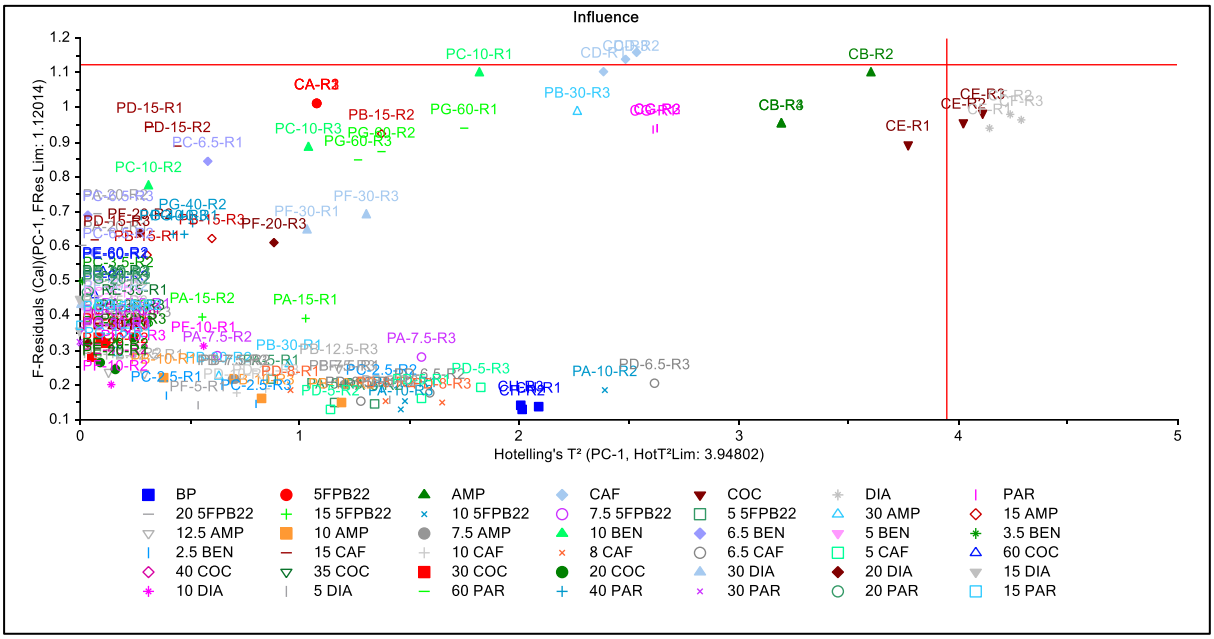

Figure A4. PC-1 F-residuals vs Hotelling T^2 influence plots of set 10 recalculated without outliers.

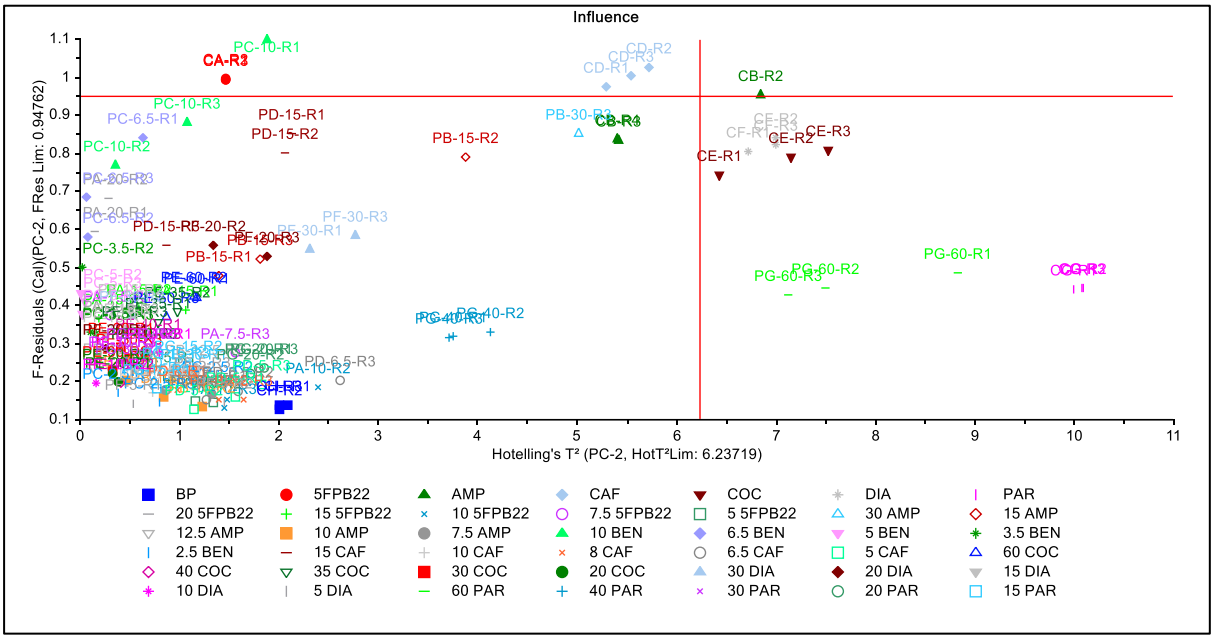

Figure A5. PC-2 F-residuals vs Hotelling T^2 influence plots of set 10 recalculated without outliers.

Appendix 4.23. Additional line plots of 5F-PB-22, amphetamine, cocaine and diazepam spectra taken with Raman Rigaku

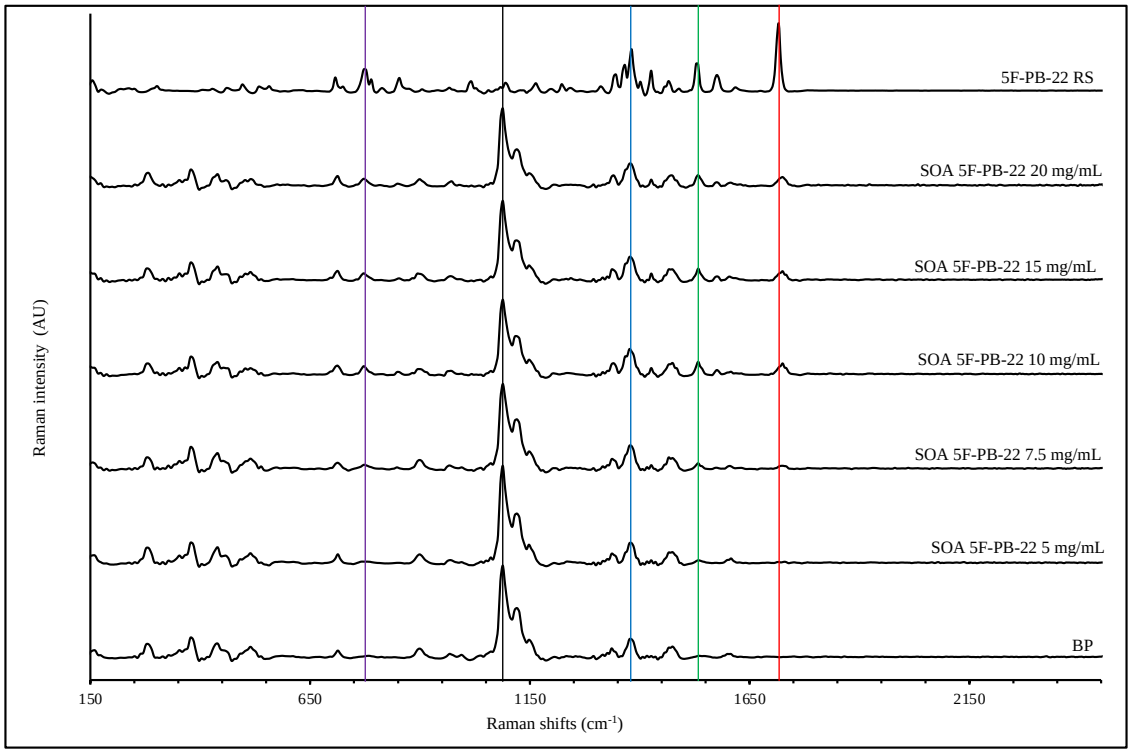

Figure A1. Raman Rigaku spectra of 5F-PB-22 reference standard, 5F-PB-22 soaked on paper at 20, 15, 10, 7.5 and 5 mg/mL and BP (from top to bottom).

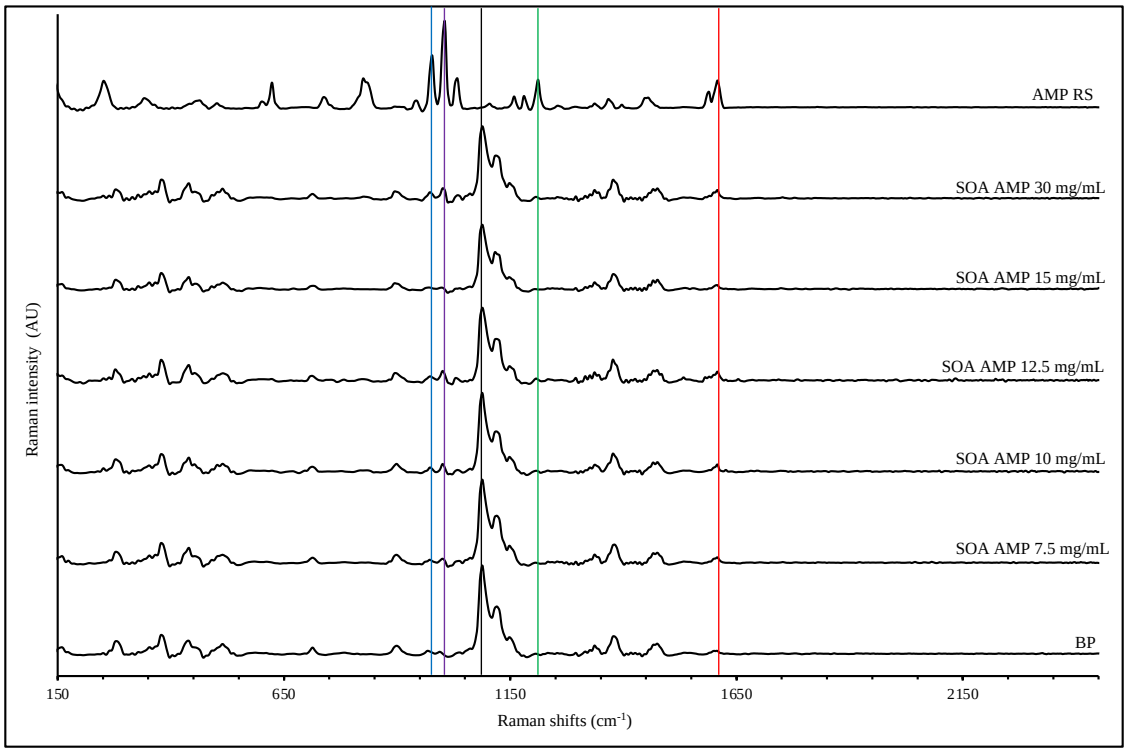

Figure A2. Raman Rigaku spectra of amphetamine reference standard, amphetamine soaked on paper at 30, 15, 12.5, 10 and 7.5 mg/mL and BP (from top to bottom).

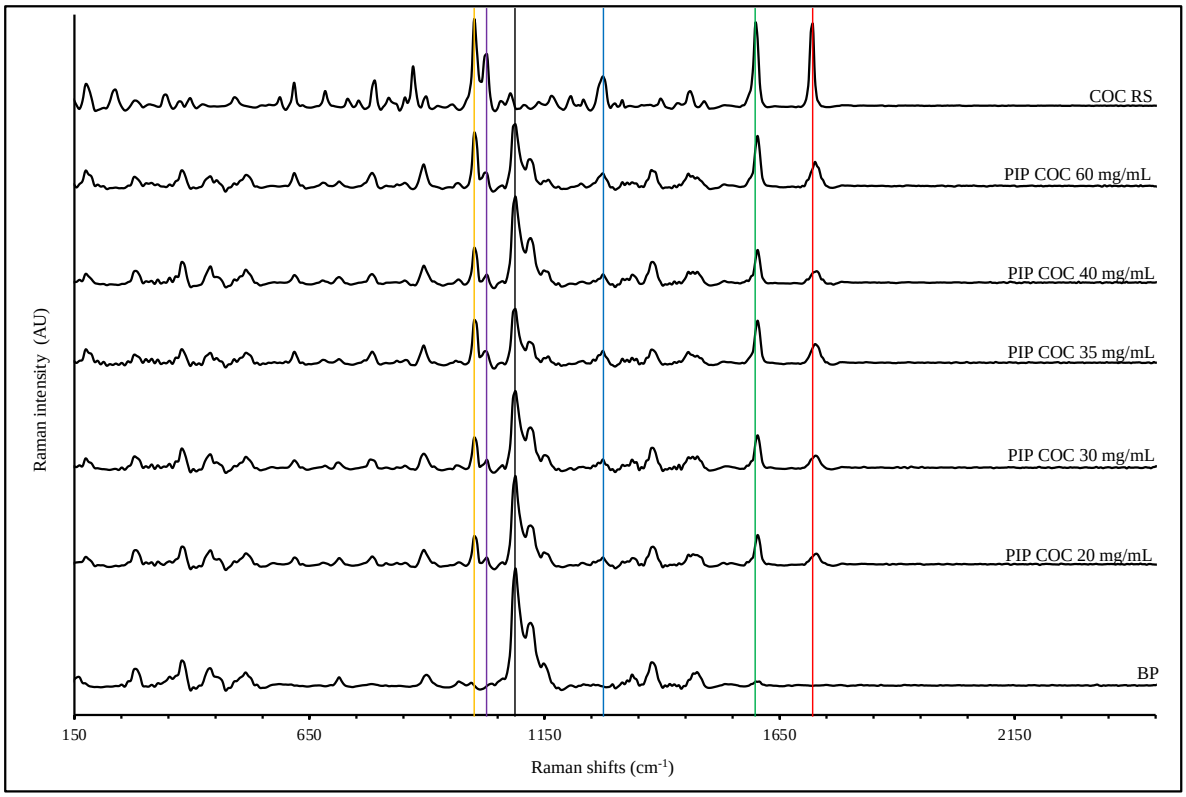

Figure A3. Raman Rigaku spectra of cocaine reference standard, cocaine soaked on paper at 60, 40, 35, 30 and 20 mg/mL and BP (from top to bottom).

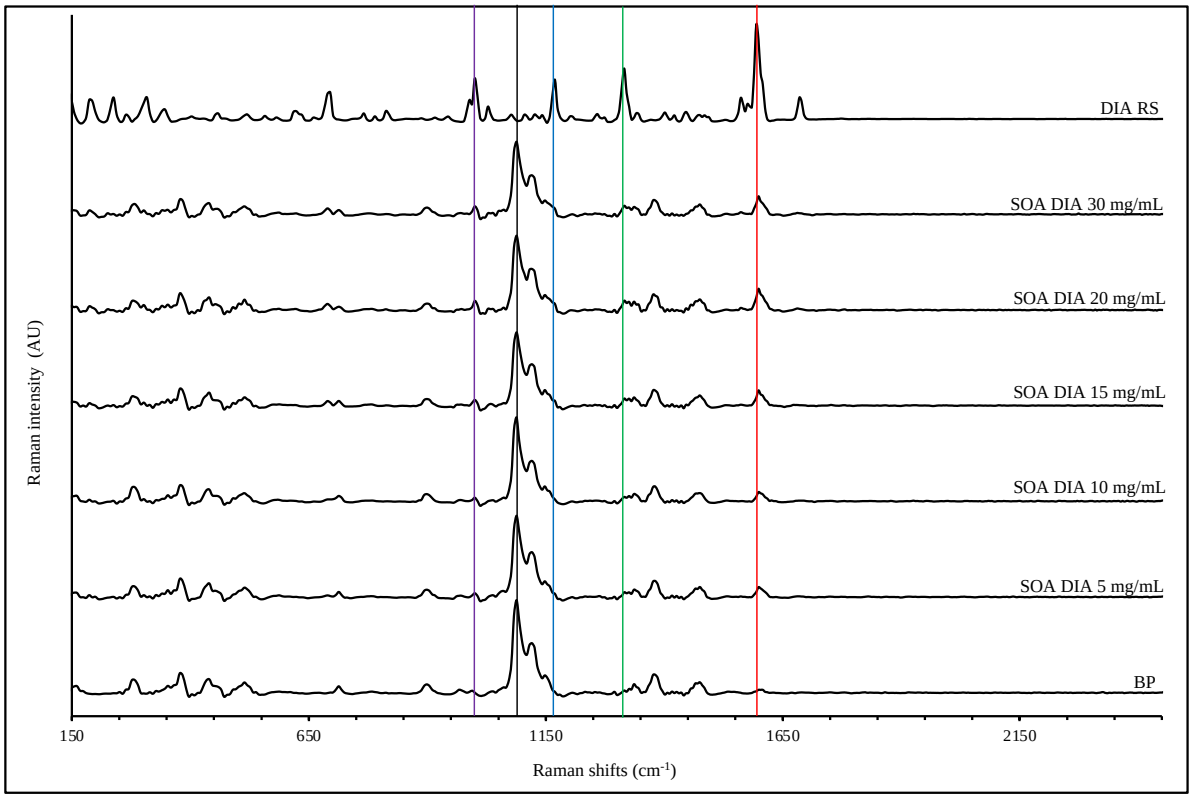

Figure A4. Raman Rigaku spectra of diazepam reference standard, diazepam soaked on paper at 30, 20, 15, 10 and 5 mg/mL and BP (from top to bottom).

Appendix 4.24. Additional line plots of 5F-PB-22, amphetamine, cocaine and diazepam spectra taken with Raman Renishaw.

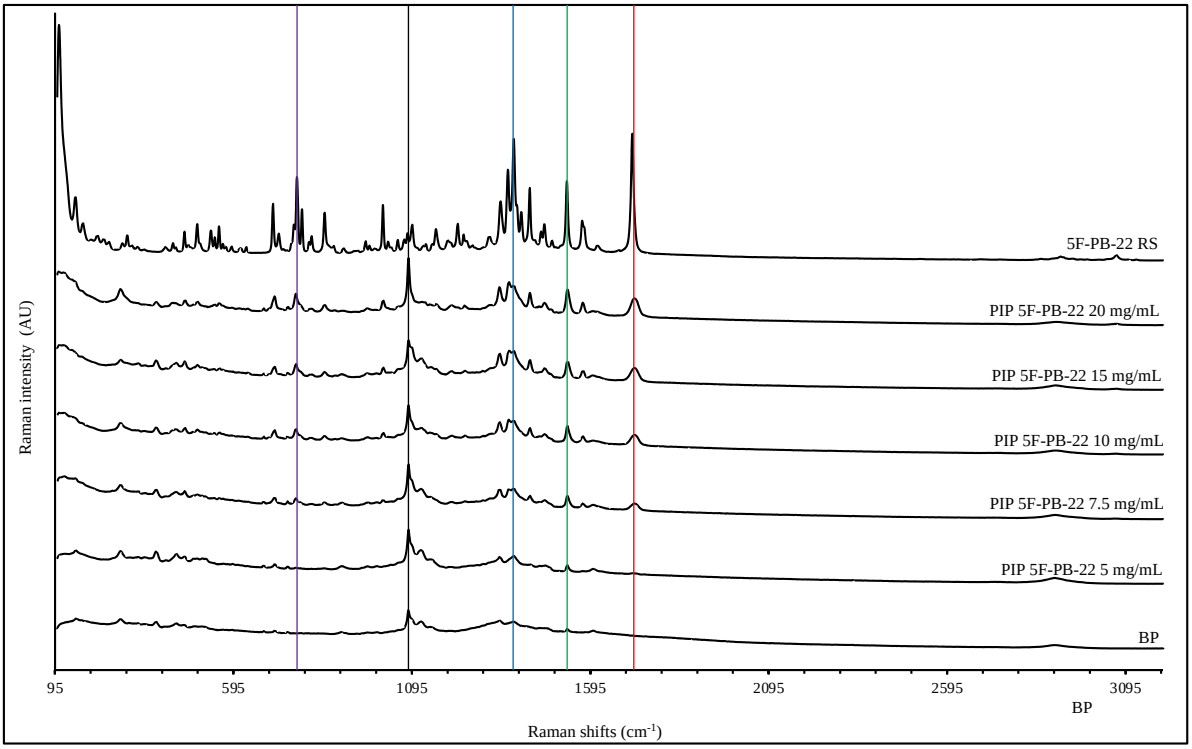

Figure A1. Raman Renishaw spectra of 5F-PB-22 reference standard, 5F-PB-22 pipetted on paper at 20, 15, 10, 7.5 and 5 mg/mL and BP (from top to bottom).

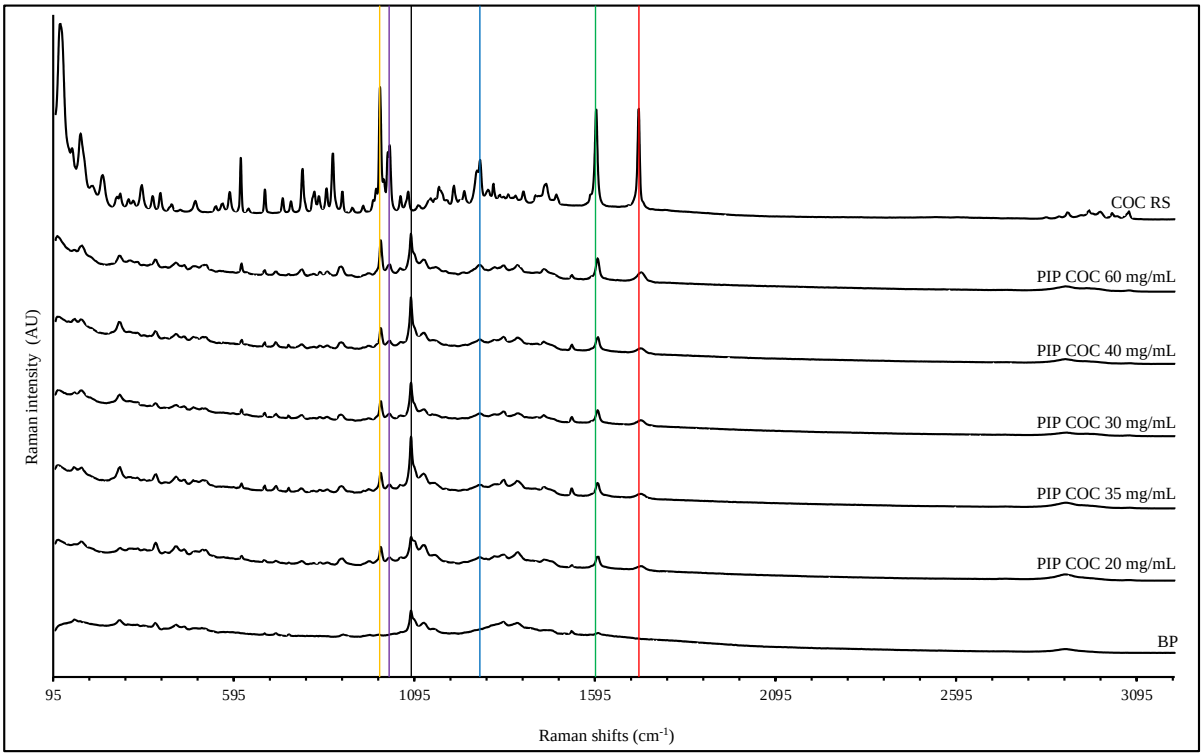

Figure A3. Raman Renishaw spectra of cocaine reference standard, cocaine pipetted on paper at 60, 40, 35, 30 and 20 mg/mL and BP (from top to bottom).

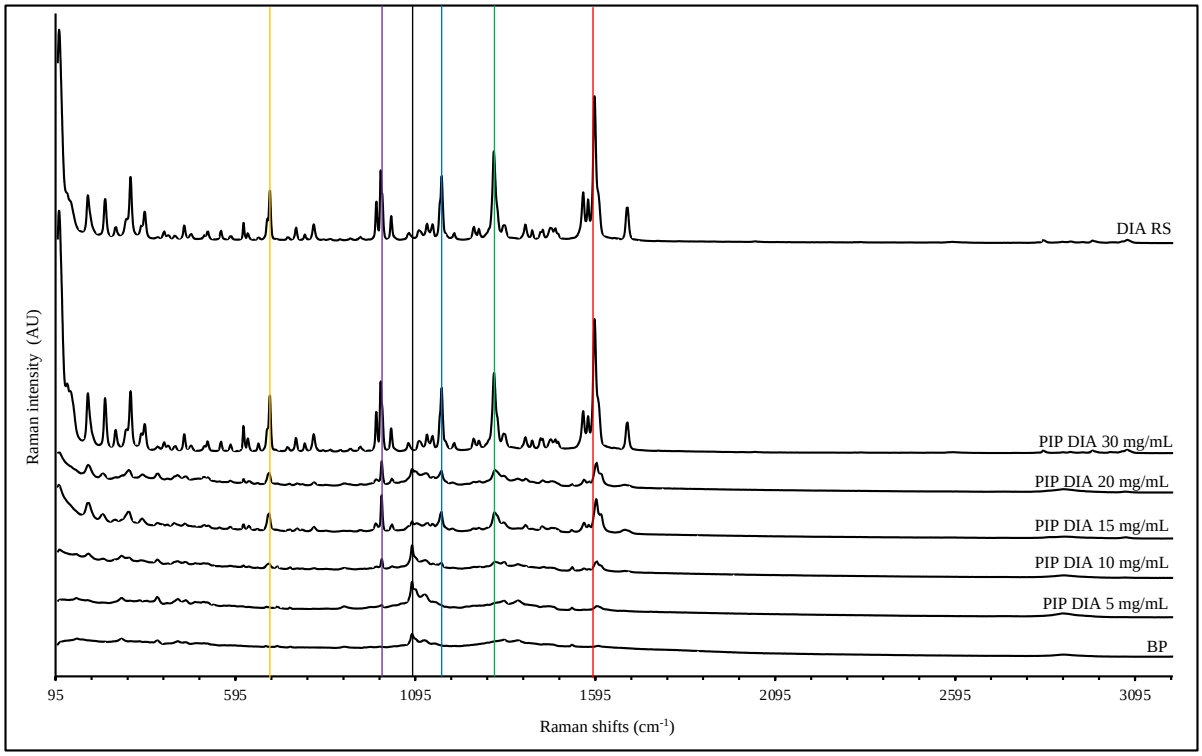

Figure A4. Raman Renishaw spectra of diazepam reference standard, diazepam pipetted on paper at 30, 20, 15, 10 and 5 mg/mL and BP (from top to bottom).

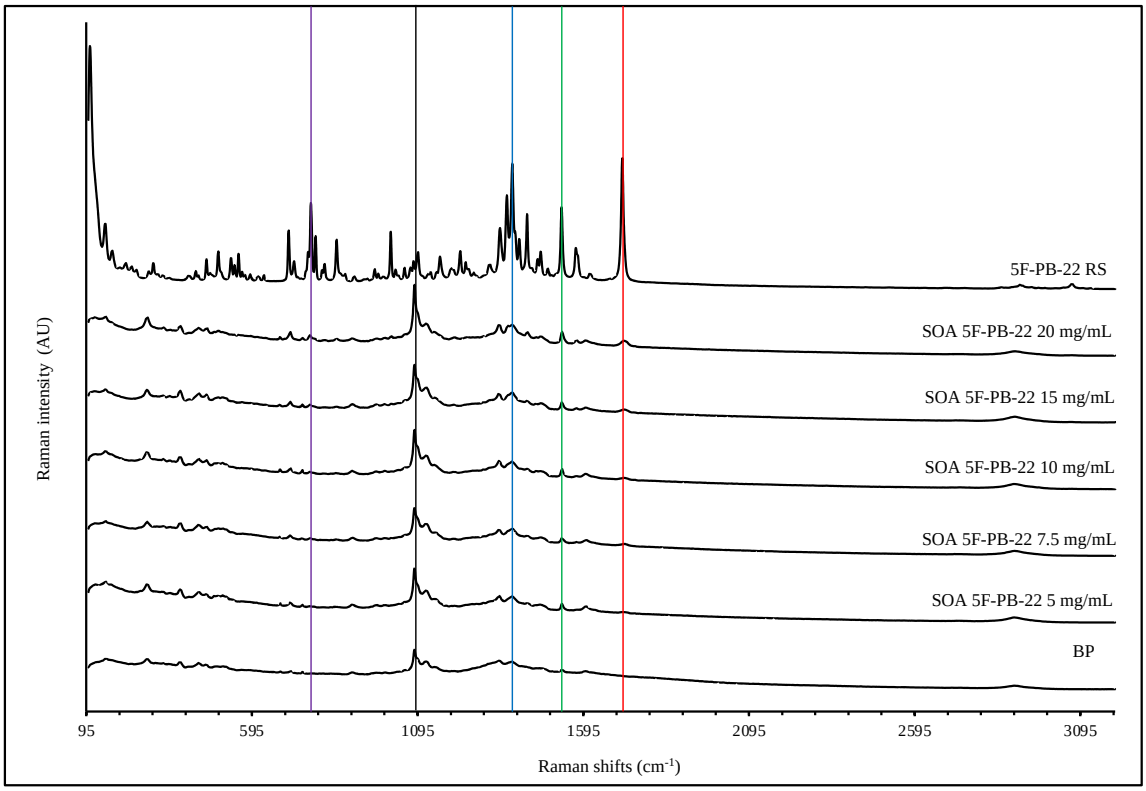

Figure A5. Raman Renishaw spectra of 5F-PB-22 reference standard, 5F-PB-22 soaked on paper at 20, 15, 10, 7.5 and 5 mg/mL and BP (from top to bottom).

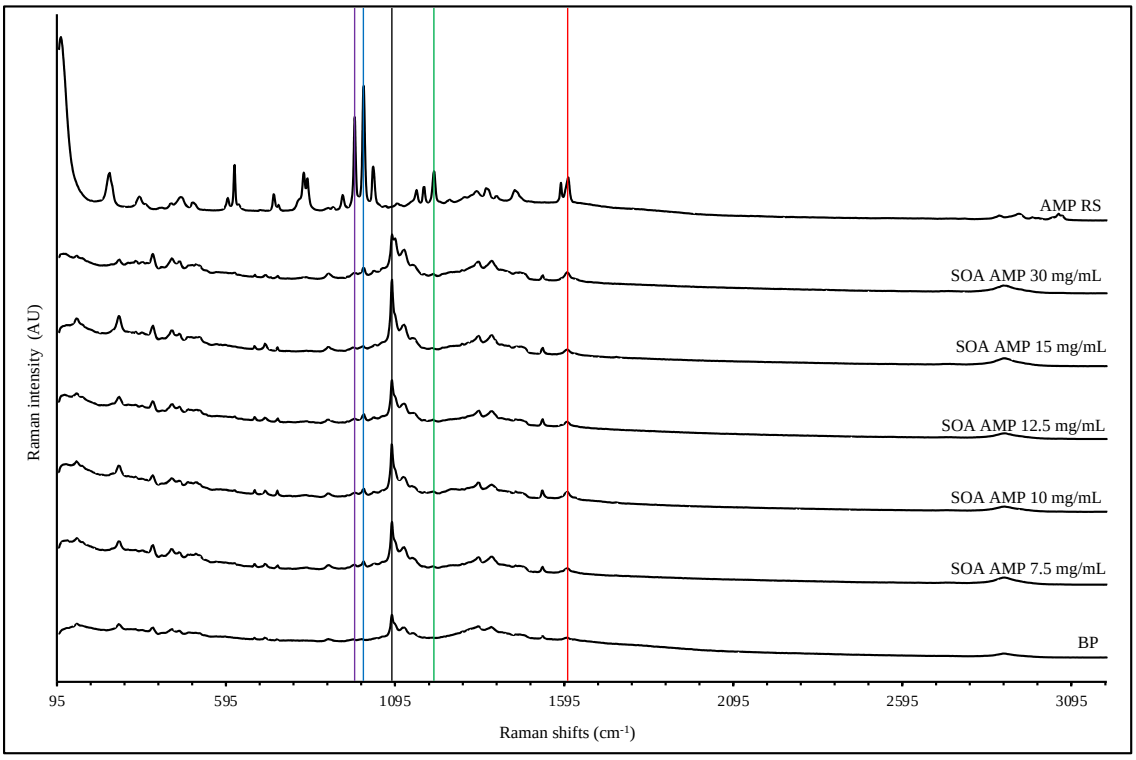

Figure A6. Raman Renishaw spectra of amphetamine reference standard, amphetamine soaked on paper at 30, 15, 12.5, 10 and 7.5 mg/mL and BP (from top to bottom).

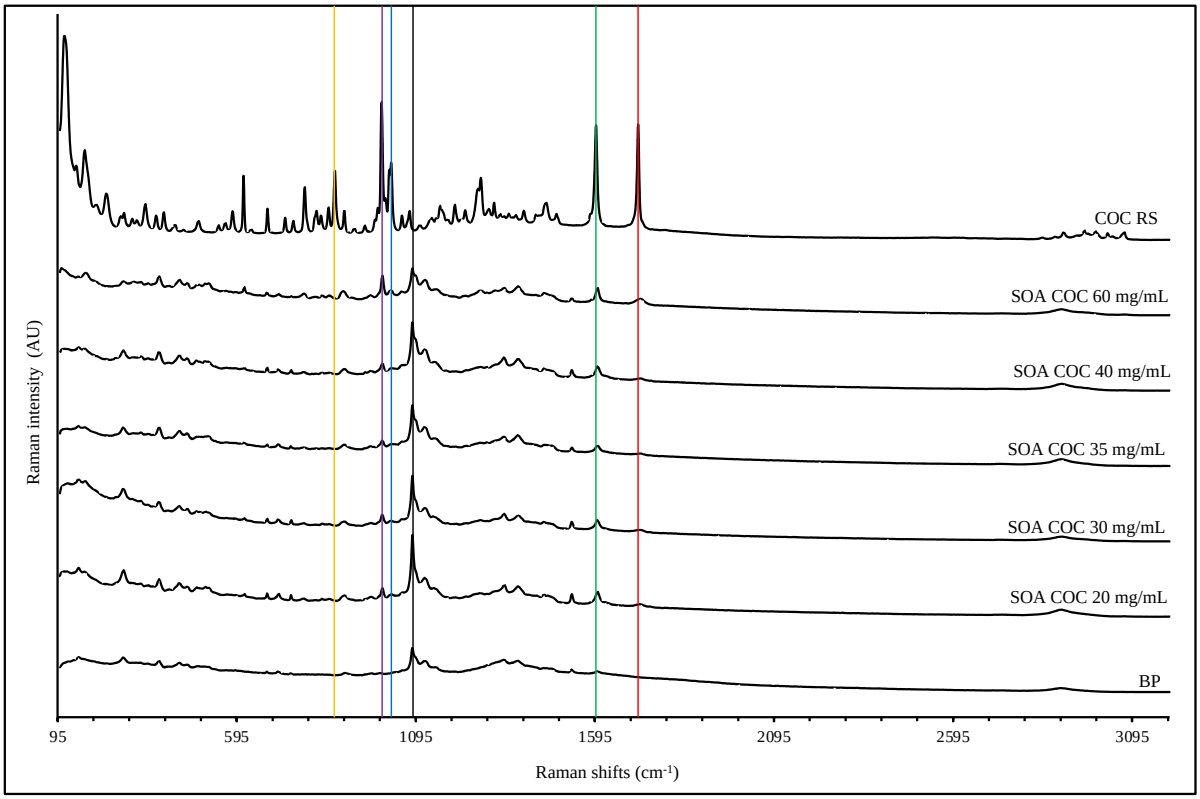

Figure A7. Raman Renishaw spectra of cocaine reference standard, cocaine soaked on paper at 60, 40, 35, 30 and 20 mg/mL and BP (from top to bottom).

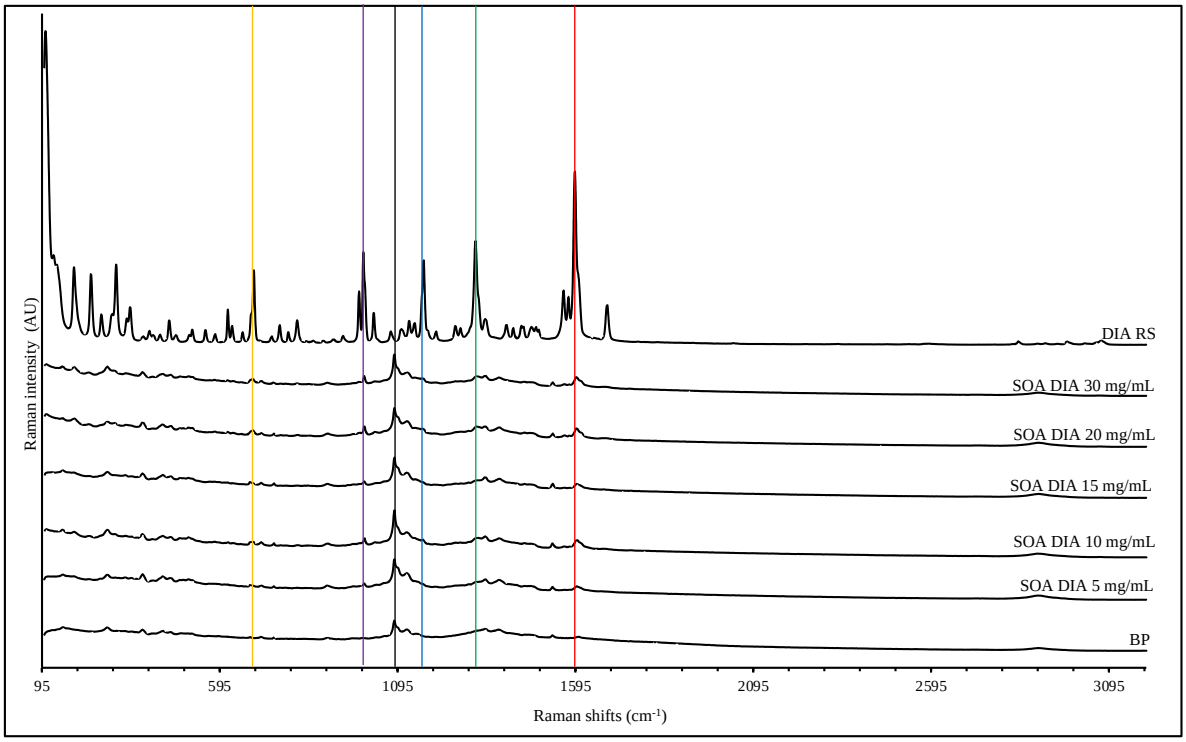

Figure A8. Raman Renishaw spectra of diazepam reference standard, diazepam soaked on paper at 30, 20, 15, 10 and 5 mg/mL and BP (from top to bottom).

Appendix 4.25. Raman Renishaw set 11 additional PCA plots

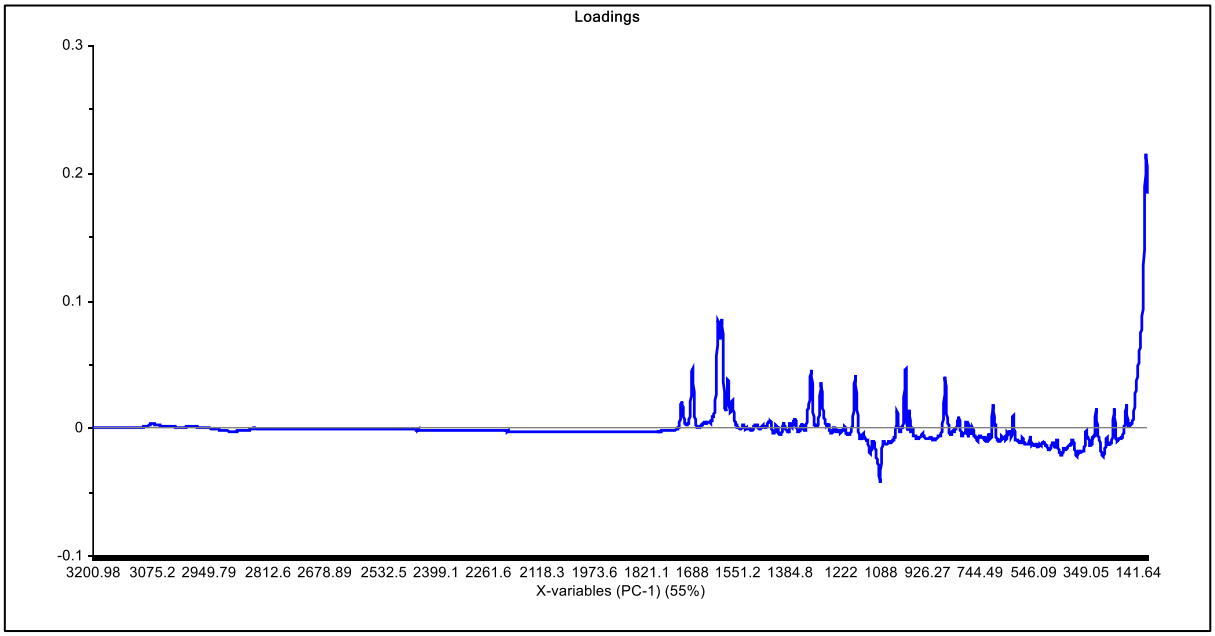

Figure A1. PC-1 loadings plot of set 11.

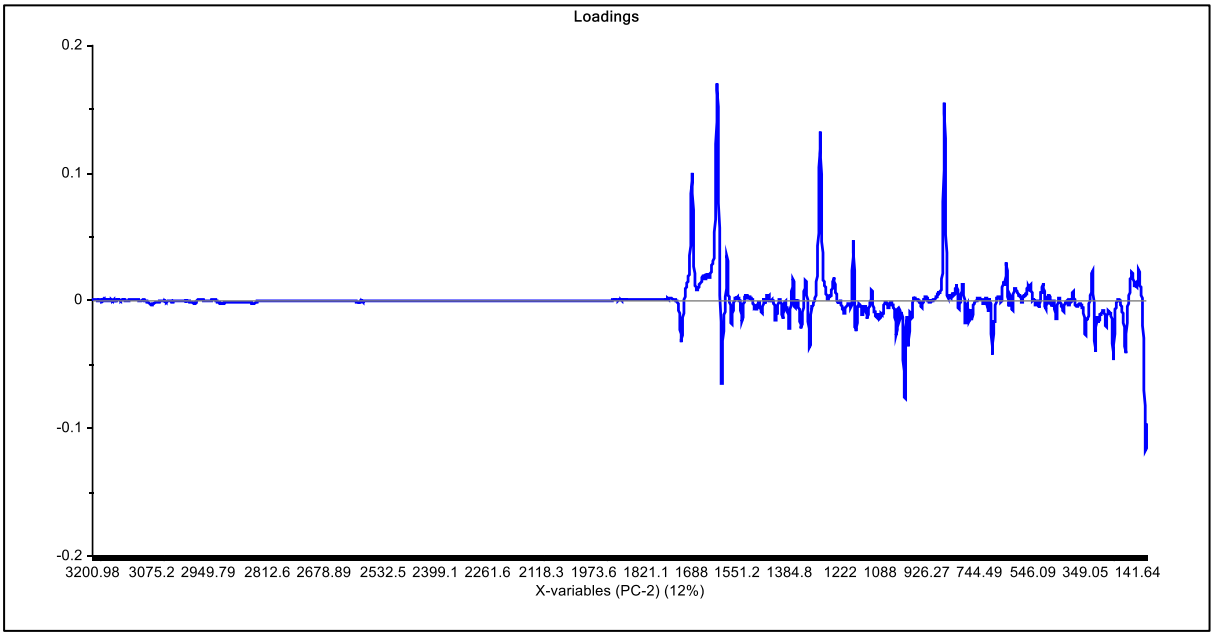

Figure A2. PC-2 loadings plot of set 11.

Appendix 4.26. Raman Renishaw additional PCA plots of set 11 recalculated without outliers

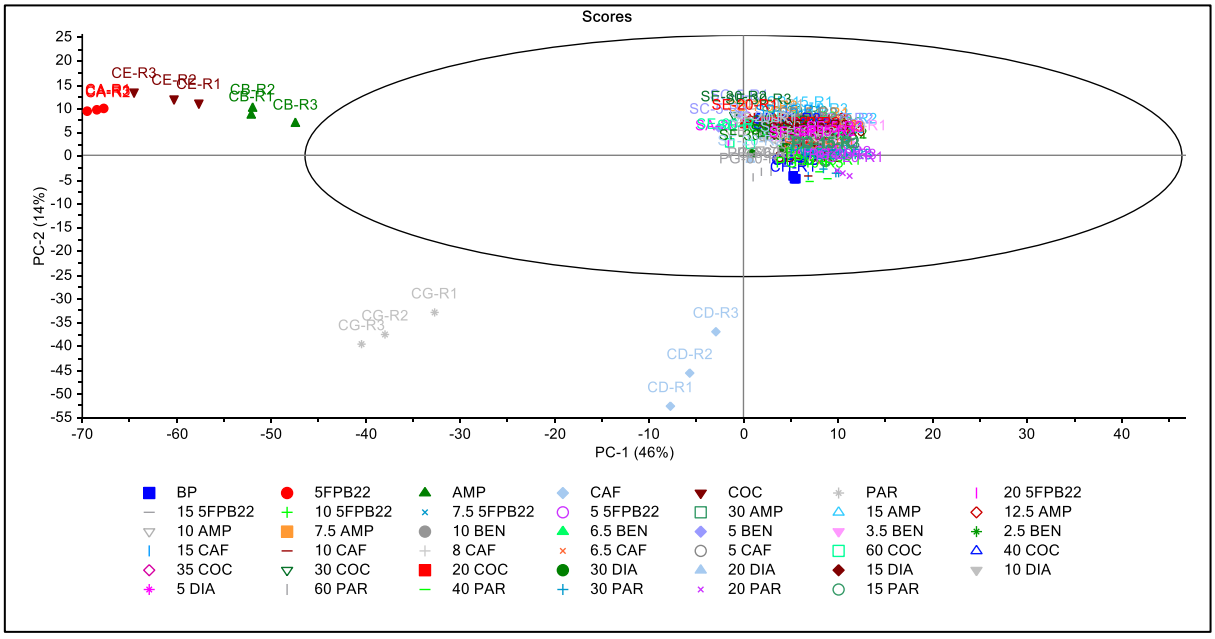

Figure A1. PC-1 vs PC-2 2D scores plot of set 11 recalculated without outliers

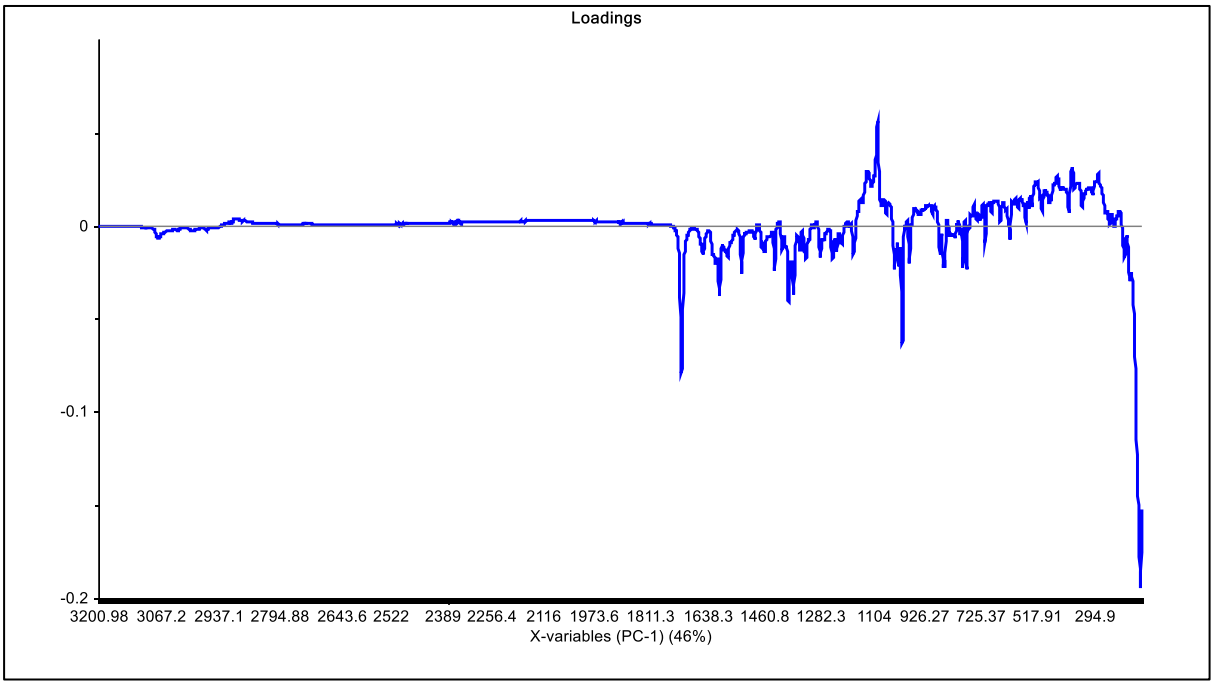

Figure A2. PC-1 loadings plot of set 11 recalculated without outliers.

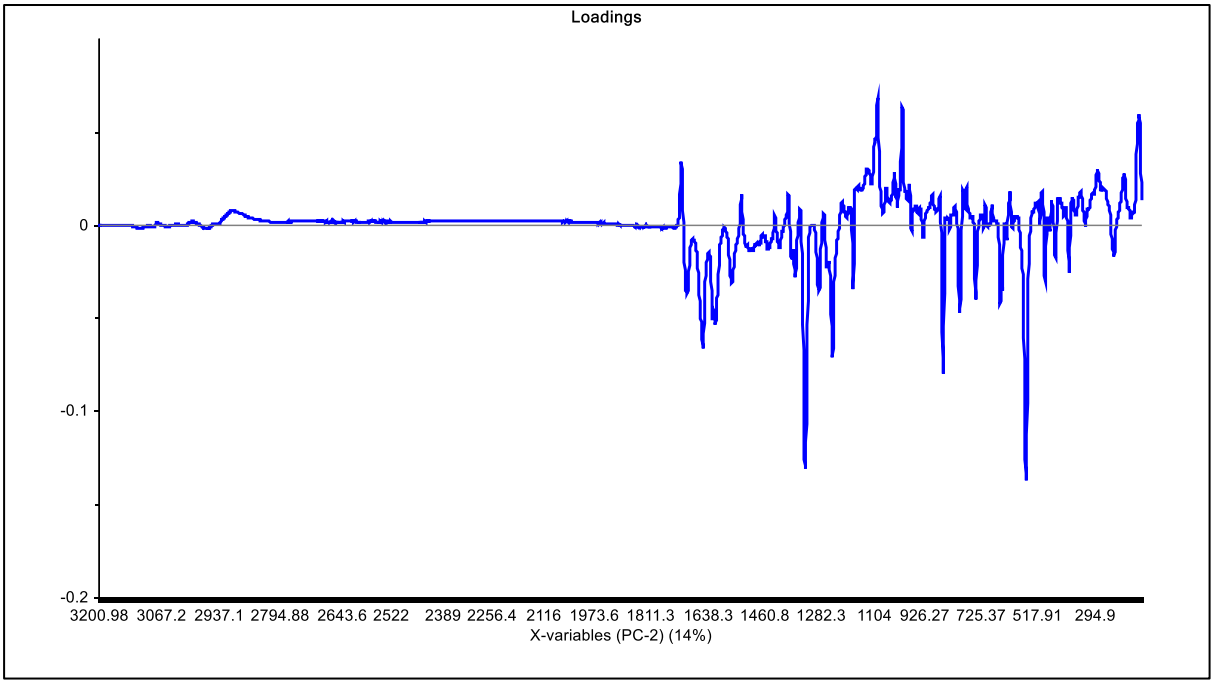

Figure A3. PC-2 loadings plot of set 11 recalculated without outliers.

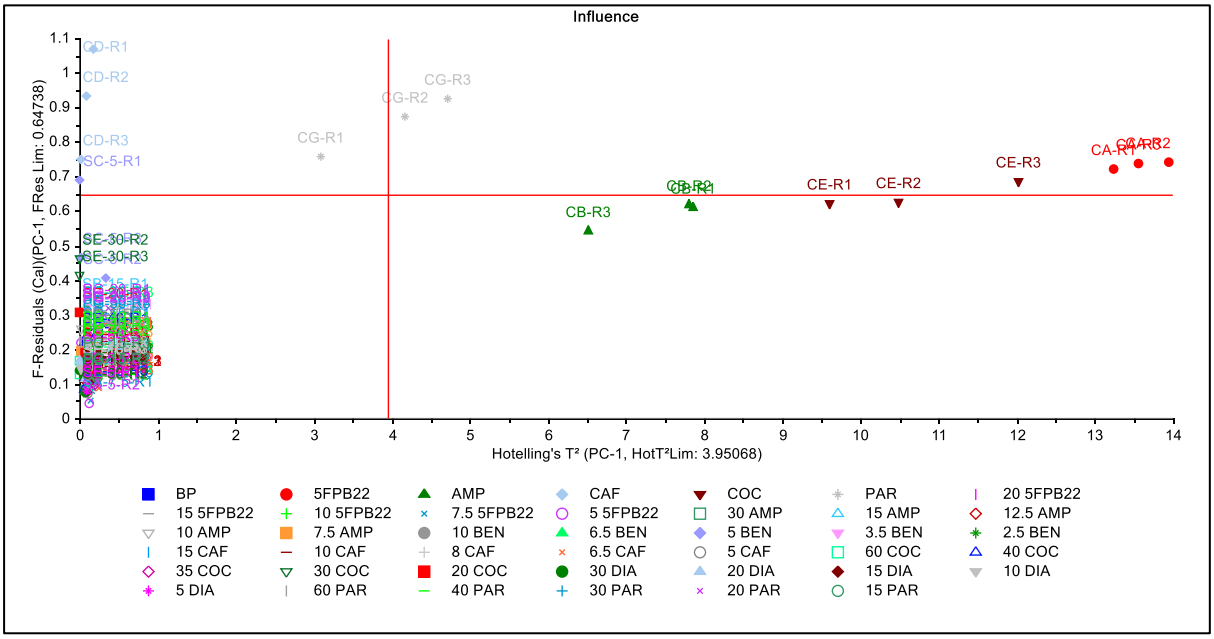

Figure A4. PC-1 F-residuals vs Hotelling T^2 influence plots of set 11 recalculated without outliers.

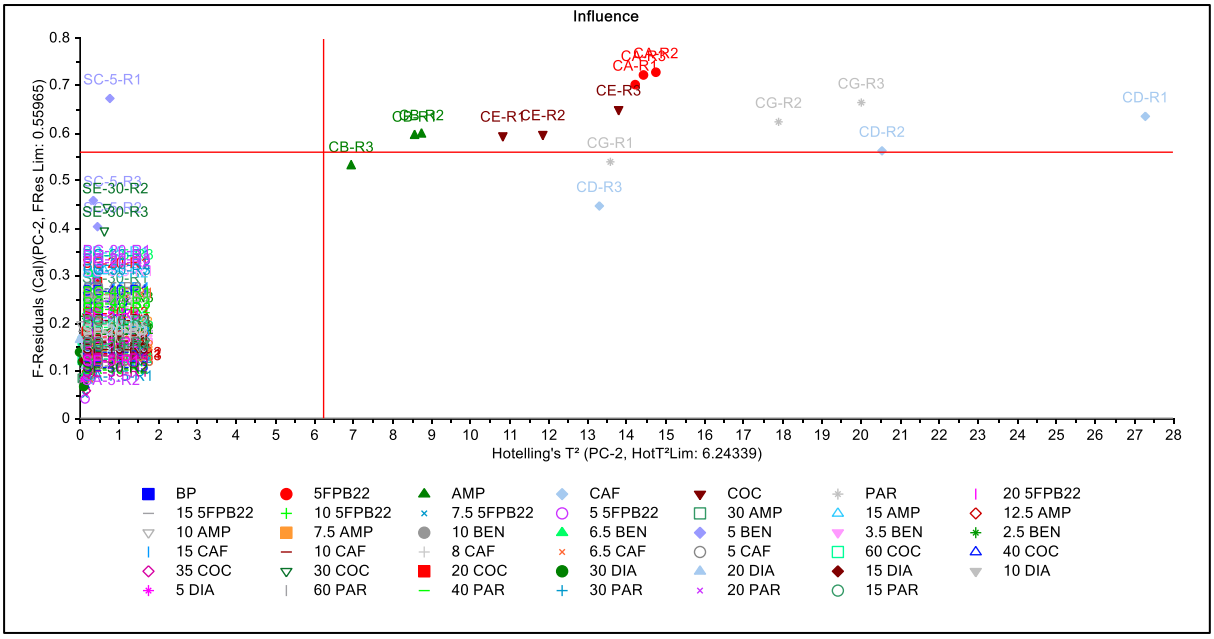

Figure A5. PC-2 F-residuals vs Hotelling T^2 influence plots of set 11 recalculated without outliers.

Appendix 4.27. Raman Rigaku set 12 additional PCA plots

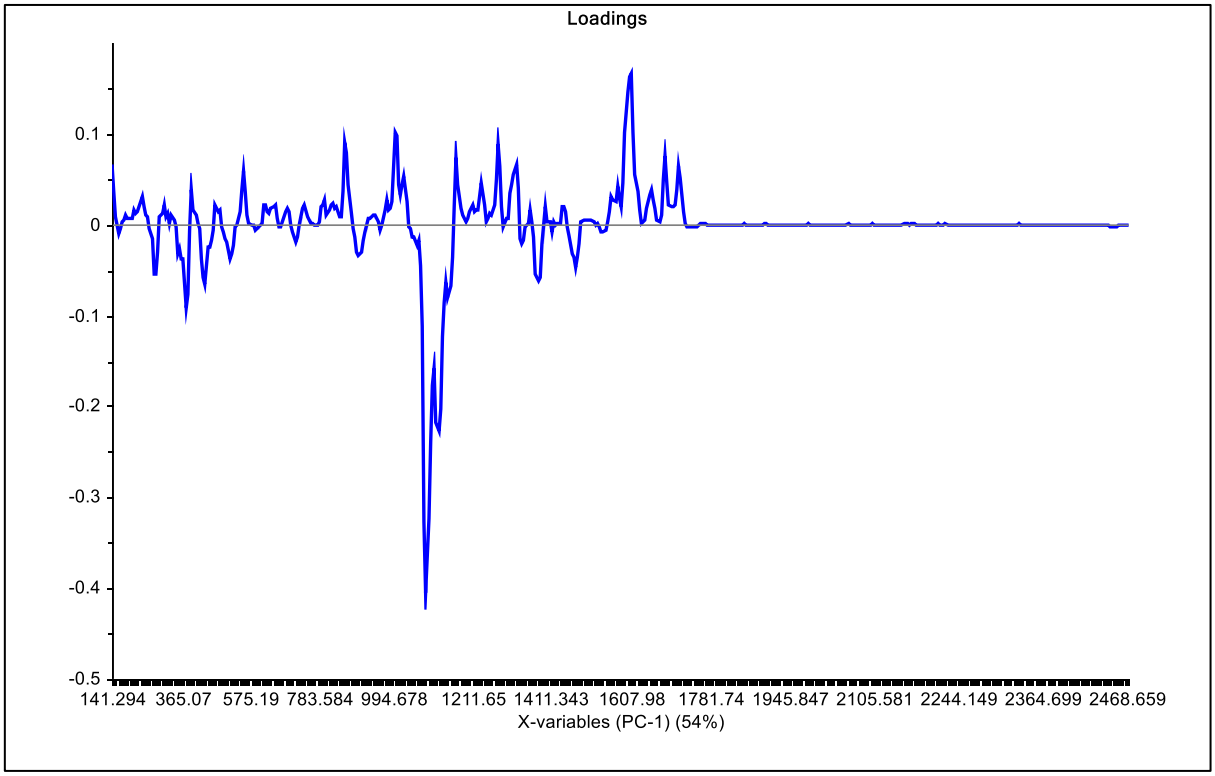

Figure A1. PC-1 loadings plot of set 12.

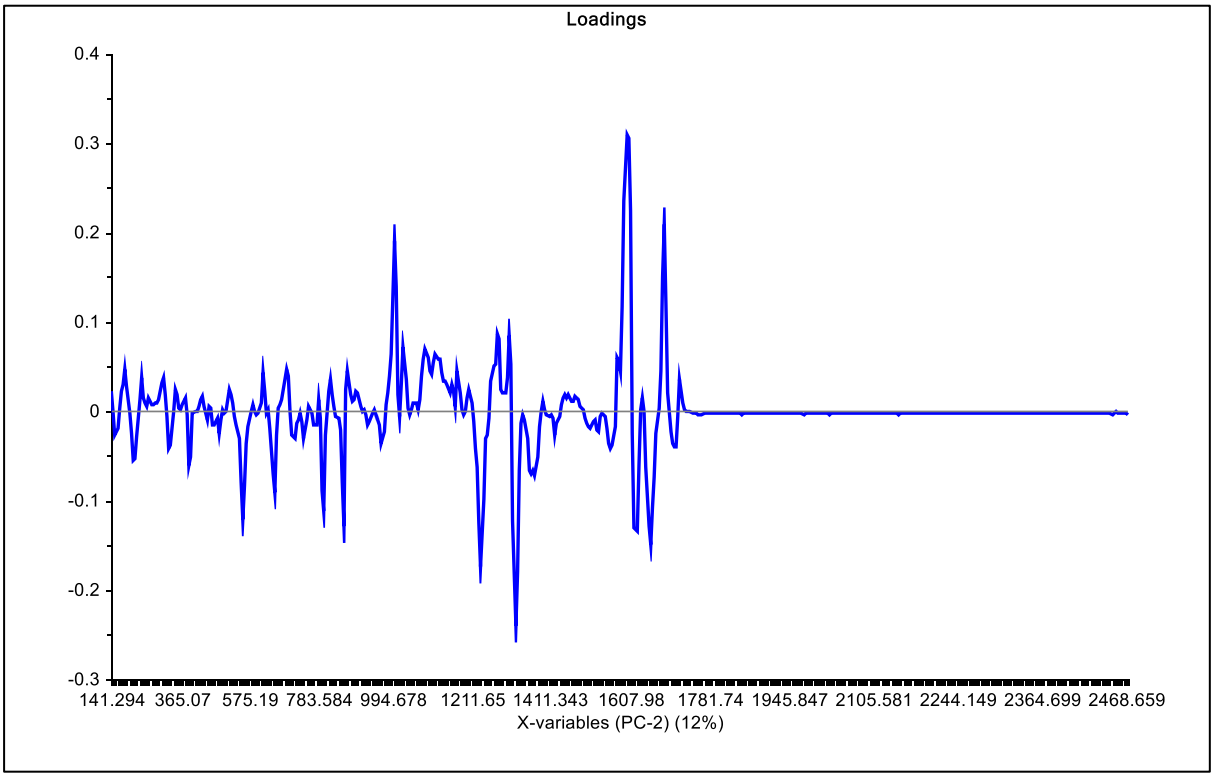

Figure A2. PC-2 loadings plot of set 12.

Appendix 4.28. Raman Rigaku additional PCA plots of set 12 recalculated without outliers

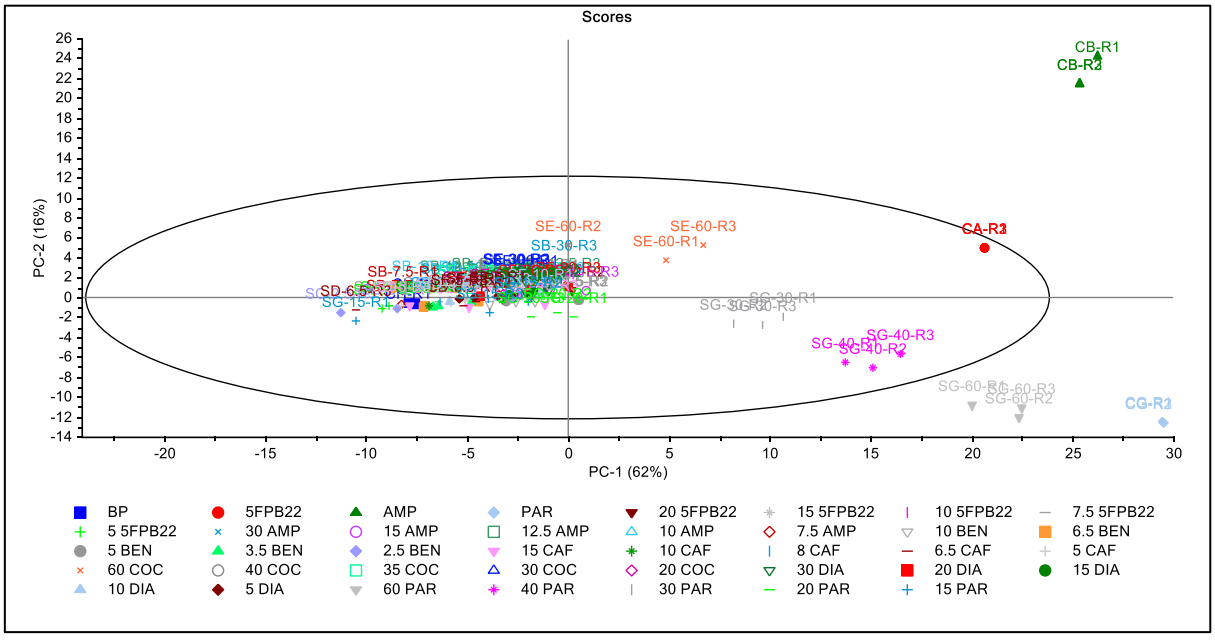

Figure A1. PC-1 vs PC-2 2D scores plot of set 12 recalculated without outliers.

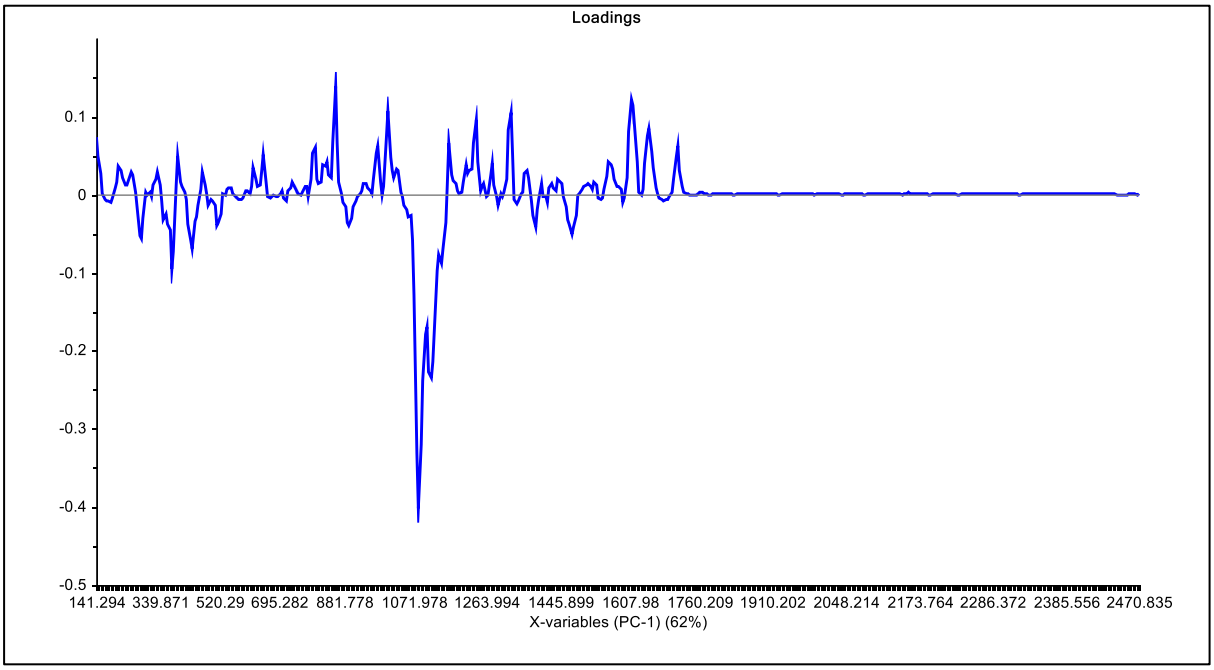

Figure A2. PC-1 loadings plot of set 12 recalculated without outliers.

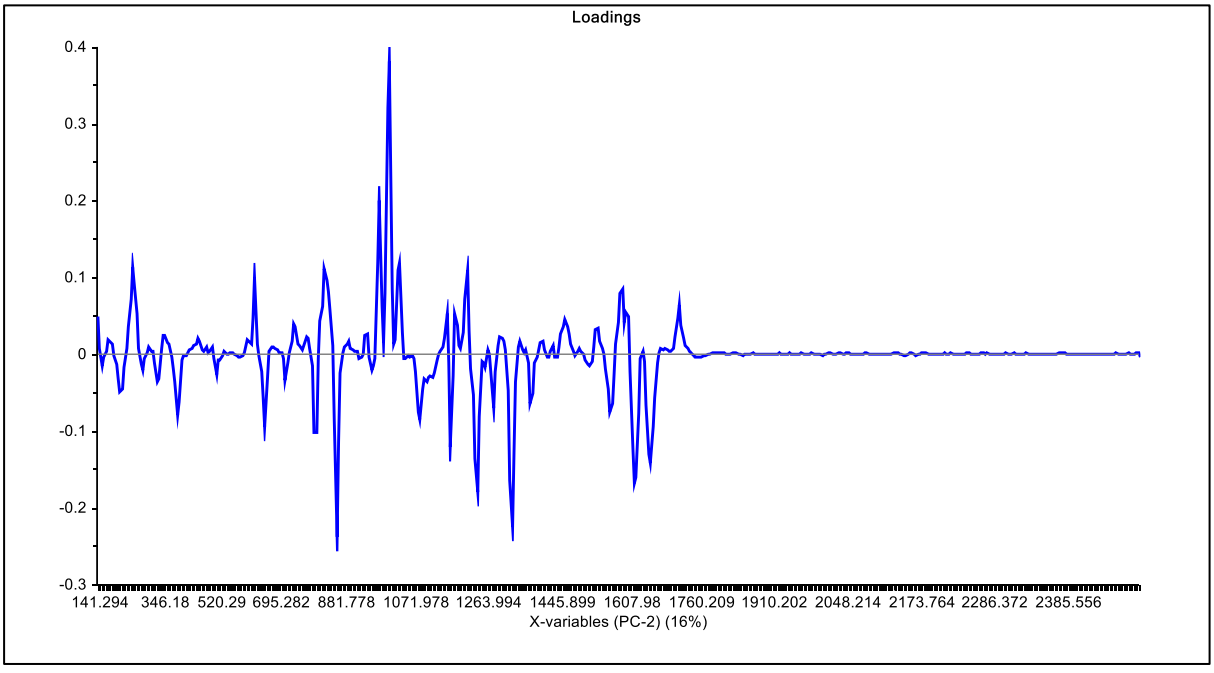

Figure A3. PC-2 loadings plot of set 12 recalculated without outliers.

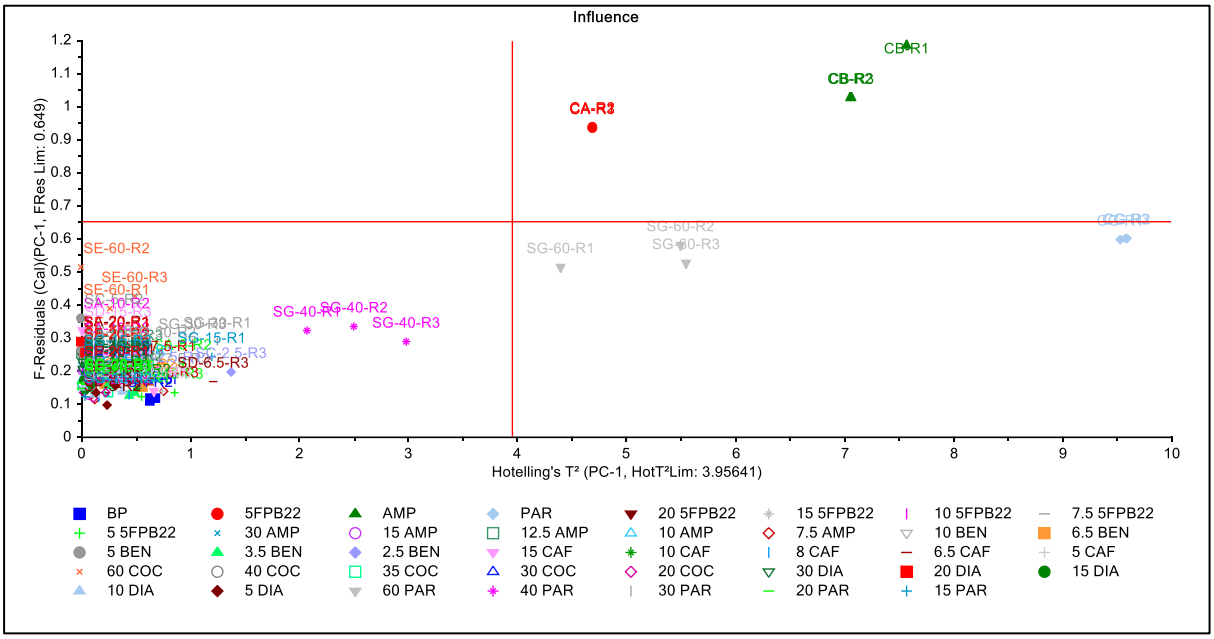

Figure A4. PC-1 F-residuals vs Hotelling T^2 influence plots of set 12 recalculated without outliers.

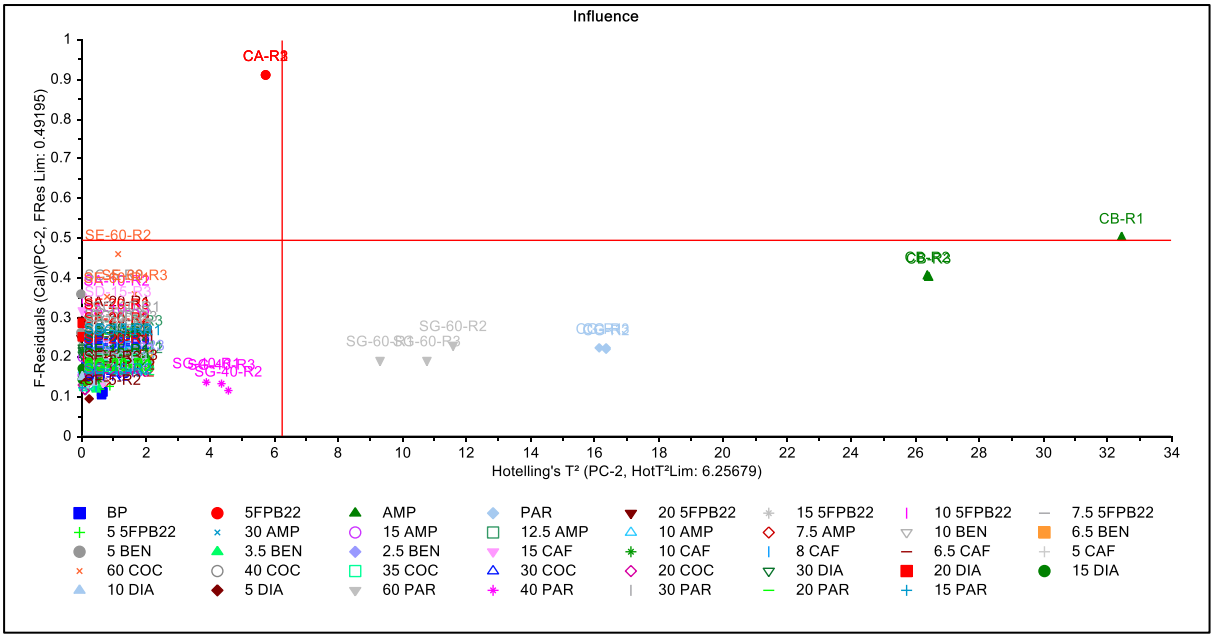

Figure A5. PC-2 F-residuals vs Hotelling T^2 influence plots of set 12 recalculated without outliers.

Appendix 4.29. Raman Renishaw set 13 additional PCA plots

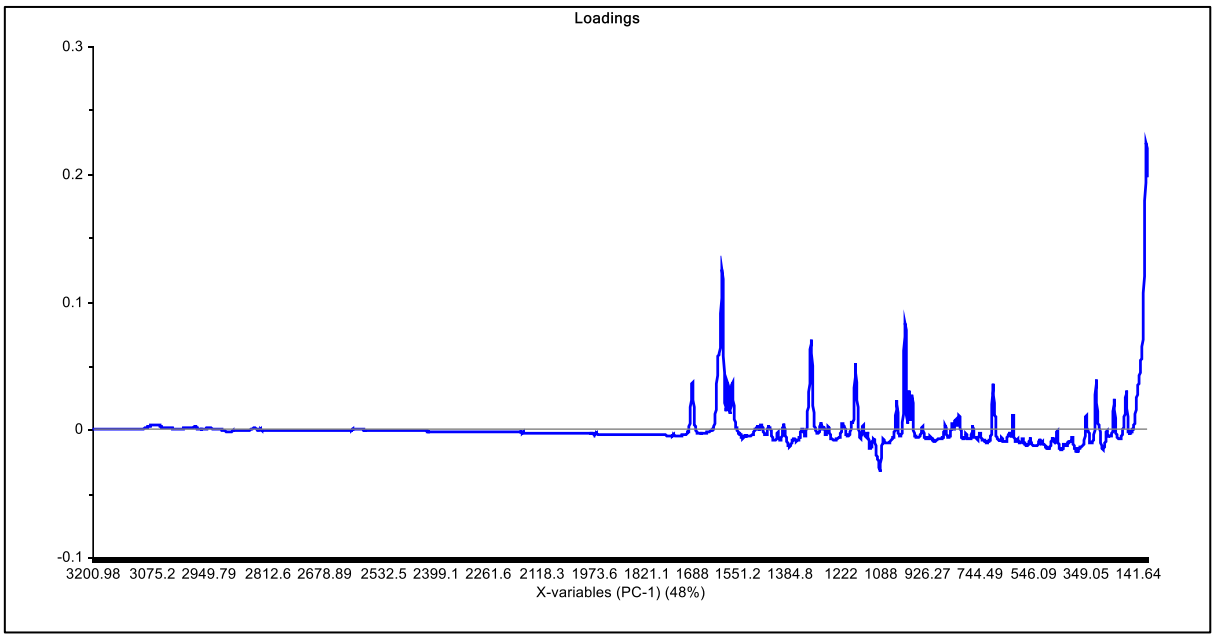

Figure A1. PC-1 loadings plot of set 13.

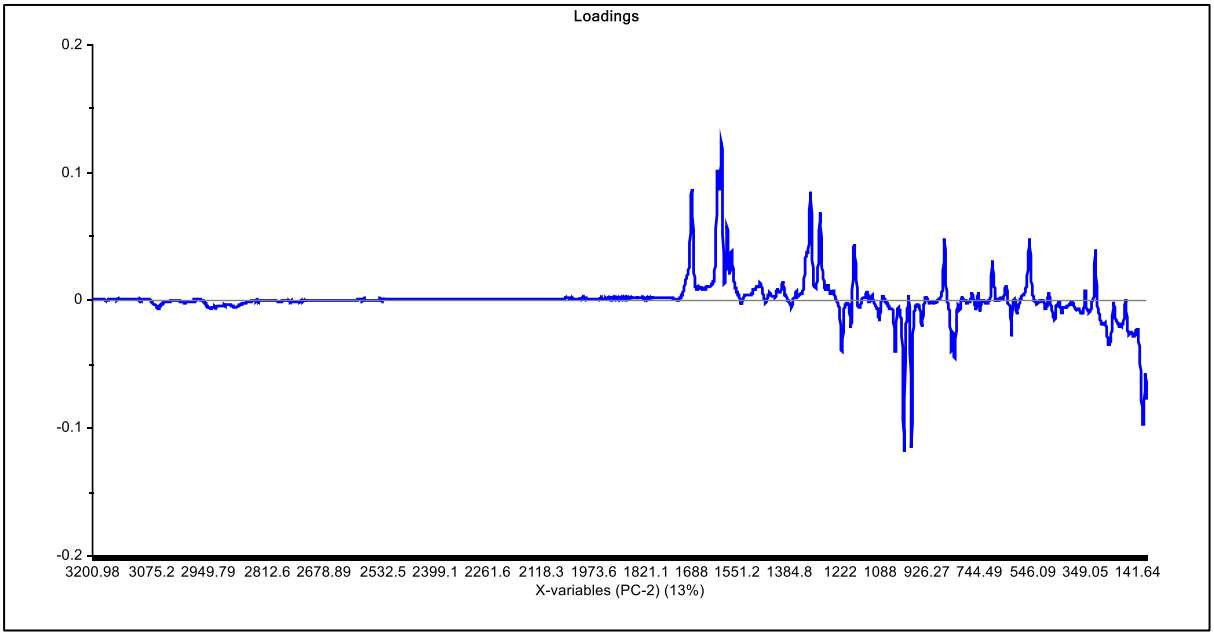

Figure A2. PC-2 loadings plot of set 13.

Appendix 4.30. Raman Renishaw additional PCA plots of set 13 recalculated without outliers

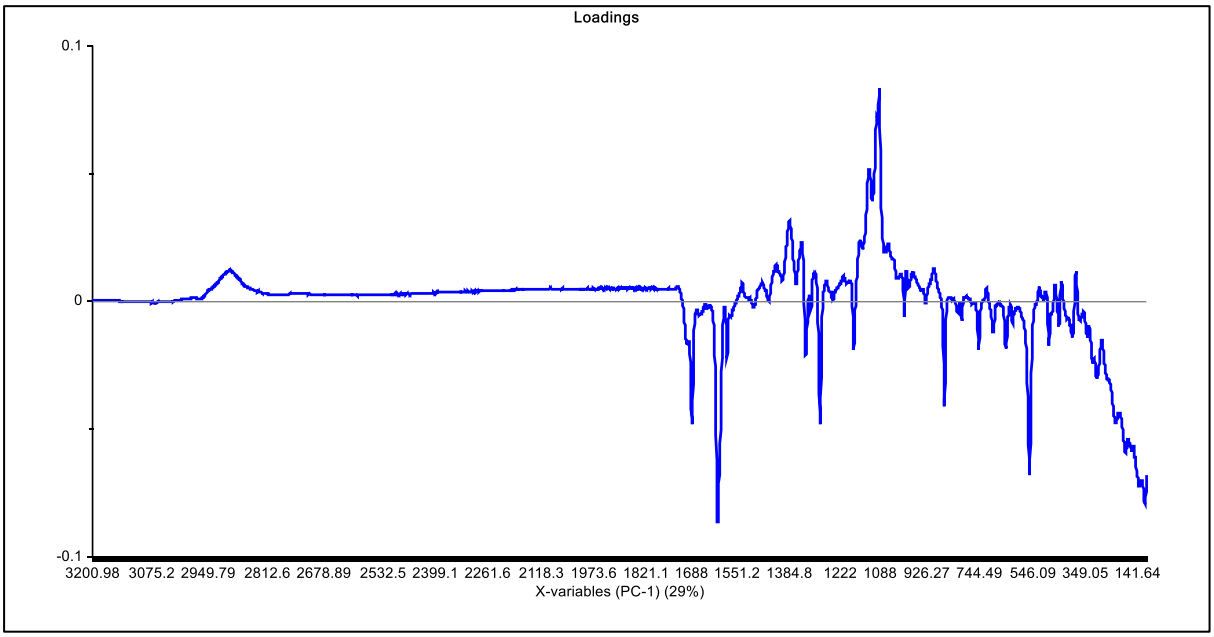

Figure A1. PC-1 loadings plot of set 13 recalculated without outliers.

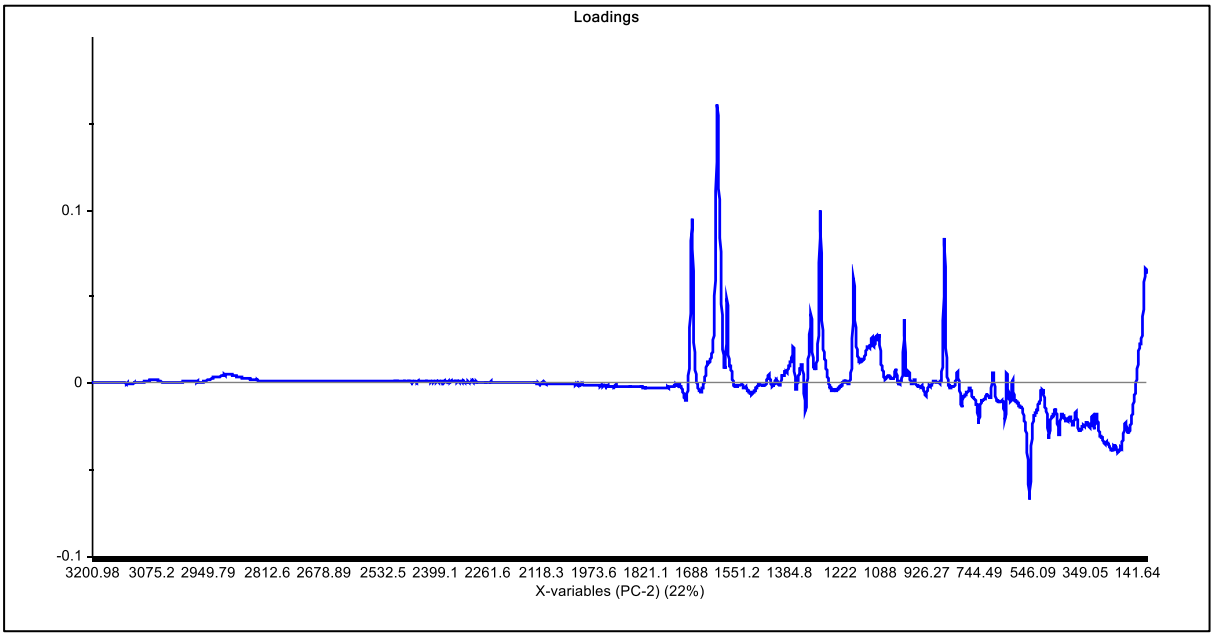

Figure A2. PC-2 loadings plot of set 13 recalculated without outliers.

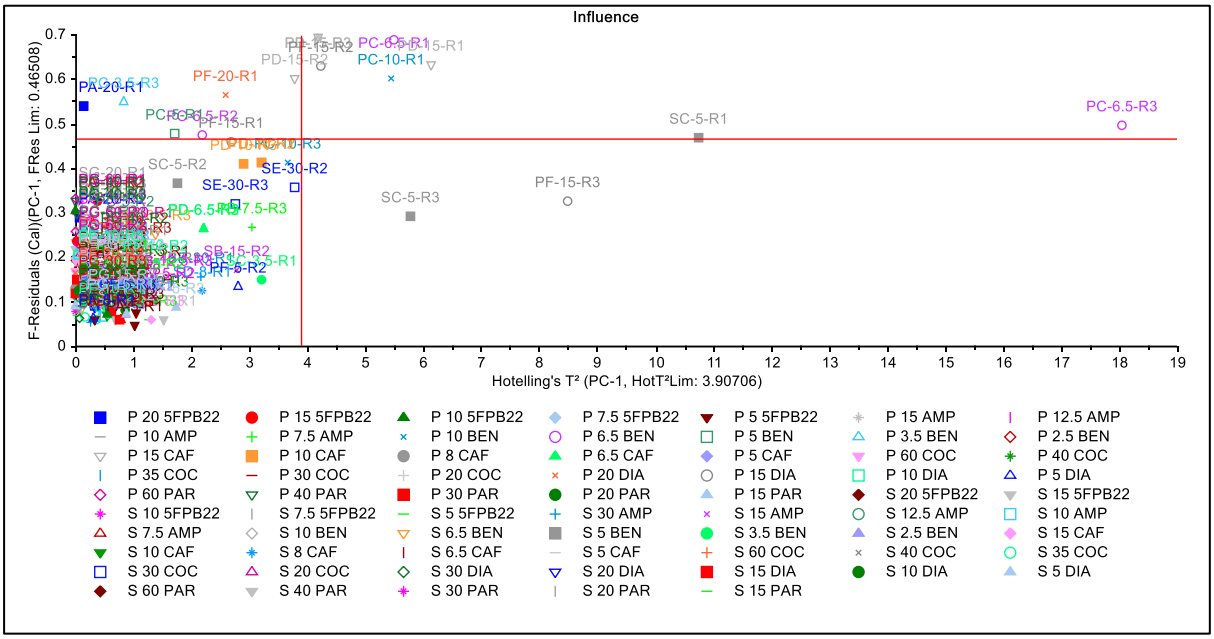

Figure A3. PC-1 F-residuals vs Hotelling T^2 influence plots of set 13 recalculated without outliers.

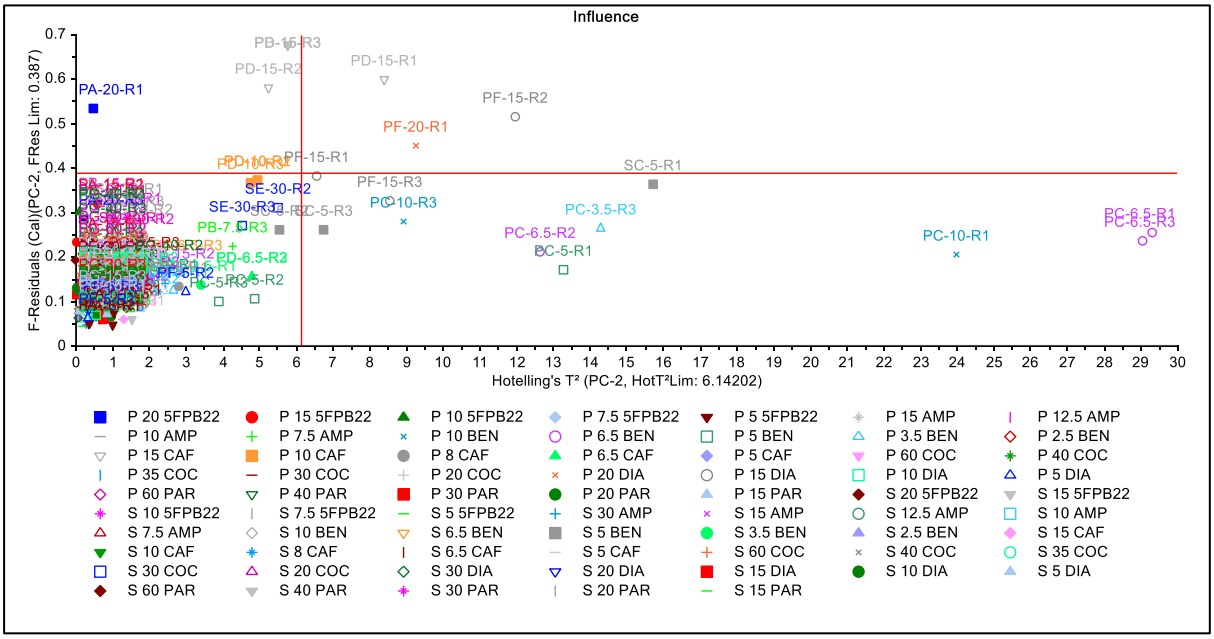

Figure A4. PC-2 F-residuals vs Hotelling T^2 influence plots of set 13 recalculated without outliers.

Appendix 4.31. Raman Rigaku set 14 additional PCA plots

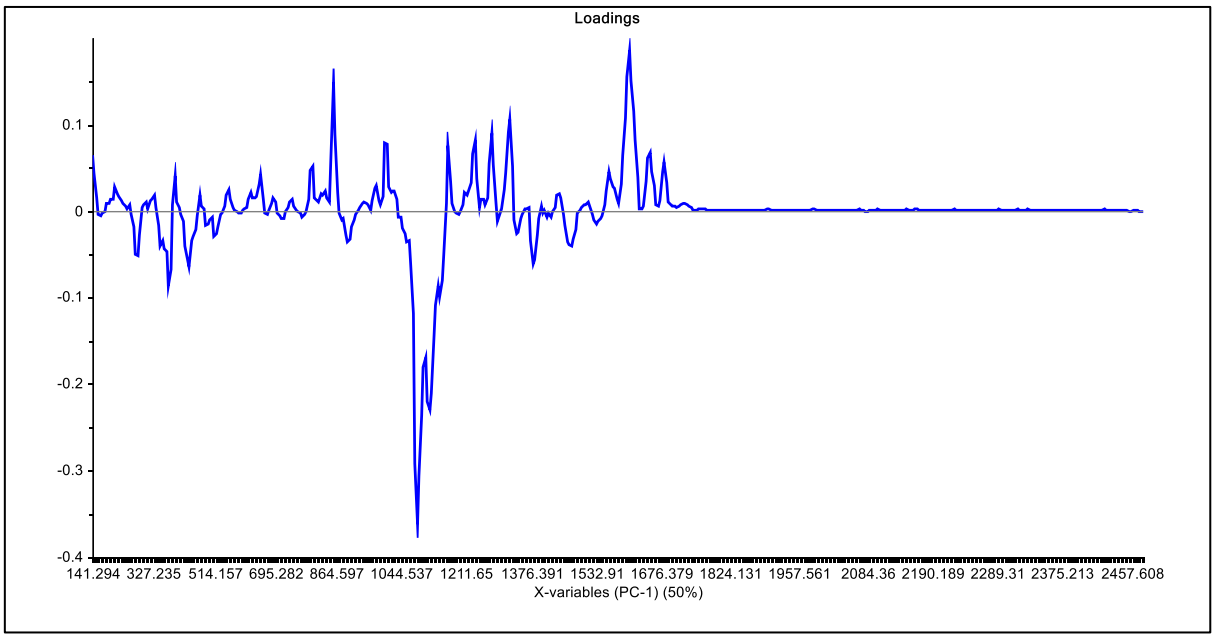

Figure A1. PC-1 loadings plot of set 14.

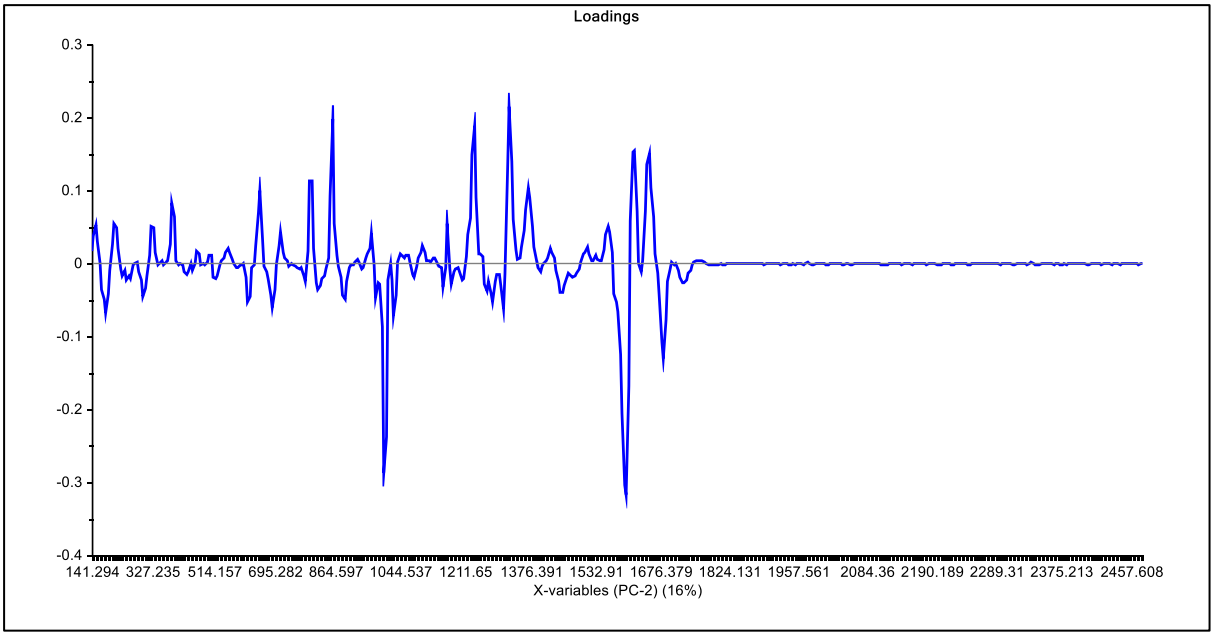

Figure A2. PC-2 loadings plot of set 14.

Appendix 4.32. Raman Rigaku additional PCA plots of set 14 recalculated without outliers

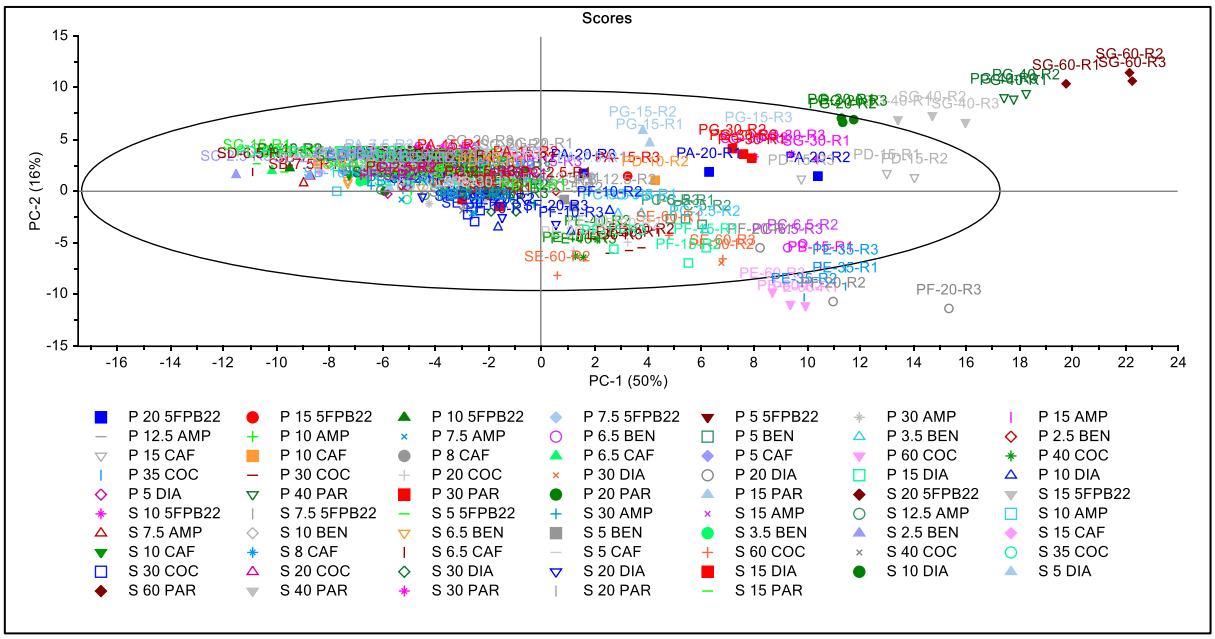

Figure A1. PC-1 vs PC-2 2D scores plot of set 14 recalculated without outliers.

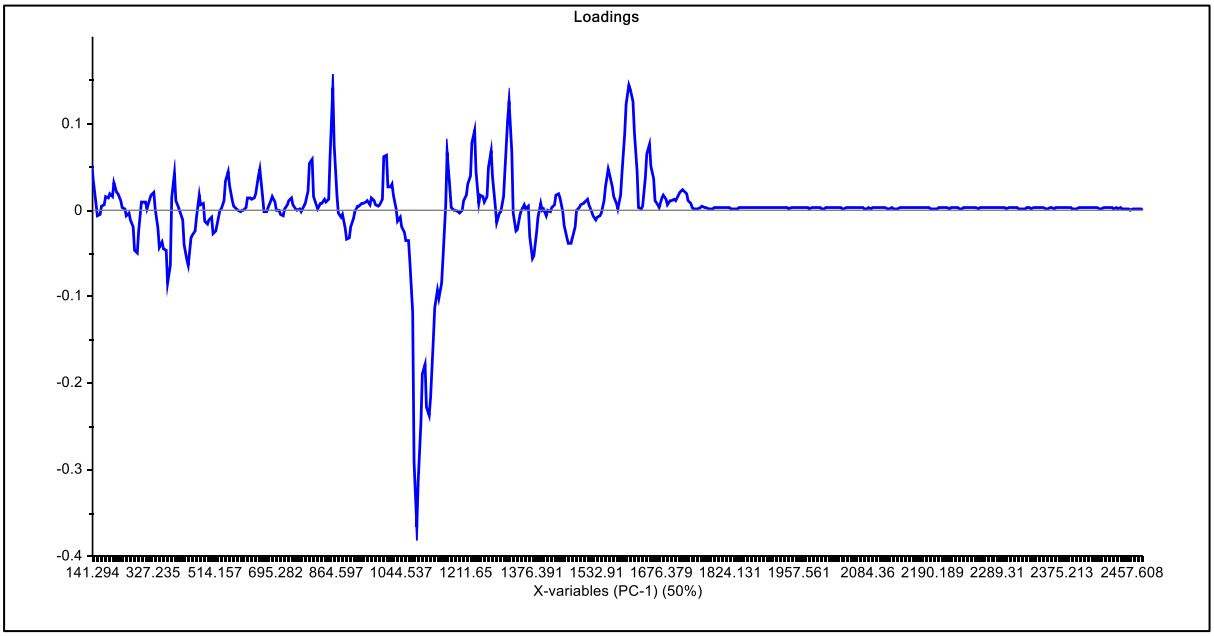

Figure A2. PC-1 loadings plot of set 14 recalculated without outliers.

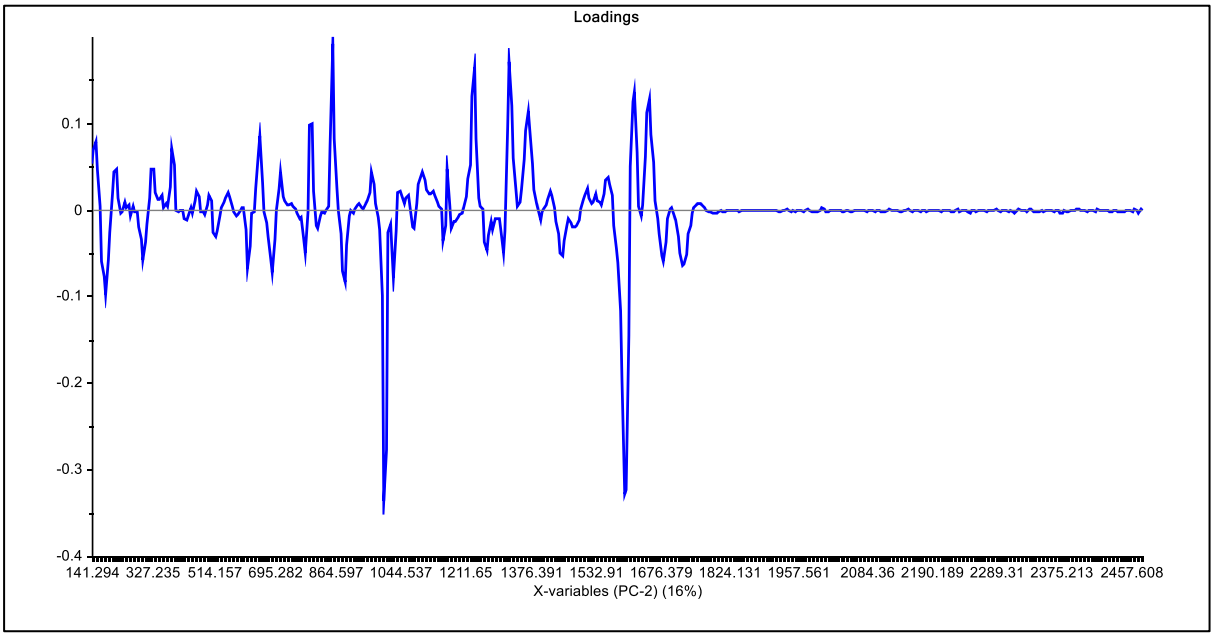

Figure A3. PC-2 loadings plot of set 14 recalculated without outliers.

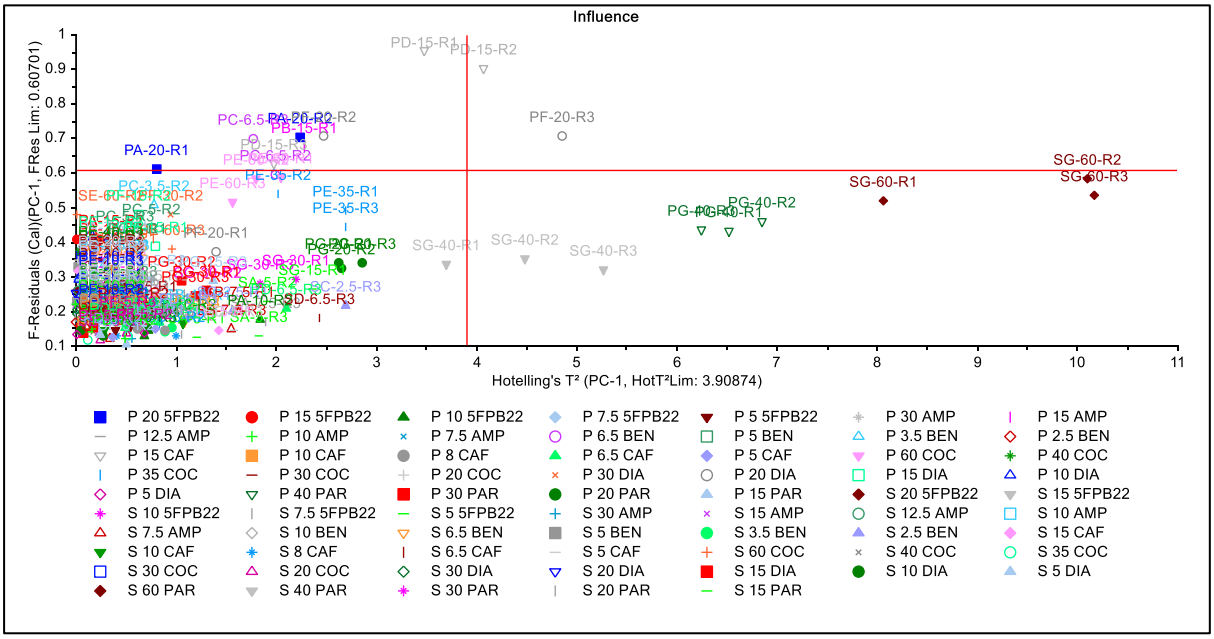

Figure A4. PC-1 F-residuals vs Hotelling T^2 influence plots of set 14 recalculated without outliers.

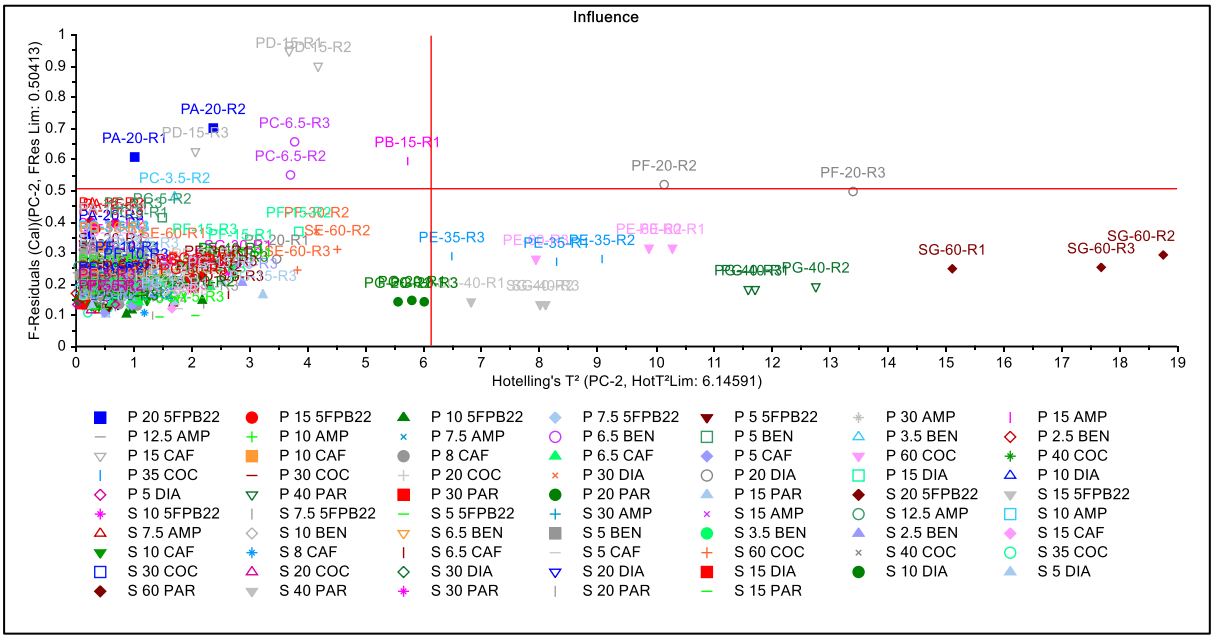

Figure A5. PC-2 F-residuals vs Hotelling T^2 influence plots of set 14 recalculated without outliers.

Appendix 4.33. Raman Rigaku set 15 additional PCA plots

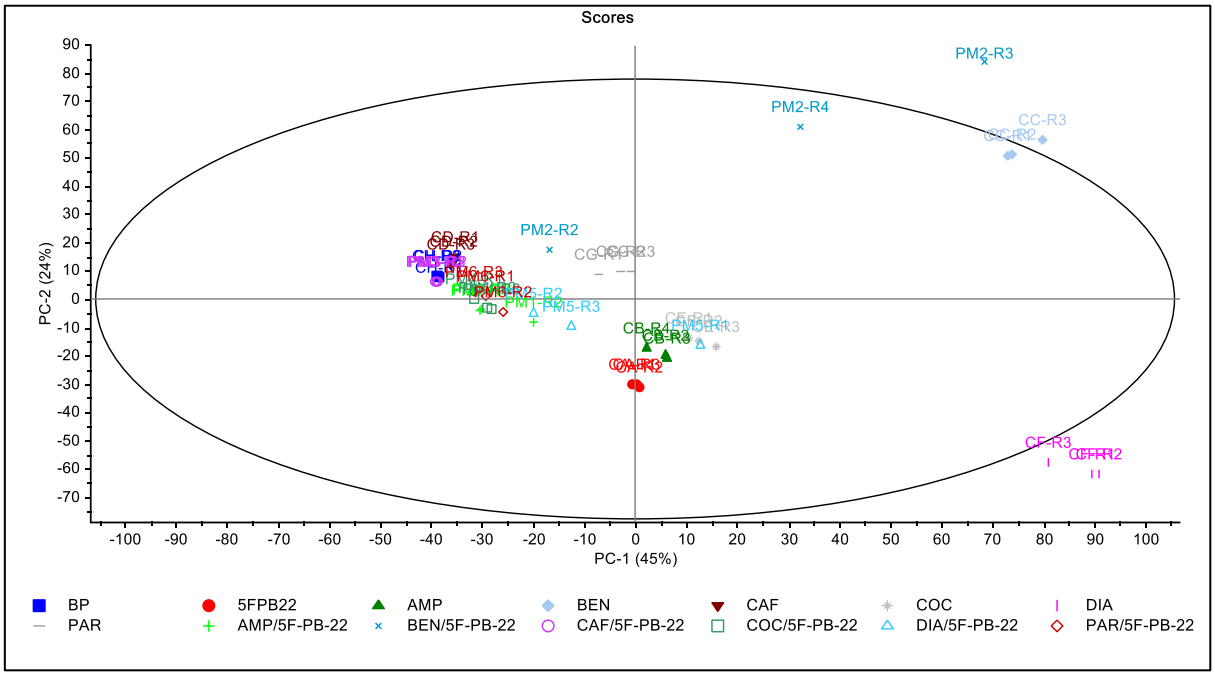

Figure A1. PC-1 vs PC-2 2D scores plot of set 15.

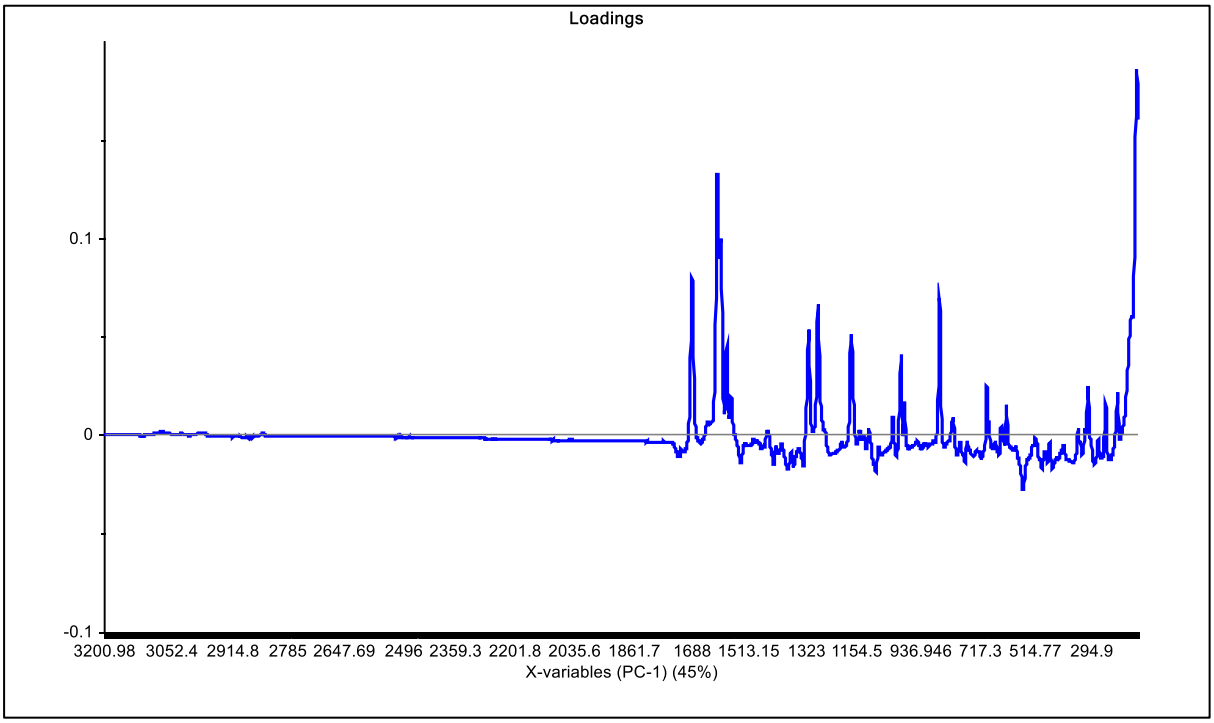

Figure A2. PC-1 loadings plot of set 15.

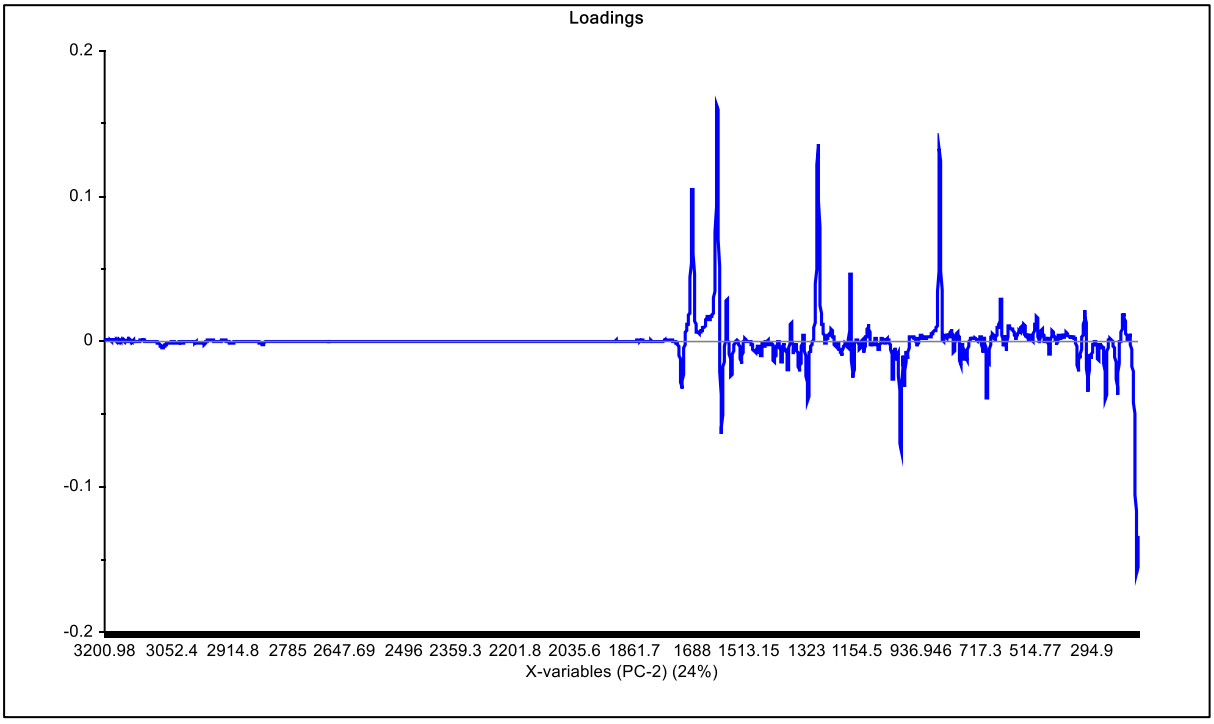

Figure A3. PC-2 loadings plot of set 15.

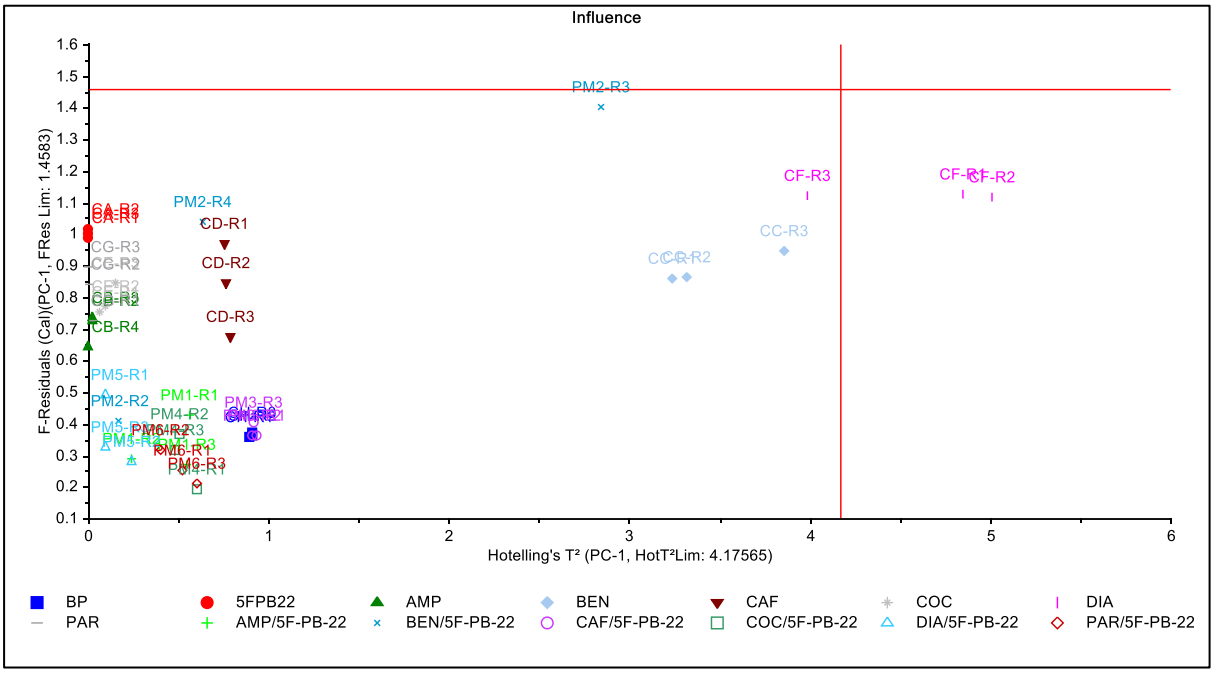

Figure A4. PC-1 F-residuals vs Hotelling T^2 influence plots of set 15.

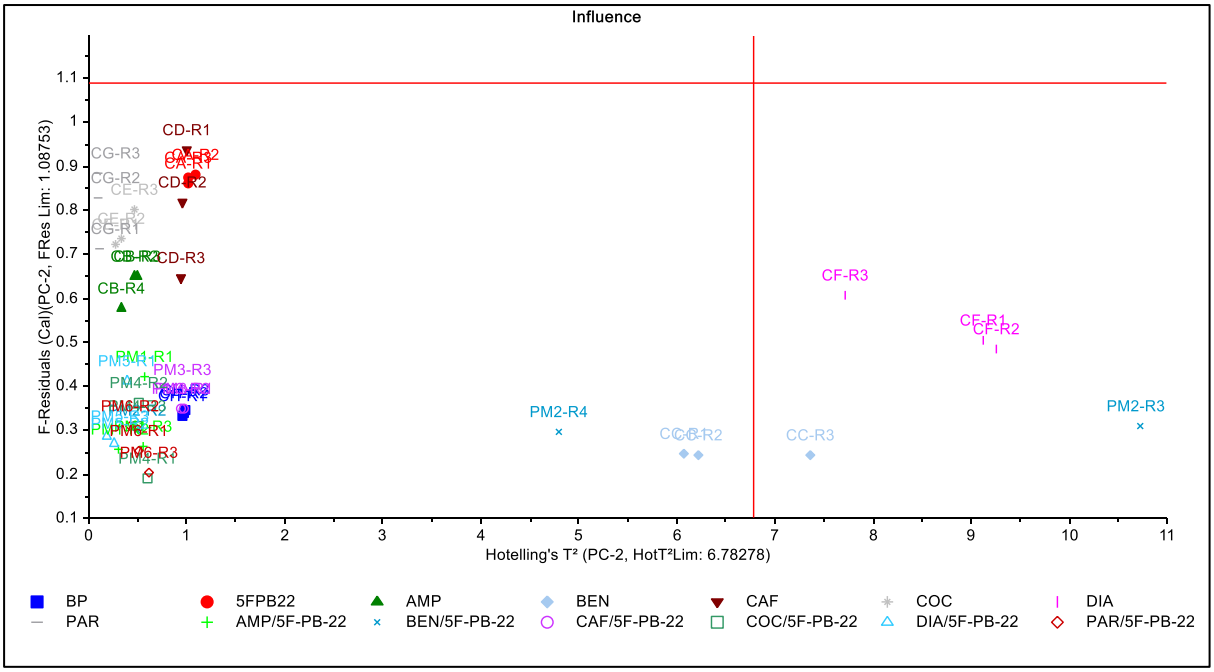

Figure A5. PC-2 F-residuals vs Hotelling T^2 influence plots of set 15.

Appendix 4.34. Raman Renishaw set 16 additional PCA plots

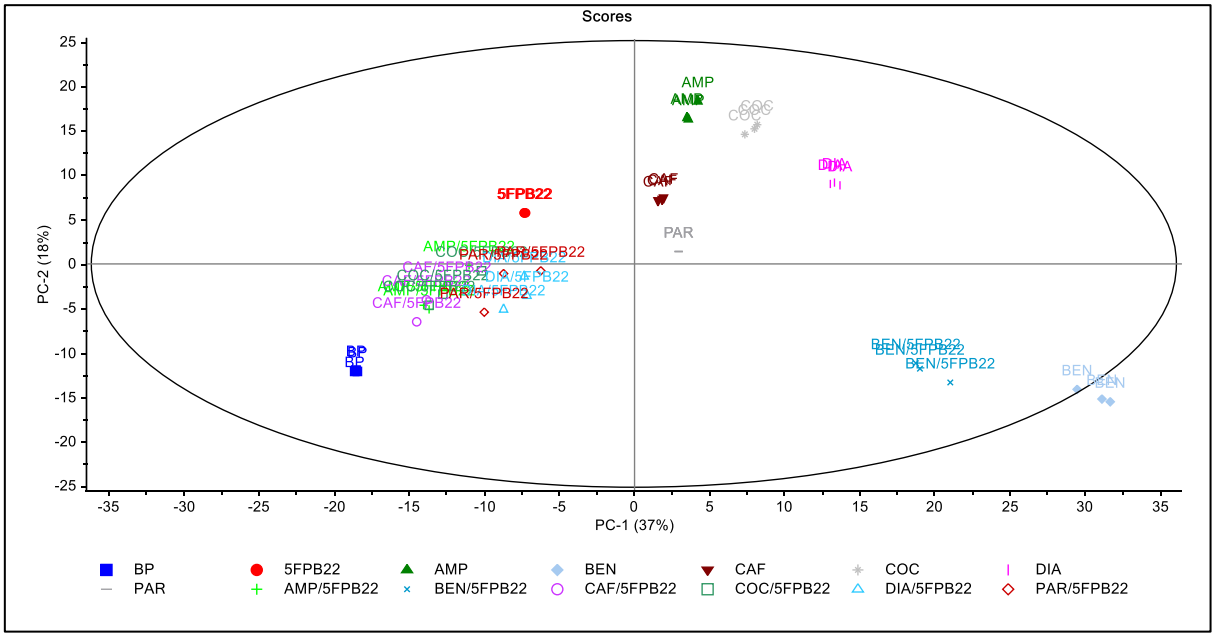

Figure A1. PC-1 vs PC-2 2D scores plot of set 16.

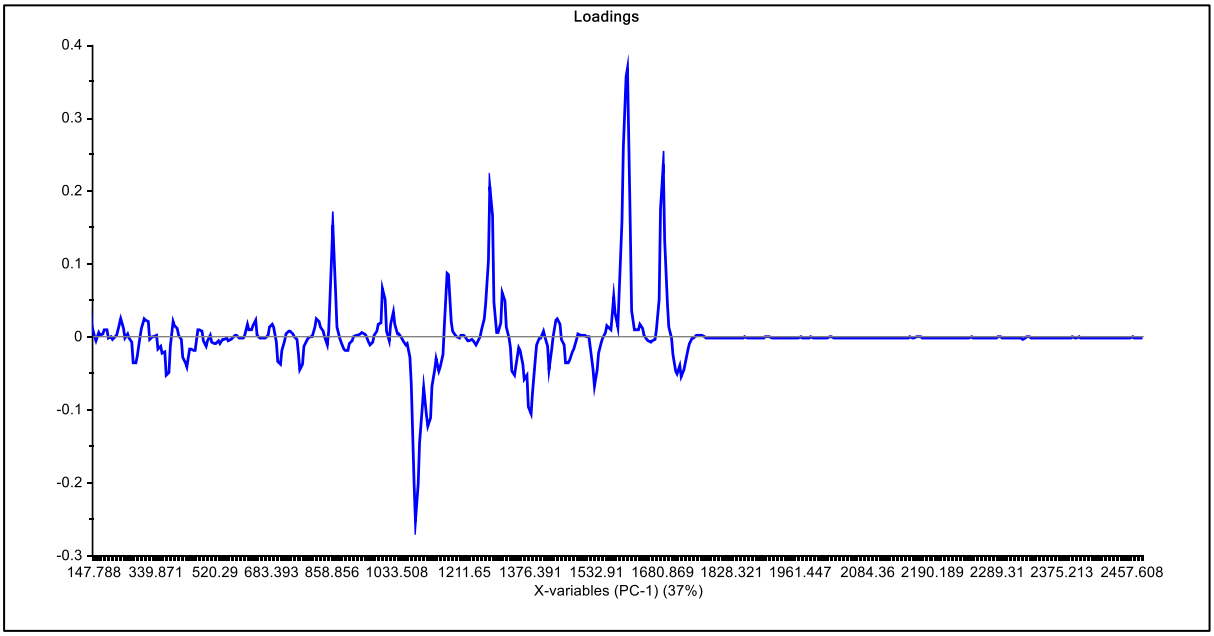

Figure A2. PC-1 loadings plot of set 16.

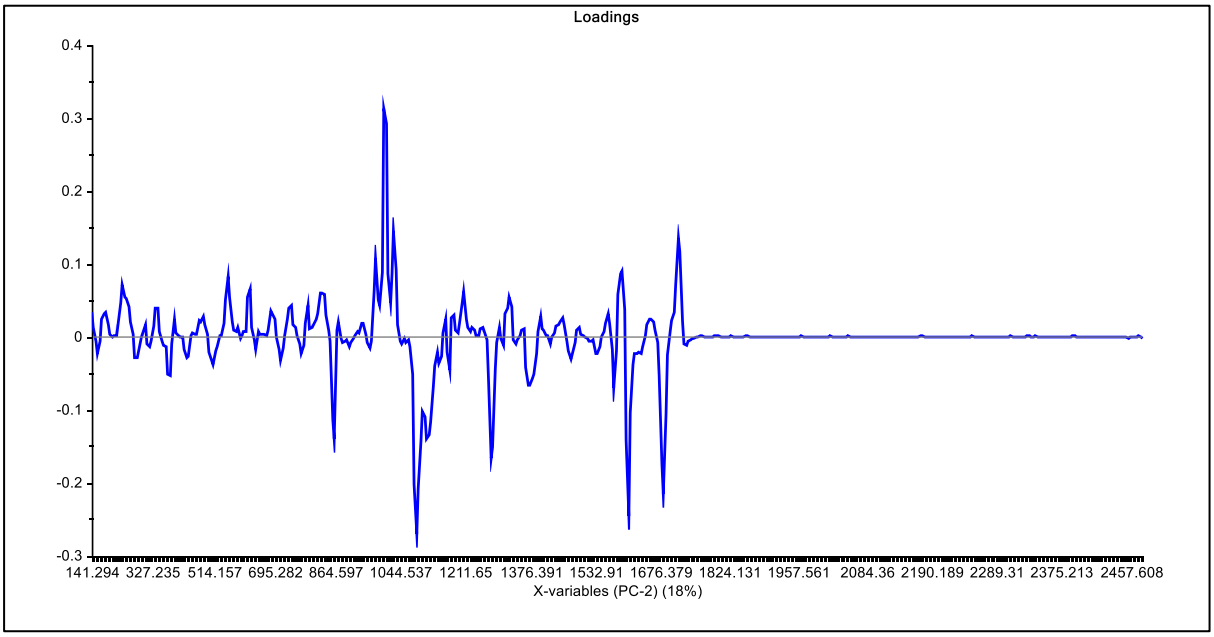

Figure A3. PC-2 loadings plot of set 16.

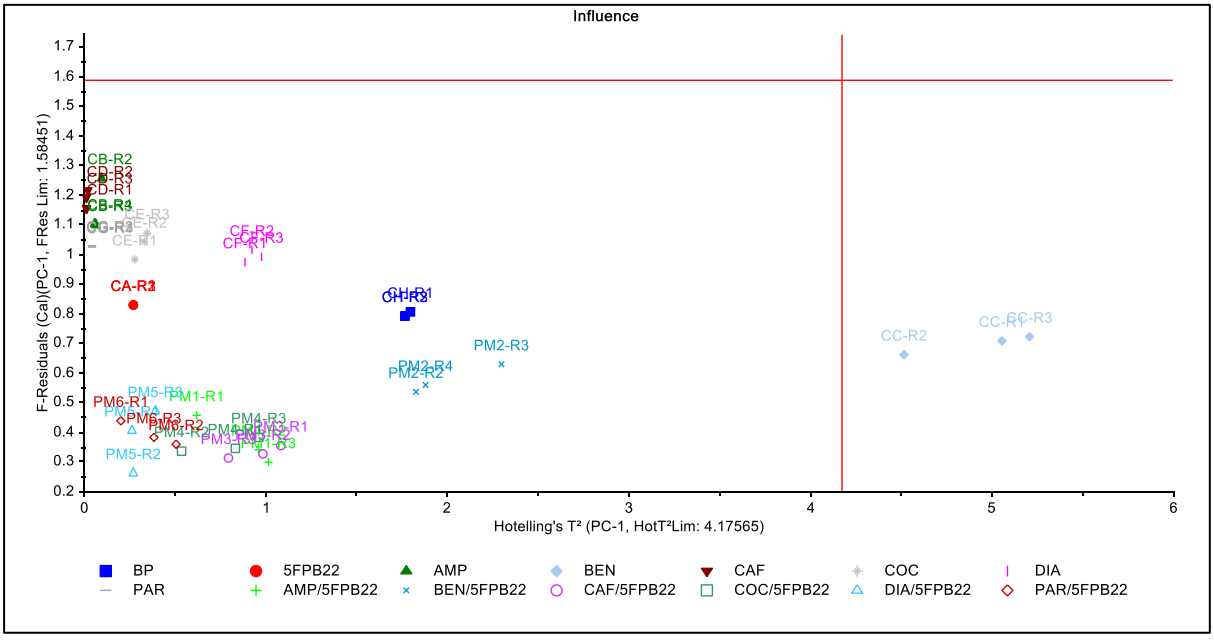

Figure A4. PC-1 F-residuals vs Hotelling T^2 influence plots of set 16.

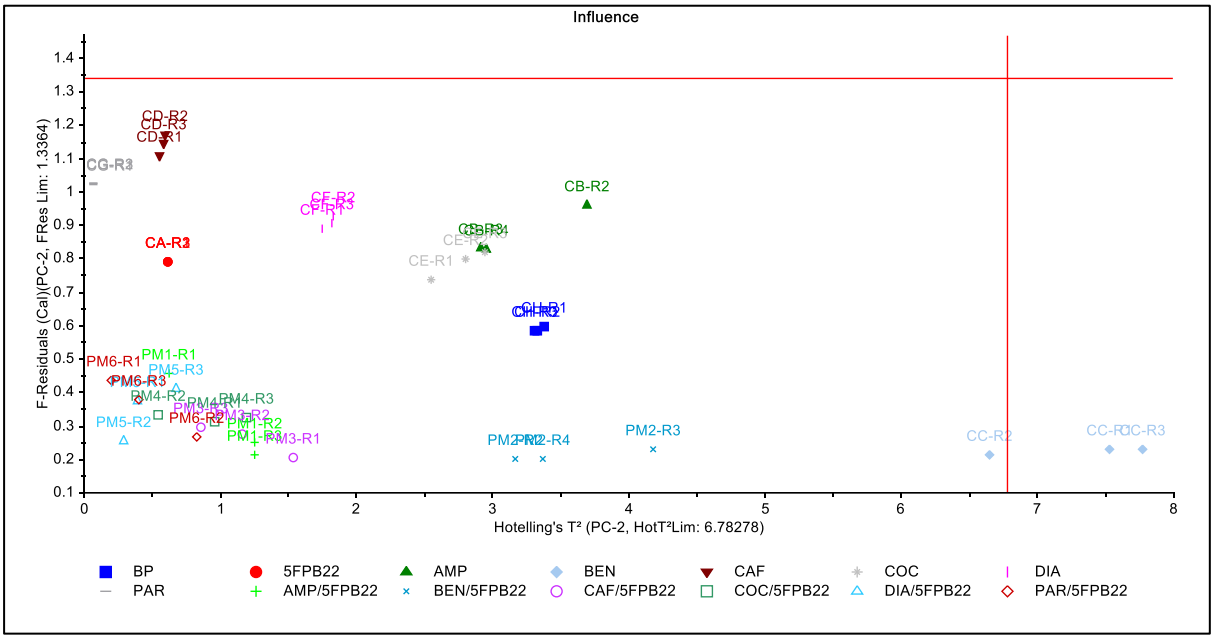

Figure A5. PC-2 F-residuals vs Hotelling T^2 influence plots of set 16.

Appendix 4.35. Raman Rigaku set 17 additional PCA plots

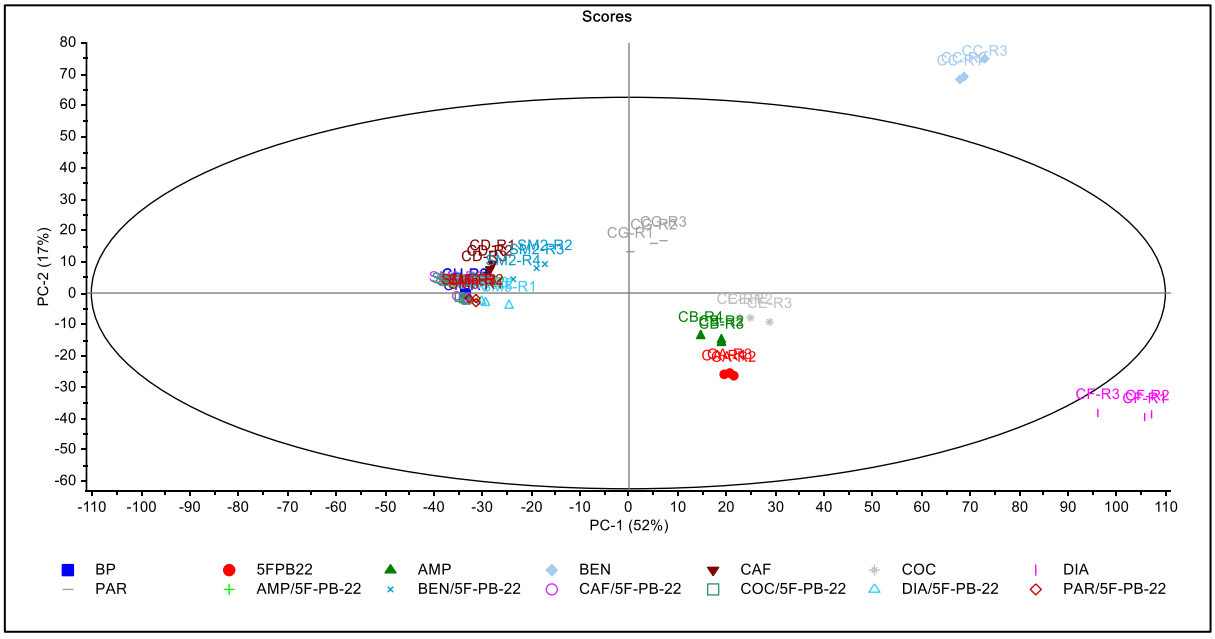

Figure A1. PC-1 vs PC-2 2D scores plot of set 17.

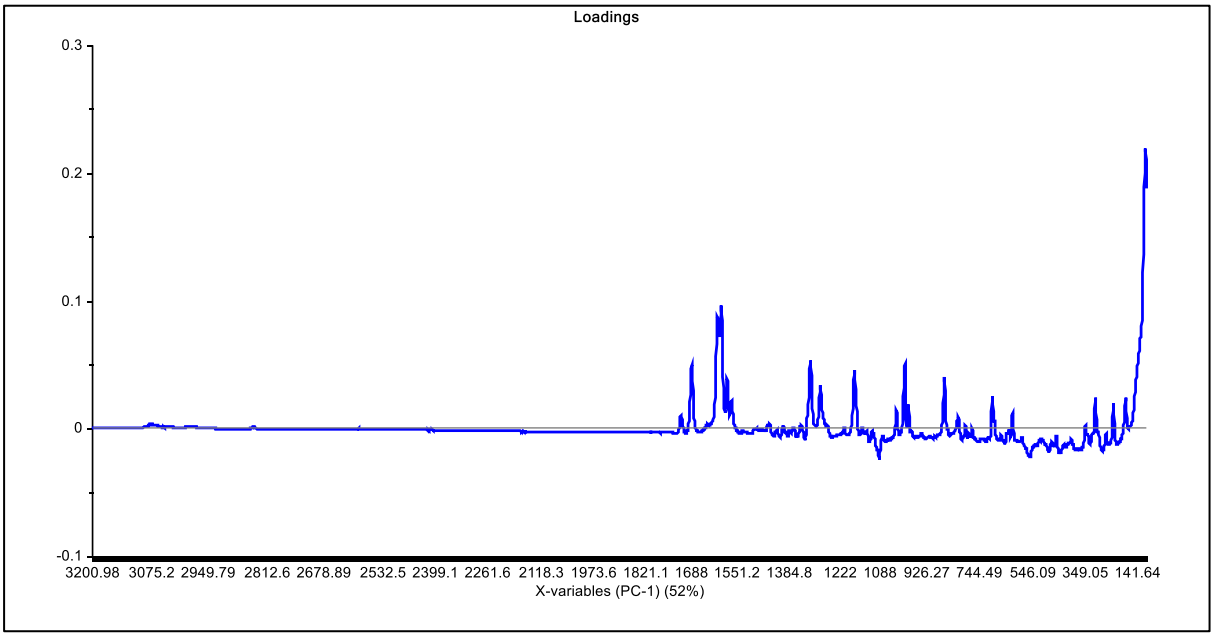

Figure A2. PC-1 loadings plot of set 17.

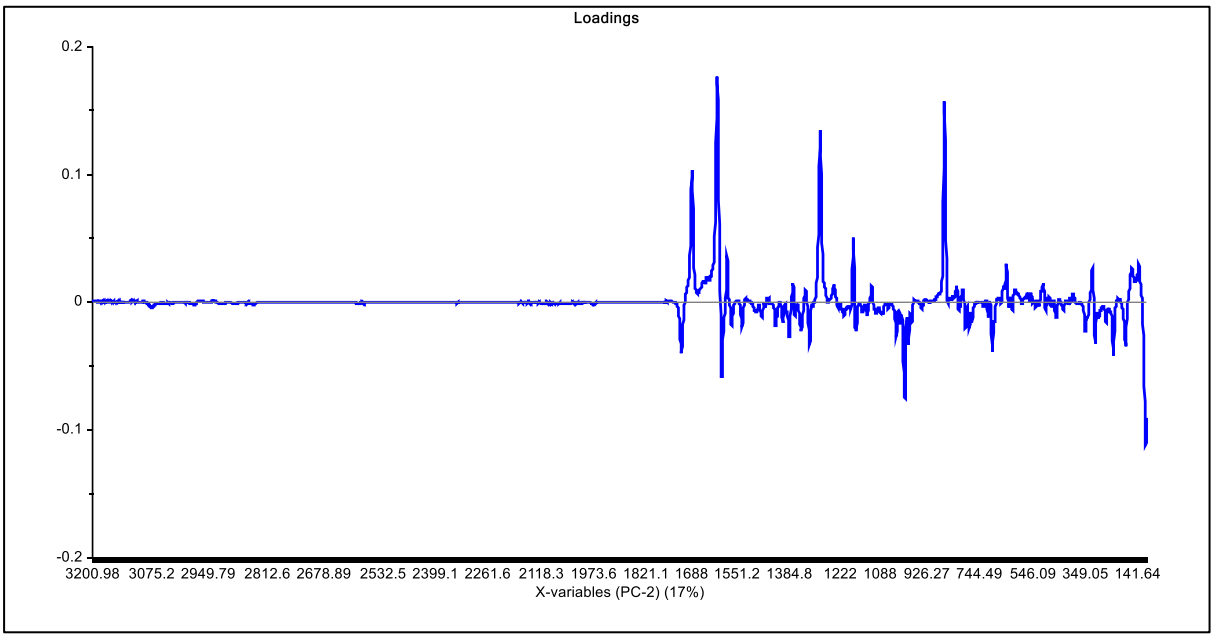

Figure A3. PC-2 loadings plot of set 17.

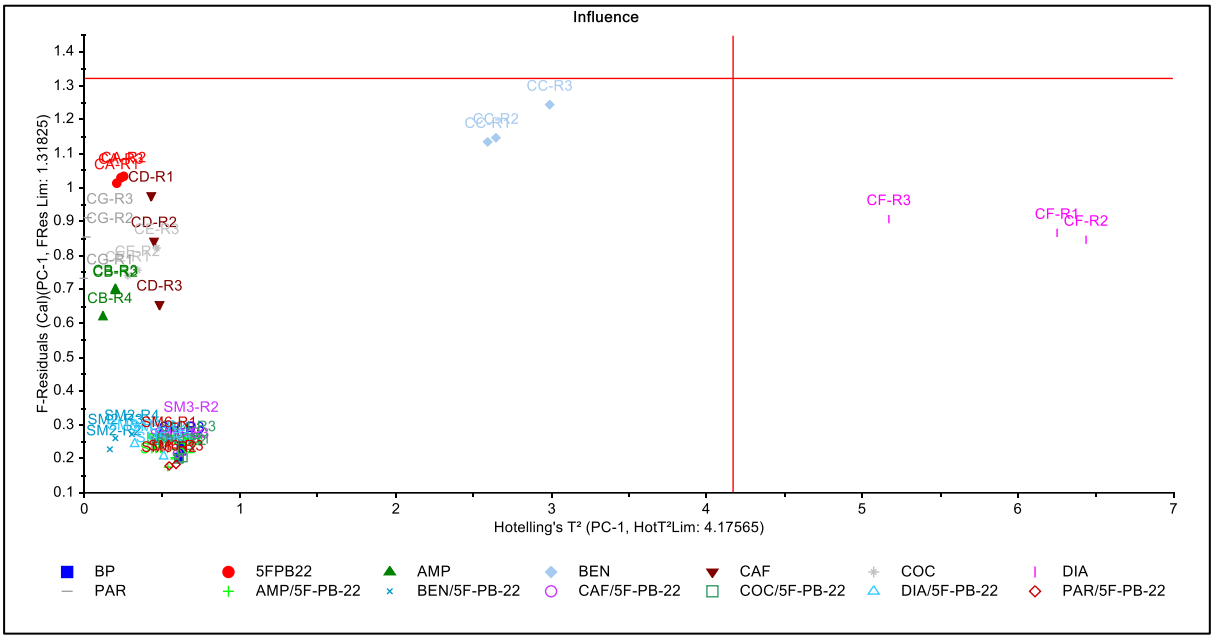

Figure A4. PC-1 F-residuals vs Hotelling T^2 influence plots of set 17.

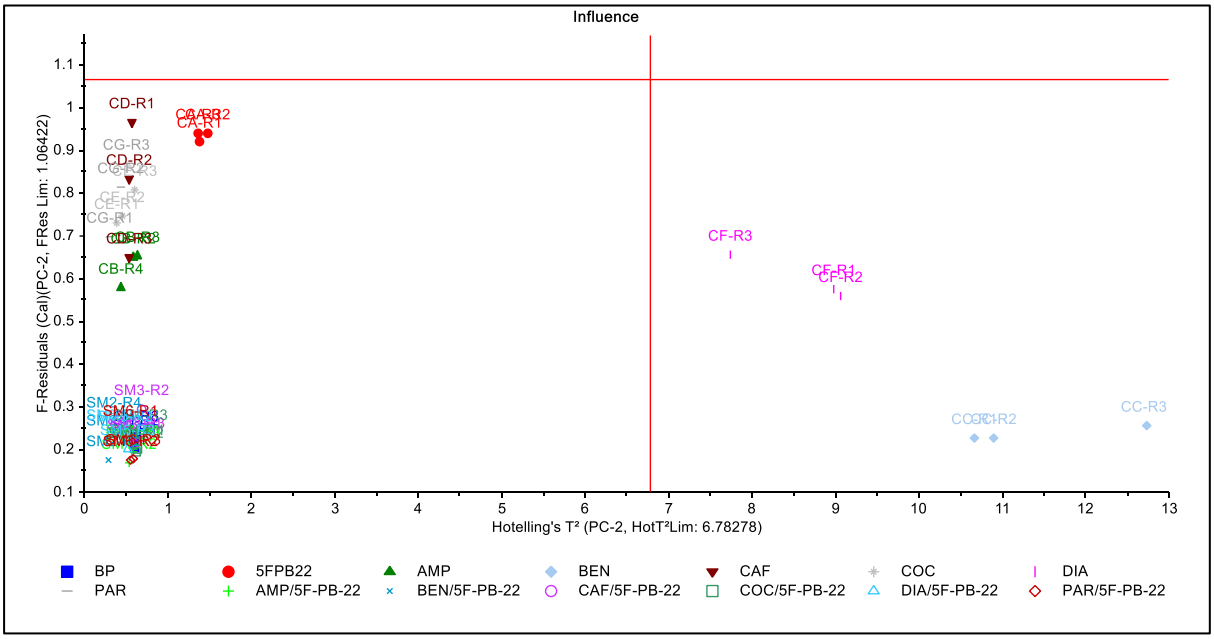

Figure A5. PC-2 F-residuals vs Hotelling T^2 influence plots of set 17.

Appendix 4.36. Raman Renishaw set 18 additional PCA plots

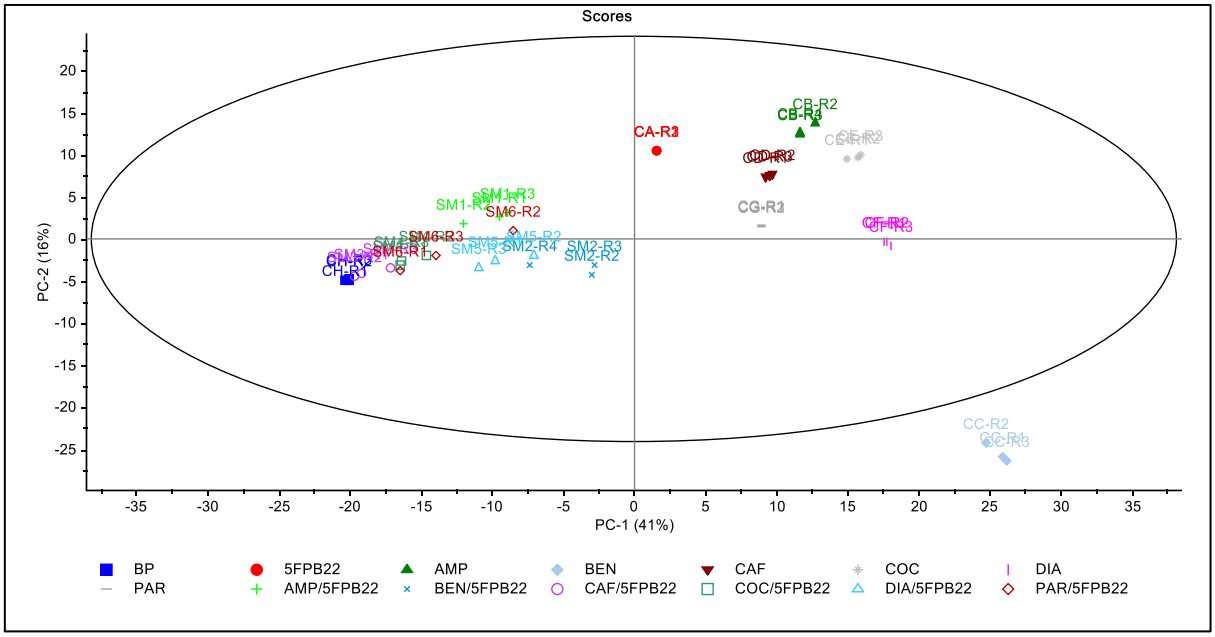

Figure A1. PC-1 vs PC-2 2D scores plot of set 18.

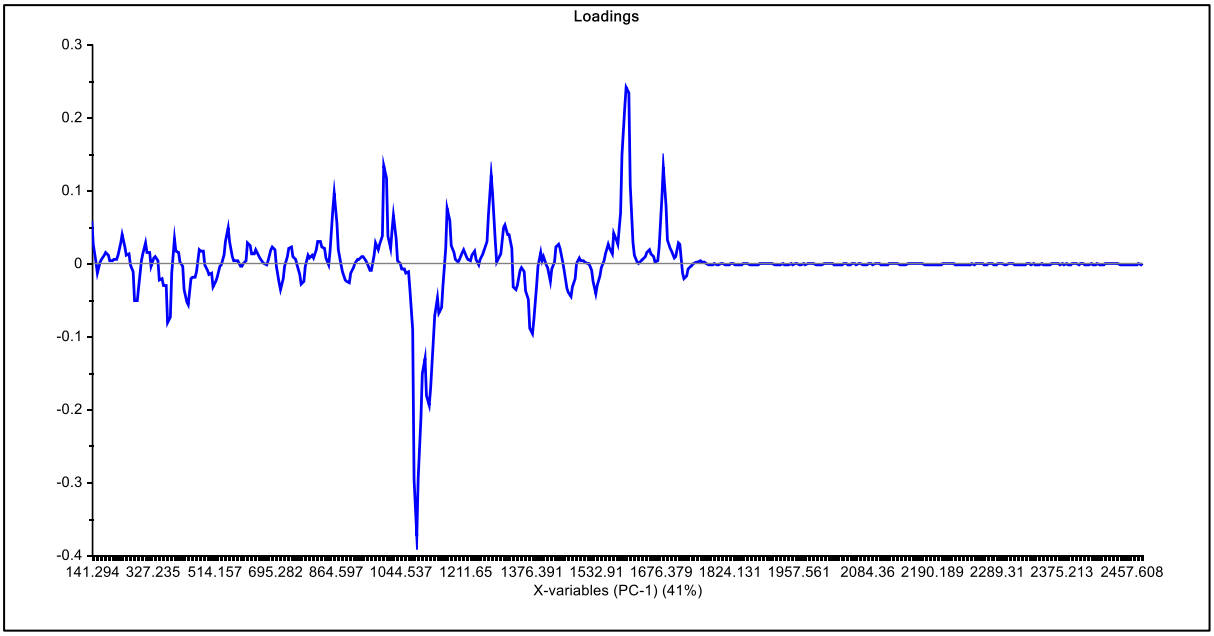

Figure A2. PC-1 loadings plot of set 18.

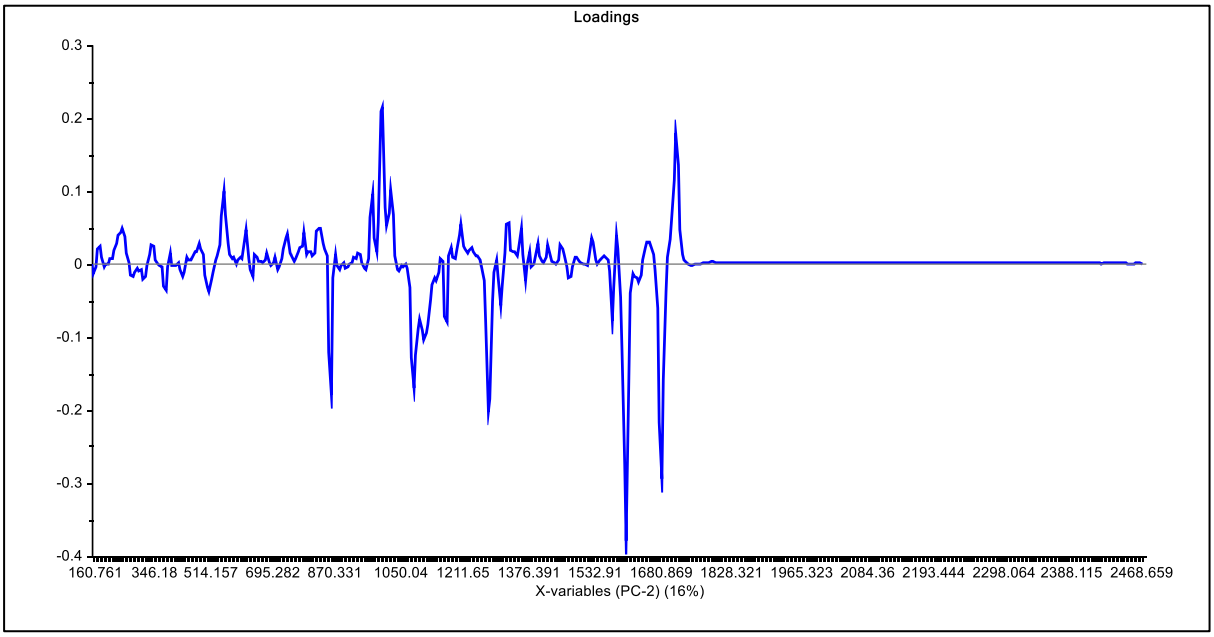

Figure A3. PC-2 loadings plot of set 18.

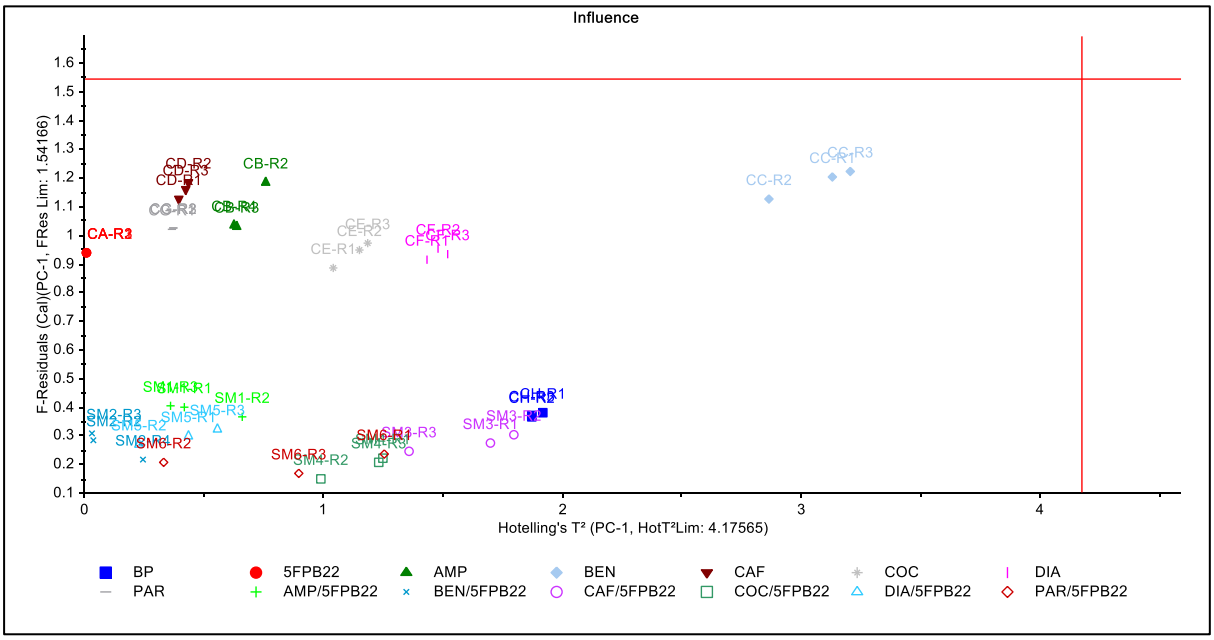

Figure A4. PC-1 F-residuals vs Hotelling T^2 influence plots of set 18.

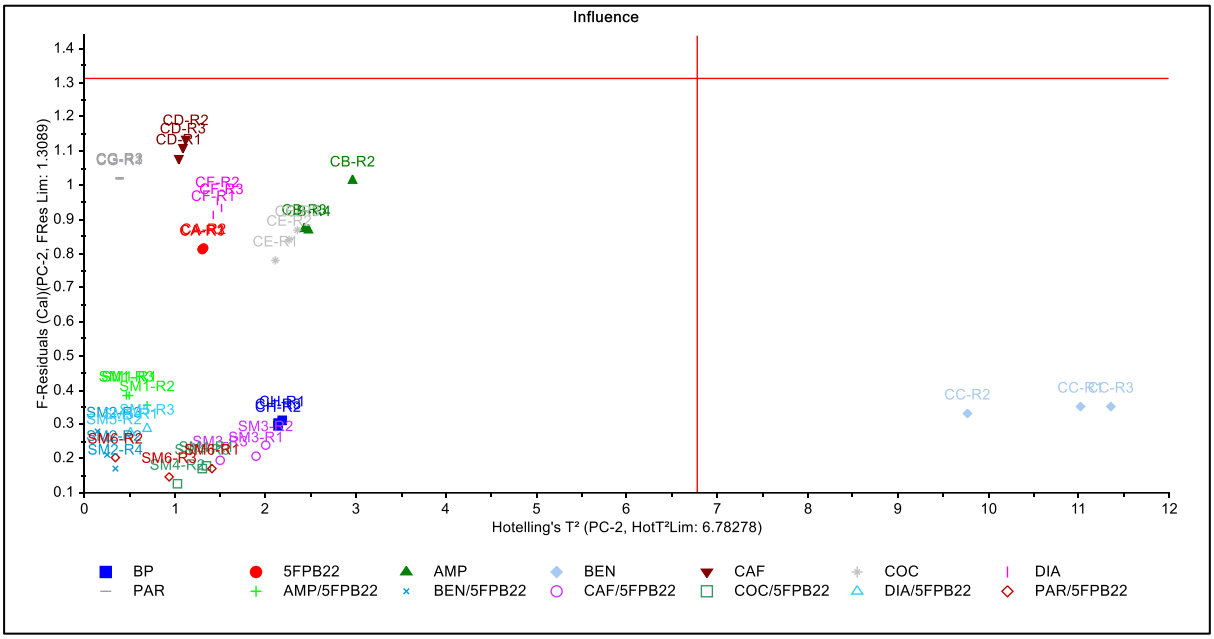

Figure A5. PC-2 F-residuals vs Hotelling T^2 influence plots of set 18.

Appendix 5. (Chapter 6)

Appendix 5.1. Additional 3D surface plots showng the interaction between (A) agar concentration and (B) extraction time, C) weight applied and (B) sonication.

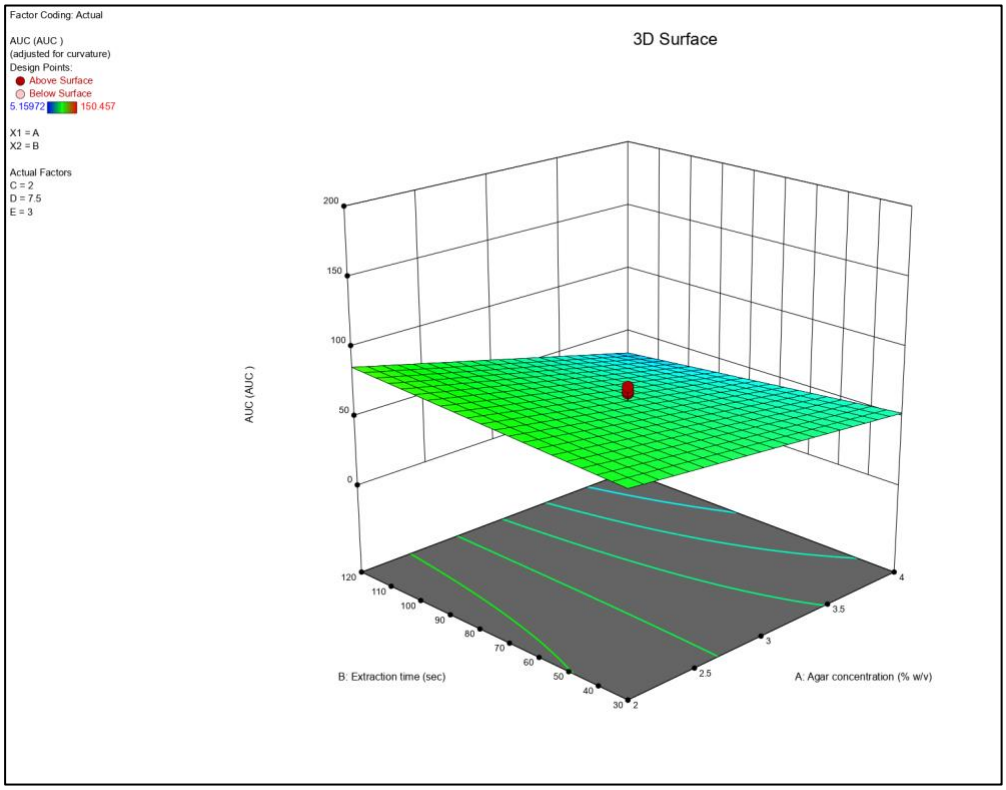

Figure A1. 3D surface plot of the interactions between the factors (A) agar concentration and (B) extraction time.

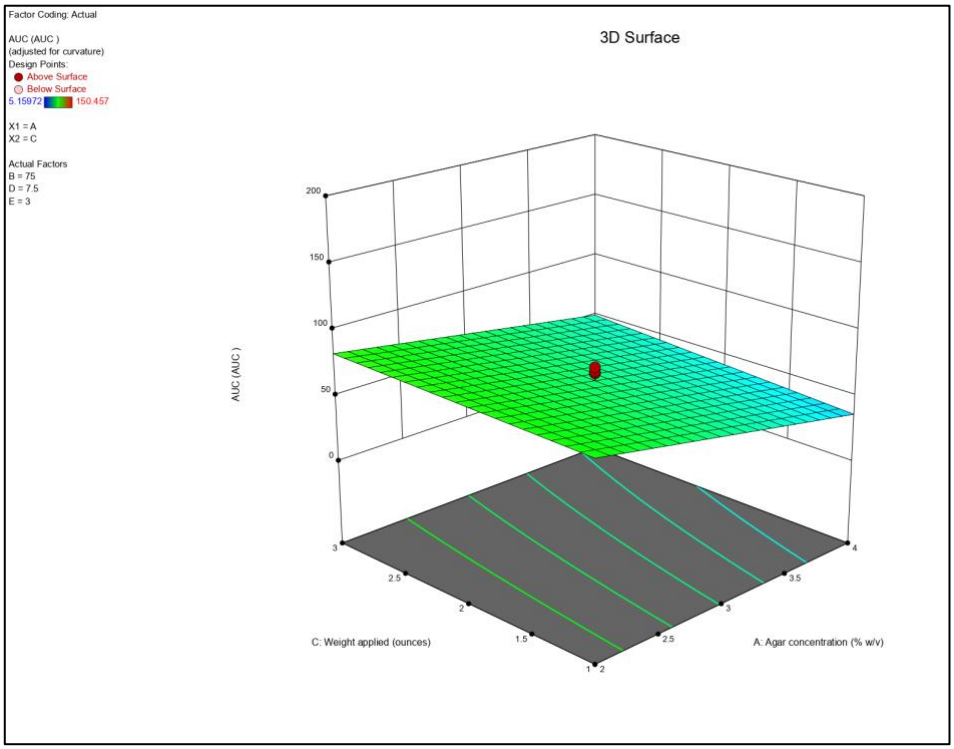

Figure A2. 3D surface plot of the interactions between the factors (A) agar concentration and (C) weight applied.

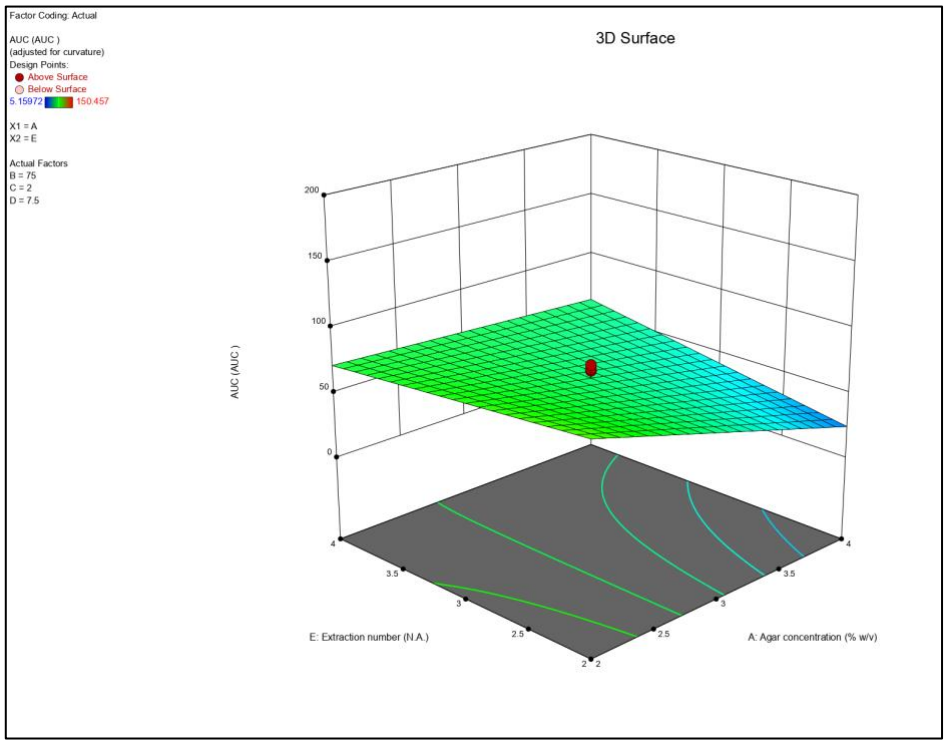

Figure A3. 3D surface plot of the interactions between the factors (A) agar concentration and (E) extraction number.

Appendix 5.1. Contour plot of the response of the interactions between the factors (A) agar concentration and (B) sonication.

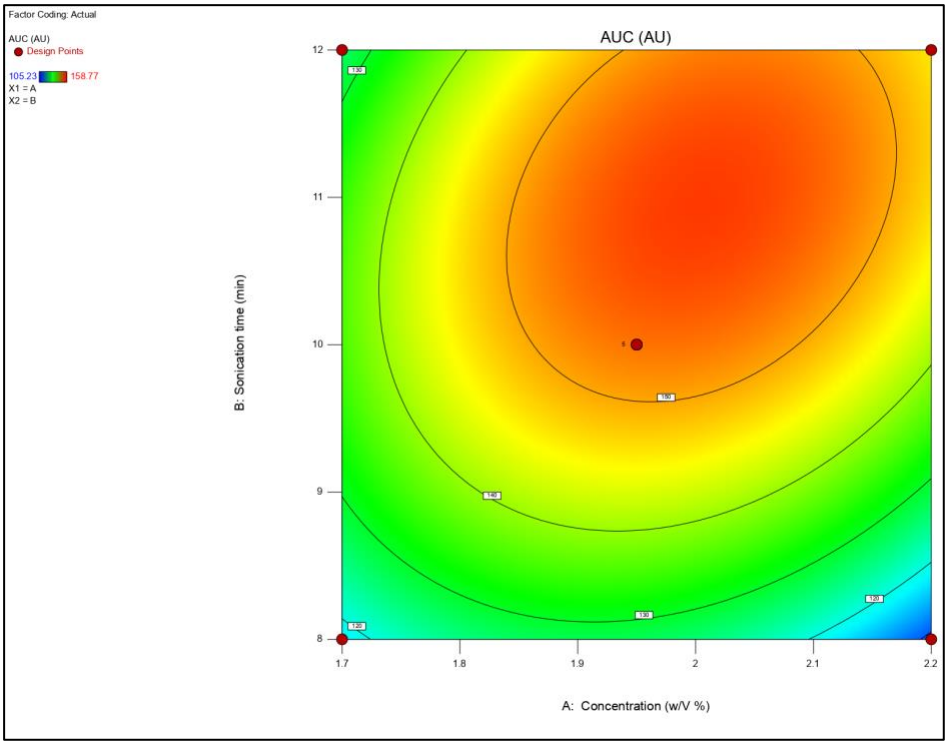

Figure A1. Contour plot of the response of the interactions between the factors (A) agar concentration and (B) sonication.

10. Achievements

10.1. Publications

- "NPS detection in Prison: A Systematic Literature Review of Use, Drug Form, and Analytical Approaches". Giorgia Vaccaro, Amira Guirguis, Stewart B. Kirton, Jacqueline L. Stair. Drug Test Anal. 2022;1-18. doi:10.1002/dta.3263

- "Characterisation of designer benzodiazepines purchased of the internet and clinical implications". Amira Guirguis, Anthony Mullin, Giorgia Vaccaro, Jacqueline Stair, Fabrizio Schifano. Drafting in progress.

- "In-Field and Laboratory-Based Analytical Characterisation of Psychoactive Substances from a UK Home Office Licensed community drug checking service". Amira Guirguis, Anthony Mullin, Giorgia Vaccaro, Rosalind Gittins, Salvatore Ferla, Fabrizio Schifano. Drafting in progress.
- "Screening and Quantitative Analysis of Psychoactive Substances from seized paper Prison sample using High Performance Liquid Chromatography- Mass Spectrometry". Giorgia Vaccaro, Daniel Baker, Amira Guirguis, Stewart B. Kirton, Jacqueline L. Stair. Drafting in progress.

10.2. Poster and oral presentations

- "Life and Medical Science Research Conference", Hatfield, 10/04/18- poster presentation.
- "Analytical Research forum 2018", London, 20/06/18- Poster presentation.
- "JPAG Pharmaceutical Analysis Research & Careers Symposium", Royal Society of Chemistry, London, 20/11/18- Poster presentation.
- "New Psychoactive Substances - Bringing diagnostics to new highs" symposium, London, 29-30/11/18- Poster presentation.
- "Life and Medical Science Research Conference" Hatfield, 17/04/19- Poster presentation.
- "Emerging Analytical Professionals 2019", Leeds, 10-12/05/19-Poster presentation.
- "Life and Medical Science Research Conference" Hatfield, 22/06/21- Oral presentation.

10.3. Awards

- "Analytical Research forum 2018", London, 20/06/18- Bursary awarded.
- "JPAG Pharmaceutical Analysis Research & Careers Symposium", Royal Society of Chemistry, London, 20/11/18- Bursary awarded.
- "New Psychoactive Substances- Bringing Diagnostics to New Highs symposium, London, 29-30/11/18- Partial bursary awarded.
- "Emerging Analytical Professionals 2019", Leeds, 10-12/05/19- Bursary awarded.
- "Analytical Research forum 2019", London, 25/06/19- Bursary awarded.
- "Postgraduate Research Student Conference 2018", University of Hertfordshire, Hatfield, 15/10/18- 1st prize in the Vision and Voice competition awarded.
- "Doctoral Training Alliance- summer school", University of Central Lancashire, Preston, 10-12/07/19, Bursary and 1st prize in the "Images of research" competition awarded.

10.4. Other achievements

- Analytical skills gained through contributions to "Nitrous oxide content analysis in canisters".
- Analytical skills gained through contributions to "In-Field and Laboratory-Based Analytical Characterisation of Psychoactive Substances from a UK Home Office Licensed community drug checking service".
- Analytical skills gained through contributions to "Characterisation of designer benzodiazepines purchased of the internet and clinical implications".

10.5. Supervision and learning teaching and assessments

- MPharm final project Erasmus students' supervision.
- First year MPharm student learning, teaching and assessments.

10.6. Specialist training

- "Renishaw Benchtop Raman training", University of Hertfordshire, Hatfield, 01/12/18.
- "Titration and High-Performance Liquid Chromatography masterclass", University of Hertfordshire, Hatfield, 21/05/18.

- “Unscrambler X Multi Variate Analysis 1 training”, Stansted, 22-23/05/18.
- “See through Portable Raman demo”, University of Hertfordshire, Hatfield, 14/06/18.
- “Naloxone administration training”, University of Hertfordshire, Hatfield, 15/06/18.
- “Malvern DLS” webinar, 19/09/19.
- “Waters Mass Spectrometry Fundamentals” webinars, 26/09/19.